THE JOURNAL
OF
CHEMICAL PHYSICS

VOLUME 21, NUMBER 11 NOVEMBER, 1953

Magnetic Study on High Polymers. I. Diamagnetic Anisotropy of Natural Rubber

AKIRA ISIHARA
Department of Physics, Faculty of Science, University of Tokyo, Japan

AND

HAZIME KUSUMOTO,* HIROSHI NAGANO, AND KEICHI OSHIMA
Institute of Science and Technology, University of Tokyo, Japan

(Received June 29, 1953)

The magnetic anisotropy of natural rubber was measured by Krishnan's oscillation method. In the first place, the anisotropy was measured by varying the time of vulcanization and was found to decrease with the time of vulcanization. In the second place, the anisotropy was measured as a function of temperature. Similar to the breadth of nuclear magnetic resonance line, an abrupt change in the slope of the anisotropy *versus* temperature curve was observed at the second-order transition temperature. Above and below this transition temperature, its change with temperature was not so strong.

1. INTRODUCTION

THERE are totally different views on the nature of second-order transitions in high polymers. Some authors believe that the transitions are true thermodynamic transitions, whereas the others consider the transitions to be apparent. To settle this point, there have been carried out many different experimental investigations on the second-order transitions. Among these, density, heat capacity, index of refraction, dielectric constant, stress temperature studies, etc. are the principal methods,[1] and magnetic studies seem to be very scarce. Selwood and Toor,[2] and Cotton-Feytis[3] have made studies on the magnetic anisotropy of natural and synthetic rubbers. However, since they have measured the anisotropy as a function of elongation, it seems worthwhile to investigate the temperature dependence of the anisotropy. Recently Guth,[4] *et al.* made a very interesting study of the second-order transitions by the method of nuclear magnetic resonance absorption. The anisotropy *versus* temperature curve obtained in our experiment was very similar to the width-temperature curves obtained by these authors. Since the physical properties of rubber-like substances are dependent on the degree of vulcanization and since we used vulcanized rubber of fixed elongation for the study of the temperature dependence of anisotropy, we first investigated the dependence of anisotropy on the degree of vulcanization.

2. EXPERIMENTAL

The composition of the rubber sample used was the following: 200 g natural rubber FAQ, 2 g stearic acid, 10 g zinc oxide, 1 g diphenylguanidine, 2 g dibenzothiazoldisulfide, and 6 g sulfur. The natural rubber was mixed with the other ingredients and rolled into a sheet. In the form of thin sheet approximately 1 mm thick, the natural rubber was vulcanized by a hot press, heated to 140±2°C by an electric heater.

A strip of rubber about 10 mm long was cut from the sheet to form a ring and the both ends of the strip, overlapping 1 to 2 mm, were joined together by rubber solution of the same composition.

Polyethylene cores of different size were put into this rubber ring to stretch the ring in different magnitudes.

The magnetic anisotropy was measured by Krishnan's oscillation method. The apparatus is illustrated in Fig. 1. The sample fixed to a glass hook, as in Fig. 1(c), was

* On leave from the Research Laboratory, Nippon Rubber Company Ltd.

[1] See, for example, *Advances in Colloid Science* (Interscience Publishers, Inc., New York, 1946), Vol. VI, pp. 1–55.

[2] E. W. Toor and P. W. Selwood, J. Am. Chem. Soc. **72**, 1269 (1950), etc.

[3] E. Cotton-Feytis, Compt. rend **214**, 485 (1942); **215**, 299 (1942). These articles were not available to us in preparing this paper. We inferred their results through the papers of Selwood *et al.*

[4] Holroyd, Codrington, Mrowca, and Guth, J. App. Phys. **22**, 696 (1951).

TABLE I. The change in the anisotropy in cgs units on varying the temperature.

Cooling agents	Room temperature	Ice and water		Ice and sodium chloride	Ice and caustic potash	Dry ice and alcohol (or ether)			Liquid air			
Temperature	9.5	5	0	−15	−30	−50	−60	−72	−90	−100	−150	−180
Δx in cgs units	13.1	13.7	13.5	14.1	15.0	15.6	16.7	16.9	21.5	24.3	27.2	28.1

attached to a glass hanger carrying a mirror, shown in Fig. 1(b), and suspended from the torsion head with a quartz fiber of 7μ in diameter and 20 cm in length. This sample was inserted in a homogeneous magnetic field and oscillated. The period of oscillation was read by the deflection of the mirror.

The magnetic field was produced by a Weiss electric magnet in a 5-cm gap with flat 10-cm diameter pole faces. A current of 8 to 10 amperes from a battery, charged by a generator during operation, produced a stable magnetic field of 3800 to 4800 gauss at the center of the field.

The temperature of the sample, calibrated previously by a thermometer inserted into its place, was controlled and maintained by the temperature and the quantities of the cooling agents in the Dewar vessel. The cooling agents used are shown in Table I.

By this method, the diamagnetic anisotropy Δx_r per repeating unit of rubber molecule is given by the formula,

$$\Delta x_r = \frac{T_0^2 - T_{pr}^2}{T_{pr}^2} \cdot \frac{CM_r}{m_r H} - \Delta x_p,$$

where: T_0 is the period of oscillation of the sample with magnetic field off, in sec; T_{pr} is the period of oscillation of the sample with magnetic field on, in sec; M_r is the molecular weight of isoprene, in grams; m_r is the weight of the rubber sample, in grams; H is the strength of the magnetic field, in gauss; Δx_p is Δx of the polyethylene core, in cgs units; and C is the torsional constant of the quartz fiber, in cgs units.

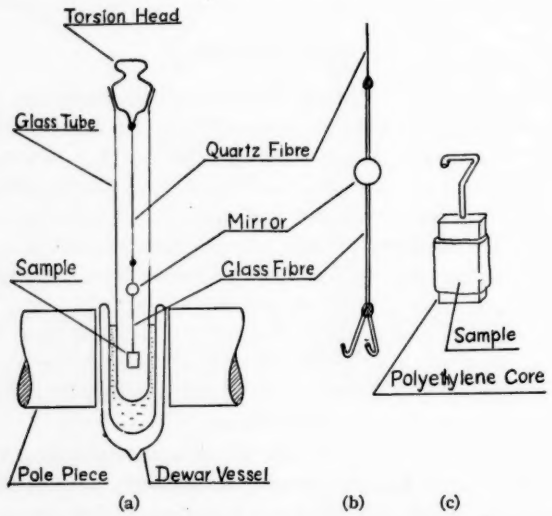

FIG. 1. (a) Apparatus for the anisotropy measurements. (b) Details of the hanger of the sample. (c) Details of the hanger of the sample.

Therefore, measurements of oscillation were made, first on the polyethylene core only and next on the sample with the polyethylene core, both in and out of the magnetic field.

3. RESULTS

1. The Anisotropy *versus* the Time of Vulcanization

In this measurement, the anisotropy was measured in the unstretched state of the sample, and the direction of the orientation of molecules of the sample caused by rolling was put parallel to the direction of the magnetic field in its initial equilibrium position. The change in the anisotropy in cgs units on varying the time of vulcanization is given in Table II and Fig. 2.

The anisotropy at the time of vulcanization zero corresponds to the effect of rolling and does not have any significant physical meaning.

2. The Anisotropy *versus* Temperature

The result of experiment on the change of Δx with temperature is illustrated in Fig. 3 and listed in Table I. In this measurement, a well-vulcanized sample, showing a saturated value of anisotropy in the first experiment, was elongated to 50 percent parallel to the direction of the magnetic field. Temperatures were controlled as described before. To establish thermal equilibrium, the sample was kept at each measuring temperature for about twelve hours before each measurement.

At higher temperatures, the variation of the anisotropy with the temperature was very slow, but increased gradually with lowering temperature. In the neighborhood of temperature of −73°C, a marked increase in the anisotropy was observed.

4. DISCUSSIONS

In the temperature range of rubber elasticity, where we can neglect the effect of crystallization, the stress dependence of the anisotropy of rubber can be treated by the same theory as that of birefringence.[5] In the

TABLE II. The change in the anisotropy in cgs units on varying the time of vulcanization.

Time of vulcanization	0	5	10	20	30	40	50	60 min
Δx in cgs units	80.3	42.9	34.0	38.7	31.7	30.7	30.3	30.8

[5] A. Isihara *et al.*, J. Appl. Phys. **23** 308 (1952).

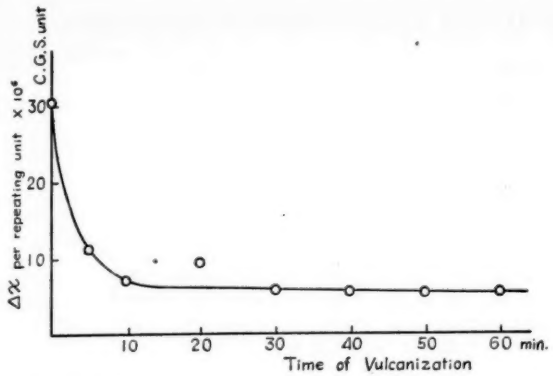

FIG. 2. Anisotropy Δx per repeating unit *versus* the time of vulcanization.

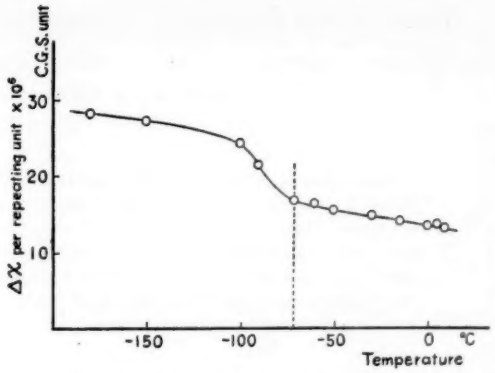

FIG. 3. Anisotropy *versus* temperature.

first approximation, it is proportional to the stress t, and the relation

$$\Delta x \sim t/kT$$

is established. Since the stress t is proportional to temperature in this range, Δx is expected to be nearly independent of temperature. In this range of temperature, the stress is not proportional to the elongation, and Δx seems not to have linear relationship with the elongation.

The theoretical formula for the anisotropy of rubber at the transition temperature is not yet given. However, the curve obtained here is very similar to the curve obtained by Guth *et al.* in their experiment on the nuclear magnetic resonance absorption line. Thus, qualitatively, we can interpret that the abrupt increase in the magnetic anisotropy is due to the sudden decrease in thermal motions of rubber molecules. From this point of view, it seems somewhat curious that in our first experiment the anisotropy was decreased with the degree of vulcanization. However, in this experiment the degree of vulcanization was determined by the time of vulcanization; so we can interpret Fig. 1(b) that the initial anisotropy produced by rolling was diminished by putting the sample at the vulcanization temperature for different duration of time. Thus, to see the effect of diminishing the thermal motions of rubber molecules on the diamagnetic anisotropy, it seems more appropriate if we could control the degree of vulcanization by the other methods, for example by controlling the quantities of accelerators or that of sulfur. However, such processes will make the degrees of initial magnetic anisotropy in each sample different, and will make the results not easy to interpret by comparison of the results with each other.

The present method is convenient in this concern, but because the result was masked by the effect of annealing, we cannot obtain knowledge about the relations between the anisotropy and the thermal motions of rubber molecules. In this connection, we wish to note that the curve of Fig. 3 resembled the rate of crystalization curves obtained by Wood and Bekkedahl.[6]

Natural rubber is known to crystalize at about 11°C and some change in the anisotropy is expected to occur at this temperature. Both in the temperature ranges of second-order transition and of the crystallization, we infer the results to be more or less dependent on the rate of decreasing or increasing temperatures. We hope to carry out further experiments on this line.

ACKNOWLEDGMENT

In conclusion, the authors wish to express their thanks to Nippon Rubber Company Ltd., especially to President Dr. K. Nagata, Vice President Dr. Y. Hori, and Director of the Research Laboratory Dr. J. Shimosato, for their kindness in giving us help in performing this work.

[6] C. A. Wood and N. Bekkedahl, J. Appl. Phys. **17**, 362 (1946).

Vapor Heat Capacities Determined by the Use of Vapor Pressure Equations

GORDON M. BARROW
Department of Chemistry, Northwestern University, Evanston, Illinois
(Received July 16, 1953)

Vapor pressure equations have proven useful in providing quantitative data on heats of vaporization but the heat capacity term, occurring in equations of the Rankine type, has been usually treated as an empirical constant. This term represents $Cp^{vap}-Cp^{liq}$ for a vapor obeying the ideal gas laws and it is shown that even for a real gas the same result may be expected to hold. This conclusion is tested for twelve compounds for which data are available. The values of Cp^0 calculated from the heat capacities of the liquid and the difference in heat capacities from the vapor pressure equation are in good agreement with those directly measured and would therefore be of use for thermodynamic calculations.

IT is well known that equations representing the temperature variation of the vapor pressure of a liquid can be used to give reliable data on the heat of vaporization. Equations of the Clausius-Clapeyron type, but assuming a linear dependence of the heat of vaporization on the temperature, can also be of use in providing, quantitatively, another term of thermodynamic importance.

The Rankine equation results from the integration of the thermodynamic relation $dP/dT=\Delta S/\Delta V$ with the assumptions that the liquid volume is negligible compared to the vapor volume, that the vapor behaves as an ideal gas, and that the heat of vaporization is a linear function of the temperature, $\Delta H=\Delta H_0+\Delta C_{sat}T$. Frost[1] has recently shown that the ideal gas assumption can be removed by the addition of a term calculable from van der Waal's constants. The resulting equation

$$\log P=A+\frac{B}{T}+C\log T+\frac{DP}{T^2}$$

adequately represents the temperature dependence of the vapor pressure and the constants have the significance that $B=-\Delta H_0/2.303R$, $C=\Delta C_{sat}/R$, and $D=a/2.303R^2$ where a is van der Waal's constant.

The term ΔC_{sat} arises from the assumption that the difference in the liquid and vapor heat capacities along the saturation curve can be represented by a constant throughout the range of the vapor pressure measurements. Since the heat capacity of a liquid is essentially independent of the pressure, for a vapor which obeys the ideal gas law the ΔC_{sat} term will also represent the difference in the heat capacities of vapor and liquid at constant pressure. Since this quantity, ΔCp, would be of use in obtaining the thermodynamically important vapor heat capacity from the more readily obtained liquid heat capacity it is of interest to consider the significance of the ΔC_{sat} term for a non-ideal vapor.

The enthalpy of a real vapor along the saturation curve will be a function of both the pressure and the temperature, as indicated by the total differential

$$dH=(\partial H/\partial T)_P dT+(\partial H/\partial P)_T dP.$$

The vapor contributions to the ΔC_{sat} term will therefore be

$$\left(\frac{\partial H}{\partial T}\right)_{sat}=Cp+\left(\frac{\partial H}{\partial P}\right)_T\left(\frac{\partial P}{\partial T}\right)_{sat}$$

and the heat of vaporization will be represented by

$$\Delta H=\Delta H_0+\Delta Cp\,T+\int\left(\frac{\partial H}{\partial P}\right)_T\left(\frac{\partial P}{\partial T}\right)_{sat}dT.$$

Here the deviation from ideal behavior has been explicitly separated, and it is apparent that on substitution in $dP/dT=\Delta S/\Delta V$ and integration this additional term will contribute to the $C\log T$ term of the vapor pressure equation only to the extent that

$$\int\left(\frac{\partial H}{\partial P}\right)_T\left(\frac{\partial P}{\partial T}\right)_{sat}dT$$

is a constant.

The variation of enthalpy with pressure is not sufficiently understood for real gases to enable a reliable form for $(dH/dP)_T$ to be written for the range of temperature and pressure of the vapor pressure measurements. To obtain some idea of the size and form of this gas imperfection term, however, we may represent the deviation from ideal behavior by $PV=RT+BP$ with $B=a+be^{c/T}$, where a, b, and c are empirical constants as discussed by Scott, Waddington, Smith and Huffman.[2]

This virial equation, with numerical values of a, b, and c for some representative hydrocarbons, leads to an additional term in the integrated vapor pressure equation which has about the same form and magnitude as Frost's[1] van der Waal correction term. We may expect therefore that this term will contribute little to the $C\log T$ term and that the C can be identified with $\Delta Cp/R$. Since different forms of the equation of state for the vapor may lead to terms in the vapor pressure equation which will interfere with this identification, a comparison of ΔCp calculated from the vapor pressure equation with that observed would be helpful in determining the general validity of this conclusion.

[1] A. A. Frost and D. R. Kalkwarf, J. Chem. Phys. **21**, 264 (1953).

[2] Scott, Waddington, Smith, and Huffman, J. Chem. Phys. 15, 565 (1947).

TABLE I. Comparison of observed vapor heat capacities (cal/mole deg) with those calculated from vapor pressure equation data.

	Range of v.p. data (°K)	T°K	Cp(liquid)	$Cp^{liq}-Cp^{vap}$ (from v.p. eq'n.)	Cp^{vap}(calc)	$Cp^{vap}-Cp^{0}$	Cp^{0}(calc)	Cp^{0}(obs)	ΔCp^{0}
Methane	90–190	95.1	(12.8)[a]	5.33	(7.5)	0.2[b]	(7.3)	8.0[c]	−0.7
Ethane	136–305	180	17.3[d]	7.09	10.2	0.35[b]	9.8	9.8[e]	0.0
Propane	180–370	250	24.3[f]	8.40	15.9	0.6[g]	15.3	15.1[g]	0.2
n-Butane	195–425	270	31.6[h]	10.00	21.6	0.4[i]	21.2	21.5[j]	−0.3
n-Pentane	245–470	298.16	40.9[k]	10.60	30.3	0.5[m]	29.8	28.7[j]	1.1
			39.6[l]		29.0		28.5		−0.2
n-Hexane	253–507	298.16	46.8[n]	11.84	35.0	0.4[p]	34.6	34.2[j]	0.4
n-Heptane	273–540	298.16	53.7[q]	12.83	40.9	0.2[r]	40.7	39.7[j]	1.0
n-Octane	263–569	298.16	60.7[q]	14.07	46.6	0.1[s]	46.5	45.1[j]	1.4
Benzene	273–353	300	32.5[t]	12.31[u]			20.2	19.6[v]	0.6
		320	33.7				21.4	21.2	0.2
		350	35.6				23.3	23.5	−0.2
Naphthalene	373–493	451.0	62.9[w]	14.88[x]	48.0	0.2[y]	47.8	48.1[y]	−0.3
Water	270–640	373.16	18.12	8.86	9.26	0.80[z]	8.46	8.13[z]	0.33
Mercury	400–700	400	6.54*	1.32†	5.22	0.00*	5.22	4.97[c]	0.25
		550	6.48		5.16	0.01	5.15	4.97	0.18
		700	6.53		5.21	0.07	5.14	4.97	0.17

[a] Estimated from the entropy data of A. Frank and K. Clusius, Z. physik. Chem. **B36**, 291 (1937).
[b] Calculated from the Berthelot equation.
[c] Calculated statistically.
[d] R. K. Witt and J. D. Kemp, J. Am. Chem. Soc. **59**, 273 (1937).
[e] J. D. Kemp and K. S. Pitzer, J. Am. Chem. Soc. **59**, 276 (1937).
[f] J. D. Kemp and C. J. Egan, J. Am. Chem. Soc. **60**, 1521 (1938).
[g] Estimated from the data of G. B. Kistiakowsky and W. W. Rice, J. Chem. Phys. **8**, 610 (1940).
[h] J. G. Aston and G. Messerly, J. Am. Chem. Soc. **62**, 1917 (1940); Huffman, Parks, and Barmore, J. Am. Chem. Soc. **53**, 3876 (1931).
[i] Estimated from the data of B. P. Dailey and W. A. Felsing, J. Am. Chem. Soc. **65**, 44 (1943).
[j] W. B. Person and G. C. Pimentel, J. Am. Chem. Soc. **75**, 532 (1953).
[k] G. H. Messerly and R. M. Kennedy, J. Am. Chem. Soc. **62**, 2988 (1940).
[l] G. S. Parks and H. M. Huffman, J. Am. Chem. Soc. **52**, 4381 (1930).
[m] Estimated from the data of K. S. Pitzer, J. Am. Chem. Soc. **63**, 2413 (1941).
[n] D. R. Douslin and H. M. Huffman, J. Am. Chem. Soc. **68**, 1704 (1946).
[p] From the data of G. Waddington and D. R. Douslin, J. Am. Chem. Soc. **69**, 2275 (1947).
[q] N. S. Osborne and D. C. Ginnings, J. Research Natl. Bur. Standards **39**, 453 (1947).
[r] Extrapolated from the data of Waddington, Todd and Huffman, J. Am. Chem. Soc. **69**, 22 (1947).
[s] Estimated from the data of G. M. Barrow, J. Am. Chem. Soc. **73**, 1824 (1951).
[t] J. S. Burlew, J. Am. Chem. Soc. **62**, 696 (1940).
[u] $Cp^{liq}-Cp$, see reference 2.
[v] "Selected Values of Properties of Hydrocarbons," Circular of the National Bureau of Standards C461, U. S. Government Printing Office, Washington, D. C., 1947.)
[w] Spaght, Thomas and Parks, J. Phys. Chem. **36**, 882 (1932).
[x] O. A. Nelson and C. E. Senseman, Ind. Eng. Chem. **15**, 621 (1923); **14**, 58 (1922).
[y] G. M. Barrow and A. L. McClellan, J. Am. Chem. Soc. **73**, 573 (1951).
[z] McCullough, Pennington and Waddington, J. Am. Chem. Soc. **74**, 4439 (1952).
* R. H. Busey and W. F. Giauque, J. Am. Chem. Soc. **75**, 806 (1953).
† A. W. C. Menzies, Z. physik Chem. **130**, 90 (1927).

Lack of constancy of ΔCp over the range of the vapor pressure measurements may also lead to a discrepancy. If ΔCp is not constant then the calculated difference in heat capacities over the temperature range of the vapor pressure measurements and the comparison with the measured heat capacities should then be made at some intermediate temperature. Although this has been done as much as possible, the availability of measured liquid and vapor heat capacities dictated the possible temperatures at which the comparison can be made.

Table I gives the data for some compounds for which reliable heat capacity and vapor pressure data are available. The vapor pressure equations are from the work of Frost[1] except where otherwise indicated. The last three columns show the ideal gas state heat capacities calculated from the liquid heat capacities by means of the vapor pressure equation, the observed or statistically calculated ideal gas state heat capacity, and the difference in the calculated and observed values. The agreement is quite satisfactory, the differences being little larger than the uncertainties in the thermal data. For *n*-heptane and *n*-octane the temperature at which the comparison can be made is sufficiently far from the average temperature of the vapor pressure measurements to account for the larger errors for these two compounds.

The gas imperfection corrections for the saturated vapors are quite large and have been estimated from experimental values except for methane and ethane for which no data are available. For these compounds, corrections have been estimated from the Berthelot equation. The vapor pressure and heat of vaporization of benzene have been discussed by Allen, Everett and Penney,[3] who used a correction term in the vapor pressure equation similar to that introduced by Frost but based on the second virial coefficient. Their treatment leads directly to the ideal gas state heat capacity, as given in Table I, rather than to that of the saturated vapor.

Since the agreement of the calculated and observed ideal gas state heat capacities of Table I is very satisfactory, it would appear that vapor pressure equations of the Rankine or Frost type can provide useful quantitative information on the vapor heat capacity when the more easily measured liquid state heat capacity is known. This treatment might be particularly useful in providing comparisons for statistical calculations on compounds whose vapor state thermodynamic properties are not easily directly measured, as a result, for example, of low stability or low vapor pressure. In any case, the physical significance of this heat capacity constant in the vapor pressure equations of this type argues for the general use of such equations rather than the more empirical equations.

[3] Allen, Everett, and Penney, Proc. Roy. Soc. (London) **A212**, 149 (1952).

Mean Dimensions of Rubber-Like Polymer Molecules

FREDERICK T. WALL
Noyes Chemical Laboratory, University of Illinois, Urbana, Illinois
(Received April 7, 1953)

The mean square end-to-end separations of coiling type polymer molecules have been calculated by two different approximate methods, taking into account the effect of excluded volumes. One of the methods is the equivalent of a first-order perturbation calculation using the unrestricted random walk as a starting approximation. The other method involves the use of certain plausible functional forms valid for large values of the chain lengths. The calculations have been carried out for three, two, and one dimensions and the results are analyzed to provide an insight into factors which might determine convergence or divergence of the quotient $\langle r_n^2\rangle_{Av}/n$ (the mean-square length divided by the number of links). It appears that the quotient converges in three (or more) dimensions, but diverges for a lower number of dimensions.

INTRODUCTION

A CONSIDERABLE amount of attention has been given to the theoretical problem of the dimensions of rubber-like polymer molecules. Assuming that such a molecule is made up of freely rotating links, completely unrestricted with respect to their orientations, then the problem of end-to-end length distribution reduces to the so-called "random walk" problem, which can be solved quite exactly by relatively simple means. The "random walk" solution is only approximately correct, however, since no restriction is made against stepping on the same spot twice, which for a polymer molecule would be equivalent to permitting two atoms (or monomer units) to occupy the same site. The purpose of the present treatment is to take into account the effect of such volume restrictions; this will be done by approximate methods which, it is hoped, are sufficiently accurate, at least for the three-dimensional problem, to correspond closely to reality.

The calculations here reported are directed toward determining the nature of the dependence of the mean-square molecular length $\langle r_n^2\rangle_{Av}$ on the number of links n with particular reference to the possible existence of a limit to the quotient $\langle r_n^2\rangle_{Av}/n$ as n becomes infinite. The convergence or divergence of this quotient is a matter of some importance about which there is no definite agreement. The calculations of Hermans *et al.*,[1,2] Grimley,[3] Hadwiger,[4] and Montroll[5] suggest convergence, whereas Flory[6] and Rubin[7] maintain that $\langle r_n^2\rangle_{Av}/n$ increases without limit as $n\rightarrow\infty$. Although the conclusions here advanced will not be deduced with absolute rigor, a plausible case will be built in favor of convergence of the aforementioned ratio for the three-dimensional case and divergence for two dimensions.

Two different approximate methods will be used, each of which, however, utilizes the same basic equations. The initial procedure to be employed is substantially equivalent to a first-order perturbation method in which the solution to the unrestricted random walk problem is utilized as the zeroth-order approximation. Taking into account the existence of excluded sites, we shall derive a difference equation relating $\langle r_n^2\rangle_{Av}$ to n, and will compare the equation so obtained with that applicable when no site restrictions are involved. An additional term appearing in the more complete equation will be considered a perturbation, and an improved value for the mean-square end-to-end separation of polymer chains will then be calculated by appropriate operation of this perturbation on the known solution of the unrestricted (i.e., unperturbed) problem. Hermans, Klamkin, and Ullman[2] have already treated the problem by another perturbation method which leads to substantially equivalent results. However, our calculations take cognizance of the density of matter within a polymer molecule in a somewhat different manner and the approximate density functions are also illustrated by contour maps. Moreover, the calculations have also been carried out for the one- and two-dimensional problems to gain a fuller insight into the general factors involved and how they affect the functional dependence of chain length upon molecular weight. The second method which we shall use will also utilize the difference equation with the perturbation term mentioned above, but a different kind of approximation will be made to evaluate the result.

DERIVATION OF DIFFERENCE EQUATION

For the sake of simplicity we shall assume that a polymer molecule can be represented by a string of beads that can be placed in a three-dimensional simple cubic lattice with each bead located at a lattice point. The bonds joining successive beads in the polymer molecule are each assumed to be parallel to one of the coordinate axes (x, y, or z), and the lattice spacing will be taken as unity. According to this model, the bond angles will be either 0, $\pi/2$ (with a weight factor of 4), or π.

Let us suppose that a particular polymer molecule consisting of n links has one end at the origin and the

[1] J. J. Hermans, Rec. trav. chim. **69**, 220 (1950).
[2] Hermans, Klamkin, and Ullman, J. Chem. Phys. **20**, 1360 (1952).
[3] T. B. Grimley, Proc. Roy. Soc. (London) **212**, 339 (1952).
[4] H. Hadwiger, Makromol. Chem. **5**, 148 (1951).
[5] E. W. Montroll, J. Chem. Phys. **18**, 734 (1950).
[6] P. J. Flory, J. Chem. Phys. **17**, 303 (1949).
[7] R. J. Rubin, J. Chem. Phys. **20**, 1940 (1952).

other end at a lattice point (x, y, z), and let $p_n(x, y, z)$ denote the probability that the molecule possesses the indicated end-to-end separation. Now let us consider the process of adding one more bead to this particular chain so that it will then have $n+1$ links with its end located at $(x\pm1, y, z)$, at $(x, y\pm1, z)$, or at $(x, y, z\pm1)$. If no excluded site restrictions are imposed, each of the six possibilities for the new end position will be equally probable, and with that premise, the change in mean-square end-to-end separation can readily be calculated. However, we must recognize that the six possibilities are not equally probable, for the last link, on the average, will tend to point in the direction of lowest bead density and away from those sites which are most likely occupied. These unequal probabilities will be related to the statistical bead density attributable to the first n links, but for the present we shall simply denote them as follows: Let

$P_n(x, y, z)$ = probability that $(n+1)$th link will be $+1$ in x direction,
$Q_n(x, y, z)$ = probability that $(n+1)$th link will be -1 in x direction,
$R_n(x, y, z)$ = probability that $(n+1)$th link will be $+1$ in y direction,
$S_n(x, y, z)$ = probability that $(n+1)$th link will be -1 in y direction,
$T_n(x, y, z)$ = probability that $(n+1)$th link will be $+1$ in z direction,
$U_n(x, y, z)$ = probability that $(n+1)$th link will be -1 in z direction.

Each of the quantities defined above refers to the probability that the $(n+1)$th link will point in the indicated direction when the nth link has ended at point (x, y, z).

Before proceeding further, it is necessary to establish the nature of P, Q, R, etc. To do so, let us consider the statistical density of beads in the neighborhood of the growing end of the polymer chain. This density, which will be denoted by ρ, must lie in the range of $0\leqslant\rho\leqslant1$, where the upper limit indicates certainty that the point is occupied and the lower limit, certainty that it is unoccupied. For reasons which will appear later, ρ must be computed without including the contribution of the last link of the chain.

We shall now make the reasonable assumption that the probability of a new link entering a certain lattice point is proportional to the probability that the point is unoccupied. In algebraic form this means that

$$P_n(x, y, z)=\lambda[1-\rho_n(x+1, y, z)], \tag{1a}$$

$$Q_n(x, y, z)=\lambda[1-\rho_n(x-1, y, z)], \tag{1b}$$

$$R_n(x, y, z)=\lambda[1-\rho_n(x, y+1, z)], \text{ etc.,} \tag{1c}$$

where λ is a normalizing factor which will be determined by assuming that $P+Q+R+S+T+U=1$. (Actually, this assumption introduces an error that is not obvious; this will be discussed in a later publication with evidence concerning it.) For simplicity we shall now write

$$\rho_n(x+1, y, z)=\rho+g_x, \tag{2a}$$

$$\rho_n(x-1, y, z)=\rho-g_x, \tag{2b}$$

$$\rho_n(x, y+1, z)=\rho+g_y, \tag{2c}$$

where ρ denotes the average density of beads in the six sites immediately surrounding the end site, the end point itself not contributing to this average; g_x, g_y, and g_z denote the components of the gradients of the density in the neighborhood of the end point, the end point likewise not contributing to this gradient.

We now observe that

$$P=\tfrac{1}{6}[1-g_x/(1-\rho)], \tag{3a}$$

$$Q=\tfrac{1}{6}[1+g_x/(1-\rho)], \tag{3b}$$

$$R=\tfrac{1}{6}[1-g_y/(1-\rho)], \text{ etc.} \tag{3c}$$

From Eqs. (3) it follows that

$$P+Q=\tfrac{1}{3}, \tag{4a}$$

$$Q-P=g_x/3(1-\rho), \tag{4b}$$

and

$$R+S+T+U=\tfrac{2}{3}. \tag{4c}$$

Our computations can most conveniently be carried out by considering the mean-square component of length along a particular axis, say the x axis. Because of symmetry it is obvious that $\langle r_n^2\rangle_{Av}=3\langle x_n^2\rangle_{Av}$, where

$$\langle x_n^2\rangle_{Av}=\int\int\int x^2 p_n dxdydz. \tag{5}$$

Let us now return to our chain of n links whose last bead is located at x, y, and z. The next bead might now be added in six different ways, which, taking probabilities into account, will contribute the following terms toward the new value of x^2:

$$P_n(x+1)^2+Q_n(x-1)^2+(R_n+S_n+T_n+U_n)x^2.$$

Making use of Eqs. (4) we rewrite the contribution toward x_{n+1}^2 as

$$x^2+\tfrac{1}{3}-2xg_x/3(1-\rho).$$

Multiplying by p_n and integrating, we obtain an expression for $\langle x_{n+1}^2\rangle_{Av}$, namely

$$\langle x_{n+1}^2\rangle_{Av}=\int\int\int p_n[x^2+\tfrac{1}{3}-2xg_x/3(1-\rho)]dxdydz, \tag{6}$$

or

$$\langle x_{n+1}^2\rangle_{Av}=\langle x_n^2\rangle_{Av}+\tfrac{1}{3}-\tfrac{2}{3}\int\int\int\frac{p_n x g_x}{(1-\rho)}dxdydz. \tag{7}$$

Defining $\Delta\langle x_{n+1}^2\rangle_{Av}$ to be equal to $\langle x_{n+1}^2\rangle_{Av}-\langle x_n^2\rangle_{Av}$, we can rewrite Eq. (7) as

$$\Delta\langle x_{n+1}^2\rangle_{Av}=\tfrac{1}{3}-\tfrac{2}{3}\int\int\int\frac{p_n x g_x}{(1-\rho)}dxdydz. \tag{8}$$

The term $\frac{1}{3}$ which appears in Eq. (8) is precisely the value to be expected for the unrestricted problem; the second term represents the effect of restrictions against double occupancy of any site. Since the atom density will tend, on the average, to be greater between the ends of the chain than beyond those extremities, the product xg_x will be negative, thus causing $\Delta\langle x_{n+1}^2\rangle_{Av}$ to be greater than $\frac{1}{3}$.

BEAD DENSITY IN A POLYMER

If ρ, g_x, and p_n were known exactly, $\Delta\langle x_{n+1}^2\rangle_{Av}$ could be calculated precisely by use of Eq. (8). Since ρ, g_x, and p_n appear only in the correction term of Eq. (8), a satisfactory approximation to $\Delta\langle x_{n+1}^2\rangle_{Av}$ might be expected by using approximate values for those quantities. For this purpose we shall assume that ρ, g_x, and p_n have the values to be expected for the unrestricted problem, for which simple solutions can be written down. The approximation for p_n is well-known, being given by

$$p_n=[3/(2\pi n)]^{\frac{3}{2}}\exp\{-(3r^2)/(2n)\}. \tag{9}$$

We shall now set up the corresponding expressions for ρ and g_x.

Consider a chain of n links (or $n+1$ beads) with ends located at $(0, 0, 0)$ and (x, y, z), and consider further any point (x', y', z') through which the chain might conceivably pass. The probability of reaching point (x', y', z') with $n-j$ links is $p_{n-j}(x', y', z')$ and the probability of going from (x', y', z') to (x, y, z) in j more steps is $p_j(x-x', y-y', z-z')$, assuming validity of the unrestricted probability expressions. The product of these probabilities is proportional to the probability that a chain of n links with the indicated end points has its $(n-j+1)$th atom at the point (x', y', z'). Summing the indicated products over all allowable values for j and dividing by the probability of attaining the specified end-to-end separation should then give the atom density. The appropriate expression for this is

$$\rho_n(x', y', z') = \frac{\sum_j p_{n-j}(x', y', z')p_j(x-x', y-y', z-z')}{p_n(x, y, z)}. \tag{10}$$

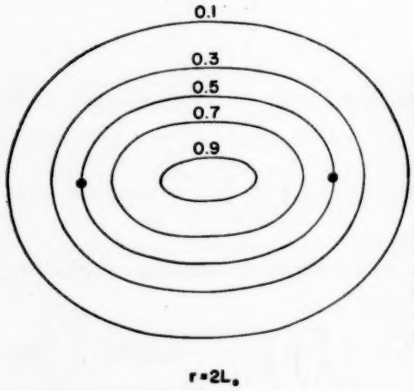

FIG. 1. Contour map showing density (ρ) of beads in chain of five links with ends separated by twice the length of a single link (L_0). Diagram also approximately valid for polymer with $r=(2/5)nL_0$, where n is large. Solid circles represent end points.

For the purpose of evaluating the integral which appears in Eq. (8), we must first obtain an expression for g_x, which is just the partial derivative $\partial\rho/\partial x'$ evaluated at $x'=x$. Since the direction to be preferred by the $(n+1)$th link will depend only upon the density of the first n beads (which correspond to $n-1$ links), we can omit from the summation indicated in Eq. (10) the term for which $j=0$. This is permissible because the density contribution of the last atom added cannot affect the direction of the next link, whereas all previous atoms contribute to the significant portion of the atom density gradient. Apparently no harm would result from including the last added atom in the expression for the density were it not that the approximate mathematical expressions used would appear to give nonexistent (infinite) gradients of density at the coordinates of the last atom. Accordingly we shall omit the term corresponding to $j=0$. (It might appear that the term for $j=n$, which represents the contribution of the first atom, might also cause difficulty because of the precisely defined position of that atom, but it does not actually lead to any trouble in the calculations.)

To arrive at the detailed expression for ρ, we now assume that

$$p_{n-j}=\left(\frac{3}{2\pi(n-j)}\right)^{\frac{3}{2}}\exp\left\{\frac{-3(x'^2+y'^2+z'^2)}{2(n-j)}\right\}, \tag{11a}$$

$$p_j=\left(\frac{3}{2\pi j}\right)^{\frac{3}{2}} \times\exp\left\{\frac{-3[(x-x')^2+(y-y')^2+(z-z')^2]}{2j}\right\}. \tag{11b}$$

If the summation indication in Eq. (10) is now carried out over the range $1\leqslant j\leqslant n$, it is found upon integration that

$$\int\int\int p_n(x', y', z')dx'dy'dz'=n. \tag{12}$$

The correctness of the last integral becomes clear when it is realized that the integrated density of n atoms over all space must be precisely equal to n.

Upon simplification, the expression to be used for ρ_n reduces to the following:

$$\rho_n=\sum_j\left[\frac{3n}{2\pi(n-j)j}\right]^{\frac{3}{2}}\exp\left\{\frac{-3n}{2(n-j)j} \times[[x'-(n-j)x/n]^2+[y'-(n-j)y/n]^2 +[z'-(n-j)z/n]^2]\right\}. \tag{13}$$

Contour maps of the approximate atom density as a function of position in the x, y plane are shown in Figs. 1–3, which correspond to various end-to-end separa-

tions. Although these maps were computed for a low value of n, (namely, $n=5$) the qualitative characteristics presumably should be preserved for higher values as well. (Thus Fig. 1 should represent a polymer with $r=(2/5)nLo$ where n is large.) Obviously if the end-to-end separation were zero, the statistical atom density would be spherically symmetrical. As the length is increased, however, there comes a point after which the density assumes a "saddle" shape, involving two maxima and a minimum symmetrically arranged along the line joining the ends. (It will be observed that an average polymer molecule of specified end-to-end separation would better be represented by ellipsoids of revolution than by spheres.) In plotting the density maps, the contributions of the end points ($j=0$ and $j=n$) cannot be indicated since they contribute infinite values at those points (and zero elsewhere).

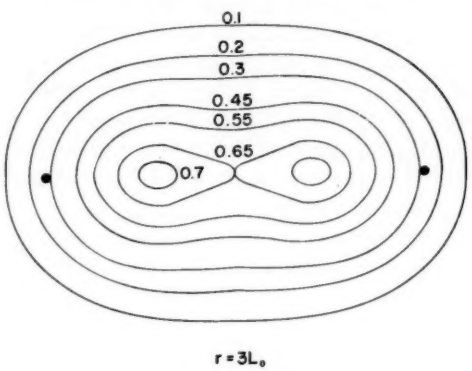

FIG. 2. Contour map showing density (ρ) of beads in chain of five links with ends separated by three times the length of a single link (L_0). Diagram also approximately valid for polymer with $r=(3/5)nL_0$, where n is large. Solid circles represent end points.

EVALUATION OF MEAN SQUARE DIMENSIONS

By differentiating Eq. (13) partially with respect to x' and then setting $x'=x$, we obtain an expression for g_x to use in Eq. (8). To facilitate approximate evaluation of the integral in Eq. (8), we will neglect ρ compared to unity, as did Hermans, Klamkin, and Ullman.[2] In this way, we obtain upon integration

$$\Delta\langle x_{n+1}^2\rangle_{Av}=\tfrac{1}{3}+\tfrac{2}{3}\left(\frac{3}{2\pi}\right)^{\frac{1}{2}}\sum_{j=1}^{n}\frac{1}{j^{\frac{1}{2}}}. \tag{14}$$

Since $\langle r_n^2\rangle_{Av}=3\langle x_n^2\rangle_{Av}$, we can write

$$\Delta\langle r_{n+1}^2\rangle_{Av}=1+2\left(\frac{3}{2\pi}\right)^{\frac{1}{2}}\left\{\frac{1}{1^{\frac{1}{2}}}+\frac{1}{2^{\frac{1}{2}}}+\frac{1}{3^{\frac{1}{2}}}+\cdots\frac{1}{n^{\frac{1}{2}}}\right\}. \tag{15}$$

Recognizing from basic considerations that $\langle r_1^2\rangle_{Av}=1$, it follows by induction that

$$\langle r_n^2\rangle_{Av}=n+2\left(\frac{3}{2\pi}\right)^{\frac{1}{2}}\times\left\{\frac{n-1}{1^{\frac{1}{2}}}+\frac{n-2}{2^{\frac{1}{2}}}+\cdots\frac{1}{(n+1)^{\frac{1}{2}}}\right\}. \tag{16}$$

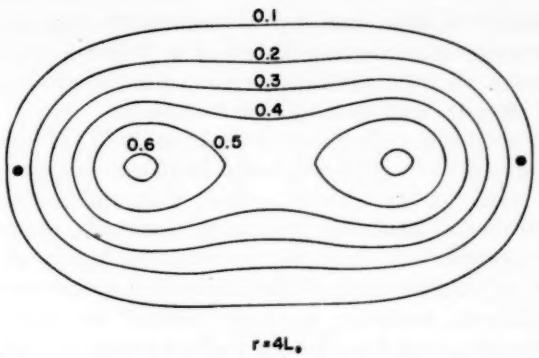

FIG. 3. Contour map showing density (ρ) of beads in chain of five links with ends separated by four times the length of a single link (L_0). Diagram also approximately valid for polymer with $r=(4/5)nL_0$ where n is large. Solid circles represent end points.

Also it will be seen that

$$\lim_{n\to\infty}\frac{\langle r_n^2\rangle_{Av}}{n}=1+2\left(\frac{3}{2\pi}\right)^{\frac{1}{2}}\times\left\{\frac{1}{1^{\frac{1}{2}}}+\frac{1}{2^{\frac{1}{2}}}+\frac{1}{3^{\frac{1}{2}}}+\cdots(\text{infinite series})\right\}=2.724. \tag{17}$$

Since the infinite series appearing in Eq. (17) converges, it appears that the mean square length of molecules divided by the number of links approaches a constant (equal to 2.724) as the number of links becomes very large. In this respect the predicted behavior for large molecules resembles the result computed for an unrestricted random configuration except for the constant factor which gives rise to an expanded molecule.

By use of a generalized trapezoidal rule, such as can be employed for purposes of numerical integration, the expression appearing in Eq. (16) can be written in functional form as follows:

$$\langle r_n^2\rangle_{Av}=n+2(3/2\pi)^{\frac{1}{2}}(2.612n-4\sqrt{n}+1.460). \tag{18}$$

This equation provides a valid representation of Eq. (16) for moderately large values of n and from it one can readily predict the asymptotic behavior of the mean-square lengths of polymer molecules.

At this time it would appear of interest to carry out the foregoing treatment for two-dimensional and one-dimensional restricted walks. Following the identical procedure employed for the three dimensional case we find the following expression for the two dimensional molecule:

$$\langle r_n^2\rangle_{Av}=n+\frac{2}{\pi}\left\{\frac{n-1}{1}+\frac{n-2}{2}+\frac{n-3}{3}+\cdots\frac{1}{n-1}\right\} \tag{19}$$

or

$$\langle r_n^2\rangle_{Av}=n+\frac{2}{\pi}\{n\ln n-0.4228n+0.5000\}. \tag{20}$$

It will be observed that unlike the result for three dimensions, the mean-square distance divided by the

number of steps does not asymptotically approach a constant value for large values of n. This is a result of the fact that the series appearing in Eq. (19), even after dividing through by n, does not converge.

For the one-dimensional problem it is, of course, unnecessary to go through any involved computations to arrive at the correct answer. With the restriction that no two beads can occupy the same site, the exact relationship will obviously be given by $\langle r_n^2\rangle_{Av}=n^2$. To get an idea as to the correctness of our approximate treatment, however, we have carried out the one-dimensional problem by our method simply to provide a basis for comparing results. If this is done, the expressions obtained are as follows:

$$\langle r_n^2\rangle_{Av}=n+\left(\frac{2}{\pi}\right)^{\frac{1}{2}}\times\left\{\frac{n-1}{\sqrt{1}}+\frac{n-2}{\sqrt{2}}+\frac{n-3}{\sqrt{3}}+\cdots\frac{1}{(n-1)^{\frac{1}{2}}}\right\} \quad (21)$$

or

$$\langle r_n^2\rangle_{Av}=n+\left(\frac{2}{\pi}\right)^{\frac{1}{2}}\times\left\{\frac{4}{3}n^{\frac{3}{2}}-1.460n+0.208-\frac{1}{24\sqrt{n}}\right\}. \quad (22)$$

It will be noted that here also the mean-square distance divided by the number of steps increases indefinitely. However, the increase predicted is roughly proportional to the square root of the number of steps instead of the first power of the number of steps, as it should be. From the character of the approximations involved, one would expect that the first-order correction would be too small for the one-dimensional problem, because too low a value of the bead density gradient is utilized in calculating the perturbation. With an increase in the number of dimensions, however, the treatment should become more exact.

DISCUSSION

Quite apart from the numerical correctness of the results is the question of convergence or divergence of the quotient $\langle r_n^2\rangle_{Av}/n$ as n becomes infinite. Since this is a matter of some importance, we can profitably examine the expressions on the right-hand sides of Eqs. (16), (19), and (21), to ascertain the underlying reasons for, and significance of, the various terms. A little reflection will disclose that terms like $(3/2\pi j)^{\frac{1}{2}}$, $(1/\pi j)$, and $(1/2\pi j)^{\frac{1}{2}}$ are simply the intrinsic probabilities of realizing closed loops of j steps in three, two, and one dimensions, respectively. Moreover, the factor $n-j$, which recurs in the aforementioned equations, is substantially equal to the number of ways of taking j successive links out of n links to form a loop. Therefore, products like $(n-j)(3/2\pi j)^{\frac{1}{2}}$, $(n-j)(1/\pi j)$, and $(n-j)\times(1/2\pi j)^{\frac{1}{2}}$ represent weighted numbers of ways in which disallowed configurations might conceivably arise to contribute to an increased mean-square length. (We might expect the factor to be $n-j+1$ instead of $n-j$, but since the loop argument is only implicit in the theory and not explicitly involved in the calculations, the slight difference can easily be a result of the approximate character of the theory.)

Since the probability of forming a loop of j links is proportional to $j^{-a/2}$, where a is the number of dimensions, it follows that an infinite series corresponding to such loops will converge only if $a>2$, and will diverge if $a\leqslant 2$. Therefore, we can expect that $\langle r_n^2\rangle_{Av}$ will approach a limit as n becomes infinite only for the three (or higher)-dimensional problem.

Montroll[5] predicted that the quotient $\langle r_n^2\rangle_{Av}/n$ approaches a finite limit in two dimensions, but his calculations did not take into account possible ring closures or loops of more than four steps. The fact that his result was finite does not constitute proof of convergence because he considered only the equivalent of a finite number of terms in an infinite series. Although our treatment gives strong reasons for believing that the two-dimensional problem gives rise to divergence, we recognize that the argument is only approximate and that it does not constitute a rigorous proof. After all, the harmonic series, which arises in connection with the two-dimensional problem, is on the threshold of convergence, and a better approximation might alter the conclusion. In the absence of such better approximations, however, the best statement we can now make is that the two-dimensional problem diverges.

For the three-dimensional problem, the result expressed by Eq. (18) can be expected to be reasonably reliable as to functional form. As a matter of fact, the form has been tested by use of statistical samples generated by an electronic digital computer, which results will soon be reported in full.

EFFECT OF ATOMIC DIMENSIONS

The theory here presented started out assuming a simple cubic lattice of unit spacing. Obviously if the bond length is L_0, let us say, instead of unity, then the mean-square end-to-end separation computed above should be multiplied by L_0^2. In adopting the lattice model it was further implied that the volume excluded by a given atom (or monomer unit) was equivalent to a unit cell, or L_0^3. If the excluded volume is represented by v instead of L_0^3, then the perturbation term should be multiplied by v/L_0^3, since the atom density will be effectively altered by that factor. With these modifications, Eq. (18) can be rewritten:

$$\langle r_n^2\rangle_{Av}/L_0^2=n+\frac{2v}{L_0^3}\left(\frac{3}{2\pi}\right)^{\frac{3}{2}}(2.612n-4\sqrt{n}+1.460) \quad (23)$$

with corresponding modifications for the other equations.

MAGNITUDE OF BEAD DENSITY

In evaluating the integral appearing in Eq. (8), it was found convenient to neglect ρ compared to unity for the sake of simplicity. Actually the true value of ρ should not be large, but as far as the expressions used are concerned, this assumption may not be valid. An answer to this question can be obtained by examination of the order of magnitude of ρ in the neighborhood of the end bead for large n. If we set $x'=x$, $y'=y$, and $z'=z$ in Eq. (13), and then pass to the limit as $n\to\infty$, we find that the limiting value of ρ, to be denoted by ρ_0, is given by

$$\rho_0=\sum_{j=1}^{n}\left(\frac{3}{2\pi j}\right)^{\frac{3}{2}}=0.862. \tag{24}$$

Now, obviously a value 0.862 is not small compared to unity, so the question arises as to what this means with respect to convergence or divergence of $\langle r_n^2\rangle_{Av}/n$. First of all, we can assert with confidence that in the neighborhood of the chain-end, ρ can never be greater than ρ_0, as given by Eq. (24). This follows because an increase in the number of beads cannot conceivably diminish the bead density for a given end-to-end separation. Hence, the value of ρ_0, representing as it does the limiting value for large n, must be an upper limit to ρ in the neighborhood of an end. (It is not an upper limit to ρ for other regions, such as those in between the two ends.) Hence, the integral appearing in Eq. (8) must still converge even if the factor $1-\rho$ is kept in the denominator of the integral. Moreover, the integral, with the term $1-\rho$ present, cannot exceed the value of the approximate integral (without $1-\rho$) by a factor greater than $1/(1-\rho_0)$ for *any* n. Hence the inclusion of $1-\rho$ cannot increase the dominant power of n appearing in the final results. Therefore, $\langle r_n^2\rangle_{Av}/n$ should still converge in three dimensions for large n, but to a different value from that calculated above.

The approximate value for ρ used in the calculations is, of course, too large for the neighborhood of an end of the molecule and for regions in between the ends. As a matter of fact, the computed values exceed unity for certain intermediate positions, which is not actually possible. An analysis of g_x, which is more important in the computation, shows that its assumed value is also too large, which means that as far as g_x is concerned, an overcorrection is made in the perturbation integral. In the treatment immediately following, a different type of approximate calculation will be carried out which appears to avoid the overcorrection.

ALTERNATIVE EVALUATION OF PERTURBATIONS

In the preceding discussion it was pointed out that ρ and g_x as calculated from Eq. (13) for the neighborhood of a chain end are each larger than they should be. However, there are certain qualitative conclusions that can be drawn from Eq. (13) that are probably correct, and by proper use of these conclusions we can evaluate the integral of Eqs. (7) and (8) in a different form. First of all, it appears from (13) that in the neighborhood of the chain end, as n becomes large, ρ approaches a constant denoted by ρ_0, which is independent of n, x, y, and z. Although the value of ρ_0 so computed is too large, the conclusion that it is constant is not unreasonable, particularly in light of statistical evidence to be reported later.

Moreover, it can readily be shown that as n becomes large, the quantity $ng_x\to-3x\rho_0$. As an asymptotic form for use in Eq. (7), we shall therefore assume that

$$g_x=-3x\rho_0/n \tag{25}$$

and $\rho=\rho_0$.

Substituting Eq. (25) into Eq. (7) we obtain

$$\langle x_{n+1}^2\rangle_{Av}=\langle x_n^2\rangle_{Av}+\tfrac{1}{3}+2\int\int\int\frac{p_n x^2\rho_0}{n(1-\rho_0)}dxdydz$$

or

$$\langle x_{n+1}^2\rangle_{Av}=\langle x_n^2\rangle_{Av}+\tfrac{1}{3}+\frac{2\rho_0\langle x_n^2\rangle_{Av}}{n(1-\rho_0)}. \tag{26}$$

Converting from x to r, it is seen that

$$\langle r_{n+1}^2\rangle_{Av}=\langle r_n^2\rangle_{Av}\left\{1+\frac{2\rho_0}{n(1-\rho_0)}\right\}+1. \tag{27}$$

By carrying the corresponding treatment out for the one- or two-dimensional problems, equations identical to Eq. (27) are obtained, so the end result is not peculiar to a particular number of dimensions. Now, it is interesting to note that Eq. (27) will give exactly the right answer to the one-dimensional problem. In one dimension, $\rho_0=\frac{1}{2}$ (the average for the sites immediately before and after the last bead). Putting $\rho_0=\frac{1}{2}$ into Eq. (27), it can readily be established that $\langle r_n^2\rangle_{Av}=n^2$ is the correct solution of the difference equation.

In general (for $\rho_0\neq\frac{1}{3}$), the solution to Eq. (27) assumes the form

$$\langle r_n^2\rangle_{Av}=\frac{n}{1-a}+Cn^a\left\{1-\frac{a(1-a)}{2n}+\cdots\right\}, \tag{28}$$

where $a=2\rho_0/(1-\rho_0)$, and C is a constant. If $\rho_0<\frac{1}{3}$, then $a<1$, and it is seen that

$$\lim_{n\to\infty}\langle r_n^2\rangle_{Av}/n=\frac{1-\rho_0}{1-3\rho_0}. \tag{29}$$

On the other hand, if $\rho_0\geqslant\frac{1}{3}$, the limit does not exist. It should be remembered that Eq. (27) is intended to be valid only for large n, so the solution given by Eq. (28) cannot be expected to hold for short molecules. The asymptotic forms, however, can be compared with machine data with particular reference to the dependence on density. This will also be the subject of a later publication.

Dielectric Properties of Hydrogen Halides. I. Hydrogen Bromide*

NORMAN L. BROWN† AND ROBERT H. COLE
Metcalf Research Laboratory, Brown University, Providence, Rhode Island

(Received July 3, 1953)

Static dielectric constants of solid hydrogen bromide have been measured from 186 to 70°K, and dispersion and loss below 89°K in the frequency range 15 cy to 5 Mc. Special cell designs minimized formation of cracks and voids in the polycrystalline sample, as such flaws were shown by several lines of evidence to cause serious errors. Static dielectric constants above 117°K are in quite good agreement with Onsager's equation. In phase II, stable below 113°K, the dielectric constant rises to a peak of 200 at 89°K, then falls to a value of 32 at 70°K in phase III. The principal dispersion below 89°K follows a circular arc locus with $\alpha=0.3$, and a rate expression with activation energy 2.7 kcal/mole. A second dispersion is observed at much higher frequencies with energy 1.59 kcal/mole, and it is suggested that the two dispersions are a consequence of crystal anisotropy.

I. INTRODUCTION

THE dielectric properties of the solid hydrogen halides have been of interest since Pauling's discussion[1] of the solid phase transitions in these crystals in terms of molecular rotations in the solid lattice. Although his interpretation of the observed specific heat anomalies in terms of a cooperative change from hindered to free rotation has been largely superseded by order-disorder models, the information obtainable from dielectric dispersion and loss measurements remains of value.

Some of the experimentally determined properties of the solid phases and phase transitions in hydrogen bromide are summarized in Fig. 1. The specific heat data of Giauque and Wiebe[2] show three sharp maxima in the heat capacity at 89°K, 113°K, and 117°K. Polarizing microscope studies by Kruis and Kaischew[3] showed that the phase stable between 117°K and the melting point at 187°K is the only optically isotropic one. X-ray studies[4] indicate a face centered cubic arrangement of bromide ions in the high-temperature phase, and an orthorhombic, nearly tetragonal, structure below 117°K.

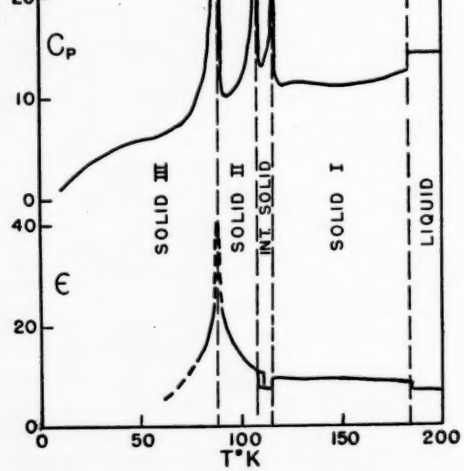

FIG. 1. Specific heat and dielectric constant of hydrogen bromide in the various solid phases.

The variation of the equilibrium dielectric constant with temperature is indicated in Fig. 1 (bottom). The conspicuous features are a gradual rise in the high-temperature phase and a slight drop in the four-degree interval between 113° and 117°K, followed by an increasingly rapid rise to a peak at 89°K, below which the dielectric constant falls off and is frequency dependent at audio frequencies.

Unfortunately, the available dielectric measurements have until recently been made over too narrow ranges of frequency to define the low-temperature dispersion properly and have also been in poor numerical agreement, particularly in the vicinity of the lowest temperature phase transition. Smyth and Hitchcock,[5] Damköhler,[6] and Powles[7] have reported peak values of the dielectric constant at low audio-frequencies of more than 35, 4 to 10, and about 20, respectively. The measurements in the lowest temperature phase agreed only in indicating the presence of dielectric dispersion at increasingly low frequencies, and only in Powles' work was the frequency range of measurement adequate to describe the dispersion.

In order better to define the dielectric behavior, we some time ago began an experimental study of solid hydrogen bromide over the temperature range 70°K

* This paper is based on a thesis submitted by Norman L. Brown in partial fulfillment of the requirements for the degree of Doctor of Philosophy from Brown University.

† Now with General Electric Company, Electronics Park, Syracuse, New York.

[1] L. Pauling, Phys. Rev. **36**, 430 (1930).

[2] W. F. Giauque and R. Wiebe, J. Am. Chem. Soc. **50**, 2193 (1928).

[3] A. Kruis and R. Kaischew, Z. Physik. Chem. **B43**, 384 (1939).

[4] G. Natta, Mem. Accad. Italia Chem. **2**, No. 3, 5 (1931); Gazz. chim. ital. **63**, 425 (1933).

[5] C. P. Smyth and C. S. Hitchcock, J. Am. Chem. Soc. **55**, 1830 (1933).

[6] G. Damköhler, Ann. Physik. **31**, 76 (1938).

[7] J. G. Powles, Nature **165**, 686 (1950); Compt. rend. **230**, 836 (1950); J. phys. radium **13**, 121 (1952).

to the melting point at 187°K in the frequency range 20 cps to 5 Mc/sec. Measurements were first made with conventional test condensers in which the dielectric sample was frozen in the annular space between two coaxial cylindrical metal electrodes. The results were unsatisfactory, however, as the apparent dielectric constant values were greatly dependent on the method of freezing the sample and on its subsequent thermal history.

An obvious explanation of this erratic behavior follows from the fact that the linear contraction of solid HBr from 186°K to 78°K, as estimated from density data, is of the order of 5 percent, a figure far larger than the corresponding change of rigid metal or glass cell structures. Formation of cracks and voids in the sample on cooling can cause serious error if these result in separation of the dielectric from one or both electrodes, as the measured capacitance of a loss-free dielectric must then be smaller than that of either dielectric or the gap. For example, a gap one-fiftieth the thickness of a sample of dielectric constant 100 would result in an apparent dielectric constant of 34. On the other hand, cracks parallel to the lines of force in the sample cause a much smaller error of the order of the fraction of the volume occupied by voids.

On the basis of these considerations, it seemed to us imperative to prevent cracks in the sample at electrode-dielectric interfaces or elsewhere across the lines of force, and to do this with a cell of design suitable for handling the material without contamination and at low temperatures. Two cells to be described accomplished these objectives quite successfully, and the results obtained show that such precautions are essential for trustworthy measurements of either equilibrium dielectric constants or dispersion and loss.

II. EXPERIMENTAL METHODS

A. Electrical

The bridge circuit used has been described elsewhere.[8] Important features of the design for the present work were the convenience and accuracy of direct capacitance and loss measurements with three terminal cells of small dimensions.

Temperatures of the cell and surrounding cooling block were measured by copper-constantan couples made from specially annealed wire kindly supplied by Professor C. S. Stephenson of the Massachusetts Institute of Technology. The calibration tables prepared by him were employed after calibrations at the CO_2 and nitrogen fixed points.

B. Cell Designs

The first arrangement to give any reproducible results was a parallel plate condenser as shown in Fig. 2(a). The high-potential electrode was supported from the top only by a right-angled strip of brass and insulating strip of Teflon, with the intent of permitting this electrode to follow lateral contraction of the frozen sample as it was cooled. A number of attempts to obtain consistent results with this arrangement failed, as indicated by failure of capacitance to change regularly on cooling and by dependence of the values on previous thermal history. For one sample, however, the measured values were reproducible and essentially in agreement with those obtained using the second design.

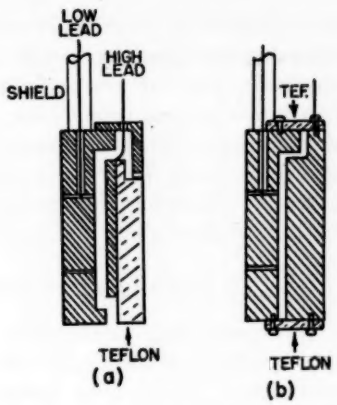

FIG. 2. Schematic diagram of cells. Each cell, shown in plan view, is of cylindrical form.

The electrode arrangement finally employed was designed to provide positive compression of the sample between the electrodes on cooling. As shown in Fig. 2(b), the parallel electrodes are attached at top and bottom to Teflon disks by screws at a distance several times the electrode separation (11.5 mm *vs* 2 mm). With no dielectric present, the decrease of this separation on cooling corresponds to a thermal expansion coefficient nearly that of Teflon multiplied by the ratio 11.5/2, the contraction of the brass electrodes being small in comparison. With a sample of smaller coefficient of expansion present, equilibration of opposing forces evidently results in a small lateral compression of the sample.

The use of parallel plate electrodes had the further advantage, which proved important, that the manner in which samples froze could be observed, as discussed in Sec. C. Nominal electrode spacings of 2 mm and effective area 5.5 cm^2 gave air capacitances of the order 2.0 $\mu\mu f$, exact values being determined by direct calibration.

Both were contained in a glass jacket consisting of two parts: a cap on a female standard taper joint through the top of which electrode and thermocouple leads were brought from the electrode assembly some 30 cm below, and a closed off lower tube with a male standard taper joint at the top and a connecting side tube for evacuation and filling. The electrode assembly was made entirely of brass after tests showed no contamination of liquid HBr if the system was thoroughly cleaned and evacuated before the dry gas was condensed in the cell. Since the gas entered the container substantially at room temperature and the upper portions of the cell were not cooled, electrode leads of gold wire were used, one of which

[8] R. H. Cole and P. M. Gross, Jr., Rev. Sci. Inst. **20**, 252 (1949).

was shielded for its entire length by a surrounding gold-plated glass tube electrically connected to the guard electrode. The thermocouple leads passed through the cap inside a glass tube whose lower end was sealed to a small brass tube which was soldered into a well in the guard electrode. Adequate thermal contact was assured by fastening the thermocouple junction in the bottom of this tube with Wood's metal.

C. Freezing and Cooling of Samples

A careful and painstaking procedure for freezing and cooling the dielectric was found essential for reproducible results with either cell. The liquid-filled cell was suspended inside a thick-walled brass tube with vertical slots to permit observation of the freezing. This tube, which surrounded the lower part of the cell, helped minimize thermal gradients inside the cell by acting as the heat sink. The cell was then slowly cooled over liquid nitrogen in a Dewar flask. By suitable adjustment the cooling rate was controlled to give complete freezing of the liquid sample in about three hours, and the solid formed at the bottom of the cell grew upward and outward from the electrodes as a perfectly colorless transparent mass, free of cracks or flaws except for a vertical interface midway between the electrodes. It was then possible to make the interface disappear from a carefully grown sample by keeping it about 0.5°K below the melting point for several hours.

That these precautions were necessary was shown by subsequent behavior of samples on cooling. Comparison of data for good samples and ones in which cracks were present or developed after freezing showed that the dielectric constants measured for the latter either did not rise as rapidly on cooling or actually decreased before again rising, the change usually occurring quite abruptly.

D. Temperature Control

After a suitable sample had been frozen and its cooling curve followed, the cell was transferred to a thermostat consisting of a massive brass cylinder inside which the cell envelope fitted, the whole being contained in a large Dewar. Cooling was effected by adding liquid nitrogen at suitable intervals to a metal tray suspended above the block, and thermocouples in the cylindrical block were used to compare block and cell temperatures. By suitable addition of coolant, isothermal equilibrium conditions were possible over periods of half an hour or more except in the immediate vicinity of second-order phase transitions, and the system had a natural warming rate of one degree per hour or less. Measurements to 70°K were made by pumping on liquid nitrogen added to the large Dewar.

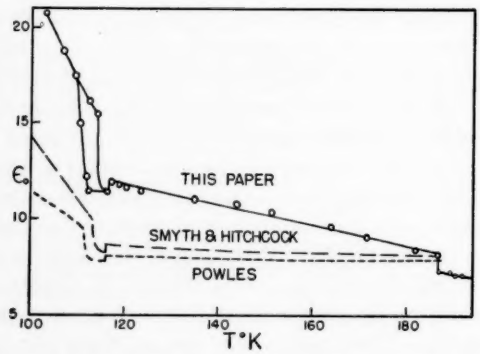

FIG. 3. Static dielectric constant above 100°K.

E. Purity and Handling of Materials

Tank hydrogen bromide gas from the Matheson Company, of 99.5 percent stated purity, was distilled twice before finally being condensed in the cell.‡ Further precautions, such as prolonged drying over P_2O_5, gave no change in dielectric properties. The melting point and phase transition temperatures agreed with Giauque and Wiebe's values[2] to within possible calibration errors.

The electrical properties also gave no evidence of significant impurity: dielectric constants of the liquid agreed with those of Smyth and Hitchcock,[5] the liquid conductivity of 3×10^{-9} mho/cm was as low as or lower than other reported values, and no anomalies of dispersion or loss near the melting point of the sort found for impure solids were observed.

F. Sources of Error

The absolute dielectric constant and loss values reported are subject to slight uncertainty because of the cell design employed. This is because contractions of the dielectric between the electrodes on cooling lead to a decreased electrode separation by design, and to a corresponding increase in geometrical capacitance of the cells which was not measured. On the basis of density data this would lead to dielectric constant values which might be as much as five percent too high at the lowest temperatures, as the cell capacitances used in calculations were measured at the temperature of the melting point of HBr. A compensating error is that from contraction of the sample in directions parallel to the electrodes forming voids parallel to the lines of force. This in effect results in less dielectric being measured and hence gives values too small by as much or more than the increase resulting from the changing separation. The combined effect of these sources of error may thus amount to some five percent at the lowest temperatures, the probable result being values which are too small.

A second source of error about which nothing as definite can be said is the effect of anisotropy of the solid in the low-temperature phases. It is reasonable to suppose that the solid sample at the melting point was a

‡ It is of interest to note that rapid freezing with liquid nitrogen produced a pink solid, much as described for HCl by Giauque and Wiebe (see reference 2) and by Johnson and Martin (J. Chem. Phys. **20**, 534 (1952)).

mosaic of crystallites of the cubic symmetry reported by Kruis and Kaischew[3] and that these became randomly oriented anisotropic regions in the low-temperature phases. Visual observations to test this last conjecture were not possible because the material between the measuring condenser and the glass cell envelope shattered enough on cooling§ to render the sample invisible at these temperatures.

III. EXPERIMENTAL RESULTS

A. Equilibrium Dielectric Constants

The dependence of the static dielectric constant on temperature is shown graphically in Figs. 3 and 4. In Fig. 3 we have plotted the values above 100°K, together with the results of Smyth and Hitchcock[5] and of Powles.[7] In phase I, stable from the melting point (186.7°K) to 117.1°K, our values show a monotonic increase with decreasing temperature, whereas Smyth and Hitchcock found an initial rise and then a slight decrease followed by a gradual rise to the transition point, and Powles found values which are a little smaller at the melting point and remain essentially constant at lower temperatures.

TABLE I. Equilibrium dielectric constants of HBr.

T°K	ϵ_0	T°K	ϵ_0
Liquid		Phase II	
191.8	7.11	109.5	17.5
187.1	7.33	101.0	23.5
		94.2	35.9
Solid Phase I		90.8	55.1
186.8	8.23	89.3	97.8
164.0	9.66	89.2	144
144.0	10.8	89.1	200
117.1	12.0		
		Phase III	
Intermediate Phase		87.5	100
116.6	11.4	86.4	79.2
114.2	11.4[a]	84.1	49.6
	15.5[b]	81.5	46.4
112.5	11.5[a]	77.7	41.6
	16.2[b]	73.1	36.4
		70.0	32.6

[a] Decreasing temperature. [b] Increasing temperature.

If the crystalline form is face centered cubic in this phase as reported by the polarization studies, there can be no question of anisotropy effects in this temperature region, and the only explanation we can find for the differences is that the lower values previously reported resulted from formation and development of flaws in the sample on cooling, as discussed in Sec. II C.

The variation of the equilibrium dielectric constant in phases II and III is, as shown in Fig. 4, characterized by a very large peak at the 89°K second-order transition. Most of the rise to the peak value of 200 occurs in very small but finite temperature intervals on either side of the transition, the value one degree above it being 65, for example.

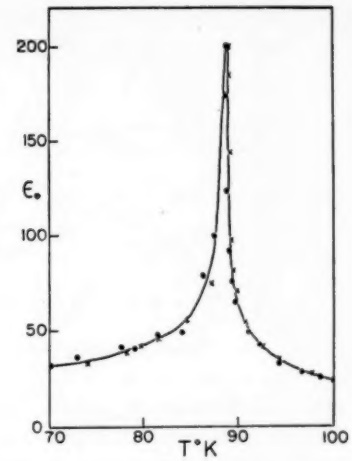

FIG. 4. Static dielectric constant below 100°K.

As one would expect, the values obtained for faulty samples are extremely variable in the transition region, and figures lying anywhere between 10 and 200 were observed. It should be emphasized that the lower figures were in every case foretold by small but definite levelling off or decrease of measured values in phase I as the samples were first cooled below the melting point.

For the two samples which were free of these effects, the peak values could be reproduced on a second passage through the transition, as could values on either side of the transition. Also, the curves measured on slow warming or cooling were the same except for a displacement of the temperatures of the maximum and points near it, the value being higher on warming by about 0.8° for Cell b. It was also noted that the indicated peak temperature on cooling was 0.3° higher for Cell b than for Cell a. Both effects are reasonably explained as a consequence of the very large heat capacity of the dielectric in this region and its poor thermal conductivity, which together make the temperature of the sample lag behind the surroundings despite the very slow warming and cooling rates used. This possible lack of thermal homogeneity may have made the apparent peak values small, but the fact that the same figure was obtained for Cell a as for Cell b would then not be expected because of the better heat transfer in the latter.

In phase III below 89°K, the equilibrium dielectric constant ϵ_0 falls off at a decreasing rate to a value of 32.6 at 70°K, as shown in Fig. 4. Representative values at various temperatures in the four phases are listed in Table I. The values at temperatures below 80°K were obtained by progressively longer extrapolations of the frequency dependent values obtained even at 20 cycles per sec, the manner of extrapolation being apparent from the discussion of this dispersion which follows.

B. Dielectric Relaxation

The results of dispersion and loss measurements in phase III are conveniently presented by the loci of the

§ It is of interest that audible cracking noises when this happened were not accompanied by any measurable change of capacitance of good samples, but with poor samples either sudden drops or levelling off of capacitance resulted on further cooling.

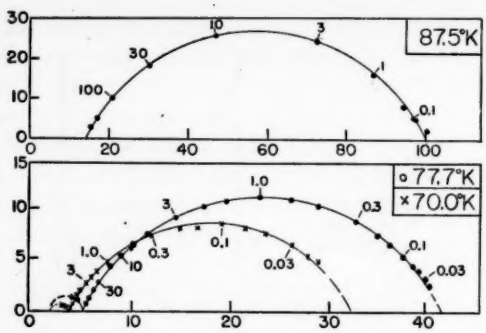

FIG. 5. Complex plane loci of ϵ'' *vs* ϵ'.

real and imaginary parts, ϵ' and ϵ'', of the complex dielectric constant ϵ^*. These were computed from measured parallel capacitance C and conductance G by the relations $\epsilon'=C/C_g$, $\epsilon''=G/\omega C_g$, where C_g is the geometrical capacitance of the cell and $\omega=2\pi$ frequency. Typical loci at 70.0, 77.7, and 87.5°K are plotted in Fig. 5.

Except at the highest frequencies, the data are accurately described by circular arc loci[9] satisfying the equation

$$\epsilon^*=\epsilon'-i\epsilon''=\epsilon_1+(\epsilon_0-\epsilon_1)/(1+(i\omega\tau_1)^{1-\alpha}), \qquad (1)$$

where ϵ_0 and ϵ_1 are the intercepts of the arc on the ϵ' axis at low and high frequencies and τ_1 is a relaxation time related to the frequency f_1 of the midpoint of the arc by $\tau_1=1/(2\pi f_1)$. The values of these parameters which fit the data are listed in Table II.

As shown by the locus at 70°K, and less completely by the others, a second dispersion is found at higher frequencies which can to the extent that it is defined be fitted by a second circular arc. Estimated values of the high-frequency intercepts ϵ_2 and central relaxation frequencies f_2 for these high-frequency values are also given in Table II.

The existence of two dispersions in phase III is in agreement with Powles' observations, but we find much larger values of dielectric constant and relaxation times, especially for the low-frequency dispersion and at higher temperatures. The differences are again primarily the result of sample voids, as we have found too small values for otherwise suspect samples in our work. One can, in fact, achieve a semi-quantitative correlation of these errors by assuming a homogeneous sample and air-gap in series as a model of the faulty samples. If the fractional width of the gap is δ and the dielectric is described by Eq. (1), it is readily shown that the apparent dielectric constant is still described by an equation of the same form as (1), but the apparent values of ϵ_0, ϵ_1, and τ_1 are all too small, and are given by

$$\epsilon_0(\text{app})=\epsilon_0/(1+\epsilon_0\delta),$$

$$\epsilon_1(\text{app})=\epsilon_1/(1+\epsilon_1\delta),$$

$$\tau_1(\text{app})=\tau_1(1+\epsilon_1\delta)/(1+\epsilon_0\delta)^{1/1-\alpha}.$$

[9] K. S. Cole and R. H. Cole, J. Chem. Phys. **9**, 341 (1941).

In the case $\epsilon_1\delta\ll 1$, one may combine the first and third equations to give

$$\epsilon_0(\text{app})=(\epsilon_0/\tau_1^{1-\alpha})\tau_1(\text{app})^{1-\alpha}.$$

Hence a logarithmic plot of ϵ_0(approx) *versus* τ_1(approx) should give a straight line of slope $1-\alpha$. A set of such values obtained for faulty samples at 78°K is plotted in Fig. 6, and the line drawn has the slope 0.7 corresponding to the observed value $\alpha=0.30$. This, together with the fact that all the complex loci were similar circular arcs, differing only in scale and frequency range of dispersion, indicates that the admittedly oversimplified model nevertheless gives a semi-quantitative description of the observed differences.

Only limited evidence could be obtained about the nature and frequency range of dispersion in phase II stable above 89°K. This evidence is based on measured values of conductance, which should increase with frequency as an absorption region is approached. For frequencies much less than the critical frequency this dependence should be as $f^{2-\alpha}$ if the empirical Eq. (1) is valid. By interpolation of measurements at frequencies of 1 kc to 1 Mc/sec with slowly decreasing temperature,

TABLE II. Parameters of dispersions below 89°K.

T°K	ϵ_1	ϵ_2	f_1 (kilocycles per sec)	f_2 (megacycles per sec)
70.0	4.0	2.4	0.113	2.1
73.1	4.4	2.4	0.290	3.2
77.7	5.4	2.4	0.995	6.5
81.5	7.2	2.4	1.85	10
84.1	7.9	...	4.20	...
86.4	10.9	...	4.70	...
87.5	13.6	...	5.65	...

it was found that the increase in conductance varied as frequency squared, corresponding to $\alpha=0$ in Eq. (1). If this functional dependence on frequency is taken as evidence for validity of Eq. (1), one can set both upper and lower limits on the relaxation time: a lower limit by the maximum total dispersion, which must be less than the value of ϵ_0, and an upper one by the absence of any appreciable departure from the limiting low-frequency dependence, which will be the case if the highest frequency f is less than say, 10 f_1. Applying these criteria to data at 89.92°K (0.85° above the transition temperature) gave 1 Mc/sec$<f_1<$7 Mc/sec. The data at higher temperatures did not extend to sufficiently high frequencies to make the upper limit significantly restrictive. The conclusions from these measurements as to character and frequency range of the dispersion in phase II are thus quite tentative, but within their limitations suggest the nature of the dispersion to be further explored.

IV. DISCUSSION

We consider first the dependence of static dielectric constant on temperature. The behavior in phase I

at and below the melting point is consistent with a simple theoretical picture, as the data are in semi-quantitative agreement with Onsager's equation.[10] This may be written

$$\epsilon_0 - n^2 = \frac{3\epsilon_0}{2\epsilon_0 + n^2}\left(\frac{n^2+2}{3}\right)^2 \frac{4\pi N \mu_0^2}{3kTV}, \qquad (2)$$

where n is the refractive index for induced polarizations, N is Avogadro's number, V the molar volume, and μ_0 the gas dipole moment. The appropriate value of n is not accurately known. However, using an electronic polarizability of 4.24×10^{-24} cm^3 and a solid density of 2.45 in the Clausius-Mossotti expression gives $n^2=2.43$, a value not far from the extrapolated high-frequency intercept $\epsilon_\infty=2.35$ found below 90°K.

Using $n^2=2.40$ in Eq. (2) together with $\mu_0=0.85$ debye gives values of 8.13 at 187°K and 12.64 at 117°K, as compared to the observed figures of 8.23 and 12.0. A more extensive and precise study of this phase by J. A. Barclay in this laboratory has given slightly higher results for ϵ_0 which are in even better agreement with the theory. These will be reported in detail later, as will similar results for solid HCl obtained by R. W. Swenson.

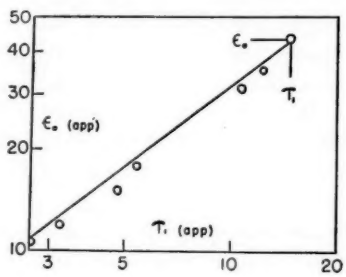

FIG. 6. Correlation of apparent dielectric constant and relaxation time of faulty samples at 78°K.

Onsager's equation (2) was originally developed for polar liquids by applying electrostatic boundary conditions to a cavity of molecular volume containing a single molecule and surrounded by uniform dielectric. One would hardly expect the result of this model to apply very generally to solids, but the agreement is reasonable in the present case of a disordered cubic close packed structure.

In view of this normal increase of ϵ_0-n^2 with $1/T$, there is no need to postulate special models of alternative lattice positions with energy differences the order of kT, as was done by Powles[11] to account for the failure of his observed values to increase at lower temperatures in phase I.

The sharp maximum observed at the low-temperature transition is similar to that found experimentally for the specific heat, and is a much more pronounced effect than predicted by the only detailed theory so far advanced. This theory due to Kirkwood[12] is based on an assumed potential energy of interaction between nearest neighbors and predicts values of ϵ_0 given by Onsager's equation for temperatures above the transition. At lower temperatures, the cooperative ordering of neighbors results in a decrease to a value characteristic of induced polarization in the limit $T\to0$. The model thus gives results qualitatively similar to those observed, but fails to account for the sharp increase to a very large peak which begins several degrees above the transition.

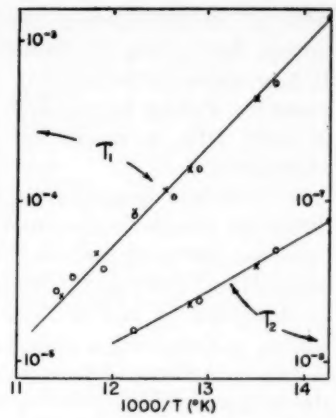

FIG. 7. Rate plots of relaxation times against temperature. Upper curve for low-frequency dispersion (τ_1), lower for high-frequency (τ_2).

These differences resemble the failure of simple order-disorder models to account for the sharpness of specific heat anomalies in second-order transitions, and point to the need for more refined models. The algebraic difficulties of Onsager's exact solution[13] of the two-dimensional Ising model suggests that adequate treatment of the molecular interactions in the present problem may be very complicated. This may be particularly true for the dielectric constant if anisotropy of the lattice is a significant factor, as both the local and long-range dipole interactions will be more difficult to treat in developing an adequate theory such as those of Kirkwood[14] and Fröhlich.[15] That anisotropy exists in solid HBr is clear from x-ray[4] and infrared[16] studies, and that it may be important is suggested both by the multiplicity of solid phases and by the multiple dielectric dispersions below 89°K.

The two dispersions at audio- and radio-frequencies found in phase III have relaxation times described by rate laws of the form $\tau=A\exp(B/RT)$, as shown by the plots of $\log\tau$ *versus* $1/T$ in Fig. 7. For the larger lower-frequency dispersion $\log A=-11.35$, $B=2.70$ kcal/mole; for the other, $\log A=-12.05$, $B=1.59$ kcal/mole.

The values of τ are not in agreement with those of Powles,[7] nor do we find any evidence of the departures from the simple rate laws which led Powles to consider proton transitions by tunneling through energy bar-

[10] L. Onsager, J. Am. Chem. Soc. **58**, 1486 (1936).
[11] J. G. Powles, Trans. Faraday Soc. **48**, 430 (1952).
[12] J. G. Kirkwood, J. Chem. Phys. **8**, 205 (1940).
[13] L. Onsager, Phys. Rev. **65**, 117 (1944).
[14] J. G. Kirkwood, J. Chem. Phys. **7**, 911 (1939).
[15] H. Fröhlich, *Theory of Dielectrics* (Oxford University Press, London, 1949).
[16] W. E. Osberg, Jr., Ph.D. thesis, Brown University, June, 1951; see also G. L. Hiebert and D. F. Hornig, J. Chem. Phys. **20**, 918 (1952).

riers. If, as we believe, these departures result from sample flaws, this mechanism need not be involved. It also seems probable that such difficulties may account for Powles having found *shorter* relaxation times in solid DBr, a result which is otherwise hard to understand.

It is evident from the dispersion loci and the great difference in relaxation times that the two dispersion processes are quite distinct. The marked anisotropy of phase III suggests that the dielectric polarization should be described by two or three principal dielectric constants, rather than a single one characteristic of an isotropic medium. If the relaxation processes giving rise to the equilibrium values differ considerably in their rates, measurements on a mosaic crystal would resolve the dispersions in time, even though the equilibrium value is an average from which individual principal values cannot be deduced.

The interesting possibility thus exists of determining principal dielectric constant and dispersion values from measurements on a polycrystalline sample, with the limitation, however, that the corresponding crystallographic directions are not identified. If the proper identification can be surmised from other evidence about the structure and molecular arrangement, the analysis would be a valuable substitute for direct determinations on single crystals. The latter are not attractive in the present case of a phase stable only below 89°K, and with three intervening solid phases below the melting point.

If the interpretation is correct, there still remain the possible difficulties that the samples as measured were not random aggregations of crystallites or that depolarization effects occurred at boundaries. Variability attributed to imperfect randomness was observed in measurements with Cell b, which consisted in a slow drift noticeable over a period of hours when the sample was left at 78°K. This was of such a nature that the extent of the high-frequency dispersion increased and the low-frequency one decreased by as much as 20 percent after 24 hours, *without* any measurable change in the relaxation times. This behavior was thus quite distinct from that of generally low values found for flawed samples, and, moreover, could be reproduced after the sample was warmed through the transition at 89°K and again cooled.

Because the initial values on reaching a steady temperature were reproducible and in agreement with those using Cell a, these values are the ones quoted in Table II. The subsequent drift can be explained as the result of change in relative arrangements of crystallites, quite possibly occasioned by slow stress relaxation of the Teflon confining disks employed in Cell b. That the initial values correspond to random arrangements cannot be concluded with certainty from the evidence, and our belief that they do is only a reasonable interpretation.

Osberg and Hornig[16] have concluded that ordered molecular arrangements in phase III of hydrogen bromide which are consistent with their infrared absorption spectra of thin films consist of parallel bonded zig-zag chains with the angle between neighboring molecules about 97° and the chains lying in parallel planes. If, as Tisza[17] has suggested, the disorder leading to the transition at 89°K is by reversal of dipole directions, one would expect marked anisotropy of the polarization with the large, low-frequency dispersion corresponding to dipole reversal in the planes of the chains and the smaller dispersion to dipole displacements at right angles to these planes.

We believe that anisotropy of the crystal is a more probable explanation of the dispersions than the hypotheses advanced by Powles, but attempts at a quantitative development are perhaps premature until a more definite decision among possible alternative structures can be made. The dielectric evidence is also incomplete in some respects. Further measurements at temperatures below 70°K would better define the dispersion in phase III, and data at sufficiently high frequencies to define the dispersion in phase II would be valuable, especially in view of the indications that the dispersion is of quite different character than in phase III. Further studies with similar techniques on the other hydrogen and deuterium halides are also desirable, and are planned or in progress.

[17] L. Tisza, M.I.T. R.L.E. Tech. Rept. 127 (1949).

The Mean Amplitudes of Thermal Vibrations in Polyatomic Molecules. II. An Approximate Method for Calculating Mean Square Amplitudes

YONEZO MORINO, KÔZO KUCHITSU, AKIRA TAKAHASHI, AND KEIJI MAEDA
Department of Chemistry, Faculty of Science, Tokyo University, Bunkyo-ku, Tokyo, Japan
(Received June 11, 1953)

A simple method of the calculation of the mean amplitudes of both directly bonded atom pairs and non-bonded ones is proposed by approximating the function $\coth x$ by $1/x+x/4$. The enumeration of the **L** matrix, the most time-consuming procedure, is replaced by the calculation of the inverse matrix $\mathbf{F}^{-1}$ from the potential energy matrix. The formulae obtained are applicable with reasonable accuracy (4 percent) to almost all the cases except the atom pairs having higher frequencies than 1200 cm^{-1}. For the latter cases modified formulas are presented by using hyperbolic cotangent function.

It is also revealed that, if some allowance be made for the errors of the mean amplitudes, a definite value can be assigned to the mean amplitude of a given pair of atoms, without referring to the structure of the other part of the molecule. Reliable values of the mean amplitudes are computed for some typical atom pairs, by the use of the force constants of Urey-Bradley type obtained by the analysis of the vibrational spectra.

I. APPROXIMATE FORMULAS FOR CALCULATION

FOR the discussion of the molecular structure by electron diffraction, it is necessary to obtain the mean amplitude for each atom pair in the molecule to be discussed. Rigorous calculation is so laborious, as shown in the preceding article,[1] that it would be desirable to introduce some approximate method.

A. Mean Amplitudes of Directly Bonded Atom Pairs

Let us consider first a pair of atoms which are linked by a chemical bond. In the treatment of normal vibration a small displacement of a bond distance is usually taken as an internal coordinate. Internal coordinates **R** are related to the normal coordinates by the transformation matrix **L**

$$\mathbf{R}=\mathbf{LQ}, \tag{1}$$

where **R** and **Q** are expressed in a column matrix. The transformation matrix **L** is obtained by solving the equation[2]

$$\mathbf{GFL}=\mathbf{L\Lambda}, \tag{2}$$

and the normalizing condition

$$\mathbf{L'FL}=\mathbf{\Lambda}, \tag{3}$$

or

$$\mathbf{LL'}=\mathbf{G}. \tag{4}$$

The **G** and **F** are the kinetic and the potential energy matrix respectively. **Λ** is the diagonal matrix, the elements of which, λ_k's, are related to the frequencies ν_k of the kth normal vibrations by the equation

$$\lambda_k=4\pi^2\nu_k^2, \tag{5}$$

and are given by solving the secular equation

$$\det|\mathbf{GF}-\mathbf{\Lambda E}|=0. \tag{6}$$

If a small displacement of a bond distance, Δr, is taken as the ith internal coordinate R_i, its mean amplitude is given by the ith diagonal element of the matrix of $\langle R_i^2\rangle$:*

$$\langle\Delta r^2\rangle=\langle R_i^2\rangle=\langle\mathbf{RR'}\rangle_{ii}=(\mathbf{L}\langle\mathbf{QQ'}\rangle\mathbf{L'})_{ii}, \tag{7}$$

where **R'** denotes the transposed matrix of **R**. Since the **Q**'s are the normal coordinates, the nondiagonal terms, $\langle\mathbf{QQ'}\rangle_{kl}$, $(K\neq l)$ vanish: in other words, the matrix $\langle\mathbf{QQ'}\rangle$ is a diagonal one, and may be written as $\langle\mathbf{Q}^2\rangle$. Thus

$$\langle\Delta r^2\rangle=(\mathbf{L}\langle\mathbf{Q}^2\rangle\mathbf{L'})_{ii}. \tag{8}$$

The kk element of $\langle\mathbf{Q}^2\rangle$ is the mean amplitude of the kth normal coordinate Q_k, and is given by[3]

$$\langle Q_k^2\rangle=\frac{1}{8\pi^2\nu_k}\coth\frac{h\nu_k}{2kT}. \tag{9}$$

In the rigorous treatment the mean amplitude $\langle\Delta r^2\rangle$ is obtained by Eqs. (8) and (9) only after the frequencies of the normal vibrations and then the elements of the **L** matrix are calculated by Eqs. (2), (3), and (6). As already stated, this procedure needs troublesome calculation, so that some approximate method would be desirable to be deduced. For this purpose it is profitable to consider the expansion of $\coth x$:

$$\coth x=\frac{1}{x}+\frac{x}{3}-\frac{x^3}{45}+\cdots. \tag{10}$$

This may be approximated by

$$\coth x=\frac{1}{x}+\frac{x}{3}, \tag{11}$$

in the region of $x<1$. Since $x=h\nu/2kT$ according to Eq. (9), $x<1$ corresponds to $\nu<415$ cm^{-1} at ordinary

[1] Morino, Kuchitsu, and Shimanouchi, J. Chem. Phys. **20**, 726 (1952).
[2] E. B. Wilson, Jr., J. Chem. Phys. **7**, 1047 (1939); **9**, 76 (1941).

* The symbol $\langle\ \rangle$ denotes the time average.
[3] F. Bloch, Z. Physik, **74**, 295 (1932); R. W. James, Physik. Z. **33**, 737 (1932).

TABLE I. The comparison of the function cothx with the approximate formulas.

x	coth$x$	$1/x+x/3$	Δ^a	$1/x+x/4$	Δ'^b
0.1	10.034	10.033	−0.001	10.025	−0.009
0.5	2.168	2.167	−0.001	2.125	−0.043
1.0	1.314	1.333	+0.019	1.250	−0.064
1.5	1.105	1.167	+0.062	1.042	−0.063
2.0	1.038	1.167	+0.129	1.000	−0.038
2.5	1.013	1.233	+0.220	1.025	+0.012
3.0	1.004	1.333	+0.329	1.083	+0.079
4.0	1.001	1.583	+0.582	1.250	+0.249

[a] $\Delta=(1/x+x/3)-\coth x$. [b] $\Delta'=(1/x+x/4)-\coth x$.

temperature ($T=298°$K), which is too narrow and insufficient for our application. Considering the accuracy of the mean amplitude necessary for electron diffraction, an alternative formula,

$$\coth x=\frac{1}{x}+\frac{x}{4}, \tag{12}$$

is more suitable, where the coefficient of the second term is replaced with $\frac{1}{4}$ instead of $\frac{1}{3}$. In Table I the values computed by Eq. (12) are compared with the true values of cothx. It will be seen that this approximation has rather larger error (at most 8 percent) but larger applicable region of $x<3$; i.e., $\nu<1200$ cm^{-1} at 298°K. The condition $\nu<1200$ cm^{-1} covers the most important region of molecular vibration, and the error of 8 percent in cothx, corresponding to the error of 4 percent in mean amplitude, may be sufficient for the present purpose.

Now inserting Eq. (12) into Eq. (9), we obtain

$$\langle Q_k^2\rangle=\frac{h}{8\pi^2\nu_k}\left(\frac{2kT}{h\nu_k}+\frac{1}{4}\frac{h\nu_k}{2kT}\right)=kT\frac{1}{\lambda_k}+\frac{h^2}{64\pi^2kT}. \tag{13}$$

With this equation, Eq. (8) becomes

$$\langle\Delta r^2\rangle=kT(\mathbf{L}\Lambda^{-1}\mathbf{L}')_{ii}+\frac{h^2}{64\pi^2kT}(\mathbf{LL}')_{ii}. \tag{14}$$

From Eq. (3) it can be easily obtained that

$$\mathbf{L}\Lambda^{-1}\mathbf{L}'=\mathbf{F}^{-1}. \tag{15}$$

This, together with Eq. (4), leads to the equation

$$\langle\Delta r^2\rangle=kTF^{-1}{}_{ii}+\frac{h^2}{64\pi^2kT}G_{ii}. \tag{16}$$

As shown by Wilson,[2] if R_i is the change of the bond distance from its equilibrium value, then $G_{ii}=\mu+\mu'$, where μ and μ' are the reciprocals of the masses of the two atoms situated at the both ends of the distance. Consequently the final equation becomes

$$\langle\Delta r^2\rangle=kTF^{-1}{}_{ii}+\frac{h^2}{64\pi^2kT}(\mu+\mu'). \tag{17}$$

Thus, without solving the secular equation and computing the elements of the matrix **L**, the mean amplitude of a bond distance can be straightforwardly calculated from the inverse matrix of **F**.

The elements of the inverse matrix $\mathbf{F}^{-1}$ are obtained by the equation

$$F^{-1}{}_{ii}=F_{ii}'/\det F, \tag{18}$$

where F_{ii}' denotes a cofactor corresponding to the ii element of the original matrix **F**. The calculation of the inverse matrix is much less laborious than the computation of the elements of the matrix **L**.

B. Mean Amplitudes of Nonbonded Atom Pairs

Similar argument can be applied to the calculation of the mean amplitude of any atom pair, whether the two atoms in the pair are separated by two chemical bonds or more. A displacement from the equilibrium distance between the nonbonded atoms Δq is expressed as a linear combination of internal coordinates such as the displacements of bond lengths and bond angles:

$$\Delta q=\sum_k a_kR_k. \tag{19}$$

Let **A** be a column matrix composed of the coefficients a_k's, then Eq. (19) may be written in a matrix form of

$$\Delta q=\mathbf{A}'\mathbf{R}. \tag{20}$$

Thus the mean amplitude is given by

$$\langle\Delta q^2\rangle=\mathbf{A}'\langle\mathbf{RR}'\rangle\mathbf{A}=\mathbf{A}'\mathbf{L}\langle\mathbf{Q}^2\rangle\mathbf{L}'\mathbf{A},$$
$$=kT\mathbf{A}'\mathbf{F}^{-1}\mathbf{A}+\frac{h^2}{64\pi^2kT}\mathbf{A}'\mathbf{GA}. \tag{21}$$

The second term of this equation can be further simplified if a new set of internal coordinates are selected in which the displacement of the distance of the said nonbonded atom pair is included in place of a bond angle. It is easily shown that by this transformation the second term of Eq. (21) is reduced to the sum of the reciprocals of the masses of the two atoms concerned, just as the cases of directly bonded atom pairs:

$$\langle\Delta q^2\rangle=kT\mathbf{A}'\mathbf{F}^{-1}\mathbf{A}+\frac{h^2}{64\pi^2kT}(\mu+\mu'). \tag{22}$$

Therefore, the mean amplitude $\langle\Delta q^2\rangle$ can be computed easily by using the matrix elements of $\mathbf{F}^{-1}$. The main difference between (22) and (17) is that in this case nondiagonal elements of the matrix $\mathbf{F}^{-1}$ have to be used, while for the directly bonded atom pairs only the diagonal ones are required.

C. Treatments for Symmetrical Molecules

If the molecule has any symmetry whatever, it is convenient to introduce symmetry coordinates $\mathfrak{R}$.

Internal coordinates are related to the symmetry coordinates by the transformation matrix $\mathbf{U}$:

$$\mathbf{R}=\mathbf{U}'\mathfrak{R}, \tag{23}$$

where $\mathbf{R}$ and $\mathfrak{R}$ are expressed in a column matrix. The matrix $\mathbf{U}$ is easily written down from the character of the symmetry of the molecule. The symmetry coordinates, on the other hand, can be transformed into the normal coordinates by the equation:

$$\mathfrak{R}=\mathfrak{L}\mathbf{Q}. \tag{24}$$

The transformation matrix $\mathfrak{L}$ is obtained by the same procedure as described in section A.

Now, from Eqs. (7) and (23)

$$\langle\Delta r^2\rangle=\langle\mathbf{R}\mathbf{R}'\rangle_{ii}=(\mathbf{U}'\langle\mathfrak{R}\mathfrak{R}'\rangle\mathbf{U})_{ii}=(\mathbf{U}'\mathfrak{L}\langle\mathbf{Q}^2\rangle\mathfrak{L}'\mathbf{U})_{ii}, \tag{25}$$

where the matrices expressed in the symmetry coordinates are distinguished by German type. Using (13)

$$\langle\Delta r^2\rangle=kT(\mathbf{U}'\mathfrak{L}\mathbf{A}^{-1}\mathfrak{L}'\mathbf{U})_{ii}+\frac{h^2}{64\pi^2kT}(\mathbf{U}'\mathfrak{L}\mathfrak{L}'\mathbf{U})_{ii}. \tag{26}$$

From the relations corresponding to (4) and (15):

$$\mathfrak{L}\mathfrak{L}'=\mathfrak{G}, \tag{27}$$

and

$$\mathfrak{L}\mathbf{A}^{-1}\mathfrak{L}'=\mathfrak{F}^{-1}, \tag{28}$$

TABLE II. The comparison of the calculated values of the mean amplitudes (in A units).

Molecule	Pair	$\langle\Delta l^2\rangle^{\frac{1}{2}}_{\text{approx}}$[a]	$\langle\Delta l^2\rangle^{\frac{1}{2}}_{\text{rig}}$[b]	$\langle\Delta l^2\rangle^{\frac{1}{2}}_{\text{obs}}$[c]
CCl_4	C−Cl	0.052_6	0.053_8	0.041
	Cl − − − Cl	0.066_4	0.067_2	0.054
$CF_2=CF_2$	C=C	0.045_3	0.039_4	···
	C−F	0.044_8	0.043_0	0.056
	F − − − F	0.053_5	0.055_4	0.087
	cis F − − − F	0.056_5	0.055_0	0.095
	trans F − − − F	0.094_8	0.093_9	0.090
		0.056_7	0.056_9	0.114
$CF_2=CH_2$	C=C	0.045_7	0.040_9	···
	C−F	0.044_8	0.043_6	0.042
	F − − − F	0.054_0	0.054_0	0.060
	C−H	0.056_3	0.057_0	0.060
	H − − − H	0.108_0	0.076_7	···
	cis H − − − F	0.152_3	0.123	···
	trans H − − − F	0.115_7	0.091	···
		0.138_8	0.135	···
		0.114_6	0.094	···

[a] Calculated by the approximate formulas.
[b] Calculated by the rigorous method given in the preceding article (reference 1).
[c] Observed by Karle and Karle (reference 5).

TABLE III. Force constants (in 10^5 dyne/cm), bond lengths (in A units), and bond angles (in degrees) used in the calculation.[a]

K_{CCl} =1.75	K_{CF} =5.5	K_{CH} =4.8
H_{ClCCl} =0.1	H_{FCF} =0.25	H_{HCH} =0.3
F_{ClCl} =0.65	H_{CCF} =0.25	H_{CCH} =0.25
F'_{ClCl} =−0.1	F_{FF} =1.15	F_{HH} =0.1
r_{CCl} =1.77A	F_{CF} =0.8	F_{CH} =0.4
α_{ClCCl} =109°28′	K_{CC} =9.2 ($CF_2=CF_2$)	K_{CC} =8.4 ($CH_2=CF_2$)
	r_{CF} =1.313A ($CF_2=CF_2$)	R_{CF} =1.321A ($CH_2=CF_2$)
	r_{C-C} =1.313A	r_{CH} =1.07A
	α_{FCF} =114°	α_{FCF} =110°
		α_{HCH} =117°

[a] The constants F' for $CF_2=CF_2$ and $CH_2=CF_2$ are assumed to be one-tenth of the corresponding constants F with negative sign.

Eq. (26) is rewritten as

$$\langle\Delta r^2\rangle=kT(\mathbf{U}'\mathfrak{F}^{-1}\mathbf{U})_{ii}+\frac{h^2}{64\pi^2kT}(\mu+\mu'). \tag{29}$$

It was already shown that the reduction of the second term can be carried out whether the molecule has symmetry or not. The mean amplitude of a nonbonded pair of atoms, which is expressed as Eq. (19) in terms of the internal coordinates R_k's, has a little more complicated form:

$$\langle\Delta q^2\rangle=kT\mathbf{A}'\mathbf{U}'\mathfrak{F}^{-1}\mathbf{U}\mathbf{A}+\frac{h^2}{64\pi^2kT}(\mu+\mu'). \tag{30}$$

At first sight these formulas seem to be more troublesome for the calculation than those developed in the preceding sections, but in actual computation they are more convenient by the following reasons: (1) the matrix $\mathbf{F}$ is factorized into sub-groups in the symmetry coordinates, so that the inverse matrix $\mathbf{F}^{-1}$ can be obtained by solving simultaneous equations of lower degrees for each sub group, and (2) the multiplication calculation of the matrix $\mathbf{A}'\mathbf{U}'\mathfrak{F}^{-1}\mathbf{U}\mathbf{A}$ is much simplified, when taking into account the fact that elements $\mathfrak{F}^{-1}_{lm}$'s are zero if the lth and mth coordinates do not belong to the same symmetry, in addition to the fact that the matrix $\mathbf{U}$ has many vanishing elements according to the symmetry of the molecule.

D. Application

By the approximate method introduced above, the mean amplitudes for CCl_4, $CF_2=CF_2$, and $CH_2=CF_2$ molecules are calculated and compared with the values obtained by the rigorous calculation and the experimental data.[4,5] These are listed in Table II, the force constants, bond lengths and bond angles used in the calculation being given in Table III. The matrices $\mathbf{U}$, $\mathfrak{G}$, and $\mathfrak{F}$ and the relations between the displacements of atom pairs and the symmetry coordinates for the latter two molecules were described in the preceding article.[1] The results are in good agreement with those obtained by the rigorous calculation, except the values for C=C and for the pairs in which a hydrogen atom participates. This will be understood if we consider the

[4] J. Karle and I. L. Karle, J. Chem. Phys. 18, 957 (1950).
[5] I. L. Karle and J. Karle, J. Chem. Phys. 18, 963 (1950).

TABLE IV. The comparison of the mean amplitudes calculated by various methods (in A units).

Molecule	Pair	$\langle\Delta l^2\rangle^{\frac{1}{2}}_{\text{mod}}$	$\langle\Delta l^2\rangle^{\frac{1}{2}}_{\text{approx}}$	$\langle\Delta l^2\rangle^{\frac{1}{2}}_{\text{rig}}$
$CF_2=CF_2$	C=C	0.039_8	0.045_3	0.039_4
	C=C	0.041_0	0.045_7	0.040_9
	C−H	0.077_2	0.108_0	0.076_7
	H − − − H	0.126_4	0.152_3	0.123
	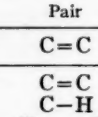			
$CF_2=CH_2$		0.102_5	0.115_7	0.091
	cis H − − − F	0.140_4	0.138_8	0.135
	trans H − − − F	0.102_3	0.114_6	0.094

fact that the frequencies of the latters are out of the region of this approximation. Strictly speaking, this method is not to be applied to the pairs including C=C bond in its part, e.g., C=C−F, cis F − − − F, and trans F − − − F. Yet Table II shows that it provides the values sufficient for our purpose also in these cases. This is due to the fact that the contribution of the C=C vibration to the mean amplitude of the said pairs is small, as shown in Tables V and VI in the preceding paper.[1] Thus it may be said that this approximation is applicable to almost all atomic pairs except the double and triple bonds themselves and the ones including a hydrogen atom which have extremely large characteristic frequencies.

II. MODIFIED FORMULAS FOR THE ATOM PAIRS HAVING HIGH CHARACTERISTIC FREQUENCIES

In Part I some approximate methods for calculating the mean amplitudes of polyatomic molecules were introduced, but it was found that they are unavailable for the atom pairs having higher frequencies, $\nu>1200$ cm^{-1}: e.g., C=C double bond and the pairs in which a hydrogen atom participates. However, electron diffraction investigation often requires to estimate the mean amplitudes for such atom pairs. So it may be desirable to modify the formulas so as to be applicable in wider region of characteristic frequencies.

In the derivation of the formulas in Part I the function $\coth x$ in the mean amplitudes of normal vibrations was approximated by $1/x+x/4$. As shown in Table I this approximation deviates appreciably in the positive direction when $x>3$. This tendency still remains in the final formulas: that is, they afford larger values than those obtained by the rigorous calculation as shown in Table II, when applied to the cases having larger characteristic frequencies ($x>3$).

Now, if we write Eq. (17) for a bonded atom pair

$$\langle\Delta r^2\rangle=\frac{h}{4\pi}[F^{-1}{}_{ii}(\mu+\mu')]^{\frac{1}{2}} \times\left\{\frac{1}{\dfrac{h}{4\pi kT}\left[\dfrac{\mu+\mu'}{F^{-1}{}_{ii}}\right]^{\frac{1}{2}}}+\frac{1}{4}\frac{h}{4\pi kT}\left[\frac{\mu+\mu'}{F^{-1}{}_{ii}}\right]^{\frac{1}{2}}\right\}, \quad (31)$$

then we may at once think of a procedure which brings back the expression in the bracket of this equation into the original hyperbolic cotangent function:

$$\langle\Delta r^2\rangle=\frac{h}{4\pi}[F^{-1}{}_{ii}(\mu+\mu')]^{\frac{1}{2}}\coth\left(\frac{h}{4\pi kT}\left[\frac{\mu+\mu'}{F^{-1}{}_{ii}}\right]^{\frac{1}{2}}\right). \quad (32)$$

Of course in this procedure there is no reason to insist upon its mathematical necessity, but, for a diatomic molecule this equation coincides exactly with the rigorous one, and, for other cases, it may cancel to some extent the error produced by the expansion of the hyperbolic cotangent function.

Similarly, corresponding to Eq. (22), we may obtain for a nonbonded atom pairs,

$$\langle\Delta q^2\rangle=\frac{h}{4\pi}[\mathbf{A}'\mathbf{F}^{-1}\mathbf{A}(\mu+\mu')]^{\frac{1}{2}} \times\coth\left(\frac{h}{4\pi kT}\left[\frac{\mu+\mu'}{\mathbf{A}'\mathbf{F}^{-1}\mathbf{A}}\right]^{\frac{1}{2}}\right), \quad (33)$$

and in a symmetrical molecule, for a bond distance, in place of Eq. (29)

$$\langle\Delta r^2\rangle=\frac{h}{4\pi}[(\mathbf{U}'\mathfrak{F}^{-1}\mathbf{U})_{ii}(\mu+\mu')]^{\frac{1}{2}} \times\coth\left(\frac{h}{4\pi kT}\left[\frac{\mu+\mu}{(\mathbf{U}'\mathfrak{F}^{-1}\mathbf{U})_{ii}}\right]^{\frac{1}{2}}\right), \quad (34)$$

and for a nonbonded atom pair

$$\langle\Delta q^2\rangle=\frac{h}{4\pi}[\mathbf{A}'\mathbf{U}'\mathfrak{F}^{-1}\mathbf{U}\mathbf{A}(\mu+\mu')]^{\frac{1}{2}} \times\coth\left(\frac{h}{4\pi kT}\left[\frac{\mu+\mu'}{\mathbf{A}'\mathbf{U}'\mathfrak{F}^{-1}\mathbf{U}\mathbf{A}}\right]^{\frac{1}{2}}\right). \quad (35)$$

In Table IV the values calculated by this approximation, $\langle\Delta l^2\rangle^{\frac{1}{2}}_{\text{mod}}$, are compared with those obtained by the rigorous calculation, $\langle\Delta l^2\rangle^{\frac{1}{2}}_{\text{rig}}$. For comparison, the values computed by the formulae described in Part I, $\langle\Delta l^2\rangle^{\frac{1}{2}}_{\text{approx}}$, are also included. It is clearly seen that these modified formulas provide the values quite nearer to the true ones even for the cases containing a hydrogen atom.

III. FURTHER APPROXIMATION

For simplicity, let us consider first a pair of directly bonded atom pairs. In the formula (17) for the mean amplitude the second term depends on the masses of the atoms at the ends of the distance and is independent of the other part of the molecule. The first term, however, depends on all the elements of the matrix $\mathbf{F}$, and consequently on all the force constants in the molecule. But it often occurs that the nondiagonal elements of the matrix $\mathbf{F}$ are small compared with the diagonal

ones, so that Eq. (18) can be approximated by

$$F^{-1}{}_{ii}=\frac{1}{F_{ii}}\left(1+\sum_i \frac{F_{ij}{}^2}{F_{ii}F_{jj}}\right). \tag{36}$$

The second terms in this expression are small quantities of the second order. Therefore, if we dare to neglect them, we have a simple expression:

$$F^{-1}{}_{ii}=1/F_{ii}. \tag{37}$$

On the other hand it was the conclusion from the study of molecular vibration[6] that the forces acting between nonbonded atoms cannot be omitted. Consequently, in order to compute the F_{ii}, the components of the forces between nonbonded atoms along the bond direction should be taken into account. For instance, in a case of a C−X bond, where the four valencies of the carbon atom are saturated with four atoms, the F_{ii} is affected by the force constants due to the three atoms attached to the carbon atom so that

$$F_{ii}=K_i+\sum_k \tfrac{2}{3}F_{ik}. \tag{38}$$

The K_i and F_{ij} are the force constants which give the contributions $\frac{1}{2}K_i(\Delta R_i)^2$ and $\frac{1}{2}F_{ik}(\Delta q_{ik})^2$ respectively to the potential energy of the molecule, where ΔR_i is the displacement of the bond distance and Δq_{ik} that of the distance between one of the pair atoms and any one of the other nonbonded atoms.† The coefficient $\frac{2}{3}$ is brought about by assuming the angles between the bonds to be tetrahedral. It is well known that the force constant K_i has a definite value for a definite atom pair, whatever molecule it belongs to. Simultaneously, it was shown that the force constants F_{ik} have almost similar values for the atom pairs, one atom of which is a definite X: for example, in the case of X=Cl, F(Cl − − − Cl)=0.65, F(Cl − − − F)=0.6, F(Cl − − − H) =0.8, and F(Cl − − − Br)=0.55. Therefore, one may assume an average value F_{AV} for all of the three atom pairs. This simplifies Eq. (38) as

$$F_{ii}=K_i+2F_{AV}. \tag{39}$$

Thus we can tentatively assign a definite value to F_{ii}, and accordingly, by Eq. (7), a definite value of mean amplitude to the C−X bond, irrespective of the structure of the other part of the molecule.

For the bond Si−X, the same formula may be applied. But in the case of the C−C bond, which has six neighboring atoms, the forces between the nonbonded atoms afford more contribution to the F_{ii}, so that

$$F_{ii}=K_i+4F_{AV}. \tag{40}$$

The mean amplitudes of the directly bonded atom pairs calculated by the use of the force constants of Urey-Bradley type obtained by Shimanouchi[6] are shown in Table V, the values of the force constants used for the calculation being listed in the same table. Needless to say, in the cases listed in the lowest two columns of the table, where a hydrogen atom takes part in the pair, Eq. (32) is used for the calculation.

In order to estimate the mean amplitude for the nonbonded atom pair which are separated by one atom, we take out the three atoms from the whole molecule, assuming the forces of Urey-Bradley type to act between them, while other atoms and forces are all disregarded. This treatment does not produce much error in the computed values; for, if we take the said nonbonded distance as one of the internal coordinates, it can be easily shown that the influence of the forces originated from the atoms attached to the central atom are of the second order, as evident from Eq. (36). The predicted values for some pairs of atoms are shown in Table VI, together with the force constants and the bond lengths used in the calculation. The angles between the bonds are assumed to be tetrahedral.

The same argument may be applied to the mean amplitudes of the nonbonded atom pairs farther apart. As an example the mean amplitudes of the trans X − − −X distances in X−Y−Y−X molecules are calculated by the assumption that the rotation about the central C−C axis is fixed. The results are listed in Table VII.

It is very interesting to see that the values observed by Karle and Karle[5,7–9] and those assumed by Hastings and Bauer[10] are in reasonably good agreement with those computed by this method. Therefore, if some allowance be made for the errors of the mean amplitudes, it may be advisable to use the values computed above, without

TABLE V. The approximate values of the mean amplitudes of some of the directly bonded atom pairs.

Pair	K_i[a]	F_{AV}[a]	$\langle\Delta r^2\rangle^{\frac{1}{2}}_{calc}$[b]	$\langle\Delta r^2\rangle_{obs}$[b]
C−C	2.8	0.5	0.050	0.055 ($C_5H_{11}Cl$)[c]
C−F	3.75	1.3	0.045	0.043 (C_2F_4)[d]
C−Me	3.7	0.5	0.049	...
C−Cl	1.75	0.6	0.050	0.055 ($C_5H_{11}Cl$)[c] 0.064 ($C_2H_4Cl_2$)[e] 0.048 (C_2Cl_4)[f]
C−Br	1.45	0.5	0.052	...
Si−Si	1.25	0.05	0.061	...
Si−F	5.8	0.3	0.039	...
Si−Me	3.05	0.03	0.049	...
Si−Cl	2.6	0.3	0.044	...
Si−Br	2.0	0.3	0.046	...
C−H	4.8	0	0.078	0.072 (C_5H_8 and C_6H_6)[g]
Si−H	2.7	0	0.089	...

[a] In 10^5 dyne/cm units.
[b] In A units.
[c] Hastings and Bauer (reference 10).
[d] Karle and Karle (reference 5).
[e] Ainsworth and Karle (reference 9).
[f] Karle and Karle (reference 7).
[g] Karle (reference 8).

[6] T. Shimanouchi, J. Chem. Phys. **17**, 245, 734, 848 (1949).
† It should be noted that F_{ik} is not the ik element of the F matrix.

[7] I. L. Karle and J. Karle, J. Chem. Phys. **20**, 63 (1952).
[8] I. L. Karle, J. Chem. Phys. **20**, 65 (1952).
[9] J. Ainsworth and J. Karle, J. Chem. Phys. **20**, 425 (1952).
[10] J. M. Hastings and S. H. Bauer, J. Chem. Phys. **18**, 13 (1950).

TABLE VI. The approximate values of the mean amplitudes of some of the nonbonded atom pairs separated by one atom.

Pair	K[a]	H[a]	F'[a]	F[a]	r[b]	$\langle\Delta q^2\rangle^{\frac{1}{2}}_{calc}$[b]	$\langle\Delta q^2\rangle^{\frac{1}{2}}_{obs}$[b]
Me---Me (C)	3.7	0.2	−0.05	0.3	1.54	0.079	0.066 ($C_5H_{11}Cl$)[c]
F---F (C)	3.75	0.15	−0.3	1.35	1.32	0.056	···
Cl---Cl (C)	1.75	0.1	−0.1	0.65	1.77	0.070	0.070 (C_2Cl_4)[d]
Br---Br (C)	1.45	0.05	−0.1	0.5	1.93	0.077	···
Me---Me (Si)	3.05	0.1	−0.02	0.03	1.88	0.119	···
F---F (Si)	5.8	0.1	−0.14	0.34	1.54	0.078	···
Cl---Cl (Si)	2.6	0.04	−0.06	0.3	2.02	0.094	···
Br---Br (Si)	2.0	0.04	−0.04	0.23	2.16	0.103	···
Cl---Br (C)	C−Cl 1.75 C−Br 1.45	0.05	−0.1	0.55	C−Cl 1.77 C−Br 1.93	0.075	···
Me---F (C)	C−C 3.7 C−Br 3.75	0.15	−0.1	1.3	C−C 1.54 C−F 1.32	0.059	···
Me---Cl (C)	C−C 3.7 C−Cl 1.75	0.1	−0.1	0.6	C−C 1.54 C−Cl 1.77	0.073	0.070 ($C_2H_4Cl_2$)[e]
Me---Br (C)	C−C 3.7 C−Br 1.45	0.1	−0.1	0.5	C−C 1.54 C−Br 1.93	0.075	···
Me---H (C)	C−C 3.7 C−H 4.2	0.15	−0.05	0.4	C−C 1.54 C−H 1.09	0.120	0.086 ($C_2H_4Cl_2$)[e]
H---H (C)	4.8	0.4	0	0.1	1.09	0.135	···
H---H (Si)	2.8	0.15	−0.03	0.04	1.47	0.166	···
H---Cl (C)	C−H 4.2 C−Cl 1.75	0.05	−0.05	0.8	C−H 1.09 C−Cl 1.77	0.114	0.093 ($C_5H_{11}Cl$)[c] 0.104 ($C_2H_4Cl_2$)[e]

[a] In 10^5 dyne/cm units.
[b] In Å units.
[c] Hastings and Bauer (reference 10).
[d] Karle and Karle (reference 7).
[e] Ainsworth and Karle (reference 9).

taking the trouble to calculate them for each molecule. In this sense Schomaker's work[11] along this line is worth while mentioning. He used some selected values of the mean amplitudes in drawing the theoretical intensity curves, but, in order to make amends for the uncertainty in the values, he had to corroborate the result

[11] W. W. Wood and V. Schomaker, J. Chem. Phys. **20**, 555 (1952).

TABLE VII. The approximate values of the mean amplitudes of the trans X - - - X atom pairs in X−Y−Y−X molecules.

Molecule	K_{YY}[a]	K_{XY}[a]	H_{XYY}[a]	F_{XY}[a]	F'_{XY}[a]	r_{YY}[b]	r_{XY}[b]	α_{XYY}	$\langle\Delta q^2\rangle^{\frac{1}{2}}_{calc}$[b]
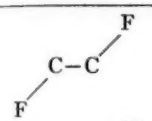	2.4	3.75	0.15	1.3	−0.1	1.54	1.36	109°28′	0.061
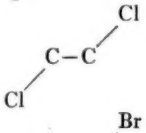	2.4	1.75	0.1	0.6	−0.1	1.54	1.77	109°28′	0.074
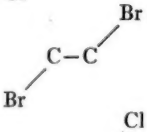	2.4	1.45	0.1	0.5	−0.1	1.54	1.92	109°28′	0.077
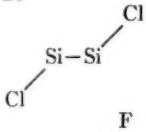	1.25	2.6	0.1	0.05	0.0	2.34	2.02	109°28′	0.119
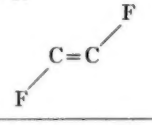	8.4	5.5	0.25	0.8	−0.08	1.313	1.313	123°	0.059
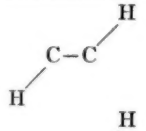	2.4	4.5	0.15	0.4	−0.05	1.54	1.10	109°28′	0.143
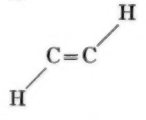	8.4	4.8	0.25	0.4	−0.04	1.313	1.07	122°	0.130

[a] In 10^5 dyne/cm units.
[b] In A units.

by the use of some sets of the values. Considering the accuracy of the calculation stated in this section, we may be able to assign reliable values to the mean amplitudes with more confidence.

Karle[8] indicated that for the radial distribution curve of cyclooctatetraene the best fit was obtained with two C−C equilibrium distances 1.35A and 1.50A with the mean amplitudes 0.055A and 0.065A respectively. At the same time there was still reasonable agreement with only one C−C bond distance of 1.42A with the larger mean amplitude 0.10A. Thus it cannot be decided by the experiment alone whether the C−C distances are equal or not. According to the conclusion obtained above (see Table V), it is safely emphasized that 0.10A is too large for the mean amplitude of the C−C bond distance, so that the model with equal distances is assuredly excluded from the consideration. In this way the accurate knowledge of the mean amplitudes enables us to determine the equilibrium distances with more accuracy.

In conclusion the authors are grateful for aid from the Scientific Research Encouragement Grant given by the Department of Education of Japan in support of this research.

The Thermal and Dielectric Properties of Crystalline Long-Chain Acetates

R. J. MEAKINS AND JOAN W. MULLEY
Division of Electrotechnology, Commonwealth Scientific and Industrial Research Organization, Sydney, Australia
(Received June 25, 1953)

This investigation deals with the normal long-chain acetates with 18, 20, 24, and 28 carbon atoms. When crystallized from the melt, these compounds first give the transparent α-phase which gradually changes to the white, opaque β-phase on standing or on cooling below a certain temperature. It is found that the acetates in the α-phase all give large dielectric absorption, whereas, in the β-phase the absorption is small, or, in some cases, negligible.

Of the long-chain compounds so far investigated, the acetates in the α-phase are unique in giving two absorption regions which appear to be the result of the rotational transitions of complete molecules. The maxima for the two regions are separated by about 7 decades in frequency. Measurements of the lower frequency absorption at various temperatures show that the associated energy barrier is very large compared with previous values for compounds of similar chain-length. To explain these results it is suggested that a molecule rotating in the crystal lattice of a long-chain compound possesses four positions of equilibrium instead of two, as previously proposed.

In addition to the two absorption regions mentioned above, the long-chain acetates in the α-phase give further absorption at still higher frequencies, which is probably caused by independent orientation of the polar groups near the ends of the molecular chains.

I. INTRODUCTION

IT has been previously reported[1–3] that many long-chain esters in the solid state give dielectric absorption maxima at radio frequencies. The variation of the frequency of the maximum loss factor with molecular weight indicates that the absorption is associated with the orientation of complete molecules.

The previous investigations in these Laboratories included the compound *n*-hexacosyl acetate, which was found to be somewhat different from the other esters in its dielectric and thermal properties.[4] It therefore seemed likely that a combined investigation of the cooling curves and dielectric properties of this compound and other long-chain acetates might prove interesting.

Another feature of the long-chain acetates to be considered is the possibility of independent orientation of the polar group due to its position near the end of the molecular chain. A similar structure is present in long-chain methyl esters, and in these has been found to result in dielectric absorption in the microwave region.[2]

II. MATERIALS

The acetates of the C_{16}, C_{18}, and C_{22} *n*-primary alcohols were prepared by heating the appropriate alcohol under reflux with acetic anhydride for 6 hours and then distilling off the excess reagent and the acetic acid formed in the reaction. The last traces of these impurities were eliminated by the addition of light petroleum and further distillation. The product was then vacuum fractionated, using a 90 cm column packed with Monel metal gauze saddles for the two lower homologs, and a spinning band column for the C_{24} compound.

The sample of *n*-hexacosyl acetate was obtained from the acetates of ceryl alcohol by vacuum fractionation through a spinning band column.

After distillation the acetates were further purified by recrystallization from methanol or ethanol. This reduced the conductivity, presumably due to the elimination of oxidative degradation products formed during the distillation.[5]

III. APPARATUS AND PROCEDURE

The method of preparation of samples and methods of electrical measurement have been previously described.[6,2]

The apparatus used for determining the melting and cooling curves was similar to that designed by Skau.[7]

The relative densities, where given, were determined from the mass and dimensions of one inch diameter disks pressed at about 12 tons per sq in. With waxy long-chain compounds this method gives results almost identical with those from x-ray crystal measurements.

IV. RESULTS AND DISCUSSION

(a) Cooling Curves

Previous workers[8,9] have found that long-chain acetates exist in at least two forms. The material first obtained on crystallization from the melt is the transparent α phase which, on further cooling, changes to the opaque β phase.

These changes can be conveniently observed with a sample of *n*-hexadecyl acetate in a glass vessel. In this

[1] R. J. Meakins, Australian J. Sci. Research **A2**, 405 (1949).
[2] J. S. Dryden and H. K. Welsh, Australian J. Sci. Research **A4**, 616 (1951).
[3] R. W. Crowe and C. P. Smyth, J. Am. Chem. Soc. **73**, 5401 (1950).
[4] R. J. Meakins, Unpublished results.
[5] B. V. Hamon and R. J. Meakins, Nature **166**, 29 (1950).
[6] B. V. Hamon and R. J. Meakins, Australian J. Sci. Research **A5**, 671 (1952).
[7] E. L. Skau, Proc. Am. Acad. Arts. Sci. **67**, 551 (1932).
[8] J. W. C. Phillips and S. A. Mumford, J. Chem. Soc. **1934**, 1657 (1934).
[9] J. D. Meyer and E. E. Reid, J. Am. Chem. Soc. **55**, 1574 (1933).

compound the transition occurs much more quickly than in the higher homologues. On cooling the liquid, the transparent crystals of the α phase begin to form at 18.5°C. This crystallization then proceeds until the commencement of the transition to the β phase which sometimes occurs before the mass has completely solidified. It is indicated by the formation of a white opaque spot in the crystalline mass. In the transition region sufficient heat is liberated to cause a local liquefaction of the low-melting α phase. This liquid then resolidifies into the more stable β phase, being seeded by the crystals already present.

These changes are shown in the cooling curve given in Fig. 1. In this particular experiment the transition commenced at 7.6°C, but different experiments gave different transition temperatures, even with the same sample. A comparison of the areas under the different portions of the cooling curve shows that the heat of transition is about half the heat of crystallization of the α phase. It is thus evident that the α phase of *n*-hexadecyl acetate possesses considerably higher energy than the β phase. Similar differences have been found in other work on α and β phases of long-chain compounds.[10]

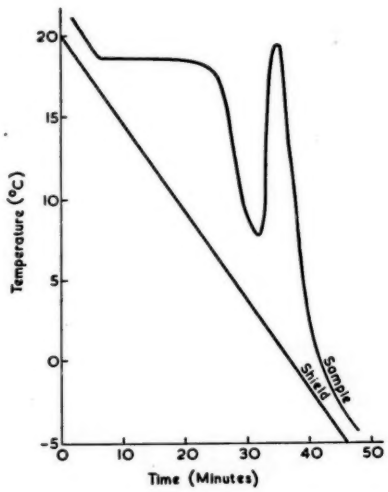

FIG. 1. Solidification and transition *n*-Hexadecyl acetate. (Readings at one minute intervals.)

The transition from α to β phase in *n*-hexadecyl acetate is not reversible. The heating curve shows that the β phase persists up to 24.0°C and then melts.

The cooling curve for *n*-octadecyl acetate is shown in Fig. 2. A superficial inspection suggests that the transition from α to β phase for this compound occurs at about 1°C. However, it is observed that the sample and shield curves are more widely separated than usual for a considerable period after solidification and it therefore seemed possible that the transition had commenced at a much higher temperature. This was confirmed by cooling a sample of *n*-octadecyl acetate from the liquid to 20°C and holding it at this temperature overnight. The cooling curve was then continued and it was found

[10] Garner, van Bibber, and King, J. Chem. Soc. **1931**, 1533 (1931).

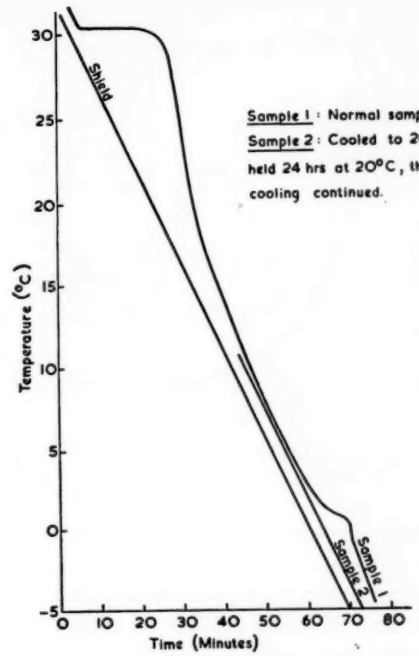
Shield
Sample 1 : Normal sample
Sample 2 : Cooled to 20°C, held 24 hrs at 20°C, then cooling continued.
Temperature (°C)
Time (Minutes)
Sample 1
Sample 2

FIG. 2. Solidification and transition of *n*-Octadecyl acetate. (Readings at one minute intervals.)

that the inflexion at 1°C was absent (see Fig. 2 sample 2). In further experiments, it was observed that samples of the transparent α-phase kept in a glass vessel at 20°C always changed to the white opaque β phase within 24 hours.

The cooling curves for *n*-docosyl and *n*-hexacosyl acetates are similar to that for *n*-octadecyl acetate. The heating curves are different, however, and show the reverse transition from the β to the α phase.

The melting and setting points of the above-mentioned long-chain acetates, determined from the cooling curves, are given in Table I.

(b) Dielectric Properties

With samples of the acetates cooled from the liquid state to room temperature in glass tubes it was found that the α phase usually persisted for at least a few hours after solidification. Attempts were therefore made to prepare disks for dielectric measurement but it was found that with the two lower homologues, the working

TABLE I. Melting and setting points of long-chain acetates.

Acetate	Formula	α Phase M. pt. (°C)	α Phase S. pt. (°C)	β Phase M. pt. (°C)	β Phase S. pt. (°C)
n-Hexadecyl	$C_{16}H_{33}O\cdot COCH_3$	18.5	18.5	24.0	23.7 (seeded)
n-Octadecyl	$C_{18}H_{37}O\cdot COCH_3$	30.3	30.3	32.4	...
n-Docosyl	$C_{22}H_{45}O\cdot COCH_3$	47.6	47.5		
n-Hexacosyl	$C_{26}H_{53}O\cdot COCH_3$	59.5	59.6	Material changes to α phase before melting, and crystallizes in α phase from melt.	

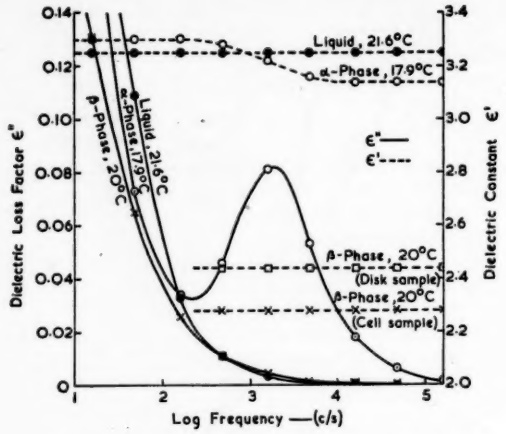

FIG. 3. Low frequency dielectric properties of *n*-Hexadecyl acetate ($C_{18}H_{36}O_2$).

of the material caused a rapid transition to the β phase. Samples of the α phases of these two compounds could be measured at frequencies up to about 10 Mc/sec, however, by allowing them to crystallize in a dielectric test cell.[6] Actually, this part of the program was limited mainly to bridge measurements up to 1.6×10^5 cps, since this frequency range was sufficient to include the whole of the low frequency absorption regions at the temperatures involved. *n*-Docosyl acetate was also included in the dielectric test cell measurements, for purposes of comparison, but there was insufficient *n*-hexacosyl acetate available to fill the cell.

In addition to the cell measurements, disks and coaxial samples were prepared from the two higher homologs in the α phase, and measured over the complete frequency range from 10^{-4} to 2.4×10^{10} cps. Similar measurements were made with all four of the acetates in the β phase.

In discussing the results it is convenient to deal first with the properties of the C_{18}, C_{20} and C_{24} compounds in the frequency range up to 160 kc/sec. This includes one important region of dielectric absorption in the α phase acetates. Further absorption regions at higher frequencies are then discussed, with reference chiefly to the C_{24} and C_{28} compounds. It is not possible to show all of the absorption regions on one diagram since some of the high frequency apparatus used in this programme was suitable for measurements only at room temperature (20°C). At 20°C, the low frequency absorption of the two higher acetates is masked by the loss due to dc conductivity.

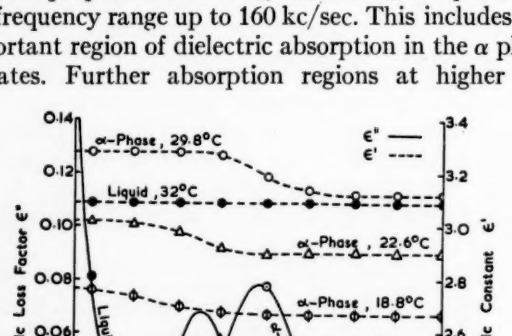

FIG. 4. Low frequency dielectric properties of *n*-Octadecyl acetate ($C_{20}H_{40}O_2$).

1. *Dielectric Properties at Frequencies below* 1.6×10^5 cps

The results of electrical measurements of the C_{18}, C_{20} and C_{24} compounds in the dielectric test cell are shown in Figs. 3–5. With each compound there is a striking difference between the loss factor curves for the α and β phases. Apart from the dc conductivity effects at the lowest frequencies, the β phases show no dielectric loss. The α phases, on the other hand, give well-defined absorption maxima at frequencies which vary between about 150 and 1000 cps according to the molecular chain-length and the temperature of measurement.

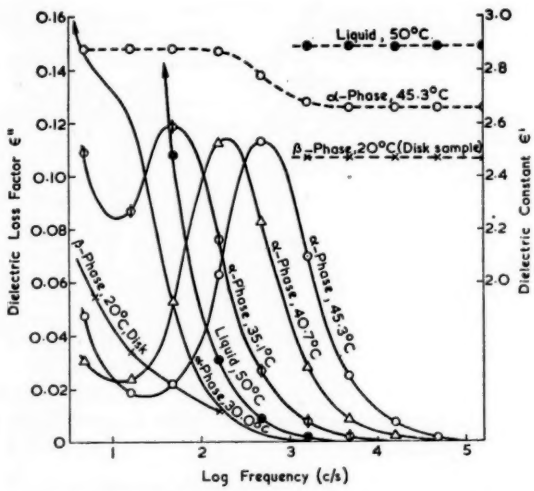

FIG. 5. Low frequency dielectric properties of *n*-Docosyl acetate ($C_{24}H_{48}O_2$).

The dielectric absorption in the α-phase acetates is accompanied by an increase in the dielectric constant with decreasing frequency. In each case, the difference between the high and low frequency values of the dielectric constant ϵ' is found to be twice the value of the maximum loss factor ϵ''_{max}, indicating that the absorption is due to a relaxation mechanism possessing a single relaxation time.[11] This is unusual in crystalline long-chain compounds, which generally give wide absorption curves indicating the presence of a range of relaxation times. It should be pointed out, however, that most previous measurements of this type have probably been made with β-phase material.[2]

As indicated in the diagrams, the C_{20} and C_{24} compounds were sufficiently stable in the α phase to enable

[11] P. Debye, *Polar Molecules* (The Chemical Catalog Co. Inc., New York, 1929).

measurements to be made at several different temperatures. From these results it is possible to determine the energy barrier H for the process causing the absorption, by applying the relationship

$$f_{max}=C\exp\left(\frac{-H}{kT}\right), \qquad (1)^{12}$$

where f_{max} is the frequency of the maximum loss factor, C is a constant, k is Boltzmann's constant, and T is the absolute temperature.

This gives the values shown in Table II.

The values of H are very much larger than those observed for methyl esters of similar molecular weight.[2] This is not unexpected, since the absorption regions indicated above in the acetates are at least 5 decades lower in frequency than those for the corresponding methyl esters.

In *n*-hexadecyl and *n*-octadecyl acetate, dielectric measurements of the α phase were made at temperatures close to 18°C. A comparison of the loss factor curves for the two compounds indicates that the maximum is considerably displaced to lower frequencies with increasing molecular weight. No direct comparison can be made with *n*-docosyl acetate, due to the higher temperature of the measurements, but an indication of the probable frequency of the maximum at 18.8°C can be obtained by extrapolation. The resulting value is included in Fig. 6, which shows the variation of $\log f_{max}$ with molecular chain-length for the three acetates. The approximately linear relationship is similar to that previously obtained for other long-chain compounds. It suggests that the absorption is due to the rotational transitions of complete molecular chains.[1,13] This conclusion is supported by the observation that the energy barrier for *n*-docosyl acetate (see Table II) is slightly larger than that for *n*-octadecyl acetate.

TABLE II.

Compound	H (kcal/mole)	C
n-Octadecyl acetate	32	5×10^{26}
n-Docosyl acetate	35	5×10^{26}

At the beginning of this Section, reference was made to the presence of dc conductivity in the acetates. This is indicated by the shape of the dielectric loss factor curves at the lowest frequencies, and by the results of further measurements which showed that, in each case, ϵ'' continued to increase with decreasing frequency down to 10^{-3} cps. The actual values of the dc conductivity, measured with disk samples between mercury electrodes[6] were all in the region of 10^{-16} mho cm^{-1}. Freshly melted material gave larger values, up to 4×10^{-14} mho cm^{-1}, but these decreased to about the initial value on standing. Similar results were obtained with all samples, irrespective of the method of preparation or purification, and also with *n*-hexacosyl acetate, which was supplied from a different laboratory (see Sec. 6). It appears that the observed dc conductivity is either an inherent property of the long-chain acetates, or is due to the presence of impurities which are very difficult to remove.

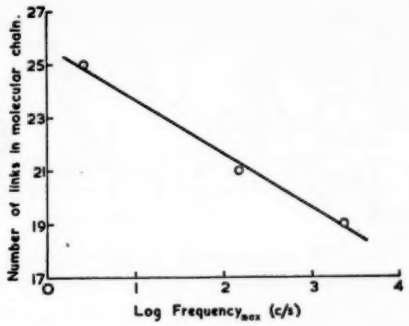

FIG. 6. Effect of molecular chain-length on frequency of maximum absorption of acetates in the α phase.

It should be mentioned that, in the loss factor curves for *n*-octadecyl acetate given in Fig. 4, ϵ''_{max} shows a progressive decrease with decreasing temperature. This is due to a partial transition to the β-phase during the measurements, which were commenced on the liquid at 32°C and continued in order of decreasing temperature. To check this point, the sample was held at 22.6°C for 1½ hours, during which period ϵ''_{max} was found to decrease from 0.077 to 0.058. With *n*-docosyl acetate the α-phase is more stable and ϵ''_{max} shows no significant decrease during the measurements.

In previous work by Crowe and Smyth[3] on the α phases of a number of long-chain esters, including *n*-octadecyl acetate, it was found that the dielectric constant varied from one experiment to another, possibly due to different rates of solidification from the melt. In the present investigation also, variations in the dielectric constant and maximum loss factor were observed in different experiments with a particular compound. Thus, with *n*-octadecyl acetate ϵ''_{max} at 29°C varied from 0.08 to 0.17 in different experiments.

Measurements of disk samples of *n*-docosyl and *n*-hexacosyl acetates in the α phase were made only at room temperature (20°C). No absorption maxima of the type shown above were observed, apparently because, at this temperature, such absorption would be completely masked by dc effects.

In the results for the dielectric constants given in Figs. 3–5, the values for the α-phase samples are appreciably larger than those for the corresponding β phases, even at frequencies above the dispersion region. This indicates that acetates in the α phase give further dielectric absorption at higher frequencies.

The dielectric constants of the β phases (disk samples) are between 2.44 and 2.50 throughout the frequency range of measurement. This is only about 10 percent larger than the value (2.25) for paraffin wax under the same conditions. Taking into account the larger specific

[12] H. Frohlich, *Theory of Dielectrics* (Oxford University Press, London, 1949).
[13] R. W. Sillars, Proc. Roy. Soc. (London) **A169**, 66 (1939).

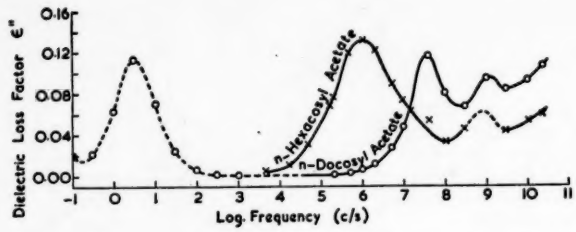

FIG. 7. Comparison of dielectric absorption in *n*-Docosyl and *n*-Hexacosyl acetates ($C_{24}H_{48}O_2$ and $C_{28}H_{56}O_2$) in the α phase at 20°C.

gravity of the acetates (0.96) compared with paraffin wax (0.87) it is evident that there can be very little dielectric absorption at higher frequencies.

The results for *n*-hexacosyl acetate are somewhat different to those for the three lower homologues. The dielectric constants of both the α and β phases (2.88 and 2.63 respectively) are larger than expected for a loss free substance, which suggests that both forms should give high frequency dielectric absorption.

2. *Dielectric Properties at Frequencies between 1.6×10^5 and 2.4×10^{10}* cps

The apparatus used for much of this frequency range was suitable only for measurements at room temperature (20°C) with disk-shaped or coaxial samples. This restricted the investigation of α-phase acetates at high frequencies mainly to the C_{24} and C_{28} compounds. The results are given in Fig. 7. Also included in the diagram is the estimated position of the low frequency absorption maximum for *n*-docosyl acetate, determined by extrapolation from the results of cell sample measurements at higher temperatures. In the actual samples measured at 20°C, the low frequency absorption maximum was masked by the loss due to dc conductivity.

The main feature of interest in the results given in Fig. 7 is the relationship between the absorption maxima for the two compounds in the frequency region between 10^5 and 10^8 cps. From previous work with long-chain compounds it seems likely that these absorption regions are due to the rotational transitions of complete molecules, the higher frequency of absorption for the lower molecular weight compound being due to the smaller energy barrier associated with the shorter molecules. Further results in support of this suggestion were obtained from some measurements, at frequencies up to 10 Mc/sec, with an α-phase sample of *n*-octadecyl acetate in the dielectric test cell. Although only a small part of the absorption region was detected, the results were sufficient to indicate that the maximum is at a higher frequency than that for *n*-docosyl acetate.

A feature of the dielectric absorption regions discussed above is the greater width of the *n*-hexacosyl acetate curve compared with that for *n*-docosyl acetate. The results for the latter are approximately in accordance with the requirements for a Debye type absorption associated with a single relaxation time, as was found also for the low frequency absorption in this compound. The wider curve for *n*-hexacosyl acetate, suggesting a range of relaxation times is more closely related to the type of absorption normally observed in β-phase long-chain compounds.

The energy barrier for the process resulting in the above absorption for the C_{24} and C_{28} acetates was not determined, owing to the instability of the α phase and the difficulty, with the present apparatus, of making measurements at a range of different temperatures in this frequency region. Some indication of the values of the energy barrier for the C_{20} and C_{24} acetates may possibly be obtained, however, from a comparison of the frequencies of the maximum loss factor of these compounds with the values previously determined for methyl esters of similar chain-length.[2] This suggests that the energy barriers for the acetates are a little less than the values of 11 and 17 kcal/mole for the corresponding methyl esters. In making the comparison it is assumed that the absorption is due to the same type of process and that the value of the constant C in Eq. (1) is approximately the same for the two series of compounds.

At frequencies above 10^8 cps, both *n*-docosyl and *n*-hexacosyl acetates give further dielectric loss. Unfortunately, with the latter compound, there was insufficient material available to prepare a sample suitable for measurement at 10^9 cps but the shape of the curve suggests that there would be a maximum in this region. *n*-Docosyl acetate is similar, and both compounds also appear to have at least one more maximum above 2.4×10^{10} cps. The similarity in the shape of the curves for the two compounds at frequencies above 10^8 cps suggests that the dielectric loss in this region is due to dipole orientation involving movement of the polar end-groups independently of the main molecular chains. The presence of more than one absorption maximum in these two acetates above 10^8 cps may be the result of different modes of orientation of the $\cdot O\cdot CO\cdot CH_3$ end-group.

High frequency measurements of β-phase samples were made with all four of the acetates, the results being in agreement with predictions from the low frequency dielectric constant values discussed in the previous part of this Section. The C_{18}, C_{20} and C_{24} compounds gave very little dielectric loss. The highest homologue, *n*-hexacosyl acetate, gave some loss, with a maximum near 1 Mc/sec, which is about the same frequency as the maximum for the α-phase material discussed above. The amount of the absorption was considerably less, however, ϵ''_{max} being only 0.026, compared with a value of about 0.13 for the α phase.

3. *Mechanisms of Dielectric Loss in Long-Chain Compounds in Relation to Results for the Acetates*

The results given in the previous Section suggest that long-chain acetates in the α phase possess two regions of dielectric absorption depending on the rotational transi-

tions of complete molecules. This has not been previously observed in long-chain compounds and it therefore seemed of interest to consider the results in relation to the proposed mechanisms of dielectric loss in crystalline solids.

A simple model explaining the presence of dielectric absorption in polar solids is that of Debye,[11] in which the dipoles are assumed to possess two positions of equilibrium, equal in energy and opposite in direction. The transitions of the dipoles from one potential minimum to another, interacting with an alternating electric field, give rise to dielectric loss and anomalous dispersion of the dielectric constant which can be described by the usual Debye equations. With this model the loss factor-frequency relationship possesses a single maximum.

If, in the above model, the potential minima differ in energy by an amount V, the dielectric absorption decreases as V increases.[12] For the systems in which V is very much larger than the thermal energy kT there is no measurable dielectric loss. This has been found to be the case in many long-chain ketones,[1] in some esters and ethers,[4] and also in the β-phase acetates described above.

Although the above model explains the electrical properties of some long-chain compounds it is not adequate to account for the two absorption peaks in the α-phase acetates which appear to be associated with the rotations of complete molecules. These can be more satisfactorily explained on the basis of a model (O'Dwyer, to be published) in which the molecules are assumed to possess four positions of equilibrium instead of two, as suggested above. This is illustrated in Fig. 8 which is a diagrammatic representation of the potential energy curve of a long-chain molecule rotating in the crystal lattice. The positions of the minima at about 0, 60, 280 and 240°, respectively, and the relatively smaller energy barriers for the rotational transitions through 60° are suggested from a study of molecular models and the available data on similar crystal structures.[14] Another point in the illustration is that the first and third positions are of equal energy differing by an amount V from the second and fourth positions which are also equal. In the results for the α-phase

[14] A. Müller, Proc. Roy. Soc. (London) **A127**, 417 (1930).

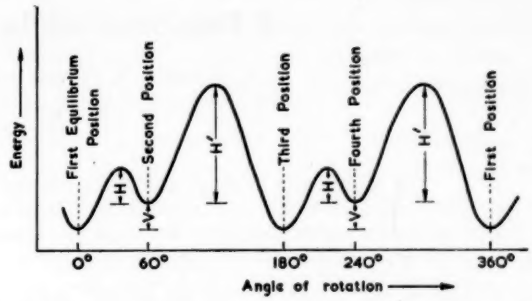

FIG. 8. Diagram illustrating potential minima and energy barriers of a long chain molecule rotating in the crystal lattice.

acetates the most important feature to be explained is the presence of two absorption regions associated with molecular rotation. On the basis of the above model, the higher frequency absorption would be due to rotational transitions between the first and second, or the third and fourth positions of equilibrium respectively, i.e., transitions involving the smaller energy barrier H. The lower frequency absorption would be associated with transitions across the larger energy barrier H' which occurs between the second and third and the fourth and first positions of equilibrium, respectively.

In the particular model described above the amounts of absorption in the two different regions would be equal, and would both depend on the value of V, the energy difference between the equilibrium positions.[12] The energy levels in the model have been arranged in this manner to account for the results for *n*-docosyl acetate, in which the values of ϵ''_{max} for the two absorption regions were found to be approximately equal. In the most general model, however, the energy levels of the equilibrium positions could be all unequal.

ACKNOWLEDGMENTS

The authors wish to thank the following officers of the Australian Commonwealth Scientific and Industrial Research Organization: Dr. J. S. Dryden, Division of Electrotechnology, for help with the electrical measurements above 10^8 cps; Mr. Davenport, Division of Food Preservation, for purifying a sample of *n*-docosyl acetate by distilling it through a spinning band column, and Mr. K. E. Murray, Division of Industrial Chemistry, for providing a sample of *n*-hexacosyl acetate.

K Fine Structure in the $2\nu_1$ Band of CHD_3†

T. A. WIGGINS, E. R. SHULL, JEAN M. BENNETT, AND D. H. RANK
Physics Department, The Pennsylvania State College, State College, Pennsylvania

(Received May 8, 1953)

The K structure in the P and R branches of the $2\nu_1$ band of CHD_3 has been resolved permitting the determination of the following molecular constants: $\nu_0=5865.02$, $B''=3.2777$, $B'=3.2396$, $A'-A''=-0.0181$, $D_J=3.9\times10^{-5}$, and $D_{JK}=-4\times10^{-5}$ cm^{-1}. The Q branch is synthesized from these data and compared with the spectrometer trace of that branch.

INTRODUCTION

THE high resolution and techniques of precision measurement that have been developed in this laboratory[1] have been used to verify additional details of the theory of symmetric top molecules. It is shown that a value for D_{JK} can be found for CHD_3 from the K structure in the P and R branches of the parallel band at 5865 cm^{-1}. The band is assigned as $2\nu_1$ on the basis of the fundamental frequencies reported by Benedict, Morikawa, Barnes, and Taylor.[2] K structure of rotational-vibrational lines has been reported in N_3H by Eyster,[3] in NH_3 by Sheng, Barker, and Dennison,[4] and in CH_3D by Boyd and Thompson.[5] However, this fine structure has not been observed before in the overtone region and none of the above authors have reported a value for D_{JK} for the molecules investigated.

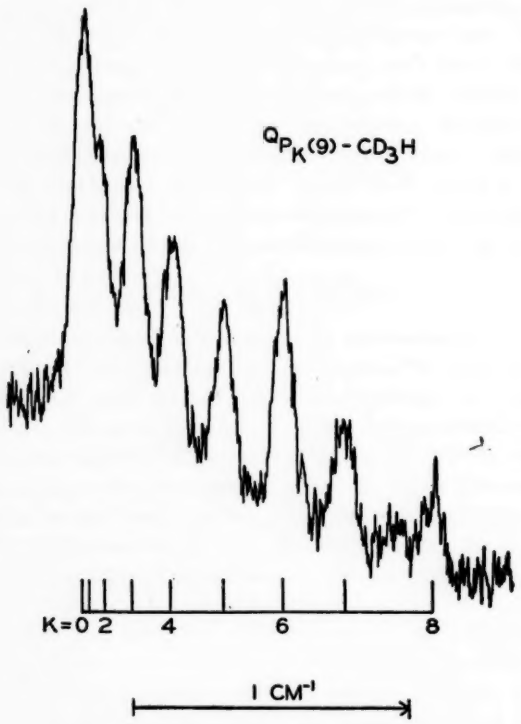

FIG. 1. Fine structure of the $^QP_K(9)$ line.

A complete description of the apparatus used for this work has been given elsewhere[1] and need not be repeated here. It is sufficient to state that the Bausch and Lomb 15 000 lines/in. plane transfer grating provides a resolution of 140 000 at 6000 cm^{-1} when used double-pass with 10-meter optics. The interferometric measurements provide an absolute accuracy of ±0.03 cm^{-1}. Relative frequencies can be measured to ±0.005 cm^{-1} using the wedge prism for scanning.

The deuteroform was contained in a one-meter absorption tube at a pressure of 8 cm. It was prepared by hydrolyzing a solution of CD_3MgBr in pure, dry di-n-butyl ether with a solution of ordinary water in pure p dioxane. The gas evolved was collected in a liquid nitrogen cooled trap and vacuum distilled twice. The CD_3Br used to prepare the Grignard reagent was obtained by the method of Shull, Oakwood, and Rank.[6]

EXPERIMENTAL RESULTS

The theory of symmetric top molecules indicates that the frequencies of the lines in the P and R branches of a parallel band can be expressed in wave numbers as

$$\nu=\nu_0+(B'+B'')m+(B'-B'')m^2-4D_Jm^3 -(A'-A''-B'+B''-2mD_{JK})K^2, \quad (1)$$

where $m=-J$ for the P branch and $J+1$ for the R branch, if it is assumed that $D_J'=D_J''$, $D_K'=D_K''$ and $D_{JK}'=D_{JK}''$. With the same assumptions, frequencies in the Q branch can be expressed as

$$\nu=\nu_0+(B'-B'')J(J+1)+(A'-A''-B'+B'')K^2. \quad (2)$$

In the P branch, K may assume integral values from zero to $J-1$, in the R branch from zero to J, while in the Q branch K takes on integral values from one to J.

Inspection of Eq. (1) shows that by using a constant value of K, the usual methods of band analysis may be applied to determine the molecular constants B', B'', and D_J. In this work the frequencies used for the determination of these constants were for the $K=0$

† This research was assisted by support from Contract N6Onr-269, Task V, of the U. S. Office of Naval Research.

[1] Rank, Shull, Bennett, and Wiggins, J. Opt. Soc. Am. **43**, 952 (1953).

[2] Benedict, Morikawa, Barnes, and Taylor, J. Chem. Phys. **5**, 1 (1937).

[3] E. H. Eyster, J. Chem. Phys. **8**, 135 (1940).

[4] Sheng, Barker, and Dennison, Phys. Rev. **60**, 786 (1941).

[5] D. R. J. Boyd and H. W. Thompson, Proc. Roy. Soc. (London) **A216**, 143 (1953).

[6] Shull, Oakwood, and Rank, submitted to J. Chem. Phys.

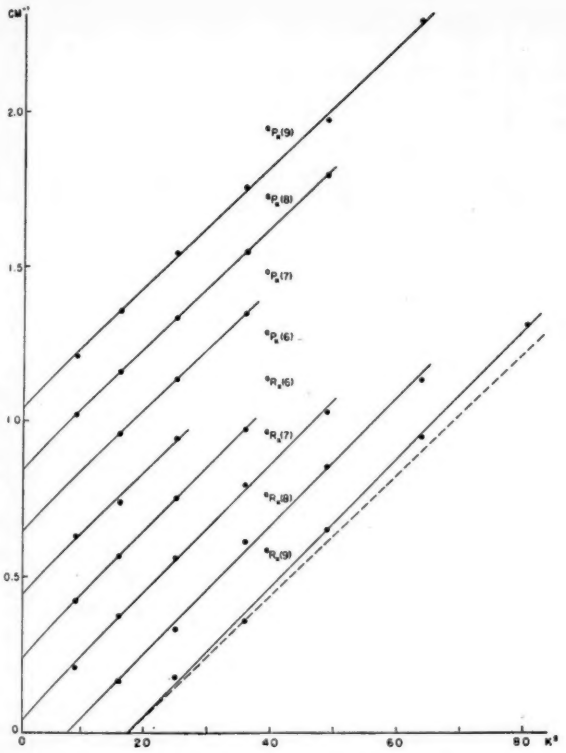

FIG. 2. Frequencies of fine structure components. The dashed line is drawn parallel to the line labeled $^QP_K(9)$.

components in each line since this is the only component that occurs in all lines of the P and R branches. These frequencies could not be measured directly since they were not resolved from the $K=1$ components. Where several K components could be measured (i.e., $J>3$) the frequency for $K=0$ was determined by plotting the frequencies of the components *versus* K^2 and noting the value of the intercept. For low J values, the frequency for $K=0$ could be estimated to within ± 0.005 cm^{-1} considering the separation and statistical weights of the component lines. Figure 1 shows the fine structure of the $^QP(9)$ line. All of the allowed components were found with intensities in agreement with the theoretical statistical weights.

Due to the large value of B for deuteroform, only a relatively small number of lines was observed in the P and R branches. For this reason it seemed that better constants could be found by fitting the observed frequencies for the $K=0$ components to an equation of the form

$$\nu=\nu_0+bm+cm^2+dm^3. \quad (3)$$

This procedure requires that the P and R branches have the same constants and origin and also provides at least twice as many data points for least squares fitting as would be available in the Δ_2F method of analysis. Comparison of Eqs. (1) and (3) indicates that $B'=(b+c)/2$, $B''=(b-c)/2$, and $D_J=-d/4$. The frequencies for $^QR(8)$ and $^QR(9)$ were not used in fitting of the data since these "lines" were displaced by some perturbation by about 0.3 cm^{-1} from their expected position. The average deviation between the computed and measured frequencies was ± 0.007 cm^{-1}.

A further inspection of Eq. (1) shows that the quantities $(A'-A'')$ and D_{JK} may be determined from the frequencies of the fine structure components. This is pointed out by Herzberg[7] but is in contradiction to the interpretation given by Boyd and Thompson[5] in a somewhat similar situation. If the frequencies of the components in one of the P or R branch lines are plotted *versus* K^2, a measurement of the quantity $(A'-A''-B'+B''-2mD_{JK})$ can be made. This indicates that the slope of the fine structure plots should change continuously from one end of the band to the other. Equation (2) indicates that, in theory, the quantity $(A'-A''-B'+B'')$ can be obtained from the Q branch if the components for a constant value of J can be resolved and identified. By plotting the slopes of the fine structure components of several lines in the P and R branches *versus* m, a straight line is obtained, the slope and

TABLE I. Vacuum wave numbers in the $2\nu_1$ band of CHD_3.

P Branch			*R* Branch		
J	*K*	ν	*J*	*K*	ν
2	0	5851.832	1	0	5877.899
3	0	45.118	2	0	84.206
4	0	38.349	3	0	90.476
5	0	31.504	4	0	96.646
6	0	24.578	5	0	5902.704
	3	24.764			
	4	24.871	6	0	8.737
	5	25.076		3	8.920
				4	9.062
7	0	17.580		5	9.248
	4	17.892		6	9.469
	5	18.069			
	6	18.280	7	0	14.631
				3	14.809
8	0	10.532		4	14.972
	3	10.704		5	15.158
	4	10.842		6	15.392
	5	11.017		7	15.626
	6	11.231			
	7	11.480	8	0	20.192
				4	20.517
9	0	3.394		5	20.683
	3	3.556		6	20.963
	4	3.701		7	21.205
	5	3.888		8	21.485
	6	4.106			
	7	4.321	9	0	25.921
	8	4.645		5	26.459
				6	26.636
10	0	5796.190		7	26.931
				8	27.226
				9	27.590

[7] G. Herzberg, *Infrared and Raman Spectra of Polyatomic Molecules* (D. Van Nostrand Company, Inc., New York, 1945), p. 434.

intercept of which are $-2D_{JK}$ and $(A'-A''-B'+B'')$, respectively.

Figure 2 shows plots of the components of lines in the P and R branches. They are constructed to the same scale but with arbitrary intercepts. It can be seen that with the exception of ${}^{Q}P(7)$, ${}^{Q}P(8)$, and ${}^{Q}R(6)$ the plotted points exhibit deviations approaching the half-width of the line. These cannot be explained as errors in measurement and may be attributed to higher order (probably Coriolis) perturbations. The measured frequencies are tabulated in Table I. Frequencies are given to thousandths of a wave number so that frequencies in a single P or R branch line can be compared.

The perturbations noted above prevented a determination of the slopes to a sufficient precision to illustrate that there is a change in slope from one line to the next. However, a value for D_{JK} can be found since a line in each of the two branches could be measured with sufficient precision. The lines drawn in Fig. 2 through the points for ${}^{Q}P(8)$ and ${}^{Q}R(6)$ are those indicated by least squares methods applied to the average frequencies from eight sets of data. These slopes are 0.01943 and 0.02036 cm^{-1} respectively. From these data, values for $(A'-A''-B'+B'')$ and D_{JK} could be found as noted in the theory above. From these constants the slopes of the other P and R branch lines were computed and used to construct the lines drawn in Fig. 2. It is observed that the lines provide a respectable fit to the measured frequencies. The dashed line near ${}^{Q}R(9)$ is drawn parallel to the line ${}^{Q}P(9)$ to illustrate the amount of change in the slope from one end of the band to the other.

This analysis of the band yields the following constants expressed in vacuum wave numbers:

$$\nu_0=5865.02, \quad A'-A''=-0.0181,$$
$$B'=3.2396, \quad B''=3.2777,$$
$$D_J=3.9\times10^{-5}, \quad D_{JK}=-4\times10^{-5}.$$

It was noted above that a value for $(A'-A''-B'+B'')$ could be obtained from the Q branch. This was not possible in this case since the K components associated with a given value of J could not be uniquely assigned due to the overlapping of the different J lines.

To illustrate this overlapping, the molecular constants determined from the P and R branches were used to predict the positions of the components that would appear in the Q branch. From Eq. (2) the frequencies are given by

$$\nu=\nu_0-0.0381J(J+1)+0.0199K^2, \quad 0<K\leqslant J.$$

The intensities of the components can be determined from the statistical weights as summarized by Herzberg[8]

$$I\sim A_{JK}\nu g_{JK}\exp[-F(J,K)hc/kT].$$

[8] See reference 7, p. 421.

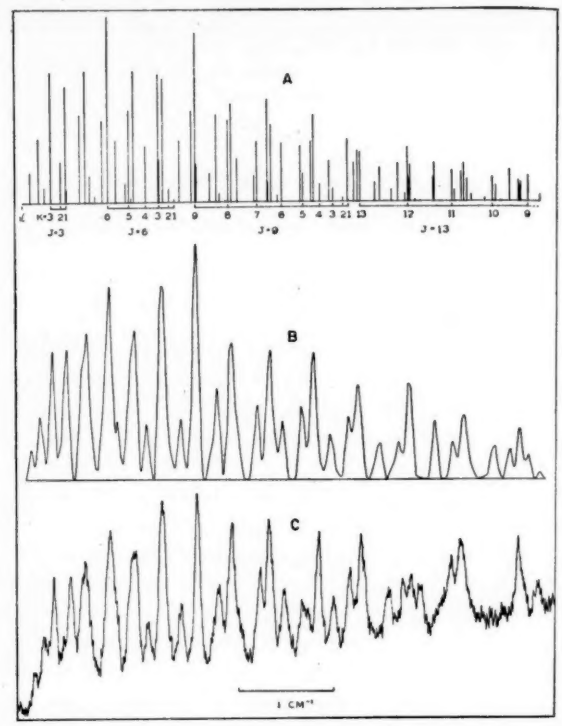

FIG. 3. The Q branch. (A) Positions and intensities of predicted components. (B) Synthetic branch assuming triangular line shape and half-width of 0.06 cm^{-1}. (C) Reproduction of spectrometer trace of the Q branch.

Using the above data,

$$I\sim\frac{K^2(2J+1)(8+X)}{J(J+1)}\times\exp[-0.01575J(J+1)]\exp[0.00302K^2],$$

where $X=3$ for $K=3, 6, 9$, etc. and $X=0$ for $K=1, 2, 4$, etc. The value for $A=2.65$ cm^{-1} is not critical and was taken from the value given for CD_4 by Herzberg.[9]

Using these frequencies and intensities, Fig. 3(A) was constructed. Several series of lines are identified. Assuming triangular line shapes with a half-width of 0.06 cm^{-1}, Fig. 3(B) was constructed as a synthetic Q branch. This can be compared with a reproduction of the actual Q branch shown in Fig. 3(C) as recorded by the spectrometer. The similarity of the figures indicates that correct quantum numbers could be assigned to the lines in the Q branch on the basis of Fig. 3(A). There would be no advantage in this, however, since the components are not completely resolved and since no new information could be obtained except for confirmation of the values of $A'-A''$ and $B'-B''$.

Note added in proof.—Since this paper was submitted, an article on CHD_3 by L. F. H. Bovey, working in the photographic infrared with higher harmonics, has appeared in the Journal of Chemical Physics **21**, 830 (1953).

[9] See reference 7, p. 456.

Dielectric Polarization and Structure of Polar Liquids under Pressure

FRANK E. HARRIS,* ERNEST W. HAYCOCK, and BERNI J. ALDER
Department of Chemistry and Chemical Engineering, University of California, Berkeley, California
(Received May 11, 1953)

The static dielectric constants of *n*-butyl alcohol, *t*-butyl alcohol, *n*-butyl chloride, *n*-butyl bromide, t-butyl chloride, and water were experimentally determined over a temperature range of 14° to 50° C and over a pressure range of 1 to 200 atmos. In addition, for glycerol, both the static dielectric constant from −18° to 14° C and the dielectric relaxation data at 0°C and up to 1.5 mc were obtained over the same pressure interval. The theory of dielectric polarization was then applied to these measurements to determine the molecular interaction. On the basis of the molecular interaction, structures and structure changes with temperature and pressure have been proposed for the various liquids studied.

INTRODUCTION

WITH the theory of dielectric polarization which involves very few restrictive conditions, it is possible to gain a large amount of information regarding the structure of polar liquids. The approximations involved in the derivation of the theory are, first, the neglect of dielectric saturation and, secondly, that the thermal energies are small compared to energies required for charge motion. These are well justified for the application to the structure of almost all pure liquids. Moreover, the experimental values of the dielectric constant ϵ of the index of refraction n of the molar volume V and of the vacuum dipole moment μ_0 are relatively easily obtained. These measurements can then be interpreted in terms of the structure of the substance and the changes of structure with temperature. Measurements of the dielectric constant under presure and a knowledge of the molar volume under these conditions allows observations to be made on how the structure of a liquid changes as it is compressed.

In the theory of dielectric polarization of a polar substance, the structure is determined from a quantity g, which indicates the extent of correlation of orientation between molecules. The dielectric constant and g are related by[1]

$$\frac{4\pi N}{V}\frac{\mu^2 g}{3kT}=\left(\frac{\epsilon-n^2}{n^2+2}\right)\left(\frac{2\epsilon+1}{\epsilon}\right), \tag{1}$$

where N is Avogadro's number, k is the Boltzmann constant, T is the absolute temperature, and μ is the dipole moment of a molecule in that substance. μ differs from μ_0 by the polarization induced through neighboring molecules. μ may be evaluated with reference to a particular model or, when conditions warrant it, by the use of the Onsager reaction field,[2]

$$\mu=\mu_0\left(\frac{n^2+2}{3}\right)\left(\frac{2\epsilon+1}{2\epsilon+n^2}\right). \tag{2}$$

In the theory $g\mu$ is defined as the average total moment of a macroscopic sample of the polar substance when an arbitrary molecule is fixed in position. Thus, g equal to unity in a liquid indicates no correlation between molecular orientations, while values of g greater than unity correspond to interactions which tend to orient the neighbors of a molecule so as to reinforce the total moment. On the other hand, values of g less than unity imply orientations such that the resultant moment is reduced. These two cases have been called co-association and anti- or contra-association, respectively.[3] More detailed knowledge of the structure can be obtained from the numerical values of g. Previous investigations along these lines have been discussed in reference 1.

EXPERIMENTAL

Materials

Baker C. P. carbon tetrachloride was shaken with redistilled mercury and fractionally distilled. The sample used had a boiling point of 76.8°C.

Union Carbide and Carbon n-butyl alcohol and Eastman Kodak *t*-butyl alcohol were treated with sodium metal and fractionally distilled. The samples of *n*-butyl alcohol and *t*-butyl alcohol used had boiling points of 116.5°C and 82.9°C, respectively.

Eastman Kodak *n*-butyl chloride and *n*-butyl bromide, and Mathieson Company *t*-butyl chloride were dried over sodium and fractionally distilled. The n-butyl chloride used had a boiling point of 77.9°C to 78.1°C, the *n*-butyl bromide had a boiling point of 101.0°C, and the *t*-butyl chloride had a boiling point of 51.3°C.

The water used was purified by distillation from potassium permanganate solution. Baker C. P. glycerol was used after distilling in a partial vacuum.

Apparatus

The low-frequency dielectric constants were measured at pressures between 1 and 200 atmos and over a temperature range of 14°C to 50°C, using the apparatus shown schematically in Fig. 1, in conjunction with a

* Predoctoral Fellow, National Science Foundation.
[1] F. E. Harris and B. J. Alder, J. Chem. Phys. **21**, 1031 (1953).
[2] L. Onsager, J. Am. Chem. Soc. **58**, 1486 (1936).
[3] J. Norton Wilson, Chem. Rev. **25**, 377 (1939).

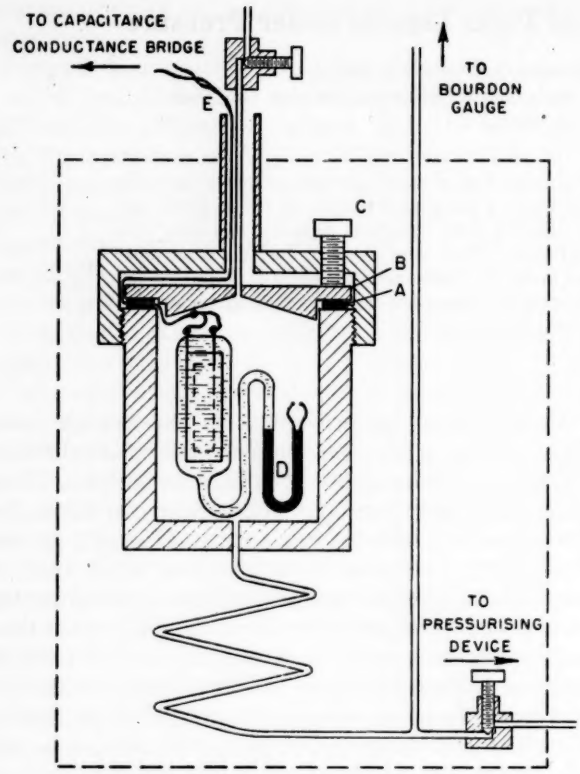

FIG. 1. Diagram of the apparatus.

wide range capacitance-conductance bridge[4] to be described elsewhere. A capacitance cell was supported in an iron pressure bomb of standard design which could be thermostated to ± 0.01°C. The cells employed were constructed of concentric cylinders of Monel metal, held rigidly in position by radial glass spacers. The outer cylinder extended beyond the ends of the inner cylinder so as to minimize fringing errors. A cell, 4.5 cm long and 2.2 cm in diameter, with a vacuum capacity of about 21 $\mu\mu$f was used for all the substances studied except water and glycerol. For these latter substances a smaller cell with a vacuum capacity of about 9 $\mu\mu$f was employed. Connections to the cells were made by sealing tungsten leads through a Pyrex container. This container was designed such that the experimental materials could be isolated from the compressing fluid in the bomb by means of the mercury plug (*D*). The pressure seal was made by compressing the Teflon gasket (A) between the coverplate (B) and the rim of the bomb by means of eight symmetrically placed steel bolts (C). Connections through the Teflon gasket to the tungsten leads were made with insulated No. 22 gauge copper wire, and a shielded cable (E) was used for connections between these copper leads and the bridge. Care was taken to keep the leads inside of the bomb as short as possible. Carbon tetrachloride was used as the compressing fluid. Experimental techniques of filling and pressurizing the bomb have been described elsewhere.[5] Pressures were applied from a cylinder of compressed air and measured on an air thermostated Heise Bourdon Laboratory Test Gauge calibrated so that it could be read to ± 1 psi.

All measurements of the low-frequency dielectric constants were taken at 20 kc and in each case it was verified that these were the static dielectric constants. The capacitance cell was calibrated, at a given temperature using a literature value[6] of the dielectric constant for each liquid studied. Dielectric relaxation measurements on glycerol were extended to 1.5 mc, the highest frequency for which sufficient accuracy could be obtained. It is estimated that the absolute accuracy of the capacitance measurements is 0.5 percent, but that relative accuracy of better than 0.05 percent was obtained over the experimental regions studied. Possible errors due to the change in dimensions of the cell with pressure have been calculated and found to be negligible.

Results

The experimental values of the low-frequency dielectric constants of carbon tetrachloride, *n*-butyl alcohol, *t*-butyl alcohol, *n*-butyl chloride, *n*-butyl bromide, *t*-butyl chloride, and water, measured at temperatures between 14°C and 50°C and at pressures between 1 and 200 atmos, are given in Tables I to VII. The low-frequency dielectric constant of glycerol, measured between -17.5°C and 14°C and between 1 and 200 atmos, and the relaxation time at 0°C as determined from measurements of both capacitance and conductance up to 1.5 mc and over the same pressure range, are given in Tables VIII and IX.

The molar volumes corresponding to the various temperatures and pressures studied are also given in the tables. These molar volumes have been calculated using data obtained in the following manner. Isothermal compressibilities at one atmosphere were calculated from velocity of sound measurements obtained by Schaaffs[7] and by Willard,[8] and heat capacity data from the *International Critical Tables* (ICT) and Timmermans.[9] Isothermal compressibilities at elevated pressures were computed using data in ICT and in some cases by reference to the original work of P. W. Bridgman. For cases where the compressibility data at elevated pressures were not available, values have been obtained by assuming a parallelism of compressibility in the ethyl alcohol-ethyl chloride-ethyl bromide and the butyl alcohol-butyl chloride-butyl bromide series. Density

[4] C. T. O'Konski and F. E. Harris, to be published. The authors are indebted to Professor C. T. O'Konski for the loan of this bridge.

[5] Haycock, Alder, and Hildebrand, J. Chem. Phys. **21**, 1601 (1953).

[6] A. A. Maryatt and E. R. Smith, *Table of Dielectric Constants of Pure Liquids* [National Bureau of Standards (U. S.), 1951].

[7] W. Schaaffs, Z. physik. Chem. **194**, 28 (1944).

[8] G. W. Willard, J. Acoust. Soc. Am. **19**, 235 (1947).

[9] J. Timmermans, *Physico-Chemical Constants of Pure Organic Compounds* (Elsevier Publishing Company, Inc., Houston, Texas, 1950).

data for all the substances studied, except water, were obtained from Timmermans.[9]

Values of $\mu^2 g$, given in Tables I to VIII, were calculated using Eq. (1). Optical refractive indices used for these calculations were obtained by extrapolating to low-frequencies data from Timmermans[9] and from Dorsey.[10] At higher pressures the indices of refraction were determined by the application of the Lorentz-Lorenz equation

$$\left(\frac{n^2-1}{n^2+2}\right)\frac{M}{\rho}=\text{const},$$

where M is the molecular weight and ρ the density. The above treatment omits atomic polarization, which is not directly determinable. This omission causes calculated values of $\mu^2 g$ to be somewhat too high, but should not affect the conclusions dependent upon the trends of $\mu^2 g$ with temperature or volume. The derivation and interpretation of other quantities given in Tables I to IX will be discussed in the next section. The values of the vacuum dipole moments used in calculating these derived quantities were obtained from the *Tables of Electric Dipole Moments* compiled by Wesson.[11]

DISCUSSION OF STATIC POLARIZATION

1. Carbon Tetrachloride

This nonpolar substance was used for calibration purposes. Application of the Clausius-Mossotti equation to the dielectric constants of carbon tetrachloride, measured at various temperatures and pressures (see Table I), leads to a molar polarization which is nearly constant. Possible deviations from the Clausius-Mossotti equation have been discussed by Kirkwood,[12] Brown,[13] and others.[14]

TABLE I. Carbon tetrachloride.

Temp. °C	Pressure atmos	Volume cc/mole	ϵ	P[a] cc/mole
25.0	1.0	97.08	2.230	28.23
	84.3	96.23	2.239	28.13
	156.1	95.58	2.248	28.08
40.0	1.0	98.92	2.207	28.38
	104.4	97.70	2.225	28.32
	203.7	96.74	2.239	28.28

[a] $P=V(\epsilon-1)/(\epsilon+2)$.

2. *n*-Butyl Alcohol

A chain model for the alcohols, first introduced by Oster and Kirkwood,[15] may be used for calculating both the average moment of the *n*-butyl alcohol molecule and the correlation parameter g. This model provides that each alcohol molecule is bonded to two neighbors through rigid hydrogen bonds, and that free rotation is permitted about these bonds. The chains formed will be of infinite length, and it is assumed that there are no interactions between molecules of different chains. If the dipole moment is calculated considering the effect of the nearest neighbors only, it is evident that the same value will be obtained regardless of the temperature and pressure. This moment differs from the one calculated by the Onsager equation. Furthermore, the latter moment increases with increasing density. In addition, the chain model predicts that g would be equal to 2.57 and would be independent of temperature since all configurations considered are weighted equally. A change of volume could be interpreted solely as a change in the separation between neighboring chains, and this would necessitate values of g being independent of pressure.

The experimental values of g are essentially in accord with the above discussion. At constant temperature, g remains very nearly constant as a function of volume. The slight decrease in g at lower volumes may be attributed either to breaking down of the relatively ordered structure at elevated pressures, or to an incidence of a restricted rotation which causes the moments of the molecules to slightly oriented in opposite directions. The same effect is observed in the case of water, where a similarly ordered structure exists. The failure to predict the decrease in g as the temperature increases is due to an inadequacy of the Oster-Kirkwood model. An improvement on the model might be the assumption of bendable hydrogen bonds, as in Pople's[16] model for water. Allowance for bending alters the Oster-Kirkwood formula to

$$g=1+2\left[\frac{(\mu_{OH}+\mu_{OR})(\mu_{OH}+\mu_{OR}\cos\beta)}{\mu_{OH}^2+\mu_{OR}^2+2\mu_{OH}\mu_{OR}\cos\beta}\right]\times\sum_{n=1}^{\infty}\cos^{2n}\frac{\beta}{2}\left[\coth\frac{q}{kT}-\frac{kT}{q}\right]^{2n},\quad(3)$$

where q is the hydrogen bond bending force constant, β is the R-O-H angle, and μ_{OR} and μ_{OH} the components of the dipole moment along the R-O and O-H directions. However, application of Eq. (3) does not permit an adequate fit to the experimental data. The inadequacy of Eq. (3) may be due to the fact that interference with neighboring chains and steric interference within the same chain causes restriction of the free motions assumed. This hindrance of motion leads to a smaller temperature coefficient of g and makes the assumption of unbendable hydrogen bonds more valid in this case than in that of water. Thus the simple model of Oster and Kirkwood is a reasonably accurate representation of

[9] N. E. Dorsey, *Properties of Ordinary Water Substance* (Reinhold Publishing Corporation, New York 1940).
[10] L. G. Wesson, *Tables of Electric Dipole Moments* (Massachusetts Institute of Technology, Cambridge, Massachusetts, 1947).
[11] J. G. Kirkwood, J. Chem. Phys. **4**, 592 (1936).
[12] W. F. Brown, J. Chem. Phys. **18**, 1193 (1950).
[13] J. Yvon, Compt. rend. **202**, 35 (1936).
[14] G. Oster and J. G. Kirkwood, J. Chem. Phys. **11**, 175 (1943).
[15] J. A. Pople, Proc. Roy. Soc. (London) **A205**, 163 (1951).

TABLE II. *n*-butyl alcohol.

Temp. °C	Pressure atmos	Volume cc/mole	n^2	ϵ	$\mu^2 g$	g
14.2	1.0	91.06	1.9569	18.50	12.297	2.69
	77.2	90.47	1.9655	18.64	12.285	2.68
	140.1	90.00	1.9724	18.76	12.281	2.68
	201.7	89.59	1.9786	18.88	12.287	2.68
27.0	1.0	92.17	1.9418	16.84	11.786	2.57
	67.0	91.60	1.9499	16.96	11.775	2.57
	128.2	91.09	1.9571	17.04	11.773	2.57
	179.2	90.70	1.9628	17.14	11.746	2.56
40.0	1.0	93.33	1.9263	15.36	11.300	2.47
	76.9	92.60	1.9362	15.49	11.282	2.46
	141.8	92.01	1.9445	15.64	11.299	2.47
	206.4	91.45	1.9511	15.73	11.279	2.46

the system, and we have therefore used the moment of 2.14 D, calculated from this model, to obtain values of g given in Table II.

3. *t*-Butyl Alcohol

The Oster-Kirkwood chain model does not adequately describe the dielectric polarization of *t*-butyl alcohol, the values of $g\mu^2$ being considerably smaller than those for the straight chain alcohol. Smaller values of g can be accounted for by assuming the chains to be of finite length. It is assumed that the chain lengths are sufficiently long to permit the use of the infinite chain model to calculate μ. However, it will be seen below that the actual chain lengths are quite short, and that therefore calculations of μ on the infinite chain model are not entirely justified, although it is a satisfactory approximation for chains of at least three molecules.

A calculation of the variation of g with chain length may be made from a rigid hydrogen bond model by extending the summation in $g=1+\sum_i w_i\langle\cos\gamma\rangle_i$ over the molecules in the finite chain. It is assumed on the basis of large steric hindrance that the effects of O-H-O bending are small. To carry out the summation, the average number of neighbors of various orders is calculated for a given chain length, and for each kind of neighbor $\langle\cos\gamma\rangle_i$ is summed with the appropriate weight w_i. Although the resultant function g is thus defined only over integral chain lengths, interpolation can be made to fractional values. Using the same value of μ as for the normal butyl alcohol, 2.14 D, the values of g obtained for *t*-butyl alcohol and the corresponding chain lengths are listed in Table III.

The chain length is seen to increase markedly with pressure, especially at the lower temperatures as the melting point of 25.5°C is approached. The short chain lengths in this alcohol must be due to the steric effects of the bulky *t*-butyl groups preventing the building up of long chains. At smaller volumes, the steric effect is seen to be somewhat overcome by an increased tendency toward association, leading to longer chains and increased values of g. This is opposite to the behavior observed for the straight chain alcohol, which already consists of large chains and suffers reduced correlation under pressure. At the higher temperatures, the chain lengthening due to decreased volume becomes less extensive. The actual values of the chain length are only approximately determined, since such effects as bending of the hydrogen bonds have been neglected. Inclusion of these effects will tend to alter all chain lengths in the same manner, and therefore qualitative conclusions dependent on changes in length should be unaffected.

TABLE III. *t*-butyl alcohol.

Temp. °C	Pressure atmos	Volume cc/mole	n^2	ϵ	$\mu^2 g$[a]	g	l[b]
27.8	1.0	95.06	1.9112	12.02	8.43	1.88	3.55
	109.3	93.82	1.9276	12.57	8.71	1.94	3.94
	149.7	93.40	1.9333	12.78	8.82	1.96	4.06
30.0	1.0	95.34	1.9076	11.54	8.14	1.82	3.22
	59.5	94.63	1.9166	11.85	8.30	1.85	3.38
	66.0	94.55	1.9176	11.90	8.33	1.86	3.44
	68.9	94.51	1.9181	11.91	8.34	1.86	3.44
	94.6	94.23	1.9216	12.03	8.39	1.87	3.49
	137.8	93.76	1.9277	12.27	8.53	1.90	3.68
	185.4	93.27	1.9340	12.50	8.65	1.93	3.87
42.1	1.0	96.91	1.8880	9.552	6.93	1.55	2.18
	64.1	96.03	1.8991	9.879	7.13	1.59	2.30
	64.8	96.02	1.8992	9.879	7.13	1.59	2.30
	128.6	95.20	1.9096	10.184	7.30	1.63	2.44
	184.5	94.53	1.9184	10.425	7.42	1.66	2.52
50.5	1.0	97.98	1.8755	8.490	6.27	1.40	1.77
	69.1	96.94	1.8881	8.795	6.45	1.43	1.85
	140.7	95.94	1.9006	9.097	6.62	1.47	1.95
	200.7	95.17	1.9104	9.328	6.74	1.50	2.04

[a] $\mu_{OH}=1.73$ D, $\mu_{OR}=.88$ D, $\mu_0=1.75$ D, $\mu=2.14$ D.
[b] l = Average number of molecules per chain.

TABLE IV. *n*-butyl chloride.

Temp. °C	Pressure atmos	Volume cc/mole	n^2	ϵ	$\mu^2 g$	g
13.6	1.0	103.62	1.9677	7.572	4.896	0.707
15.2	1.0	103.82	1.9652	7.532	4.905	0.709
	78.4	102.95	1.9764	7.557	4.861	0.699
	142.7	102.27	1.9855	7.665	4.900	0.702
	202.7	101.67	1.9935	7.731	4.908	0.700
28.55	1.0	105.54	1.9442	7.147	4.919	0.720
	75.6	104.59	1.9561	7.221	4.915	0.716
	139.1	103.83	1.9657	7.270	4.902	0.711
	222.1	102.89	1.9779	7.334	4.888	0.706
42.45	1.0	107.36	1.9231	6.770	4.920	0.731
	76.5	106.25	1.9363	6.849	4.915	0.726
	144.9	105.31	1.9478	6.909	4.904	0.720
	227.5	104.24	1.9612	6.988	4.898	0.715

4. *n*-Butyl Halides

The Onsager field was used to calculate dipole moments of both *n*-butyl chloride and *n*-butyl bromide. Values of g for these substances were then calculated and are tabulated in Tables IV and V. The values of g considerably below unity indicate anti-association, the effects being more marked in the case of the bromide. However, the small change in g with pressure and temperature implies no large specific interactions which are strongly dependent upon the separation of the molecules.

An explanation of the observed phenomenon is possible in terms of the van der Waals interactions between the highly polarizable halide groups in conjunction with steric considerations. Because of the relatively large van der Waals interaction, there is a higher than random probability that the halide groups of neighboring molecules will be close together. Otherwise, all relative orientations of pairs of neighboring molecules are permissible except that there is no chance of finding configurations where both molecules occupy the same space. This model would result in a net anti-association, the magnitude of which would depend upon the size of the excluded region. If a halide molecule had four neighbors orientated such that the halides groups point toward each other, values of g can be accounted for if the excluded region between a pair of molecules considered as line dipoles were about 30°. Since the repulsive potential defining the forbidden configurations rises steeply when the molecules start to overlap, the change in available space with energy will not be large, and hence, the change in g with temperature will be small. The observed temperature dependence of g can

TABLE V. *n*-butyl bromide.

Temp. °C	Pressure atmos	Volume cc/mole	n^2	ϵ	$\mu^2 g$	g
14.1	1.0	106.72	2.0713	7.227	4.545	0.609
	69.7	105.99	2.0820	7.272	4.532	0.604
	135.7	105.34	2.0915	7.317	4.522	0.601
	203.7	104.71	2.1009	7.357	4.511	0.597
27.4	1.0	108.30	2.0491	6.875	4.552	0.618
27.1	72.4	107.44	2.0611	6.940	4.549	0.614
27.1	138.4	106.71	2.0715	6.985	4.537	0.610
27.2	204.4	106.02	2.0815	7.030	4.527	0.606

be qualitatively accounted for by the change in van der Waals interaction which alters the probability of the halide-halide groups coming together. Also, a small compression would only cause a slight decrease in g, as there are no orienting forces which would be greatly intensified by shorter intermolecular distances; however, pressure has the effect of somewhat increasing the halide-halide attraction.

The van der Waals attraction between bromide groups is larger than that between the chlorides, and therefore the decrease of g below unity should be more marked for the bromide, in accord with experiment. Such orientations due to halide-halide interactions has been previously postulated by Hildebrand.[17] It might also be remarked that such a picture as the one described above is consistent with the use of the Onsager reaction field for calculating the dipole moment.

5. *t*-Butyl Chloride

The Onsager reaction field was used to calculate the dipole moment of *t*-butyl chloride, since the values of g near unity preclude any model with a large degree of orientational structure. Values of g thus calculated and shown in Table VI are, in fact, sufficiently close to unity that the difference may be attributed to the neglect of atomic polarization in n or a small error in μ_0. Values of g slightly above unity are to be expected from the dipole forces and can be calculated by methods previously developed.[18] The results indicate that *t*-butyl chloride may be regarded as a point dipolar, spherical molecule with very weak directional interaction. The very small decrease in g with increasing pressure suggests that any such directional interaction would be of an anti-associative nature. It should be noted that some anti-association does occur, but to a far less extent than in the straight chain halides. Further evidence of weak interaction as compared to the normal halides is indicated by the lower boiling point of the tertiary compound and is to be expected because of the greater shielding of the chloride by the methyl groups in the tertiary halide.

TABLE VI. *t*-butyl chloride.

Temp. °C	Pressure atmos	Volume cc/mole	n^2	ϵ	$\mu^2 g$	g
14.1	1.0	109.12	1.9203	10.147	7.55	1.039
	75.8	108.01	1.9332	10.308	7.59	1.040
	145.6	107.10	1.9441	10.443	7.61	1.038
	204.1	106.41	1.9512	10.531	7.61	1.034
25.0	1.0	110.84	1.9017	9.574	7.48	1.046
	78.2	109.54	1.9163	9.710	7.48	1.039
	142.5	108.59	1.9272	9.832	7.50	1.035
	202.6	107.77	1.9369	10.007	7.58	1.040
37.55	1.0	112.87	1.8808	8.943	7.38	1.048
	69.4	111.52	1.8956	9.097	7.40	1.043
	144.6	110.16	1.9106	9.219	7.38	1.032
	216.3	109.01	1.9215	9.380	7.43	1.032
50.1	73.3	113.30	1.8774	8.524	7.27	1.038
	140.1	111.82	1.8920	8.700	7.32	1.036
	199.3	110.60	1.9054	8.782	7.28	1.025

6. Water

The dipole moment calculated using the bendable hydrogen bonded model[16] for liquid water was employed in the evaluation of g. The effect of pressure on the water would be expected to be a breaking down of the relatively highly coordinated tetrahedral structure, resulting in a less rigidly bonded configuration. The effect of the structure change with pressure on the dipole moment of water was not calculated, but is expected to be small.

TABLE VII. Water.

Temp. °C	Pressure atmos	Volume cc/mole	n^2	ϵ	$\mu^2 g$	g
25.6	1.0	18.072	1.7686	78.34	12.084	2.634
	77.2	18.008	1.7721	78.66	12.077	2.632
	127.2	17.968	1.7744	78.78	12.068	2.630

[17] J. H. Hildebrand, Trans. Faraday Soc. **33**, 145 (1937).

[18] F. E. Harris and B. J. Alder, J. Chem. Phys. **21**, 1351 (1953)

TABLE VIII. Static polarization of glycerol.

Temp. °C	Pressure atmos	Volume cc/mole	n^2	ϵ	$\mu^2 g$
−17.5	108.8	71.519	2.1989	52.99	24.486
	181.3	71.413	2.2013	53.10	24.490
0.0	1.0	72.299	2.1808	48.20	24.047
	66.3	72.196	2.1832	48.44	24.121
	198.3	71.992	2.1878	48.67	24.131
14.1	1.0	72.802	2.1695	45.11	23.834
	100.3	72.640	2.1731	45.28	23.855
	172.4	72.525	2.1757	45.42	23.874

Values of g calculated from the moment corresponding to the above model are listed in Table VII. These values are consistent with a small degree of transformation toward a less rigid structure as the water is compressed.

7. Glycerol

Values of $\mu^2 g$ for glycerol are shown in Table VIII. The dipole moment to be used in order to obtain values of g depends on the model to be adopted for glycerol. The use of the Onsager field is not justified for such a highly associated substance. Any approximate value of the dipole moment results in values of g of the order of 1.8. This indicates a degree of co-association somewhat less than that of water and the straight chain alcohols, but in view of the low compressibility and high viscosity of glycerol the total amount of association must be large. The above considerations imply a small pressure coefficient of $\mu^2 g$. The trend in $\mu^2 g$ with pressure is such as to indicate small increased co-association as the substance is compressed and slightly decreased co-association as the temperature is raised.

Dielectric Relaxation of Glycerol

The Debye theory of dielectric relaxation states that

$$\epsilon' = \epsilon_\infty + \frac{\epsilon_0 - \epsilon_\infty}{1+(\omega\tau)^2}, \tag{4}$$

$$\epsilon'' = \frac{(\epsilon_0 - \epsilon_\infty)\omega\tau}{1+(\omega\tau)^2}, \tag{5}$$

where ϵ_0 and ϵ_∞ are the static and high-frequency limiting values of the dielectric constant, respectively. ω is the angular frequency, and τ is the relaxation time. ϵ' and ϵ'', the so-called real and imaginary parts of the dielectric constant, are related to the experimental quantities by

$$\epsilon' = C/C_0, \quad \epsilon'' = G/\omega C_0, \tag{6}$$

where C and C_0 are the capacitance with and without the sample, respectively, and G is the conductance. Values of G must be corrected for the dc conductance.

Previous studies by Davidson and Cole[19] at atmospheric pressure show that the simple behavior implied by the Debye theory is not followed by glycerol, but that the data may be explained by assuming a distribution of Debye relaxation times. Measurements in this research have only been extended to 1.5 mc, which at the temperatures studied is too low a frequency to accurately determine the character of the relaxation. However, fair agreement with Cole's[19] and Litovitz and Sette's[20] data was obtained, and the trend in relaxation times with pressure was observed as shown in Table IX. Individual values of ϵ' and ϵ'' were substituted into Eqs. (4) and (5) to determine a "Debye relaxation time" for each experimental point. This procedure is necessary because the data do not extend over a sufficient range of frequency. The apparent dependence of relaxation time on frequency is due to the non-ideal nature of the relaxation and will cause the times listed to differ from those obtained over a wider frequency range.

TABLE IX. Dielectric relaxation of glycerol.

Temp. °C	Pressure atmos	Freq. mc	ϵ'	ϵ''	τ
0	1.0	0.5	48.20	0.99	7.07×10^{-9}
	66.3	0.5	48.15	1.02	7.50
	198.3	0.5	48.15	1.07	7.74
0	1.0	1.0	48.10	2.14	7.76
	66.3	1.0	48.06	2.27	8.18
	198.3	1.0	48.06	2.42	8.82
0	1.0	1.5	47.86	3.59	8.73
	66.3	1.5	47.82	3.84	9.34
	198.3	1.5	47.77	4.03	9.79

The behavior of the relaxation time as the pressure is increased can, however, be gauged from the results. They show that an increase of pressure causes an increase in the relaxation time which may be attributed to stronger association at the lower volumes. Similar behavior was observed by Danforth.[21] These observations are consistent with the remarks made in the discussion of the static polarization.

The authors wish to thank Professor J. H. Hildebrand for his continued interest and valuable discussions. This work was supported in part by the U. S. Atomic Energy Commission.

[19] D. W. Davidson and R. H. Cole, J. Chem. Phys. **19**, 1484 (1951).
[20] T. A. Litovitz and D. Sette, J. Chem. Phys. **21**, 17 (1953).
[21] W. E. Danforth, Jr., Phys. Rev. **38**, 1224 (1931).

The Vibrational Spectrum of Chlorotrifluoroethylene*

D. E. MANN, N. ACQUISTA, AND EARLE K. PLYLER
National Bureau of Standards, Washington 25, D. C.

(Received March 23, 1953)

The infrared spectrum of gaseous $F_2C:CFCl$ has been reinvestigated in greater detail and over a more extensive region than in earlier work. Three hitherto unobserved bands have been found at 369, 338, and 194 cm^{-1}. These data, together with the previously available Raman spectrum, have made possible the achievement of a new and more satisfactory fundamental assignment: 1792 (ν CC), 1336 (ν CF), 1215 (ν CF), 1058 (ν CF), 689 (ν CCl), 517 (δ CF_2), 463 (ρ CF_2), 338 (δ CFCl), 194 (ρ CFCl) for the planar vibrations; and 538 (β CF_2), 369 (β CFCl), 158 (τ) for the out-of-plane modes. The ideal-gas entropy value based on the present assignment agrees with that obtained calorimetrically.

INTRODUCTION

THE infrared and Raman spectra of chlorotrifluoroethylene,[1] $F_2C:CFCl$, have been observed and interpreted by Smith *et al.*[2] More recently the ideal-gas entropy of CTFE at its boiling point, 244.80°K, has been determined[3,4] and is 73.28±0.1 eu. The corresponding entropy value calculated on the basis of the assignment made by Smith *et al.* is about 1.1 eu smaller than that obtained calorimetrically. This discrepancy suggests that their assignment is in part incorrect. The present work was undertaken with the hope that a more nearly correct interpretation of the spectra could be achieved.

This paper is the first of a series on the vibrational spectra of the halogenated ethylenes. In subsequent papers our investigations of the spectra of $F_2C:CF_2$, $F_2C:CFH$, $F_2C:CFBr$, $FClC:CCl_2$, and $Cl_2C:CCl_2$ will be reported and discussed in the light of the new results presented here for CTFE.

EXPERIMENTAL

Two samples of CTFE were made available to us by Dr. R. C. Downing of the "Kinetic" Chemicals Division of E. I. du Pont de Nemours and Company. One of these had been specially purified and was used in the spectroscopic work. The purity of the gas was probably 99.9 mole percent.[4]

The infrared absorption spectrum of gaseous CTFE was measured from 2.5 to about 54μ. To ensure good resolution over the entire range prisms of LiF, CaF_2, NaCl, KBr, CsBr, and CsI were employed. A Perkin-Elmer 12C spectrometer was used with all but the NaCl and KBr prisms. The former was used with a Perkin-Elmer 21, the latter with a Baird Associates instrument. The general method of measurement has been described previously.[5] In addition the regions 1925–2000 cm^{-1} and around 2160 cm^{-1} were examined with a grating instrument similar to one already described.[6] The results of these measurements are given in Figs. 1–3 and in Table I. The Raman spectrum of CTFE was not redetermined. The lines found by Smith *et al.*[2] are given in Table II.

RESULTS

The infrared spectrum of CTFE reported here agrees well with that obtained by Smith *et al.*[2] Toward higher frequencies the measured wave numbers differ somewhat from those given in the earlier work, but the discrepancies are not serious.

A survey of the region between 400 and 185 cm^{-1} revealed three hitherto unobserved bands at 369, 338, and 194 cm^{-1}. The band at 338 cm^{-1} corresponds to the Raman line found at 340 cm^{-1}. No Raman lines related to the 369 and 194 cm^{-1} bands were reported by Smith *et al.*[2] Apart from these three new bands, the prism spectra revealed very little not already apparent in the earlier traces.

The exploration of the regions 1925–2000 and around 2160 cm^{-1} with a grating instrument has disclosed type *C* combination bands at 2164, *ca* 1977, 1962, 1952, and probably several in the vicinity of 1936 cm^{-1}. A type $A-B$ band at 1982 cm^{-1} is clearly revealed. On subtraction of the absorption by the background and the *R* wing of the 1982 cm^{-1} band from the observed trace a band at about 1989 cm^{-1} is disclosed. Its contour suggests that it is of type *C*. The significance of these observations is discussed in the following sections.

INTERPRETATION

Assignment of Fundamentals

No electron diffraction, x-ray, or microwave data are available for CTFE. The structural parameters required for the calculation of its moments of inertia were guessed

* This work has been supported in part by the U. S. Office of Naval Research under contract NAonr 112–51.

[1] Chlorotrifluoroethylene will be abbreviated hereafter to CTFE.

[2] Smith, Nielsen, Berryman, Claassen, and Hudson, NRL Report 3567, "Spectroscopic Properties of Fluorocarbons and Fluorinated Hydrocarbons," Washington, D. C., September 15, 1949, p. 57.

[3] Oliver, Grisard, and Cunningham, J. Am. Chem. Soc. **73**, 5719 (1951).

[4] Furukawa, McCoskey, and Reilly, J. Am. Chem. Soc. **75**, 4339 (1953).

[5] Plyler, Stair, and Humphreys, J. Research Natl. Bur. Standards **38**, 211 (1947).

[6] E. K. Plyler and N. Gailar, J. Research Natl. Bur. Standards **47**, 248 (1951). The present instrument has a 7500 lines/inch grating, ruled at Johns Hopkins, and a cooled lead telluride cell as the detecting element. In the 3–4μ region the resolution achieved is equivalent to about 0.2 cm^{-1}.

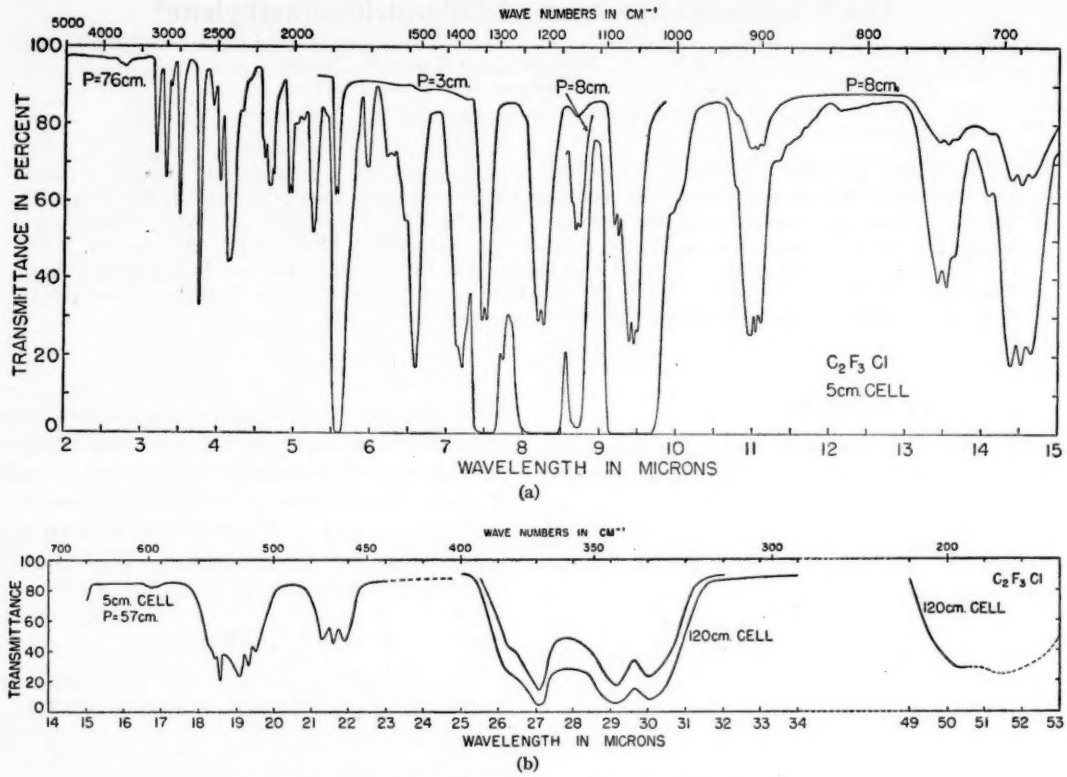

FIG. 1. Infrared absorption spectrum of chlorotrifluoroethylene.

with the aid of the recently evaluated constants for $F_2C:CF_2$,[7] $F_2C:CH_2$,[7] and $Cl_2C:CCl_2$,[8] and the older results for other chloroethylenes.[9] The CC, CF, and CCl distances are assumed to be 1.31, 1.32, and 1.68A, respectively. The molecule is of course supposed to be planar with symmetry C_s, while the FCC and ClCC angles are taken to be 124° and 122°, respectively. The three moments of inertia are then 186.6, 363.7, and 550.3×10^{-40} g cm^2.

The 12 fundamental vibrations of CTFE fall into two distinct groups: nine planar modes in species a' of C_s, and three out-of-plane motions in a''. The latter give rise to type C infrared bands and depolarized Raman lines, while the former result in hybrid $A-B$ bands and polarized Raman lines. For most of the a' fundamentals it may be supposed that the type A character will predominate. From Badger and Zumwalt's curves[10] the contours for the type C and mixed $A-B$ bands can be roughly estimated. The former are characterized by prominent Q branches and rather washed out P and R wings. The hybrid bands may partake of the usual A and B contours. It is to be expected, therefore, that the stronger type C bands can be easily distinguished from those of type $A-B$. Indeed, inspection of the spectrum displayed in Fig. 1 indicates that of the more intense bands only those at 538 and 369 cm^{-1} have the appearance anticipated for type C while that at 194 cm^{-1} has too indistinct a contour to permit definite classification.

The assignment of the very strong bands at 1792, 1336, 1215, and 1058 cm^{-1} to the CC and the three CF stretching fundamentals respectively is quite straightforward. The band at 1080 cm^{-1} is readily explained as the overtone of the fundamental at 538 cm^{-1}. Similarly, the CCl stretching is associated with the strong infrared band at 689 cm^{-1} and the very strong Raman at 690 cm^{-1}, while the much weaker Raman line at 748 cm^{-1} and the somewhat less intense infrared band

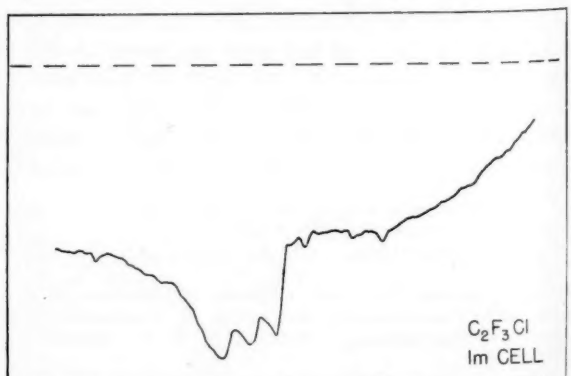

FIG. 2. Grating spectrum of the 2164 cm^{-1} band of chlorotrifluoroethylene. The dotted line indicates background level.

[7] I. L. Karle and J. Karle, J. Chem. Phys. **18**, 963 (1950).
[8] I. L. Karle and J. Karle, J. Chem. Phys. **20**, 63 (1952).
[9] P. W. Allen and L. E. Sutton, Acta Cryst. **3**, 46 (1950).
[10] R. M. Badger and L. R. Zumwalt, J. Chem. Phys. **6**, 711 (1938).

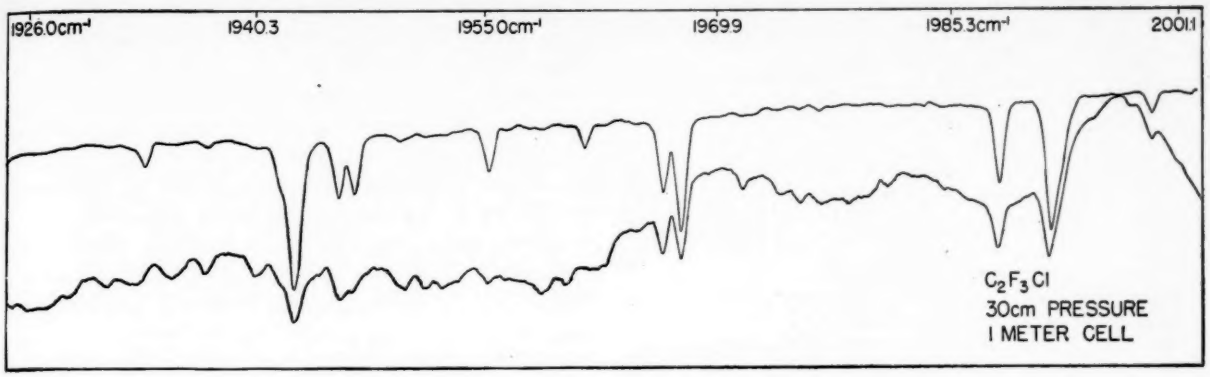

FIG. 3. Grating spectrum of chlorotrifluoroethylene in 1925–2000 cm^{-1} region. Peaks in background curve are due to water absorption.

TABLE I. Infrared spectrum of $F_2C:CFCl$(gas).

Wave number (cm^{-1})	Intensity	Interpretation
194	m	$\nu_9(a'; \rho$ CFCl)[a]
333	m	P
338	m	Q $\nu_8(a'; \delta$ CFCl)
342	m	R
369	m	$\nu_{11}(a''; \beta$ CFCl)
457	s	P
463	s	Q $\nu_7(a'; \rho$ CF_2)
469	s	R
512	s	P
517	s	Q $\nu_6(a'; \delta$ CF_2)
524	s	R
538	s	Q $\nu_{10}(a''; \beta$ CF_2)
543	s	R
593	vvw	P
598	vvw	Q $1058(a')-463(a')=595(A')$.
602	vvw	R
682	s	P
689	s	Q $\nu_5(a'; \nu$ CCl)
695	s	R
709	vw	$338(a')+369(a'')=707(A'')$; $194(a')+517(a')=711(A')$.
734	w	P
739	m	Q $2\times369(a'')=738(A')$.
745	m	R
805–825[b]	vvw	$369(a'')+463(a')=832(A'')$; $338(a')+463(a')=801(A')$.
847–881[b]	vvw	$194(a')+689(a')=883(A')$; $338(a')+517(a')=855(A')$. $338(a')+538(a'')=876(A'')$; $369(a'')+517(a')=886(A'')$; $158(a'')+689(a')=847(A'')$.
899	m	P
905	m	Q $369(a'')+538(a'')=907(A')$.
912	m	R
ca 929	vvw	$2\times463(a')=926(A')$.
ca 994[b]	vvw	$194(a')+338(a')+463(a')=995(A')$; $1336(a')-338(a')=998(A')$.
ca 1008[b]	vvw	$463(a')+538(a'')=1001(A'')$.
1052	vs	P
1058	vs	Q $\nu_4(a'; \nu$ CF)
1065	vs	R
1080	vs	Q $2\times538(a'')=1076(A')$.
1086	vs	R
1116	vw	$3\times369(a'')=1107(A'')$.
1147	s	P
1153	s	Q $463(a')+689(a')=1152(A')$.
1157	s	R
1209	vs	P ν_3
1220	vs	R $(a'; \nu$ CF)
1280	vvw	$2\times538(a'')+194(a')=1270(A')$.
1290	vvw	$2\times369(a'')+538(a'')=1276(A'')$.
1330	vs	P ν_2
1339	vs	R $(a'; \nu$ CF)
ca 1374	m	$158(a'')+1215(a')=1373(A'')$.
1383	m	$2\times689(a')=1378(A')$.
1399	m	$194(a')+1215(a')=1409(A')$; $338(a')+1058(a')=1396(A')$.
ca 1466	vw	$2\times463(a')+538(a'')=1464(A'')$.
1517	m	$463(a')+1058(a')=1521(A')$.
1550	vw	$338(a')+1215(a')=1553(A')$.
ca 1570	vw	$517(a')+1058(a')=1575(A')$.
ca 1585	vw	$369(a'')+1215(a')=1584(A'')$.
1605	vw	$538(a'')+1058(a')=1596(A'')$.
1669	w	$338(a')+1336(a')=1674(A')$.
1677	w	$463(a')+1215(a')=1678(A')$.
1792	vs	$\nu_1(a'; \nu$ CC)
1845	vvw	$517(a')+1336(a')=1853(A')$.
1898	w	$689(a')+1215(a')=1904(A')$.
ca 1936[c,d,e]	vw	
ca 1952[d]	vw	$158(a'')+1792(a')=1950(A'')$.
1962[d]	vw	
1977[d]	vw	
1982[d]	vw	$194(a')+1792(a')=1986(A')$.
1989[d]	vw	
2012	w	$689(a')+1336(a')=2025(A')$.
(2025)[f]	w	
2077	vvw	$2\times369(a'')+1336(a')=2074(A')$.
2119	w	$2\times1058(a')=2116(A')$.
(2131)	w	$338(a')+1792(a')=2130(A')$.
(2137)	w	
2164[d]	w	$369(a'')+1792(a')=2161(A'')$.
2257	vvw	$463(a')+1792(a')=2255(A')$.
2304	vw	$517(a')+1792(a')=2309(A')$.
(2334)	vvw	$538(a'')+1792(a')=2330(A'')$.
2394	m	$1058(a')+1336(a')=2394(A')$.
2415	m	$2\times1215(a')=2430(A')$.
2481	w	$689(a')+1792(a')=2481(A')$.
2543	vw	$1215(a')+1336(a')=2551(A')$.
2650	m	$2\times1336(a')=2672(A')$.
(2713)	vvw	$2\times689(a')+1336(a')=2714(A')$.
2857	m	$1058(a')+1792(a')=2850(A')$.
(2946)	vvw	$463(a')+689(a')+1792(a')=2944(A')$.
2999	w	$1215(a')+1792(a')=3007(A')$.
3115	w	$1336(a')+1792(a')=3128(A')$.
(3172)	vvw	$2\times689(a')+1792(a')=3170(A')$.
3311	vvw	$463(a')+1058(a')+1792(a')=3313(A')$.
(3340)	vvw	$338(a')+1215(a')+1792(a')=3345(A')$.
ca 3425	vvw	$2\times1058(a')+1336(a')=3452(A')$.
ca 3559	vvw	$2\times1792(a')=3584(A')$.
(*ca* 3620)	vvw	$3\times1215(a')=3645(A')$; $517(a')+1336(a')+1792(a')=3645(A')$.
ca 3676	vvw	$538(a'')+1336(a')+1792(a')=3666(A'')$.
ca 3922	vvw	$2\times1058(a')+1792(a')=3908(A')$.
ca 4115	vvw	$2\times1058(a')+689(a')+1336(a')=4141(A')$; $2\times1792(a')+538(a'')=4122(A'')$.
ca 4329	vvw	$1215(a')+1336(a')+1792(a')=4343(A')$.

[a] The notation used to designate the most characteristic aspects of the various normal modes is the following: for the in-plane motions ν refers to bond stretching, δ to the CF_2 or CFCl group deformation, ρ to rocking; for the out-of-plane vibrations β means wagging or bending, while τ implies a twisting or torsional motion. Of course, these conventional terms have only approximate meanings for CTFE. See, however, Y. Morino and K. Kuchitsu, J. Chem. Phys. **20**, 1809 (1952).

[b] A number of impurity bands found in earlier spectra of CTFE[2] are absent or much diminished in intensity in the present work. The chief impurity bands have been found at the following (approximate) frequencies: 639, 751, 803, 816, 840, 845, 856, 965, 972, 978, 997, 1742, 1755, and possibly 2311 cm^{-1}. The extremely weak and indistinct absorption around 805–825, 847–881, 994, and 1008 cm^{-1} may be due in whole or in part to impurities.

[c] The frequency 1936 cm^{-1} refers to the approximate center of the weak and complex absorption bands observed in this region in the grating traces.

[d] These frequencies are taken from the grating curves.

[e] See the text for a discussion of the possible assignments for the 1936, 1952, 1962, 1977, and 1989 cm^{-1} type C bands.

[f] Frequencies in parentheses refer to bands reported by Smith *et al.* (reference 2) but not found or resolved in our work.

TABLE II. Raman spectrum of F_2C:CFCl(liquid).[a]

Wave number (cm^{-1})	Intensity	Interpretation
340	m	$\nu_8(a'; \delta$ CFCl)
462.3	s	$\nu_7(a'; \rho$ CF_2)
537	vs, d	$\nu_{10}(a''; \beta$ CF_2)
690.4	vs, sh	$\nu_5(a'; \nu$ CCl)
748	w	$2\times\nu_{11}(a''; \beta$ CFCl)$=738(A')$
1054	vw	$\nu_4(a'; \nu$ CF)
1078	w	$2\times\nu_{10}(a''; \beta$ CF_2)$=1076(A')$
1225	vvw	$\nu_3(a'; \nu$ CF)
1323	vvw	$\nu_2(a'; \nu$ CF)
1380	vvw	$2\times\nu_5(a'; \nu$ CCl)$=1378(A')$
1794	s	$\nu_1(a'; \nu$ CC)
2099	vw	$2\times\nu_4(a'; \nu$ CF)$=2116(A')$

[a] The experimental data in this table are those reported by Smith *et al.* (reference 2).

at 739 cm^{-1} are interpreted as 2×369 cm^{-1}. All the stretching modes have now been accounted for, and the remaining fundamentals may be expected at lower frequencies.

The assignment of the angular vibrations is facilitated once it is admitted that the intensities and shapes of the 538 and 369 cm^{-1} bands require their interpretation as the two wagging fundamentals, β CF_2 and β CFCl,† respectively. Indeed, the presence of the overtones of the wagging frequencies with appreciable intensity in both the infrared and Raman spectra seems to be characteristic of a number of halogenated ethylenes, as has been remarked by Smith *et al.*,[2] and lends further support to the present assignment. Moreover, it is noteworthy that the binary sum band $369(a'')+538(a'')=907(A')$ occurs with considerable intensity in the infrared spectrum. High infrared intensity of the combination frequency $\beta_i+\beta_j$ also seems to be characteristic of a fair number of halogenated ethylenes.‡

The angular modes which remain unassigned are, with the exception of the torsion, the planar vibrations δ CF_2, δ CFCl, ρ CF_2, and ρ CFCl. These motions may without doubt be correlated in some order with the moderately intense bands at 517, 463, 338, and 194 cm^{-1}. Indeed, the first three clearly have type $A-B$ contours. Unfortunately, the shape of the 194 cm^{-1} band is too indistinct to be of aid in its classification. To be sure, its intensity alone would preclude its interpretation as τ since this mode is unlikely to give rise to a strong infrared band. Nevertheless, it was considered desirable to determine the type of the 194 cm^{-1} band more directly. From Fig. 3 it will be seen that the grating record of the region 1925–2000 cm^{-1} reveals a type $A-B$ contour centered at 1982 cm^{-1}. The interpretation of this combination as $194+1792=1986$ identifies the species of the low-frequency fundamental as a'. Since it seems to be generally true for halogenated ethylenes that the planar mode with the lowest frequency is one of the rockings the assignment of 194 cm^{-1} to ρ CFCl is indicated. Similar correlations suggest that the other rocking and the corresponding deformation mode are to be expected at much higher frequencies. On this basis the 517, 463, and 338 cm^{-1} bands may be assigned to the δ CF_2, ρ CF_2, and δ CFCl modes, respectively. Probably, final judgment on this point should be reserved until more extensive and reliable correlations become available. All that is needed now to complete the assignment is a value for the torsional frequency.

The Torsion Frequency

The torsion frequency can be evaluated approximately with the aid of the experimental entropy value for CTFE. At 244.80°K the translational and rotational contributions to S^0 amount to 66.017 eu.[14] The fundamentals at 1792, 1336, 1215, 1058, 689, 538, 517, 463, 369, 338, and 194 cm^{-1} add 5.058 eu. The difference Δ between the calorimetric value, 73.28 ± 0.1 eu,[3,4] and the sum of the translational, rotational, and vibrational contribution (for 11 frequencies) is therefore about 2.205 eu. This value of Δ leads to 158 cm^{-1} for the torsion frequency. It must be recognized, however, that the value of Δ on which this frequency is based is uncertain by at least ±0.1 eu and perhaps as much as ±0.2 eu if generous allowance is made for small inaccuracies in the structural and spectroscopic constants of the molecule. Admission of an uncertainty of ±0.2 eu in Δ places the torsion frequency between the limits 140–175 cm^{-1}. It is desirable to attempt to locate this value more definitely. Since binary combinations of the CC stretching with every other fundamental occur it is reasonable to expect that the sum band

$$[140-158-175](a'')+1792(a') = [1932-1950-1967](A'')$$

should also appear, albeit feebly.

In order to determine the appearance of a known type C combination band under high dispersion the 2164 cm^{-1} band was examined with the grating instrument. Reference to Fig. 1 will show that even the prism trace leaves no doubt as to the contour of this sum band. In Fig. 2 the grating record of the 2164 cm^{-1} band is displayed. Apart from the occurrence of three Q branches the envelope has the expected appearance, and it may be used as a guide to pick out the type C bands in the grating spectrum shown in Fig. 3.

The region 1925–2000 cm^{-1} displays, under high dispersion, three or four prominent and well defined

† For a description of this notation see Table I (footnote a).

‡ In the infrared spectrum of $F_2C:CF_2$ (reference 11) the binary combination $407(b_{1u})+510(b_{2g})=917(B_{3u})$ appears as a strong type A band at 913 cm^{-1}. For $Cl_2C:CCl_2$ (reference 12) the corresponding sum band $288(b_{1u})+512(b_{2g})=800(B_{3u})$ occurs as a strong band at 802 cm^{-1}. For F_2C:CClH the strong band at 1319 cm^{-1} is explained as $572(a'')+751(a'')=1323(A')$ (reference 13).

[11] Nielsen, Claassen, and Smith, J. Chem. Phys. **18**, 812 (1950).

[12] H. J. Bernstein, J. Chem. Phys. **18**, 478 (1950).

[13] Nielsen, Liang, and Smith, J. Chem. Phys. **20**, 1090 (1952).

[14] The fundamental constants used in this and subsequent thermodynamic calculations in this paper are taken from the recent compilation by Rossini, Gucker, Johnston, Pauling, and Vinal. [J. Am. Chem. Soc. **74**, 2699 (1952).]

groups of Q branches: one at about 1977, another around 1962, a third at 1952, and a less distinct set in the neighborhood of 1936 cm^{-1}. On several other records made of this region the bands at 1952 and 1962 cm^{-1} appear more clearly and prominently than is evident in Fig. 3, while that at 1977 cm^{-1} is revealed less well. At any rate it is clear that any one of these could be explained as the combination $[\tau+\nu-CC]$, so that the precise value of the torsion frequency remains elusive. But since they must all be assigned it is necessary to consider the binary, ternary, and even quaternary combinations which are at least numerically satisfactory as explanations for the observed type C bands in the 1925–2000 cm^{-1} region.

Binary sum:

$$158(a'')+1792(a')=1950(A'').$$

Ternary sums:

$$338(a')+369(a'')+1215(a')=1922(A'').$$
$$338(a')+538(a'')+1058(a')=1934(A'').$$
$$369(a'')+517(a')+1058(a')=1944(A'').$$
$$194(a')+538(a'')+1215(a')=1947(A'').$$
$$158(a'')+463(a')+1336(a')=1957(A'').$$

TABLE III. Fundamental vibration frequencies for $F_2C:CFCl$.

Species	Number	Designation	Assignment Smith *et al.*[b]	Assignment present work
a'	1	ν CC	1802 cm^{-1}	1792 cm^{-1}
	2	ν CF	1336	1336
	3	ν CF	1217	1215
	4	ν CF	1058	1058
	5	ν CCl	739	689
	6	δ CF_2	691	517
	7	ρ CF_2	463	463
	8	δ CFCl	517	338
	9	ρ CFCl	(215)[a]	194
a''	10	β CF_2	538	538
	11	β CFCl	340	369
	12	τ	(180?)	158

[a] Frequencies in parentheses were determined from combination bands as described in reference 2.
[b] See reference 2.

Ternary differences:

$$517(a')+1792(a')-369(a'')=1940(A'').$$
$$689(a')+1792(a')-538(a'')=1943(A'').$$
$$2\times1058(a')-158(a'')=1958(A'').$$
$$369(a'')+1792(a')-194(a')=1967(A'').$$
$$338(a')+1792(a')-158(a'')=1972(A'').$$
$$538(a'')+1792(a')-338(a')=1992(A'').$$

Quaternary sums:

$$194(a')+369(a'')+2\times689(a')=1941(A'').$$
$$338(a')+3\times538(a'')=1952(A'').$$
$$158(a'')+2\times369(a'')+1058(a')=1954(A'').$$
$$369(a'')+517(a')+2\times538(a'')=1962(A'').$$
$$2\times369(a'')+538(a'')+689(a')=1965(A'').$$
$$369(a'')+2\times463(a')+689(a')=1984(A'').$$

TABLE IV. Calculated thermodynamic functions for $F_2C:CFCl$ in dimensionless units.

$T°K$	$C_p°/R$	$(H°-E_0°)/RT$	$-(F°-E_0°)/RT$	$S°/R$
244.80	9.190	6.316	30.559	36.875
300	10.123	6.934	31.906	38.840
400	11.435	7.904	34.038	41.941
500	12.409	8.712	35.891	44.603
600	13.139	9.392	37.541	46.933
700	13.689	9.968	39.033	49.002
800	14.108	10.461	40.397	50.858
900	14.429	10.885	41.655	52.539
1000	14.679	11.252	42.821	54.073
1100	14.877	11.573	43.909	55.481
1200	15.035	11.855	44.928	56.783
1300	15.163	12.105	45.887	57.992
1400	15.268	12.327	46.792	59.119
1500	15.355	12.526	47.650	60.176

There are several things about this compilation that are worthy of note. It will be noticed that the combination values are more or less grouped about the observed frequencies. Secondly, the only combinations which on a numerical basis alone can be used to explain the observed band at 1977 and the overlapped band at about 1989 cm^{-1} are either ternary differences or quaternary sums. This suggests that perhaps a few of them have sufficient intensity to be revealed under high dispersion. Thirdly, consideration of the binary and ternary sums involved in the quaternary combinations shows that two are particularly favored: 1962 and 1965 cm^{-1}. In the former both the 907 and 1076 cm^{-1} binary sums are involved, while in the latter the relatively intense 738 and 907 cm^{-1} sums are present. On the other hand, there do not seem to be any equally plausible explanations for the 1952 cm^{-1} band apart from the sum $158(a'')+1792(a')=1950(A'')$. These considerations are offered, therefore, as possible though admittedly tenuous grounds for accepting 158 cm^{-1} as the torsion frequency. It would indeed be gratifying to observe this fundamental directly. The final assignment for CTFE is given in Table III, where the earlier one made by Smith *et al.*[2] is also shown.

Thermodynamic Functions

The fundamental assignment and molecular constants given in the preceding sections were used to compute the thermodynamic functions, to the rigid-rotator, harmonic-oscillator approximation, for CTFE regarded as an ideal gas. The condensed tabulation given in Table IV is taken from a more complete table calculated with the aid of the SEAC at the National Bureau of Standards and to be published elsewhere.

ACKNOWLEDGMENT

The authors are indebted to Dr. R. C. Downing of the "Kinetic" Chemicals Division of du Pont for providing us with a specially purified sample of CTFE.

Heat Capacity of Chain Polymeric Crystals*

W. H. STOCKMAYER AND C. E. HECHT†
Department of Chemistry, Massachusetts Institute of Technology, Cambridge, Massachusetts
(Received June 23, 1953)

A crude calculation of the frequency spectrum and heat capacity has been made for a simple model of a large crystal composed of long parallel polymer chains. The heat capacity is very unlike that of a cubic crystal but can be represented quite well with a simple two-parameter equation recently proposed by Tarasov.

1. INTRODUCTION

IN the past several years there has been a revival of interest in the heat capacities of anisotropic crystalline solids, particularly of elementary substances at rather low temperatures where they may deviate widely from the Debye equation. For example, new measurements on graphite[1] confirm and extend the older data[2] in indicating that the heat capacity is rather closely proportional to the square of the temperature over a considerable range; and similar behavior has been observed for other solids with layer lattices, including gallium,[3] boron nitride,[4] and black phosphorus.[5] Another class of solids with abnormal low-temperature heat capacities comprises those known or presumed to consist of polymeric chains, such as selenium,[6] tellurium,[6,7] several forms of red phosphorus,[5] and organic polymers like natural rubber.[8] In these solids there is a fairly long temperature range over which the heat capacity is close to a linear function of the temperature.

There is nothing fundamentally surprising in the fact that crystals containing polymeric units should have frequency distributions differing markedly from those of cubic crystals. The numerical computation of the frequency spectrum for any detailed model of such a crystal by the general method of Born and von Karman[9] is in principle straightforward, and with modern high-speed computing machines would in many cases be entirely feasible. However, a less complete but more generally useful aim would be the construction of an approximate theory, involving perhaps two or at most three parameters, which would serve as a norm for polymeric solids much as Debye's theory has served for cubic crystals. Such a limited theory would at least be of value in the empirical representation of heat-capacity measurements, and if given a sound physical basis, might also permit the derivation of approximate structural information from observed heat capacities.

Previous efforts toward the objective above indicated have followed several lines. Some investigators, impressed by the known small thickness of graphite crystals, have treated these as essentially two-dimensional elastic continua, thus arriving immediately at the desired T^2 law for the heat capacity at low temperatures. The best discussion of this type is probably that of the late Gurney.[10] This argument, however, invokes essentially a surface contribution to the thermodynamic properties that is not confined to special lattice types but is present whenever the crystals are sufficiently small.[11] Although this may be a major factor in the case of graphite and perhaps other substances, it is clearly necessary also to understand the behavior of crystals of macroscopic size containing sheet or chain polymeric structures.

Tarasov[12] attempted a discussion of polymeric crystals on the apparently naive supposition that they could be represented as two- or one-dimensional elastic continua, irrespective of crystal dimensions. While this simple treatment results in moderate empirical success at not too low temperatures, it is scarcely satisfying physically. Any macroscopic three-dimensional crystal must necessarily give rise to a lattice heat capacity varying as T^3 at sufficiently low temperature, though perhaps over a short range. In a valid theory the coupling forces between the polymeric sheets or chains must therefore be recognized explicitly. More recently, Tarasov[13] proposed a simple two-parameter heat-capacity equation which satisfies this dictum and gives[6,13] much improved agreement with experiment.

As a step toward an approximate theory, we carried

* This work was supported in part by the Office of Ordnance Research (Contract DA-19-020-ORD-1545). It is largely based on a thesis submitted by C. E. Hecht in partial fulfillment of the requirements for the degree of Bachelor of Science in Chemistry from the Massachusetts Institute of Technology, June, 1952.

† Present address: Department of Chemistry, University of Chicago, Chicago, Illinois.

[1] W. DeSorbo and W. W. Tyler, Phys. Rev. **83**, 878 (1951).
[2] W. Nernst, Ann. Physik **36**, 395 (1911).
[3] W. DeSorbo, J. Chem. Phys. **21**, 168 (1953).
[4] Dworkin, Sasmor, and Van Artsdalen, J. Chem. Phys. **21**, 954 (1953).
[5] Stephenson, Morrow, Maple, and Potter (unpublished measurements in this laboratory).
[6] W. DeSorbo, J. Chem. Phys. **21**, 764 (1953).
[7] C. M. Slansky and L. V. Coulter, J. Am. Chem. Soc. **61**, 564 (1939).
[8] N. Bekkedahl and H. Matheson, J. Research Natl. Bur. Standards **15**, 503 (1935); J. Rehner, Jr., J. Polymer Sci. **2**, 263 (1947).
[9] M. Born and T. von Karman, Physik. Z. **13**, 297 (1912); **14**, 15 (1913).
[10] R. W. Gurney, Phys. Rev. **88**, 465 (1952).
[11] For other discussions of surface contributions, see E. W. Montroll, J. Chem. Phys. **18**, 183 (1950); H. Koppe, J. Chem. Phys. **18**, 638 (1950); J. T. Law, J. Chem. Phys. **20**, 1329 (1952); G. Jura and K. S. Pitzer, J. Am. Chem. Soc. **74**, 6030 (1952).
[12] V. V. Tarasov, Compt. rend. U.R.S.S. **46**, 20, 110 (1945).
[13] V. V. Tarasov, Zhur. Fiz. Khim. **24**, 111 (1950); Doklady Akad. Nauk S.S.S.R. **84**, 321 (1952); see Chem. Abstr. **46**, 10841g (1952).

out the calculations described below, being at the time unaware of Tarasov's modified equation. Briefly, we have made a crude evaluation of the frequency spectrum of the simplest possible chain polymer crystal, following essentially the procedure used by Blackman[14] for simple cubic crystals. Since the vibrations of isolated chains are also easily determined, the effect of the coupling forces in the crystal can be directly seen. Although our results are numerical and restricted to a single plausible set of force constants, it was considered that they might aid in the search for some relatively simple function to represent the heat capacity. It turns out that the frequency distribution corresponding to Tarasov's two-parameter equation gives fairly good agreement with the results of our model calculation.

2. MODEL AND FREQUENCY SPECTRUM

The simple tetragonal lattice used here as a model for a crystal of long-chain molecules is indicated in Fig. 1. Atoms of mass m are assigned to lattice points identified by three integers n_1, n_2, n_3. Each integer has a range $-N_j/2 \leqslant n_j \leqslant N_j/2$, so that the crystal consists of N_1N_2 parallel chains of N_3 atoms each.

Force constants governing the interactions between first and second neighbors are assigned as follows. The constant for relative displacements of first neighbors along the x and y directions (perpendicular to the chains) is α, while that for the z direction (valence force) is β. The forces between second neighbors are assumed to act along the diagonals connecting them, the associated force constants being 2γ for diagonals lying in XZ or YZ planes and $2\gamma'$ for those in XY planes. Finally, the force constant for displacements of the valence angles from 180° is κ. All the forces are, of course, taken to be linear in the displacements.

The equations of motion are obtained in conventional fashion and need not be given here. The displacement $\mathbf{r}_{n_1n_2n_3}$ of a specified atom from its equilibrium position has the periodic solution

$$\mathbf{r}_{n_1n_2n_3}=\boldsymbol{\sigma}\exp i(2\pi\nu t+\sum_{j=1}^{3} n_j\phi_j); \tag{2.1}$$

$$\phi_j=2\pi a_j/N_j; \quad (j=1, 2, 3)$$

$$-N_j/2\leqslant a_j\leqslant N_j/2,$$

where a_j is integral and $\boldsymbol{\sigma}$ is an amplitude vector. When substituted into the equations of motion, this solution yields the following secular determinant:

$$\begin{vmatrix} A-E & D_{12}' & D_{13} \\ D_{12}' & B-E & D_{23} \\ D_{13} & D_{23} & C-E \end{vmatrix}=0, \tag{2.2}$$

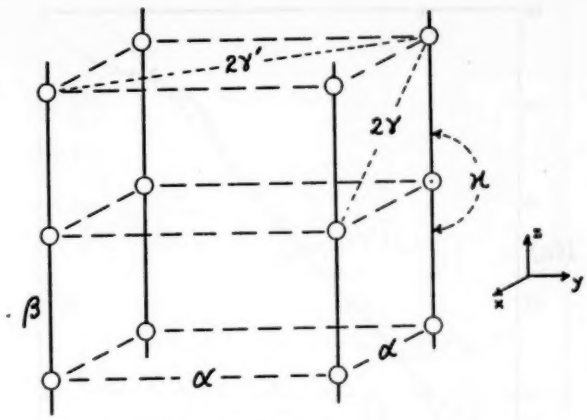

FIG. 1. Model of chain polymer crystal, indicating the various force constants.

where

$$\begin{aligned} A&=(\alpha/2)(1-\cos\phi_1)+\gamma'(1-\cos\phi_1\cos\phi_2)\\ &\quad+\gamma(1-\cos\phi_1\cos\phi_3)+\kappa(1-\cos\phi_3)^2;\\ B&=(\alpha/2)(1-\cos\phi_2)+\gamma'(1-\cos\phi_2\cos\phi_1)\\ &\quad+\gamma(1-\cos\phi_2\cos\phi_3)+\kappa(1-\cos\phi_3)^2;\\ C&=(\beta/2)(1-\cos\phi_3)+\gamma(1-\cos\phi_3\cos\phi_1)\\ &\quad+\gamma(1-\cos\phi_3\cos\phi_2); \end{aligned} \tag{2.3}$$

$$D_{ij}=\gamma\sin\phi_i\sin\phi_j; \quad D_{12}'=\gamma'\sin\phi_1\sin\phi_2;$$

$$E=\pi^2m\nu^2.$$

If we put $\alpha=\beta$, $\gamma=\gamma'$ and $\kappa=0$, we recover the equations for the simple cubic lattice.[14]

Since $\beta>\alpha$ when there are strong valence forces in the chains, the maximum frequency occurs at the point $\phi_1=\phi_2=0$, $\phi_3=\pi$, and is given by

$$\pi^2m\nu_m^2=\beta+4\gamma. \tag{2.4}$$

Since we are interested only in relative values of the frequencies, it is convenient to work with a dimensionless reduced frequency $\nu_r=\nu/\nu_m$. Accordingly, we divide each element of the determinant (2.2) by $\pi^2m\nu_m^2$, so that the reduced elements become

$$E_r=\nu_r^2 \tag{2.5}$$

$$\begin{aligned} A_r&=(\alpha_r/2)(1-\cos\phi_1)+\gamma_r'(1-\cos\phi_1\cos\phi_2)\\ &\quad+\gamma_r(1-\cos\phi_1\cos\phi_3)+\kappa_r(1-\cos\phi_3)^2, \text{ etc.,} \end{aligned}$$

with reduced force-constants

$$\alpha_r=\alpha/\pi^2m\nu_m^2; \quad \gamma_r=\gamma/\pi^2m\nu_m^2; \text{ etc.} \tag{2.6}$$

For the numerical computations, the following value of the reduced force-constants were chosen:

$$\begin{aligned} &\alpha_r=0.03968; \quad \beta_r=0.992\\ &\kappa_r=0.0992; \quad \gamma_r=\gamma_r'=0.002. \end{aligned} \tag{2.7}$$

These were dictated by the following considerations: the ratio $\beta/\alpha=25$ corresponds to a large but still reasonable ratio of valence to van der Waals forces between

[14] M. Blackman, Proc. Roy. Soc. (London) **A148**, 384 (1935); **A159**, 416 (1937).

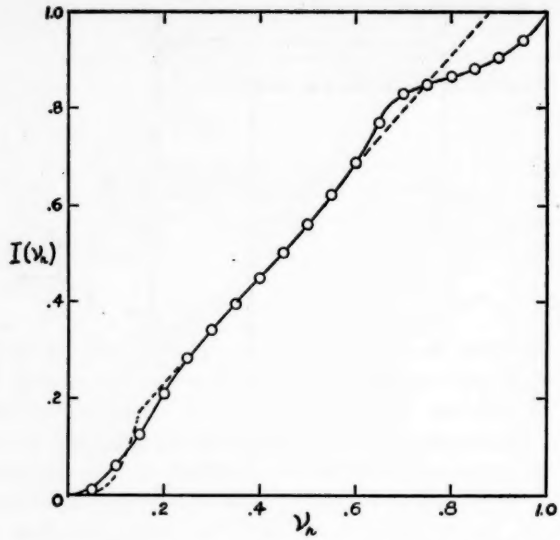

FIG. 2. Integral frequency distribution of a chain polymer crystal: circles and solid curve from calculations of Table I; dashed curve from Eq. (5.1) with $\nu_3=0.15\nu_m$ and $\nu_1=0.88\nu_m$.

nearest neighbors; the ratio $\kappa/\beta=0.1$ of bending to stretching constants is approximately that for paraffin chains; and the ratio $\gamma/\alpha\simeq 0.05$ has been used by Blackman and others as typical of the second-neighbor contributions. The choice $\gamma=\gamma'$ was made for convenience; probably we should have $\gamma>\gamma'$, but the effect would be trivial. The above ratios, plus the reduced form of Eq. (2.4), serve to fix the numerical values of the reduced constants.

To shorten the numerical work considerably further, we follow Blackman[14] by neglecting the off-diagonal elements of the secular determinant, a step which has been shown to give little error in the case of the simple cubic lattice. The three branches[15] of the frequency spectrum are then given (for $\gamma=\gamma'$) by the relations

$$\begin{aligned}
\nu_{1r}^2&=(\alpha_r/2)(1-\cos\phi_1)+\gamma_r(2-\cos\phi_1\cos\phi_2\\
&\qquad-\cos\phi_1\cos\phi_3)+\kappa_r(1-\cos\phi_3)^2;\\
\nu_{2r}^2&=(\alpha_r/2)(1-\cos\phi_2)+\gamma_r(2-\cos\phi_2\cos\phi_1\\
&\qquad-\cos\phi_2\cos\phi_3)+\kappa_r(1-\cos\phi_3)^2;\\
\nu_{3r}^2&=(\beta_r/2)(1-\cos\phi_3)+\gamma_r(2-\cos\phi_3\cos\phi_1\\
&\qquad-\cos\phi_3\cos\phi_2).
\end{aligned}\tag{2.8}$$

The symmetry of these equations makes it sufficient to consider in the ϕ-space a five-sided prism bounded by the planes $\phi_3=0$, $\phi_3=\pi$, $\phi_2=0$, $\phi_2=\phi_1$, and $\phi_1=\pi$. For a large crystal the number of reduced frequencies (in a specified branch of the spectrum) no greater than any assigned value ν_r is proportional to the volume enclosed between these planes (and including the origin) and the surface of constant frequency in ϕ space found from the appropriate one of Eqs. (2.8). Denoting the *fraction* of such frequencies in a given branch by $I_j(\nu_r)$, we then have

$$I_j(\nu_r)=(2/\pi^3)\int\int\int_{0\leqslant\nu_{jr}\leqslant\nu_r} d\phi_1 d\phi_2 d\phi_3;\quad j=1,2,3. \tag{2.9}$$

To get the functions I_j approximately, we computed values of the frequencies ν_{1r}, ν_{2r}, ν_{3r} from Eqs. (2.8) at intervals of $\pi/6$ along each of the three coordinates ϕ_1, ϕ_2, ϕ_3 and within the prism defined above. Although 196 points in ϕ space are thus included, some of these lie at vertices, edges, or faces of the prism and must be given fractional weights (1/16 or 1/8 for vertices, 1/4 for edges, 1/2 for faces, as compared to unity for interior points). With the interval $\pi/6$, the sum of these weights is 108, and thus for a specified branch of the spectrum we obtain:

$$I_j(\nu_r)\simeq\frac{1}{108}\sum_k w_k;\quad \nu_{jr}(k)\leqslant\nu_r, \tag{2.10}$$

where the index k describes a point with weight w_k and

TABLE I. Integral frequency distribution of a chain polymer crystal.

ν_r	$I(\nu_r)$	ν_r	$I(\nu_r)$
0.05	0.010	0.55	0.623
0.10	0.061	0.60	0.688
0.15	0.124	0.65	0.772
0.20	0.208	0.70	0.831
0.25	0.283	0.75	0.848
0.30	0.338	0.80	0.864
0.35	0.394	0.85	0.883
0.40	0.448	0.90	0.907
0.45	0.503	0.95	0.940
0.50	0.562	1.00	1.000

j-branch reduced frequency $\nu_{jr}(k)$. For the first two branches, the curves of I_j against ν_r thus obtained were fairly smooth, but not for the third branch, because of the high value of β_r. Accordingly, an interval of $\pi/12$ was used for this branch in the lower-frequency range, while the analytical result obtained by setting $\gamma_r=0$ was sufficient for $\phi_3>\pi/6$ (see below).

The total integral frequency distribution, $I(\nu_r)=(I_1+I_2+I_3)/3$, determined to the approximation described above, is given in Table I for intervals of 0.05 in ν_r. A graph of $I(\nu_r)$ against ν_r, plotted as open circles in Fig. 2, shows that quite a smooth curve has been obtained.

The corresponding differential distribution, defined by

$$g(\nu_r)=dI/d\nu_r, \tag{2.11}$$

cannot be obtained with any precision from our results, but fortunately this circumstance does not prevent consideration of the heat capacity. Nevertheless, there is some interest in comparing even the crude difference approximation $g(\nu_r)\simeq\Delta I/\Delta\nu_r$ with Blackman's result for the simple cubic crystal[14] and with the limiting

[15] As shown clearly by Blackman, the three equations obtained do not give separately the true branches of the spectrum, but since we are concerned only with the total spectrum, we can ignore this complication.

case of uncoupled chains considered in the next section. These comparisons are given in Fig. 3, where the crude $g(\nu_r)$ for the polymer crystal is given by the full lines and the simple cubic crystal by the dashed lines. From both Fig. 2 and Fig. 3 it is evident that the Debye approximation would be very poor for the polymeric crystal.

3. LIMITING CASES

To see the effect of coupling between the chains, imposed by the constants α_r and γ_r, we may treat the case when these parameters are allowed to vanish. The frequencies then become

$$\begin{aligned} &\nu_{1r}^2=\nu_{2r}^2=\kappa_r(1-\cos\phi_3)^2;\\ &\nu_{3r}^2=(\beta_r/2)(1-\cos\phi_3), \end{aligned} \tag{3.1}$$

so that the surfaces of constant frequency are all planes perpendicular to the ϕ_3 axis. Analytical solution is thus easy and gives

$$\begin{aligned} &I_1=I_2=(1/\pi)\cos^{-1}(1-\kappa_r^{-1}\nu_r);\\ &I_3=(2/\pi)\sin^{-1}(\beta_r^{-\frac{1}{2}}\nu_r). \end{aligned} \tag{3.2}$$

The corresponding differential distribution $g(\nu_r)$ is shown by the smooth curve in Fig. 3. Comparison with the distribution for the polymer crystal shows how coupling between the chains eliminates the large number of very low frequencies (singularity at the origin) for uncoupled chains.[16]

If we return to the crystal treated in the previous section, we can obtain the limiting distribution at low frequencies by expanding the trigonometric functions and retaining only square terms. Equations (2.8) then become

$$\begin{aligned} \nu_{1r}^2&=\phi_1^2(\gamma_r+\alpha_r/4)+\phi_2^2\gamma_r/2+\phi_3^2\gamma_r/2;\\ \nu_{2r}^2&=\phi_1^2\gamma_r/2+\phi_2^2(\gamma_r+\alpha_r/4)+\phi^2{}_3\gamma_r/2;\\ \nu_{3r}^2&=\phi_1^2\gamma_r^*/2+\phi_2^2\gamma_r/2+\phi_3^2(\gamma_r+\beta_r/4). \end{aligned} \tag{3.3}$$

Thus, at sufficiently low frequencies the bending forces play no role, and the constant-frequency surfaces are ellipsoids. From Eq. (2.9) we then find

$$\begin{aligned} I_1=I_2&=\frac{4}{3\pi^2}\frac{\nu_r^3}{\gamma_r(\alpha_r+4\gamma_r)^{\frac{1}{2}}};\\ I_3&=\frac{4}{3\pi^2}\frac{\nu_r^3}{\gamma_r(\beta_r+4\gamma_r)^{\frac{1}{2}}}. \end{aligned} \tag{3.4}$$

If we insert the numerical constants, sum, and differentiate, we find the total differential distribution at low frequencies to be

$$g(\nu_r)=342.8\nu_r^2, \tag{3.5}$$

which allows the calculation of the limiting form of the specific heat curve at low temperatures. Most of the contribution to $g(\nu_r)$ in this region comes from the first two (low frequency) branches.

[16] In a rigorous calculation for the crystal, the two infinities in $g(\nu)$ at higher frequencies shown by the uncoupled chains would be reduced to finite cusps. See L. Van Hove, Phys. Rev. **89**, 1189 (1953).

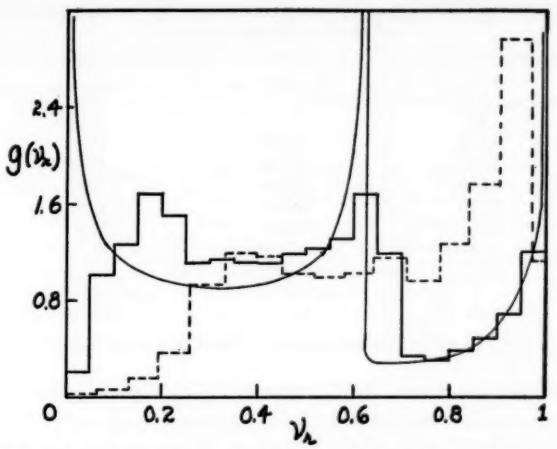

FIG. 3. Differential frequency distributions. Solid smooth curve, single uncoupled chain according to Eq. (3.2); full rectangles, chain polymer crystal according to Table I; dashed rectangles, simple cubic crystal (Blackman).

It should, however, be emphasized that the frequency range over which the limiting forms (3.4) and (3.5) are adequate is extremely short. If expansion of Eqs. (2.8) is carried one step farther, a large fourth-order contribution appears in the valence-angle term. Indeed, a range is reached (say $0.05<\nu_r<0.13$) in which the equation

$$\nu_{1r}^2=\phi_1^2(\gamma_r+\alpha_r/4)+\phi_2^2\gamma_r/2+\phi_3^4\kappa_r/4 \tag{3.6}$$

gives a good representation of the low-frequency branches, and it is readily shown that in this range $g(\nu_r)$ for these branches varies as $\nu_r^{\frac{1}{2}}$. We may thus expect deviations from a Debye heat capacity function at quite low temperatures.

4. HEAT CAPACITY

The constant-volume heat capacity of the crystal is given by the familiar integral

$$\begin{aligned} &C_v/k=\int_0^{\nu_m} f(\nu, T)dN(\nu);\\ &f(\nu, T)=f(x)=x^2e^x/(e^x-1)^2;\quad x=h\nu/kT, \end{aligned} \tag{4.1}$$

where $dN(\nu)$ is the number of normal modes in the frequency range $d\nu$ at ν. In terms of our reduced integral distribution $I(\nu_r)$, we may rewrite this expression as

$$\begin{aligned} &C_v/3Nk=\int_{\nu_r=0}^{\nu_r=1} f(x)dI(\nu_r);\\ &x=(T_m/T)\nu_r;\\ &T_m=h\nu_m/k. \end{aligned} \tag{4.2}$$

Here $N=N_1N_2N_3$ is the number of atoms in the crystal, and the heat capacity is clearly a function of the di-

TABLE II. Heat capacities and equivalent Debye temperatures of chain polymer crystal.

T/T_m	$C_v/3Nk$	Θ_D/T_m
0	0	0.206
1/64	0.0187	0.25
1/32	0.0742	0.32
1/16	0.209	0.42
1/10	0.358	0.51
1/8	0.446	0.55
1/4	0.738	0.64
1/2	0.914	0.68
1	0.977	0.68
∞	1	0.69

mensionless ratio T/T_m, where T_m is the characteristic temperature related to the maximum frequency. From Eq. (4.2) we see that $C_v/3Nk$ at any reduced temperature T/T_m can be determined as the area under a curve of the Einstein function against $I(\nu_r)$. The results of a series of such graphical integrations are given in Table II. For each temperature we also give the Debye temperature Θ_D (in ratio to T_m) that would be required to fit the heat capacity at that point, as determined from the tabulation of Beattie.[17] The limiting value of Θ_D at 0°K follows at once from the low-frequency distribution of Eq. (3.5), while the high-temperature limit follows from a graphical integration of the limiting form of (4.2):

$$C_v/3Nk=\int_{\nu_r=0}^{1}\left(1-\frac{1}{12}x^2+\cdots\right)dI(\nu_r)$$

$$=1-0.0235(T_m/T)^2+\cdots, \quad (4.3)$$

which is then compared with the limiting Debye equation:

$$C_v/3Nk=1-(\Theta_D^2/20T^2)+\cdots. \quad (4.4)$$

Values of the heat capacity at other temperatures are easily found by interpolating in a plot of Θ_D/T_m against T/T_m and then using a table of the Debye function.

It is clear from the values of Θ_D/T_m shown in Table II that the heat capacity shows large deviations from the behavior of a Debye crystal, particularly at lower temperatures. The range over which a T^3 law is obeyed is extremely short, as expected, and indeed the two lowest values of C_v calculated happen to follow a T^2 law almost exactly. This accident shows that adherence of the heat capacity to a T^2 law over a short range of low temperatures does not necessarily imply a layer lattice structure. In general, it would be necessary to examine the data over a fairly wide temperature range before drawing inferences about the structure of the solid.

[17] J. A. Beattie, J. Math. Phys. (M.I.T.) **6** (1926).

5. THE TARASOV FUNCTION

The two-parameter heat-capacity equation recently proposed by Tarasov[13] for chain polymeric crystals corresponds to the integral frequency distribution:

$$\begin{aligned} I(\nu)&=\nu^3/\nu_1\nu_3^2 \quad \text{for} \quad 0\leq\nu\leq\nu_3; \\ &=\nu/\nu_1 \quad \text{for} \quad \nu_3<\nu\leq\nu_1. \end{aligned} \quad (5.1)$$

We shall not attempt to fit the heat capacities of Table II directly with their equation, but Fig. 2 shows that it would give a rather good approximation except possibly at rather low temperature. The dashed curve there shown corresponds to Eq. (5.1) with $\nu_3=0.15\nu_m$ and $\nu_1=0.88\nu_m$. The deviation at the highest frequencies would have very little effect on the heat capacity, but at low frequencies our distribution definitely varies less rapidly than ν^3 except extremely near the origin. The details of the curve in this region will depend on the values of the force-constant ratios κ/γ and κ/α [compare Eq. (3.6)], but we have not pursued the question further. Since these ratios may be expected not to range widely among crystals of the type considered, a single two-parameter distribution such as (5.1) will probably be fairly successful. On the basis of the present calculations we may, therefore, consider the Tarasov equation to have received some additional justification.[18]

For sheet-polymer crystals, we may analogously expect the distribution

$$\begin{aligned} I(\nu)&=\nu^3/\nu_2^2\nu_3 \quad \text{for} \quad 0\leq\nu\leq\nu_3; \\ &=\nu^2/\nu_2^2 \quad \text{for} \quad \nu_3<\nu\leq\nu_2 \end{aligned} \quad (5.2)$$

to give improvement over the simple two-dimensional continuum model.

[18] W. DeSorbo and R. H. Pry (private communication) have reached conclusions similar to ours by more general arguments. We are indebted to Drs. DeSorbo and Pry (General Electric Research Laboratory) for helpful criticism of our manuscript.

Paramagnetic Resonance Absorption in Solutions of K and Na in Liquid NH_3*

CLYDE A. HUTCHISON, JR. AND RICARDO C. PASTOR
Institute for Nuclear Studies and Department of Chemistry, University of Chicago, Chicago, Illinois
(Received August 2, 1953)

Paramagnetic resonance absorption in solutions of K and Na in liquid NH_3 has been investigated. The resonance has been studied at a frequency of approximately $7.0 \cdot 10^6$ cycle sec^{-1} and a magnetic field of 2.5 gauss. The measurements have been made at 240°K, 274°K, and 298°K and over a concentration range from 0.004 *M* to 0.7 *M*. The intensities and susceptibilities, spectroscopic splitting factors, widths, shapes, and extents of saturation of the resonances have been determined. The paramagnetic parts of the magnetic susceptibilities in static fields have been calculated from the rf data and have been compared with the susceptibilities measured in static fields by other investigators. The relations of the trapped electron model of such solutions to these quantitative measurements on the paramagnetic resonance absorption have been considered.

INTRODUCTION

As a result of extensive investigations[1] of the physical properties of solutions of alkali metals in liquid NH_3, it is clear that the metal is, in these systems dissociated into positive metal ions and electrons, the latter being trapped in the solvent. One of the important lines of evidence leading toward the development of a satisfactory model of these solutions has resulted from the study of their magnetic susceptibilities in static fields. These susceptibilities have been investigated by Freed and Sugarman[2] for the case of K and by Huster[3] for the case of Na. Measurements were made at 240°K and 220°K in the case of K and at 238°K and 198°K in the case of Na. In the concentrated solutions and down to concentrations of a few tenths molar, the static magnetic susceptibility is quite small, of the order found in the metal. As the concentration is decreased, the molar susceptibility increases. It approaches in dilute solutions something in the vicinity of the value of the susceptibility of an Avogadro's number of free electron spins. The susceptibilities increase with increasing temperature at all concentrations which were investigated. (In the extremely dilute solutions the susceptibilities presumably obey Curie's law with variation of temperature.) It is apparent from these measurements that increasing the concentration or lowering the temperature results in a pairing of electron spins. This is qualitatively the behavior to be expected of a metal. But not only is the behavior of the magnetic susceptibility not quantitatively that to be expected for a metal, but also the electrical conductivity at the concentrations for which the susceptibilities were measured corresponds to electron mobilities at least 100 times smaller than those of electrons in a metallic conduction band. It was proposed by Freed and Sugarman[2] that the electrons were trapped by the solvent and that there were pairwise interactions between these trapped electrons similar to those which lead to the F' centers in crystals in which two electrons are trapped in a single vacancy.[4] These pairs would be expected to be diamagnetic and would thus lead to lowered susceptibilities. This model was elaborated by Ogg[5] who postulated the existence of cavities in the liquid which served to trap single electrons and pairs of electrons. He calculated the radius of these cavities to be 10A. The large size of these traps has been the subject of both experimental and theoretical controversy. More recent detailed calculations by Lipscomb[1(d)] have shown that the cavities which form the traps would be expected to have sizes about the same as that of an NH_3 molecule, and that such a model is in agreement with the experimental data on the volumes of the solutions. Kaplan and Kittel[1(c)] have considered the cavity trapping model in some detail and have shown that it successfully correlates much of the experimental knowledge of these solutions.

Hutchison and Pastor[6] first reported the observation of paramagnetic resonance absorption in solutions of K in liquid NH_3 at microwave frequencies. Observations of the resonance have also been made by Garstens and Ryan[7] and by Levinthal, Rogers, and Ogg.[8] This resonance was found to be extremely sharp and to have the smallest width of any known paramagnetic resonance absorption. In fact the width, 0.1 gauss, initially reported by Hutchison and Pastor[6] proved to be caused largely by field inhomogeneities.

In view of the intrinsically interesting features of this paramagnetic resonance absorption and because of the importance for an understanding of these solutions of

* This work was assisted by the U. S. Office of Naval Research.
[1] For summaries of the results of these investigations with reference to suitable models of such systems and for references to the literature see:
(a) C. A. Hutchison, Jr., and R. C. Pastor, Revs. Mod. Phys. **25**, 285 (1953);
(b) C. A. Hutchison, Jr., J. Phys. Chem. **57**, 546 (1953);
(c) J. Kaplan and C. Kittel, J. Chem. Phys. **21**, 1429 (1953);
(d) W. N. Lipscomb, J. Chem. Phys. **21**, 52 (1953);
(e) T. L. Hill, J. Chem. Phys. **16**, 394 (1948);
(f) W. Bingel, Ann. Physik **12**, 57 (1953).
[2] S. Freed and N. Sugarman, J. Chem. Phys. **11**, 354 (1943).
[3] E. Huster, Ann. Physik **33**, 477 (1938).
[4] F. Seitz, Revs. Mod. Phys. **18**, 384 (1946).
[5] R. A. Ogg, Jr., J. Chem. Phys. **14**, 295 (1946); **14**, 114 (1946); J. Am. Chem. Soc. **68**, 155 (1946); Phys. Rev. **69**, 668 (1946).
[6] C. A. Hutchison, Jr. and R. C. Pastor, Phys. Rev. **81**, 282 (1951).
[7] M. A. Garstens and A. H. Ryan, Phys. Rev. **81**, 888 (1951).
[8] Levinthal, Rogers, and Ogg, Phys. Rev. **83**, 182 (1951).

the detailed magnetic information which such experiments yield, the investigations were extended over a wide range of temperatures and concentrations. Preliminary results of such experiments with K in liquid NH_3 were reported in two symposia held recently.[1(a), 1(b)] This paper gives a detailed report and discussion of the data on intensities and susceptibilities, spectroscopic splitting factors, widths, shapes, and saturation, for the paramagnetic resonance absorption in solutions of K and Na in liquid NH_3, and preliminary results on K in ND_3.

EXPERIMENTAL PROCEDURES AND APPARATUSES. PREPARATIONS AND ANALYSES OF SAMPLES

The solutions of alkali metals in liquid NH_3 were prepared by distillation, first of alkali metal and then of NH_3 into Pyrex capsules which were subsequently sealed. The samples were prepared in an evacuated system. The storage vessel for the NH_3 was made of steel, and it was joined to the Pyrex preparation system proper by means of a copper-to-glass seal. The capsules, 1 cm in diameter and 3 cm in length, were attached to the lower ends of vertical tubes 1 cm in diameter by means of constrictions which facilitated the sealing. Just above every constriction was a side arm, 0.5 cm in diameter and 10 cm in length leading to a bulb in which approximately 0.5 g of metal was placed before the evacuation of the system. The side arms were constructed with five right angle bends. The system was evacuated, the alkali metal was fused and heated to remove occluded gases, and the vacuum system was baked by heating nearly to the softening point. Tank NH_3 had originally been placed in the steel storage cylinder with a large quantity of sodium metal. The hydrogen which was evolved had been released from the cylinder. NH_3 from this cylinder was now condensed in a glass bulb containing alkali metal in the preparation system. This was the final step of purification of the solvent. The metal in the bulbs at the end of the bent side arms was then heated and moved along the walls to form mirrors just above the constrictions. The side arms were removed. The walls of the tubes on which the mirrors were located were cooled with a swab which had been dipped in a dry ice-acetone mixture, and the proper amounts of metal were washed down into the capsules. Additional NH_3 was distilled into the capsules until the desired levels of liquid were obtained. The contents of the capsules were frozen in liquid N_2 and sealed off from the vacuum system. The capsules were stored at dry ice temperature when they were not being used for measurements.

The contents of the capsules were analyzed chemically. The capsules were weighed and placed one at a time in a stainless steel bomb which contained 25 cm^3 of H_2O. The bomb was placed in hot water causing the capsules to explode. The contents of the bomb were filtered. The residue of broken glass was dried, ignited, and weighed. The filtrate was boiled down to such a small volume that all NH_3 was removed. An excess of standard HCl solution was added quantitatively, and the solution was titrated at about 98°C to 100°C with a standard solution of NaOH, using methyl red as the indicator. The standard HCl was usually 0.005 M. Blank analyses were made which indicated the presence of about $5.0 \cdot 10^{-7}$ mole of alkali, and this was deducted from the determined numbers of moles in the samples. It is believed that the errors were largely those of the titration, and that they were equal in all cases to about 0.1 cm^3 of 0.005 M HCl or $5.0 \cdot 10^{-7}$ mole. This would be an error of about 10 percent for a 0.005 M solution of alkali metal in liquid NH_3 or an error of 0.5 percent for a 0.100 M solution. Analyses of known solutions of NaOH mixed with NH_3 carried through all steps of the analytical procedure except the breaking of the capsules confirmed this viewpoint. The errors introduced by the procedure of breaking the glass capsules were probably much smaller than the errors of titration.

The tris-*p*-nitrophenylmethyl samples, used as standards, were made by the reaction between tris-*p*-nitrophenylmethyl sodium and tris-*p*-nitrophenylmethyl bromide in an atmosphere of dry N_2. The former compound was obtained by filtering the dark blue product which resulted on treating a pyridine solution of tris-*p*-nitrophenylmethane with sodium ethoxide dissolved in alcohol. The latter compound was the residue left on refluxing tris-*p*-nitrophenylmethane with an excess of Br_2 for 24 hr and then evaporating the Br_2 in a vacuum. The residue was recrystallized from chloroform-ether. The method used was a modification of the procedure of Ziegler and Boye.[9] The free radical content of a given sample was determined from the volume uptake of O_2 by a weighed portion, 1 mole of O_2 being equivalent to 2 moles of tris-*p*-nitrophenylmethyl.

MEASUREMENT AND RECORDING OF THE ABSORPTIONS

a. The Static Field

Since the resonance was extremely narrow, the width at the points of maximum slope being as small as $20 \cdot 10^{-3}$ gauss, it was necessary to have a static magnetic field that was homogeneous to better than $1 \cdot 10^{-3}$ gauss over the volume of the sample. The resonance was first observed at $23\,700 \cdot 10^6$ cycle sec^{-1} the associated field strength being approximately 8500 gauss. A field of this value with sufficient homogeneity was not available. The width of the resonance being essentially independent of the field strength the investigations were carried out at approximately $7 \cdot 10^6$ cycle sec^{-1}. The associated magnetic field was approximately 2.5 gauss, and it was not difficult to obtain such a field with sufficient homogeneity. Moreover because of the narrowness, the intensity was sufficiently great to permit the use of these very low field strengths. (In the case of large fields and frequencies difficulties were also encountered

[9] K. Ziegler and E. Boye, Ann. **458**, 248 (1927).

because of the relatively large conductivity of the solutions.)

The static field was supplied by a solenoid of circular cross section 96.16 cm long and 12.591±0.002 cm in outside diameter. The solenoid was wound with 33.225 ±0.045 turns per cm as determined by means of a travelling microscope and scale. (33.225 is 50 times the average of the reciprocals of the lengths of 50 50-turn sections of the solenoid and 0.045 is 50 times the mean deviation from the mean of these reciprocals.) The current for the solenoid came from an electronically regulated supply. A motor driven potentiometer in the supply circuit provided a very slow and nearly linear variation of current with time. The voltage across a resistor in series with the solenoid was measured and recorded for 5 sec at intervals of 30 sec by a recording potentiometer throughout each determination of a magnetic resonance curve. The recording potentiometer was calibrated by comparison with another potentiometer, and the resistor was calibrated by comparison with a resistor which had been calibrated by the National Bureau of Standards. The recorder chart was calibrated in terms of the output of the other potentiometer immediately after each scanning of the magnetic resonance signal. For K or Na in liquid NH_3 the current through the solenoid was scanned from 0.054 to 0.070 amp or a resultant field of 2.0 to 2.8 gauss and for tris-*p*-nitrophenylmethyl, 0.000 to 0.120 amp or −0.6 to 5.2 gauss. The solenoid was mounted so that it could be rotated both horizontally and vertically and maintained in a desired position. The axis of the solenoid was aligned parallel to the magnetic field of the laboratory by means of the resonance signal from a solution of K in NH_3. The direction of the solenoid was varied until the difference between the currents at constant frequency required to produce maximum resonance absorption with (a) the angle between the solenoid field and lab field less than $\pi/2$, and (b) this angle greater than $\pi/2$ was a maximum.

b. The Modulating Field

The static field was modulated by means of an auxiliary coil. The auxiliary coil was a short solenoid (2 cm in length) with a single layer of 12 turns. It was located just inside and at the midpoint of the main solenoid. The center of the rf coil was located at the center of the auxiliary modulating coil. The auxiliary coil was transformer coupled to a power amplifier whose input signal was a 50-cycle sec^{-1} sine wave from an audio oscillator. The potential across a resistor in series with the modulating coil was measured with an ac voltmeter which had been calibrated against an electrodynamometer. The field modulation H_w equivalent to a given voltmeter reading was determined by employing the magnetic resonance of K in NH_3. The change in voltage across the calibrated resistor in series with the solenoid which was required to move the resonance from one extreme of the modulation to the other at fixed frequency was determined. This together with the geometrical constants of the solenoid and the calibration of the resistor in series with the solenoid was sufficient to determine the amplitude of the modulation field as a function of the reading on the voltmeter which was across the resistor in series with the auxiliary coil. The range of peak to peak modulation for solutions of alkali metals in liquid NH_3 was from 0.0025 to 0.0218 gauss at 298°K, 0.0059 to 0.0238 gauss at 274°K, and 0.0198 to 0.0594 gauss at 240°K.

c. The Radio-frequency Field

The radio-frequency field was supplied by a coil which together with a variable condenser formed the grid tank circuit of a regenerative oscillator-detector. The coil consisted of 30 turns of number 20 Formex coated copper wire, was 3.0 cm long and 1.27 cm in outside diameter. The capsules containing the solutions were fitted inside this coil. The coil was mounted with its midpoint at the center of the static field solenoid and with its axis perpendicular to that of the solenoid. It was connected by a coaxial line to the remainder of the circuit outside the solenoid. It was completely surrounded by a copper box which served as a shield. The frequency of the radio-frequency field was in the range $6.0 \cdot 10^6$ to $8.0 \cdot 10^6$ cycle sec^{-1} and was usually $7.0 \cdot 10^6$ cycle sec^{-1}. The voltage across the coil was controlled by varying the regeneration and was measured continuously during measurements of magnetic resonance by means of an electronic voltmeter. The loaded Q of the coil and the shunt capacitance C at resonance at the working frequency were determined with a Q meter. The frequency of oscillation was determined with a heterdyne-type frequency meter and the measurements of frequency were found to be accurate to 1 part in 20 000.

All measurements of magnetic resonances with K or Na in liquid NH_3 were made with 0.05 rms volt across the coil. At circuit resonance, for a frequency of $7.0 \cdot 10^6$ cycle sec^{-1} and a capacitance of $1.43 \cdot 10^{-10}$ f, this potential corresponds to 0.0051 gauss at the center of the coil, and the rf field should be proportional to the coil voltage. At room temperature, for a frequency of $7.0 \cdot 10^6$ cycle sec^{-1}, the Q of the coil plus sample varied from 90 to 120 for the range of concentration (0.65 M to 0.004 M) of K in liquid NH_3 investigated, and the capacitance needed for circuit resonance was about $1.43 \cdot 10^{-10}$ f. The Q's obtained using the low-temperature apparatus were about 20 percent lower. With solutions of Na in liquid NH_3 the Q's were about 10 percent lower at room temperature than those obtained with equivalent concentrations of solutions of K in liquid NH_3.

d. The Detecting and Recording System

The detected 50-cycle sec^{-1} audio signal from the oscillator-detector circuit passed through three tuned

stages of amplification followed by a phase-sensitive detector. The reference signal for the phase-sensitive detector was supplied from the generator for the auxiliary modulating coil. The rectified output of the amplification system was fed to a recording potentiometer. By means of an automatic switch the same potentiometer was used for recording both the magnetic signal and the current through the solenoid. A Watkins-Pound[10] calibrator was used for determining signal intensities. The regenerative oscillator-detector-amplifier-recorder system was used to compare the magnetic signal with the calibrator signal produced when a 50-cycle sec^{-1} signal of known amplitude was placed on the grid of the calibrator tube at known fixed plate current. The calibrator signal was supplied from the modulation generator and measured with an electronic voltmeter which had been calibrated against an electrodynamometer. The recorder chart was calibrated in terms of calibrator gird voltage immediately after each scanning of the magnetic resonance signal. In experiments in which the Watkins-Pound[10] radio-frequency spectrometer was substituted for the regenerative oscillator-detector, the magnetic signals were not detectably different in shape from those obtained with the regenerative oscillator-detector. The regenerative circuit was used because of its much greater signal to noise ratio.

For all measurements the amplitude of the modulation of the static field of the solenoid was sufficiently small that the output of the phase-sensitive detector was proportional to the first derivative of the magnetic signal with field strength. The ratio of (a) af calibrator volts necessary to simulate the magnetic derivative signal to (b) the field modulation amplitude, was equal to the slope of the curve of hypothetical dc calibrator grid voltage *versus* field strength, i.e., to the slope of the curve of magnetic signal *versus* field strength.

THE DATA AND THEIR TREATMENT

The data consisted of (a) curves drawn by the recording potentiometer showing the variation of the magnetic derivative signal and of the current through the solenoid with time; (b) meter readings showing the rf coil voltage and frequency, field modulation amplitude, calibrator ac grid voltage, Q of the rf coil and capacitance across the coil; (c) thermometer and thermocouple readings; (d) results of chemical analyses of the solutions and standards; (e) data obtained during the calibration of the recording potentiometer, meters, resistors, etc.

The magnetic derivative signal and the solenoid current signal were both recorded along the width of the chart of the recording potentiometer. The length of the chart was proportional to time. At the conclusion of each recording of the magnetic derivative signal, records of a series of calibrator signals and records of a series of known voltages from another potentiometer were made on the same chart paper. The calibrator signals were produced by known ac grid voltages. Hence, the number of calibrator ac grid volts per nominal in. of chart width was determined. The calibration against the other potentiometer gave the number of volts per nominal in. of width of chart and this combined with (a) the measured slope of the current signal *versus* length of chart, (b) the calibration of the resistor in series with the solenoid (the voltage across which gave the current signal), and (c) the geometrical constants of the solenoid, determined the number of gauss variation of field at the center of the solenoid per nominal in. of length of chart. The width of the chart, thus, could be converted to a calibrator ac grid volt scale and the length to a magnetic field scale. The length of the chart was divided into small intervals convenient for numerical integration. The areas of these strips were converted to volt gauss by use of the calibration factors measured as just described. Summations of the volt gauss, corresponding to these strips, up to a given field strength gave a quantity which when divided by the constant field modulation amplitude was the number of hypothetical calibrator dc grid volts that would simulate the magnetic signal (not derivative signal) at that given field strength. A plot of these first integrals up to given field strengths *versus* the field strengths gave the magnetic resonance absorption line. A second numerical integration gave the areas under these curves of calibrator dc grid volts *versus* field strength. These second integral areas were proportional, in the absence of magnetic saturation, to numbers of absorbers in the samples being investigated, other things such as sizes and positions of samples, frequency, etc., being kept constant.

This may be seen as follows: The calibrator was coupled to the rf coil in such a manner that if the rf resistance of the coil is represented by $\mathfrak{R}$, the voltage placed on the grid of the calibrator was proportional to $\Delta\mathfrak{R}/\mathfrak{R}^2$ where $\Delta\mathfrak{R}$ was the change in $\mathfrak{R}$ produced by this voltage. It is also true that if the $\Delta\mathfrak{R}$ was produced by a magnetic resonance absorption, then for a coil with large Q, $\Delta\mathfrak{R}/\mathfrak{R}^2 = -\xi\omega C/Q_{mag}$ where ξ is the ratio of (a) the field energy stored within the boundary of the sample to (b) the total energy stored in the field, and Q_{mag} is the ratio of (a) the energy stored in unit volume of the field in the sample to (b) the magnetic energy absorbed per unit volume and per radian in the sample. Now since Q_{mag}^{-1} is equal to 4π times χ'', the imaginary component of the susceptibility, then $\Delta\mathfrak{R}/\mathfrak{R}^2$ was equal to $-4\pi\xi\omega C\chi''$. The area obtained as the second integral $\int_0^\infty$ (calibrator dc grid voltage) dH, described above was proportional to $\int_0^\infty(\Delta\mathfrak{R}/\mathfrak{R}^2)dH$. (The integral $\int_0^\infty$ is written assuming that the only contribution to spin resonance absorption was in the region investigated.) Therefore, from the immediately preceding discussion it

[10] G. D. Watkins and R. V. Pound, Phys. Rev. 82, 343 (1951).

is seen that

$$\frac{1}{\xi\omega C}\int_0^\infty (\text{calibrator dc grid voltage})\, dH \propto \int_0^\infty \chi''(H)dH.$$

The experiment was carried out at a constant frequency. For a sharp symmetrical absorption the integral, $\int_0^\infty \chi''(H)dH$, for the present experiments may be equated to the corresponding integral, $H_{max}\int_0^\infty \times(\chi''(\nu)/\nu)d\nu$, for an experiment in which the field is kept constant and the frequency is varied. (H_{max} is the value of H in the constant ν experiment at which the absorption is a maximum.) But $\int_0^\infty(\chi''(\nu)/\nu)d\nu$ is, according to the Kronig-Kramers[11] relation, just χ the susceptibility in a static field (magnetic moment per unit volume divided by field strength). Therefore it is seen that

$$\chi \propto \frac{g\beta}{\xi\omega^2 Ch}\int_0^\infty (\text{calibrator dc grid voltage})\, dH.$$

It should be noted that this χ is just the paramagnetic part of the susceptibility. χ is proportional to the number of absorbers per unit volume. It is therefore clear that the numbers of absorbers per unit volume in the samples were proportional to $(\xi\omega^2C)^{-1}$ times the results of the second numerical integrations of the recorder charts described above. The second integrals for the samples of alkali metal in liquid NH_3 were compared with those for the standard substance, tris-*p*-nitrophenylmethyl, and the proportionality constant was thereby eliminated. Since only the part of the imaginary susceptibility χ'' caused by the flipping of spins in the static field was observed, it is clear that the static susceptibilities calculated from the rf data were just the paramagnetic parts of the susceptibilities and did not depend upon any diamagnetic effects of the systems.

ξ was not determined but instead a quantity R was measured. R was defined as the ratio of the magnetic energy stored within the boundaries of the sample to the energy that would have been stored if the energy density were everywhere the same as at the center of the coil. It will be seen that the previous relation may then be transformed so as to read

$$\chi_m \propto \frac{1}{mR\omega^2 C}\int_0^\infty (\text{calibrator dc grid voltage})\, dH,$$

in which m is the number of moles in the sample and χ_m is the molar susceptibility. Calling the right-hand side of this proportionality $A/mR\omega^2C$, the static paramagnetic susceptibilities of the samples of alkali metals in liquid NH_3 were calculated by means of the relation,

$$\chi_m = \frac{N_{Av}\beta^2}{kT_{st}}\left(\frac{A}{mR\omega^2C}\right)\left(\frac{A}{mR\omega^2C}\right)^{-1}\cdot f.$$

$N_{Av}\beta^2/kT_{st}$ is the magnetic susceptibility of the standard substance at the temperature at which its curve of calibrator ac grid voltage *versus* field was recorded and the subscript st everywhere refers to the standard substance. (A_{LF}, the integral from zero up to maximum absorption was actually employed for the comparisons rather than A.) f is a factor which corrected for the saturation. f was determined by measuring the maximum deflections of the phase-sensitive detector as a function of rf coil voltage at various concentrations of K in liquid NH_3. Since the width and shape did not vary in the region 0.05 volt (operating voltage) and less, the second integrals were proportional to these maximum deflections. f is the ratio of the area extrapolated to zero voltage to the area at 0.05 volt. The f values determined at room temperature for K were used in the treatment of the data for both K and Na at all temperatures. A curve drawn through the measured values of f *versus* concentration was employed to interpolate the values of f for given concentrations.

The experimental data entering into the calculation of χ_m and the values obtained for χ_m are listed in Tables I and II. (The data in these tables were obtained from a series of measurements employing techniques which were considerably improved over those used in the measurements referred to as Series I and II in the symposia mentioned above. None of the rf data of these Series I and II is included in Figs. 1 to 4. Figs. 5 and 6 give results of all series of runs.) In Figs. 1 and 2 the static molar susceptibilities χ_m of K and Na in liquid NH_3 calculated from the rf data as described above are plotted against the concentration at the three different temperatures. The curves through the points were visually fitted to them, and these curves were all drawn so as to pass through the points, $N_{Av}\beta^2/kT$, at zero concentration which are shown as horizontal bars on ordinate axes. In Figs. 3 and 4 these visually fitted curves are given, without the experimental points, together with curves that were visually fitted to the data of Freed and Sugarman[2] and of Huster[3] obtained from measurements made in static fields.

The values of χ were obtained by multiplying $10^{-3}\cdot\chi_m$ by the concentrations M.

The lengths of recorder charts from the maxima of the magnetic derivative signal to the minima were measured. These lengths when multiplied by the factor equal to the number of gauss variation of static field per unit length of chart gave the widths ΔH_{MS} between the points of maximum and minimum slopes of the magnetic resonance curves. In Fig. 5 these widths are plotted as a function of concentration. To avoid confusion caused by overlapping of curves and points three separate graphs are given corresponding to the three temperatures. In Fig. 6 just the visually fitted curves are presented without the experimental points and all with the same ordinate scale. Data on widths for two concentrations of solutions of K in ND_3 are given in Table III.

[11] H. A. Kramers, Atti congr. intern. fisica, Como, **2**, 545 (1927); R. de L. Kronig. J. Opt. Soc. Am. **12**, 547 (1926).

TABLE I. Experimental data for K in liquid NH_3.

1 Serial No.	2 Sample No.	3 Concentration M mole l^{-1}	4 Amount Alkali Metal $\cdot 10^5$ $m \cdot 10^5$ mole	5 Temperature Celsius deg	6 Geometrical factor $\cdot 2$ $2R$	7 Capacitance $\cdot 10^{12}$ C farad	8 Modulation amplitude H_w gauss	9 Width maximum slope ΔH_{MS} gauss	10 Low field half area A_{LF} volt gauss	11 Molar susceptibility $\cdot 10^6$ $\chi_m \cdot 10^6$ mole l^{-1} cm^3	12 Susceptibility $\cdot 10^9$ $\chi \cdot 10^9$
1	K141	0.00402	0.3358	−33.2	1.82	124.6	0.0317	0.057	0.00979	981	3.94
2	K149	0.0138	1.183	−33.2	1.85	124.1	0.0475	0.059	0.0210	595	8.21
3	K143	0.0195	1.589	−33.2	1.85	124.5	0.0317	0.056	0.0275	574	11.2
4	K148	0.0267	2.306	−33.2	1.87	124.2	0.0594	0.062	0.0276	395	10.5
5	K142	0.0337	2.326	−33.2	1.88	124.6	0.0317	0.055	0.0226	315	10.6
6	K145	0.0361	2.797	−33.2	1.86	124.7	0.0317	0.055	0.0298	349	12.6
7	K150	0.0793	6.686	−33.2	1.87	124.3	0.0317	0.055	0.0363	176	14.0
8	K155	0.155	14.00	−33.2	1.86	124.1	0.0317	0.052	0.0576	131	20.3
9	K144	0.177	16.42	−33.2	1.86	124.3	0.0317	0.049	0.0587	113	20.0
10	K151	0.203	19.98	−33.2	1.82	124.2	0.0317	0.049	0.0715	115	23.3
11	K146	0.219	16.78	−33.2	1.87	124.7	0.0198	0.044	0.0632	117	25.6
12	K147	0.312	27.57	−33.2	1.83	124.4	0.0198	0.046	0.0770	86	26.8
13	K153	0.419	33.63	−33.2	1.90	124.2	0.0317	0.051	0.0569	48	20.1
14	K156	0.728	62.01	−33.2	1.90	124.8	0.0396	0.125	0.1089	50	36.4
15	K157	1.551	130.7	−33.2	1.88	...	...	...	...	...	...
16	K141	0.00376	0.3358	0.8	1.79	124.3	0.0238	0.040	0.01489	1549	5.82
17	K149	0.0129	1.183	0.8	1.81	124.3	0.0198	0.036	0.0337	978	12.6
18	K143	0.0182	1.589	0.8	1.81	124.3	0.0238	0.036	0.0399	869	15.8
19	K148	0.0250	2.306	0.7	1.85	123.8	0.0158	0.032	0.0517	763	19.1
20	K142	0.0315	2.326	0.8	1.87	124.2	0.0238	0.039	0.0479	687	21.6
21	K145	0.0338	2.797	0.8	1.83	123.9	0.0158	0.031	0.0615	750	25.4
22	K150	0.0742	6.686	1.2	1.85	124.2	0.00792	0.030	0.0826	406	30.1
23	K155	0.145	14.00	0.8	1.83	124.2	0.00594	0.030	0.1191	277	40.2
24	K144	0.166	16.42	0.8	1.83	123.7	0.00594	0.030	0.1275	256	42.5
25	K151	0.190	19.98	0.7	1.79	124.2	0.00792	0.030	0.1311	217	41.2
26	K146	0.204	16.78	0.8	1.85	124.7	0.00792	0.032	0.1123	217	44.3
27	K147	0.291	27.57	0.8	1.81	123.8	0.01190	0.039	0.1456	170	49.5
28	K153	0.392	33.63	0.7	1.87	124.2	0.00594	0.039	0.1462	129	50.6
29	K156	0.681	62.01	0.8	1.87	122.8	0.0792	0.190	0.2572	121	82.4
30	K157	1.451	130.7	0.8	1.87	...	...	...	...	...	...
31	K141	0.00356	0.3358	25.5	1.75	142.9	0.02176	0.024	0.01426	1301	4.63
32	K149	0.0123	1.183	24.6	1.79	142.4	0.01474	0.025	0.0415	1054	13.0
33	K143	0.0172	1.589	25.2	1.79	142.6	0.01123	0.022	0.0490	919	15.8
34	K148	0.0237	2.306	25.2	1.83	142.4	0.00878	0.023	0.0606	767	18.2
35	K142	0.0299	2.326	25.2	1.84	142.7	0.01123	0.025	0.0616	766	22.9
36	K145	0.0320	2.797	25.0	1.81	142.5	0.00632	0.020	0.0738	778	24.9
37	K150	0.0703	6.686	24.2	1.83	142.4	0.00562	0.023	0.1144	496	34.9
38	K155	0.137	14.00	24.2	1.81	141.2	0.00316	0.025	0.1750	363	49.7
39	K144	0.157	16.42	25.0	1.81	142.3	0.00421	0.027	0.2209	385	60.4
40	K151	0.180	19.98	25.3	1.75	142.3	0.00246	0.026	0.2280	336	60.5
41	K146	0.193	16.78	25.2	1.83	142.0	0.00351	0.032	0.2091	349	67.4
42	K147	0.276	27.57	25.2	1.77	141.3	0.00702	0.046	0.2487	255	70.4
43	K153	0.371	33.63	25.0	1.86	142.3	0.0176	0.061	0.2497	193	71.6
44	K156	0.645	62.01	26.5	1.86	...	...	...	...	...	...
45	K157	1.375	130.7	25.0	1.84	...	...	...	...	...	...

Graphs of the first integrals of the recorder curves which give the shapes of the resonance absorption lines have been given by Hutchison and Pastor.[1(a)]

Ratios of the spectroscopic splitting factors g for different samples were determined by means of an experimental procedure which involved reversal of the direction of the current through the solenoid, thereby cancelling the effect of the earth's field. With the solenoid's axis aligned parallel or antiparallel to the earth's field, the output of the phase-sensitive detector was observed as the current through the solenoid was varied. The value of the voltage across the resistor in series with the solenoid at which this output passed through zero on its way from maximum to minimum derivative signal was called E. The ratio of g for one sample g_y to that of another g_x was then given by

$$g_y/g_x=\left(\nu_f/\left[|E_f|+\left|E_r\frac{\nu_f}{\nu_r}\right|\right]\right)_y\left(\nu_f/\left[|E_f|+\left|E_r\frac{\nu_f}{\nu_r}\right|\right]\right)_x^{-1},$$

in which the subscripts f and r denote the forward and reverse directions of the current in the solenoid. From 5 to 8 pairs E_f, E_r were measured for each of a number of samples. The results are summarized in Table IV along with the results on other substances and at other frequencies.

The magnetic saturation was investigated in a series of measurements in which the maximum magnetic derivative signal with variation of field was examined as a function of the voltage on the rf coil. The results of

TABLE II. Experimental data for Na in liquid NH_3.

1 Serial No.	2 Sample No.	3 Concentration M mole l^{-1}	4 Amount alkali metal $\cdot 10^5$ $m \cdot 10^5$ mole	5 Temperature Celsius deg	6 Geometrical factor $\cdot 2$ $2R$	7 Capacitance $\cdot 10^{12}$ C farad	8 Modulation amplitude H_w gauss	9 Width maximum slope ΔH_{MS} gauss	10 Low field half area A_{LF} volt gauss	11 Molar susceptibility $\cdot 10^6$ $\chi_m \cdot 10^6$ mole l^{-1} cm^3	12 Susceptibility $\cdot 10^9$ $\chi \cdot 10^9$
1	Na135	0.0558	4.801	−33.1	1.91	124.3	0.0198	0.051	0.0355	215	12.0
2	Na138	0.0563	5.273	−33.2	1.90	124.3	0.0198	0.056	0.0393	217	12.2
3	Na137	0.0784	8.134	−33.2	1.87	124.3	0.0198	0.052	0.0448	163	12.8
4	Na136	0.210	19.45	−33.2	1.89	124.3	0.0198	0.043	0.0763	111	23.3
5	Na124	0.347	35.65	−33.2	1.84	124.4	0.0139	0.043	0.0994	77	26.7
6	Na139	0.982	104.2	−33.2	1.90	...	...	...	...	...	...
7	Na135	0.0521	4.801	0.6	1.89	124.2	0.00594	0.030	0.0876	539	28.1
8	Na138	0.0526	5.273	1.0	1.86	124.6	0.00594	0.033	0.1086	615	32.3
9	Na137	0.0732	8.134	0.8	1.84	123.9	0.00792	0.031	0.1242	463	33.9
10	Na136	0.1962	19.45	0.8	1.87	124.0	0.00594	0.030	0.1856	276	54.2
11	Na124	0.324	35.65	0.7	1.81	124.1	0.00594	0.037	0.1922	154	49.9
12	Na139	0.919	104.2	0.8	1.86	...	...	...	...	...	...
13	Na135	0.0495	4.801	24.1	1.88	127.8	0.00351	0.025	0.1196	718	35.5
14	Na138	0.0499	5.273	24.2	1.86	128.2	0.00351	0.025	0.1722	947	47.3
15	Na137	0.0696	8.134	23.8	1.82	128.0	0.00351	0.023	0.2248	816	56.8
16	Na136	0.1864	19.45	23.8	1.85	127.1	0.00351	0.028	0.370	539	100.0
17	Na124	0.3080	35.65	24.3	1.78	128.6	0.00351	0.032	0.354	278	85.6
18	Na139	0.873	104.2	24.0	1.86	...	...	...	...	...	...

these measurements at room temperature for several concentrations of K in liquid NH_3 are summarized in Table V along with data on the width of the resonance as a function of coil voltage.

In order to calculate T_1, the spin-lattice relaxation time, the maximum magnetic derivative signal at zero rf field was calculated by extrapolation of the measurements at finite fields. The ratio

$$D_{ex}=\frac{\text{maximum derivative signal}}{\text{maximum derivative signal at zero rf voltage}}$$

was equated to $(1+r^2H_{rf}^2T_1T_2)^{-\frac{1}{2}}$ according to Eq. (17) of Bloembergen, Purcell, and Pound.[12] T_1 was then calculated from the relation

$$T_1=\frac{D_{ex}^{-2}-1}{r^2H_{rf}^2T_2},$$

in which H_{rf}^2 was obtained from coil geometry and circuit constants and T_2 is equal to $2/3^{\frac{1}{2}}r\Delta H_{MS}$. ΔH_{MS} is the width at point of maximum slope.

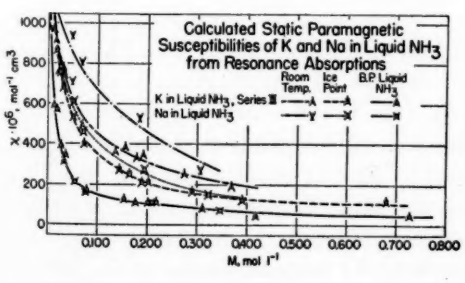
Calculated Static Paramagnetic Susceptibilities of K and Na in Liquid NH3 from Resonance Absorptions
Room Temp.
Ice Point
B.P. Liquid NH3
K in Liquid NH3, Series III
Na in Liquid NH3
χ·10^6, mol^-1 cm^3
M, mol l^-1

FIG. 1.

[12] Bloembergen, Purcell, and Pound, Phys. Rev. **73**, 679 (1948).

The T_1's so calculated varied from 2 to 5 times the inverse line width time T_2.

The errors in the determinations of the integrals of the recorder curves were essentially all in the intensity determinations the measurement of the field making a negligible contribution. The measurements of the integrals for the solutions of K in NH_3 were most precise in two intermediate concentration ranges from 0.06 M to 0.1 M and from 0.2 M to 0.3 M where the errors were probably of the order of 3 percent or less. The errors in the determinations of relative amounts of tris-*p*-nitrophenylmethyl in various independently chemically analyzed samples was about 2 percent. Three factors were responsible for loss of precision in the low, middle, and high ranges of concentration of K in NH_3. These were (a) the fact that χ decreased very rapidly in the more dilute solutions although χ_m was increasing rapidly and this resulted in very weak signals; (b) at the high concentrations although χ was large, the width was also large and this lowered all the intensities

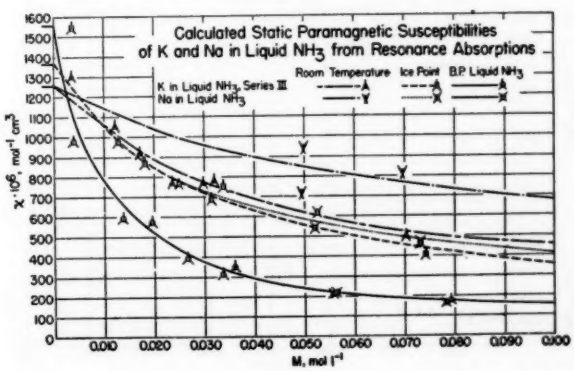
Calculated Static Paramagnetic Susceptibilities of K and Na in Liquid NH3 from Resonance Absorptions
Room Temperature
Ice Point
B.P. Liquid NH3
K in Liquid NH3, Series III
Na in Liquid NH3
χ·10^6, mol^-1 cm^3
M, mol l^-1

FIG. 2.

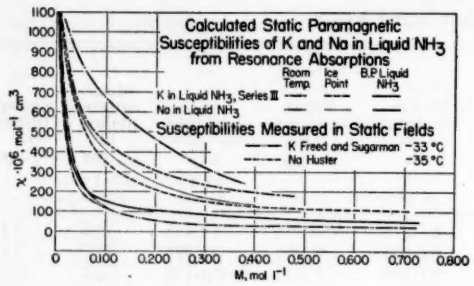
Calculated Static Paramagnetic Susceptibilities of K and Na in Liquid NH3 from Resonance Absorptions
Room Temp.
Ice Point
B.P. Liquid NH3
K in Liquid NH3, Series III
Na in Liquid NH3
Susceptibilities Measured in Static Fields
K Freed and Sugarman -33 °C
Na Huster -35 °C
χ·10^6, mol^-1 cm^3
M, mol l^-1

FIG. 3.

and gave small derivative signals; (c) at the middle concentrations the magnetic derivative signals were very intense, and in order to avoid overloading the calibrator, the derivative signals had to be decreased by means of reducing the field modulation amplitudes and

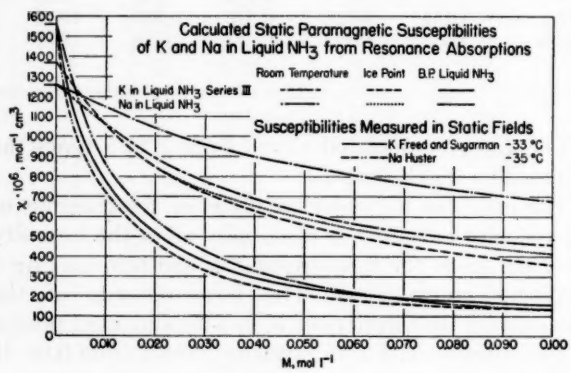
Calculated Static Paramagnetic Susceptibilities of K and Na in Liquid NH3 from Resonance Absorptions
Room Temperature
Ice Point
B.P. Liquid NH3
K in Liquid NH3 Series III
Na in Liquid NH3
Susceptibilities Measured in Static Fields
K Freed and Sugarman -33 °C
Na Huster -35 °C
χ·10^6, mol^-1 cm^3
M, mol l^-1

FIG. 4.

this led to errors in the determination of the modulation amplitudes. The errors in the low, middle, and high ranges were probably about 5 percent or 6 percent except in the very dilute region where the errors of chemical analysis predominated.

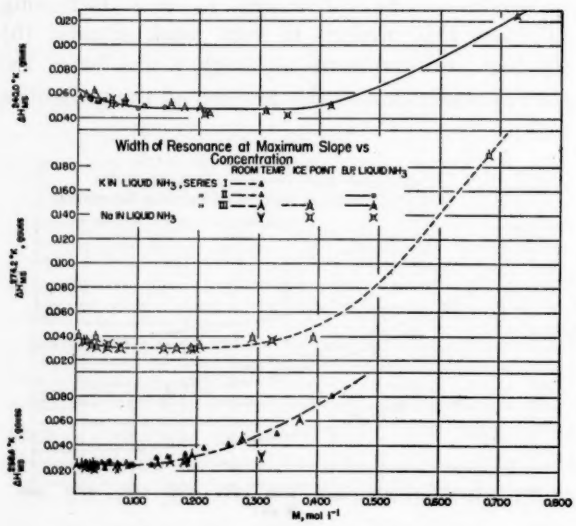

FIG. 5.

DISCUSSION. SUSCEPTIBILITIES

Figures 1–4 summarize the calculations of the paramagnetic susceptibilities in static fields from the rf data and compare the values so obtained with the susceptibilities measured in static fields by other workers.[2, 3] The essential features of these curves are the following. (a) At all temperatures and for both K and Na the static molar magnetic susceptibilities calculated from the rf data are relatively small at the higher concentrations and increase with decreasing concentration until they reach something near the value, $N_{Av}\beta^2/kT$ in the very dilute solutions. In this respect the behavior is similar to that observed in static fields.[2, 3] (b) At all concentrations which were examined the molar magnetic susceptibilities increase with increasing temperatures. Although presumably at the extremely low concentrations the reverse would be true the lowest concentrations which were employed were still above the crossover point. In this respect the behavior is similar to that observed in static fields.[2, 3] In the present experiments the range of temperatures is larger than was the case for the static field measurements. (c) At the higher concentrations, for the temperature at which both rf and static field data are available (bp of NH_3), the curves for the two approach a small approximately constant difference, the quantities obtained from the rf measurements being larger. In the dilute solutions the smooth curves which have been drawn visually through the points show the static field data for K slightly higher and the static field data for Na slightly lower than the values from the present research. (The rf curves for K and Na are indistinguishable at this temperature.) However, this happens only below 0.065 molar, and at these low concentrations the possibilities of analytical errors affecting all the curves (rf and dc) become much more important, and the errors in the recorder curves become larger because of the weak signals. The difference between the rf curve for Na and K and the dc curve for Na is just about constant over almost the entire concentration range. (d) The rf curves for K and Na are identical at the bp of NH_3. At 274°K, the Na curve is slightly higher than the K curve, and at the highest temperature 298°K the Na curve is very much higher than the K curve throughout the range from a few thousandths to a few tenths molar.

The attempts to correlate the optical, chemical, electrical, thermodynamic, and magnetic properties of the solutions of alkali metals in liquid NH_3 by means of a model capable of quantitative analysis have been numerous. One model which has received considerable attention in recent years has consisted in supposing that the metal is dissociated into positive metal ions and electrons and that the electrons are trapped in cavities in the solvent. Moreover, it has been supposed that the electrons may be trapped singly or in pairs in these cavities, there being a reversible dissociation of the pairs on diluting the solutions. The pairs would pre-

TABLE III. Experimental data for K in liquid ND_3.

1 Serial No.	2 Sample No.	3 Concentration M mole l^{-1}	4 Amount alkali metal $\cdot 10^5$ $m \cdot 10^5$ mole	5 Temperature Celsius deg	6 Geometrical factor $\cdot 2$ $2R$	7 Capacitance $\cdot 10^{12}$ C farad	8 Modulation amplitude H_w gauss	9 Width maximum slope ΔH_{MS} gauss	10 Low field half area A_{LF} volt gauss	11 Molar susceptibility $\cdot 10^6$ $\chi_m \cdot 10^6$ mole l^{-1} cm^3	12 Susceptibility $\cdot 10^9$ $\chi \cdot 10^9$
1	K161	0.0329	2.05	29.5	...	...	0.0176	0.039	...	...	...
2	K162	0.0648	2.15	29.2	...	...	0.0176	0.035	...	...	...

sumably be in singlet states and therefore not contribute to the paramagnetism of the solutions. Such a model has its origins in the work of Kraus, was explicitly discussed by Freed and Sugarman[2] and was elaborated by Ogg.[5] Detailed discussions of the cavity trapping model and calculations based on it have been presented by Hill[1(e)] and quite recently by Lipscomb.[1(d)] Most recently, Kaplan and Kittel[1(c)] have discussed the model giving particular attention to the spin resonance results.

One of the questions on which light is shed by results of the paramagnetic resonance absorption experiments is that concerning the diamagnetism of these solutions. The diamagnetism of the electrons in the cavities is an effect which is inherent in the cavity model of the paramagnetic absorbers and one which cannot be measured in static field experiments or rf experiments taken by themselves. In the static field experiments, only the sum of the diamagnetic and paramagnetic susceptibilities is measured. The paramagnetic resonance experiment, as explained previously, gives just the paramagnetic part of the susceptibility. Comparison of the latter with the static measurements gives the diamagnetism associated directly with the paramagnetic species. On the basis of the cavity trapping model one may then form some opinion concerning the radii of the cavities which contain the electrons.

At the highest concentration for which there are available data from both the rf and static field experiments ($\sim 0.5\ M$) the value of χ_m from the former is $55 \cdot 10^{-6}$ and from the latter is $29 \cdot 10^{-6}$. At this concentration the pairing of the electrons is nearly complete, the rf data showing that the pairs are only 0.035 dissociated. (The temperature in question is the bp of NH_3.) We may, therefore, calculate the mean-square radius for the electron's distribution in the cavities in which the pairs are trapped assuming that the diamagnetism of two electrons in a cavity of given size is just twice that of a single electron in a cavity of the same size. Qualitative calculations have shown that a quite large correlation between the positions of the two electrons has only a small effect on the diamagnetism and the assumption is therefore probably quite good. Since $e^2 N_{Av}/6mc^2 = 2.829 \cdot 10^{10} \langle r^2 \rangle_{Av}$ we see that the difference in susceptibilities $26 \cdot 10^{-6}$ corresponds to $\langle r^2 \rangle_{Av} = 3.0A$. If now it is postulated that the cavities are spherical boxes and the electrons have vanishing probabilities of occurrence outside the boxes, it is found that the boxes must have a radius of $5.7A$. On the other hand, if one imagines the situation which must actually exist in which the wave functions pene-

TABLE IV. Spectroscopic splitting factors.[a]

1	2 Concentration mole l^{-1}	3 23 600 $\cdot 10^6$ cycle sec^{-1}	4 14 $\cdot 10^6$ cycle sec^{-1}	5 7 $\cdot 10^6$ cycle sec^{-1}
g_H/g_T	...	...	0.99973	0.99788 $\pm$0.00012
g_K/g_H	...	...	0.99882 $\pm$0.00007	...
g_K/g_T	0.0036	...	...	0.99906 $\pm$0.00012
g_K/g_T	...	...	0.99855 $\pm$0.00010	...
g_K/g_T	0.157	...	...	0.99909 $\pm$0.00006
g_K/g_T	0.180	...	...	0.99904 $\pm$0.00010
g_K/g_T	0.276	...	...	0.99906 $\pm$0.00006
$g_{K\ relT}$	...	...	2.0008	...
$g_{K\ relH}$	...	...	2.0013	...
$g_{K\ relP}$	...	2.0012	...	...
$g_{H\ relP}$	...	2.0037–2.0041[a]	...	...
$g_{T\ relP}$	...	2.0039	...	...

[a] Depending upon orientation of crystals.

Column — Entries

1 These are the symbols for the ratios of g factors and for relative g's. The symbols have the following meanings:
g_H g factor of hydrazyl.
g_T g factor of tris-p-nitrophenylmethyl.
g_K g factor of K in liquid NH_3.
$g_{K\ relY}$ where Y is H (hydrazyl) or T (tris-p-nitrophenylmethyl) $(g_K/g_Y) \cdot 2.0037$. (See references 13, 6, 14.)
$g_{X\ relP}$ where X is H (hydrazyl), T (tris-p-nitrophenylmethyl), or K (K in liquid NH_3) $\frac{\nu_{electron}}{\nu_{proton}} \cdot 3.0420 \cdot 10^{-3}$. (See references 15, 16.) (Proton and electron resonances were both measured in the same field.)
2 These are the concentrations of solutions of K in liquid NH_3; unit, mole l^{-1}.
3 These are the values of the corresponding entries in column 1 measured at a frequency of 23 600 $\cdot 10^6$ cycle sec^{-1}.
4 These are the values of the corresponding entries in column 1 measured at a frequency of 14 $\cdot 10^6$ cycle sec^{-1}.
5 These are the values of the corresponding entries in column 1 measured at a frequency of 7 $\cdot 10^6$ cycle sec^{-1}.

[13] Holden, Kittel, Merritt, and Yager, Phys. Rev. **77**, 147 (1950).
[14] Hutchison, Pastor, and Kowalsky, J. Chem. Phys. **20**, 524 (1952).
[15] H. Taub and P. Kusch, Phys. Rev. **75**, 1481 (1949).
[16] J. Schwinger, Phys. Rev. **73**, 416 (1948).

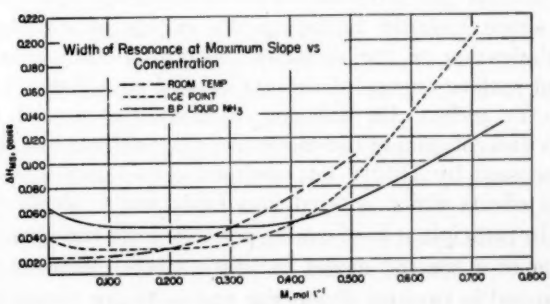

FIG. 6.

TABLE V. Experimental values of saturation factor f and width at maximum slope ΔH_{MS} as a function of concentration at room temperature for K in liquid NH_3.

1 Sample No.	2 Concentration mole l^{-1}	3 rf Field gauss	4 *Max. Defl.* Mod. Amp. volt gauss^{-1}	5 ΔH_{MS} gauss	6 f
K57	0.0135	(0.000)	(43.5)[a]	···	1.127
		0.010	33.6	0.022	
		0.021	25.5	0.027	
K53	0.0138	0.037	18.2	0.028	
		0.048	14.8	0.034	
		0.080	5.42	0.048	
K73	~0.02	(0.000)	(42.6)[a]	···	1.124
		0.005	37.9	0.021	
		0.010	33.7	0.021	
		0.021	24.8	0.024	
		0.031	18.4	0.031	
		0.041	13.2	0.033	
		0.062	4.0	0.044	
K88	0.152	(0.000)	(178.0)[a]	···	1.094
		0.004	166.0	0.031	
		0.010	147.0	0.033	
		0.021	116.0	0.034	
		0.041	68.8	0.039	
K166	0.380	(0.000)	(55.7)[a]	···	1.016
		0.005	54.8	0.058	
		0.010	53.7	0.058	
		0.021	50.5	0.059	
		0.041	38.9	0.065	
		0.062	28.4	0.073	
		0.072	22.4	0.078	
		0.082	18.1	0.084	

[a] By extrapolation.

trate the dielectric to some distance it will be seen that the cavities would be somewhat smaller than this.

The experimental data on volumes of dilute solutions of Na in liquid NH_3 show an increase in volume of $71A^3$ per dissolved Na.[1(d)] If this volume is increased by amounts necessary to account for the difference in volumes of Na^+ and Na and also to take account of the electrostriction caused by the Na^+ the volume to be accounted for by cavities in the NH_3 is $143A^3$ according to Lipscomb.[1(d)] This leads to $3.2A$ as the experimental cavity radius of the singly trapped electrons. If one minimizes the sum of the electron energy and dielectric polarization energy of a single electron trapped in a box in a dielectric he finds $h^2/2me^2$ or $10.3A$ as the radius of the cavity with a single electron, and the size of the cavities containing two such electrons would be considerably larger. However, Lipscomb[1(d)] has carried out a detailed calculation of the size of the cavity containing a single electron including the effects of electronic polarization of the dielectric, electrostriction energy, and surface energy of the cavity and gets about $4.8A$ as the radius. He did not calculate the size of the cavities containing two electrons; this problem has been discussed by Hill[1(e)] but without consideration of all the effects which entered into Lipscomb's calculation.

In principle it is of course possible from the assumption of a specific model in which single electrons are trapped in cavities of one size and pairs are trapped in cavities of another size, to determine the sizes of both by means of a comparison of the static and rf data. The slope of the plot of (a) the difference between the molar susceptibility calculated from rf data and the static molar susceptibility *versus* (b) the ratio of the rf molar susceptibility to $N_{Av}\beta^2/kT$ is just $N_{Av}e^2/6mc^2$ times the difference between the mean-square radii of the two different cavities. Unfortunately, however, the static field data in the region from 0.1 M to 0.5 M are not sufficiently numerous to fix the curve of susceptibility *versus* concentration with sufficient precision for any meaningful comparison with the rf data. It is clear that if the single traps and double traps are of the same size, then the difference between the susceptibilities calculated from rf data and the static molar susceptibilities should be constant over the entire range of concentrations which have been investigated. This is just about the case for the difference between the rf data on Na or K and the static data on Na, the latter being available over a much wider range of concentrations than are the static K data. However the Na static data are apparently less precise than the corresponding data on K.

It may be said that the value for the size of the cavities in which pairs are trapped, $\langle r^2\rangle_{Av}^{\frac{1}{2}}=3.0A$, as determined from comparison of the rf and static field susceptibility data are in reasonably good agreement with Lipscomb's calculated value $4.8A$[1(d)] for the radius of the cavities containing single electrons assuming no penetration of the dielectric or with the experimental value $3.2A$ for the radius of these cavities as determined from measurements of volume changes.

The question of the manner in which the susceptibility should vary with concentration is one which has been examined in detail by Hill[1(e)] and very recently by Kaplan and Kittel.[1(c)] Hill[1(e)] has considered the transition from trapped pairs to trapped single electrons to be a simple dissociation equilibrium and has given both a classical and a quantum-mechanical discussion of the manner in which the extent of dissociation and hence the magnetic susceptibility should vary with concentration. Hill[1(e)] evaluated the interaction energy for two electrons in a cavity using first order perturbation theory, and was led to the conclusion that the energy of trapped pairs was greater than the energy of trapped single electrons. He pointed out, however, that treating the species involved as ideal classical gases the extent of dissociation would still increase with temperature. It should also be remarked that he neglected the surface energy and electrostriction effects which were considered by Lipscomb.[1(d)] He then made a calculation using Bose-Einstein statistics for the pairs and Fermi-Dirac statistics for the single electrons and found that at a temperature equal to 220°K, a concentration equal to 0.1 M and a ratio of the energy of trapped pair to twice that of a singly trapped electron equal to 4, that 0.28 of the trapped electrons are singly trapped and the remainder are held as pairs. The rf value of $\chi_m kT/N_{Av}\beta^2$

TABLE VI. Experimental values of degree of dissociation α; α times the square root of concentration, $\alpha M^{\frac{1}{2}}$; and one half the square root of the equilibrium constant for the reaction $e_2^{=}=2e^{-}$, $\alpha M^{\frac{1}{2}}/(1-\alpha)^{\frac{1}{2}}$, as functions of concentration and temperature.

1	2	3	4	5	6	7	8	9	10	11
Concentration M mole l^{-1}	α 240°K	α 274°K	α 298°K	$\alpha M^{\frac{1}{2}}$ 240°K mole$^{\frac{1}{2}}$ $l^{-\frac{1}{2}}$	$\alpha M^{\frac{1}{2}}$ 274°K mole$^{\frac{1}{2}}$ $l^{-\frac{1}{2}}$	$\alpha M^{\frac{1}{2}}$ 298°K mole$^{\frac{1}{2}}$ $l^{-\frac{1}{2}}$	$\frac{\alpha M^{\frac{1}{2}}}{(1-\alpha)^{\frac{1}{2}}}$ 240°K mole$^{\frac{1}{2}}$ $l^{-\frac{1}{2}}$	$\frac{\alpha M^{\frac{1}{2}}}{(1-\alpha)^{\frac{1}{2}}}$ 274°K mole$^{\frac{1}{2}}$ $l^{-\frac{1}{2}}$	$\frac{\alpha M^{\frac{1}{2}}}{(1-\alpha)^{\frac{1}{2}}}$ 298°K mole$^{\frac{1}{2}}$ $l^{-\frac{1}{2}}$	W ev
0.002	0.822	0.953	0.968	0.0367	0.0426	0.0433	0.0970	0.195	0.243	0.101
0.006	0.616	0.858	0.905	0.0477	0.0665	0.0701	0.0760	0.176	0.228	0.120
0.012	0.455	0.735	0.816	0.0498	0.0805	0.0893	0.0675	0.156	0.208	0.122
0.020	0.331	0.620	0.709	0.0469	0.0877	0.1003	0.0573	0.142	0.186	0.129
0.028	0.255	0.541	0.630	0.0426	0.0905	0.106	0.0494	0.134	0.174	0.138
0.036	0.205	0.483	0.573	0.0388	0.0915	0.109	0.0435	0.127	0.166	0.147
0.045	0.168	0.431	0.517	0.0357	0.0913	0.110	0.0391	0.121	0.158	0.154
0.060	0.134	0.364	0.446	0.0327	0.0891	0.109	0.0351	0.112	0.147	0.158
0.080	0.112	0.305	0.390	0.0317	0.0862	0.110	0.0337	0.103	0.141	0.156
0.100	0.0979	0.258	0.359	...	...	...	...	...	...	...
0.120	0.0883	0.229	0.328	0.0306	0.0793	0.114	0.0320	0.0903	0.139	0.167
0.160	0.0768	0.186	0.281	0.0307	0.0743	0.113	0.0319	0.0824	0.133	0.153
0.200	0.0697	0.155	0.246	0.0312	0.0693	0.110	0.0324	0.0754	0.127	0.146
0.300	0.0544	0.113	0.188	0.0298	0.0621	0.103	0.0306	0.0659	0.115	0.140
0.400	0.0435	0.0928	0.157	0.0275	0.0587	0.100	0.0281	0.0617	0.108	0.142
0.500	0.0352	0.0848	0.143	0.0249	0.0600	0.101	0.0254	0.0627	0.109	0.137

is (extrapolating the data to 220°K from the plots of $d\ln[\alpha M^{\frac{1}{2}}/(1-\alpha)^{\frac{1}{2}}]/dt$ *versus* $1/T$ mentioned below) found to be 0.063 which is considerably lower than Hill's estimate. On the other hand, Hill finds that if the energy ratio be taken as 1/1.4 instead of 4 the fraction of the electrons that are singly trapped is 0.14 which is considerably closer to the observed value. At 300°K for the first choice of the energy ratio Hill gets 0.36 as the fraction dissociated and the rf experiments give 0.36 for this fraction. The smaller value of the energy ratio would give a much smaller fraction. For a solution with concentration 0.2 M but with other conditions the same as in the first case Hill gets 0.16 dissociation and the experimental results are about 0.05. The classical calculation for the first set of conditions gives 0.42 as the fraction of electrons singly trapped which is in much worse disagreement with the rf data than is the other calculation. The value 1/1.4 for the energy ratio used above corresponds to 0.14 ev for the difference between $\frac{1}{2}$ the energy of a trapped pair and the energy of a singly trapped electron. This is in quite good agreement with the value of this energy calculated from the temperature dependence of the rf data as discussed below.

Kaplan and Kittel[1(c)] have proposed a detailed model for which minimization of the free energy leads to the expression

$$[1+\alpha^2(e^{2w/kT}-1)]/(1-\alpha)=2N/n, \qquad (1)$$

in which α is the ratio of χ_m as determined in the rf experiments to the free electron spin susceptibility, namely $N_{Av}\beta^2/kT$; $2W$ is the difference in energy between a pair of trapped electrons and two singly trapped electrons; N is the total available number of trapping sites, and n is the total number of trapped electrons, i.e., the total number of dissolved alkali metal atoms. Since at all concentrations investigated in the present rf work $e^{2w/kT}\gg 1$ we may write

$$(1+\alpha^2e^{2w/kT})/(1-\alpha)\simeq 2N/n. \qquad (2)$$

From the lowest concentrations up to somewhat higher than 0.5 M it is true that $\alpha^2e^{2w/kT}\gg 1$ and with error no greater than 10 percent over this range one may write

$$\alpha^2e^{2w/kT}/(1-\alpha)\simeq 2N/n. \qquad (3)$$

This is just the expression, as far as concentration dependence is concerned, that would result from the consideration of a simple dissociation equilibrium between doubly and singly trapped electrons, i.e.,

$$\alpha^2M/(1-\alpha)=\text{constant}$$

in which M is the concentration and α is the fraction dissociated which in the present case on the basis of the cavity trapping model is just $\chi_m kT/N_{Av}\beta^2$. The constancy of this product is examined in Table VI. Kaplan and Kittel[1(c)] have in their paper chosen to discuss their model in terms of a still further approximation $\alpha\ll 1$ which is seen from Table VI to be good to within 10 percent only down to 0.1 M. The constancy of $\alpha M^{\frac{1}{2}}$ is examined in Table VI. It will be seen that this last approximation gives considerably better agreement than does the better approximation mentioned above.

It is to be noted that at the bp of NH_3 the static magnetic susceptibilities calculated from rf data are indistinguishable for K and Na within the errors of the experiments in the range of concentration investigated. This fact is, of course, in agreement with the predictions of all of the models that have been discussed inasmuch as they assume the metal to be completely dissociated into positive ions and trapped electrons and the magnitude of the paramagnetism is determined

only by the extent of the electron pairing. Thus, the positive ions play no role in determining the magnetization. It will be seen, however, from Tables I and II and Figs. 1 and 2 that as the temperature is raised, a difference between the Na and K appears which increases with temperature. At 0.100 M the susceptibility of Na is about 15 percent greater than that of K at 274°K and about 50 percent at 298°K. Apparently some effect of the alkali metal ions on the relative numbers of singly and doubly trapped electrons must be taken into consideration. Whether Debye-Huckel type interactions would be sufficient to account for these pronounced effects or whether it would be necessary to introduce the idea of electrons trapped on positive metal ions to form metal atoms, and in equilibrium with singly and doubly trapped electrons, is not clear.

The variation of the susceptibility with temperature is of interest in the examination of any of the models. The Hill[1(e)] relation requires that

$$d\ln\frac{\alpha^2M}{1-\alpha}\Big/dT=d\ln K/dT=1/T(\tfrac{3}{2}+2W/kT),$$

whereas Kaplan and Kittel[1(c)] speak only of the exponential term in T and one would write in this case for the approximation (3) the expression

$$d\ln\frac{\alpha^2M}{1-\alpha}\Big/dT=2W/kT^2.$$

Plots of $\log[\alpha M^{\frac{1}{2}}/(1-\alpha)^{\frac{1}{2}}T^{\frac{3}{4}}]$ *versus* $1/T$ and $\log[\alpha M^{\frac{1}{2}}/(1-\alpha)^{\frac{1}{2}}]$ *versus* $1/T$ gave only slightly curved lines over the range of three temperatures and the slopes were about the same in either case and varied very little with concentration. The values of W calculated from the plots of $\log[\alpha M^{\frac{1}{2}}/(1-\alpha)^{\frac{1}{2}}]$ *versus* $1/T$ are given in Table VI. The values for $\frac{1}{2}$ the dissociation energy of pairs to form singly trapped electrons according to these plots range from 0.10 ev at the lowest concentrations to a maximum of about 0.17 ev at about $0.1M$ and then drop to slightly lower values at the higher concentrations. The plots of $\log[\alpha M^{\frac{1}{2}}/(1-\alpha)^{\frac{1}{2}}T^{\frac{3}{4}}]$ *versus* $1/T$ gave values of W which were essentially the same as those in Table VI.

SPECTROSCOPIC SPLITTING FACTORS

Three important observations concerning the spectroscopic splitting factors or g's for K are that (a) they are independent of concentration in the vicinity of $7\cdot10^6$ cycle sec^{-1}; (b) they are the same at the frequencies $23\,500\cdot10^6$ cycle sec^{-1} and $7\cdot10^6$ cycle sec^{-1} if the g's of the standard comparison substances are not different at these two frequencies; and (c) they have the value 2.0012 ± 0.0002. The fact that they are independent of concentration over a rather wide range is indicative of the fact that the electron is bound in the same manner at all concentrations. The value of the g is about 0.0011 lower than the free electron value 2.0023. As has been indicated by Kaplan and Kittel[1(c)] this is compatible with binding on the protons of the NH_3 molecules surrounding the cavity in analogy with the binding that has been found by magnetic resonance experiment to exist for the electrons trapped in vacancies in alkali halide crystals to form F centers.[17,18] The Bloch-Siegert[19] effect which results in a shift of the center of resonance by the factor

$$1-[(2H_1)^2/16H_0^2]=1-1.6\cdot10^{-7}$$

is too small to be of importance in this connection.

WIDTHS

One of the most striking features of this resonance is its extreme sharpness. There is evidently an extraordinarily large narrowing associated with exchange effects and with the great mobility of the electrons in these solutions. Abrahams and Kittel[20] find that for n_1 spins per cm^3 distributed randomly on a simple cubic lattice the dipole-dipole width should be about $n_1\cdot10^{-19}$ gauss. This would give as the width 4.3 gauss at 0.5 M, 2.16 gauss at 0.1 M and 0.84 gauss at 0.02 M which makes it clear that the narrowing is very large. Kaplan and Kittel[1(c)] discuss the effect of the rapid diffusion of the singly trapped electrons on the dipole-dipole width using the methods of Bloembergen, Purcell, and Pound[12] and find that below 0.1 M the diffusion narrowed dipole-dipole broadening is very small compared with the observed widths, but that such broadening might be responsible for the increased widths at the higher concentrations.

It has been seen that the spin-lattice relaxation time T_1 is of such a magnitude that it is not more than 2 to 5 times greater than the inverse line width time T_2. Kaplan and Kittel[1(c)] have considered the problem of the broadening caused by nuclear hyperfine structure which has proved to be very important in the case of the electrons trapped in vacancies in the alkali halides.[21] Motional narrowing must be considered here also and the conclusion reached is that the broadening for electrons trapped on the protons surrounding the cavity might be expected to be of order 10 gauss for a rigid structure. However, Kaplan and Kittel[1(c)] estimate that the rotational relaxation fluctuations might narrow the line to 0.03 gauss at the bp of NH_3. This is not too far from the observed widths. They also estimate that the characteristic frequency ω_c of the fluctuations is about 10^{11} radian sec^{-1}. Since in the present experiments ω is approximately $4\cdot10^7$ radian sec^{-1}, it is clear that $\omega\tau_c\ll1$. Bloembergen, Pound, and Purcell[12] have

[17] A. H. Kahn and C. Kittel, Phys. Rev. **89**, 315 (1953).
[18] C. A. Hutchison, Jr. and G. A. Noble, Phys. Rev. **87**, 1125 (1952).
[19] F. Bloch and A. Siegert, Phys. Rev. **57**, 522 (1940).
[20] C. Kittel and E. Abrahams, Phys. Rev. **90**, 171 (1953).
[21] Kip, Kittel, Levy, and Portis, Phys. Rev. **91**, 1066 (1953).

shown that when this condition obtains one would expect that $T_1 \cong T_2$. This is seen to be in agreement with the present experimental observation that for K in liquid NH_3 T_1 is not much larger than T_2.

It should be pointed out that the variation of the width at infinite dilution would be expected to vary with temperature inversely as the ratio of the temperature to the viscosity. This relation will be seen to be nearly quantitatively obeyed for the three temperatures which were investigated.

It should also be remarked that the rapid rise of the widths at the higher concentrations may perhaps be associated with the increasing electrical conductivity. Actually the very rapid rise begins at each temperature at just the concentration at which the skin depth is about 1 cm and this is the order of the linear dimensions of the samples.

The preliminary data on solutions of K in ND_3 gave at two concentrations widths which are considerably greater than those for K in NH_3. Two effects at least are to be considered. One is that the deuteron nuclear magnetic moment is much smaller than that of the proton, and we might therefore expect somewhat sharper absorptions because of residual effects of the nuclear hyperfine structure which are not washed out by the motional processes mentioned above. The other is that the zero-point vibrational frequency of the deuterons is very much less than that of the protons and that the inversion frequency of ND_3 is very much less than that of NH_3 and these effects might result in considerably less motional narrowing and thus lead to broader lines. Actually the interpretation of the experimental results is very much beclouded by the fact that the viscosity of ND_3 is unknown and in particular the viscosities of solutions of K in ND_3 must be measured before an interpretation of the results can be given. In any event there is probably no marked narrowing of the line at comparable viscosities and the two effects on the width probably cancel each other to a considerable extent.

The change of width with rf coil voltage begins only at voltages considerably higher than that employed in the determination of the rf susceptibilities. In the case of a resonance as sharp as that of the alkali metals in liquid NH_3 one must consider the Rabi width associated with the flipping of the spin by the perturbing rf magnetic field. For very small rf fields such as were used in these experiments the Rabi width is just $\sqrt{2}\cdot$rms rf field strength or for the conditions of the present experiments $0.147\cdot$rms coil voltage. The operating coil voltage was 0.05 volt so that the Rabi width was about 0.006 gauss. This is not less by a very great factor than the width of the narrowest resonances, namely 0.020 gauss.

SHAPES

The shapes of the resonances are very close to Lorentzians and deviate greatly from the Gaussians.[1(a)] For absorptions down to 0.2 to 0.1 of the maximum the Lorentzian curve is followed closely and then at lower absorptions the experimental curve drops appreciably below the Lorentzian. This is in agreement with the theory of Anderson and Weiss.[22]

SATURATION

The spin-lattice relaxation times determined by the method of Bloembergen, Purcell, and Pound[12] from the variation of the output voltage of the phase-sensitive detector with rf coil voltage are several times as large as the times corresponding to the widths of the absorption lines. The fact that these determinations give relaxation times of the same order of magnitude as the inverse line width times indicates that the spin-lattice relaxation may make a considerable contribution to the observed widths. No calculations of spin-lattice relaxation times on the basis of the cavity trapping model have been made.

ACKNOWLEDGMENTS

Most of the electronic equipment employed in these experiments was designed and constructed by Clarence Arnow. Edward Bartal constructed the solenoid and its mounting and did other necessary machine work. Jack Boardman carried out a large part of the numerical integrations and other calculations. Arthur Kowalsky synthesized the tris-*p*-nitrophenylmethyl and analyzed it. Their help and assistance is gratefully acknowledged.

[22] P. W. Anderson and P. R. Weiss, Revs. Mod. Phys. **25**, 269 (1953).

Temperature Independent Factor in the Relative Rates of Isotopic Three Center Reactions*

JACOB BIGELEISEN AND MAX WOLFSBERG
Chemistry Department, Brookhaven National Laboratory, Upton, Long Island, New York

(Received June 15, 1953)

It is shown that the theoretical equation for the ratio of the rate constants of isotopic molecules is essentially independent of whether the crossing of the barrier is treated as a translation or a vibration. The temperature independent factor in this equation is evaluated for the case of substitution or displacement reactions. Calculations are presented for several cases involving the isotopes of carbon where there is simultaneous bond rupture and bond formation.

INTRODUCTION

IN a previous publication by one of us[1] (hereinafter referred to as BI) a general expression was derived for the relative rates of reaction of isotopic molecules. The basis for the derivation is the transition state hypothesis. If one neglects the effect of isotopic substitution on the transmission coefficient, K, the equation for the ratio of the specific rate constants,

$$k_1/k_2=(K_1/K_2)(m_2^*/m_1^*)^{\frac{1}{2}}(f/f^{\neq}) \tag{1}$$

consists of a temperature independent factor, $S(m_2^*/m_1^*)^{\frac{1}{2}}$, and a temperature dependent one, $(1/S)(f/f^{\neq})$. S is a classical statistical factor, and the other symbols have been previously defined in BI.

In the applications of Eq. (1) to specific systems,[2] the ratio $(m_2^*/m_1^*)^{\frac{1}{2}}$ has usually been evaluated by the consideration of simple bond rupture or bond formation processes. The method of evaluation, furthermore, utilizes a correspondence pointed out by Slater[3] between the "effective mass" in the transition state formalism and the mass coefficient associated with the Pelzer-Slater reaction coordinate in the kinetic energy expression. Since many reactions, such as substitution and displacement, involve simultaneous bond formation and rupture, we have investigated the form of the "effective mass" term for such reactions. We also consider it appropriate to state explicitly the relationship between Eq. (1) and essentially similar equations which are derivable with different assumptions.

THE CROSSING OF THE BARRIER

In addition to the usual assumptions of the transition state hypothesis, Eq. (1) results from the treatment of the crossing of the barrier as a translation while the partition function corresponding to this motion is treated as a vibration. This apparent inconsistency, which is not unique in this application, can be shown to be of little consequence in the present case. The principal reason for this is simply that the usual potential surfaces lead to a low imaginary frequency, which then behaves like a translation. If we treat both the motion across the barrier[4] and its associated partition function as a vibration, then the method discussed in BI leads to

$$k_1/k_2=(K_1/K_2)(\nu_{1i}/\nu_{2i})(f/f^{\neq}), \tag{2}$$

where ν_i is the imaginary frequency obtained from the solution of the secular equation. If the "effective mass" is defined as the mass coefficient of ν_i, Eqs. (1) and (2) are identical.

We may alternately treat both the motion across the barrier and its associated partition function as a translation. In this case it is convenient to start with the Eyring equation[5]

$$k=K\frac{kT}{h}\frac{Q'^{\neq}}{Q_AQ_B\cdots}, \tag{3}$$

where Q_A, Q_B, etc., are the complete partition functions of the reactants and $Q'^{\neq}$, the partition function of the activated complex, includes translations, rotations and $3n-7$ real vibrations but excludes the motion across the barrier.

If we limit the potential functions of the reactants and the activated complex to quadratic terms, then for isotopic substitution one obtains from Eq. (3) by the method of BI

$$k_1/k_2=(K_1/K_2)(\nu_{1i}/\nu_{2i})f/f_N^{\neq}, \tag{4}$$

where

$$f_N^{\neq}\equiv S_1^{\neq}/S_2^{\neq}\prod^{3n-7}\frac{u_{2j}^{\neq}}{u_{1j}^{\neq}}e^{\Delta u_j^{\neq}/2}\frac{(1-e^{-u_{1j}^{\neq}})}{(1-e^{-u_{2j}^{\neq}})}. \tag{5}$$

If, in the evaluation of Eq. (3), one utilizes the Pelzer[6]-Slater[3] treatment of the transition state vibrations, a result similar to (4) is obtained but the significance of the terms is altered.

The Pelzer-Slater potential takes the form

$$V=V_0+\tfrac{1}{2}b_Lx_L^2+\tfrac{1}{2}\sum_{i,j}^{n}b_{ij}x_ix_j, \tag{6}$$

where the b's are force constants, x_i and x_j are internal

* Research carried out under the auspices of the U. S. Atomic Energy Commission.

[1] J. Bigeleisen, J. Chem. Phys. **17**, 675 (1949).

[2] For a recent summary see J. Bigeleisen, J. Phys. Chem. **56**, 823 (1952).

[3] N. B. Slater, Proc. Roy. Soc. (London) **A194**, 112 (1948).

[4] See Glasstone Laidler, and Eyring, *The Theory of Rate Processes*. (McGraw-Hill Book Company, Inc., New York, 1941), p. 189.

[5] H. Eyring, J. Chem. Phys. **3**, 107 (1935).

[6] H. Pelzer, Z. Elektrochem. **39**, 608 (1933).

coordinates not involving motion across the barrier, and x_L is the coordinate for crossing of the barrier. Solution of the secular equation at a fixed value of x_L with this potential leads to $3n-7$ solutions, $\omega_i^{\neq}$'s, which are not quite normal vibrations in the usual sense and involve no motion along the reaction coordinate.[7] The Pelzer-Slater method, together with Eq. (3), and the method outlined in BI leads to

$$k_1/k_2=(K_1/K_2)(\nu_{1L}/\nu_{2L})f/f_L^{\neq} \tag{7}$$

for the ratio of the rate constants of isotopic molecules. $f_L^{\neq}$ is similar to $f_N^{\neq}$ except that the normal frequencies used in $f_N^{\neq}$ are replaced by the $\omega^{\neq}$'s discussed above. ν_L is the ratio of the $3n-6$ normal vibrations, obtained by allowing x_L to vary, to the $3n-7\omega^{\neq}$'s obtained at a fixed x_L. Alternately ν_L is the frequency obtained when all the coordinates, x_i, except x_L are constrained to a fixed value. Both Eqs. (4) and (7) differ formally from Eqs. (1) or (2) by a factor of

$$1\Big/\left(\frac{\nu_{2\,i,\,L}^{\neq}}{\nu_{1\,i,\,L}^{\neq}}e^{\Delta u_{i,L}^{\neq}/2}\frac{(1-e^{-u_{1i,L}^{\neq}})}{(1-e^{-u_{2i,L}^{\neq}})}\right).$$

For an imaginary frequency where $u_{i,L}$ is less than $3i$, this factor becomes

$$\left\{1+\frac{1}{24}(|u_{2i,L}^{\neq}|-|u_{1i,L}^{\neq}|)\right\}.$$

This is just equal to the Wigner tunnelling correction, and it might be argued that Eqs. (1) and (2) contain a quantum correction for the crossing of the barrier. This quantum correction is negligible except in the case of the isotopes of hydrogen. In the latter case the Wigner tunnelling correction may be inadequate *per se*.

These considerations serve to establish the essential equivalence of the different methods of approach, but point out an intrinsic difference between the Pelzer-Slater coordinates and the usual normal coordinates.

THREE CENTER REACTIONS

Consider three atoms A, B, and C, involved in a chemical reaction, which breaks a bond between atoms B and C and forms the $A-B$ bond. Since the reaction coordinate, x_L, increases monotonically as the reaction proceeds, it may be written by the extension of a method developed by Slater[7] for simple bond rupture,

$$x_L=\alpha|\mathbf{r}_B-\mathbf{r}_C|-\beta|\mathbf{r}_B-\mathbf{r}_A| \tag{8}$$

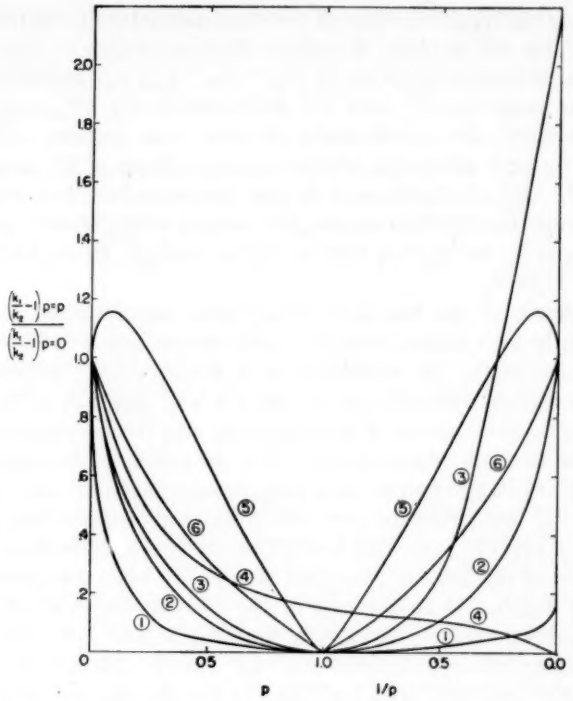

FIG. 1. Plot of the ratio $(k_1/k_2-1)_{p=p}/(k_1/k_2-1)_{p=0}$ as a function of p or $1/p$. The curves are for the following cases:

(1) $m_B=m_C=12$, $m_A=1$, $m_{B'}=14$

(2) $m_A=m_B=m_C=12$, $m_{B'}=14$

(3) $m_B=m_C=12\ll m_A$, $m_{B'}=14$

(4) $m_B=m_C=12$, $m_A=1$, $m_{C'}=13, 14$

(5) intramolecular isotope effect $m_A=m_B=m_C=12$, $m_{A'}=m_{C'}=13, 14$

(6) intramolecular isotope effect $m_B\gg m_A=m_C=12$, $m_{A'}=m_{C'}=13$.

where r_B-r_C and r_B-r_A are the separation of B and C and B and A, respectively, and β/α determines the relative amount of bond formation between A and B to bond extension between B and C. Then irrespective of the nature of the other coordinates, the reaction coordinate, x_L, leads to a frequency, ν_L, which depends on the masses of A, B, and C alone.

$$\nu_L\alpha\{\alpha^2(m_B^{-1}+m_C^{-1})+\beta^2(m_B^{-1}+m_A^{-1})-2\alpha\beta m_B^{-1}\}^{\frac{1}{2}}. \tag{9}$$

For simultaneous bond rupture and bond formation Eq. (7) therefore takes the form

$$k_1/k_2=K_1/K_2\left\{\frac{(m_{B1}^{-1}+m_{C1}^{-1})+p(m_{B1}^{-1}+m_{A1}^{-1})-2p^{\frac{1}{2}}m_{B1}^{-1}}{(m_{B2}^{-1}+m_{C2}^{-1})+p(m_{B2}^{-1}+m_{A2}^{-1})-2p^{\frac{1}{2}}m_{B2}^{-1}}\right\}^{\frac{1}{2}}f/f_7^{\neq} \tag{10}$$

where $p=\beta^2/\alpha^2$. The method can analogously be extended to systems of greater complexity.

When p is equal to zero, Eq. (9) reduces to the simple case of bond rupture, while, when $1/p$ is equal to zero, it becomes the combination of two atoms, molecules, or radicals. The case of p equal to unity is of interest for this involves no motion of the atom B. ν_L will, therefore, show no effect on isotopic substitution for atom B when p equals unity.

In Fig. 1 we present a graph of the ratio $(\nu_{1L}/\nu_{2L}^{-1})_{p=p}/$

[7] See reference 3 and N. B. Slater, Proc. Leeds Philosophical Soc. 5, 75 (1949).

$(\nu_{1L}/\nu_{2L}^{-1})_{p=0}$ for some of the most important cases involving the isotopes of carbon. It is interesting to note that the ratio $(\nu_{1L}/\nu_{2L})_{p=p}/(\nu_{1L}^{-1}/\nu_{2L}^{-1})_{p=0}$ is practically the same for C^{13} and C^{14} substitution for C^{12}, and, therefore, the consideration of three atom systems will in no way affect the relative isotope effects of C^{14} and C^{13}. Also of significance is the fact that in all cases, except for the intramolecular isotope effect shown as curve 5, the curves fall off rather steeply from $p=0$ or $1/p=0$.

Some of the reactions which have been studied recently for carbon, nitrogen, and oxygen isotope effects which might be considered as a three center reaction are the decarboxylation of malonic and mesitoic acids, the deammonation of phthalamide, and the decomposition of ammonium nitrate.[8] The decarboxylation studies are in agreement with calculations based on simple C—C bond rupture and, therefore, correspond closely to p equal to zero. This is also the case in the deammonation of phthalamide and has previously been discussed on this basis.[9] In the case of the decomposition of ammonium nitrate, Friedman and Bigeleisen[10] give two theoretical calculations for the kinetic fractionation of O^{18} between N_2O and H_2O in the decomposition of ammonium nitrate. The fractionation factor of 1.034 corresponds to p equal to zero, while the one 1.026 corresponds to p equal to 0.012. The experimental fractionation factor of 1.023 corresponds to p equal to 0.021. In essence their calculations show that p is very close to zero. The steep dependence of k_1/k_2 on p in this case makes the theoretical fractionation factor a sharp function of p. Precise agreement between an *a priori* model and experiment is, therefore, not to be expected. There is, however, little difference in the motion described by $p=0.012$ and $p=0.021$.

[8] See reference 2 for references to the literature on these studies.
[9] J. Bigeleisen, Can. J. Chem. **30**, 443 (1952).
[10] L. Friedman and J. Bigeleisen, J. Chem. Phys. **18**, 1325 (1950).

The reaction coordinate parameter, $p^{\ddagger}$, which determines the relative amount of bond formation to bond rupture is by definition independent of the masses of the adjoining atoms A, B, and C. A similar ratio can also be calculated from the normal coordinate corresponding to the imaginary frequency, ν_i, in the conventional manner. In the latter method the normal coordinate changes with isotopic substitution, and therefore the ratio of the amount of bond formation to bond rupture also varies with isotopic substitution. This is, therefore, an inherent difference in the two methods, which is, however, of little consequence. A comparison of the two methods can readily be made for the extreme case of the reactions of the isotopic hydrogen atoms and molecules. The potential energy surface of Eyring and Polanyi,[11] as well as subsequent ones, gives a large value for p (about 75) at the activation point. If we intercompare the relative values of ν_L, calculated from Eq. (9), with those of ν_i, from the potential surfaces of Hirschfelder, Eyring and Topley[12] or Farkas and Wigner,[13] good agreement is found between the ν_L's and the ν_i's irrespective of whether p is kept constant in accord with definition or is varied to coincide with the normal coordinate corresponding to the ν_i of each isotopic reaction. A similar result is obtained for the reactions of halogen atoms with the isotopic hydrogen molecules. In view of the insensitivity of ν_L to possible variations of p which might result from a change in the normal modes by isotopic substitution, as well as the fact that the assumption of harmonic motion is clearly a crude one, the definition of p as independent of isotopic substitution appears to be a fairly good approximation.

[11] H. Eyring and M. Polanyi, Z. physik. Chem. **B12**, 279 (1931).
[12] Hirschfelder, Eyring, and Topley, J. Chem. Phys. **4**, 170 (1936).
[13] L. Farkas and E. Wigner, Trans. Faraday Soc. **32**, 708 (1936).

THE JOURNAL OF CHEMICAL PHYSICS VOLUME 21, NUMBER 11 NOVEMBER, 1953

Lattice Dynamics of Body-Centered and Face-Centered Cubic Metallic Elements

JULES DE LAUNAY
Naval Research Laboratory, Washington, D. C.
(Received June 19, 1953)

The body-centered and face-centered cubic monatomic metals are represented by a model consisting of an ion point lattice embedded in an electron gas. The Born-von Kármán lattice dynamics are modified to include the role which the conduction electrons play in acoustical wave motion. This leads to relations connecting the dynamic parameters with the elastic constants, and yields the Fuchs relations in an elementary manner. The discrepancy in the Cauchy relation is shown to be just the bulk modulus of the electron gas.

In studying the contribution of the conduction electrons to the thermal motion, two extreme cases are treated: 1.—the electron gas does not partake of the thermal motion appreciably; 2.—the electron gas follows the ion motion almost exactly. The secular equations are given for both cases. The Debye characteristic temperature in the T^3 region of atomic heat is computed analytically for both cases when the departure of the elastic constants from the isotropy condition is not too large.

I. INTRODUCTION

THE Born-von Kármán theory of lattice dynamics[1] was revived by Blackman[2] in 1935, some twenty-three years after its inception. The simplicity of the rival Debye theory as well as its immediate success in representing early data distracted attention from the more complicated treatment of Born and von Kármán. But as more and more low-temperature calorimetric data became available during the period 1912–1935, it became apparent that the Debye theory could not be made to fit the experimental data adequately. One sensitive way to demonstrate how well the data fit the Debye theory is to compute the Debye characteristic temperature Θ for each value of the atomic heat at constant volume, C_V, and plot Θ *versus* the temperature T. If the Debye theory satisfactorily represents the data, the result is a straight line parallel to the T axis indicating a constant Θ. It became important to know whether the observed deviations from constant Θ should all be sought in special phenomena, or whether some deviation was to be expected from the simple fact that the Debye theory is not completely adequate to account for the contribution of the lattice vibrations. Thus, Blackman[2] made some computations for a two-dimensional square lattice using the Born-von Kármán theory and showed qualitatively that deviations from Θ=constant could be expected from lattice theory alone. These computations were later supported by the exact solutions of the two-dimensional square lattice by Montroll[3] and by Bowers and Rosenstock.[4]

Calculations of the vibration spectrum and atomic heat of actual crystals have been hampered in the past by the great labor required to obtain numerical solutions. Furthermore, since comparison between theory and experiment can be made most sensitively at low temperatures, accurate experimental data on the elastic constants and atomic heats at low temperatures are required. It seems that these difficulties are on the verge of being surmounted. Computing machines capable of making the numerical calculations now exist. The elastic constants of solids have been measured at low temperatures by ultrasonic pulse techniques to an accuracy of a few tenths of a percent.[5,6] Also, it now appears that sufficiently accurate calorimetric data near 0°K may be obtained to give quantitative comparison with the theoretical results.[7,8] Consequently, it is the purpose of this article to re-examine the present position of the Born-von Kármán theory when applied to the cubic metallic elements.

It is customary to consider interactions between nearest neighbors and next-nearest neighbors of a lattice. The effect of the more distant neighbors is supposed to be negligible due to screening by the closer neighbors. The atoms are assumed to vibrate under Hooke's law forces. If we denote the Hooke's constant between nearest neighbors by α and between next-nearest neighbors by γ, then the result is a two-constant theory involving α and γ. For cubic crystals there are three independent elastic constants, c_{11}, c_{12}, and c_{44}, from which α and γ must be determined. This means that there must be an additional relation between the three elastic constants in order that the two constants α and γ be uniquely determined by the three. If central forces are the only type present, it can be shown that the Cauchy relation, $c_{12}=c_{44}$, must follow. Thus, it may appear that the constants, c_{11}, c_{12}, and c_{44}, together with the Cauchy relation constitute two independent quantities. Unfortunately for this pleasant situation, the results of experiment show that the Cauchy relation does not generally hold for metals.

[1] M. Born and Th. v. Kármán, Physik. Z. **13**, 297 (1912); Physik. Z. **14**, 15 (1913).
[2] M. Blackman, Proc. Roy. Soc. (London) **A148**, 365, 385 (1935); Proc. Roy. Soc. (London) **A149**, 117, 126 (1935).
[3] E. W. Montroll, J. Chem. Phys. **15**, 575 (1947).
[4] W. A. Bowers and H. B. Rosenstock, J. Chem. Phys. **18**, 1056 (1950).
[5] W. C. Overton, Jr., J. Chem. Phys. **18**, 113 (1950).
[6] W. C. Overton and R. T. Swim, Phys. Rev. **84**, 758 (1951).
[7] J. R. Clement and E. H. Quinnell, Rev. Sci. Instr. **23**, 213 (1952).
[8] J. R. Clement and E. H. Quinnell, Phys. Rev. **85**, 502 (1952).

Fuchs[9] has attributed the failure of the Cauchy relation to the presence of the conduction electrons. According to Fuchs, the electron gas would contribute to those combinations of elastic constants involved in volume changes but not in shearing strains. Thus, if c_{11}, c_{12}, and c_{44} are the measured elastic constants of the metal and c_{11}', c_{12}', and c_{44}' are those for the ion lattice alone, Fuchs finds that

$$c_{11}-c_{12}=c_{11}'-c_{12}' \tag{1}$$

and

$$c_{44}=c_{44}'. \tag{2}$$

The Born-von Kármán theory has been applied to the body-centered lattice by Fine[10] and to the face-centered cubic lattice by Leighton.[11] Fine did not make use of Fuchs' relation; he avoided the issue by limiting his treatment to tungsten for which the isotropy condition $c_{44}=(c_{11}-c_{12})/2$ seems to hold. Thus, he already had a two-constant theory. However, since the Cauchy relation is not obeyed for tungsten, one is not justified in ignoring the electron gas. Leighton took account of electron gas with the following argument. "Fuchs' result (Eqs. (1) and (2)) was used in the evaluation of the atomic constants α and γ, because the Born-von Kármán boundary condition, which was used in the derivation of the secular determinant, requires that the volume of the crystal remain constant so that the conduction electrons have no effect upon the motion of the lattice." Against this, one could counter with the argument that a standing compression (longitudinal) wave can be imagined in which there are periodic compressions and rarefactions along the wave without the total volume of the solid being affected.

In this paper, we consider as a model of a monatomic metallic crystal, a body-centered or face-centered cubic ion point lattice embedded in an electron gas. The ion point lattice is the customary Born-von Kármán type in which nearest and next-nearest neighbors interact. The electron gas is assumed to be a continuum possessing a bulk modulus K_e but no shear modulus. When acoustical measuring waves (wavelengths of the order of millimeters) pass through the combination of point lattice and electron gas, the conduction electrons are assumed to follow the motion of the ions in order that no large space charge develop. This requires the gas to undergo the same volume changes which the ion lattice experiences. When considering the much shorter thermal waves which occur in the metal, even in the T^3 region of atomic heat, we assume that the electron gas must again follow the motion of the ion lattice on the *average* in order that no large space charge develop (Bethe[12]). However, the electron gas may not keep in exact phase with the ion motion. For simplicity in the analysis of the lattice vibrations, the following two extremes are treated: 1.—the gas does not partake appreciably of the lattice motion; 2.—the gas keeps in phase with the lattice motion. Thus, the calculations based on these two extremes can be compared with the low-temperature atomic heat measurements and perhaps some conclusions drawn concerning the effect of the conduction electrons on the "lattice term" of the atomic heat.

II. ACOUSTICAL WAVES IN CUBIC CRYSTALS

We shall have occasion to express the dynamic parameters in terms of the elastic constants obtained from velocity of sound measurements. In this section we discuss the propagation of plane waves through an infinite medium whose elastic properties have cubic symmetry.

The stress tensor (P_{ij}) is symmetrical and generally has 6 independent elements. Similarly, the strain tensor (e_{ij}) is symmetrical and has 6 independent elements. The elements P_{11}, P_{22}, P_{33}, P_{23}, P_{13}, and P_{12} are each assumed to be linearly related to the elements e_{11}, e_{22}, e_{33}, e_{23}, e_{13}, e_{12}. When the elements are linearly related in the order just given, the coefficients c_{ij} of the e_{ij} terms in these 6 linear equations form the following matrix, for crystals of cubic symmetry,[13]

$$\begin{pmatrix} c_{11} & c_{12} & c_{12} & 0 & 0 & 0 \\ c_{12} & c_{11} & c_{12} & 0 & 0 & 0 \\ c_{12} & c_{12} & c_{11} & 0 & 0 & 0 \\ 0 & 0 & 0 & c_{44} & 0 & 0 \\ 0 & 0 & 0 & 0 & c_{44} & 0 \\ 0 & 0 & 0 & 0 & 0 & c_{44} \end{pmatrix}. \tag{3}$$

The linear relations between the P_{ij} and the e_{ij} elements form a generalized Hooke's law, and the coefficients c_{11}, c_{12}, and c_{44} are elastic constants. The frame of reference (x, y, z) for Eq. (3) has been chosen to coincide with the crystallographic axes (the four-fold axes) of the cubic system.

The textbook *Theoretical Physics* by Joos[14] contains the basic equations needed for a derivation of the differential equations of wave motion in cubic crystals. As the book is widely available, we shall use the notation and some of the formulas of Joos' treatment of elasticity in the short derivation which follows.

The symbols e_{11}, e_{22}, $\cdots$ are defined by

$$e_{11}=\frac{\partial u}{\partial x}, \quad e_{22}=\frac{\partial v}{\partial y}, \quad e_{33}=\frac{\partial w}{\partial z},$$

$$e_{23}=\frac{\partial v}{\partial z}+\frac{\partial w}{\partial y}, \quad e_{13}=\frac{\partial w}{\partial x}+\frac{\partial u}{\partial z}, \quad e_{12}=\frac{\partial u}{\partial y}+\frac{\partial v}{\partial x},$$

where u, v, and w are the components of a displacement representing strain. Putting these into the linear relations between P_{ij} and e_{ij} represented by the matrix (3)

[9] K. Fuchs, Proc. Roy. Soc. (London) **A153**, 622 (1935); Proc. Roy. Soc. (London) **A157**, 444 (1936).
[10] P. C. Fine, Phys. Rev. **56**, 355 (1939).
[11] R. B. Leighton, Revs. Modern Phys. **20**, 165 (1948).
[12] A. S. Sommerfeld and H. Bethe, *Handbuch der Physik* **24.2**, 333 (Verlag. Julius Springer, Berlin, 1933), middle of p. 506.
[13] C. Zener, *Elasticity and Anelasticity* (University of Chicago Press, Chicago, Illinois, 1948), Chap. I.
[14] G. Joos, *Theoretical Physics* (G. E. Stechert & Co., New York, 1934), Chap. VIII.

we obtain

$$
\begin{aligned}
P_{11}&=(c_{11}-c_{12})\frac{\partial u}{\partial x}+c_{12}\left(\frac{\partial u}{\partial x}+\frac{\partial v}{\partial y}+\frac{\partial w}{\partial z}\right),\\
P_{22}&=(c_{11}-c_{12})\frac{\partial v}{\partial y}+c_{12}\left(\frac{\partial u}{\partial x}+\frac{\partial v}{\partial y}+\frac{\partial w}{\partial z}\right),\\
P_{33}&=(c_{11}-c_{12})\frac{\partial w}{\partial z}+c_{12}\left(\frac{\partial u}{\partial x}+\frac{\partial v}{\partial y}+\frac{\partial w}{\partial z}\right),\\
P_{12}&=c_{44}\left(\frac{\partial u}{\partial y}+\frac{\partial v}{\partial x}\right),\\
P_{13}&=c_{44}\left(\frac{\partial u}{\partial z}+\frac{\partial w}{\partial x}\right),\\
P_{23}&=c_{44}\left(\frac{\partial v}{\partial z}+\frac{\partial w}{\partial y}\right).
\end{aligned}
\tag{4}
$$

If g_x, g_y, and g_z are the components of the body forces acting on unit volume, the condition for elastic equilibrium between these and the surface forces P_{ij} is

$$
g_x+\frac{\partial P_{11}}{\partial x}+\frac{\partial P_{12}}{\partial y}+\frac{\partial P_{13}}{\partial z}=0,
$$

and two similar equations containing g_y, g_z. In the kinetic case, $g_x=-\rho\partial^2u/\partial t^2$, the inertia force, where ρ is the density. Thus, the equations of motion for the "elasto-kinetic" case are

$$
\rho\frac{\partial^2u}{\partial t^2}=\frac{\partial P_{11}}{\partial x}+\frac{\partial P_{12}}{\partial y}+\frac{\partial P_{13}}{\partial z},
\tag{5}
$$

and similar equations for $\rho\partial^2v/\partial t^2$ and $\rho\partial^2w/\partial t^2$. Substitution from Eqs. (4) into Eqs. (5) gives the wave equations for crystals of cubic symmetry:

$$
\begin{aligned}
&(c_{11}-c_{12})\frac{\partial^2u}{\partial x^2}+c_{12}\left(\frac{\partial^2u}{\partial x^2}+\frac{\partial^2v}{\partial x\partial y}+\frac{\partial^2w}{\partial x\partial z}\right)\\
&\qquad+c_{44}\left(\frac{\partial^2u}{\partial y^2}+\frac{\partial^2u}{\partial z^2}+\frac{\partial^2v}{\partial x\partial y}+\frac{\partial^2w}{\partial x\partial z}\right)=\rho\frac{\partial^2u}{\partial t^2},\\
&(c_{11}-c_{12})\frac{\partial^2v}{\partial y^2}+c_{12}\left(\frac{\partial^2u}{\partial x\partial y}+\frac{\partial^2v}{\partial y^2}+\frac{\partial^2w}{\partial y\partial z}\right)\\
&\qquad+c_{44}\left(\frac{\partial^2v}{\partial x^2}+\frac{\partial^2v}{\partial z^2}+\frac{\partial^2u}{\partial x\partial y}+\frac{\partial^2w}{\partial y\partial z}\right)=\rho\frac{\partial^2v}{\partial t^2},\\
&(c_{11}-c_{12})\frac{\partial^2w}{\partial z^2}+c_{12}\left(\frac{\partial^2u}{\partial x\partial z}+\frac{\partial^2v}{\partial y\partial z}+\frac{\partial^2w}{\partial z^2}\right)\\
&\qquad+c_{44}\left(\frac{\partial^2w}{\partial x^2}+\frac{\partial^2w}{\partial y^2}+\frac{\partial^2u}{\partial x\partial z}+\frac{\partial^2v}{\partial y\partial z}\right)=\rho\frac{\partial^2w}{\partial t^2}.
\end{aligned}
\tag{6}
$$

To solve these equations, we substitute the expressions for a plane wave:

$$
\begin{aligned}
u&=A_1\exp[2\pi i(\nu t-k_1x-k_2y-k_3z)],\\
v&=A_2\exp[2\pi i(\nu t-k_1x-k_2y-k_3z)],\\
w&=A_3\exp[2\pi i(\nu t-k_1x-k_2y-k_3z)],
\end{aligned}
\tag{7}
$$

into Eqs. (6). $\mathbf{k}$ is the propagation vector with components k_1, k_2, k_3 and magnitude equal to the reciprocal of the wavelength. From this substitution, three simultaneous homogeneous equations are obtained in the components of amplitude, A_1, A_2, A_3. If the wave exists (not all components A_1, A_2, A_3 vanish), the determinant of the coefficients must vanish. Thus, we arrive at a secular equation restricting the possible frequencies:

$$
\begin{vmatrix}
(c_{11}-c_{44})k_1^2+c_{44}k^2-\rho\nu^2 & (c_{12}+c_{44})k_1k_2 & (c_{12}+c_{44})k_1k_3\\
(c_{12}+c_{44})k_1k_2 & (c_{11}-c_{44})k_2^2+c_{44}k^2-\rho\nu^2 & (c_{12}+c_{44})k_2k_3\\
(c_{12}+c_{44})k_1k_3 & (c_{12}+c_{44})k_2k_3 & (c_{11}-c_{44})k_3^2+c_{44}k^2-\rho\nu^2
\end{vmatrix}=0.
\tag{8}
$$

It might be thought that the three roots of the secular equation in ν^2, Eq. (8), separate into a branch of solutions for longitudinal waves and two branches for transverse waves. Such is not the case except under special conditions: either the medium is isotropic or the direction of $\mathbf{k}$ is normal to one of the planes {100}, {110}, {111}.

The demonstration of this will be carried out for one case only, namely the case of a longitudinal wave with none of the components k_1, k_2, k_3 of the propagation vector equal to zero.

Let p, q, r be the direction cosines of $\mathbf{k}$, none of which vanish. Then the amplitude $\mathbf{A}$ must have the same direction cosines if the wave is to be longitudinal. Thus, we put $A_1=pA$, $A_2=qA$, $A_3=rA$, and $k_1=pk$, $k_2=qk$, $k_3=rk$ into Eqs. (7) and substitute the resulting expressions for u, v, w into the differential Eqs. (6). Since p, q, r are not zero, we have the conditions on $\rho\nu^2/k^2$:

$$
\left.
\begin{aligned}
\rho\nu^2/k^2&=c_{12}+2c_{44}+(c_{11}-c_{12}-2c_{44})p^2,\\
\rho\nu^2/k^2&=c_{12}+2c_{44}+(c_{11}-c_{12}-2c_{44})q^2,\\
\rho\nu^2/k^2&=c_{12}+2c_{44}+(c_{11}-c_{12}-2c_{44})r^2.
\end{aligned}
\right\}
\tag{9}
$$

These conditions are satisfied either if $c_{44}=(c_{11}-c_{12})/2$ (the isotropy condition) or if $p^2=q^2=r^2$ ($\mathbf{k}$ normal to the {111} plane).

By letting *one* of the direction cosines p, q, r be zero, we can show that either the isotropy condition must be satisfied or $\mathbf{k}$ is normal to the {110} plane. Further, by allowing *two* of the direction cosines to be zero, we get

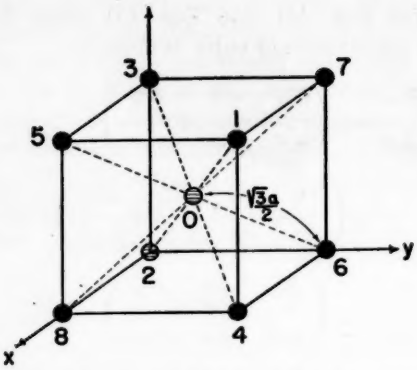

FIG. 1. The eight nearest neighbors of the atom at l, m, and n of the body-centered cubic lattice. $0=l,\ m,\ n$. $1=l+\frac{1}{2},\ m+\frac{1}{2},\ n+\frac{1}{2}$. $2=l-\frac{1}{2},\ m-\frac{1}{2},\ n-\frac{1}{2}$. $3=l-\frac{1}{2},\ m-\frac{1}{2},\ n+\frac{1}{2}$. $4=l+\frac{1}{2},\ m+\frac{1}{2},\ n-\frac{1}{2}$. $5=l+\frac{1}{2},\ m-\frac{1}{2},\ n+\frac{1}{2}$. $6=l-\frac{1}{2},\ m+\frac{1}{2},\ n-\frac{1}{2}$. $7=l-\frac{1}{2},\ m+\frac{1}{2},\ n+\frac{1}{2}$. $8=l+\frac{1}{2},\ m-\frac{1}{2},\ n-\frac{1}{2}$.

that either the isotropy condition must be satisfied or **k** is normal to the {100} plane. The same conditions hold for purely transverse waves.

We can obtain the velocity of sound ($U=\nu/k$) in the special directions {100}, {110}, {111} for longitudinal and transverse plane waves by following a procedure analogous to that just employed. A few of the relations obtained in this manner follow.

Wave Incident to {100} Surface, $\mathbf{k}_1=\mathbf{k}$, $\mathbf{k}_2=\mathbf{k}_3=0$

In this case, $A_1=A$, $A_2=A_3=0$, describe the longitudinal wave. Using these values and Eqs. (7) and (6), we find the longitudinal velocity, U_l, to be given by

$$\rho U_l^2=c_{11}. \tag{10}$$

The transverse velocity U_t of a plane wave polarized parallel to the y or z axis is

$$\rho U_t^2=c_{44}. \tag{11}$$

Wave Incident to {110} Surface, $\mathbf{k}_1=\mathbf{k}_2=\mathbf{k}/\sqrt{2}$, $\mathbf{k}_3=0$

The longitudinal velocity U_l is

$$\rho U_l^2=(c_{11}+c_{12}+2c_{44})/2. \tag{12}$$

The transverse velocity U_t of a wave polarized parallel to the z axis is

$$\rho U_t^2=c_{44}. \tag{13}$$

The transverse velocity $U_t'^2$ of a wave polarized perpendicular to the z axis is

$$\rho U_t'^2=(c_{11}-c_{12})/2. \tag{14}$$

III. THE ELASTICITY OF THE ELECTRON GAS

A. The Bulk Modulus of a Sommerfeld Gas

The Sommerfeld electron gas has a large zero-point pressure of about 10^5 atmospheres. Such pressures give rise to a large bulk modulus of the same order of magnitude as the elastic constants of the lattice. This pressure can be shown to be $\frac{2}{3}$ the energy density of the electron gas, or

$$p=\frac{2}{3}\frac{E_{\text{total}}}{V}, \tag{15}$$

where E_{total} is the total energy (kinetic) of the electron gas in a gram atomic weight of metallic element, and V is the atomic volume. Let N be Avogadro's number, n_0 the number of free electrons per atom, and ζ_0 the Gibbs' potential per electron. Then

$$E_{\text{total}}=\tfrac{3}{5}Nn_0\zeta_0 \tag{16}$$

and

$$\zeta_0=V^{-\frac{2}{3}}\frac{h^2}{2m}\left(\frac{3Nn_0}{8\pi}\right)^{\frac{2}{3}}, \tag{17}$$

which can be found in texts on the subject.

The temperature dependence of these quantities is minute at low temperatures and so it is neglected. Thus, we need not distinguish between adiabatic and isothermal bulk moduli. The bulk modulus is defined by

$$K_e=-V\frac{dp}{dV}.$$

From Eqs. (15), (16), (17) we find that

$$K_e=\frac{5}{3}p=\frac{2}{3}\frac{Nn_0\zeta_0}{V}. \tag{18}$$

As an example of the magnitude of K_e, let $n_0\zeta_0\sim 6$ electron-volts$\sim 10^{-11}$ ergs, and $V=10$ cc. Then

$$K_e\sim 4\times 10^{11}\ \text{dynes/cm}^2,$$

which is of the order of the measured elastic constants of the common metals.

B. Acoustical Waves in a Gas

If we set $c_{11}=c_{12}$ and $c_{44}=0$ in the matrix (3), we obtain the matrix of elastic coefficients for a gas. The secular Eq. (8) becomes considerably simplified, yielding the roots

$$\frac{\rho\nu^2}{c_{11}}=k^2,\ 0,\ 0.$$

There can be no transverse waves. The longitudinal waves have the velocity U given by

$$\rho U^2=c_{11}=K_e. \tag{19}$$

C. Additivity of the Bulk Moduli of Lattice and Electron Gas (Static Measurements)

If a change in volume ΔV accompanies a change in pressure Δp, the bulk modulus K is defined by

$$\Delta p=-K\frac{\Delta V}{V}.$$

When a pressure Δp is applied to a metal, a part Δp_L will compress the lattice and a part Δp_e will compress the electron gas. Both media undergo the same change of volume ΔV. Thus, for the lattice,

$$\Delta p_L = -K_L \frac{\Delta V}{V},$$

and for the electron gas,

$$\Delta p_e = -K_e \frac{\Delta V}{V},$$

which, when added, give

$$\Delta p = \Delta p_L + \Delta p_e = -(K_L + K_e)\frac{\Delta V}{V}.$$

Hence, in static measurements, the total bulk modulus is the sum of the lattice and electron gas bulk moduli.

In dynamic velocity of sound measurements, the bulk modulus of the electron gas can be expected to enter the expressions for the velocities of the compression waves additively. For example, in a direction normal to the {100} surface, the longitudinal velocity of sound would be

$$\rho U^2 = (c_{11})_{\text{lattice}} + K_e. \qquad (20)$$

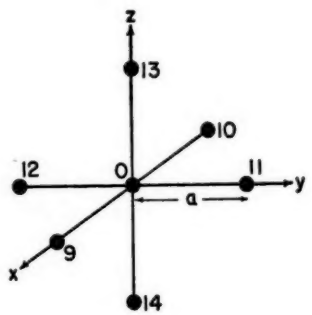

FIG. 2. The six next-nearest neighbors of the atom at l, m, and n of the body-centered cubic lattice. $0=l, m, n$. $9=l+1, m, n$. $10=l-1, m, n$. $11=l, m+1, n$. $12=l, m-1, n$. $13=l, m, n+1$. $14=l, m, n-1$.

IV. ACOUSTICAL LATTICE DYNAMICS

In part A of this section, the Born-von Kármán theory is used to derive the dynamic equations for the body-centered cubic (bcc) lattice and the face-centered cubic (fcc) lattice. The calculations include nearest neighbor interactions, with Hooke's constant α, and next-nearest neighbor interactions, with Hooke's constant γ. Then passage to the long wavelength limit is made, yielding a set of differential equations similar to Eqs. (6). In part B, these differential equations are modified to include the electron gas. Comparison of the resulting equations with those of section II leads to the determination of the dynamic parameters (α, γ, etc.) in terms of the elastic constants.

A. Acoustical Lattice Dynamics without Electron Gas Participation

The nearest and next-nearest neighbors of an atom located at $x=la$, $y=ma$, $z=na$ are shown in Figs. 1 and 2, respectively, for the bcc lattice; l, m, and n are integers. Each atom may undergo an arbitrary displacement from equilibrium with components u, v, w, subscripts being added to denote the atom considered. We identify an atom by its coordinates, in units of a: $u_{l,m,n}$, $v_{l,m,n}$, $u_{l+\frac{1}{2},m+\frac{1}{2},n+\frac{1}{2}}$ etc. However, these subscripts do not aid in expressing the equations in compact form. Thus, $u_{l,m,n}$ is *also* labeled u_0, $u_{l+\frac{1}{2},m+\frac{1}{2},n+\frac{1}{2}}$ is labelled u_1, and so forth, the order of the subscripts 0, 1, 2, $\cdots$ being chosen to aid the writing of the equations. Each figure contains a table relating the actual coordinates (in units of a) with the numbering on the diagram. It should be noticed that the numbers are ordered in pairs at the ends of diagonals through the atom at 0.

The usual approximation is made that the relative displacements are quite small compared to the distance between neighbors. Thus, components of displacements normal to the line joining the equilibrium positions of the atoms concerned are assumed to give no contribution to the restoring force acting between them. Only components of the displacements parallel to the line joining the atoms are considered as being effective.

Using the notation of Figs. 1 and 2 and denoting the mass of an atom by M, we arrive at the equation for $M(\partial^2 u/\partial t^2)_{l,m,n} (\equiv M(\partial^2 u/\partial t^2)_0)$:

$$M\left(\frac{\partial^2 u}{\partial t^2}\right)_0 = -\frac{\alpha}{3}(8u_0 - \sum_1^8 u_j - \sum_1^4 v_j + \sum_5^8 v_j - \sum_1^2 w_j + \sum_3^4 w_j - \sum_5^6 w_j + \sum_7^8 w_j) - \gamma(2u_0 - \sum_9^{10} u_j). \quad \text{(bcc)} \quad (21)$$

There are two similar equations for $M(\partial^2 v/\partial t^2)_{l,m,n}$,

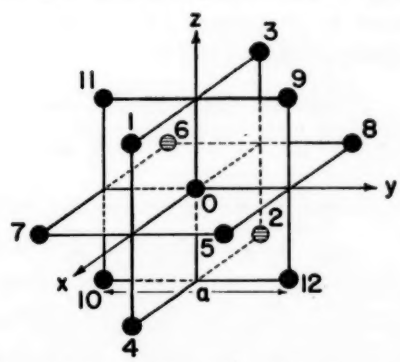

FIG. 3. The twelve nearest neighbors of the atom at l, m, and n of the face-centered cubic lattice. $0=l, m, n$. $1=l+\frac{1}{2}, m, n+\frac{1}{2}$. $2=l-\frac{1}{2}, m, n-\frac{1}{2}$. $3=l-\frac{1}{2}, m, n+\frac{1}{2}$. $4=l+\frac{1}{2}, m, n-\frac{1}{2}$. $5=l+\frac{1}{2}, m+\frac{1}{2}, n$. $6=l-\frac{1}{2}, m-\frac{1}{2}, n$. $7=l+\frac{1}{2}, m-\frac{1}{2}, n$. $8=l-\frac{1}{2}, m+\frac{1}{2}, n$. $9=l, m+\frac{1}{2}, n+\frac{1}{2}$. $10=l, m-\frac{1}{2}, n-\frac{1}{2}$. $11=l, m-\frac{1}{2}, n+\frac{1}{2}$. $12=l, m+\frac{1}{2}, n-\frac{1}{2}$.

$M(\partial^2 w/\partial t^2)_{l,m,n}$, which can be written down from symmetry.

Figures 3 and 4 show the nearest and next-nearest neighbors, respectively, of an atom at the position l, m, and n in units of a, for the fcc lattice; l, m, and n are integers. The equation for $M(\partial^2 u/\partial t^2)_{l,m,n}$ $(\equiv M(\partial^2 u/\partial t^2)_0)$ is

$$M\left(\frac{\partial^2 u}{\partial t^2}\right)_0 = -\frac{\alpha}{2}(8u_0 - \sum_1^8 u_j - \sum_1^2 v_j + \sum_3^4 v_j - \sum_5^6 w_j + \sum_7^8 w_j) - \gamma(2u_0 - \sum_{13}^{14} u_j). \quad \text{(fcc)} \quad (22)$$

There are two similar equations for $M(\partial^2 v/\partial t^2)_{l,m,n}$ and $M(\partial^2 w/\partial t^2)_{l,m,n}$, which can be obtained from symmetry.

For sufficiently long waves (i.e., acoustical waves), the difference Eqs. (21) and (22) become differential equations. To illustrate the manner of passing from

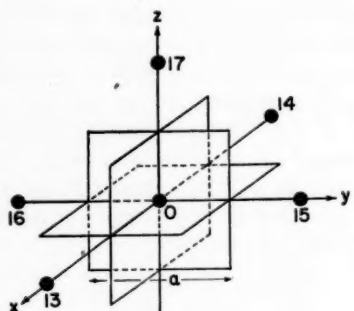

FIG. 4. The six next-nearest neighbors of the atom at l, m, and n of the face-centered cubic lattice. $0=l, m, n$. $13=l+1, m, n$. $14=l-1, m, n$. $15=l, m+1, n$. $16=l, m-1, n$. $17=l, m, n+1$. $18=l, m, n-1$.

differences to differentials with one set of terms of Eq. (21) of the bcc lattice, we select the u-displacement terms of atoms lying along the line joining the points 1, 0, 2 of Fig. 1. The neighboring points along this line are separated by a distance $\sqrt{3}a/2$, designated by s. Then, in the limit of long waves,

$$\frac{s^2[(u_1-u_0)-(u_0-u_2)]}{s^2} \rightarrow s^2\frac{\partial^2 u}{\partial s^2}. \quad (23)$$

Now

$$\frac{\partial}{\partial s} = \frac{\partial x}{\partial s}\frac{\partial}{\partial x} + \frac{\partial y}{\partial s}\frac{\partial}{\partial y} + \frac{\partial z}{\partial s}\frac{\partial}{\partial z}$$

and also,

$$\frac{\partial x}{\partial s} = \frac{\partial y}{\partial s} = \frac{\partial z}{\partial s} = \frac{a/2}{\sqrt{3}a/2} = \frac{1}{\sqrt{3}},$$

from geometry. Thus,

$$\frac{\partial}{\partial s} = \frac{1}{\sqrt{3}}\left(\frac{\partial}{\partial x} + \frac{\partial}{\partial y} + \frac{\partial}{\partial z}\right)$$

and

$$s^2\frac{\partial^2 u}{\partial s^2} = \frac{a^2}{4}\left(\nabla^2 + 2\frac{\partial^2}{\partial x\partial y} + 2\frac{\partial^2}{\partial x\partial z} + 2\frac{\partial^2}{\partial y\partial z}\right).$$

Grouping the various terms of the difference equations in a manner similar to Eq. (23) and transforming the differences to differentials, as just illustrated, we obtain the long-wave differential equations of a bcc lattice:

$$M\frac{\partial^2 u}{\partial t^2} = \frac{\alpha a^2}{3}\left[\nabla^2 u + 2\frac{\partial}{\partial x}\left(\frac{\partial u}{\partial x} + \frac{\partial v}{\partial y} + \frac{\partial w}{\partial z}\right)\right] - a^2\left(\frac{2\alpha}{3} - \gamma\right)\frac{\partial^2 u}{\partial x^2}, \quad \text{(bcc)} \quad (24)$$

the expressions for $M\partial^2 v/\partial t^2$ and $M\partial^2 w/\partial t^2$ being obtainable by permutation of u, v, w and permutation of x, y, z.

In a similar manner, we obtain the long-wave differential equations of the fcc lattice,

$$M\frac{\partial^2 u}{\partial t^2} = \frac{\alpha a^2}{4}\left[\nabla^2 u + 2\frac{\partial}{\partial x}\left(\frac{\partial u}{\partial x} + \frac{\partial v}{\partial y} + \frac{\partial w}{\partial z}\right)\right] - a^2\left(\frac{\alpha}{4} - \gamma\right)\frac{\partial^2 u}{\partial x^2}. \quad \text{(fcc)}. \quad (25)$$

The equations for $M\partial^2 v/\partial t^2$ and $M\partial^2 w/\partial t^2$ can be obtained by permuting u, v, and w and permuting x, y, and z.

B. Acoustical Lattice Dynamics with Electron Gas Participation

In Sec. II it was shown that purely longitudinal and purely transverse waves can exist only under rather special circumstances. Therefore, we cannot use the device of separating the modes into a longitudinal branch and two transverse branches (as in Debye theory) and then correcting the longitudinal branch with the electron gas bulk modulus. We are left with the conclusion that the solutions $\mathbf{A}(u, v, w)$ of the wave equations are neither longitudinal nor transverse but combinations of both. This suggests the alternative of separating *each* wave into a longitudinal and a transverse component, then correcting the longitudinal component for the electron gas. Let ψ be the angle between the amplitude vector $\mathbf{A}$ and the propagation vector $\mathbf{k}$. Furthermore, let $\mathbf{n}$ and $\mathbf{e}$ be unit vectors perpendicular and parallel to $\mathbf{k}$, respectively (Fig. 5). If $\mathbf{A}_L = A_L\,\mathbf{e}$ denotes the longitudinal part of $\mathbf{A}$ and $\mathbf{A}_T = A_T\,\mathbf{n}$ denotes the transverse part, then

$$\mathbf{A} = A_L\mathbf{e} + A_T\mathbf{n}.$$

The magnitudes A_L and A_T are simply $A\cos\psi$ and

$A\sin\psi$, respectively. Thus,

$$\mathbf{A}_L=A\frac{\mathbf{k}}{k}\cos\psi, \tag{26}$$

and

$$\mathbf{A}_T=\mathbf{A}-\mathbf{A}_L=\mathbf{A}-A\frac{\mathbf{k}}{k}\cos\psi.$$

Let p, q, and r denote the direction cosines of $\mathbf{k}$ and p', q', and r', those of $\mathbf{A}$. Then

$$\cos\psi=pp'+qq'+rr'. \tag{27}$$

In place of the components u, v, w of $\mathbf{A}$, we write those of $\mathbf{A}_L$ and $\mathbf{A}_T$ as

$$u_L=Ap\cos\psi,\quad v_L=Aq\cos\psi,\quad w_L=Ar\cos\psi$$
$$u_T=A(p'-p\cos\psi),\quad v_T=A(q'-q\cos\psi),$$
$$w_T=A(r'-r\cos\psi). \tag{28}$$

In the treatment which follows, A always cancels out of the equations, so we can set $A=1$ for convenience.

Suppose that a wave of the type represented by Eqs. (28) propagates through the crystal. The Hooke's constant α and γ of the lattice are unmodified for the transverse portion of the wave (u_T, v_T, w_T). But the portion u_L, v_L, w_L should experience a stiffening of the Hooke's forces due to the elasticity of the electron gas. Because of this, we write α' and γ' for the Hooke's constants including the electron effect. Details of the derivation of the new equations of motion will be shown only for Eq. (24).

Equations (7) for a plane wave are modified by putting for the amplitude

$$u=u_L+u_T,\quad v=v_L+v_T,\quad w=w_L+w_T,$$

where u_L, v_L, $\cdots$ are defined by Eqs. (28). When these modified forms of Eqs. (7) are substituted into Eqs. (24) and (25), and into the similar equations for $M\partial^2v/\partial t^2$ and $M\partial^2w/\partial t^2$, the understanding will be that the differential operators acting on u_L, v_L, w_L will have the α and γ in the coefficients primed to α' and γ'. But in operations on u_T, v_T, w_T the α and γ are left unprimed. Equation (24) becomes

$$\alpha'\nabla^2u_L+2\alpha'\frac{\partial}{\partial x}\left(\frac{\partial u_L}{\partial x}+\frac{\partial v_L}{\partial y}+\frac{\partial w_L}{\partial z}\right)-(2\alpha'-3\gamma')\frac{\partial^2u_L}{\partial x^2}$$
$$+\alpha\nabla^2u_T+2\alpha\frac{\partial}{\partial x}\left(\frac{\partial u_T}{\partial x}+\frac{\partial v_T}{\partial y}+\frac{\partial w_T}{\partial z}\right)$$
$$-(2\alpha-3\gamma)\frac{\partial^2u_T}{\partial x^2}=\frac{3M}{a^2}\frac{\partial^2u}{\partial t^2}. \tag{29}$$

Substituting from Eqs. (7) and (28) into (29) and making use of (27) and the relation

$$p^2+q^2+r^2=p'^2+q'^2+r'^2=1,$$

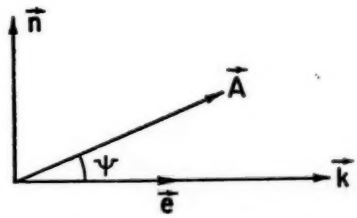

FIG. 5. The relation between $\mathbf{A}$ and $\mathbf{k}$ and the unit vectors.

we get for the modified form of Eq. (24)

$$[\alpha+3(\alpha'-\alpha+\gamma)p^2-\eta p^4-\Omega_b^2]p'$$
$$+[(3\alpha'-\alpha-\eta p^2)pq]q'$$
$$+[(3\alpha'-\alpha-\eta p^2)pr]r'=0, \tag{30}$$

where $\eta=(2\alpha'-3\gamma')-(2\alpha-3\gamma)$ and $\Omega_b^2=3Mv^2/a^2k^2$.

In like manner, we can obtain two other linear equations in p', q' and r' from the equations in $M\partial^2v/\partial t^2$ and $M\partial^2w/\partial t^2$ similar to (24). Thus, the secular equation for the bcc crystal corrected for the electron gas is tentatively

$$\begin{vmatrix}\alpha+3(\alpha'-\alpha+\gamma)p^2-\eta p^4-\Omega_b^2 & (3\alpha'-\alpha-\eta p^2)pq & (3\alpha'-\alpha-\eta p^2)pr\\ (3\alpha'-\alpha-\eta q^2)pq & \alpha+3(\alpha'-\alpha+\gamma)q^2-\eta q^4-\Omega_b^2 & (3\alpha'-\alpha-\eta q^2)qr\\ (3\alpha'-\alpha-\eta r^2)pr & (3\alpha'-\alpha-\eta r^2)qr & \alpha+3(\alpha'-\alpha+\gamma)r^2-\eta r^4-\Omega_b^2\end{vmatrix}=0.$$

Comparison of this secular equation with Eq. (8) shows at once that we must put $\eta=0$. The implication of setting $\eta=0$ is that the electron gas does not modify the form of the secular equation for acoustical waves, Eq. (8). Since we have four constants α, α', γ, and γ' and only three elastic constants, we need such a condition ($\eta=0$) in order to determine these four constants in terms of the elastic constants.

This leads to the secular equation of the acoustical waves for the bcc metallic element which we have been seeking:

$$\begin{vmatrix}\alpha+3(\alpha'-\alpha+\gamma)p^2-\Omega_b^2 & (3\alpha'-\alpha)pq & (3\alpha'-\alpha)pr\\ (3\alpha'-\alpha)pq & \alpha+3(\alpha'-\alpha+\gamma)q^2-\Omega_b^2 & (3\alpha'-\alpha)qr\\ (3\alpha'-\alpha)pr & (3\alpha'-\alpha)qr & \alpha+3(\alpha'-\alpha+\gamma)r^2-\Omega_b^2\end{vmatrix}=0. \quad \text{(bcc)} \tag{31}$$

Following the same procedure with Eq. (25) and the companion equations for $M\partial^2 v/\partial t^2$ and $M\partial^2 w/\partial t^2$, we find the secular equation of the acoustical waves for the fcc metallic crystal to be

$$\begin{vmatrix} \alpha+(3\alpha'-2\alpha+4\gamma)p^2-\Omega_f^2 & (3\alpha'-\alpha)pq & (3\alpha'-\alpha)pr \\ (3\alpha'-\alpha)pq & \alpha+(3\alpha'-2\alpha+4\gamma)q^2-\Omega_f^2 & (3\alpha'-\alpha)qr \\ (3\alpha'-\alpha)pr & (3\alpha'-\alpha)qr & \alpha+(3\alpha'-2\alpha+4\gamma)r^2-\Omega_f^2 \end{vmatrix}=0, \quad \text{(fcc)} \quad (32)$$

where $\Omega_f^2=4Mv^2/a^2k^2$.

Comparison of the secular equations just obtained, (31) and (32), with secular Eq. (8) yields the following values for the dynamic parameters in terms of the measured elastic constants. Body-centered cubic lattice:

$$\begin{aligned} \alpha&=\frac{3a}{2}c_{44}, \\ \gamma&=\frac{a}{2}(c_{11}-c_{12}), \\ \alpha'&=\frac{a}{2}(c_{12}+2c_{44}), \\ \gamma'&=\gamma+2(\alpha'-\alpha)/3. \end{aligned} \quad \text{(bcc)} \quad (33)$$

Face-centered cubic lattice:

$$\begin{aligned} \alpha&=ac_{44}, \\ \gamma&=\frac{a}{4}(c_{11}-c_{12}-c_{44}), \\ \alpha'&=\frac{a}{3}(c_{12}+2c_{44}), \\ \gamma'&=\gamma+(\alpha'-\alpha)/4. \end{aligned} \quad \text{(fcc)} \quad (34)$$

In Eqs. (33) and (34), we see that $c_{11}-c_{12}$ and c_{44} are independent of the electron gas (do not depend on α', γ') for both lattices. Thus, we have obtained, from our relatively elementary treatment, the same relations which Fuchs found by considering the static deformations of the "unit polyhedron" about an atom.[9]

If $\alpha'=\alpha$ and $\gamma'=\gamma$, then $c_{12}-c_{44}$ vanishes in both types of lattices and we have Cauchy's relation. If this is not so, then the relations are

$$\begin{aligned} c_{12}-c_{44}&=2(\alpha'-\alpha)/a \quad \text{(bcc)} \\ \text{and} \\ c_{12}-c_{44}&=3(\alpha'-\alpha)/a. \quad \text{(fcc)} \end{aligned} \quad (35)$$

The effect of the electron gas ($\alpha'>\alpha$) is to replace Cauchy's relation by these equations.

Let us consider the velocity of a longitudinal sound wave incident normally to the {100} plane. The velocity U of this wave is given by Eq. (10):

$$\rho U^2=c_{11}.$$

Since it is assumed that the electron gas follows the ion motion exactly, the wave compresses the lattice and gas to the same extent (Sec. III C), and thus

$$\rho U^2=(c_{11})_{\text{lattice}}+(c_{11})_{\text{electron}}=(c_{11})_{\text{lattice}}+K_e.$$

Now, taking $p=1$, $q=r=0$, $p'=1$, $q'=r'=0$ and $\rho=2M/a^3$ for the bcc lattice and $\rho=4M/a^3$ for the fcc lattice, we get

$$\begin{aligned} \rho U^2&=2(3\alpha'-2\alpha+3\gamma)/3a, \quad \text{(bcc)} \\ \rho U^2&=(3\alpha'-\alpha+4\gamma)/a. \quad \text{(fcc)} \end{aligned} \quad (36)$$

The right-hand side of Eqs. (36) is $(c_{11})_{\text{lattice}}$ when $\alpha'=\alpha$. With this in mind, Eqs. (36) are rearranged to

$$\begin{aligned} \rho U^2&=2(\alpha+3\gamma)/3a+2(\alpha'-\alpha)/a, \quad \text{(bcc)} \\ \rho U^2&=2(\alpha+2\gamma)/a+3(\alpha'-\alpha)/a. \quad \text{(fcc)} \end{aligned}$$

Hence, it follows that

$$\begin{aligned} K_e&=2(\alpha'-\alpha)/a, \quad \text{(bcc)} \\ K_e&=3(\alpha'-\alpha)/a. \quad \text{(fcc)} \end{aligned} \quad (37)$$

The quantity $c_{12}-c_{44}$ becomes in both cases [see Eqs. (33) and (34)],

$$c_{12}-c_{44}=K_e. \quad \text{(bcc and fcc)} \quad (38)$$

The discrepancy in the Cauchy relation is just the bulk modulus of the electron gas.

V. THERMAL LATTICE DYNAMICS

A. Thermal Lattice Dynamics without Electron Gas Participation

Although the electron gas has been assumed to follow the ion motion exactly in acoustical waves, the time constant associated with the interaction between the electron gas and the ion lattice may be such that the electron gas cannot keep up with the rapid motion of the ionic thermal oscillations. In the extreme case of no electron gas participation, the motion of the ions of the bcc lattice is represented by the unmodified Eq. (21) and its two companions for $M(\partial^2 v/\partial t^2)_{l,m,n}$ and $M(\partial^2 w/\partial t^2)_{l,m,n}$. The motion of the ions of the fcc lattice is represented by the unmodified Eq. (22) and its two companions.

To solve these equations, we substitute the expression for a plane wave

$$\begin{aligned} u_{l,m,n}&=A_1\exp[2\pi i(\nu t-k_1 la-k_2 ma-k_3 na)], \\ v_{l,m,n}&=A_2\exp[2\pi i(\nu t-k_1 la-k_2 ma-k_3 na)], \\ w_{l,m,n}&=A_3\exp[2\pi i(\nu t-k_1 la-k_2 ma-k_3 na)]. \end{aligned} \quad (39)$$

These expressions differ from those for the plane waves

of a continuum given by Eqs. (7) in that the wave is defined in Eqs. (39) only at the lattice points $x=la$, $y=ma$, $z=na$. The secular equations for the two types of cubic lattice are then

$$\begin{vmatrix} 1-C_1C_2C_3+(3\beta S_1^2/2)-\Omega_B^2 & S_1S_2C_3 & S_1C_2S_3 \\ S_1S_2C_3 & 1-C_1C_2C_3+(3\beta S_2^2/2)-\Omega_B^2 & C_1S_2S_3 \\ S_1C_2S_3 & C_1S_2S_3 & 1-C_1C_2C_3+(3\beta S_3^2/2)-\Omega_B^2 \end{vmatrix}=0, \quad \text{(bcc)} \quad (40)$$

and

$$\begin{vmatrix} 2-C_1(C_2+C_3)+2\beta S_1^2-\Omega_F^2 & S_1S_2 & S_1S_3 \\ S_1S_2 & 2-C_2(C_1+C_3)+2\beta S_2^2-\Omega_F^2 & S_2S_3 \\ S_1S_3 & S_2S_3 & 2-C_3(C_1+C_2)+2\beta S_3^2-\Omega_F^2 \end{vmatrix}=0, \quad \text{(fcc)} \quad (41)$$

where $S_i=\sin(\pi k_i a)$, $C_i=\cos(\pi k_i a)$, $\beta=\gamma/\alpha$, $\Omega_B^2=3\pi^2\nu^2M/2\alpha$, and $\Omega_F^2=2\pi^2\nu^2M/\alpha$.

The constants α and γ are determined in terms of the elastic constants, for the appropriate lattice, by Eqs. (33) and (34).

B. Thermal Lattice Dynamics with Electron Gas Participation

To modify Eq. (21) and its two companions and Eq. (22) and its companions so as to include the electron gas bulk modulus in the longitudinal components of the waves, one proceeds as in Sec. IV B. The secular equations are obtained by substitution of the plane waves of Eqs. (39) (expressed in terms of $\mathbf{A}_L$ and $\mathbf{A}_T$ defined in Sec. IV B) into these modified equations of motion. Using the same definitions for S_i, C_i, Ω_B, Ω_F, β as in Part V A, putting $\xi=(\alpha'-\alpha)/\alpha$, we obtain

$$\begin{vmatrix} 1-C_1C_2C_3+3\beta S_1^2/2+\xi pR_1-\Omega_B^2 & S_1S_2C_3+\xi qR_1 & S_1C_2S_3+\xi rR_1 \\ S_1S_2C_3+\xi pR_2 & 1-C_1C_2C_3+3\beta S_2^2/2+\xi qR_2-\Omega_B^2 & C_1S_2S_3+\xi rR_2 \\ S_1C_2S_3+\xi pR_3 & C_1S_2S_3+\xi qR_3 & 1-C_1C_2C_3+3\beta S_3^2/2+\xi rR_3-\Omega_B^2 \end{vmatrix}=0, \quad \text{(bcc)} \quad (42)$$

where

$$R_1=p(1-C_1C_2C_3+S_1^2)+qS_1S_2C_3+rS_1C_2S_3,$$
$$R_2=pS_1S_2C_3+q(1-C_1C_2C_3+S_2^2)+rC_1S_2S_3,$$
$$R_3=pS_1C_2S_3+qC_1S_2S_3+r(1-C_1C_2C_3+S_3^2);$$

and

$$\begin{vmatrix} 2-C_1(C_2+C_3)+2\beta S_1^2+\xi pT_1-\Omega_F^2 & S_1S_2+\xi qT_1 & S_1S_3+\xi rT_1 \\ S_1S_2+\xi pT_2 & 2-C_2(C_1+C_3)+2\beta S_2^2+\xi qT_2-\Omega_F^2 & S_2S_3+\xi rT_2 \\ S_1S_3+\xi pT_3 & S_2S_3+\xi qT_3 & 2-C_3(C_1+C_2)+2\beta S_3^2+\xi rT_3-\Omega_F^2 \end{vmatrix}=0, \quad \text{(fcc)} \quad (43)$$

where

$$T_1=p[2+S_1^2/2-C_1(C_2+C_3)]+qS_1S_2+rS_1S_3,$$
$$T_2=pS_1S_2+q[2+S_2^2/2-C_2(C_1+C_3)]+rS_2S_3,$$
$$T_3=pS_1S_3+qS_2S_3+r[2+S_3^2/2-C_3(C_1+C_2)].$$

The constants α, γ, and α' for the appropriate type of lattice are given in terms of the measured elastic constants by Eqs. (33) and (34).

VI. THE T^3 ATOMIC HEAT OF NEARLY ISOTROPIC LATTICES

It is not very fruitful to compute many special cases before the velocity of sound data have become available. However, the case in which the isotropy condition is fulfilled, or nearly so, is particularly simple. So the low-temperature atomic heat for this case will be computed as an illustration of the method.

The first step is to find the roots of the secular equations in the long wave approximation. Equations (42) and (43) reduce to Eqs. (31) and (32) when the wavelength greatly exceeds the interatomic distance. Equations (31) and (32) can be brought to the same form by dividing each row of the determinant by $3\alpha'-\alpha$ and putting

$$x=\frac{\Omega_b^2-\alpha}{3\alpha'-\alpha}, \quad s=\frac{3(\alpha'-\alpha+\gamma)}{3\alpha'-\alpha} \quad \text{(bcc)} \quad (44)$$

in Eq. (31), and

$$x=\frac{\Omega_f^2-\alpha}{3\alpha'-\alpha}, \quad s=\frac{3\alpha'-2\alpha+4\gamma}{3\alpha'-\alpha} \quad \text{(fcc)}$$

in Eq. (32).

This brings the two equations to the simpler common form

$$\begin{vmatrix} sp^2-x & pq & pr \\ pq & sq^2-x & qr \\ pr & qr & sr^2-x \end{vmatrix}=0,$$

which expands to

$$x^3-sx^2+(s-1)(s+1)K_{22}x-(s-1)^2(s+2)K_\pi=0, \quad (45)$$

where

$$K_{22}=p^2q^2+p^2r^2+q^2r^2,$$
$$K_\pi=p^2q^2r^2.$$

When the isotropy condition $c_{44}=(c_{11}-c_{12})/2$ is satisfied, then $\gamma/\alpha=\frac{2}{3}$ for the bcc lattice and $\frac{1}{4}$ for the fcc lattice. This can be seen to follow from Eqs. (33) and (34). In this event, s in Eqs. (44) reduces to unity and Eq. (45) becomes

$$x^3-x^2=0$$

with roots

$$x=1, 0, 0.$$

Now, we let $s=1+\sigma$, where σ is small compared to unity and has the explicit values

$$\sigma=\frac{3\gamma-2\alpha}{3\alpha'-\alpha}, \quad \text{(bcc)}$$
$$\sigma=\frac{4\gamma-\alpha}{3\alpha'-\alpha}, \quad \text{(fcc)} \quad (46)$$

and obtain the roots in powers of σ to σ^2. We thus arrive at the approximate values of the roots x_1, x_2, x_3:

$$\left.\begin{aligned} x_1&=1+(1-2K_{22})\sigma+A\sigma^2,\\ x_2&=(K_{22}+B)\sigma\\ &\quad-(1/2)\left[A+\frac{K_{22}A+2K_\pi(3K_{22}-1)}{B}\right]\sigma^2,\\ x_3&=(K_{22}-B)\sigma\\ &\quad-(1/2)\left[A-\frac{K_{22}A+2K_\pi(3K_{22}-1)}{B}\right]\sigma^2, \end{aligned}\right\} \quad (47)$$

with

$$A=K_{22}-4K_{22}^2+3K_\pi,$$
$$B=(K_{22}^2-3K_\pi)^{\frac{1}{2}}.$$

Using Eqs. (44) and substituting for Ω_b^2 and Ω_f^2, we get for the bcc lattice

$$\left.\begin{aligned} \frac{3Mv^2}{a^2k^2}&=3\alpha'+(3\alpha'-\alpha)(1-2K_{22})\sigma+(3\alpha'-\alpha)A\sigma^2,\\ \frac{3Mv^2}{a^2k^2}&=\alpha+(3\alpha'-\alpha)(K_{22}+B)\sigma-(1/2)(3\alpha'-\alpha)\\ &\quad\times\left[A+\frac{K_{22}A+2K_\pi(3K_{22}-1)}{B}\right]\sigma^2,\\ \frac{3Mv^2}{a^2k^2}&=\alpha+(3\alpha'-\alpha)(K_{22}-B)\sigma-(1/2)(3\alpha'-\alpha)\\ &\quad\times\left[A-\frac{K_{22}A+2K_\pi(3K_{22}-1)}{B}\right]\sigma^2, \end{aligned}\right\} \quad (48)\ (\text{bcc})$$

with $\sigma=(3\gamma-2\alpha)/(3\alpha'-\alpha)$; and for the fcc lattice,

$$\left.\begin{aligned} \frac{4Mv^2}{a^2k^2}&=3\alpha'+(3\alpha'-\alpha)(1-2K_{22})\sigma+(3\alpha'-\alpha)A\sigma^2,\\ \frac{4Mv^2}{a^2k^2}&=\alpha+(3\alpha'-\alpha)(K_{22}+B)\sigma-(1/2)(3\alpha'-\alpha)\\ &\quad\times\left[A+\frac{K_{22}A+2K_\pi(3K_{22}-1)}{B}\right]\sigma^2,\\ \frac{4Mv^2}{a^2k^2}&=\alpha+(3\alpha'-\alpha)(K_{22}-B)\sigma-(1/2)(3\alpha'-\alpha)\\ &\quad\times\left[A-\frac{K_{22}A+2K_\pi(3K_{22}-1)}{B}\right]\sigma^2, \end{aligned}\right\} \quad (49)\ (\text{fcc})$$

with $\sigma=(4\gamma-\alpha)/(3\alpha'-\alpha)$.

The constant-frequency surfaces in **k** space are spheres only in the case of isotropy where $\sigma=0$. When σ differs slightly from zero, in accord with our approximation, the surfaces become "nearly spherical" surfaces.

Our immediate purpose is to find the volume in **k** space contained within a constant-frequency surface. This enables us to obtain the number of modes up to that frequency. From this volume, one can obtain by differentiation with respect to the frequency and multiplication by the atomic volume, the number of modes $g(\nu)$ between ν and $\nu+d\nu$. When $g(\nu)$ has been obtained, the energy E and, therefore, the atomic heat C_V are found by

$$C_V=\frac{\partial E}{\partial T}=\frac{\partial}{\partial T}\int\frac{h\nu g(\nu)d\nu}{e^{h\nu/kT}-1}. \quad (50)$$

Since the computations are restricted to the T^3 region of atomic heat, we may set the limits of the integral at zero and infinity.

The volume in **k** space contained in a constant-frequency surface is

$$(1/3)\int k^3 d\omega, \quad (51)$$

where $d\omega$ is the element of solid angle. Three such integrals must be added, one for each branch of the secular equation. The quantity k^3 is a function of the spherical coordinate angles θ and ϕ and is obtained from Eqs. (48) and (49). The integrations to be performed involve the integrals

$$\int K_{22}d\omega=4\pi/5, \quad \int K_{22}^2 d\omega=4\pi/21,$$
$$\int K_\pi d\omega=4\pi/105.$$

Using these, and introducing the atomic volume V,

the distribution of modes with frequency, $g(\nu)$, becomes

$g(\nu)$ for bcc

$$=4\pi V\nu^2\frac{M^{\frac{3}{2}}}{a^3}\left\{\left(\frac{1}{\alpha'}\right)^{\frac{3}{2}}\left[1-\frac{3}{5}\left(\frac{3\gamma-2\alpha}{2\alpha'}\right)+\frac{567\alpha'-205\alpha}{630(3\alpha'-\alpha)}\left(\frac{3\gamma-2\alpha}{2\alpha'}\right)^2\right]+2\left(\frac{3}{\alpha}\right)^{\frac{3}{2}}\left[1-\frac{3}{5}\left(\frac{3\gamma-2\alpha}{2\alpha}\right)+\frac{3(35\alpha'-9\alpha)}{70(3\alpha'-\alpha)}\left(\frac{3\gamma-2\alpha}{2\alpha}\right)^2\right]\right\}, \quad (52)$$

$g(\nu)$ for fcc

$$=4\pi V\nu^2\frac{(4M/3)^{\frac{3}{2}}}{a^3}\left\{\left(\frac{1}{\alpha'}\right)^{\frac{3}{2}}\left[1-\frac{3}{5}\left(\frac{4\gamma-\alpha}{2\alpha'}\right)+\frac{567\alpha'-205\alpha}{630(3\alpha'-\alpha)}\left(\frac{4\gamma-\alpha}{2\alpha'}\right)^2\right]+2\left(\frac{3}{\alpha}\right)^{\frac{3}{2}}\left[1-\frac{3}{5}\left(\frac{4\gamma-\alpha}{2\alpha}\right)+\frac{3(35\alpha'-9\alpha)}{70(3\alpha'-\alpha)}\left(\frac{4\gamma-\alpha}{2\alpha}\right)^2\right]\right\}. \quad (53)$$

The quantities $g(\nu)$ are of the form $D\nu^2$, where D is a constant of the material. Therefore, Eq. (50) becomes

$$C_V=\frac{\partial E}{\partial T}=\frac{\partial}{\partial T}hD\int_0^\infty\frac{\nu^3d\nu}{e^{h\nu/kT}-1}=\frac{4\pi^4k^4D}{15h^3}T^3. \quad (54)$$

(k here is Boltzmann's constant, not to be confused with the magnitude of the wave vector $\mathbf{k}$.)

Debye's formula for the T^3 region is

$$C_V=\frac{12\pi^4}{5}\frac{Nk}{\Theta^3}T^3. \quad (55)$$

Comparing Eqs. (54) and (55), we find the equivalent Debye Θ of Eq. (54) to be

$$1/\Theta^3=k^3D/9Nh^3, \quad (56)$$

with

$$D=g(\nu)/\nu^2 \quad (57)$$

for both lattices.

If we place the values of α, α', and γ, expressed in terms of the elastic constants [Eqs. (33) and (34)], into the expressions for D and use the densities $\rho=2M/a^3$ (bcc) and $\rho=4M/a^3$ (fcc), the two equations for D merge to a single relation. Putting this new relation into Eq. (56), we obtain

$$\frac{1}{\Theta^3}=\frac{4\pi Vk^3\rho^{\frac{3}{2}}}{9Nh^3}\left\{(c_{12}+2c_{44})^{-\frac{3}{2}}\left[1-\frac{9}{10}\frac{c_{11}-c_{12}-2c_{44}}{c_{12}+2c_{44}}+\frac{189c_{12}+173c_{44}}{280(c_{12}+c_{44})}\left(\frac{c_{11}-c_{12}-2c_{44}}{c_{12}+2c_{44}}\right)^2\right]+2(c_{44})^{-\frac{3}{2}}\left[1-\frac{3}{10}\frac{c_{11}-c_{12}-2c_{44}}{c_{44}}+\frac{35c_{12}+43c_{44}}{280(c_{12}+c_{44})}\left(\frac{c_{11}-c_{12}-2c_{44}}{c_{44}}\right)^2\right]\right\} \quad (58)$$

for both the bcc and fcc lattices, when $|c_{11}-c_{12}-2c_{44}/c_{44}|<$ about $\frac{1}{2}$.

Equation (58) includes the bulk modulus of the electron gas. The corresponding equation excluding the electron effect is

$$\frac{1}{\Theta^3}=\frac{4\pi Vk^3\rho^{\frac{3}{2}}}{9Nh^3}(c_{44})^{-\frac{3}{2}}\times\left\{\frac{\sqrt{3}}{9}\left[1-\frac{3}{10}\frac{c_{11}-c_{12}-2c_{44}}{c_{44}}+\frac{181}{2520}\left(\frac{c_{11}-c_{12}-2c_{44}}{c_{44}}\right)^2\right]+2\left[1-\frac{3}{10}\frac{c_{11}-c_{12}-2c_{44}}{c_{44}}+\frac{39}{280}\left(\frac{c_{11}-c_{12}-2c_{44}}{c_{44}}\right)^2\right]\right\} \quad (59)$$

for both the bcc and fcc lattices, when $|c_{11}-c_{12}-2c_{44}/c_{44}|<$ about $\frac{1}{2}$.

The general terms of Eqs. (58) and (59) are unknown. We are *assuming* that the series converge, at least asymptotically, and that the value of the coefficient of the neglected term in σ^3 follows the trend of the known coefficients of σ, σ^2. Thus, the limits set at "$<$ about $\frac{1}{2}$" indicate a guess at one percent error due to the neglect of the unknown remainder. If the error is really less than one percent, then the Θ determined by these expressions will possess an error of less than a third of one percent.

The elastic constants for aluminum at *room temperature* have been found by Lazarus[15] to be $c_{11}=10.56$, $c_{12}=6.39$, $c_{44}=2.853$ in units of 10^{11} dynes/cm^2. These constants substituted into Eqs. (58) and (59) lead to

$\Theta=401$°K with electron gas [Eq. (58)]

$\Theta=395$°K without electron gas [Eq. (59)].

[15] D. Lazarus, Phys. Rev. **76**, 545 (1949).

The experimental values of Θ from atomic heat data yield 394°K for temperatures near room temperature and 419°K for the T^3 region of atomic heat. The only satisfaction we can derive from this comparison is that the two calculated values fall in the range 394°K to 419°K. A fair comparison can be made only after the elastic constants have been determined in the liquid helium range of temperature.

VII. SUMMARY AND DISCUSSION

We have taken as the model representing the crystal of a monatomic cubic metal an ion point lattice immersed in an electron gas. The electron gas is assumed to possess a bulk modulus K_e but no shear modulus. The long acoustical waves used in measuring the elastic constants would produce large space charges if the electron gas did not follow the volume changes closely. Therefore, we assumed that the electron gas does follow the motion of the ions and we included its effect in the longitudinal components of the waves. This enabled us to obtain explicit relations between the dynamic parameters and the elastic constants. We have shown that the discrepancy in the Cauchy relation is just K_e [Eq. (38)]. In the absence of the electron gas, the Cauchy relation holds for both types of cubic lattice. In addition, we have found that the quantities $c_{11}-c_{12}$ and c_{44} are independent of K_e, in agreement with Fuchs' calculations based on a static model.

Turning our attention to thermal waves, we then distinguished two extreme cases. In the first case, the electrons do not participate in the lattice motion. This led to the secular Eqs. (40) and (41) for the bcc and fcc lattices, respectively. If the elastic constants nearly satisfy the isotropy condition, the Debye Θ in the T^3 region is deduced from Eqs. (40) and (41) and is given by Eq. (59), for both lattices. In the second case, the electrons participate in the lattice motion. From this hypothesis, we get the secular Eqs. (42) and (43) for the bcc and fcc lattices, respectively. The Debye Θ in this instance is given by Eq. (58), in the T^3 region, for both lattices.

It may be that neither extreme is correct. But by comparing the results of the calculations for both extreme cases with experiment, one may be able to draw conclusions which will give direction toward a better theory. However, the data entering the theory and the data used in comparing the results with experiment must be more precise than that existing at the time of this writing.

An interesting by-product of these calculations is the determination of the number of free electrons per atom (for monovalent elements) from the velocity of sound measurements, in combination with data such as can be obtained from soft x-ray measurements. For example, the width of the occupied part of the conduction band for Cu has been determined from soft x-ray measurements by Gyorgy and Harvey to be 7.1 ± 0.5 electron volts.[16] Using Eqs. (18) and (38), we find that

$$\frac{2}{3}\frac{Nn_0\zeta_0}{V}=K_e=c_{12}-c_{44}.$$

Putting $c_{12}=12.3$ and $c_{44}=7.5$ in units of 10^{11} dynes/cm^2 (as cited by Leighton[11]), and with $V=7.1$ cc, we obtain

$$n_0=0.75$$

free electrons per atom, a reasonable figure for Cu.

Note added in proof.—The elastic constants of Al have been measured recently by P. M. Sutton, Phys. Rev. **91**, 816 (1953), down to 63°K. The values of c_{11}, c_{12}, c_{44} extrapolated to 0°K are 12.30, 7.08, 3.090 in units of 10^{11} dynes/cm^2. These constants substituted into Eqs. (58) and (59) lead to

$\Theta=429$°K with electron gas [Eq. (58)],

$\Theta=423$°K without electron gas [Eq. (59)].

[16] E. M. Gyorgy and G. G. Harvey, Phys. Rev. **87**, 861 (1952).

The Distribution of Solute in Crystals Grown from the Melt. Part I. Theoretical

J. A. BURTON, R. C. PRIM, and W. P. SLICHTER
Bell Telephone Laboratories, Murray Hill, New Jersey

(Received May 18, 1953)

The incorporation of solute elements into single crystals of germanium grown from the melt is examined in terms of a simple model. The theory takes account of the contribution of solute transport in the melt, owing to diffusion and fluid motion, to the over-all process of impurity incorporation during steady-state crystallization. The analysis is extended to treat the transient inclusion of solute which results when the composition of the melt is abruptly changed.

HETEROGENEOUS chemical reactions are comprised of several processes. One of these is the chemical transformation itself, and associated with it the adsorption and desorption processes, occurring at the interface of the two phases. Elsewhere the transport of reactants or products to or from the interface may be a significant factor. Diffusion is a consideration in the transport process, particularly with solid-liquid reactions.

Nernst[1] postulated that the chemical change itself occurs almost instantaneously, and supposed the over-all rate of the reaction to be set by a diffusion-dominated transport process. This viewpoint has been endorsed by some workers, but others have argued for the importance of other processes, sometimes to the extent of denying that transport contributes to the reaction rate at all. It is now widely believed that the importance of a given process, such as transport, to the over-all rate depends critically upon the system under study, and for a given system may even depend upon the experimental conditions. The subject of heterogeneous reactions has been reviewed by Moelwyn-Hughes,[2] and by Bircumshaw and Riddiford[3] with special attention to transport processes.

The present paper treats theoretically the incorporation of impurity elements into single crystals of germanium grown from the melt.[4] The paper which follows describes some experimental studies of such crystals. The crystallization is viewed as a heterogeneous reaction. The chemical process consists of the incorporation of impurity at the solid-liquid interface. It depends strongly upon the impurity, and possibly upon some conditions of crystallization. The transport process is particularly sensitive to crystallization conditions, and is the chief subject of this discussion.

1. DISTRIBUTION COEFFICIENT

The incorporation of impurity in the crystal may be characterized by a distribution coefficient. In treating a binary solution having solid and liquid phases, one may define an equilibrium coefficient k_0 as the ratio of the concentration of solute in the solid C_S to that in the liquid C_L, when equilibrium exists between the two phases at a given temperature. When the solute composition of the system is decreased, so that the equilibrium temperature approaches the melting point of the pure solvent, k_0 converges to a constant value. With solutions in germanium, k_0 is ordinarily less than unity and depends markedly upon the impurity. When crystallization occurs very slowly, the solid forming at any moment from the melt has composition $C_S = k_0 C_L$, provided one may assume diffusion in the solid to be negligible. As the crystallization proceeds, the rejection of solute by the solid enriches the melt, and so the solid formed in the later stages becomes progressively richer, in a manner which has been described by several authors.[5]

However, if crystallization does not proceed slowly, solute atoms are rejected by the advancing solid at a greater rate than they can diffuse into the bulk of the melt. A concentration gradient thus develops just ahead of the advancing crystal. It is this enriched region which directly determines the rate of solute incorporation into the solid. If C_L is the solute concentration in the bulk of the liquid, where stirring and convection currents keep the composition virtually uniform, one may define an effective distribution coefficient k as the ratio C_S/C_L at any moment.

The equilibrium value of the distribution coefficient, k_0, may of course be regarded as the ratio α/β, where α and β are rate constants, expressed in cm sec^{-1}, for two exchange processes occurring at the phase interface which have reached equilibrium. Here α describes the entrance of solute into the crystal and β describes the exit process into the melt. True equilibrium presumably occurs only if the crystallization speed is essentially zero. When crystallization occurs at measurable speed, doubtless the equilibrium at the interface will be disturbed at least to some degree. Thus the effective distribution coefficient k, which describes the over-all reaction of solute incorporation into the crystal at nonzero growth speed, may vary with the crystallization

[1] W. Nernst, Z. physik. Chem. **47**, 52 (1904).
[2] E. A. Moelwyn-Hughes, *The Kinetics of Reactions in Solution* (Oxford University Press, London, 1947), second edition.
[3] L. L. Bircumshaw and A. C. Riddiford, Quart. Rev. Chem. Soc. (London), **6**, 157 (1952). See also A. C. Riddiford, J. Phys. Chem. **56**, 745 (1952).
[4] G. K. Teal and J. B. Little, Phys. Rev. **78**, 647 (1950).
[5] E. Scheuer, Z. Metallekunde, **23**, 237 (1951); A. Hayes and J. Chipman, Trans. Am. Inst. Mining Met. Engs. **135**, 85 (1939); R. H. McFee, J. Chem. Phys. **15**, 856 (1947); W. G. Pfann, J. Metals **4**, 747 (1952).

rate due to two factors: (a) the contribution of transport processes in the melt, mentioned in the preceding paragraph; (b) the effect upon the exchange process at the interface, i.e., upon the chemical process itself.

The present paper will be devoted chiefly to (a), since transport of solute in the melt is found experimentally to be of major importance. Hall[6] has postulated a mechanism for the dependence of k upon growth rate which in effect ascribes the behavior to (b). He has taken (a) to be unimportant in practice, but this view is not in accord with our own experience.[7] Some mention will be made presently of the effect of nonzero growth rate upon the exchange process at the interface, but a detailed discussion will be reserved for later presentation.

2. ANALYSIS OF FLUID FLOW

For any type of fluid flow, whether laminar or turbulent, the fluid velocity tends toward zero with approach to the solid-liquid interface, except for the flow normal to the interface due to crystallization. There is thus some region of the melt, next to the crystal, in which the principal transport of solute away from the interface occurs by diffusion. Fluid motion dominates solute transport in more remote regions. Crystallization from the melt according to the method of Teal and Little[4] involves continual rotation of the crystal, the purpose being in part to yield symmetrical growth. This rotation tends to produce ordered, laminar flow in the melt. If turbulence and random convection currents are small enough in comparison, the fluid flow is essentially that due to the stirring. Experimentally, there is no superficial evidence of turbulence in the liquid, nor would turbulence be expected from general considerations[8] of the conditions of stirring. Hence, it is presumed that the fluid flow is laminar, and that it can be analyzed in the following way, which is similar to the treatment used by Levich[9] in his study of diffusion-limited electrode reactions.

The interface of a rotating crystal pulled from the melt is approximately a plane disk. As is well known, a disk rotating upon a liquid acts as a centrifugal fan, spinning fluid radially and tangentially, and hence drawing material toward the rotating surface from the body of the liquid. The fluid flow pattern produced by an infinite disk rotating upon a semi-infinite liquid has been calculated by Cochran,[10] solely in terms of the angular velocity of the disk and the kinematic viscosity of the liquid. In Cochran's example the flow velocity normal to the disk is independent of radial distance from the rotation axis, and falls off rapidly in proximity to the disk. Crystal and crucible dimensions are typically of the order of centimeters, whereas the diffusion-dominated region of present interest is probably only about 10^{-2} or 10^{-3} cm thick. Therefore Cochran's analysis should give a reasonable approximation for flow in the melt, provided the analysis is confined to regions of the melt which lie close to the crystal and separated from the edges of the crystal and crucible. Since the melt is not infinitely deep, an analysis like that made by Batchelor,[11] treating the flow between two parallel rotating disks with finite separation, should be more exact. However this last approach is more difficult than seems warranted.

Conservation of solute atoms in the melt is expressed by the continuity equation

$$\partial C/\partial t = -\nabla\cdot(C\mathbf{V} - D\nabla C), \tag{1}$$

where $\mathbf{V}$ is the vector fluid velocity, and D is the diffusion coefficient of the solute, assumed to be independent of concentration in the dilute solutions which are encountered. A one-dimensional treatment is appropriate, since the solid solute concentration is found experimentally to be virtually uniform in the radial direction, perpendicular to the growth direction. Then, since the fluid is incompressible, Eq. (1) reduces to the following in the steady state:

$$D\frac{d^2C}{dx^2} - V_x\frac{dC}{dx} = 0. \tag{2}$$

The coordinate system is fixed with respect to the solid-liquid interface, which is located at $x=0$, with the positive x direction extending into the melt. Velocity V_x is taken to be the sum of the normal fluid velocity W, and the growth velocity f. The latter is chosen to be positive for growth and negative for melting. The boundary conditions for steady-state growth are:

$$C \to C_L \quad \text{as} \quad x \to \infty, \tag{3}$$

$$(C_0 - C_s)f + D\frac{dC}{dx} = 0 \quad \text{at} \quad x=0, \tag{4}$$

where as before C_L and C_0 are the melt concentrations in the bulk of the liquid and at the interface, respectively.

Relations (2)–(4) can be solved numerically, using Cochran's tables for W. For the small values of x which are of interest here, however, Cochran gives the following approximation,

$$W = 0.51\omega^{\frac{3}{2}}\nu^{-\frac{1}{2}}x^2 \quad \text{for} \quad x < \nu^{\frac{1}{2}}\omega^{-\frac{1}{2}}, \tag{5}$$

where ω is the angular velocity of crystal rotation and ν is the kinematic viscosity of the liquid. The following solution is obtained.*

$$\frac{C_0 - C_L}{C_0 - C_S} = \int_0^\infty e^{-(X+BX^3)}dX, \tag{6}$$

where $B = 0.17 f^{-3}\omega^{\frac{3}{2}}D^2\nu^{-\frac{1}{2}}$ and $X = fx/D$.

[6] R. N. Hall, Phys. Rev. **88**, 139 (1952).
[7] See Part II, J. Chem. Phys. **21**, 991 (1953).
[8] See *Modern Developments in Fluid Dynamics*, edited by S. Goldstein (Oxford University Press, London, 1938), pp. 113, 367.
[9] B. Levich, Acta Physicochim. U. R. S. S. **17**, 257 (1942).
[10] W. G. Cochran, Proc. Camb. Phil. Soc. **30**, 365 (1934).
[11] G. K. Batchelor, Quart. J. Mech. Appl. Math. **4**, 29 (1951).

* Strictly speaking, the integration may not be carried beyond $x = \sqrt{(\nu/\omega)}$, but practically the matter is unimportant, since with the physical constants of the present process there is virtually no contribution to the integral for $x > \sqrt{(\nu/\omega)}$.

For practical purposes it is more convenient, however, to make an approximation not unlike Nernst's approach. Thus, it is assumed that beyond a distance δ, from the growing interface the fluid flow keeps the concentration uniformly equal to C_L. Within δ the normal flow velocity is merely f, and here diffusion likewise contributes to the transport. Thus Eq. (3) becomes

$$D\frac{d^2C}{dx^2}+f\frac{dC}{dx}=0 \tag{7}$$

and (3) is replaced by

$$C=C_L \quad \text{at} \quad x=\delta. \tag{8}$$

The following solution results for the concentration at the interface.

$$\frac{C_0-C_S}{C_L-C_S}=e^{\Delta}, \tag{9}$$

where $\Delta=f\delta/D$. The somewhat arbitrary quantity δ may be characterized by defining it so that it yields the same dependence of the composition upon the growth parameters that is given by the more exact solution, (6). Thus, δ is required to vary in such a way that

$$e^{-\Delta}=1-J, \tag{10}$$

where J is the integral standing on the right in Eq. (6).

For small enough values of the growth rate, δ depends simply upon the rotation rate and certain physical properties of the liquid phase.

$$\delta=1.6D^{1/3}\nu^{1/6}\omega^{-1/2}. \tag{11}$$

Thus it is seen that if the growth rate is small enough, Δ varies linearly with f and with $\omega^{-\frac{1}{2}}$. The variation of Δ with $B^{-\frac{1}{2}}$, i.e., its dependence upon the term $f\omega^{-\frac{1}{2}}$, is shown in Fig. 1.

The foregoing treatment has described steady-state solute transport in the fluid for both crystal growth and for melting. In the case of growth there exists an additional relation between C_S and C_0, which is given in its simplest form by the equilibrium distribution coefficient

$$C_S/C_0=k_0. \tag{12}$$

The relation is described more generally as depending upon f, and possibly also upon other quantities such as acceleration:

$$C_S/C_0=k^*(f, \partial f/\partial t, \cdots). \tag{13}$$

As has been stated, no attempt will be made here to explore the manner in which k^* depends upon these factors. Suffice it to say that one would expect the behavior to be qualitatively similar to that postulated by Hall,[6] in that the process at the interface should shift toward an enhanced tendency for solute incorporation at higher growth rates.

In any case, whatever the form of k^*, Eqs. (9) and (13) lead to the following expression for the effective distribution coefficient in the steady state:

$$k=\frac{k^*}{k^*+(1-k^*)e^{-\Delta}}. \tag{14}$$

For the important case in which equilibrium prevails at the interface virtually independently of growth rate,

$$k=\frac{k_0}{k_0+(1-k_0)e^{-\Delta}}. \tag{15}$$

The variation of k with growth rate is shown in Fig. 2 for two rates of crystal rotation, and for three values of k_0. Reasonable values have been assumed here for D and ν: $D=5\times10^{-5}$ cm^2 sec^{-1} and $\nu=2.5\times10^{-3}$ cgs units. The variation described by Eq. (15), for equilibrium at the interface, is given in each case. If this equilibrium were disturbed by the use of nonzero growth rate, the steady-state variation described by Eq. (14) would of course cause the curves to stand above those in Fig. 2.

3. TRANSIENT ANALYSIS

Transient behavior in the melt will now be examined for the case of rapid exchange at the interface, i.e., $k^*=k_0$. The transient case to be considered is that in which the solute concentration in the bulk of the melt is abruptly increased. Because of the linearity of the problem, one may deal solely with the case in which this concentration jumps from zero to a final value at $t=0$.

Retaining the concept of diffusion-dominated region of thickness δ, beyond which the melt composition is uniform, the partial differential equation and boundary

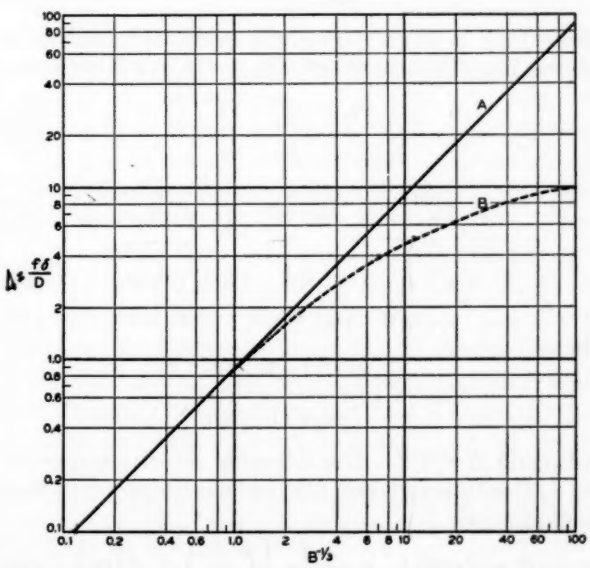

FIG. 1. Variation of $f\delta/D$ with $B^{-\frac{1}{2}}$, i.e., with $f\omega^{-\frac{1}{2}}$. Curve A neglects the dependence of δ upon f. Curve B gives the exact variation.

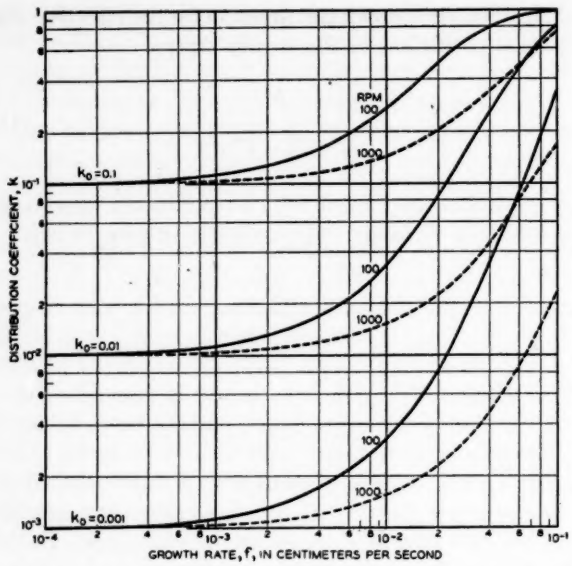

FIG. 2. Dependence of the effective distribution coefficient upon growth rate and rotation rate, for several values of equilibrium distribution coefficient.

conditions for $0 \leq x \leq \delta$ become

$$D\frac{\partial^2 C}{\partial x^2}+f\frac{\partial C}{\partial x}=\frac{\partial C}{\partial t}, \tag{16}$$

$$-D\frac{\partial C}{\partial x}=(1-k_0)fC_0 \quad \text{at} \quad x=0, \tag{17}$$

$$C=0 \quad \text{for} \quad 0<x<\delta, \quad t=0, \tag{18}$$

$$C=C_L \quad \text{for} \quad x=\delta, \quad t=0. \tag{19}$$

It is convenient to change to variables $\bar{C}$ and y:

$$\bar{C}\equiv C-C_{ss} \tag{20}$$

$$y\equiv\delta-x, \tag{21}$$

where C_{ss} is the steady-state result obtained from solving Eq. (7). Accordingly, Eqs. (16)–(19) become

$$D\frac{\partial^2 \bar{C}}{\partial y^2}-f\frac{\partial \bar{C}}{\partial y}=\frac{\partial \bar{C}}{\partial t} \tag{22}$$

$$D\frac{\partial \bar{C}}{\partial y}=(1-k_0)f\bar{C} \quad \text{at} \quad y=\delta \tag{23}$$

$$\bar{C}=-C_{ss}(y) \quad \text{for} \quad y>0, \quad t=0 \tag{24}$$

$$\bar{C}=0 \quad \text{for} \quad y=0, \quad t\geq 0, \tag{25}$$

where

$$C_{ss}=C_L\frac{k_0+(1-k_0)e^{-\Delta}e^{-fy/D}}{k_0+(1-k_0)e^{-\Delta}},$$

and again $\Delta=f\delta/D$. The following set of solutions to Eq. (22) satisfies relation (25) and has the property that $\bar{C}\to 0$ as $t\to\infty$.

$$\bar{C}_\mu=e^{fy/2D}\sin\mu y\cdot\exp\left\{-\left[\left(\frac{f}{2D}\right)^2+\mu^2\right]Dt\right\}. \tag{26}$$

Here the μ's are positive numbers which, in order for condition (23) to be obeyed, must be the roots of the equation

$$(\mu\delta)\cot(\mu\delta)=(\tfrac{1}{2}-k_0)\Delta. \tag{27}$$

Let $\mu_i\delta(i=1, 2, 3, \cdots)$ denote the ith positive root of (27). Condition (24) is obeyed by proper choice of multipliers B_i in a series of terms from the solution set (26).

$$e^{fy/2D}\sum_{i=1}^{\infty}B_i\sin\mu_i y=-C_{ss}(y) \quad \text{for} \quad 0<y\leq\delta. \tag{28}$$

Since the solutions $\bar{C}_{\mu_i}$ are orthogonal over the interval

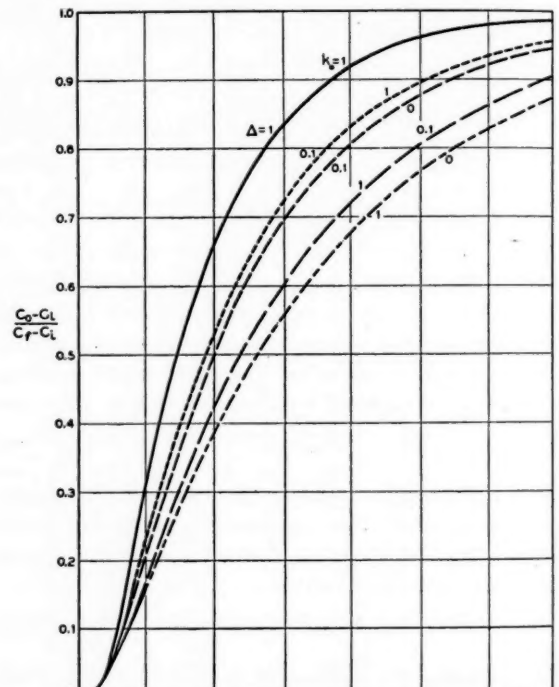

FIG. 3. Concentration at a crystal interface as a function of time following a step-function change in solute concentration in the melt.

$0\leq x\leq\delta$, the B_i's are given by

$$B_i=\frac{\int_0^\delta -\exp\left(-\frac{fy}{2D}\right)\cdot C_{ss}(y)\sin\mu_i y\,dy}{\int_0^\delta \sin^2\mu_i y\,dy}. \tag{29}$$

From this one can compute

$$\frac{\bar{C}}{C_L}=-2e^{fy/2D}\times\sum_{i=1}^{\infty}\frac{\mu_i\delta\sin\mu_i y\cdot\exp\left\{-\left[\left(\frac{\Delta}{2}\right)^2+(\mu_i\delta)^2\right]\frac{Dt}{\delta^2}\right\}}{\left(1-\frac{\sin 2\mu_i\delta}{2\mu_i\delta}\right)\left[\left(\frac{\Delta}{2}\right)^2+(\mu_i\delta)^2\right]}. \tag{30}$$

Then the concentration of solute in the melt next to the interface is found to be

$$\frac{C_0(t)}{C_L}=\frac{1}{k_0+(1-k_0)e^{-\Delta}}-2e^{\Delta/2}\times\sum_{i=1}^{\infty}\frac{\mu_i\delta\sin\mu_i\delta\cdot\exp\left\{-\left[\left(\frac{\Delta}{2}\right)^2+(\mu_i\delta)^2\right]\frac{Dt}{\delta^2}\right\}}{\left(1-\frac{\sin 2\mu_i\delta}{2\mu_i\delta}\right)\left[\left(\frac{\Delta}{2}\right)^2+(\mu_i\delta)^2\right]},\quad(31)$$

$\mu_i\delta$ being the ith positive root of

$$(\mu\delta)\cot(\mu\delta)=(\tfrac{1}{2}-k_0)\Delta.$$

More generally, let C_i be the initial concentration at the interface just before a step-function change is made in C_L at $t=0$, and let C_f be the final concentration at the interface after a new steady state is reached. Then from Eq. (31) it follows that the concentration at the interface, C_0, varies with time as shown in Fig. 3, for several values of k_0 and Δ.

ACKNOWLEDGMENT

It is a pleasure to express appreciation to Dr. H. Reiss and Dr. J. A. Lewis for several valuable discussions.

THE JOURNAL OF CHEMICAL PHYSICS VOLUME 21, NUMBER 11 NOVEMBER, 1953

Distribution of Solute in Crystals Grown from the Melt. Part II. Experimental

J. A. Burton, E. D. Kolb, W. P. Slichter, and J. D. Struthers
Bell Telephone Laboratories, Murray Hill, New Jersey

(Received May 18, 1953)

Experiments have been performed on the distribution coefficients of a number of solute elements in germanium crystals grown from the melt. The variation of distribution coefficient with conditions of crystallization is examined in the light of the theory of Part I. The incorporation of solute elements into the crystal is shown to depend critically upon the transport processes occurring in the melt.

THE distribution of solute atoms in germanium crystals grown from the melt was examined in Part I, with particular attention to the effect of transport processes in the melt. The distribution coefficient, defined as the ratio of the solute concentration in the solid to that in the body of the liquid, was related by a simple model to the growth parameters and to certain physical constants characteristic of the solvent-solute system. In Part II, the distribution coefficient in germanium is examined experimentally.

1. EQUILIBRIUM DISTRIBUTION COEFFICIENT

The equilibrium distribution coefficient was defined in Part I. For most elements in germanium the solid solubility is small, so that solute atoms are ordinarily present in germanium crystals to the extent of about $1:10^8$ to $1:10^6$. At these small concentrations, the laws of dilute solutions should apply, and the liquidus and solidus lines in the phase diagram should be virtually straight. Thus, the equilibrium distribution coefficient is usually independent of concentration in this concentration range.

Phase diagrams of many binary germanium alloys have been determined by Klemm and his co-workers.[1] However, this work has been done for concentrations of the order of one percent or greater, and affords little information on the distribution coefficients in this low concentration region.

For germanium crystals containing impurities less than a part per million, the ordinary methods of direct chemical analysis are too insensitive. Radioactive tracer techniques are applicable, however, for any element having a radioactive isotope with a suitably long half-life and a sufficiently high specific activity. Such measurements have been made with the following radioactive isotopes:* (60 day Sb^{124}), (26.8 hr As^{76}), (14.3 hr Ga^{72}), (14.3 day P^{32}), (50 day In^{114}), (12.9 hr Cu^{64}), (85 yr Ni^{63}), (2.7 day Au^{198}), (270 day Ag^{110}), (2.7 yr Tl^{204}), (250 day Zn^{65}), and (5.3 yr Co^{60}). The concentration of conventional donor or acceptor elements in solid germanium can also be determined from electrical conductivity measurements, combined with a knowledge of the electron and hole mobilities.† Both methods of analysis have been applied to single crystals

[1] W. Klemm and H. Stohr, Z. anorg. u. allgem. Chem. **241**, 305 (1939); *ibid.* **244**, 205 (1940). W. Klemm *et al.*, *ibid.* **256**, 239 (1948). See also M. Zumbush *et al.*, *ibid.* **242**, 237 (1939); also, M. Hansen, *Der Aufbau der Zweistofflegierunger*, (Springer, Berlin, 1936).

* The isotopes were obtained from Brookhaven and Oak Ridge National Laboratories on allocation from the Isotopes Division, U. S. Atomic Energy Commission.

† Distribution coefficients have been determined at the Bell Telephone Laboratories, from conductivity measurements, by H. C. Theuerer, M. Sparks, W. G. Pfann, G. L. Pearson, and W. P. Slichter.

TABLE I.

Element	Tetrahedral covalent radius (Pauling)	Approximate C_S/C_L	Notes
P	1.10	0.12	a
As	1.18	0.04	a
Sb	1.36	0.003	a
Bi	1.46	4×10^{-5}	b
B	0.88	>1	c
Al	1.26	0.10	d
Ga	1.26	0.10	a
In	1.44	0.001	e
Tl	1.47	4×10^{-5}	a
Cu	1.35	1.5×10^{-5}	a
Ag	1.53	10^{-4}	f
Au	1.50	3×10^{-5}	f
Ni	...	5×10^{-6}	a
Zn	1.31	0.01	a
Co	...	10^{-6}	f
Ge	1.22	1.0	...

[a] Both radioactive tracer and conductivity measurements.
[b] Conductivity measurements only.
[c] Conductivity measurements only. This value for boron is based on work by R. N. Hall, Phys. Rev. **78**, 645 (1950) and by W. G. Pfann (unpublished).
[d] Conductivity measurements only. This value for aluminum is based on work by H. C. Theurer.
[e] Both radioactive tracer and conductivity measurements. This value has been confirmed by J. J. Dowd and R. L. Rouse, Proc. Phys. Soc. (London) **6**, 60 (1953).
[f] Radioactive tracer measurements only.

prepared by the method of Teal and Little,[2] and to polycrystalline ingots.[3]

The techniques used to measure the absolute concentrations of tracer elements were essentially the same as those used by Pearson, Struthers, and Theuerer.[4] A known quantity of tracer element is added to the melt from which a crystal is grown. The analytical technique gives the concentration of solute, C_S in a given region of the crystal. The concentration of solute in the melt, C_L, at the time when that part of the crystal was formed is obtainable from the sum of the tracer content of the subsequent portions of the solid; or it is obtainable by subtracting the tracer content of the previous portions from the original quantity of solute added to the melt (assuming none to have been lost by evaporation). The ratio C_S/C_L gives the distribution coefficient for the given region of the crystal.

The use of conductivity measurements to determine concentration of donor and acceptor elements is convenient for most Group III-A and Group V-A elements, and is particularly valuable for elements like boron and aluminum which lack radioactive isotopes of long half-life. Use is made of the well known relation

$$\sigma = ne\mu_n + pe\mu_p, \tag{1}$$

where σ is the conductivity, e is the electronic charge, μ is the mobility of electrons (or holes), and n (or p) is the density of electrons (holes). If only one donor or acceptor element is present in significant amount, and if there is one donor or acceptor level per impurity atom, n (or p) is identified with C_S, at room temperature. Conductivity is readily measured, but some uncertainty exists concerning the value of μ,[5] for high conductivity samples.

Table I summarizes the distribution coefficients[6] for a number of solute elements in germanium, obtained from radioactive tracer and conductivity measurements. In Fig. 1, the measured values of C_S/C_L are plotted against the tetrahedral covalent radius[7] of the solute atom. It can be seen that C_S/C_L covers a wide range for the different solutes, and that there is a fairly consistent relation between the distribution coefficient and the atomic radius. As would be expected, the larger solute atoms are difficult to incorporate in the germanium lattice, and tend to remain in the liquid phase. The Group III-A and V-A elements are believed to enter the germanium lattice substitutionally with tetrahedral covalent bonds. Hence, the tetrahedral radius should be an approximate measure of atomic size for these elements. It is not known whether the other elements are incorporated substitutionally or interstitially. However, the distribution coefficients seem to depend on tetrahedral radius in much the same way, with the exception of copper. Since copper has an unusually large diffusion constant in germanium,[8] it is not surprising that copper should show singular behavior in other respects compared with other solute elements of comparable radius. Thus, it is seen that the distribution coefficient of copper is also irregular, being about 1/200 as large as that for antimony, an atom of like tetrahedral radius.

It should be emphasized that the values for C_S/C_L given in Table I are only approximate. These measurements were made on crystals grown at appreciable rates. Where possible, such measurements have been corrected to the zero growth rate values, using the theory of Part I. The uncertainties in this procedure and the experimental errors are of the order of a factor of two. In most cases, the errors are probably in the direction to cause the values quoted here to be larger than the true equilibrium values.

2. DISTRIBUTION COEFFICIENT AT FINITE GROWTH RATE

The steady-state distribution coefficient was found in Part I to depend upon growth conditions in the

[2] G. K. Teal and J. B. Little, Phys. Rev. **78**, 647 (1950).
[3] H. C. Theuerer and J. H. Scaff, Trans. Am. Inst. Mining Met. Engrs., **189** (1951). J. Metals, 59 (1951).
[4] Pearson, Struthers, and Theuerer, Phys. Rev. **77**, 809 (1950).
[5] W. Shockley, *Electrons and Holes in Semiconductors* (D. Van Nostrand Company, New York, 1950), p. 336. Mobility has been studied recently by P. P. Debye and E. M. Conwell, Phys. Rev. **87**, 1131 (1952). See also J. R. Haynes and W. Shockley, Phys. Rev. **81**, 835 (1951).
[6] Preliminary values of distribution coefficients have been reported previously by Struthers, Buehler, Theuerer, and Burton, J. Metals **4**, 149 (1952); and by J. A. Burton at the Inst. Radio Engrs. and Am. Inst. Elec. Engrs. Conference on Semi-conductor Device Research, June, 1952.
[7] L. Pauling, *Nature of the Chemical Bond* (Cornell University Press, Ithaca, 1945), p. 179.
[8] C. S. Fuller and J. D. Struthers, Phys. Rev. **87**, 526 (1952); W. P. Slichter and E. D. Kolb, Phys. Rev. **87**, 527 (1952).

following manner:

$$k=\frac{k^*}{k^*+(1-k^*)e^{-\Delta}}, \quad \Delta=\frac{f\delta}{D}, \quad k^*=k^*(f). \qquad (2)$$

Here again k is the effective distribution coefficient and k^* is the ratio C_S/C_0, describing the solute distribution at the solid-liquid interface. The thickness, δ, of the diffusion-dominated region depends upon growth rate, f, upon the diffusion coefficient in the liquid, D, and upon the crystal rotation rate. The quantity k^* depends in general upon f. The dependence of k upon growth conditions, for steady-state crystallization, has been examined experimentally for the solutes gallium and antimony. In these studies, single crystals were pulled[2] from a melt of germanium which had been purified by the molten zone technique.[9] The crystallization apparatus is shown schematically in Fig. 2.‡ When the desired crystal diameter was attained, about 2 cm, the heat input to the apparatus was regulated to keep the diameter uniform for the rest of the crystallization. Constancy of diameter was considered to be indicative of a steady state. When the proper diameter control was in effect, a known quantity of the solute element was added to the melt during the course of growth. In the case of gallium, which has a fairly large value of k_0 ($\sim$0.1), the solute was added in the form of a weighed pellet composed about 99.9 percent of germanium. The gallium content of the admixture was found by chemical analysis. In the case of antimony, which has a very small value of k_0($\sim$0.003), the solute was added in pure form. Arsenic is a common impurity in antimony, and since k_0 for arsenic is relatively large ($\sim$0.04), even a small contamination by this element

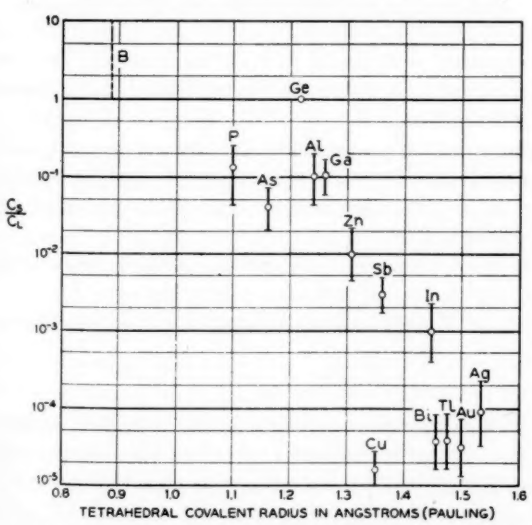

FIG. 1. Experimental values of the distribution coefficients of solute elements between liquid and solid germanium, plotted against the tetrahedral covalent radii of the elements.

[9] W. G. Pfann and K. M. Olsen, Phys. Rev. **89**, 322 (1953).

‡ The apparatus and methods used were those developed by G. K. Teal and his co-workers (see reference 2).

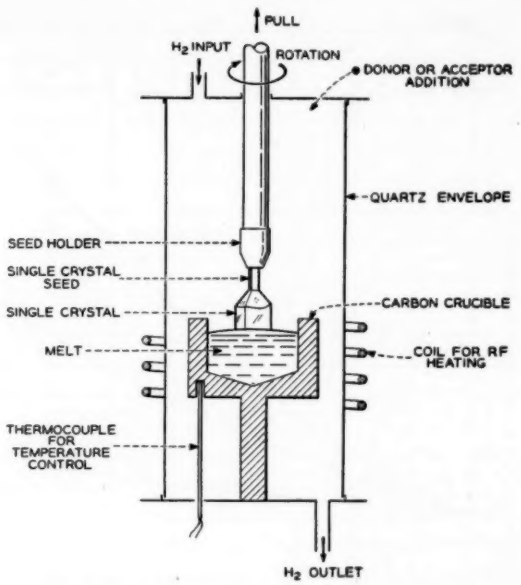

FIG. 2. Schematic diagram of the apparatus used to grow single crystals of germanium for the melt.

can markedly increase the apparent distribution coefficient of the antimony. In the present case, however, spectrochemical analysis showed the antimony to be free of arsenic. With both the gallium and the antimony, the quantity of solute was limited so as to keep the resulting resistivity not less than about one ohm-cm, in order to minimize the uncertainty concerning the mobility of the current carriers.

The concentration of solute in the solid before and just after the impurity addition was found by conductivity measurements. The volume of solid previous to impurity addition was measured, and from this were determined the melt volume and hence the value of C_L at the time of addition. The ratio of C_S, the solid solute concentration due to the added impurity, to C_L gave the effective distribution coefficient.

Crystals were grown under a variety of growth rates and rotation rates. Figure 3 displays the results for the case of antimony in germanium. The curves were fitted to the experimental points by the method of trial and error. The curves were calculated on the basis of Eq. (15) of Part I, which involves the assumption that equilibrium exists at the solid-liquid interface ($k^*=k_0$), virtually independently of growth rate. An appropriate value for k_0 (0.003) was adopted, and by trial a value of δ/D was chosen for one rotation rate. The values of δ/D for the other rotation rates were then found from this first value by means of Eq. (10) of the theory in Part I. Figure 4 shows similar data for the case of gallium, with k_0 taken to be 0.085, and with the curves computed in like manner.

With both solutes, it appears that reasonable agreement is obtainable between experiment and the simple theory, within the limits of experimental uncertainty. This uncertainty is seen to be not less than $\pm$10 percent.

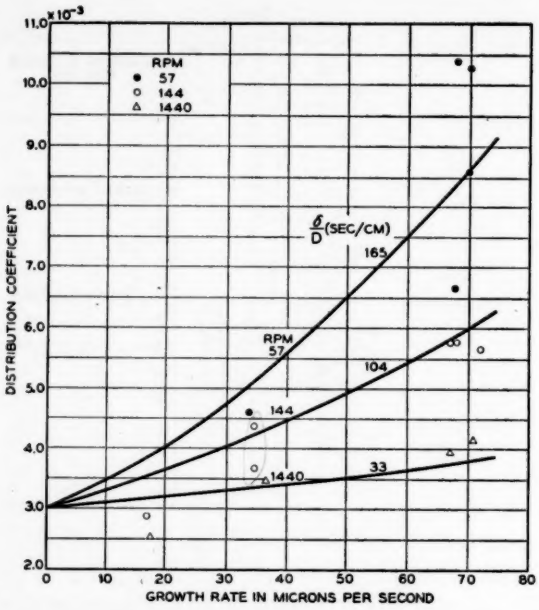

FIG. 3. Distrubution coefficient of antimony in germanium, as a function of crystal growth rate and rotation rate.

Although it may be true that k^* depends in some degree upon f, one is not forced to conclude that the effect is important with the solutes investigated. Indeed, if the theory used to plot the curves is correct, the data do not entitle one to a conclusion which is any more detailed than the simple relation $k^*=k_0$.

It is quite obvious that the effective distribution coefficient depends critically upon the intensity of stirring. This fact shows that diffusion in the liquid contributes significantly to the over-all kinetics. This finding is in conflict with Hall's belief[10] that he had obtained virtually complete mixing in the melt, with a crystal rotation rate of only 200 rpm.

The experiments on distribution coefficient lead to the choice of values of the ratio δ/D which for a given solute depend upon the rotation rate and are independent of growth if f is small enough. The physical constants required for the exact calculation of δ/D from the theory evidently have not been investigated. But it is proper to ask whether the values for δ/D found somewhat artificially from the present experiments lead to reasonable figures for the diffusion coefficients. Equation (11) of Part I may be rewritten to yield an expression for the diffusion coefficient, D, in terms of the angular velocity, ω, and the corresponding value of δ/D.

$$D=2.0\left(\frac{\delta}{D}\right)^{-\frac{1}{3}}\nu^{\frac{1}{6}}\omega^{-\frac{1}{2}}. \tag{3}$$

Taking a reasonable value for the kinematic viscosity, (0.0025 cgs unit), and the experimental values of δ/D, it then develops from (3) that D for gallium in molten germanium is 7.5×10^{-5} cm^2 sec^{-1}, and for antimony D is 5.5×10^{-5} cm^2 sec^{-1}. It is interesting to note that the values thus obtained from the theory are of the same magnitude as diffusion coefficients reported in the literature for a wide variety of solutes in molten elements.

[10] R. N. Hall, Phys. Rev. 88, 139 (1952).

3. UNIFORM DISTRIBUTION OF SOLUTE

The validity of the theory of Part I may be tested in another way. It is well known that when freezing proceeds at a constant rate, the solute concentration generally increases markedly in the direction of freezing.[11] An extension of the theory permits one to derive the growth conditions required to keep the concentration uniform over a large part of the solid. Experiments following this approach reflect on the correctness of the basic theory.

For a given fraction of crystal grown, the greater the rate of freezing, the greater is the concentration of solute brought into solid solution. For the early stages of crystallization, therefore, let a fairly high growth speed be used, so that the rate at which impurity is frozen into the solid will be enhanced, compared with the amount obtainable at reduced speeds. Then, as the accumulation of solute in the melt tends to increase the concentration in the solid still more, let the growth rate be progressively decreased. By the proper program for the decrease of growth speed, uniform solute concentration is in principle obtainable over an extended region of the crystal.[12]

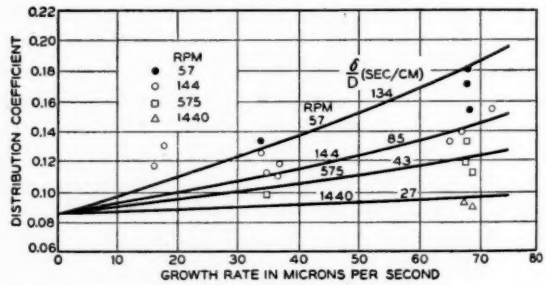

FIG. 4. Distrubition coefficient of gallium in germanium, as a function of cyrstal growth rate and rotation rate.

If the mean concentration of solute in the system is C_M, the following relation exists between C_L and the fraction of melt frozen, X, since C_S is to be constant:

$$C_L(1-X)+C_SX=C_M. \tag{4}$$

(The small amount of solute in the boundary layer next to the crystal is neglected.) Let the maximum extent of uniform solid obtained when the growth rate has been progressively reduced to zero be termed X_0. At this point, Eq. (4) becomes

$$C_L^0(1-X_0)+C_SX_0=C_M. \tag{5}$$

[11] See reference 5 in Part I.

[12] This technique was first investigated empirically by G. K. Teal and E. Buehler (unpublished).

Equating (4) and (5), and using (2), one can obtain a relation which defines the required variation of growth rate with fraction of material solidified, for a crystal grown under steady-state conditions.

$$\frac{1-k^*}{k^*}\cdot e^{-\Delta}=\frac{1-k_0}{k_0}\cdot\frac{1-X_0}{1-X}. \tag{6}$$

Both Δ and k^* depend upon f, but if there is virtual equilibrium at the solid-liquid interface ($k^*=k_0$), Eq. (6) assumes a simple form:

$$e^{-\Delta}=(1-X_0)/(1-X). \tag{7}$$

It is evident that the fraction X_0 cannot be reached in finite time. However one can choose a hypothetical X_0, and can in practice approach this value quite closely within a convenient time. For a chosen value of X_0, one has some freedom in the selection of crystal rotation rate and initial growth rate. Figure 5 shows the variation of resistivity along the length of a representative

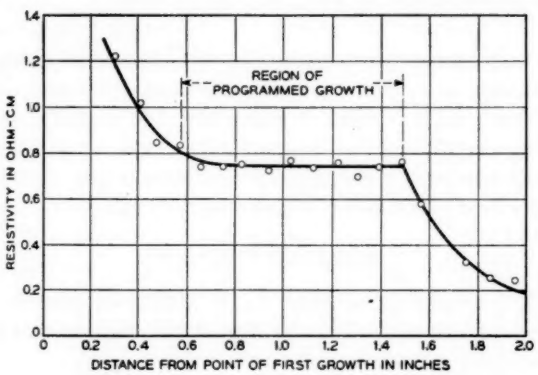

FIG. 5. Example of the variation of resistivity with distance in a crystal grown with a programmed growth rate.

crystal, a portion of which was grown as specified by Eq. (7). In this case, arsenic was used as the solute. The crystal diameter was kept constant over the region of programmed growth, as a criterion for steady-state growth. It is seen that the solute concentration is quite uniform over the programmed region. This result offers further substantiation of the basic theory.

4. STRIATED CONCENTRATION DISTRIBUTIONS

The importance of transport processes in the melt to the over-all reaction of solute incorporation during crystallization is further seen from a study of the effects which prevail when the mechanical stirring of the melt is deliberately made negligible. Then fluid motion comes only from thermal convection currents which doubtless fluctuate, and so the contribution of diffusion to the transport process continually changes. Thus the crystal is grossly inhomogeneous in its solute composition. Variations in concentration can also result from fluctuations in growth rate, caused by cyclic or erratic variations in the temperature control.

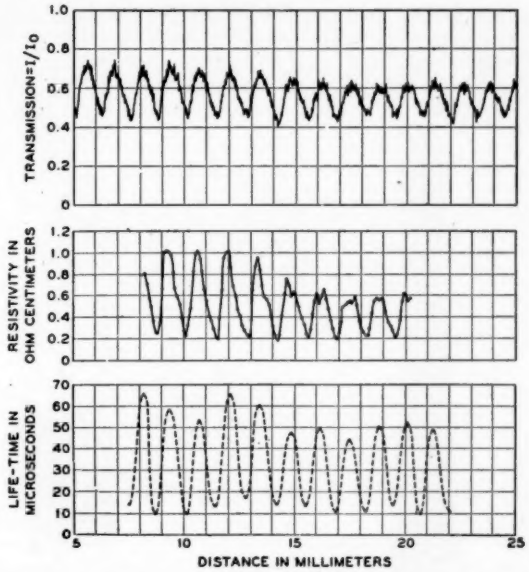

FIG. 6. Optical transmission of radioautograph, electrical resistivity, and hole lifetime for a germanium crystal exhibiting a straited distribution of antimony (data of J. D. Struthers, G. L. Pearson, and J. R. Haynes).

The concentration fluctuations are best seen with the aid of radioautographs, which are made by cutting the crystal longitudinally along the direction of growth, and placing this flat ground surface in contact with a photographic plate. The radiations from the tracer element expose the emulsion to a degree which is roughly proportional to the concentration of tracer in the crystal. J. R. Haynes and G. L. Pearson[13] have shown that accompanying irregularities occur in the lifetime of injected current carriers and in the resistivity. Figure 6 shows the corresponding variations in solute concentration, hole lifetime and resistivity in one of these irregular crystals.

Figure 7 shows crystals grown from a poorly stirred melt, where the speed of crystal rotation was only four rpm, so that the fluid flow was probably largely the result of uncontrolled convection currents. Growth rates were in the range 1 to 2 mils/sec. In both cases shown, the radioautographs reveal bands or striations of high and low solute concentration parallel to the solid-liquid interface, and spaced about 0.5 to 2 mm apart.

In contrast, Fig. 8 shows radioautographs of two germanium crystals which were prepared with good stirring. Both crystals were grown at 2 mils/sec. For the crystal shown on the left, both the crystal and the crucible containing the melt were rotated at 120 rpm, in opposite directions. The crystal shown on the right was rotated at 60 rpm, with a stationary crucible. It is noteworthy that the more intense stirring produced homogeneous concentrations in the crystals, except for normal segregation in the direction of growth.

In Fig. 7 (left) and Fig. 8 (right), one can detect crystallographic twins; these regions are quite distinct

[13] Unpublished studies.

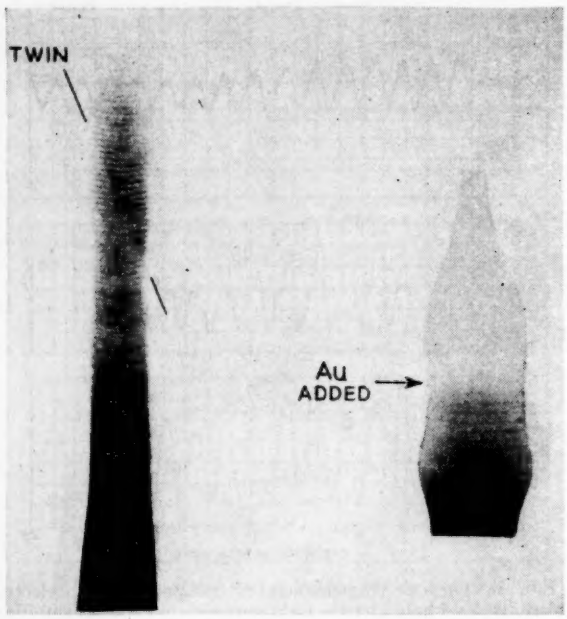

FIG. 7. Radioautographs of germanium crystals prepared from poorly stirred melts (crystal rotated at 4 rpm): (left) radioactive antimony added; (right) radioactive gold added.

in the original radioautographs. It is seen that a change in solute concentration, and hence a change in the effective distribution coefficient, accompanies the shift in crystal orientation. From measurements of the optical density of the radioautographs, it is estimated that the distribution coefficient changed by not more than five percent. It is not clear whether this change is to be attributed to a change in the dependence of $k^*(f)$ upon

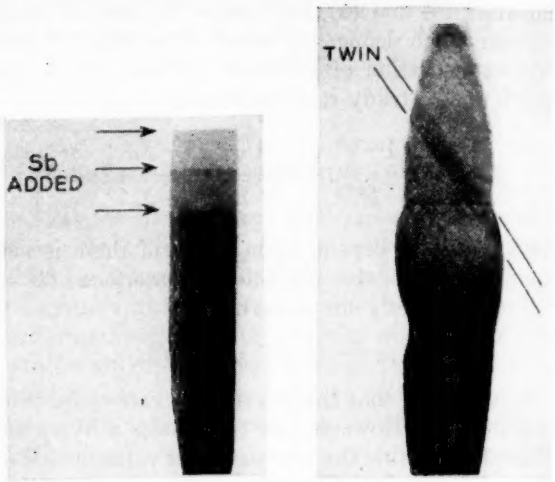

FIG. 8. Radioautographs of germanium crystals prepared from well-stirred melts: (left) germanium single crystal rotated at 120 rpm and grown from a melt to which three antimony pellets were added; (right) twinned germanium crystal containing radioactive phosphorus and grown with a rotation of 60 rpm.

growth rate, which is essentially Hall's viewpoint,[10] or to a change in k_0 with crystallographic orientation.

Thus, Figs. 7 and 8 point out the importance of adequate stirring to the growth of homogeneous crystals and by inference show the importance of the transport process in the melt to the over-all reaction.

ACKNOWLEDGMENT

The assistance of Miss A. D. Mills and Miss K. B. Wolfstirn in making a number of the measurements is gratefully acknowledged.

The Infrared Spectra of the Methyl Chlorosilanes

A. Lee Smith
Spectroscopy Laboratory, Dow Corning Corporation, Midland, Michigan
(Received May 4, 1953)

The infrared spectra of the series $SiCl_4$ through $SiMe_4$ have been obtained in the gas phase over the range 2–25 microns using CaF_2, NaCl, and KBr prisms. The spectra are compared with Raman data for these compounds, and vibrational assignments are made. The methyl band at about 8 microns is shown to be associated with the symmetrical CH_3 deformation, the bands around 12 microns with the methyl rocking and Si–C stretching vibrations, and the bands between 16 and 25 microns with the SiCl stretching modes. A comparison of frequencies for the members of the series has made it possible to assign fundamentals for all motions except those involving torsion of the Me group around its axis.

INTRODUCTION

ALTHOUGH the methyl chlorosilanes are both industrially important and theoretically interesting, they have received very little attention from infrared spectroscopists. There is no question as to the structures of these molecules since silicon is known to form tetrahedral bonds analogous to carbon. Electron diffraction studies[1] also show results consistent with tetrahedral bonding. Nevertheless, the infrared spectra of silicon-containing organic compounds present many interesting features, of which one of the most arresting is the constancy of certain frequencies,[2,3] even at longer wavelengths where empirical correlations often break down. It was therefore thought profitable to study a series of compounds containing different distributions of the same groups, since in this way absorption bands arising from a particular motion of a given group can be traced throughout the series and vibrational assignments made. In this paper the infrared spectra for the series $Me_xSiCl_y(x+y=4)$ are shown from 2–25μ and the infrared bands correlated with the Raman data.

EXPERIMENTAL DETAILS

The compounds studied were plant grade products which were purified by fractional distillation. The infrared spectra of the resulting materials did not show any bands which could be attributed to other members of the series from which they had been separated. A Baird Associates double-beam infrared spectrometer equipped with a NaCl prism, and a Perkin-Elmer Model 12-C spectrometer equipped with KBr and CaF_2 prisms were used to record the spectra. The instruments were calibrated with polystyrene, water vapor, ammonia, and methyl alcohol vapor bands.[4] The calibration error should be less than ± 2 cm^{-1} from 400–650 cm^{-1}, and ± 4 cm^{-1} from 650–3200 cm^{-1}. A 10-cm gas cell was used throughout. The intensity of the infrared absorption was therefore limited in some cases by the vapor pressure of the sample.

[1] R. L. Livingston and L. O. Brockway, J. Am. Chem. Soc. **66**, 94 (1944); *ibid.* **68**, 719 (1946).
[2] N. Wright and M. J. Hunter, J. Am. Chem. Soc. **69**, 803 (1947).
[3] Young, Servais, Currie, and Hunter, J. Am. Chem. Soc. **70**, 3758 (1948).
[4] E. K. Plyler and C. W. Peters, J. Research Natl. Bur. Standards **45**, 462 (1950).

INTERPRETATION OF THE SPECTRA

Experience has shown that the skeletal vibrations of the alkyl chlorosilanes fall into fairly well defined regions of the spectrum. The C–H stretching frequencies, of course, occur at about 3000 cm^{-1}, and the bending frequencies in the region 1100–1500 cm^{-1}; and vibrations involving Si–Cl stretching lie in the region 400–625 cm^{-1}. The Si–Cl bending frequencies are found in the range 0–400 cm^{-1}.

1. $SiCl_4$

This molecule belongs to point group T_d and has four fundamental vibrations, of which one is doubly degenerate and two are triply degenerate. Only the latter are infrared active, but all vibrations are active in the Raman effect. The Raman spectrum of liquid silicon tetrachloride has been studied by several investigators.[5] Raman shifts are shown in Table I along with the infrared data. It will be noted that ν_3 is shifted appreciably on going from the liquid to the gas. The infrared spectrum is shown in Fig. 1. It is interesting that no strong bands appear in the sodium chloride range, but in thick layers a number of absorptions appear which

Table I. Assignment and symmetry of $SiCl_4$ bands.

Infrared Freq.	Infrared Intensity[a]	Raman[5] Freq.	Raman[5] Intensity	Interpretation
1232	MW			$2\nu_3(=1242)(A_1+E+F_2)$
1064	VW			$2\nu_1+\nu_4(=1069)(F_2)$
1044	MW			$\nu_1+\nu_3(=1045)(F_2)$
838	VVW			$\nu_3+\nu_4(=842)(A_1+E+F_2)$
798	VVW			$\nu_1+\nu_2+\nu_4(=795)(F_1+F_2)$
765	M			$\nu_2+\nu_3(=771)(F_1+F_2)$
647	M			$\nu_1+\nu_4(=645)(F_2)$
621	VS	610	(2b)	ν_3 (F_2 fundamental)
		424	(5), P	ν_1 (A_1 fundamental)
		221	(4)	ν_4 (F_2 fundamental)
		150	(4)	ν_2 (E fundamental)

[a] V = Very. W = Weak. M = Medium. S = Strong. P = Polarized. b = Broad.

[5] See, for example, Delwaulle, Buisset, and Delhaye, J. Am. Chem. Soc. **74**, 5768 (1952); J. Goubeau and R. Warneke, Z. anorg. u. allgam. Chem. **138**, 233 (1949).

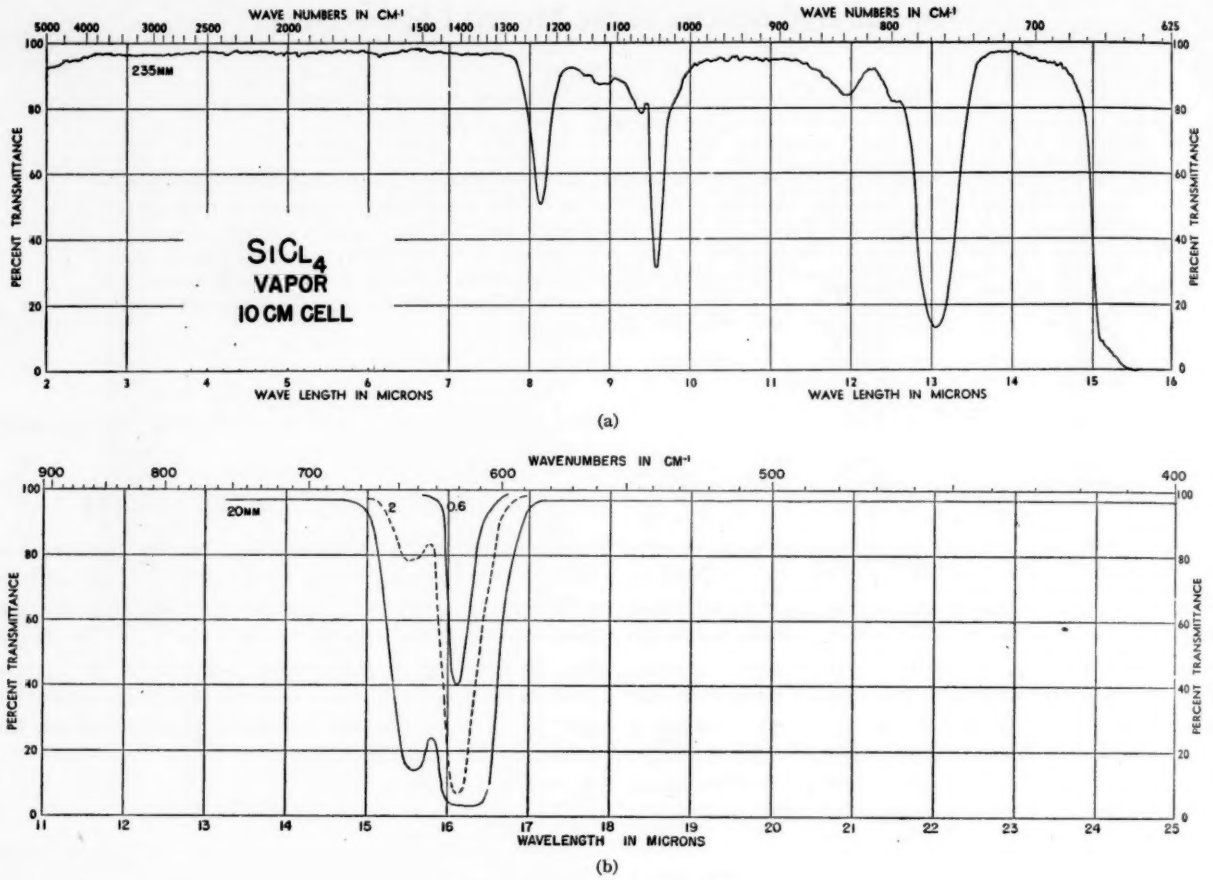

FIG. 1. Infrared spectrum of $SiCl_4$.

are satisfactorily explained as combination and overtone bands. The asymmetry of the 621 cm^{-1} fundamental is no doubt the result of the presence of Cl^{37} isotopes. The numbering of the fundamentals follows the suggestion of Herzberg.[6]

2. CH_3SiCl_3

Methyl trichlorosilane is the simplest of the methyl chlorosilanes. It belongs to point group C_{3v} whether the molecule has the staggered or eclipsed configuration. It has 12 fundamental vibrations of which five belong to species A_1, one to species A_2, and six to species E (doubly degenerate). All vibrations except the A_2 twisting mode are both infrared and Raman active. The molecule is a symmetric top rotator, with the center of mass lying within the $SiCl_3$ pyramid. The moments of inertia are $I_x = I_y = 466.2 \times 10^{-40}$ gm cm^2 and $I_z = 639.5 \times 10^{-40}$ gm cm^2, assuming tetrahedral angles and $r_{Si-Cl} = 2.01$A, $r_{C-H} = 1.09$A, and $r_{Si-C} = 1.88$A[1]. The infrared spectrum is shown in Fig. 2.

Several assignments can be made unambiguously. The C—H stretching bands at 2923 and 2990 cm^{-1} are obviously the symmetrical and unsymmetrical stretching modes.[7] The bands between 400 and 650 cm^{-1} occur in all chlorosilanes and must arise from the Si—Cl stretching vibrations. The band at 458 cm^{-1} shows PQR structure which means for this point group that it is a parallel band and belongs to species A_1. It arises from the symmetrical Si—Cl stretching motion. The strong absorption at 577 cm^{-1} has the shape of a perpendicular band, has a corresponding broad Raman line, and therefore arises from the unsymmetrical Si—Cl stretching.

There has been some disagreement about the origin[2,3,8] of the band at 1271 cm^{-1}. This band is found in all compounds containing one or more methyl groups on silicon. The spectrum of gaseous methyl trichlorosilane shows clearly that this is a parallel band (see Figs. 2 and 3). Further evidence that it is a parallel band is obtained by calculating the separation of the P—R maxima.[9] This can be done quite accurately for a molecule with large moments of inertia. The calculated separation of the rotational wings, 14.9 cm^{-1}, agrees very well with the observed separation shown in Fig. 3. The band at 1271 cm^{-1} therefore must be the result of the symmetrical deformation of the methyl group.

[6] G. Herzberg, *Molecular Spectra and Molecular Structure II*, (D. van Nostrand Company, Inc., New York, 1945), p. 272.

[7] J. J. Fox and A. E. Martin, Proc. Roy. Soc. (London) **A175**, 208 (1940).

[8] R. E. Richards and H. W. Thompson, J. Chem. Soc. **1949**, 124.

[9] S. L. Gerhard and D. M. Dennison, Phys. Rev. **43**, 197 (1933).

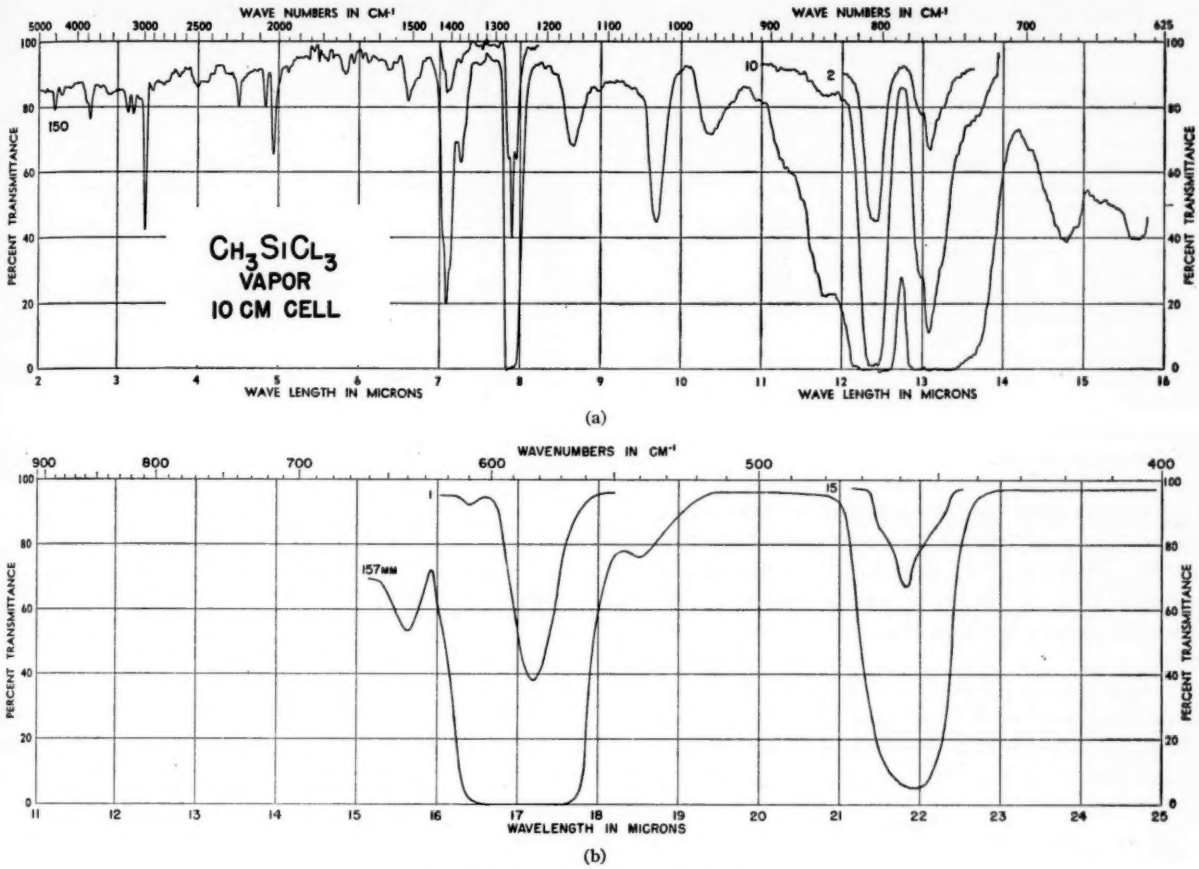

FIG. 2. Infrared spectrum of $MeSiCl_3$.

The 1417 cm^{-1} fundamental can be assigned as the unsymmetrical deformation. A parallel structure is shown by the band at 764 cm^{-1} which may therefore be roughly characterized as a Si—C stretching mode. The perpendicular band at 804 cm^{-1} is assigned as methyl rocking.

This leaves four vibrations to be assigned. The symmetrical $SiCl_3$ deformation is the lowest totally symmetric frequency, and can be assigned to the Raman band at 229 cm^{-1} by analogy with $HSiCl_3$, which has a polarized Raman line[10] at 250 cm^{-1}. The unsymmetrical $SiCl_3$ deformation is also assigned to the 229-cm^{-1} band, since this is a broad Raman line, and such lines arise from nontotally symmetric vibrations.[11] The broad Raman line at 164 cm^{-1} is the result of a motion which is essentially $SiCl_3$ rocking. The twisting frequency ν_6 is inactive in both the infrared and Raman effect, and no convincing assignment can be made in the absence of supplementary data. There is a possibility that the weak infrared band at 537 cm^{-1} is $2\nu_6$ (which is of species A_1), so that ν_6 would have a frequency of approximately 270 cm^{-1}. This frequency seems rather high, however. All observed infrared and Raman bands and their assignments are given in Tables II and III. Raman shifts are average values except where otherwise noted. The assignment of the fundamentals is essentially the same as that of Burnelle and Duchesne,[12] although it was made independently of their results.

3. Me_2SiCl_2

Dimethyl dichlorisilane has two vertical planes of symmetry (point group C_{2v}), analogous to propane. The molecule is an asymmetric top rotator, with the center of mass lying within the $SiCl_2$ triangle. Coordinate axes have been chosen such that the methyl groups

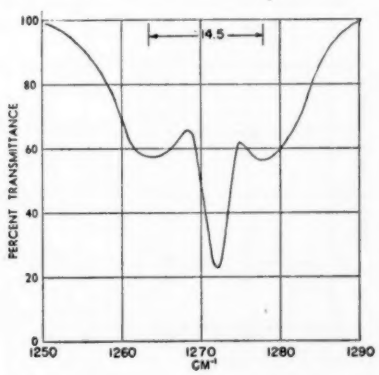

FIG. 3. 8μ band of $MeSiCl_3$ under high resolution.

[10] M. deHemptinne and J. Wouters, Nature **138**, 884 (1936).
[11] See reference 6, p. 446.
[12] L. Burnelle and J. Duchesne, J. Chem. Phys. **20**, 1324 (1952).

TABLE II. Description of vibrational modes and frequency assignment for $MeSiCl_3$.

Approximate description	A_1	A_2	E	Frequency
CH_3 nonsym. str.			ν_7	2990
CH_3 sym. str.	ν_1			2923
CH_3 nonsym. deform.			ν_8	1417
CH_2 sym. deform.	ν_2			1271
CH_3 rocking			ν_9	804
Si−C str.	ν_3			764
Si−Cl nonsym. str.			ν_{10}	577
Si−Cl sym. str.	ν_4			458
$SiCl_3$ nonsym. deform.			ν_{11}	229
$SiCl_3$ sym. deform.	ν_5			229
$SiCl_3$ rocking			ν_{12}	164
Si−Me torsion		ν_6		?
Activity[a]	I, R		I, R	

[a] I = Infrared. R = Raman.

TABLE III. Assignment of CH_3SiCl_3 bands.

Infrared Freq.	Intensity	Raman[a,b] Freq.	Intensity	Interpretation	
3800	VW[c]			$\nu_7+\nu_9$	(=3794)
3722	VW			$\nu_1+\nu_9$	(=3727)
3213	VW			$\nu_7+\nu_5$	(=3219)
3151	VW			$\nu_1+\nu_5$	(=3152)
2990	M	2982	(6)	ν_7 (E fundamental)	
2923	VW	2912	(8)	ν_1 (A_1 fundamental)	
2072	W			$\nu_2+\nu_9$	(=2075)
2028	MW			$\nu_2+\nu_3$	(=2035)
1940	VW			$\nu_2+\nu_4+\nu_5$	(=1958)
1710	W			$\nu_2+\nu_4$	(=1729)
1520	M			$2\nu_3$	(=1528)
1417	MW	1405	(2)	ν_8 (E fundamental)	
1383	S			$\nu_9+\nu_{10}$	(=1381)
1271	W	1268	(1)	ν_2 (A_1 fundamental)	
1155	M			$2\nu_{10}$	(=1154)
1032	W			$\nu_4+\nu_{10}$ (=1035) and/or $\nu_5+\nu_9$	(=1033)
964	W			$\nu_9+\nu_{12}$	(=967)
804	VS			ν_9 (E fundamental)	
764	VS	760	(5)	ν_3 (A_1 fundamental)	
730	VW			$(\nu_4+\nu_6)$?	(=728)
678	W			$\nu_4+\nu_5$	(=687)
640	W			$\nu_9-\nu_{12}$	(=641)
577	VS	577	(4b)	ν_{10} (E fundamental)	
537	VW			$(2\nu_6?)$ (Impurity?)	
458	M	450	(9)	ν_4 (A_1 fundamental)	
		229	(9b)	ν_5, ν_{11} (A_1, E fundamentals)	
		163	(9b)	ν_{12} (E fundamental)	

[a] Shimanouchi, Tsuchiya, and Mikawa, J. Chem. Phys. **18**, 1306 (1950).
[b] Goubeau, Siebert, and Winterwerb, Z. anorg. u. allgem. Chem. **259**, 240 (1949).
[c] See reference a, Table I.

lie in the x−z plane and the chlorines in the y−z plane. The moments of inertia are approximately $I_x=637\times10^{-40}$, $I_y=218\times10^{-40}$, and $I_z=576\times10^{-40}$ gm cm^2. Therefore type A, B, or C bands will arise from a change in moments along the y, z, or x axis, respectively.

The spectrum is shown in Fig. 4. The CH_3 stretching and deformation bands have about the same frequency as they did in $MeSiCl_3$, and the Si−Cl stretching bands are also easy to assign. The rather peculiar looking envelope at about 820 cm^{-1} contains three bands, as is shown by the spectrum of the liquid (see Fig. 5). The methyl rocking and Si−C stretching frequencies are expected in this region. The two bands having sharp Q

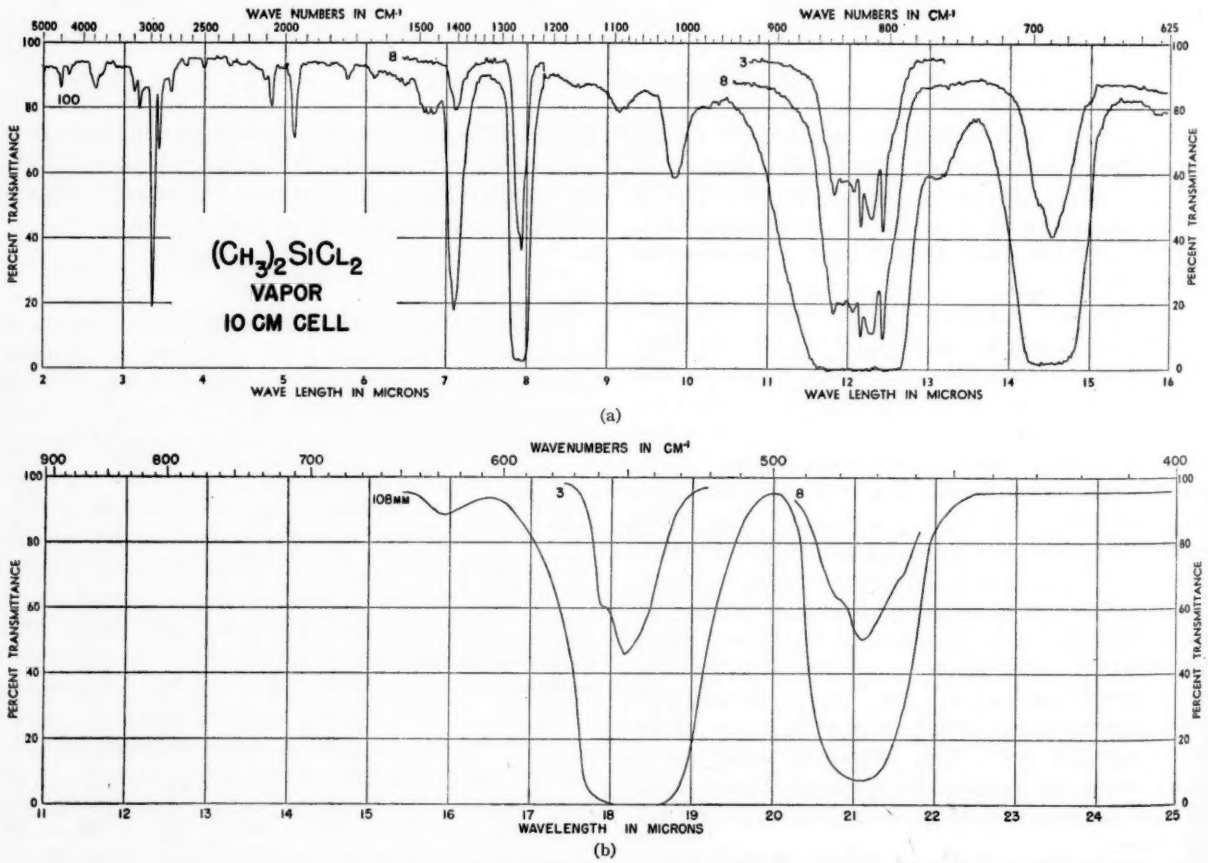

FIG. 4. Infrared spectrum of Me_2SiCl_2.

TABLE IV. Description of vibrational modes and frequency assignment for Me_2SiCl_2.

Approximate description	A_1	A_2	B_1	B_2	Frequency
CH_3 nonsym. str.	ν_1	ν_{10}	ν_{15}	ν_{22}	2984 cm^{-1}
CH_3 sym. str.	ν_2		ν_{16}		2918
CH_3 nonsym. deform.	ν_3	ν_{11}	ν_{17}	ν_{23}	1412
CH_3 sym. deform.	ν_4		ν_{18}		1261
CH_3 rocking (sym.)	ν_5	ν_{12}			847
CH_2 rocking (nonsym.)			ν_{19}	ν_{24}	823
Si−C nonsym. str.			ν_{20}		805
Si−C sym. str.	ν_6				688
Si−Cl nonsym. str.				ν_{25}	553
Si−Cl sym. str.	ν_7				473
Si−Me_2 rocking			ν_{21}		298
Si−Cl_2 rocking				ν_{26}	241
Si−Me_2 deformation	ν_8				232
Si−Cl_2 twisting		ν_{13}			177
Si−Cl_2 deformation	ν_9				168
Si−Me torsion		ν_{14}		ν_{27}	?
Activity[a]	I, R	R	I, R	I, R	

[a] I = Infrared. R = Raman.

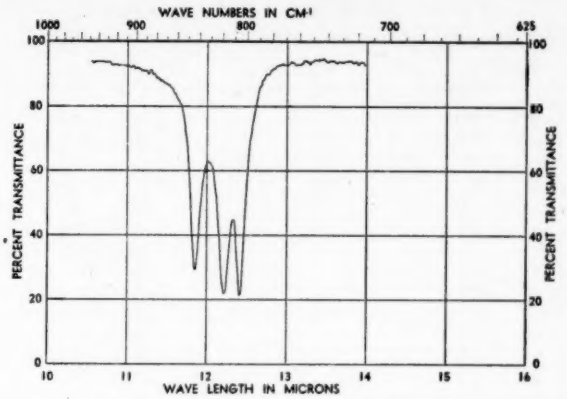

FIG. 5. Infrared spectrum of liquid Me_2SiCl_2.

branches at 805 cm^{-1} and 823 cm^{-1} must be of approximately the same type (A or C) and are therefore assigned to the nonsymmetrical methyl rocking and nonsymmetrical Si−C stretching motions, respectively. The fact that combination 532+805=1337 cm^{-1} ($B_2 \cdot B_1 = A_2$) appears in the Raman spectrum but not in the infrared (vibrations of species A_2 are infrared inactive) supports this assignment. The symmetrical methyl rocking is assigned as 847 cm^{-1}, and the symmetrical Si−C stretch as 688 cm^{-1}. These assignments are consistent with the observed band envelopes, the Raman intensities, and the noncrossing rule (see the concluding discussion). A complete fundamental frequency assignment is given in Table IV, and the overtone and combination bands are listed in Table V. The description of the vibration is, of course, very approximate, especially in the case of the lower frequencies.

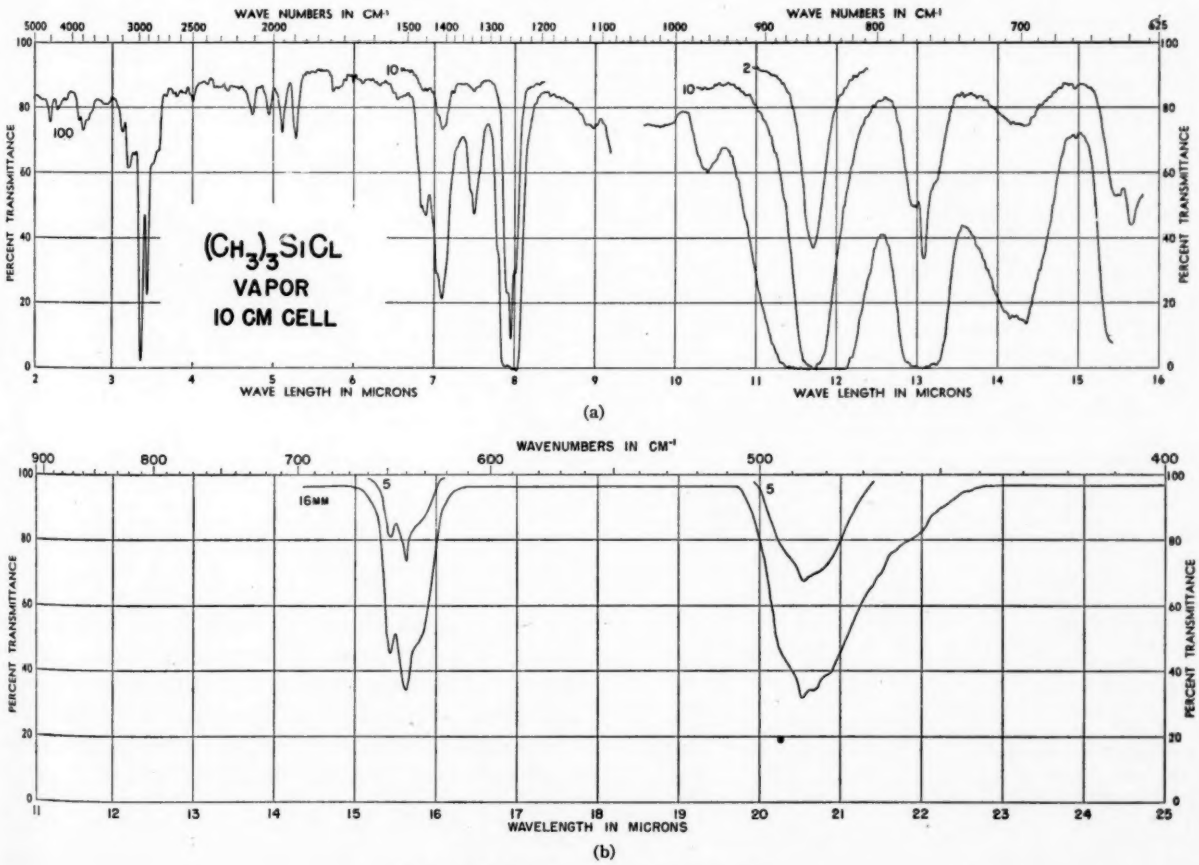

FIG. 6. Infrared spectrum of Me_3SiCl.

TABLE V. Assignment of $(CH_3)_2SiCl_2$ bands.

Infrared Freq.	Infrared Intensity[b]	Raman[a] Freq.	Raman[a] Intensity	Interpretation
~3208	VW			232+2984=3216
~3147	VW			168+2984=3152
2984	MS	2979	10b	ν_1, ν_{15}, ν_{22}
2918	W	2908	10b	ν_2, ν_{16}
2802	VW			2984−168=2816
~2750	VVW			2918−168=2750
~2650	VVW			1261+1412=2673
~2500	VW			2×1261=2522
~2100	VVW			688+1412=2100
~2069	W			805+1261=2066
~1958	W			560+1412=1972
1730	VW			473+1261=1734
1630	VVW			805+823=1628
1540	VVW			298+1261=1559
1475	W	1472[c]	1	688+805=1493
1412	MS	1400	6b	ν_3, ν_{17}, ν_{23}
		1335[c]	2	532+805=1337
1261	S	1267	2	ν_4, ν_{18}
1093	W	1123[c]	1	1261−168=1093
1016	M			168+847=1015
847	S			ν_5, ν_{12}
823	S			ν_{19}, ν_{24}
805	S	803	5b	ν_{20}
760	VW	758[c]	1	298+473=771
688	M	690	8	ν_6
553	S	532	4b	ν_{25}
473	M	463	10	ν_7
		323[c]	1	2×168=336?
		298	2	ν_{13}
		241	5b	ν_{21}
		232	7	ν_8
		177	10sb	ν_{26}
		168	12	ν_9

[a] See references a and b, Table III.
[b] See reference a, Table I.
[c] Observed only by Goubeau, *et al.*

4. Me_3SiCl

This molecule is again a symmetric top rotator with a threefold symmetry axis. The approximate moments of inertia are $I_x = I_y = 374 \times 10^{-40}$ gm cm^2, and $I_z = 238 \times 10^{-40}$ gm cm^2. The infrared spectrum is shown in Fig. 6, and the vibrational assignments are given in Table VI. The assignments are straightforward when the spectrum of Me_3SiCl is considered along with those of the other methyl chlorosilanes. Parallel vibrations give rise to bands showing P–Q–R structure, as expected, except for the SiCl stretching frequency where the Cl^{37} isotope introduces some asymmetry in the 487 cm^{-1} band. Also, totally symmetric vibrations (487 and 640 cm^{-1}) give the most intense Raman lines (see Table VII).

TABLE VI. Description of vibrational modes and frequency assignment for Me_3SiCl.

Approximate description	A_1	A_2	E	Frequency
CH_3 nonsym. str.	ν_1	ν_9	ν_{13}, ν_{14}	2977 cm^{-1}
CH_3 sym. str.	ν_2		ν_{15}	2912
CH_3 nonsym. deform.			ν_{16}, ν_{17}	1454
CH_3 nonsym. deform.	ν_3	ν_{10}		1415
CH_3 sym. deform.	ν_4		ν_{18}	1260
CH_3 rocking (nonsym.)			ν_{19}, ν_{20}	857
CH_3 rocking (sym.)	ν_5	ν_{11}		767
Si−C nonsym. str.			ν_{21}	700
Si−C sym. str.	ν_6			640
Si−Cl str.	ν_7			487
Si−C nonsym. deform.			ν_{22}	330
Si−C sym. deform.	ν_8			242
Si−Cl bending			ν_{23}	188
Si−Me torsion		ν_{12}	ν_{24}	?
Activity[a]	I, R		I, R	

[a] I = infrared. R = Raman.

5. Me_4Si

The infrared spectrum of tetramethyl silane has been observed, with different interpretations, by Young, Koehler, and McKinney;[13] and by Rank, Sakensa, and Shull.[14] Our interpretation of the spectrum, which is shown in Fig. 7, agrees with that of the former authors, and therefore no data are tabulated in this paper. It seems clear that Rank, *et al*[14] have erred in their assignment of 863 cm^{-1} as a combination band, since this fre-

TABLE VII. Assignment of $(CH_3)SiCl$ bands.

Infrared Freq.	Infrared Intensity	Raman[a,b] Freq.	Raman[a,b] Intensity	Interpretation
~3213	VW			242+2977=3219
~3145	VW			188+2977=3165; 242+2912=3154
~3102	VVW			188+2912=3100
~3060	VW			242+2×1415=3072
2977	M	2970	8b	ν_1, ν_9, ν_{13}, ν_{14}
2912	W	2902	8b	1415+1454=2869
~2857	VW			1415+1454=2869
~2800	VW			2×1415=2830
~2730	VW			1260+1454=2714
~2660	VVW			1260+1415=2675
~2500	VVW			2×1260=2520
2114	VW			857+1260=2117; 700+1415=2115
2022	VW			767+1260=2027
1958	VW			700+1260=1960
1900	VW			640+1260=1900; 487+1415=1902
1725	VVW			330+1415=1745
1454	VW	1451	3	ν_{16}, ν_{17}
1415	W	1412	3	ν_3, ν_{10}
1335	VW	1326	1	487+857=1344; 640+700=1340
1260	S	1263	2	ν_4, ν_{18}
		1132[c]	1	Impurity?
		1030[c]	1	330+700=1030
		998[c]	1	242+760=1002
966	W	947[c]	1	188+760=948; 330+640=970
		909[c]	1	Impurity?
857	S	848	3	ν_{19}, ν_{20}
767	W	760	3	ν_5, ν_{11}
700	M	700	4	ν_{21}
640	M	636	10	ν_6
519	M			188+330=518
487	S	470	10	ν_7
		330	1	ν_{22}
		242	7	ν_8
		188	7	ν_{23}

[a] See reference b, Table III.
[b] J. Duchesne, J. Chem. Phys. **16**, 1006 (1948).
[c] Observed only by Goubeau, *et al.*

[13] Young, Koehler, and McKinney, J. Am. Chem. Soc. **69**, 1410 (1947).
[14] Rank, Saksena, and Shull, Trans. Faraday Soc. **9**, 187 (1950). See also p. 216.

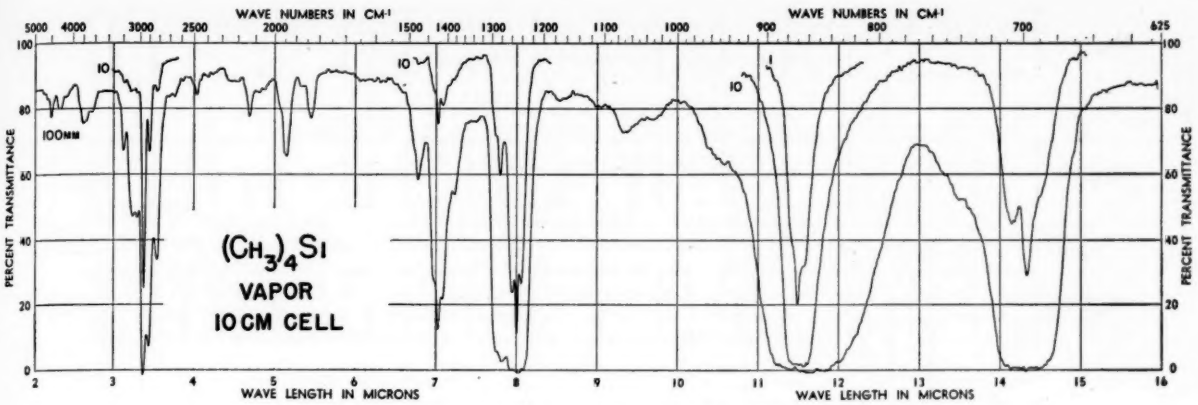

FIG. 7. Infrared spectrum of Me_4Si.

quency fits in very nicely as a degenerate methyl rocking fundamental.

DISCUSSION

Raman polarization data and Raman shifts for the gas phase would have been helpful in interpreting the spectra of the methyl chlorosilane series. However, by considering the series as a whole, it has been possible to arrive at a very reasonable assignment for all the strong infrared and Raman bands. A condensed plot of the fundamentals for all members of the series, correlated according to group frequencies, is shown in Fig. 8. The same type of plot, correlated according to symmetry species, is shown in Fig. 9. Totally symmetric species are joined by solid lines, and nonsymmetric species by broken lines. No lines of the same type may cross. The height of the lines is roughly proportional to their intensity. In almost every case, the nonsymmetrical motions of a group occur at higher frequencies than the symmetrical motions.

The only frequencies remaining unassigned are those involving a twisting of the methyl group against the rest of the molecule. In Me_4Si, heat capacity data[15] gives a potential barrier of 1300 ± 200 cal/mole, which corresponds to a twisting frequency of approximately 150 cm^{-1}. It is probable that the potential barrier is changed upon introduction of chlorine into the molecule, so no extrapolation to the other members of the series can be made. It is interesting, however, that the value $\nu=150$ cm^{-1} for the twisting vibrations in Me_3SiCl would explain the Raman band at 909 cm^{-1}

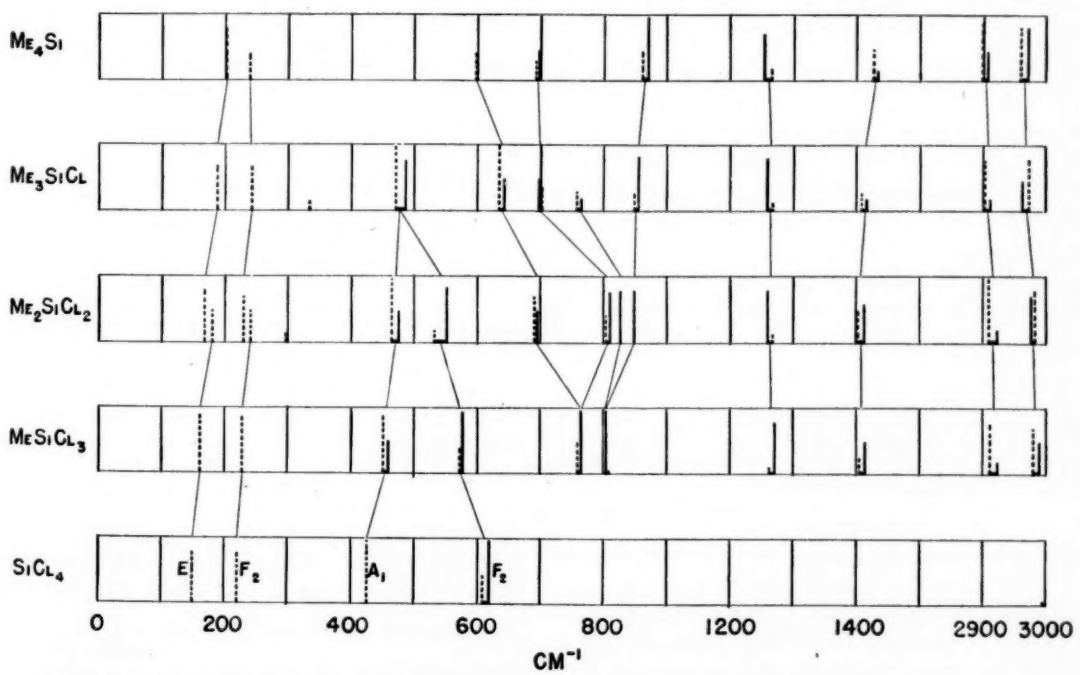

FIG. 8. Frequencies of the methyl chlorosilanes correlated according to "group frequencies."

[15] Aston, Kennedy, and Messerly, J. Am. Chem. Soc. 63, 2343 (1941).

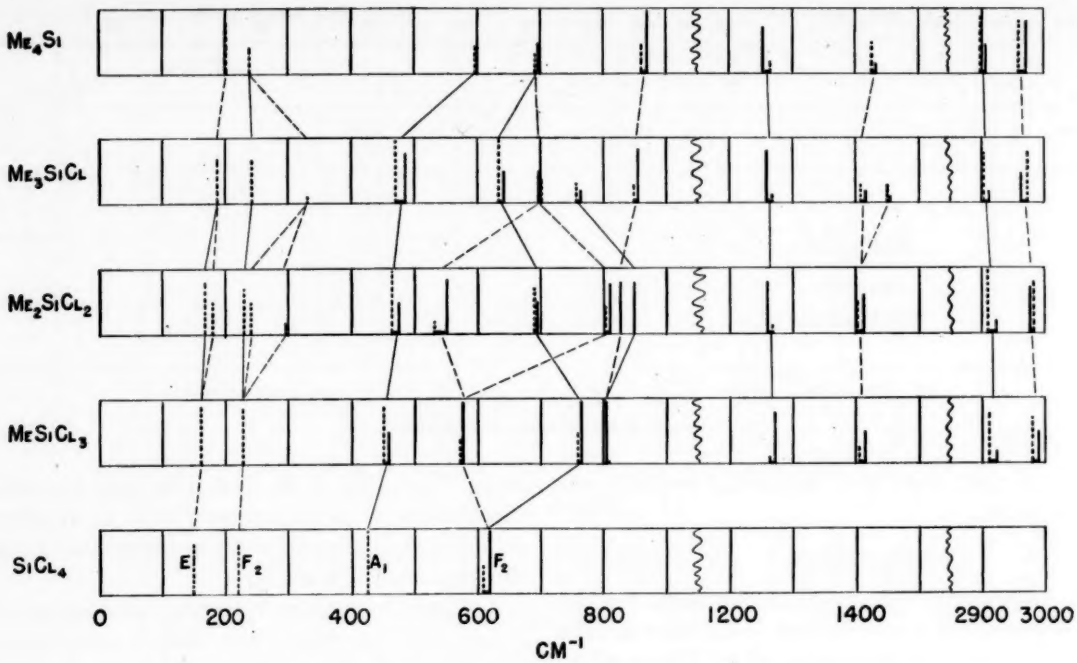

FIG. 9. Frequencies of the methyl chlorosilanes correlated according to symmetry species.

(760+150=910 cm^{-1}) which is otherwise ascribed to an impurity. In the absence of more convincing data, however, it seems best to delay calculation of thermodynamic quantities for these molecules.

A few general observations may be of interest. The assignment of motions involving the methyl group should be valid for siloxanes also, since unlike the corresponding carbon compounds, the frequencies remain quite constant as long as the methyl to silicon bond is present, regardless of what else is present in the molecule. It will be noted also that stretching frequencies involving atoms or groups bonded to silicon always occur at lower frequencies than the corresponding frequencies in carbon compounds. This is probably due not only to the greater mass of the silicon atom, but also to the greater ionic character of the bond.

Ground and Excited Electronic States and Molecular Vibrations of Some Polyatomic Molecules

JULES DUCHESNE AND LOUIS BURNELLE
Institut d'Astrophysique, University of Liège, Cointe-Sclessin, Belgium
(Received April 27, 1953)

The vibration potential functions of electronic ground and excited states of molecules of C_{2v} and D_{6h} symmetry are computed and compared. From this, quantitative characteristics of the molecular orbitals belonging to the correlated angular molecules and to a negative ion are deduced and, in this connection, the structure of the CF_2 and CH_2 radicals is discussed. The behavior of the interaction terms is examined, and a rule concerned with their sign is obtained in the case of $n\rightarrow\pi^*$ and $\pi\rightarrow\pi^*$ transitions. Various other effects, such as the $\sigma-\pi$ resonance and the part played by the lone-pair electrons, are studied.

THE aim of this paper is to extend to molecules of C_{2v} and D_{6h} symmetry, such as ClO_2, ClO_2^-, SO_2, CF_2, and C_6H_6, the application of a method already used by one of us[1] in the case of thiophosgene. The method consists essentially in comparing the general vibration potential functions characterizing different electronic states with a view to getting quantitative information about the molecular orbitals. In the present work, electronic transitions of the type $n\rightarrow\pi^*$ and $\pi\rightarrow\pi^*$ will be considered. The angular molecules, including the chlorite ion, will be correlated from a diagram recently given by Mulliken.

$Cl^{35}O_2$

If r_1, r_2, and θ are the bond lengths and angle at the equilibrium position, the most general potential function may be written

$$2V=f_1(\Delta r_1^2+\Delta r_2^2)+r_1^2 f_\theta \Delta\theta^2+2f_{12}\Delta r_1\Delta r_2 +2r_1 g_c\Delta\theta(\Delta r_1+\Delta r_2).$$

This function will be used for all the angular molecules dealt with in this paper, and the parameters will be expressed in 10^5 dynes/cm.

The fundamental vibrations and the OClO angle corresponding to the A_2 excited state which results from the transition $1a_2\rightarrow 2b_1$ are as follows:[2]

$$\nu_1=722.0\ \text{cm}^{-1},\quad \nu_2=296.1\ \text{cm}^{-1},\quad \nu_3=804.4\ \text{cm}^{-1},\quad \text{OClO}=104°.$$

The species symbols a_2, b_1 are those which are now standard for molecules of the symmetry C_{2v}. Their exact meaning is to be found in a paper recently given by Mulliken.[3] Using a method which has been followed for the analysis of the ground states,[4] the ellipses representing the real values of the f_1, f_θ, and f_{12}, in terms of g_c, have been deduced from these data. In Table I, we report selected values of the force constants which are deduced from the inspection of the curves, and as a comparison, we also give the data previously obtained for the ground state.[5] The value of g_c has been arbitrarily chosen, but in spite of that, f_1 and f_θ are satisfactorily determined as being rather insensitive to changes in g_c. From the large decrease of the ClO bond force constant (f_1) by about half its value with respect to the ground state, it appears that the $2b_1$ orbital has a strong antibonding character. The reasonable assumption that g_c is positive and at least 0.2 is sufficient to establish the positive sign of f_{12}, which is invariable for both states. The value of 0.066 is an upper limit for f_{12}, and this shows that whatever the inaccuracy, f_{12} is certainly much smaller than in the ground state, as expected if the a_2 orbital is strongly O↔O antibonding.

ClO_2^-

The ground state $A_1(a_2^2b_1^2)$ of the chlorite ion in $NaClO_2$ will now be examined. The fundamental frequencies and the OClO angle are as follows:[6]

$$\nu_1=797\ \text{cm}^{-1},\quad \nu_2=396\ \text{cm}^{-1},\quad \nu_3=844\ \text{cm}^{-1},\quad \text{OClO}=110°.$$

In Table II the selected values of the force constants are reported. In spite of the arbitrariness in the choice of g_c, f_1 and f_θ are rather precise as in the former case. Furthermore, even for $g_c=0$, f_{12} is still +0.12 which definitely proves its relative importance as compared with the A_2 excited state of ClO_2. This may be explained as due to the presence in the ion of an additional electron in the antibonding a_2 orbital of this state. On the other hand, the fact that the ground state of this ion,

TABLE I.

	f_1	f_θ	f_{12}	g_c
Upper state $A_2(a_2b_1^2)$	3.955	0.442	+0.066	+0.6
Ground state $B_1(a_2^2b_1)$	7.4	0.74	+0.261	+0.8

TABLE II.

	f_1	f_θ	f_{12}	g_c
Ground state $A_1(a_2^2b_1^2)$	4.597	0.563	+0.416	+0.5

[1] J. Duchesne, J. Chem. Phys. **21**, 548 (1953); Bull. acad. roy. sci. Belg. (to be published).
[2] J. B. Coon and E. Ortiz, Phys. Rev. **82**, 766 (1951); J. B. Coon, Phys. Rev. **85**, 746 (1952).
[3] R. S. Mulliken, Revs. Modern Phys. **14**, 204 (1942).
[4] J. Duchesne and L. Burnelle, J. Chem. Phys. **19**, 1191 (1951).
[5] J. Duchesne and A. H. Nielsen, J. Chem. Phys. **20**, 1968 (1952).
[6] J. P. Mathieu, C. R. Paris **234**, 2272 (1952); Duval, Lecomte, and Morendat, Bull. soc. chim. France, **18**, 745 (1951).

TABLE III.

	f_1	f_θ	f_{12}	g_c
Upper state $B_2(a_2b_1)$	4.297	0.426	+0.090	+0.3
Ground state $A_1(a_2^2)$	10.170	0.816	+0.187	+0.4

and the A_2 excited state of the ClO_2 molecule are characterized by valency-deformation forces quite close to one another, shows that the a_2 orbital is little bonding for ClO.

It is to be noticed that, in the ground state of ClO_2, the ClO bond is nearly twice as strong as in ClO_2^-, where it is like a single bond. This favors a double bond, in agreement with the views already developed by Dunitz and Hedberg.[7]

SO_2

The zero-order fundamental frequencies and the OSO angle of the B_2 excited state are as follows:[8]

$$\nu_1=794\ \text{cm}^{-1},\quad \nu_2=345\ \text{cm}^{-1},\quad \nu_3=833\ \text{cm}^{-1},$$
$$\text{OSO}=96°.$$

The angle may not be known with great precision, but this would not significantly alter the results. In Table III, the selected values for both the excited $B_2(a_2b_1)$ and ground $A_1(a_2^2)$ states are given. In the latter case, values have been recalculated from an earlier work by one of us.[9] As for ClO_2, the SO bond force constant decreases considerably. Furthermore, the sign of the cross terms is positive and remains invariant if it is assumed that $g_c>0.15$. This similitude in the behavior of both ClO_2 and SO_2 molecules strongly indicates that the electronic transitions are the same nature, in agreement with Mulliken's assignment.[3] The large change in f_{12} shows that also in this case the O↔O antibonding property of the a_2 orbital is strong.

CF_2

This molecule which has been shown to belong to the C_{2v} point group[10] has the following symmetrical fundamental vibrations in the ground state:

$$\nu_1=1162\ \text{cm}^{-1},\quad \nu_2=666.5 \text{ or } 344\ \text{cm}^{-1}.$$

Using the first assignment, no satisfactory values are obtained for the force constants whichever the bond angle chosen, and the solutions become less acceptable for the largest angles. On the other hand, with $\nu_2=344$ cm^{-1}, and when θ is varied within the range of 90°–110°, reasonable values are deduced as shown in Table IV. Indeed the CF bond in molecules such as CH_3F, CF_3H, and C_2H_4 is respectively 5.6,[11] 6.2,[12] and 7.[13]

On account of the increase of f_1 in terms of θ, the value of 110° must be considered as an upper limit. As a consequence of this, it is practically certain that CF_2 is a nonlinear symmetrical molecule with a singlet ground electronic state. The rather high value of the valency force constant indicates that there is some hybridization of the sp^2 type in which the nonbonding pair at the carbon atom occupies an orbit which is much more nearly s than otherwise. As CF_2 and CH_2 have presumably similar normal states,[10] the present investigation also favors a singlet state for CH_2. If so, it may be expected that the first electronic transition of CH_2 is considerably shifted towards the shortest wavelength region with respect to CF_2 and may even reach the far ultraviolet in the region of 1800A. This would explain why the CH_2 spectrum has not been discovered so far.

In the upper state corresponding to the 3250–2400A band system, the fundamental frequencies are as follows:[10]

$$\nu_1=750\ \text{cm}^{-1}\quad \nu_2=495.5\ \text{cm}^{-1}.$$

The characteristics of the fine structure of the bands show that the bond angle is increased with respect to the ground state.[10] Furthermore, it may now be estimated that the increase amounts to about 30°,* and if it is

TABLE IV.

θ	f_1	f_θ	f_{12} (assumed)	g_c (assumed)
90°	5.489	0.438	0	0
	5.977	0.411	0.3	0.3
110°	7.001	0.343	0	0
	7.628	0.326	0.3	0.3

assumed, as a working hypothesis, that the ground state value is 90°, we may adopt 120°. In these conditions, the selected values for the force constants are $f_1'(\equiv f_1+f_{12})=4.205$, $f_\theta=0.591$, $g_c=0.452$. Here we are confronted with a new behavior of the excited molecular orbital as the decrease of the CF bond is accompanied by an increase in the FCF rigidity. The band system which would result from a transition $A_1\leftrightarrow B_2$,[10] would therefore be due to the excitation of an a_2 electron to a b_1 orbital, as for the other molecules. Then, the decrease of the CF bond is quite obvious. The behavior of f_θ as being strengthened should, however, not follow the same rule.

C_6H_6

We will consider the B_{2u} first excited state of plane-hexagonal symmetry due to the promotion of one of the six π electrons to an antibonding π^* orbital.[14,15] The fundamental frequencies of the corresponding A_{1g} class

[7] J. D. Dunitz and K. Hedberg, J. Am. Chem. Soc. **72**, 3108 (1950).
[8] N. Metropolis, Phys. Rev. **60**, 295 (1941).
[9] J. Duchesne, Mém. soc. roy. sci. Liège **11**, 429 (1943).
[10] P. Venkateswarlu, Phys. Rev. **77**, 676 (1950); Laird, Andrews, and Barrow, Trans. Faraday Soc. (London) **46**, 803 (1950); K. Wieland, Z. Physik. **133**, 229 (1952).
[11] D. M. Dennison, Revs. Modern Phys. **12**, 175 (1940).
[12] Decker, Meister, and Cleveland, J. Chem. Phys. **19**, 784 (1951).
[13] A. Monfils and J. Duchesne, C. R. Paris **236**, 685 (1953).
* A corresponding increase of the CF bond from 1.38A to 1.43A which is compatible with the change in the CF force constant in going from the lower to the upper state, gives inertia moments which account approximately for the K structure studied by Venkateswarlu (see reference 10).
[14] M. Goeppert-Mayer and A. L. Sklar, J. Chem. Phys. **6**, 645 (1938).
[15] Garforth, Ingold, and Poole, J. Chem. Soc. **1948**, 491, 508.

for C_6H_6 and C_6D_6 are as follows:[15]

$$C_6H_6 \quad \nu_1=923 \quad \nu_2=3130$$
$$C_6D_6 \quad \nu_1=879 \quad \nu_2=2325.$$

It is to be noticed that $\nu_2(C_6D_6)$ was not observed and that the value given at 2340 was estimated.[15] We have slightly modified the latter in order to verify exactly the isotopic ratio. The most general potential function used is due to Manneback:[16]

$$2V=6[F^+\Delta a^2+\phi^+\Delta c^2+2\rho^+\Delta a\Delta c].$$

a and c are respectively the CC and CH bond distances at the equilibrium position. The force constants are defined as follows:

$$F^+=F+2F_0+2F_M+F_P, \quad \phi^+=\phi+2\phi_0+2\phi_M+\phi_P,$$
$$\rho^+=\rho_0+\rho_M+\rho_P.$$

The symbols 0, M, P designate interaction terms which refer to bonds in ortho, meta, and para position. From the frequency relations, which do not involve the molecular dimensions, the values obtained are: $F^+=6.597$; $\phi^+=5.312$; $\rho^+=-0.056$.

In the ground electronic state the experimental values for the fundamental frequencies do not satisfy the isotopic ratio, so that they have been modified through a least square calculation. Finally it is found:

$$C_6H_6 \quad \nu_1=986 \quad \nu_2=3062$$
$$C_6D_6 \quad \nu_1=932 \quad \nu_2=2293.$$

The final values differ from the experimental ones by 1 percent in one case and by only 0.4 percent on the average. The force constants deduced are: $F^+=7.660$; $\phi^+=5.020$; $\rho^+=-0.356$. The fact that a similar method was used for solving, in both excited and ground states, the difficulty arising from anharmonicity, lends support to the relative validity of the results. The negative sign obtained in the ground state for the bond-bond interaction ρ^+ is, moreover, in agreement with what was expected according to a rule formulated earlier,[17] and this reinforces confidence. Then, in this type of transition ($\pi\rightarrow\pi^*$) the sign of the cross term still remains invariant. The decrease of ρ^+ seems to be real, in spite of the fact that it could be overestimated here. This should indicate that the excitation of the π electron is able to modify to a certain extent the electrostatic interactions between the CC and CH bonds. In fact, a reduction of the repulsive forces, the nature of which is perfectly compatible with a negative sign for ρ^+,[17] would determine a shortening of the CH bonds in the excited state. The corresponding strengthening of these bonds, already shown by the work of Garforth, Ingold, and Poole[15] and confirmed by the present investigation, would therefore be explained.

Among the remaining planar vibrations of the excited state, the E_g^+ class seems the best known. The four frequencies are as follows for C_6H_6:[15]

$$\nu_1=521 \text{ cm}^{-1}, \quad \nu_2=3080 \text{ cm}^{-1},$$
$$\nu_3=1470 \text{ cm}^{-1}, \quad \nu_4=1130 \text{ cm}^{-1}.$$

ν_4 has been estimated indirectly and may not be very precise. The molecular dimensions adopted are 1.43A and 1.07A, respectively.[15] The potential function which we will use contains only four force constants F_S, ϕ_S, G_S, Γ_S, where $F_S=F-F_0-F_M+F_P$, with similar expressions for the other constants. G and Γ are the bending force constants for the CCC and HCC angles respectively.[16] Several cross terms are neglected and in particular a bond-angle one, between CC and CCC, whose importance has been revealed by the work of Bernard, Manneback, and Verleysen for the ground state.[18] In these conditions no real values are obtained. This may depend upon the inaccuracy in ν_4 and also upon the restrictions in the potential function. It is found that the limit from which real values are obtained is given by $\nu_4=1020$ cm^{-1}. The change may not be very significant for the part played by other cross terms on account of the incertitude concerned with the value of ν_4. The following values are deduced: $F_s=3.958$; $G_s=0.500$; $\phi_s=5.163$; $\Gamma_s=0.830$. It is seen from the general expressions that F_s is smaller than F^+ by $3(F_0+F_M)$. If we neglect F_M on account of its relative smallness, it is immediately deduced that F_0 is positive and equals 0.88. This compares favorably with the corresponding ground state values of 0.811 and 1.14, respectively obtained by Duchesne and Penney,[19] and by Coulson and Longuet-Higgins.[20] The results, as far as the sign of F_0 is concerned, would not be altered by taking F_M into consideration. But this and the dependence of F_S upon ν_4 do not allow a satisfactory precision in the absolute value. Similarly, ϕ_S is smaller than ϕ^+, and if we neglect ϕ_M and ϕ_P, $\phi=5.212$ and $\phi_0=0.049$ are deduced. The positive sign of ϕ_0 is also the same as that obtained for the ground state.[18,19] The increase of ϕ with respect to its normal value of 5.06[18] which had already been indicated by Garforth, Ingold, and Poole[15] is now confirmed. As ϕ_S is practically independent of ν_4, the value given for ϕ_0 is accurate. G_s is strongly affected with respect to the normal state (0.68), whereas Γ_s is practically unaffected (0.83).[18] The former result is unquestionable, G_s being little sensitive to ν_4, whereas the latter one seems less certain.

GENERAL CONCLUSIONS

It is now quite clear that the analysis of the potential function of the excited electronic states of polyatomic molecules is useful for the understanding of valence. It is shown, as was already anticipated in thiophosgene,[1] that the bond-bond and bond-angle interactions are

[16] C. Manneback, Ann. soc. sci. Bruxelles **B55**, 129, 237 (1935).
[17] J. Duchesne and A. Monfils, J. Chem. Phys. **19**, 586 (1949); J. Duchesne and L. Burnelle, J. Chem. Phys. **19**, 1191 (1951); J. Duchesne, Mém. acad. roy. sci. Belg. **26**, 1 (1952).
[18] Bernard, Manneback, and Verleysen, Ann. soc. sci. Bruxelles **B59**, 376 (1939); **60**, 45 (1940).
[19] J. Duchesne and W. G. Penney, Bull. soc. roy. sci., Liège **11**, 514 (1939).
[20] C. A. Coulson and H. C. Longuet-Higgins, Proc. Roy. Soc. (London) **193**, 456 (1948).

invariant in the case of $n\rightarrow\pi^*$ and $\pi\rightarrow\pi^*$ transitions of a number of molecules. According to the recent work of Duchesne and Monfils,[17] it is well-known that changes in the repulsive forces of the end atoms may modify the sign of the cross terms. Therefore, the rule which seems operative here might in some cases suffer exceptions on account of the change of antibonding forces between the end atoms in the excited states. The excitation of the π electrons in benzene, which determines a decrease of the bond-bond interactions p^+, does, therefore, affect the electrostatic interactions between the CC and CH σ bonds. This effect is therefore a particularly striking one showing the interdependence of the σ and π electrons. This is in agreement with the theoretical work of Coulson, March, and Altmann,[21] who show that $\sigma-\pi$ resonance is important even in the ground state of aromatic molecules. On the other hand, the great part played by the interactions between the long-pair electrons and the bonding ones in the determination of the bond angles is revealed by the considerable change of deformation forces and cross terms in the upper level, as in thiophosgene.[1] This is also supported by theoretical conclusions recently reached by Pople[22] and by Coulson, Greenwood, Danielsson, and Orgel.[23]

[21] S. L. Altmann, Proc. Roy. Soc. (London), **A210**, 327 (1951); Coulson, March, and Altmann, Proc. Nat. Acad. Sci. **38**, 372 (1952).

ACKNOWLEDGMENT

We are greatly indebted to Professors C. A. Coulson and C. Manneback for a helpful correspondence and to Professor R. S. Mulliken for interesting discussions and criticism.

We wish to acknowledge the help given by Mr. Y. Ottelet in the computational part of this work.

[22] J. A. Pople, Proc. Roy. Soc. (London) **A202**, 323 (1950).
[23] C. A. Coulson, private communication.

THE JOURNAL OF CHEMICAL PHYSICS VOLUME 21, NUMBER 11 NOVEMBER, 1953

Conjugation and the Intensity of the Infrared Carbonyl Band

GORDON M. BARROW
Department of Chemistry, Northwestern University, Evanston, Illinois
(Received April 15, 1953)

Data are given for the absolute intensities, in chloroform and carbon tetrachloride solutions and in the vapor state, of the carbonyl infrared absorption bands of a number of compounds in which the carbonyl group is conjugated by varying amounts. The absolute intensity differs in the different solvents and in the vapor, but the increase in intensity of a conjugated carbonyl over that of a simple ketone or aldehyde seems to be independent of the state. For most of these compounds a simple relation is shown to exist between this increase in carbonyl intensity with conjugation and the resonance energy of conjugation. This relation is expected from a consideration of the electronic configurations available to the normal and distorted molecule. That such compounds as the amides do not necessarily fit this trend is attributed to the geometric requirements on the molecule of these electronic configurations.

THE intensity of an infrared absorption band is proportional to the square of the oscillating dipole moment for that vibration of the molecule giving rise to the absorption band. This dipole moment change is given by $(\partial\mu)/(\partial Q)$, where μ is the molecular dipole moment and Q is the normal coordinate describing the particular vibration. The correlation of this quantity $(\partial\mu)/(\partial Q)$ with known or calculable molecular properties has not as yet proven very satisfactory. The concept that the change in dipole moment with bond stretching might be interpreted on the basis of fixed electronic charges on the nuclei was immediately shown to be insufficient by the large values, i.e., greater than an electronic charge, found for $(\partial\mu)/(\partial r)$, where r is a bond length, for certain multiply bonded molecules.[1-7] In fact, such measurements quickly led to the suggestion that the increased contribution of charge separated resonance forms expected in distorted molecules would explain the high values of the change in dipole moment with bond stretching. Furthermore the importance of nonbonding electrons in determining the molecular dipole,[8] and the dependence of such orbitals on the hybridization, and therefore on the nature and length of the bonding orbitals, also leads to the view that the molecular dipole will vary with bond stretching as a result of a change in the electronic configuration.

The dependence of the carbonyl intensity on possible alternate electronic configurations might be expected to show up in a study of the intensities of the carbonyl bands of a series of molecules with carbonyl groups in varying degrees of conjugation. Some results of this type have already been reported by Richards and

[1] A. M. Thorndike, J. Chem. Phys. **15**, 868 (1947).
[2] D. F. Eggers and B. L. Crawford, J. Chem. Phys. **19**, 1554 (1951).
[3] Callomon, McKean, and Thompson, Proc. Roy. Soc. (London) **A208**, 341 (1951).
[4] D. Z. Robinson, J. Chem. Phys. **19**, 881 (1951).
[5] McKean, Callomon, and Thompson, J. Chem, Phys. **20**, 520 (1952).
[6] Thorndike, Wells, and Wilson, Jr. J. Chem. Phys. **15**, 157 (1947).
[7] E. R. Nixon and P. C. Cross, J. Chem. Phys. **18**, 1316 (1950).
[8] D. Z. Robinson, J. Chem. Phys. **17**, 1022 (1949).

TABLE I. Observed frequencies and intensities of carbonyl bands.

	$CHCl_3$ solution		CCl_4 solution		Vapor	
	(cm^{-1})	A ($mole^{-1}$ liter cm^{-2})	(cm^{-1})	A ($mole^{-1}$ liter cm^{-2})	(cm^{-1})	A ($mole^{-1}$ liter cm^{-2})
Acetone	1709	1.9×10^4		1.55×10^4	1747	1.2×10^4
Methyl ethyl ketone					1743	1.3
Diethyl ketone	1710	1.9	1727	1.55		
Propionaldehyde	1730	2.1	1738	1.55		
Acrolein	1696	2.2				
Benzaldehyde	1702	2.6	1710	2.1		
Benzophenone	1659	2.4	1668	2.2		
Acetophenone	1685	2.7	1692	2.1		
Methyl acetate	1738	2.8	1751	2.2	1776	1.9
Ethyl propionate	1726	3.2	1741	2.8		
Ethyl acetate	1734	3.2	1745	2.6	1772	2.1
Methyl crotonate	1717	3.4	1729	3.1		
Ethyl benzoate	1711	3.6	1721	3.4		
Methyl carbonate	1756	4.2	1763	3.8	1781	2.9
Ethyl carbonate	1744	4.7	1750	4.1		
p-hydroxybenzaldehyde	1689	3.2				
m-hydroxyacetophenone	1684	2.7				
Acetyl chloride	1805	3.1	1805	2.5		
Phenyl acetate	1770	3.1	1780	2.9		
Acetanilide	1695	3.6	1705	3.1		
Dimethyl acetamide	1639	5.7				
Diethyl acetamide	1633	5.7				

Burton.[9] For a carbonyl conjugated to an electron donor group the most important resonating forms are usually considered to be, in addition to the ionic form inherent in the carbonyl group itself, of the types

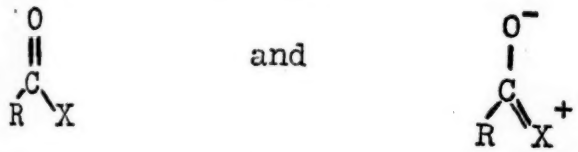

It is, therefore, to be expected that stretching of the carbonyl bond will lead to an electronic structure of the molecule with a larger contribution of the charge separated canonical form than in the molecule with equilibrium bond lengths and this increase will depend on the availability of such a charge separated electronic configuration. Intensity measurements are reported for the carbonyl bands of a series of compounds on which this type of interpretation can be tested.

EXPERIMENTAL

The intensities of the carbonyl bands were determined in both carbon tetrachloride and chloroform solutions and for a few compounds in the vapor state. For the solution measurements a 1-mm cell was used and the concentrations ranged between 0.005 and 0.02 molar. The materials used, mostly reagent grade, were freshly distilled and a middle cut used for the measurements or were recrystallized. All spectra were obtained on a Beckman Model IR-2T instrument with rock salt optics and with a fixed slit of 0.1 mm. For the set of curves representing three or four different concentrations of a given compound, a background trace of the pure solvent was run so that it was superimposed and a point by point measurement of $\log[(I_0)/I]$ was made at intervals of about 0.025 microns. These data were then plotted against the wavelength, and the area under the curve was graphically determined. The bands were followed out to about 100 cm^{-1} on either side of the band center. The values of $1/Cl\int\log(I_0/I\,d\nu$, calculated from an average conversion factor from microns to cm^{-1} for each band, were then plotted against the measured value of $\log[(I_0)/I]$ at the band maximum, as suggested by Ramsay.[10] The true intensity was then given by a linear extrapolation to $\log[(I_0)/I]_{max}$ equal to zero using a slope $A(-0.013)$ estimated for our instrument and slit width from the work of Ramsay, A being the true intensity. In effect this extrapolation gives a value for the true intensity, which is only about 2 percent higher than the average of the measured band intensities for a given compound. The average deviations of the experimental points from the extrapolation curve was less than 2 percent.

Table I gives the extrapolated intensities as measured in carbon tetrachloride and chloroform solutions and in the gas phase. These values are estimated to be reliable to about 5 percent. The vapor phase measurements were made in both a 1-cm and a 10-cm cell with dry nitrogen added to give a total pressure of one atmosphere. The deviations from Beer's Law were no larger than the solution spectra and it was therefore assumed that no incomplete pressure broadening difficulties existed. These data were therefore treated in the same way as the solutions results to obtain the true intensities.

Also included in Table I are the frequencies of the band maxima. These were obtained by direct comparison with the overlapping 6-micron water band and are reliable to within about 3 cm^{-1}.

[9] R. E. Richards and W. R. Burton, Trans. Faraday Soc. **45**, 874 (1949).

[10] D. A. Ramsay, J. Am. Chem. Soc. **74**, 72 (1952).

TABLE II. Resonance energies and additional $(\partial\mu)/(\partial Q)$, divided by a charge separation distance, for carbonyl conjugation.

	Resonance energy		$1/r_{+-}(\partial\mu/\partial Q)$conjugation		
	Wheland	Pauling	$CHCl_3$ solution	CCl_4 solution	Vapor
Acetone	0	0	0	0	0
Methyl ethyl ketone	0	0			0
Diethyl ketone	0	0	0	0	
Propionaldehyde	0	0	0	0	
Acrolein	(3)	—	4		
Benzaldehyde	6	4	9	8	
Benzophenone	10	10	7	10	
Acetophenone	13	7	10	8	
Methyl acetate	18		17	14	16
Ethyl propionate	24	24	24	24	
Ethyl acetate	25		24	21	21
Methyl crotonate	32	—	25	27	
Carbon dioxide	33	33			33
Ethyl benzoate	38	(28)	26	30	
Methyl carbonate	43	42	41	43	37
Ethyl carbonate	53		47	46	

DISCUSSION

If available electronic configurations exist such that the electronic structure of the molecule can shift to accommodate a change in length of the carbonyl bond, the value of $\partial\mu/\partial Q$ for the carbonyl vibration is expected to be greater than for a molecule in which changes of electronic configuration are necessarily localized in the carbonyl group itself. If the resonance energy due to carbonyl conjugation is taken to be some measure of the availability of such canonical forms it can be shown that a correlation can indeed be made between the intensities of the carbonyl absorption bands and the resonance energy.

In Table II, the values for the resonance energies given by Wheland[11] and by Pauling[12] are listed. For compounds containing phenyl groups the resonance energy of benzene has been subtracted from that of the molecule to give the resonance energy of the carbonyl conjugation. The resonance energy of methyl crotonate was calculated from the heat of combustion data of Schjanberg[13] by Wheland's method, while that of acrolein was estimated from Wheland's value for crotonaldehyde. A value for ethyl benzoate appropriate to Pauling's resonance energies was estimated from his values for benzoic acid and the esters.

The values of $(\partial\mu)/(\partial Q)$ contain, in addition to the change in dipole moment with carbonyl stretching, contributions from the other bond stretchings and angle bendings that make up the "carbonyl" vibration. Although some work on "characteristic intensities" of groups has been reported by Ramsay[10] and by Francis,[14] it is not well established that such intensities will be sufficiently independent of the nature of the rest of the molecule so that this approach will be as satisfactory for intensities as it is for frequencies. In the case of the intensity of the carbonyl band, therefore, although we specifically expect contributions to the intensity of this band from forms depicted as having a formal charge on a conjugated group, variations in the contribution of other bond stretchings or angle bendings to the intensity will disturb an interpretation of the intensity in terms of only the nature of the carbonyl group and the extent of its conjugation. Since it is not feasible to carry out detailed normal coordinate calculations on these molecules, it has been assumed that these additional contributions will not be large enough to obscure the expected relationship.

The values of $(\partial\mu)/(\partial Q)$ are obtained from the intensities A of Table I by the relation

$$\frac{\partial\mu}{\partial Q}=\pm\left(\frac{3c^2 1000}{N\pi}A\right)^{\frac{1}{2}},$$

where c is the velocity of light and N is Avogadro's number and A is the intensity in mole^{-1} liter cm^{-2}. If the increase in $(\partial\mu)/(\partial Q)$ for resonating molecules is attributed to the presence of the formal charge separation then the increase of $(\partial\mu)/(\partial Q)$ over that of a nonconjugated carbonyl must be calculated by means of a vector subtraction. The angles around the carbonyl carbon atom were taken to be 120° and the bond lengths were from electron diffraction data or were calculated from Pauling's atomic radii. Furthermore, again using a formal charge concept, the increase in $(\partial\mu)/(\partial Q)$ will depend on the charge separation distance, and this has been allowed for by dividing the vectorial increase in $(\partial\mu)/(\partial Q)$ by the distance, in angstroms, to which the charges are separated in the usually written resonating forms. For a phenyl group conjugated to the carbonyl the charge separation distance was taken as the distance from the carbonyl oxygen to the center of the benzene ring. For compounds with two different groups conjugated to the carbonyl, as ethyl benzoate, the net direction of the conjugation effect was calculated from an estimate of the relative contributions of the conjugated groups. Neither the vector addition nor the

[11] G. W. Wheland, *The Theory of Resonance and its Application to Organic Chemistry* (John Wiley and Sons, Inc., New York, 1945).
[12] Linus Pauling, *The Nature of the Chemical Bond* (Cornell University Press, Ithaca, 1945).
[13] E. Schjanberg, Z. physik. Chem. **A175**, 342 (1936).
[14] S. A. Francis, J. Chem. Phys. **18**, 861 (1950); **19**, 942 (1951).

division by the charge separation distance are necessary to show the correlation with resonance energy; the correlation being only slightly poorer without this treatment. These data are shown, along with the resonance energies in Table II. The results calculated for the carbon tetrachloride and chloroform solutions and the vapor phase data are very similar and in Fig. 1 a plot is shown of the average value of $1/r_{+-}[(\partial\mu)/(\partial Q)]$ conjugation against the resonance energies tabulated by Wheland. For compounds containing phenyl groups the benzene resonance energy 41 kcal was subtracted for each phenyl group to give a value of the carbonyl conjugation resonance energy. For the compounds considered the agreement is seen to be quite satisfactory.

Furthermore, the increase in intensity for *p*-hydroxybenzaldehyde over benzaldehyde and the lack of such an increase for *m*-hydroxyacetophenone over acetophenone, as seen in Table I, is in qualitative agreement* with the relation exhibited in Fig. 1. Likewise for acetyl chloride, for which a resonance energy is not available, the intensity data indicate a resonance energy of about 22 kcal, which seems reasonable.

The alkyl substituted amides are not included in Table II since it is immediately apparent from the data of Table I that for these substituted acetamides the carbonyl intensities are very much greater than would be expected on the basis of their resonance energy, which is about equal to that of the esters. Although no detailed explanation is now offered for this behavior, we attribute it to the fact that the resonating and nonresonating structures of the amides require different geometric arrangements of the groups on the nitrogen atom, and a simple relation can no longer be expected between stretching of the carbonyl bond and the increase in the contribution of the charge-separated planar form. Some support for this general view is found in the fact that the carbonyl intensity of acetanilide fits very satisfactorily the resonance energy relation of Fig. 1, and for this molecule the planarity of the groups on the nitrogen atom is assisted by resonance involving the phenyl group. The presence of the phenyl group does not produce any unexpected effects on the resonance energy and the decrease in carbonyl intensity can therefore not be attributed to an inhibition of resonance. Furthermore, the carbonyl intensity of phenyl acetate is unchanged from that of the alkyl esters.

It is interesting also to note the lack of dependence of the frequencies of the carbonyl vibrations upon the intensities on the one hand or, on the other hand, upon the resonance energies. Although conjugation is generally said to lower the carbonyl frequency, this trend is reversed for conjugation with sufficiently electronegative groups. This effect, however, plays little or no part in the carbonyl intensity as is seen, for example, in the very high frequency, but normal intensity, of acetyl chloride.

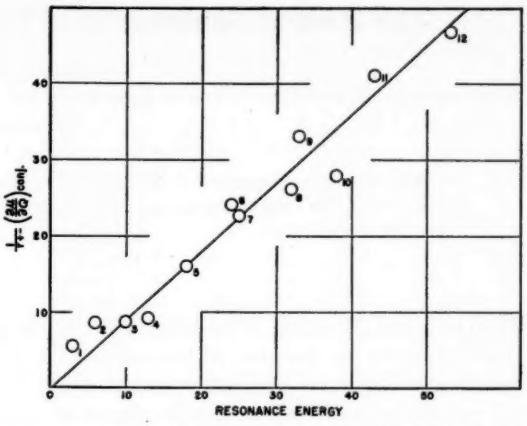

FIG. 1. Average of the measured $1/r_{+-}(\partial\mu/\partial Q)$ conjugation *versus* the resonance energy from Wheland for 1—acrolein, 2—benzaldehyde, 3—benzophenone, 4—acetophenone, 5—methyl acetate, 6—ethyl propionate, 7—ethyl acetate, 8—methyl crotonate, 9—carbon dioxide, 10—ethyl benzoate, 11—methyl carbonate, 12—ethyl carbonate.

No attempt has been made to include here any data on compounds with more than one carbonyl group, except carbon dioxide, or on cyclic compounds. Although the application of the approach used here to interpret the carbonyl intensities of such compounds will be of interest, it is expected that certain additional factors will be involved. For compounds with two carbonyl groups the relative orientation of these groups will need to be considered in cases of appreciable coupling, and for ring compounds the size and strain in the ring will affect the carbonyl intensity. In addition, of course, groups other than the carbonyl group can be studied for different degrees of conjugation and, of such groups, the carbon halogen bonds and the nitrile group appear to be most susceptible to this treatment.

SUMMARY

The intensities of the carbonyl absorption bands of compounds containing conjugated carbonyl groups can be considered in terms of resonating forms. The increase in the carbonyl band intensity can be interpreted as due to the availability of a charge-separated electronic configuration. The resonance energy of conjugation, being some measure of the availability of such configurations, is shown to be related to this increase in carbonyl intensity. This simple relationship does not necessarily hold, however, for compounds such as the amides, where the resonating and nonresonating forms of the molecule require a different geometry.

*For substituted benzaldehyde or acetophenone coupling of the carbonyl vibration with a phenyl vibration appears to be appreciable, leading to a band, almost as strong as that of the carbonyl, at about 1610 cm^{-1}. The intensities listed in Table I for the two compounds of this type are for the carbonyl band only and therefore cannot be directly compared with the other intensities, for which no unusual coupling occurs. The sum of the intensities for these two adjacent bands is, however, considerably greater for *p*-hydroxybenzaldehyde and *p*-hydroxyacetophenone than for *m*-hydroxyacetophenone.

The Heat of Sublimation of Tin and the Dissociation Energy of SnO

LEO BREWER AND RICHARD F. PORTER
Department of Chemistry and Chemical Engineering and Radiation Laboratory, University of California, Berkeley, California
(Received August 3, 1953)

The heat of sublimation of tin has been redetermined and found to be 70±2 kcal/mole. This value combined with the heat of formation of gaseous SnO agrees with the linear Birge-Sponer extrapolation to the ground-state atoms.

BREWER and Mastick[1] have reviewed the data in the literature on the heat of formation of gaseous SnO and have combined this value with a value of the heat of sublimation of tin to obtain the heat of dissociation of the SnO molecules to the gaseous atoms. This value was found to be in close agreement with the linear Birge-Sponer extrapolation[2] of the vibrational levels of SnO. Barrow and Drummond[3] have recently reconsidered these calculations and, by use of a lower heat of sublimation of tin, have claimed that the data indicate a linear Birge-Sponer extrapolation to an excited tin state rather than to the ground-state tin atom.

In an effort to resolve this difference the heat of sublimation of tin was redetermined by measurements of the vapor pressure using the Knudsen method. The vapor pressure of tin has been determined previously by Wartenberg,[4] Greenwood,[5] Harteck,[6] Ruff and Bergdahl,[7] and Granovskaya and Lyubimov.[8]

Table I indicates the temperature ranges used in some of the previous investigations, the method of study, and the average heat of sublimation at 298°K derived from these results using free-energy functions. Heats calculated from the vapor pressure data of Ruff and Bergdahl and Granovskaya and Lyubimov are 64 and 65 kcal, respectively. Of these previous determinations, all of the methods used except that by Harteck and Granovskaya and Lyubimov are subject to a very serious error because tin forms a volatile oxide SnO which is much more volatile than the metal. Thus any method which does not completely eliminate the presence of oxygen in the form of elemental oxygen or water or carbon dioxide is liable to give results which are much too high. Comparison of the results of Table I shows that the methods which do not rigorously eliminate oxygen do in fact give much too high vapor pressure. Hartick used an effusion method in vacuum which can avoid this error because the oxygen can be completely removed by evacuation. Since the Knudsen method appears to be the only one which is likely to give reliable results it was used also in this work.

TABLE I.

Investigator	Temperature range °K	Method	Averaged ΔH_{298} in kcal
von Wartenberg	1400–1640	Flow system	61
Greenwood	2240–2380	Observation of boiling point	65
Harteck	1300–1450	Knudsen	73

EXPERIMENTAL

The apparatus and procedure described by Brewer and Mastick[1] were also used for this work. The Knudsen cell was made of graphite. Graphite, tantalum carbide, and tantalum with varying hole sizes were used for the lids. The vapor pressure was determined by measuring the weight loss of the Knudsen cell after diffusion had proceeded for approximately two hours in the average run. The results are tabulated in Table II.

The crucible covers in runs 1 and 2 did not have knife-edge holes in them, and consequently the flow of gas was restricted and lower pressures were observed with correspondingly higher heats.

The free energy functions used for these calculations were obtained from Brewer.[9] It was assumed that monatomic tin was the main gaseous species. The recent study of tin vapor in the mass spectrometer by Honig[10] would substantiate the assumption that monatomic tin is the main species. Averaging the results of Table II yields $\Delta H^\circ_{298}=70\pm2$ kcal for $Sn(s)=Sn(g)$. This new result agrees quite closely with that obtained by Harteck and is the same heat of sublimation of tin as that used by Brewer and Mastick.[1] Thus the validity of the linear Birge-Sponer extrapolation[2] for tin oxide is substantiated.

Brewer and Mastick[1] have pointed out that the fourth-group oxides appear to give very satisfactory linear Birge-Sponer extrapolations assuming that the extrapolations go to the ground atomic state. The present work reconfirms this for SnO. Also, as pointed out by Brewer,[11] recent work on GeO by Jolly and Latimer and work by Gilles and Wheatley on TiO

[1] L. Brewer and D. F. Mastick, J. Chem. Phys. **19**, 834 (1951).
[2] R. T. Birge and H. Sponer, Phys. Rev. **28**, 259 (1936).
[3] G. Drummond and R. F. Barrow, Proc. Phys. Soc. (London) **A65**, 148 (1952).
[4] H. von Wartenberg, Z. Elektrochem. **19**, 482 (1913).
[5] H. C. Greenwood, Proc. Roy. Soc. (London) **A83**, 483 (1910).
[6] P. Harteck, Z. physik. Chem. **134**, 9 (1928).
[7] O. Ruff and G. Bergdahl, Z. anorg. Chem. **106**, 76 (1919).
[8] A. Granovskaya and A. Lyubimov, J. Phys. Chem. (U.S.S.R.) **22**, 527 (1948).
[9] L. Brewer, Paper 3, *National Nuclear Energy Series*, Vol. 19B, edited by L. L. Quill (McGraw-Hill Book Company, Inc., New York, 1950).
[10] R. E. Honig, J. Chem. Phys., **21**, 573 (1953).
[11] L. Brewer, Chem. Rev. **52**, 62 (1953).

TABLE II.

Run	Temperature °K	Lid	Hole area (in sq cm)	Press. (atmos.)	$-\left(\frac{\Delta F-\Delta H_{298}}{T}\right)$	ΔH_{298} (kcal)
1	1556	C	0.0314	1.94×10^{-5}	25.32	72.94
2	1621	C	0.0314	4.70×10^{-5}	25.29	73.10
3	1753	TaC	0.0177	8.83×10^{-4}	25.23	68.73
4	1713	Ta	0.0177	3.51×10^{-4}	25.26	70.33
5	1548	Ta	0.0177	5.93×10^{-5}	25.32	69.14
6	1688	Ta	0.0177	2.87×10^{-4}	25.27	70.01
7	1583	Ta	0.0804	3.83×10^{-5}	25.31	72.0
8	1688	Ta	0.0804	2.05×10^{-4}	25.27	71.14

have confirmed the validity of the linear Birge-Sponer extrapolations for these molecules. In every instance where data are available for fourth-group oxides this extrapolation appears to work quite well.

THE JOURNAL OF CHEMICAL PHYSICS VOLUME 21, NUMBER 11 NOVEMBER, 1953

The Crystal Momentum as a Quantum Mechanical Operator

E. N. ADAMS II*
Institute for Nuclear Studies, University of Chicago, Chicago, Illinois
(Received July 6, 1953)

The Schroedinger equation for a particle moving in a perturbed periodic potential is transformed into a representation called the "Crystal momentum representation." It is shown that by use of this representation previous approximate "effective mass" equations can be readily derived and extended to arbitrarily high approximation. A theorem concerning weak space dependent perturbations is discussed.

I. INTRODUCTION

MANY theoretical studies of solids are carried out using that form of the Hartree or Hartree-Fock approximation which represents the electronic wave function as a determinantal product of one electron wave functions, each of which has a definite wave number k. Such an approximation is particularly important for studies of electrical or thermal properties because of the relatively simple way in which current carrying states can be described in terms of determinantal products of Bloch wave functions. In practice it is important to be able to assume that in the one electron Schroedinger equation from which the one electron wave functions are obtained, the one electron potential is independent of the wave number of the Bloch state. Many of the most useful qualitative notions about the electronic structure of solids have their foundations in the belief that simple combinations of products of such Bloch functions can be used to obtain a rather accurate description of electronic behavior.

A most important idea has been to set up a correspondence according to which an electron which occupies a Bloch state ψ_{pn} may be spoken of as a free "effective" electron which occupies a state of momentum $p\equiv\hbar k$. Then given the relation between energy and wave number from quantum mechanical considerations, one can develop such subjects as electrical conduction, magnetic susceptibility, thermal conduction, etc. as classical statistical theories of the charged "effective" particles.

The application of the effective particle idea has not been limited to problems in which the behavior of the effective particle is classical. Theoretical studies of, e.g., the exciton, show that a quantum mechanical theory of the effective particle is meaningful and useful. It is probable that several of the important current problems of solid state physics are best thought of in terms of the quantum mechanics of effective particles.

Deductive demonstrations of the properties of the effective particle have had the common feature that they yielded equations which are only approximately correct.[1] While these equations often were entirely adequate for the problems to which they were applied, it was generally true that the manner of derivation provided no simple means for the progressive refinement of the theory to obtain higher approximation or greater generality.

It is the purpose of the present paper to demonstrate a simple way of obtaining the quantum mechanical effective particle theory directly from the Schroedinger equation. The deduction is exact and completely general. It consists in showing that the representation of

* This work supported in part by the Chicago Midway Laboratories under AF contract 33(038)-25913.

[1] E. N. Adams II, Phys. Rev. 85, 41 (1952). References to a number of such treatments can be found in this article.

the Schroedinger equation which is obtained using the Bloch functions as basic states affords a natural matrix representation for the general effective particle theory. We will call this representation the "crystal momentum representation" (CMR), because it is one in which an operator corresponding to what is called the "crystal momentum" or "pseudo momentum" is diagonal.

II. MATRIX ELEMENTS OF OPERATORS

By the ordinary conventions of representation theory a state vector $|A\rangle$ is represented by a wave function $\langle q'|A\rangle$ when the basic vectors in the space are taken to be the eigenvectors $|q'\rangle$ of the operator q. What we need in order to express the hamiltonian in the q representation is the set of matrix elements $\langle q'|o|q''\rangle$ of every operator o which occurs in the Hamiltonian. From these matrix elements we can calculate the matrix elements of the Hamiltonian and write the Schroedinger equation as

$$\sum_{q''}\langle q'|H|q''\rangle\langle q''|A\rangle = i\hbar\partial\langle q'|A\rangle/\partial t. \tag{2-1}$$

We will write the Hamiltonian in the form

$$H = H_0 + V(x_e, p_e). \tag{2-2}$$

H_0 is of the form $(p_e^2/2m)+V_p(x_e)$ with $V_p(x_e)$ a periodic function having the periodicity of the three dimensional space lattice. The operators x_e, p_e are the operators for the electron coordinate and electron momentum, respectively. The subscript e is used to avoid subsequent notational confusion.

The well-behaved eigenfunctions of H_0 are the Bloch functions ψ_{pn} which satisfy

$$H_0\psi_{pn} = E_n(p)\psi_{pn}. \tag{2-3}$$

Here ψ_{pn} denotes that function with energy in the nth allowed band which has the translational symmetry of $\exp(ip\cdot x/\hbar)$. We will define a quantum mechanical operator p which we call the "crystal momentum" and whose matrix elements are

$$\langle p'n'|p|pn\rangle = \delta_{nn'}\delta(p-p')p'. \tag{2-4}$$

Thus the Bloch function $\psi_{p'n}$, is an eigenfunction of the crystal momentum with eigenvalue p'.

In order to write the Schroedinger equation in the CMR we need the matrix elements of x_e, p_e and H_0 between various Bloch functions. These may be found in various places.[1] We will write them down here simply to establish a notation.

$$\langle p'n'|p_e|pn\rangle = \delta(p-p')P(p)_{n'n}, \tag{2-5}$$

$$\langle p'n'|H_0|pn\rangle = \delta_{nn'}\delta(p-p')E_n(p), \tag{2-6}$$

$$\langle p'n'|x_e|pn\rangle = (\hbar/i)\delta_{n'n}\partial\delta(p-p')/\partial p + \delta(p-p')X_{n'n}(p). \tag{2-7}$$

With the choice of normalization made so that

$$(\psi_{p'n'}, \psi_{pn}) = \delta_{nn'}\delta(p-p'),$$

the definitions of matrix elements above are

$$\delta(p-p')P_{n'n}(p) = \int d^3x\psi_{p'n'}^*(x)(2\nabla/i)\psi_{pn}(x), \tag{2-8}$$

$$\delta(p-p')X_{n'n}(p) = \int d^3x\psi_{p'n'}^*(x) \times[x-(\hbar\nabla_p/i)]\psi_{pn}(x). \tag{2-9}$$

It follows from the commutation rules for p_e, x_e that

$$X_{n'n}(p) = (\hbar/mi)P_{n'n}(p)/[E_{n'}(p)-E_n(p)] \quad (n'\neq n). \tag{2-10}$$

No such relation holds for X_{nn}, but if the lattice has an inversion center it seems possible by a proper choice of phases to arrange that the X_{nn} all vanish.[2]

In the CMR the wave function has the argument n which takes on discrete values and the argument p which takes on all real vector values. As a regularity condition we must require that the wave functions be a periodic function of p with the period of the reciprocal lattice. The basis for the requirement is that the wave functions ψ_{pn} have that periodicity and the wave function $\Psi^{(A)}(p, n)$ is just the coefficient of ψ_{pn} in the expansion of the state $|A\rangle$ in Bloch functions.

For the purpose of seeing most clearly the relationships of the various effective particle approximations, it is helpful to think in terms of a certain matrix formalism. In this formalism the wave function representing a state $|A\rangle$ is given as a vector $\mathbf{\Psi}^{(A)}$ which has a component in each band.

$$\mathbf{\Psi}^{(A)} = \begin{pmatrix} \Psi_1^{(A)} \\ \Psi_2^{(A)} \\ \cdot \\ \cdot \\ \cdot \end{pmatrix}. \tag{2-11}$$

The components $\Psi_n^{(A)}$ are functions of p, t. If the perturbing potential $V(X_e, p_e)$ has a Taylor series we can express the perturbed hamiltonian in terms of the following three matrices:

$$H_0 \rightarrow \mathbf{E} \equiv \begin{bmatrix} E_1(p) & 0 & \cdots \\ 0 & E_2(p) & \cdots \\ \cdots & \cdots & \cdots \end{bmatrix} \tag{2-12}$$

$$p_e \rightarrow \mathbf{P} \equiv \begin{bmatrix} P_{11}(p) & P_{12}(p) & \cdots \\ P_{21}(p) & P_{22}(p) & \cdots \\ \cdots & \cdots & \cdots \end{bmatrix} \tag{2-13}$$

$$x_e \rightarrow x + \mathbf{X} \equiv x + \begin{bmatrix} X_{11}(p) & X_{12}(p) & \cdots \\ X_{21}(p) & X_{22}(p) & \cdots \\ \cdots & \cdots & \cdots \end{bmatrix}. \tag{2-14}$$

In (2-14) we have written x for the operator $i\hbar\partial/\partial p$. This quantity x can, by a natural extension of nomen-

[2] In reference 1 it is stated that X_{nn} can always be made to vanish. However, the supposed proof given of the statement is incorrect.

clature, be called the "crystal coordinate," since it has the commutation relations of the coordinate conjugate to the crystal momentum p. We are using boldface type to indicate that an object is to be considered a matrix in the bands. Thus in the CMR the Schroedinger equation for the perturbed Hamiltonian takes the form

$$[\mathbf{E}+V(x+\mathbf{X},\mathbf{P})-i\hbar\partial/\partial t]\mathbf{\Psi}=0. \tag{2-15}$$

Equation (2-15) was previously shown[1] by a complicated argument to be approximately correct with the interpretation that $\mathbf{\Psi}$ was a function of x which gave the perturbed wave function in terms of the unperturbed by the expansion

$$\psi=\sum_{nR}\Psi_n(R)a_{nR}(x_e), \tag{2-16}$$

with $a_{nR}(x_e)$ the Wannier function for the nth band and Rth cell. Here we see that (2-15) is exact if we regard $\mathbf{\Psi}$ as a function of p which gives the perturbed wave function by means of

$$\psi=\sum_{np}\Psi_n(p)\psi_{pn}(x_e). \tag{2-17}$$

Thus the result (2-15) is a new one, and does not involve the approximations which the old one did.

III. PERTURBATIONS DEPENDING ONLY ON POSITION

We will now examine the form which (2–15) takes if the perturbation V depends only on the position of the electron. We use the Fourier integral form.

$$V(x_e)=\int d^3\kappa v(\kappa)\exp(i\kappa\cdot x_e). \tag{3-1}$$

In the CMR the exponential is replaced by the operator $\exp(i\kappa\cdot x+\mathbf{X})$ which is a function of p and a matrix in the bands. Purely as a matter of notation we will define the "effective charge" $\mathbf{q}(p,\kappa)$ by

$$\mathbf{q}(p,\kappa)\equiv\exp(i\kappa\cdot x+\mathbf{X})\exp(-i\kappa\cdot x). \tag{3-2}$$

Using (3-3) we can then write the potential V as

$$V=\int d^3\kappa v(\kappa)\mathbf{q}(p,x)\exp(i\kappa\cdot x). \tag{3-3}$$

We will now investigate the nature of the operator $\mathbf{q}(p,\kappa)$. Define $q(s)$ by

$$q(s)\equiv\mathbf{q}(p,s\kappa) \tag{3-4}$$

$q(s)$ satisfies

$$\partial q(s)/\partial s=\exp(is\kappa\cdot x+\mathbf{X})[i\kappa\cdot\mathbf{X}(p)]\exp(-is\kappa\cdot x). \tag{3-5}$$

Using the fact that $\exp(-is\kappa\cdot x)\equiv\exp(s\hbar\kappa\cdot\nabla_p)$ it is easily seen that (3-5) becomes

$$\partial q(s)/\partial s=q(s)[i\kappa\cdot\mathbf{X}(p-\hbar\kappa s)]. \tag{3-6}$$

The differential Eq. (3-6) can be converted to an integral equation

$$q(s)=1+i\int_0^s ds_1 q(s_1)\kappa\cdot\mathbf{X}(p-\hbar\kappa s_1). \tag{3-7}$$

Iteration of (3-7) yields the following expression for the effective charge:

$$q(1)\equiv\mathbf{q}(p,\kappa)=1+i\int_0^1 ds\kappa\cdot\mathbf{X}(p-\hbar\kappa s)+(i)^2\times\int_0^1 ds_1\int_0^{s_1} ds_2\kappa\cdot\mathbf{X}(p-\hbar\kappa s_2)\kappa\cdot\mathbf{X}(p-\hbar\kappa s)+\cdots. \tag{3-8}$$

The expression (3-8) may be denoted as an "ordered exponential."[3]

$$\mathbf{q}(p,\kappa)=\exp\left[i\int_0^1 ds\kappa\cdot\mathbf{X}(p-\hbar\kappa s)\right]_{(-)}. \tag{3-9}$$

$\mathbf{q}(p,\kappa)$ has two properties which we want to remark on. The first is that it has no "scattering" matrix elements, i.e., it causes only "vertical" transitions in which n changes but p does not. The second property is that for small κ, $\mathbf{q}(p,\kappa)\approx\delta_{nn'}$ for all p.

Let us adopt a pictorial language in which we consider the different values of the index n as denoting different kinds of "effective particle," so that an off diagonal matrix element nn' relates to a process in which an effective electron of type n' is annihilated and one of type n created. In these terms we can say that of the factors in (3-3), $\mathbf{q}(p,\kappa)$ describes creation-annihilation without scattering while $\exp(i\kappa\cdot x)$ describes scattering without creation-annihilation.

If the factor $\mathbf{q}(p,\kappa)$ in (3-3) is set equal to unity (2-15) reduces in each band to Wannier's equation in the form described by Slater.[4] Retaining the exact form of $\mathbf{q}(p,\kappa)$ allows one to correct Wannier's equation for the virtual creation-annihilation processes. As an example we will carry through the procedure to eliminate coupling of bands to the lowest order in V. We transform the Hamiltonian $\mathbf{H}$ to $\mathbf{H}^1=\mathbf{u}\mathbf{H}\mathbf{u}^{-1}$ with $\mathbf{u}=\exp(i\mathbf{S}/\hbar)$. $\mathbf{S}$ is chosen in the following manner.

$$S_{nn'}(p)=(\hbar/i)\times\int d^3\kappa v(\kappa)q_{nn'}(p,\kappa)e^{i\kappa\cdot x}/E_n(p+\hbar\kappa)-E_{n'}(p) \tag{3-10}$$
$$S_{nn}=0.$$

It may be verified that $\mathbf{S}^+=\mathbf{S}$.

By construction $\mathbf{S}$ satisfies

$$(i/\hbar)[\mathbf{S},\mathbf{E}]_{nn'}=-\int d^3\kappa v(\kappa)q_{nn'}(p,\kappa)e^{i\kappa\cdot x}. \tag{3-11}$$

[3] M. L. Goldberger and E. N. Adams, J. Chem. Phys. **20**, 240 (1952).

[4] J. C. Slater, Phys. Rev. **76**, 1952 (1949).

The transformation $\mathbf{u}$ is thus seen to remove from $\mathbf{H}^1$ all creation-annihilation terms of order V. As a consequence the new potential consists of two parts. One comes from the diagonal-in-bands part of $\mathbf{q}$ and is proportional to the first and higher powers of V. The other comes from the virtual creation-annihilation effects and is proportional to the second and higher powers of V.

For the sake of brevity we will not give the second-order terms explicitly although they are easily obtained. The transformed potential in the nth band is

$$V_n=\int d^3\kappa v(\kappa)q_{nn}(p,\kappa)e^{i\kappa\cdot x}+O(v^2/\Delta E). \quad (3\text{-}12)$$

The term $O(v^2/\Delta E)$ is proportional to $\sum|q_{nn'}|^2/E_{nn'}$ which is, in lowest approximation $\sum|\kappa\cdot X_{nn'}|^2/E_{nn'}$.

We will now discuss two cases when the theory yields relatively simple results. The first case is that the potential is slowly varying, but not necessarily weak. The approximation is to set $\mathbf{q}=1$. There are two conditions which must be met in order that the approximation be usable. One is the condition

$$\sum_{n'}'|\kappa\cdot X_{n'n}|^2\ll 1, \quad (3.13a)$$

which is necessary for $q_{nn}\sim 1$. This condition is the dominant condition when the potential strength is smaller than the separation between bands, ΔE.

The other condition is the more restrictive one when the potential strength exceeds the separation between bands. It is

$$|\sum_{n'}'|\kappa\cdot X_{nn'}|^2/E_{nn'}|\ll 1/V. \quad (3\text{-}13b)$$

When neither of the conditions (3-13) is violated the potential (3-12) can be approximated by

$$V_n=\int d^3\kappa v(\kappa)e^{i\kappa\cdot x}\equiv V(x). \quad (3\text{-}14)$$

Equation (3-14) is Wannier's approximation.[4] Wannier's approximation requires that the potential be slowly varying but not necessarily that it be weak.

There is a different kind of approximation possible, which requires that the potential be weak but not necessarily slowly varying. If the potential is weak ($V/\Delta E\ll 1$) we can neglect the second-order terms of (3-12) even for such values of κ that q_{nn} cannot be taken as unity. In order to see what new qualitative behavior may be expected let us replace the ordered exponential $\mathbf{q}$ by a regular exponential (this is equivalent to ignoring the p dependence of $\mathbf{X}$). Then

$$q(p,\kappa)_{nn}=[\exp(i\kappa\cdot X)]_{nn}. \quad (3\text{-}15)$$

In many cases it is a good approximation to say that the even terms in the power series for (3-15) are much larger than the odd, especially for lattices such that $X_{nn}=0$. Thus if the origin of coordinates is chosen at the center of charge of unit cell, we may expect that (3-15) becomes

$$q_{nn}(p)\doteq[\cos(\kappa\cdot\mathbf{X})]_{nn}, \quad (3\text{-}16)$$

and that in any case the relation (3-16) is quite generally good until third or fourth power terms in the exponential are required.

The approximation (3-16) gives for the potential (3-12) the approximation

$$V_{nn}\doteq\int d^3\kappa v(\kappa)[\cos(\kappa\cdot\mathbf{X})]_{nn}e^{i\kappa\cdot x}. \quad (3\text{-}17)$$

We have examined the meaning of (3-17) for a simple example and will state the qualitative results which we have found. If n in (3-17) denotes an s band then the cosine factor describes a "cut off" of the Fourier components at some κ_c value, the precise value of which depends on the dipole matrix elements. For κ_c values which are not too large the cutoff is substantially isotropic in a cubic lattice. Thus (3-17) describes a potential which differs qualitatively from the Wannier potential in that all of the fine detail has been smeared out.

As an illustration we consider the potential due to a charged interstitial or impurity ion in a lattice. We represent the effect of the $\cos\kappa\cdot\mathbf{X}$ factor by a guillotine at wave number κ_c. Then the potential function (3-17) becomes

$$V(x)=(2e^2/\pi r)\int_0^{\kappa_c r}dy(\sin y/y), \quad (3\text{-}18)$$

where r denotes $(x_1^2+x_2^2+x_3^2)^{\frac{1}{2}}$. The potential (3-18) is a Coulomb potential for large r but is parabolic for small r, going to the constant value $2e^2\kappa_c/\pi$ at small distances.

While we do not know that such guillotine behavior is general, it seems plausible on the basis of the following argument. When the potential is weak it is not energetically feasible to have strong mixing of states in different bands. In that case the electron is not able to react to the fine details of the perturbation since within one band it is not possible for the electron to achieve localization into a volume smaller than that of a single cell. Thus the short wavelength details of the perturbation are ineffective and according to (3-17) are to be ignored completely.

The case of a potential which is not either weak or slowly varying is very difficult to treat in any general way. The nature of at least part of the difficulty is that the problem is "atomic" in nature, i.e., the solution to the perturbed problem involves the same kind of mixing as occurs for the energy levels of an atom under the influence of a strong perturbation. Such problems clearly must be treated individually.

IV. RELATION TO THE WANNIER THEORY

The effective mass equation derived herein differs from previously derived similar equations in that it is

written in a momentum representation, the CMR, rather than a coordinate representation. If one transforms the Eq. (2-15) to a crystal coordinate representation (CCR) he finds that certain difficulties arise. These difficulties make the CCR much less satisfactory to use than the formulation which has already been presented. We will go through this briefly in order to establish the connection between the CMR and previous effective mass equations.

We transform to a CCR by the simple rule

$$\Phi_n^{(A)}(x)=[\Delta/(2\pi\hbar)^3]^{\frac{1}{2}} \int d^3p \exp(ip\cdot x/\hbar)\Psi_n^{(A)}(p). \quad (4\text{-}1)$$

Δ denotes the volume of unit cell, and the p integral goes over all momentum space. Because of the periodicity properties of the function $\Psi_n^{(A)}(p)$, (4-1) can be written

$$\Phi_n^{(A)}(x)=[\hbar^3/\Delta]^{\frac{1}{2}}\sum_R \delta(x-R) \int_{B.Z} d^3p \exp(ip\cdot R/\hbar)\Psi_n^{(A)}(p). \quad (4\text{-}2)$$

The p integral now runs only over the Brillouin zone. The form (4-2) shows a sharp line spectrum of the wave function in the CCR. Thus if one calculates expectation values with the CCR wave function all of the contributions come from the points of a space lattice. This situation is to be compared with the situation which arises when the wave function is expanded in terms of Wannier functions, since the Wannier functions are labeled by the same label R which labels the points of the space lattice above.

A close examination shows the function (4-1) is just the generalized Wannier function previously introduced by this writer[1] in an attempt to extend Slater's derivation of the Wannier equation to higher approximation. If (2-15) is transformed by the rule (4-1) one gets a difference-differential equation of considerable complexity, an equation which is not easily solved using standard methods. Thus we conclude that while the Schroedinger equation can be obtained in the CCR by purely formal means, the CMR is much better suited to the solution of problems.

Various approximate effective mass equations can be obtained by neglecting $\mathbf{X}$ with respect to x. Doing so, one avoids the difficulties with the CCR but limits himself to a zero order approximation. This matter is discussed in reference (1).

V. CONCLUSIONS

The "effective mass" Schroedinger equation is most easily derived by making use of the CMR. In the form obtained here it can be applied to a wide variety of problems. The only detailed applications which have been made up to the present are to certain problems connected with motion in a magnetic field.[1,5] However, we shall note below another and very important problem to which application is being presently studied.

We are examining the problem of the Coulomb correlation energy in substances other than a free electron gas. While the general problem presents some points of difference from the free electron gas calculation, there are a number of points of similarity. No quantitative results exist at present. However, we have become convinced that by throwing the problems into the CMR we can gain new insights into the process of correlation in complicated solids.

[5] E. N. Adams, Phys. Rev. **89**, 633 (1953). Most of the calculations in connection with the magnetic problems are free of the approximation inherent in the Wannier theory since only commutation relations are used to get the results. Thus the principal results of reference (1) and (5) do not involve the Wannier approximation.

A Study in the Mechanics of Crystal Growth from a Supersaturated Solution*

G. C. KRUEGER† AND C. W. MILLER
Brown University, Providence, Rhode Island
(Received January 8, 1953)

An experimental investigation of the concentration field during crystallization is made using an improved modification of W. F. Berg's interference technique. $Na_2S_2O_3 \cdot 5H_2O$ is crystallized at 23°C; concentrations between 40 percent and 55 percent. Graphing the positions of the growing faces *versus* time indicates, in all cases, a uniform rate of growth with occasional abrupt changes. These discontinuities were, in general, correlated with changes in the perfection of the growing face, the disappearance of a region of poor growth being associated with a decrease rate, whereas the appearance of an imperfection led to a higher rate. A minimum of concentration is observed near the face center, corroborating previous investigations with $NaClO_3$. A diffusion coefficient of 1.26×10^{-5} cm²/sec was calculated for $Na_2S_2O_3$ corresponding to 0.80×10^{-5} cm²/sec extrapolated from J. D. R. Scheffer's data.

There is no strict correlation between maximum, minimum, or average concentration at a crystal face and its rate of growth. It appears that the variations in concentration revealed by interferometer maps are to be interpreted as a consequence of solution depletion occasioned by the crystal's growth.

I. INTRODUCTION

THIS experimental study deals with the mechanics of the crystal growth process in a supersaturated solution. In particular those phenomena are dealt with which take place in the stages of growth that follow nucleation and precede the very slow, approximately equilibrium, growth occurring later in the crystal's history.

One aspect of the problem of the growth of a crystal from solution is the role assumed by the solution surrounding the growing crystal. There have been a number of studies dealing with this problem. Those of Lehmann are representative.[1] His techniques of investigation included the use of crystals which produce strongly colored solutions, e.g., CHI_3. By observing changes in solution color during crystalization, a qualitative picture of the concentration field could be obtained because the more concentrated salt solution was more strongly colored. He also used a modified schlieren technique designed by Toepler[2] for use with a microscope. Although this method was more sensitive than the colored solution technique, its sensitivity was still not great enough to yield more than qualitative information about the concentration field. Another technique employed by Lehmann consisted of introducing into the crystallizing solution a small amount of colloidal material which would not interfere with crystallization. The circulation of solution around the growing crystal could then be ascertained by following the colloidal particles which appeared as points of light under strong dark field illumination. Lehmann was able to obtain from these experiments a rather good qualitative picture of the concentration field surrounding a growing crystal.

A two-beam optical interference method, utilizing the Fizeau fringes which are formed in the film of crystallizing solution, has also been tried with little success. The interference fringes obtained were too broad to reveal detailed structure in the concentration field.

Berg,[3] using a sensitive multiple-beam interference technique, was able to plot in detail the concentration field surrounding a growing crystal. His experimental method consisted of placing a small seed crystal in a thin wedge-shaped film of supersaturated solution confined between two partially silvered optical flats. The multiple-beam Fizeau fringes map the concentration field established by the growing crystal. This assumes, of course, that the relationship between the index of refraction and the solution concentration is known. Berg used $NaClO_3$ for which these data had been determined by Miers and Isaac.[4]

In 1949 Berg's investigation of $NaClO_3$ was extended by Humphreys-Owen.[5] The interpretation of the concentration field was greatly facilitated by a modification of Berg's method introduced by Humphreys-Owen. The geometrical thickness of the film of crystallizing solution is held constant. The interference fringes map, then, the actual contours of equal concentration, and a qualitative examination of the field can be accomplished quickly and easily.

II. EXPERIMENTAL CONSIDERATIONS

The crystal selected for this study is the primary pentahydrate of sodium thiosulfate. This modification of the salt is stable at temperatures below 48.2°C and is the form always observed when crystallization occurs

* Part of a thesis submitted by G. C. Krueger in partial fulfillment of the requirements for the Ph.D. degree from the Graduate School of Brown University, Providence, Rhode Island.

† Now at University of Maine, Orono, Maine.

[1] O. Lehmann, *Molecularphysik* (Tuebner Leipzig, Leipzig, 1889), Vols. 1 and 2.

[2] A. Toepler, Nr. 157 and Nr. 158 von Ostwald's *Klassiker Der Exakten Wissenschaften*.

[3] W. F. Berg, Proc. Roy. Soc. (London), **164A**, 79 (1938).

[4] H. A. Miers and F. Isaac, J. Chem. Soc. **89**, 413 (1906).

[5] S. P. F. Humphreys-Owen, Proc. Roy. Soc. (London) **197A**, 218 (1949).

at room temperature in an open vessel.[6] Sodium thiosulfate crystallizes in the monoclinic system. Prisms and thin 010 plates constitute the common habits (Fig. 1).[7] From moderately supersaturated solutions (solutions which contain sufficient salt to cause saturation at approximately 8°C above crystallizing temperature) approximately two-thirds of the crystals formed are the 010 plates, the rest are the familiar prisms. For some of these crystal plates, growth at certain stages is confined to a single face.

Supersaturated solutions of $Na_2S_2O_3$ are easily prepared, and if the solution is maintained at a temperature of from 60°C to 90°C for several hours, it will remain indefinitely in a supersaturated state at room temperature. Even moderate agitation will not induce crystallization.

The data obtained in this study are the optical interference patterns formed in the film of crystallizing solution. This Fizeau interference pattern maps the contours of equal optical path. Relative index of refraction and the index of refraction gradient may be ascertained

TABLE I. Index of refraction as a function of concentration for $Na_2S_2O_3$ at $T=20$°C.

$\Delta n/\Delta T = 0.00018$ per °C, in neighborhood of 20°C.

% $Na_2S_2O_3$ in solution	Index of refraction $\lambda=5461$A	$\lambda=5890$A
43.5±1.0	1.43660	1.43418
44.2±1.0	1.43724	1.43475
44.3±0.1	1.43817	1.43550
46.0±1.0	1.44253	1.44008
46.5±0.1	1.44307	1.44049
47.7±1.0	1.44765	1.44512
49.1±1.0	1.45125	1.44890
49.5±0.1	1.45231	1.44975
50.4±1.0	1.45424	1.45163
51.0±0.1	1.45648	1.45380
52.0±1.0	1.45848	1.45585

for various points in the field. The index of refraction, during crystallization, is a maximum far from the crystal and attains its minimum value at the crystal face. The gradient is proportional to the number of fringes per centimeter, a large number of fringes indicating a steep gradient. The concentration field surrounding the growing crystal can be derived from the interference pattern, provided the relationship between the index of refraction and the concentration of the crystallizing solution is known. These data were obtained for sodium thiosulfate and are given in Table I. An empirical equation expressing the concentration for $\lambda=5461$A° at $T=23$°C is $C=42.0+(365.92)\Delta n$ for 42 percent $<C<52$ percent. $(\Delta n/\Delta T)$ in this range of temperatures is 0.00018 per °C. This information was

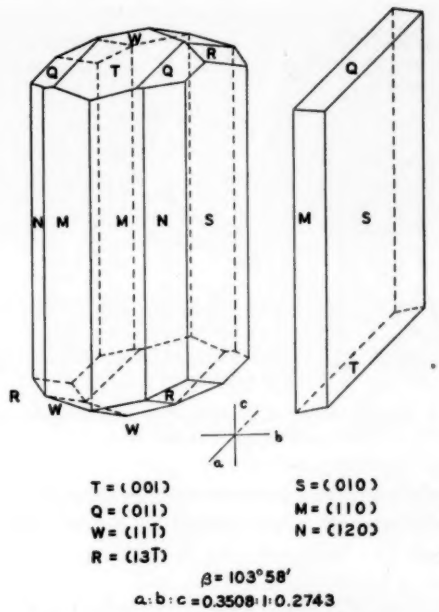

FIG. 1. Crystal habit of $Na_2S_2O_3 \cdot 5H_2O$.

obtained by measuring the index of refraction as a function of temperature of solutions of known density. We used the density *versus* concentration data available in the critical tables,[8] to obtain the concentrations of the solutions. A concentration *versus* index of refraction curve at a particular temperature is then obtained directly from these data.

The optical interference technique employed in this study is similar to that used by Berg, Humphreys-Owen, and Bunn in their studies of crystal growth from solution.[3,4] Two significant modifications have, however, been introduced. First, higher reflection coefficients have been used on the interferometer plates, and second, the thickness of the film of solution has been reduced. Optically these modifications result in sharper fringes with a consequent increase in precision of the measurements. Reducing the film thickness makes the process more nearly one of two-dimensional growth, and reduces to negligible proportions the amount of evaporation of the solution. The thickness of the film of crystallizing solution was determined by using the channeled spectrum method.[9]

To obtain sufficient exposure to record photographically the changing interference pattern, it was necessary to use (1) a high pressure mercury arc (a low-pressure arc was occasionally used during the slow growth stages), (2) a Wratten No. 77 filter, (3) Kodak Fluorographic film (Green sensitive, 35-mm, x-ray film), and (4) Kodak SD-19a high contrast developer.[10]

[6] S. W. Young and J. P. Mitchell, J. Am. Chem. Soc. **26**, 1389 (1904); S. W. Young and W. E. Burke, J. Am. Chem. Soc. **26**, 1413 (1904); **28**, 315 (1906).

[7] A. N. Winchell, *The Optic and Microscopic Characters of Artificial Minerals* (University of Wisconsin Studies in Science No. 4, 1927).

[8] Int. Critical Tables **3**, 81; **4**, 236; **4**, 248, 1928 and Tables Annuells Int. de Constantes de Donees Numeriques **4**, 16 (1910–1922).

[9] H. Fizeau and L. Foucault, Ann. chim. et phys. **26** (3), 138 (1849); **30** (3), 145 (1850).

[10] Miller, Henn, and Crabtree, J. Phot. Soc. Amer. **12**, 586 (1946).

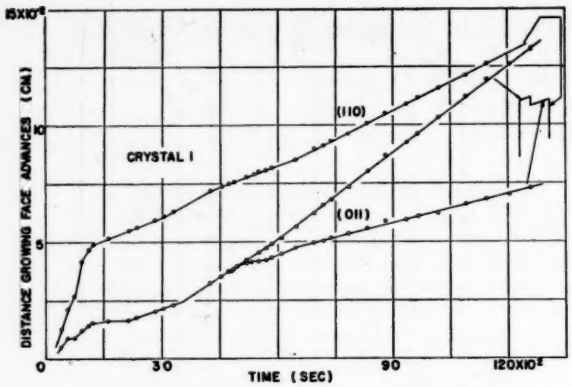

FIG. 2. Displacement of growing face as a function of time for Crystal 1.

The photographic records were evaluated by making measurements on a magnified image of the original negative.

III. EXPERIMENTAL RESULTS AND DISCUSSION

The distance advanced by the crystal face is plotted, in Figs. 2 and 3, against the time for three different experiments typical of many such studies made in the course of the investigation. The origin of the time scale on these graphs does not necessarily coincide with the instant at which the crystal first appeared, as the most interesting cases of growth seldom were the ones for which the initial appearance was even observed.

In all cases, as the graphs indicate, the rate of growth is uniform, with occasional abrupt changes, usually to lower rates but occasionally to an increased rate. Where more than one face was growing at a time, abrupt changes were frequently although not always observed to occur simultaneously on all of the growing faces, indicating a close interaction between their growth mechanisms.

Small changes in concentration which occur at the growing face do not appear to influence the rate of growth. The growing face of the crystal shown in Fig. 2 encountered an air bubble in the solution which caused the face to divide into two sections. Both sections continued to grow but at different rates. Twenty minutes after the face split the slower growing face settled down to a steady rate of growth. The rate of advance of the growing face was, within the precision of the measurements, exactly twice that of the slower growing face. There is some evidence from other experiments that the exact twofold ratio of the rates of growth of the two faces is not just a coincidence but results from the fundamental conditions at the surface (or corners) of the crystal which determine the rate of advance. It is not unusual, for example, when the rate of growth of a face changes for it to change by an amount which approximates closely to an integral ratio (see, e.g., Crystal 2, Fig. 3). At no time did the average concentration at the two faces of Crystal 1, Fig. 2, differ by more than 0.06 percent‡ although the absolute value of the concentration increased by as much as 0.25 percent. This ability of a particular crystal face to grow at two different rates under substantially the same conditions, in so far as the concentration field is concerned, is a general rather than an exceptional phenomenon.

There appears to be no strict correlation between the maximum, minimum, or average concentration of the solution contiguous to the crystal face and the rate of growth of this face. In general, however, the concentration is higher at the more rapidly growing faces.

Pasteur was one the the first to report the accelerated growth shown by imperfect crystals.[12] Experiments performed in this laboratory afford further insight into this behavior. The efficient optical arrangement used made it possible to obtain interferometer records of the concentration fields even of very rapidly advancing crystal faces.

In the first of two experiments to be considered (Crystal 2), the growing face began as an imperfect face and remained so throughout most of its history,

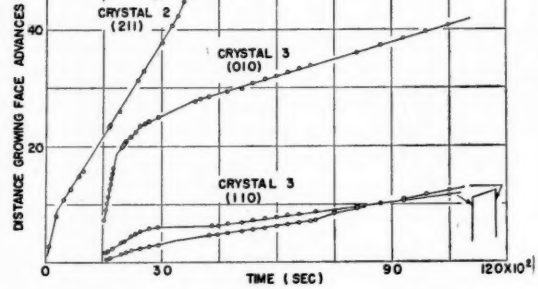

FIG. 3. Displacement of growing face as a function of time for Crystals 2 and 3.

healing over and becoming perfect only a few minutes before its growth terminated at the edge of the drop of solution. The graph for this crystal (Fig. 3) shows that the rate of growth maintained by it during most of its history is between three and six times larger than that exhibited by a crystal in which the growing face is a perfect face. These high rates of growth are probably to be attributed to the broken and therefore very imperfect face. The rate of growth remains constant between $t=3\times10^2$ sec and $t=3.3\times10^3$ sec, although the size of the break was by no means constant. However, when the break extended to the corner of the crystal the rate of growth increased to 1.6 times its previous value [Figures 4(a) and 4(b) show the crystal just before and just after the break extended to the corner].

In general, the imperfect area of the growing face is rarely centered on the face. It is usually displaced to-

‡ All concentrations are given in grams of solute per 100 grams of solution.

[12] L. Pasteur, Ann. chim. et phys. **49**, 5 (1857).

ward the obtuse-angled corner. This may well be due to the fact that the minimum value of concentration on the growing face is usually displaced toward the acute-angled corner of the crystal. The fact that low concentration favors perfect growth would make this side of the crystal less likely to develop imperfections.

The concentration field of this crystal does not differ in its general character from the fields usually observed for a crystal of this type. The nature of the asymmetry of the concentration field near the face is rather clearly shown by the shape of the fringe nearest the face. The steeper gradient at the acute corner persisted throughout the experiment but was most marked during the periods of most rapid growth. A shallower gradient is found at the obtuse corner, i.e., the corner nearest the imperfect region of the growing face. This may be due to higher temperatures prevailing in the region where rapid growth is in progress. These higher temperatures are accompanied by a higher diffusion coefficient which in turn would account for the shallower gradient. As this crystal approached the edge of the drop, it became increasingly difficult to supply the volume of fresh

(a) (b)

FIG. 4. Two successive stages in the growth of an $Na_2S_2O_3 \cdot 5H_2O$ crystal. Figure 4(a) taken just before rate of growth changed, Fig. 4(b) just after rate changed. Flare spot in center of photograph is not significant and is due to optical arrangement.

crystallizing solution needed to maintain the existing rate of growth. The fringe nearest the crystal moved further from the face indicating that the concentration there was decreasing. An examination of the advancing face shows that the break is beginning to heal. This must certainly be due to the decrease in concentration. It is important to note that the rate of growth has not yet changed. About a minute later the rate of growth abruptly decreased by approximately 300 percent, although the concentration during the preceding period of steady growth (lasting about 10 minutes) decreased by only 0.5 percent. This 0.5 percent decrease in concentration has permitted the new material to deposit as perfect crystal.

The crystal of the second experiment (Crystal 3) also grew from a solution in which initially the concentration was not quite low enough to sustain perfect growth. During the periods of imperfect growth the well-formed portion of the face is an 010 face; after healing over, the face was still an 010 face. The crystal's rate of growth during the first two stages of its history changed several

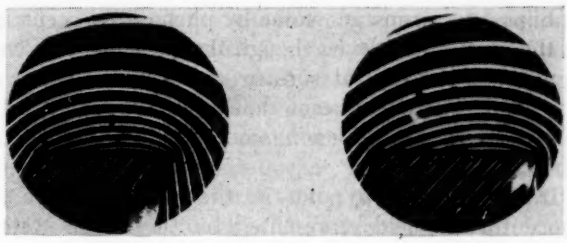

(a) (b)

FIG. 5. Detailed fringe pattern at the growing face of Crystal 3. Fringes indicate that the concentration attains a minimum near the face center. Note slight imperfections within the body of the crystal. Rate of growth is the same for both Figs. 5(a) and 5(b).

times. To each change in rate it was possible to correlate a change in the perfection of the growing face, i.e., each time a break appeared on the face the rate increased, and when the break healed over the rate dropped. Once the crystal face attained the degree of perfection shown in Fig. 5(a) it maintained a uniform rate of growth for nearly two hours, after which the experiment was terminated. Both Figs. 5(a) and 5(b) were taken during this long period of uniform rate of growth.

In Figs. 5(a) and 5(b) the three innermost fringes terminate on the crystal face and so give evidence of a decrease in concentration at the surface of the crystal, as one moves from either corner toward the center of the face. This phenomenon is also apparent, though in much less detail, in the earlier photographs of Humphreys-Owen. The improved detail is a direct consequence of the refined multiple-beam technique.

In the graph in Fig. 6 the minimum value of the concentration at the growing face is plotted as a function of time. The vertical broken lines indicate the times at which the rate of growth changed. In general, the appearance of an imperfect area is accompanied by an abrupt decrease in concentration, whereas an increase in concentration attends the healing of an imperfect area. During the final interval, 40 minutes$<t<$120 minutes, the rate of growth remains constant at 2×10^{-5} cm/sec, whereas the minimum concentration at the growing face varied by as much as 1 percent. This behavior indicates that the rate of growth is

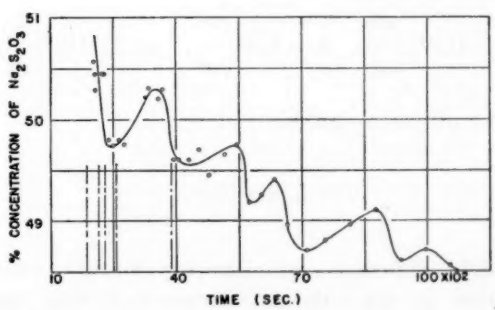

FIG. 6. Variation in concentration with time for Crystal 3. These variations can be correlated with the appearance and disappearance of the slight imperfections shown in Fig. 5.

stabilized to a constant value by phenomena occurring at the crystal face, even though the concentration contiguous to the crystal surface varies by as much as 1 percent. There can be no doubt, however, that sufficiently large deviations in concentration do change this rate.

It is appropriate to point out the extent to which the concentration field represented by the fringe system shown in Fig. 5 is able to account for the observed rate of growth. There seems to be no reason to doubt that the material which enters into the growing crystal is supplied by diffusion, particularly during the long periods of constant rate of growth. It is possible from rather fundamental considerations to obtain the condition which should be satisfied at the boundary of the crystal for a steady state of growth. Consider a system of coordinates which is fixed with respect to the crystal face.

Let M = molecular weight of crystal,
I = molecular weight of crystal minus water of crystallization,
W = molecular weight of water of crystallization,
v = velocity of advance of crystal face,
m_s = mass of solute deposited per second per cm^2,
m_w = mass of water deposited per second per cm^2,
ρ_c = density of crystal,
ρ_s = density of solution at crystal face,
c = concentration of solute (gm/cm^3),
c_w = concentration of solvent (gm/cm^3),
v_s = velocity of solute relative to crystal,
v_w = velocity of water relative to crystal,
D = diffusion coefficient.

Then

$$m_s=\frac{I}{M}\rho_c v,$$

$$m_s=cv_s;$$

therefore,

$$v_s=\frac{I}{M}\frac{\rho_c}{c}v.$$

Similarly,

$$v_w=\frac{W}{M}\frac{\rho_c}{c_w}v,$$

but

$$c_w=\rho_s-c;$$

therefore,

$$v_w=\frac{W}{M}\frac{\rho_c}{\rho_s-c}v.$$

The velocity of the solute ions with respect to the water (v_r), which is the significant velocity for the diffusion of ions relative to a solvent, is then given by the relationship

$$v_r=\frac{\rho_c}{M}\left[\frac{I}{c}-\frac{W}{\rho_s-c}\right]v.$$

$$D\frac{dc}{dx}=cv_r$$

$$=\frac{\rho_c}{M}\left[I-\frac{cW}{\rho_s-c}\right]v,$$

where

$$\frac{dc}{dx}=\frac{\text{(Change in concentration between two successive fringes)}}{\text{(Distance between two successive fringes)}}.$$

Substituting the values appropriate to Crystal 3 at $t=42.6$;

$$\frac{dc}{dx}=\frac{.00466\ \text{gm}}{.0078\ \text{cm}^4};\quad \rho_c=1.68\frac{\text{gm}}{\text{cm}^3},$$

$$M=248.2,\quad I=158.1,\quad W=90.1,$$

$$c=0.497\frac{\text{gm}}{\text{cm}^3},\quad \rho_s=1.50\frac{\text{gm}}{\text{cm}^3},\quad v=2\times10^{-5}\frac{\text{cm}}{\text{sec}},$$

yields a diffusion coefficient of

$$D=1.26\times10^{-5}\frac{\text{cm}^2}{\text{sec}}.$$

The only diffusion coefficient for $Na_2S_2O_3$ which is available in the existing literature is that due to Scheffer.[13] His measurements were made at 10.5°C and the concentrations of the solutions used were 15.2 percent and 3.6 percent. If we assume a temperature coefficient of diffusion of 0.026,[14] which is appropriate for salts of this type, the diffusion coefficient extrapolated from Scheffer's data and reduced to $T=23$°C and a concentration of 49.7 percent is found to be 0.80×10^{-5} (cm^2/sec). The value of D computed for Crystal 3 exceeds this extrapolated value by approximately 50 percent, an amount considerably greater than could be accounted for by errors in the experimental measurements. This calculation assumes that the growing crystal face is sufficiently large so that the influence of the corners may be neglected. It is not yet possible to assess with any certainty the limitations imposed by this assumption.

IV. SUMMARY

An improved technique is described for mapping the concentration field surrounding a growing face of a

[13] J. D. R. Scheffer, Z. physik. Chem. 2, 397 (1888).

[14] W. Nernst, *Theoretical Chemistry* (Macmillan Company, New York, 1916), fourth English edition, p. 403.

crystal. This technique is applied to the study of $Na_2S_2O_3 \cdot 5H_2O$ growing at temperatures of approximately 23°C, from supersaturated solutions ranging in concentration from 40 percent to 55 percent. Certain of these crystals exhibited growth on a single face, whereas others grew simultaneously on two or three faces. Photographs of the growing crystals with associated Fizeau fringes, which mapped their concentration field, were made at frequent intervals. Graphs plotted to show the positions of the various growing faces as a function of time indicated, in all cases, a uniform rate of growth with occasional abrupt changes. Where more than one face was growing at a time abrupt changes were frequently, although not always, observed to occur simultaneously on all of the growing faces. These discontinuities were in many cases correlated with obvious changes in the perfection of the growth, the disappearance of a region of imperfect growth being generally associated with a decreased rate of growth, whereas the appearance of an imperfection usually led to a higher rate of growth. An analysis was made of the fringe pattern with one of the slower growing crystals. This study corroborated previous similar work done with $NaClO_3$ in showing that the concentration is a minimum at some point in the central region of the growing face and increases toward both corners. A diffusion coefficient, $D=1.26\times10^{-5}$ cm^2/sec at $T=23$°C was calculated from these interferometer maps. Scheffer's experimental data extrapolated to the same temperature and concentration yield a value of 0.80×10^{-5} cm^2/sec.

The rate of growth is not a sensitive function of the concentration at the growing face, e.g., at any one time the difference in concentration between face center and face corner was approximately 1 percent, and during a period of constant rate of growth the minimum concentration at this face varied by as much as 1 percent. In fact, it would appear that the variations in concentration which the interferometer maps display are to be interpreted as a consequence of solution depletion occasioned by the growth of the crystal.

A number of investigators have suggested that the rate of growth of a crystal face is a function of the degree of supersaturation at that face.[15] This study indicates that diffusion may set an upper limit to the rate at which a crystal face grows, but that when the face grows at a lower rate, this rate is determined by conditions existing at the growing face. If the centers of growth are identified with dislocations, as suggested by Frank,[16] the general picture becomes clearer. Long periods of constant rate of growth would be a consequence of the domination of a particular dislocation. Abrupt changes in rate of growth suggest the overrunning of the principal dislocation and its replacement by another dislocation which then assumes the dominant role. Large fluctuations in concentration which occur during a period of constant rate of growth (Fig. 6) further strengthen the impression that it is the dislocation which is the rate controlling factor during this stage of growth. It appears that a structure-sensitive theory of crystal growth such as Frank's is required to explain the phenomena observed during a crystal's growth.

[15] C. W. Bunn, Discussions Faraday Soc. No. **5** (Crystal Growth), 132–144 (1949) reviews this approach. S. P. F. Humphreys-Owen, Discussions Faraday Soc. No. **5** (Crystal Growth), 144–149 (1949).

[16] F. C. Frank, Discussions Faraday Soc. No. **5** (Crystal Growth), 48–54, 66–67, 76–77, 189–191 (1949).

Infrared and Raman Spectra of Tetramethylmethane-d_{12}*

E. R. SHULL, T. S. OAKWOOD, AND D. H. RANK
School of Chemistry and Physics, The Pennsylvania State College, State College, Pennsylvania
(Received May 4, 1953)

In order to study further the molecular vibrations of tetramethylmethane and of hydrocarbons in general, tetramethylmethane-d_{12} was synthesized, and its Raman and infrared absorption spectra were obtained. The missing nondegenerate mode, $\nu_2(a_1)$, in ordinary tetramethylmethane was predicted by the Teller-Redlich product rule to lie at about 1430 cm^{-1} where it would be obscured by a strong depolarized Raman band at 1451 cm^{-1}. A unique narrowness in the 1200 cm^{-1} infrared absorption bands of tetramethylmethane and tetramethylmethane-d_{12} and double maxima of small separation in the band of tetramethylmethane resulted in assigning these frequencies to methyl wagging modes of unsymmetrical character. The over-all results of this investigation cast doubt on the validity of extending theoretical considerations of tetrahedral XY_4 systems to the tetrahedral tetramethyl molecules with the assumption of the methyl groups as point masses.

THE molecule tetramethylmethane because of its highly symmetrical character has received a great deal of attention in discussion of the vibrations of the paraffins. Certain problems with regard to the assignment of the molecular vibrations of this molecule still remain to be solved. Rank, Saksena, and Shull[1] have prepared monodeutero tetramethylmethane and also monodeutero silicon tetramethyl. The Raman and infrared spectra of these molecules were obtained in an attempt to clear up some of the uncertainties concerning the assignment of the vibrations of the tetramethylmethane molecule. A rather complete bibliography of the previous work on tetramethylmethane is contained in the above mentioned paper. Sheppard, Simpson, and Sutherland[2] have raised certain questions with regard to the assignments of Rank, Saksena, and Shull.[1] Because of the fundamental nature of this problem with regard to the assignment of vibrational frequencies of the paraffins, it was thought desirable to prepare tetramethylmethane-d_{12} and study its infrared and Raman spectra.

The totally deuterated tetramethylmethane molecule because of the simplicity of its spectrum might, among other things, throw light upon the limitations of making the assumption that the CH_3 group can be treated as a single atom in calculation of the so-called "framework" vibrations of the paraffins.

SYNTHESIS

Preparation of a deuterated molecule containing 12 deuterium atoms in its structure will require a very high degree of deuteration of the reagents used in effecting the synthesis. The percentage of the deuterated molecule containing one hydrogen, in general, will be 12 times as great as the over-all hydrogen percentage.

The synthesis of tetramethylmethane-d_{12} was carried out by means of the following well-known reactions:

$$CD_3Br \xrightarrow[(3)\ H_2O]{(1)\ Mg,\ ether;\ (2)\ CD_3COCD_3} CD_3-\underset{\displaystyle CD_3}{\overset{\displaystyle CD_3}{\overset{|}{\underset{|}{C}}}}-OH \xrightarrow{\text{conc. HCl}} CD_3-\underset{\displaystyle CD_3}{\overset{\displaystyle CD_3}{\overset{|}{\underset{|}{C}}}}-Cl \xrightarrow[\text{toluene}]{CD_3MgBr} CD_3-\underset{\displaystyle CD_3}{\overset{\displaystyle CD_3}{\overset{|}{\underset{|}{C}}}}-CD_3.$$

The first Grignard reaction was carried out in anhydrous diethyl ether as solvent. The Grignard complex was decomposed with ordinary water. The second Grignard reaction was carried out in dry toluene as solvent.[3]

For reasons which will appear later, isobutane-d_{10} was prepared by the reaction

$$(CD_3)_3CMgCl + D_2O \rightarrow (CD_3)_3CD.$$

The above reactions are common organic preparative reactions which all proceed with reasonably good yields. Our experiments demonstrate conclusively that no exchange between deuterium and the hydrogen present in the solvents and reagents takes place in any of these reactions. Thus it is apparent that the percentage of deuteration of the final product depended upon the completeness of the deuteration of the acetone-d_6 and the methyl-d_3 bromide used in the synthesis.

EXCHANGE REACTIONS

Acetone-d_6 was prepared by the well-known method of exchanging acetone with D_2O.[4] The CD_3Br was pre-

* This research was assisted by support from Contract N6onr-269, Task V of the U. S. Office of Naval Research.

[1] Rank, Saksena, and Shull, Discussions Faraday Soc. No. 9, 187 (1950); D. H. Rank, *ibid* No. 9, 219 (1950).

[2] Sheppard, Simpson, and Sutherland, Discussions Faraday Soc. No. 9, 216 (1950).

[3] G. H. Fleming, Ph.D. dissertation, The Pennsylvania State College, June, 1933; F. C. Whitmore and G. H. Fleming, J. Am. Chem. Soc. 55, 3803 (1933).

[4] Halford, Anderson, Bates, and Swisher, J. Am. Chem. Soc. 57, 1663 (1935).

pared from CD_3COOD which had been prepared by exchanging malonic acid with D_2O and subsequently heating the heavy malonic acid, which process produces the heavy acetic acid[5] in quantitative yields.

The acetone exchange was carried out by mixing acetone with D_2O, making a solution slightly alkaline with a very small amount of anhydrous K_2CO_3, refluxing for about one half hour and then separating the acetone from the water by fractional distillation by means of a suitable fractionation column. Malonic acid was put into solution in D_2O and a good vacuum produced in the apparatus. The water was separated by vacuum distillation condensing the water in a liquid air trap. In the final stages the solution was heated on a water bath to remove the D_2O from the malonic acid as completely as possible.

We have followed the course of the exchange reactions by determining the density of the water removed from the solution after each exchange. In calculating the progress of the exchange process step by step, we have made the assumption that statistical distribution of H and D atoms among the two components of the solution takes place.[6] The results of our density determinations on the recovered water showed that this assumption was valid to a high degree of approximation. Furthermore, the spectroscopic evidence showed that the assumption of statistical distribution was completely justified.

The production of nearly completely deuterated material by exchange processes is very extragavant in the use of D_2O when compared to direct synthesis, if synthesis is possible. However, it should be pointed out that this extravagance only occurs in the preparation of the first batch of highly deuterated material. Successive batches can be produced by only expending amounts of high purity D_2O equivalent to the highly deuterated product removed from the process.

METHYL-d_3 BROMIDE PREPARATION

The methyl-d_3 bromide in good yield was prepared by a modification of Böckemüller and Hoffman's method of preparing the ordinary compound.[7] Bromine in carbon tetrachloride was added to a suspension of finely ground silver acetate-d_3 (prepared by the reaction of silver oxide with acetic-d_3 acid-d) in carbon tetrachloride in the presence of light. The product was recovered by careful fractional distillation of the reaction mixture. Anhydrous conditions were strictly observed.

EXPERIMENTAL

The Raman spectrum of tetramethylmethane-d_{12} in the liquid phase was obtained using 2 ml of a sample which had been vacuum distilled and sealed off in a suitable scattering tube. Excitation was effected by means of the mercury blue line, Hg λ4358A, produced by a pair of low-pressure mercury arcs[8] using a filter consisting of saturated aqueous sodium nitrite solution in two cylindrical condensers. Spectrograms were obtained with a three-prism spectrograph.[9] A comparison spectrum using a stainless steel arc was obtained with a 20-inch $f/8$ camera which gave a linear dispersion of 19 A/mm at λ4600A. Qualitative depolarization measurements were obtained photographically by the method of polarized incident light[1,10] using a 5-inch $f/2$ camera.[11]

The infrared absorption spectra of tetramethylmethane and tetramethylmethane-d_{12} were obtained in the gas phase with a Perkin-Elmer infrared spectrometer Model 12C, modified to the Walsh double-pass system,[12] and equipped with prisms of lithium fluoride, sodium chloride, and potassium bromide. A 10-cm path gas cell of Pyrex glass was cemented silver chloride windows was used. The vapor pressure of the gas was varied according to the degree of absorption required to best define the respective bands.

The Raman and infrared absorption spectra of isobutane-d_{10} were obtained in a similar manner.

RESULTS AND DISCUSSION

The spectroscopic results are shown in Figs. 1–3. Figure 1 presents the comparison spectrograms of the Raman spectrum of $(CD_3)_4C$ with those of $(CH_3)_4C$ and $(CH_3)_4Si$ for comparison. Figure 2 presents the polarization spectrograms of these compounds. Trans-

[5] J. O. Halford and L. C. Anderson, J. Am. Chem. Soc. **58**, 736 (1936).

[6] For the benefit of other investigators, it might be in order to write out the elementary general theory for the quantitative progress of such an exchange reaction when the process is stepwise and statistical distribution is assumed.

Let A and B be the number of moles of H_2 and D_2 respectively present in the material to be exchanged with heavy water. C and D represent the number of moles of H_2 and D_2 contributed to the mixture $A+B+C+D$ by the heavy water component of the mixture. If statistical distribution of H and D in the mixture is achieved, the fractional deuteration K_D is obviously

$$K_D=(B+D)/(A+B+C+D);\ K_D+K_H=1.$$

It can easily be seen that repetitive operation of such a stepwise process to achieve large values of K_D is a powerful method of testing the assumption of statistical distribution of H and D in the process. Our results have shown very conclusively that such statistical distribution is achieved in the acetone and malonic exchange processes. Furthermore, after the completion of the synthesis of tetramethylmethane-d_{12}, a very sensitive test of the completeness of deuteration in the absence of further exchange of reagents is available. The statistical distribution of isotopic molecules of the various species present will be proportional to the terms of the expansion of $(K_D+K_H)^n$ where n is the number of hydrogen atoms present in the molecule. In all probability the expression just given is strictly valid only for equal K_D in the acetone and the methyl bromide reagents. The relative abundance of the species containing one hydrogen ($nK_HK_D^{n-1}$), can easily be estimated from the spectrum with considerable certainty.

[7] W. Böckemüller and F. W. Hoffman, Ann. d Chem. **519**, 165 (1935).

[8] D. H. Rank and J. S. McCartney, J. Opt. Soc. Am. **38**, 279 (1948); Rank, Sheppard, and Szasz, J. Chem. Phys. **16**, 698 (1948).

[9] Rank, Scott, and Fenske, Ind. Eng. Chem. Anal. Ed. **14**, 816 (1942).

[10] A. E. Douglas and D. H. Rank, J. Opt. Soc. Am. **38**, 281 (1948).

[11] D. H. Rank, J. Opt. Soc. Am. **40**, 462 (1950).

[12] A. Walsh, J. Opt. Soc. Am. **42**, 96 (1952).

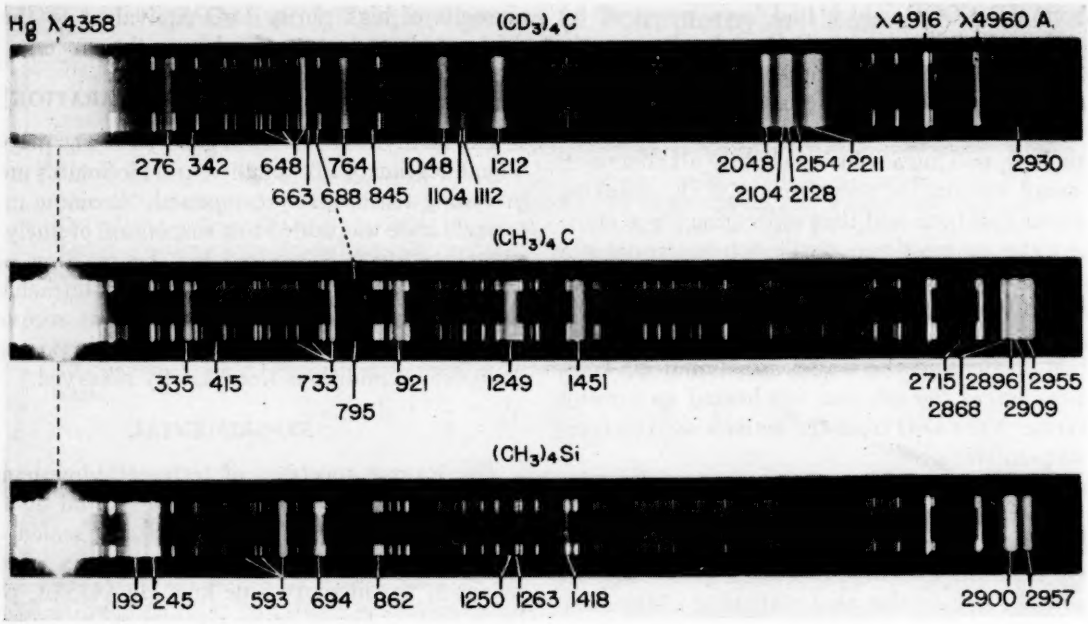

FIG. 1. Reproductions of comparison spectrograms of Raman spectra. The Raman lines $\Delta\nu=688$ and 2154 cm^{-1} from the tetramethylmethane-d_{12} sample and $\Delta\nu=795$ cm^{-1} from the tetramethylmethane sample arise from isobutane-d_{10} and isobutane, respectively.

mission curves of their infrared absorption spectra are shown in Fig. 3.

With regard to the hydrogen content in the tetramethylmethane-d_{12}, it should be pointed out that a polarized Raman line, $\Delta\nu=663.7$ cm^{-1}, attributable to the totally symmetric vibrational mode of the monohydrogen species, was observed. The intensity of this line approximated that of the totally symmetric frequency of the completely deuterated molecule excited by Hgλ4347A, which is about 1/50th as intense as the primary exciting line, Hgλ4358A.[8] The results of Rank and Bordner[13] showing that the totally symmetric Raman lines of the ordinary and monodeutero tetramethylmethanes were of approximately equal intensity in a 1:1 mixture of the two molecules suggest the relative abundance of the monohydrogen species considered here to be about 2 percent.

Because of previous observations of isobutane lines in the Raman spectrum of tetramethylmethane and the observation of suspicious lines in the Raman spectrum of the tetramethylmethane-d_{12} sample, the spectrum of a sample of isobutane-d_{10} was obtained. It was found that the Raman lines $\Delta\nu=688$ and 2154 cm^{-1} as well as "wings" on $\Delta\nu=764$, 1048, and 1212 cm^{-1} could be discounted as arising from vibrations of this molecule. Also, re-examination of the comparison plate of the Raman spectrum of tetramethylmethane revealed the totally symmetric frequency, $\Delta\nu=795$ cm^{-1}, of isobutane was present but very weak.

As in tetramethylmethane, the assignment of the observed frequencies to the respective symmetry types in the completely deuterated molecule can be made on the basis of selection rules requiring three polarized Raman active A_1 modes, one spectroscopically inactive A_2 mode, four depolarized Raman active E modes, four spectroscopically inactive F_1 modes, and seven depolarized Raman active and infrared active F_2 modes. The vibrational assignments of the active modes of tetramethylmethane-d_{12} together with those for tetramethylmethane and tetramethyl silicon based on the experimental results of this investigation are presented in Table I.

The Teller-Redlich product rule[14] predicts the following relationships between the zero order frequencies of tetramethylmethane and its d_{12} analog for the spec-

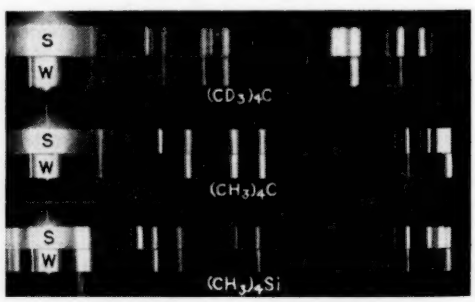

FIG. 2. Reproductions of polarization spectrograms of Raman spectra.

[13] D. H. Rank and E. R. Bordner, J. Chem. Phys. 3, 248 (1934).

[14] See G. Herzberg, *Infrared and Raman Spectra of Polyatomic Molecules* (D. Van Nostrand Company, Inc., New York, 1947), p. 231.

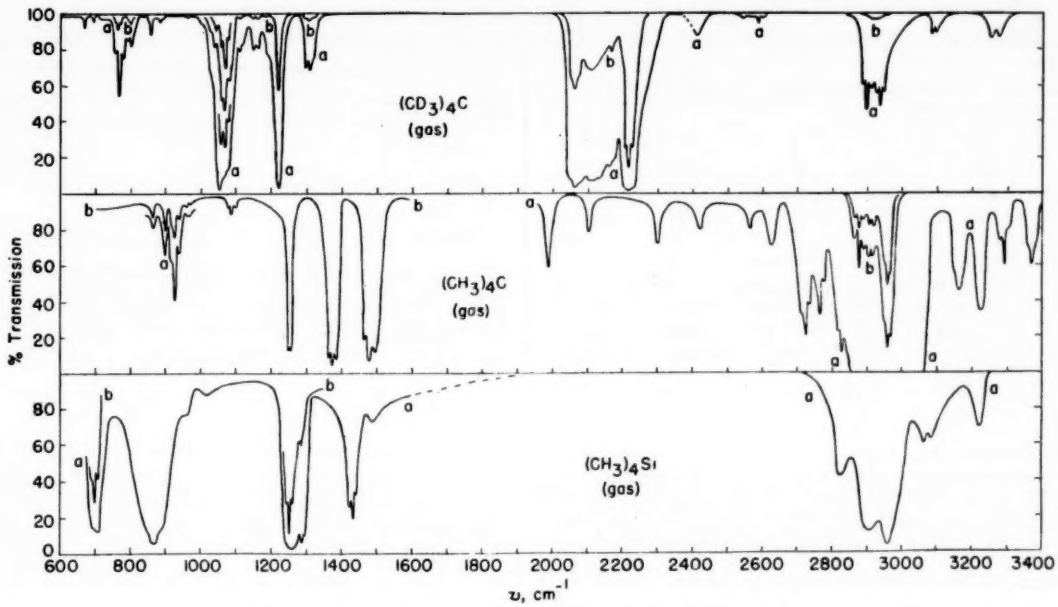

FIG. 3. Transmission curves of infrared absorption spectra.

troscopically active modes:

(1) A_1 modes $\pi(\omega_f{}^i/\omega_f)=[(m_H/m_D)^2]^{\frac{1}{2}}=0.5000$;

(2) E modes $\pi(\omega_f{}^i/\omega_f)=[(m_H/m_D)^3]^{\frac{1}{2}}=0.3536$;

(3) F_2 modes $\pi(\omega_f{}^i/\omega_f)=[(m_H/m_D)^5(M_D/M_H)^3]^{\frac{1}{2}}=0.2228$,

where π signifies the product of the frequencies f, m_H, and m_D are the masses of the H and D atoms, respectively, and M_H and M_D are the molecular weights of the respective isotopic molecules.

All three A_1 modes for tetramethylmethane-d_{12}, $\Delta\nu=648$, 1104, and 2128 cm^{-1}, were observed. The observation of 1104 cm^{-1} as well as the two more easily observable frequencies permits the calculation of the frequency of the missing A_1 mode in the ordinary compound by the Teller-Redlich product rule.[14] The predicted frequency for $\nu_2(a_1)$ at 1430 cm^{-1} would place the Raman line at a position where it would be obscured by the broad depolarized Raman band at 1451 cm^{-1}.

As in tetramethylmethane and tetramethyl silicon, only two of the four doubly-degenerate E modes are observed, $\Delta\nu=276$ and 1048 cm^{-1}. Although our present infrared facilities do not permit study of the region below 400 cm^{-1}, it is felt certain that the choice of the depolarized Raman frequency at 276 cm^{-1} is justified. Similar to the analogous situation in tetramethylmethane and tetramethyl silicon, only one depolarized Raman band, $\Delta\nu=2211$ cm^{-1}, was observed in the 2000-cm^{-1} "C–D" region. Although an E mode is to

TABLE I. Vibrational assignments for the active modes of the tetramethyl molecules.[a]

$(CD_3)_4C$						$(CH_3)_4C$						$(CH_3)_4Si$						
Raman (1)			Infrared (g)			Raman (1)			Infrared (g)				Raman (1)			Infrared (g)		
$\Delta\nu$	Int	Pol	ν	Int		$\Delta\nu$	Int	Pol	ν	Int		ν^i/ν	$\Delta\nu$	Int	Pol	ν	Int		Assignment
648	*vs*	*p*	In.	—		733	25	*p*	In.	—		0.8840	593	40	*p*	In.	—		$\nu_1(a_1)$ Skel.
1104	*m*	*p*	In.	—		(1430)	—	—	In.	—		(0.7731)	1263	8	*p*	In.	—		$\nu_2(a_1)\delta_+$(CH)
2128	*s*	*p*	In.	—		2909	100	*p*	In.	—		0.7315	2900	100	*p*	In.	—		$\nu_3(a_1)\nu_+$(CH)
276	*m*	*dp*	In.	—		335	22	*dp*	In.	—		0.8239	199	80	*dp*	In.	—		$\nu_1(e)$ Skel.
—	—	—	In.	—		—	—	—	In.	—		—	—	—	—	In.	—		$\nu_2(e)\gamma$ (CH)
1048	*sb*	*dp*	In.	—		1451	55	*dp*	In.	—		0.7223	1418	40	*dp*	In.	—		$\nu_3(e)\delta_-$(CH)
—	—	—	In.	—		—	—	—	In.	—		—	—	—	—	In.	—		$\nu_4(e)\nu_-$(CH)
342	*w*	*dp*	—	—		415	4	*dp*	418	*w*	?	0.8241	245	46	*dp*	—	—		$\nu_1(f_2)$ Skel.
764	*m*	*dp*	765	*w*	*PQR*	921	40	*dp*	925	*w*	*PQR*	0.8295	694	33	*dp*	696	*vs*	*PQR*	$\nu_2(f_2)$ Skel.
1212	*m*	*dp*	1218	*s*	"*Q*"	1249	60	*dp*	1256	*s*	*dbl*	0.9697	1250	8	*dp*	1253	*s*	*PQR*	$\nu_3(f_2)\gamma$ (CH)
—	—	—	1037	*s*	*PQR*	—	—	—	1372	*s*	*PQR*	0.7536	—	—	—	1285	*m*	?	$\nu_4(f_2)\delta_+$(CH)
—	—	—	1066	*s*	*PQR*	—	—	—	1475	*s*	*PQR*	0.7227	—	—	—	1430	*s*	*PQR*	$\nu_5(f_2)\delta_+$(CH)
—	—	—	2058	*vs*	*PQR*	—	—	—	2876	*s*	*PQR*	0.7156	—	—	—	—	—		$\nu_6(f_2)\nu_-$(CH)
2211	*vs*	*dp*	2218	*vs*	*PQR*	2955	88	*dp*	2959	*vs*	*PQR*	0.7482	2957	88	*dp*	2957	*vs*	?	$\nu_7(f_2)\nu_-$(CH)

[a] Notation: *p* = polarized; *dp* = depolarized; *s* = strong; *m* = medium; *w* = weak; *b* = broad; *dbl* = double-headed; δ = deformation; ν = stretching; γ = bending; subscripts (+) and (−) indicate symmetrical and antisymmetrical respectively. Frequencies in cm^{-1}. The Raman intensities for $(CH_3)_4C$ and $(CH_3)_4Si$ are integrated intensities obtained photoelectrically and reported previously. (See reference 1.)

TABLE II. Results of "skeletal" mode calculations.[a]

Assignment of observed fundamentals to "skeletal" modes

Molecule	ν_1	ν_2	ν_3 I	ν_3 II	ν_4
Np-h_{12}	733	335	921	1249	415
Np-d_{12}	648	276	764	1212	342
$SiMe_4$	593	199	694	862	245

Isotope shifts

Isotopic molecule	$\nu_1^i-\nu_1$ Calc.[a]	Obs.	Choice of ν_3 assign.	$\nu_3^i-\nu_3$ Calc.[d]	Obs.
Np-d_{12}	−63.8	−85	I	+80	−157
			II	+115	−37
Np-d_{11}	−58.3	−69			
Np-d_1	−5.3	−13.7			
$SiMe_4$-d_1	−4.7	−23			

Calculations based on simple valence force field considerations of XY_4 systems[b,c]

Molecule		$\frac{\nu_3\cdot\nu_4}{\nu_1\cdot\nu_2}$	$\frac{\omega_3\cdot\omega_4}{\omega_1\cdot\omega_2}$	$(\nu_3^2+\nu_4^2)$ $\times 19^{-5}$	$(\omega_3^2+\omega_4^2)$ $\times 10^{-5}$
Np-h_{12}	I	1.557	2.000	10.20	17.57
	II	2.111		19.32	
Np-d_{12}	I	1.461	2.158	7.01	15.14
	II	2.329		16.00	
$SiMe_4$	I	1.441	1.448	5.42	6.67
	II	1.790		8.03	

Choice of ν_3 assign.		ν_1^i/ν_1	ν_2^i/ν_2	ω_1^i/ω_1 $=\omega_2^i/\omega_2$	$\frac{\nu_3^i\cdot\nu_4^i}{\nu_3\cdot\nu_4}$	$\frac{\omega_3^i\cdot\omega_4^i}{\omega_3\cdot\omega_4}$
Np-d_{12}	I	0.884	0.824	0.9129	0.684	0.9001
	II				0.804	

[a] Except in the block listing Isotope Shifts, the columns headed by expressions of n pertain to the results from the experimental data, while those headed by expressions of ω give the results from the theoretical equations. Calculated isotopic shifts of ν_1 were obtained from simple valence force field considerations (see references 14 and 16), while those for ν_3 are from Rosenthal's more general force field expressions (see reference 17). Np = neopentane (tetramethylmethane); Me = methyl; I and II refer to alternative assignments of ν_3; the superscript i refers to the heavier isotopic molecule.
[b] See reference 14. [c] See reference 16. [d] See reference 17.

be expected in this 2000-cm^{-1} region, none is found with certainty since an infrared band at 2218 cm^{-1} is observed which definitely shows that this frequency is F_2 in character. Whether an E mode is superimposed upon the F_2 mode cannot be decided from the spectrum, and thus the product rule is completely useless for dealing with the E modes.

The infrared activity of the F_2 modes permits their distinction from the doubly-degenerate modes which are likewise depolarized in the Raman effect. The observation by Fitz[15] of an infrared absorption band for tetramethylmethane at 418 cm^{-1} has definitely established the degree of degeneracy of the 415-cm^{-1} frequency.[1] The 342-cm^{-1} depolarized band is taken as the analogous mode in the deuterated compound. On the basis of the infrared band character in the Raman effect, 764 cm^{-1} is the analogous band to 921 cm^{-1} in tetramethylmethane. The 1050-cm^{-1} region is complicated, and two frequencies are chosen at 1037 and 1066 cm^{-1} on the basis of the behavior of the absorption with decreasing vapor pressure. Although no corresponding depolarized Raman band is observed in the 2000-cm^{-1} region, the infrared absorption band at 2058 cm^{-1} is taken as $\nu_6{}^i(f_2)$ and, similarly, $\nu = 2876$ cm^{-1} is chosen as $\nu_6(f_2)$ in tetramethylmethane.

The character of the respective infrared bands *circa* 1200 cm^{-1} in both the ordinary and deuterated compounds is unique. Both are strong, narrow bands but definitely broader than unequivocally observed Q branches, and depart from the expected envelope with definite PQR branches. (A separation of about 18–20 cm^{-1} between the P and R branches in the other bands in the spectra was observed.) Because of the unique appearance of these two 1200-cm^{-1} bands, it must be assumed that they arise from analogous vibrations. In addition, the 1251-cm^{-1} band of tetramethylmethane has two definite maxima with a separation of about 4 cm^{-1} and a definite minimum separating them. This anomalous character could conceivaly arise from a vibration in the molecule which transforms it into an asymmetric rotor when executing the vibration. It can be seen upon inspection that the skeletal F_2 mode, namely "ν_3" (Herzberg,[14] p. 100), would be expected to yield an excellent spherical top pattern (PQR branching). The anomalous character of the 1200-cm^{-1} infrared bands in tetramethylmethane and the d_{12} derivative forces us to assign these frequencies to methyl wagging modes of unsymmetrical character. An apparent difficulty to the above assignment is the small isotope effect. However, the dynamic situation is so complex when one must treat the molecule as a whole that even a qualitative estimate of the isotope effect enters the realm of pure speculation.

Application of the Teller-Redlich product rule[14] to the F_2 modes does not help in choice of frequency assignment of $\nu_2{}^{C-C}(f_2)$ since both questionably assigned bands (921 and 1249 cm^{-1}) belong to the F_2 class. It is felt that the experimental evidence presented by us earlier,[1] i.e., very weak infrared absorption of $\nu = 929$ cm^{-1} of tetramethylmethane compared to that of the analogous band, $\nu = 696$ cm^{-1}, in tetramethyl silicon, gives strong support to our assignment. (The substitution of a silicon atom for a carbon atom in the tetramethyl framework greatly enhances the intensity of the infrared bands arising from indisputable "framework" vibrations, relative to bands arising from known "hydrogen" vibrations.) As we have pointed out previously,[1] the appearance of the polarized lines 815 cm^{-1} and 609 cm^{-1} in the monodeutero derivatives of tetramethylmethane and tetramethyl silicon seem to demand the present assignments of the highest skeletal mode.

Our present results again raise the question posed previously[1] as to the validity of extending theoretical considerations of tetrahedral XY_4 systems to the tetrahedral tetramethyl molecules with the assumption of the methyl groups as point masses. As can be seen in the

[15] E. D. Fitz, M. S. thesis, The Pennsylvania State College, August, 1951.

tabulated isotopic frequency ratios (ν^i/ν) in Table I, the isotope effect on the frequencies which are well accepted as carbon "skeletal" modes is much greater than would be expected a priori. In Table II, the results of a number of calculations based on theoretical treatments of tetrahedral XY_4 systems[16–18] are summarized. The closer agreement of the results of the simple theory calculation on the triply-degenerate modes with the 1200-cm^{-1} frequencies for n_3 and $n_3{}^i$ is felt to be fortuitous in view of the disagreement, except for the hydrides, for the tetrahedral pentatomic molecules[18] (Herzberg,[14] p. 183). The results of calculation of isotope shifts on the totally symmetric modes for various isotopic molecules and of the isotopic ratios for the totally symmetric and doubly-degenerate modes of tetramethylmethane and its deuterated molecules are in poor agreement wish experiment. It is felt that the inability to obtain more reliable agreement between experiment and theory is a real indication that the methyl group cannot be considered as a single point mass in theoretical considerations.†

[16] F. Lechner, Wien Anz. (1933), No. 14; quoted by Herzberg (reference 14) p. 182.
[17] J. E. Rosenthal, Phys. Rev. 45, 538 (1934).
[18] J. E. Rosenthal, Phys. Rev. 46, 730 (1934).

† *Note added in proof*.—Since this paper was written, one of us (D. H. R.) has had the benefit of discussion and correspondence with Dr. D. M. Simpson with regard to the general subject of this paper. Miss Simpson very helpfully pointed out several errors in our manuscript for which we are grateful. It appears that the authors and the Cambridge school still have some slight disagreements with regard to the interpretation of the vibrational spectra of this type molecule. Unfortunately our experiments are not as conclusive as might have been hoped since total deuterium substitution still leaves certain points without a specific and direct answer. Miss Simpson has pointed out to us three papers by Hans Siebert [Z. anorg. Chem. **263**, 82 (1950); **268**, 177 (1952); **271**, 75 (1952)] which tend to show on semitheoretical grounds that resonance between the $F_2CH_2\gamma$ and skeletal ν frequencies makes it impossible to distinguish between them in tetramethylmethane (this coupling is also shown to be significant in tetramethylsilicon). It is not surprising that these complications to first-order theory arise in the case of molecules as complex as those considered here. During the past year, our experience in dealing with the rotation-vibration spectra of very simple molecules has been as follows. Various perturbing phenomena appear which make interpretation of these molecules less satisfactory than might be desirable.

THE JOURNAL OF CHEMICAL PHYSICS VOLUME 21, NUMBER 11 NOVEMBER, 1953

Calculation of the Heats of Formation of Gaseous Free Radicals and Ions*

J. L. FRANKLIN
Humble Oil and Refining Company, Baytown, Texas
(Received July 1, 1953)

A simple method of calculating the heats of formation of gaseous free radicals and carbonium ions is presented, and a number of examples are given which show good agreement of calculated values with experiment. It is shown that the method permits ready calculation of bond strengths, including the strength of bonds in alicyclics, and the ionization potential of olefins, aromatics, and other unsaturates. The method is not directly applicable to the calculation of the ionization potentials of saturates.

IN an earlier paper[1] an empirical method was described by which various thermodynamic properties of organic compounds could be computed quite simply. It was shown that a thermodynamic property such as the heat of formation can be represented as the sum of a set of values or group equivalents characteristic of the various groups that make up the molecule. In this paper it will be shown that this method may also be employed to calculate the heat of formation of gaseous free radicals and positive ions. The principle is expressed mathematically in Eq. (1)

$$\Sigma\Delta H_{g_i}+\Delta H_g\cdot+\Delta H_g{}^+ + R=\Delta H_f{}^\circ, \qquad (1)$$

where ΔH_{g_i} is that part of the heat of formation assignable to the ith group, and $\Delta H_g{}^\circ$ and $\Delta H_g{}^+$ are, respectively, the group equivalent values for groups to which an unpaired electron and a positive charge are formally assigned. R is resonance energy. As was the case for molecules, a value for $\Delta H_g\cdot$ or $\Delta H_g{}^+$ for a group has to be calculated from the known heat of formation of a radical or ion containing that group.

FREE RADICALS

Table I gives ΔH_g values for several groups having an unpaired electron. With these and the values for ΔH_g in Table II, $\Delta H_f{}^\circ$ for radicals containing any of these groups is readily calculated provided the radical is not capable of π-electron resonance. If π-electron resonance is possible, it is necessary, as is to be expected from Eq. (1), to include a value for the resonance energy, R. The technique of calculating such resonance energies has been developed by Wheland,[2] and others. The resonance energies for a number of free radicals involving π-electron resonance have been calculated by Field and Franklin[3] and by Roberts, Streitweiser, and Regan.[4]

The heats of formation of several radicals have been calculated and are compared in Table III with measured

* Presented at the Southwest Regional Meeting of the American Chemical Society, Austin, Texas, December, 1951.
[1] J. L. Franklin, Ind. Eng. Chem. 41, 1070 (1949).
[2] G. W. Wheland, J. Am. Chem. Soc. 63, 2025 (1941).
[3] J. L. Franklin and F. H. Field, J. Am. Chem. Soc. 75, 2819 (1953).
[4] Roberts, Strietweiser, and Regan, J. Am. Chem. Soc. 74, 4579 (1952).

TABLE I. Group equivalents for radicals at 298°K.

	ΔH, kcal/mole-group	Calculated from
$-\dot{C}H_2$	34	$n\dot{C}_3H_7$[a]
$\diagup\!\!\diagdown\!\!\dot{C}H$	34	$2\dot{C}_3H_7$[a]
$\diagup\!\!\diagdown\!\!\dot{C}-$	33	$t\dot{C}_4H_9$[a]
$-\dot{O}$	7.5	$\begin{matrix} & C & \\ CC & \dot{O} & \\ & C & \end{matrix}$[b]
$-O-\dot{O}$	7.5	$\begin{matrix} & C & \\ CC & O-\dot{O} & \\ & C & \end{matrix}$[b]
$-\dot{S}$	43	$CH_3\dot{S}$[c]

[a] J. S. Roberts and H. A. Skinner, Trans. Faraday Soc. **45**, 339 (1949).
[b] Murowski, Roberts, and Szwarc, J. Chem. Phys. **19**, 698 (1951).
[c] J. L. Franklin and H. E. Lumpkin, J. Am. Chem. Soc. **74**, 1023 (1952).

values as taken from the compilation of Szwarc.[5] The agreement is generally quite good and in all cases it is within the accuracy of the measurements.

The application of heats of formation of radicals to the calculation of bond strengths is readily apparent for the common situation in which the breaking of a bond results in the formation of two separate molecular fragments. The measurement of the strength of a single bond in a cyclic compound is less readily determined and, indeed, the author knows of no such measurement. It is of interest that, with the aid of the group equivalents shown in Tables II and I, some quite reasonable values for the strength of bonds in certain ring compounds are readily calculated. Consider, for example, the case of cyclohexane. If a single bond is broken symmetrically, we write the following equation:

$$\text{Cyclo } C_6H_{12} \rightarrow \dot{C}H_2(CH_2)_4\dot{C}H_2$$

$$\Delta Hf^0_{(\text{cyclohexane})} = \Delta H_{f(\dot{C}H_2(CH_2)_4\dot{C}H_2)} - D_{C-C}$$

$$= 4\Delta H_{g(\diagup\!\!\diagdown\!\!CH_2)} + 2\Delta H_{g(-\dot{C}H_2)} - D_{C-C}$$

$$D_{C-C} = 78 \text{ kcal/mole.}$$

Cyclohexane is an unstrained ring, and so we would expect the energy required to rupture a single bond to be comparable to that required to rupture the bond joining the two n-C_3H_7 groups in n-hexane. Szwarc[5] gives the strength of this bond as 76 kcal, which compares closely with that calculated for cyclohexane. Table IV gives the strengths of single bonds in several ring compounds calculated by the above method.†

[5] M. Szwarc, Chem. Revs. **47**, 75 (1950).

† In order to employ the group equivalent method with cyclic compounds, a correction factor characteristic of the ring must be employed. Subsequent to the publication of the original paper (reference 1) on this subject, new and probably more accurate values for the heat of combustion of cyclopropane, cyclobutane, and several of their derivatives have been obtained by G. W. Knowlton and F. D. Rossini [J. Research Natl. Bur. Standards **43**, 113 (1949)] and by G. L. Humphrey and R. Spitzer [J. Chem. Phys. **18**, 902 (1950)]. From these correction factors for cyclopropane and cyclobutane, rings have been calculated. The new corrections for ΔH_f are +28 and +18, respectively, for the cyclopropane and cyclobutane rings. Heats of formation of cyclic sulfur compounds have been taken from S. Sunner (thesis, University of Lund, Sweden, 1949) and that of ethylene oxide from *Selected Values of Chemical Thermodynamic Properties* (Circ. 500, U. S. Bureau of Standards, Washington, D. C., 1952).

It is of interest that Genaux and Walters[6] found that cyclobutane decomposes to two ethylene molecules with an activation energy of 61 kcal/mole. This agrees closely with our calculated D_{C-C} in cyclobutane of 61 kcal/mole, and suggests that the thermal decomposi-

TABLE II. Group equivalent values at 298°.

Group	ΔH_f kcal/mole group
$-CH_2-$	−10.1
$\diagup\!\!\diagdown\!\!CH_2$	−5.0
$\diagup\!\!\diagdown\!\!CH-$	−1.1
$-\overset{\vert}{C}-$	+0.8
$-\overset{H}{C}=CH_2$	15
$-\overset{H}{C}=\overset{H}{C}-$ (cis)	19
$\diagup\!\!\diagdown\!\!C=CH_2$	17
$\diagup\!\!\diagdown\!\!C=\overset{H}{C}\diagup\!\!\diagdown$	20
$\diagup\!\!\diagdown\!\!C=C\diagup\!\!\diagdown$	24
−OH (primary)	−41.9
−Cl	−10
$\diagup\!\!\diagdown\!\!C=O$	−31.6
−SH	6
−S−	11
Corrections for various rings:	
Cyclopropane	28
Cyclobutane	18
Thia Cyclopropane	16
Ethylene Oxide	22

[6] C. T. Genaux and W. D. Walters, J. Am. Chem. Soc. **73**, 4497 (1951).

tion of cyclobutane may be initiated by rupture of the C–C bond. Further, the values for the strength of ring C–C bonds agree qualitatively with our experience that the extent of strain in the ring increases as the ring becomes small. It may be that the values shown represent upper limits of the strength of individual bonds since it is quite possible that some interaction may occur between the electrons formally assigned to atoms that are separated by only one or two CH_2 groups. Such interaction would reduce the heat of formation of the diradical and thus the strength of the bond in the ring.

CARBONIUM IONS

Almost the only information available on the energetics of organic positive ions derives from the measurement of their appearance potentials under electron impact in a mass spectrometer. Such measurements are made by subjecting a suitable compound to bombardment by electrons at various energies and determining the lowest energy at which a certain ion fragment from the molecule appears in the mass spectrum. This technique has been employed by Stevenson and Hipple,[7] Honig,[8] and others. The appearance potential of an ion measured in this way can be considered as the endothermicity or heat of reaction for the process. If the appearance potential is employed in the thermochemical equation for the process, the heat of formation of the ion can be calculated if that of the nonionized fragment is known. For example, the appearance potential of the C_2H_5+ ion from ethane is given by Stevenson and Hipple[7a] as 12.84 volts or 296.1 kcal,

$$e+C_2H_6 \rightarrow C_2H_5^+ + H + 2e - 296.1.$$

If we use -20.2 and 52 as the heat of formation of C_2H_6 and H, respectively, we calculate a value of "ΔH_f" for $C_2H_5^+$ of 223.9 kcal/mole.

Where the ion formed has its charge at the most stable position as in the case of the *t*-butyl and *i*-propyl ions, it seems clear that the value calculated in this way is a true heat of formation. However, carbonium ions rearrange very rapidly, and it is possible that ions such as *n*-propyl and isobutyl would, respectively, rearrange during the process of ionization to the more stable *i*-propyl or *t*-butyl isomers. If this be true, the activation energy for the rearrangement is such that the nominally primary ions above ethyl are formed with approximately the same amount of energy. Consequently, pseudo-group equivalents can be employed with primary ions that are capable of rearrangement. Data are not available on secondary ions capable of rearrangement.

Group equivalent values have been computed for several groups to which a positive charge is formally assigned. Table V gives these group equivalents.

One would expect from Eq. (1) and from the experience with free radicals that it would be necessary to include a term for π-electron resonance in ions where

TABLE III. Comparison of measured and calculated heats of formation of radicals ΔH_R, kcal/mole at 298°K.

	Calc	Meas[a]
$\dot{C}_2H_5$	24	26
$n\dot{C}_4H_9$	14	12
	10	12.5
$\dot{C}Cl_3$	12	15.5, 13
$\dot{C}H_2Br$	37	39
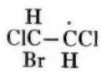	16	15.3
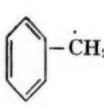	38	37.5
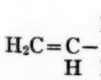	31	29.5

[a] M. Szwarc, Chem. Revs. **47**, 75 (1950).

[7] (a) D. P. Stevenson and J. A. Hipple, J. Am. Chem. Soc. **64**, 1588 (1942); (b) 2766 (1942); J. A. Hipple and D. P. Stevenson, Phys. Rev. **63**, 121 (1943).

[8] R. E. Honig, J. Chem. Phys. **16**, 105 (1948).

TABLE IV. Calculated bond strengths in cyclic compounds.

		D, kcal/mole
	→ $\dot{C}-C-\dot{C}$	50
	→ $\dot{C}C\dot{C}C$	60
	→ $\dot{C}-C-C-C-\dot{C}$	72
	→ $\dot{C}-C-C-C-C-\dot{C}$	78
	→ $\dot{C}-C-\dot{S}$	52
	→ $\cdot C-S-C\cdot$	59
	→ $\cdot C-C-O\cdot$	49
	→ $\cdot C-O-C\cdot$	53

TABLE V. Group equivalents for ions at 298°K.

Group	"ΔH_f" kcal/mole-group	From
$-\overset{+}{C}H_2$	212	nC_4H_{10}[a]
	209	iC_4H_{10}[a]
	195	IC_4H_9Cl[b]
$-\overset{+}{C}=CH_2$	240	t-C_4H_8[c]
$-C(H)=\overset{+}{C}H$	245	butene-2[d]
$-S+$	232	CH_3SH[e]

[a] D. P. Stevenson and J. A. Hipple, J. Am. Chem. Soc. **64**, 1588 (1942).
[b] D. P. Stevenson and J. A. Hipple, J. Am. Chem. Soc. **64**, 2766 (1942).
[c] D. P. Stevenson and J. A. Hipple, J. Am. Chem. Soc. **64**, 2769 (1942).
[d] V. H. Dibeler, J. Research Natl. Bur. Standards **38**, 324 (1947).
[e] J. L. Franklin and H. E. Lumpkin, J. Am. Chem. Soc. **74**, 1023 (1952).

such resonance is possible. Franklin and Lumpkin[9] have shown that the appearance potentials of the *n*-propyl, allyl and benzyl ions from the corresponding chlorides are equal and further, that the appearance potentials of the dimethyl-cyclohexyl carbinyl and the dimethyl-phenyl carbinyl ions from *t*-butyl cyclohexane and *t*-butyl benzene, respectively, are equal. Franklin and Lumpkin[9] concluded, on the basis of this information, that no resonance energy results from the interaction of a π bond and a vacant orbital on an adjacent atom.

From the values for the group equivalents given in Table V, and assuming that resonance energy does not stabilize ions such as allyl and benzyl, the heats of formation of several ions have been calculated and are compared with measured values in Table VI. The agreement is well within the accuracy of experiment in all cases except the $C_2H_5^+$ ion, where the predicted value is much too low. This is attributable to the fact that *n*-alkyl ions are stabilized by the addition of a CH_3 or a C_2H_5, group but that further increases in the length of the alkyl chain gives no added stability. The reason for this behavior is far from clear and is the subject of investigation in this laboratory.

IONIZATION POTENTIALS OF UNSATURATED MOLECULES

The ionization potential of unsaturated compounds presents certain interesting aspects and perhaps throws some additional light upon the question of resonance in ions. Suppose we consider the ionization of butene-2. Since the π electrons are more loosely held than any of the others in the molecule, it would seem reasonable to expect that ionization would occur by the release of a π electron. This is borne out by the fact that the ionization potentials of olefins are considerably lower than that of the corresponding paraffins. For example, Honig[8] gives the ionization potential of 2-butene as 9.3 electron volts as compared to 10.8 volts for *n*-butane. In the case of the ion resulting from 2-butene, one would expect the possibility of resonance between the two forms shown below:

$$CH_3-\underset{H}{\overset{\cdot}{C}}-\underset{H}{\overset{+}{C}}-CH_3 \leftrightarrow CH_3-\underset{H}{\overset{+}{C}}-\underset{H}{\overset{\cdot}{C}}-CH_3.$$

Suppose, now, that we calculate the heat of formation of the ion using the group equivalents chosen from Tables I, II, and V. The resulting value is 221 kcal/mole. If this value, together with the heat of formation of butene-2 is used to calculate the ionization potential, we obtain a value of 9.6 electron volts which is to be compared with a value of 9.3 electron volts obtained by Honig.[8]

Table VII compares calculated and measured values for the ionization potentials of several olefins and oxygen compounds, and it will be noted that the agreement is rather good in all cases except ethylene where the calculated value is somewhat low, as was true with the $C_2H_5^+$ ion. The reason for this discrepancy is no doubt the same as that for $C_2H_5^+$. If we recall that the group

TABLE VI. Comparison of calculated and measured heats of formation of ions at 298°K.

Ion	From	"H_f" ion, kcal/mole calc	meas
$CCCC+$	$CCCCBr$	192	196[a]
$CC+$	C_2H_6	202	224[b]
$CCCCC\overset{+}{C}C$	$CCCCC(Br)C$	169	169[a]
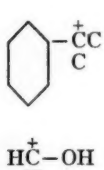	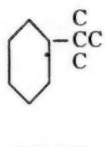	149	153[c]
$H\overset{+}{C}(H)-OH$	C_2H_5OH	170	171[d]
$CCS+$	$CCSCC$	217	213[e]
$C=C-\overset{+}{C}$	$C=C-CCl$	227	227[e]
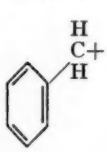		234	234[e]
$(C_6H_5)_2\overset{+}{C}H$	$(C_6H_5)_3CH$	253	257[a]

[a] F. H. Field and J. L. Franklin, unpublished value.
[b] D. P. Stevenson and J. A. Hipple, J. Am. Chem. Soc. **64**, 1588 (1942).
[c] J. L. Franklin and H. E. Lumpkin, J. Chem. Phys. **19**, 1073 (1951).
[d] C. S. Cummings and W. Bleakney, Phys. Rev. **58**, 787 (1940).
[e] J. L. Franklin and H. E. Lumpkin, J. Am. Chem. Soc. **74**, 1023 (1952).

[9] J. L. Franklin and H. E. Lumpkin, J. Chem. Phys. **19**, 1073 (1951).

equivalents used were determined from free radicals and carbonium ions in which no π-electron resonance could occur, it would appear from the close agreement between calculated and measured values, that the ions in question are not stabilized by resonance. Now an olefin ion can be produced by removing a hydrogen from a position adjacent to the charged carbon in an alkyl ion, thus

$$CH_3CH_2-\overset{+}{C}H-CH_3 \rightarrow CH_3\dot{C}H-\overset{+}{C}H-CH_3+H.$$

The C–C bond in the olefin ion is probably shorter than that in the alkyl ion. The σ bond is thus compressed and its energy raised. On the other hand, resonance of the electron between the two carbons would tend to lower the energy. Quantitatively, the effects tend to offset each other, and it may be that over a quite extended range the offsetting tendency is nearly quantitative.

When an electron is removed from benzene, the remaining ion consists of a system of 5π electrons and 6 carbon atoms. The single unpaired electron is capable of resonance with the two remaining double bonds with a resonance energy similar to that of the cyclopentadienyl radical. The heat of formation of the benzene ion is readily calculated with the aid of this resonance energy and the pertinent group equivalent values. Franklin and Field[3] have calculated these resonance energies and shown how they could be used to calculate the ionization potential of aromatics.

From the results presented so far, it is quite apparent that the method of group equivalents is applicable to calculation of ionization potentials and the heats of formation of ions and free radicals. It should be pointed out, however, that some caution must be observed in the application of this technique. For example, it does not seem to apply in the case of the ionization potential of saturated compounds such as paraffins, alkyl halides, and the like. At least in the case of parent ions of this kind, we have no way of knowing which electrons are removed, and so we cannot formally locate the charge on the molecule. As a consequence, we are not in a position to calculate group equivalents. Indeed, the recent work of Lennard-Jones[10] and his colleagues shows that the ionization potential of such compounds is a function of the entire molecule and not of any single group in it. This is probably true also in the case of the ionization potential of olefins, but the reduction in ionization potential of olefins with increasing molecular weight is fairly small, and so we can assume that the method of group equivalents gives quite satisfactory values.

The method of group equivalents must be used with reservation also when strongly electrophyllic groups are present in the ion near the point where the charge is formally located. For example, the heat of formation of the $H_3C-\overset{+}{C}(CH_3)-Cl$ ion may be calculated from the data of Stevenson and Hipple[7b] to be 174 kcal. If we use the group equivalents given in Tables I and VI, we would calculate this value to be 165 kcal. McDowell and Warren[11] found the appearance potential of the $\overset{+}{C}H_2-C\equiv N$ ion from $CH_3C\equiv N$ to be 14.3 volts from which the heat of formation of the ion is computed to be 297 kcal/mole. The method of group equivalents gives only 242 kcal/mole for the heat of formation. The measured values are higher than the calculated ones as would be expected from the presence of the electrophyllic chlorine atom and $-C\equiv N$ groups. One must infer then that to use the method of group equivalents in such cases it would be necessary first to determine the characteristic values for groups such as $\overset{Cl}{\underset{|}{C}}+$. Unfortunately, enough data are not available in the literature to permit this and so this conclusion must be tentative pending further experiment.

TABLE VII. Ionization potentials of unsaturates.

Compound	Ionization potential, volts calc	meas
C=C	10.2	10.5[a]
C–C–C=C	9.8	9.8[b]
C–C=C–C	9.6	9.3[b]
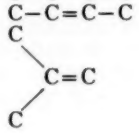	9.2	9.4[b]–8.9[e]
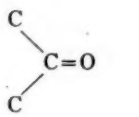	10.2	10.26[d]
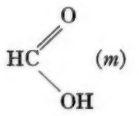 (*m*)	11.3	11.51[e]

[a] W. C. Price and W. T. Tutte, Proc. Roy. Soc. (London) **A174**, 207 (1940).
[b] R. E. Honig, J. Chem. Phys. **16**, 105 (1948).
[c] D. P. Stevenson and J. A. Hipple, J. Am. Chem. Soc. **64**, 2769 (1942).
[d] A. B. F. Duncan, J. Chem. Phys. **3**, 131 (1935).
[e] J. D. Morris and A. J. C. Nicholson, J. Chem. Phys. **20**, 1021 (1952).

ACKNOWLEDGMENTS

The writer wishes to express his appreciation to Dr. F. H. Field for many helpful discussions and to the Humble Oil and Refining Company for permission to publish this paper.

[10] Lennard-Jones and Hall, Discusssions Faraday Soc. **10**, 18 (1951).

[11] C. A. McDowell and J. W. Warren, Trans. Faraday Soc. **48**, 1084 (1952).

Exchange Between Rotational and Translational Energy in Gas Molecules*

JOHN C. BECKERLE†
The Catholic University of America, Washington, D. C.
(Received June 18, 1953)

Rotational relaxation times for the gases H_2 and D_2 have been calculated with the quantum mechanical method of distorted waves using a one-dimensional collision model and an exponential repulsive interaction potential. The potential constants were determined by fitting to the data of Hirschfelder, *et al.* and certain theoretical potential calculations for H_2 by Margenau.

The calculations indicate that more than one relaxation time is required to describe rotational relaxation phenomena in these gases. The theoretical relaxation times are 15 to 35 times shorter than the experimental values when one averages with the velocity distribution for a Maxwellian beam of particles. The relative values of the calculated relaxation times compare favorably with those obtained from experiments. Averaging with a one-dimensional velocity distribution instead of that of a Maxellian beam of prticles at temperature T yields calculated values of the relaxation times that are a factor 7 to 19 shorter than the experimental values. One expects the calculated values to be shorter than the experimental values in view of the one-dimensional collision model.

The method used in treating H_2 collisions is not applicable to N_2 and O_2. Results of another approximation method for these gases indicate that more complicated techniques must be used.

INTRODUCTION

THE study of the dispersion and absorption of ultrasonic waves in gases has led to increased interest in calculations of the probability of energy exchange between internal and translational degrees of freedom of colliding molecules. According to the thermodynamical treatment of ultrasonic dispersion and absorption in a gas, a relaxation equation relating the time rate of change of energy of internal degrees of freedom with energy of translational degrees of freedom is required in addition to the usual conservation equations and equation of state of the gas. The relaxation equation contains time constants associated with the different degrees of freedom of the gas molecules, and these are referred to as relaxation times. Since energy transfer occurs only through collisions, these relaxation times have values proportional to the time between collisions. Their proportionality factors are the probabilities of certain energy transfers during collisions.

Most ultrasonic velocity and absorption measurements in diatomic and polyatomic gases have been attributed to vibrational relaxation phenomena.[1] Landau and Teller[2] have shown from theoretical considerations of the transfer between vibrational and translational energy in pure diatomic gases that ultrasonic dispersion resulting from vibrational relaxation is the effect of a single vibrational relaxation time. Recently, attempts have been made to calculate vibrational relaxation times in gaseous mixtures using quantum mechanical methods.[3] Experimental work performed at The Catholic University of America and elsewhere seems to indicate that more than one relaxation time is required to describe rotational relaxation phenomena. However, there have been only a few attempts to compute rotational relaxation times using quantum mechanical methods.

Zener[4] (1931) discussed quantum mechanical procedures for calculating the probability of energy transfer between rotational and translational degrees of freedom of diatomic molecules. Using a simplified interaction energy, he made estimates of the order of magnitude of the collision cross sections for some diatomic molecules.

In 1935, Roy and Rose[5] applied quantum theory to estimate the probability of rotational energy transfer between colliding H_2 molecules. Their calculations, as was pointed out by Massey,[6] indicate that the rotational relaxation time for H_2 at room temperatures is of the order of 10^{-8} seconds. As more information about the angle dependence of the interaction energy between H_2 molecules is now available, further calculations of rotational transition probabilities for colliding H_2 molecules are presented in this paper. The results permit interpretation of recent ultrasonic experiments.

While the present paper was being readied for publication, Takayanagi[7] published a quantum mechanical calculation of the rotational relaxation time for H_2 gas at the temperature $T=197.7°K$. His calculation yielded a result in close agreement with the experimental value.

The validity of the application of the method employed in treating H_2 to the heavier molecules O_2 and N_2 is doubtful because information about the angle dependence of the interaction energy for these molecules

* A dissertation presented to the Faculty of the Graduate School of The Catholic University of America in partial fulfillment of the requirements for the degree of Doctor of Philosophy.

† Now at Bell Telephone Laboratories, Whippany, New Jersey.

[1] L. Bergmann, *Ultrasonics* (John Wiley and Sons, Inc., New York, 1938), p. 154.

[2] L. Landau and E. Teller, Physik. Z. Sowjetunion **10**, 34 (1936).

[3] Schwartz, Slawsky, and Herzfeld, J. Chem. Phys. **20**, 1591 (1952).

[4] C. Zener, Phys. Rev. **37**, 556 (1931).

[5] R. S. Roy and M. E. Rose, Proc. Roy. Soc. **A149**, 511 (1935).

[6] H. S. W. Massey, *Reports on Progress in Physics* (Cambridge University Press, Cambridge, 1949), Vol. XII, p. 248.

[7] K. Takayanagi, Progr. Theoret. Phys. (Japan) **8**, 497 (1952).

is vague. For this reason the treatment of O_2 and N_2 collisions is presented in the latter part of this paper.

PROCEDURE IN TREATING COLLISIONS OF H_2 MOLECULES

In order to compute rotational transition probabilities, one first sets up a collision model that renders the calculations mathematically feasible and yet which contains the essential features of the actual collision. Information concerning the interaction energy must be put into a form suitable to the collision model. An investigation based on this information leads one to expect that Zener's[4] quantum mechanical method of distorted waves should give reasonable results in the case of H_2 collision at room temperature and at 90°K. Using this method, the probability of a rotational transition, $P_{mm'}(v, v')$, from rotational state m to the lower state m' as a function of initial and final relative velocities v and v' is calculated. These relative velocities are related by energy conservation. The expression $P_{mm'}(v, v')$ is then averaged over the appropriate velocity distribution of the gas to obtain the probability of rotational energy transfer to translational energy $\mathcal{P}_{mm'}$, involving the rotational states m and m' on collisions in the gas. The probability $\mathcal{P}_{m'm}$ for the opposite process is related to this by equilibrium considerations. The relaxation time associated with the pair of rotational states m and m' is then given by

$$\tau_{mm'}=\frac{\tau_c}{\mathcal{P}_{mm'}+\mathcal{P}_{m'm}},$$

where τ_c is the time between collisions. The time between collisions can be computed using the kinetic theory relation $\eta=1.27p\tau_c$, developed by Kohler,[8] where η is the viscosity in poise and the pressure p is in dynes per cm^2.

When the equilibrium population of rotational states is only slightly altered in the presence of a disturbance, such as an ultrasonic wave, the expression for the relaxation time can be written

$$\tau_{mm'}=\frac{\tau_c}{\mathcal{P}_{mm'}[1+N_m{}^0/N_{m'}{}^0]}, \tag{1}$$

where $N_m{}^0$ and $N_{m'}{}^0$ are the equilibrium numbers of molecules in the rotational states m and m', respectively.

SIMPLIFIED COLLISION MODEL FOR H_2 MOLECULES

The mathematical difficulties encountered by Roy and Rose[5] in their attempt to use the quantum mechanical method of distorted waves to calculate rotational transition probabilities for colliding H_2 molecules suggest that one should seek a simpler model for the collision. The collision model chosen here is one-dimensional. Two molecules having their axes lying in the same plane are pictured as approaching each other along the line joining their centers of mass. One is rotating, its orientation measured by an angle φ between the line of approach and the line joining its nuclei; the other is taken to be not rotating, and its axis lies coincident with the line of approach. This second molecule may be thought of as spherical in shape since no dependence on its orientation is included in the interaction energy that is used in the calculations in this paper. One should expect rotational transition probabilities to be greatest for this kind of impact.

INTERACTION ENERGY BETWEEN H_2 MOLECULES

An interaction potential between two H_2 molecules appropriate to the collision is required. Some information about the interaction potential has been obtained by Hirschfelder, *et al.*[9] from analysis of viscosity experiments. Their results have been expressed in terms of the parameters x_0 and ϵ_0 of the Lennard-Jones Potential,

$$E(x)=4\epsilon_0\left[\left(\frac{x_0}{x}\right)^{12}-\left(\frac{x_0}{x}\right)^{6}\right].$$

These constants are $x_0=2.968$A and $\epsilon_0=33.3$k. However, very little experimental information about the angle dependence of the interaction energy is available. De Boer[10] (1942) and Margenau[11] (1943) independently evaluated Coulomb exchange integrals to obtain the interaction potential between H_2 molecules. Their results indicate that an exponentially decreasing dependence on the distance between the centers of mass of the molecules, in which the angle dependence is principally contained in the multiplying factor of the exponential, should be a good approximation of the interaction energy for positions near the classical distance of closest approach.

The form of the interaction energy chosen for calculations in the present paper is

$$V(x, \varphi)=V_0e^{-x/a}\cosh(b\cos\varphi),$$

where V_0 and a are constants obtained by curve fitting to the Lennard-Jones potential and b is obtained from results of certain calculations by Margenau.[11] This has the same form as the interaction energy employed by Jackson and Howarth[12] in their calculation of energy transfer of molecules to a crystal lattice, except that they took $b=L/2a$, where L is the equilibrium separation of the diatomic molecules considered. This choice follows from their assumption that the exponentially repulsive interaction energy acts along lines parallel to the line of approach from each nucleus of the diatomic

[8] M. Kohler, Z. Physik **5**, 715 (1949).

[9] Hirschfelder, Bird, and Spotz, J. Chem. Phys. **16**, 968 (1948), see Table IV, p. 974.

[10] J. de Boer, Physica **9**, 363 (1942).

[11] H. Margenau, Phys. Rev. **64**, 131 (1943), see Table IV, p. 143, and Fig. 2, p. 145.

[12] J. M. Jackson and A. Howarth, Proc. Roy. Soc. (London) **A152**, 515 (1935).

molecule to the position of the vibrating atom of the wall. As will be shown later, their choice leads to a stronger angle dependence than is appropriate to the collision model used here.

H_2 gas at room temperature or below has practically no vibrational states excited in view of the high characteristic temperature for vibration of H_2, *viz.*, 6140°K. For this reason one can safely treat rotational energy transfer in H_2 gas at room temperature without including a dependence of the interaction energy on the vibrational state of the molecule.

EVALUATION OF THE CONSTANTS IN THE H_2 INTERACTION ENERGY

The parameter a of the interaction energy was determined by equating the partial derivative of $V(x, \varphi)$ with respect to x, to the derivative of the Lennard-Jones potential, $E(x)$, at the classical turning point for the collision. When the parameter ϵ_0 of the Lennard-Jones potential is not small compared to the average relative kinetic energy of the collision, it is important to require during the curve fitting that the interaction energy, $V(x, \varphi)$, tend to $-\epsilon_0$ at large separation.[13] This will usually result in a smaller value for the parameter a such that the potential $V(x, \varphi)$ will best represent the repulsive portion of the Lennard-Jones potential near the classical distance of closest approach.

Since the average kinetic energy of a Maxwellian beam of particles at temperature T°K is $2k$T, where k is the Boltzmann constant, the classical turning point was defined as x' by the condition that $E(x')=2k$T. The values of a for H_2 gas at temperature 290°K and at 90°K are 0.162A and 0.141A, respectively. The additional requirement that $V(x, \varphi)$ tend to $-\epsilon_0$ at large x was significant in determination of a for H_2 at 90°K. These values show clearly that the interaction energy rises rapidly in a distance that is very small compared to the distances of closest approach which were $x'=2.52$A at 290°K and $x'=2.70$A at 90°K. The parameter a will be referred to as the interaction distance.

The form of the interaction energy that can be put into good numerical agreement with the results of calculations by Margenau for values of x near the distance of closest approach is:

$$V(x, \varphi, \varphi')=V_0 e^{-x/a}\cosh(b\cos\varphi)\cosh(b\cos\varphi'),$$

where φ' is the angle that specifies the orientation of the second H_2 molecule just as φ, the angle used previously, measures the orientation of the first H_2 molecule. This interaction energy has the properties of Margenau's potential calculations, i.e., for the orientation $\varphi=\varphi'=0$ the potential energy is strongest, while for the orientation $\varphi=\varphi'=\pi/2$, it is weakest. The interaction energy lies between these extremes for the orientation $\varphi=0$, $\varphi'=\pi/2$, or $\varphi=\pi/2$, $\varphi'=0$.

The parameter b in $V(x, \varphi, \varphi')$ was obtained after noticing in Margenau's paper[11] that the ratio of the repulsive potential energy for the two extreme orientations $\varphi=0$ and $\varphi=\pi/2$, with $\varphi'=0$ does not vary much with separation for energies around $2k$T, T=290°K and T=90°K, and has a value of about 1.7. One expects that the relative magnitudes of Margenau's results should be more accurate than the absolute values. His calculations for the mean potential are in satisfactory agreement with what one expects from the Lennard-Jones potential between H_2 molecules as obtained from experiments. One finds the constant b by requiring that

$$\frac{V(x, \varphi=0)}{V(x, \varphi=\pi/2)}=\cosh(b)=1.7,$$

where x is near the classical turning point. This leads to a value of $b=1.13$. Equating $b=$L*$/2a$ and using the value of $a=0.162$A which was previously found, one finds L*=0.366A, which is 0.488 of the internuclear separation of H_2. If one uses $a=0.141$A, obtained for T=90°K, a smaller value of L* results indicating that the parameter b is not given merely by a fixed fraction of L/a.

Margenau also calculated the interaction energy for the case wherein both H_2 molecules have their axes perpendicular to the line of approach. This potential was not used in computing b because this orientation is not appropriate to the collision model used here. It would have to be considered in a collision description using more than one dimension or involving the possibility of interchange of rotational energy without change of relative translational energy. The mathematics of such collisions becomes considerably more difficult than the one-dimensional case treated in this paper.

Using the potential $V(x, \varphi, \varphi')$, one finds that the same parameter $b=1.13$ can be used equally well to fit the three curves of Margenau which represent $\varphi=\varphi'=0$; $\varphi=\pi/2$, $\varphi'=0$; and $\varphi=\pi/2$, $\varphi'=\pi/2$, as when one omits the last.

It is reasonable to suppose that the interaction energy, $V(x, \varphi)$, using the same values of the parameters a and b determined above, would be approximately correct for the potential between an H_2 molecule and an atom of about the same size.

It was shown that the parameter b is about half of $L/2a$ in the case of H_2. $L/2a$ was used by Jackson and Howarth for the parameter b in the case of a one-dimensional collision of diatomic molecules with surface atoms of a wall. Their value clearly would lead to a stronger angle dependence than is appropriate for the case of an H_2 molecule striking a free atom. Probably $L/4a$ would also be a better choice for the parameter b when treating the collisions of diatomic molecules other than H_2 with free atoms.

The change in the distance of closest approach defined by energy $2k$T, for a fixed orientation which will

[13] This additional condition on the determination of a is discussed by R. Schwartz, *et al.*, reference 3, p. 1594.

produce a change in the repulsive potential by the factor 1.7 is only $0.53a$. This indicates that the H_2 molecule is only slightly nonspherical in shape when it strikes an atom of about the same size or another H_2 molecule oriented so that its axis lies along the line of approach. In fact, even for the case wherein both H_2 molecules rotate, the change in the distance of closest approach that would produce a change of potential equal to that resulting from the rotation of the molecules is approximately equal to the interaction distance. Since a is only 0.162A, while the distance of closest approach is about 2.52A at T=290°K, the H_2 molecule is almost spherical in shape.

PRELIMINARY INVESTIGATION RELEVANT TO METHODS SUITABLE FOR THE H_2 COLLISION

Since the interaction energy between H_2 molecules appropriate to the collision model chosen has been obtained, it should now be possible to decide what method is suitable for the calculation of the probability of rotational energy transfer during collision. One finds that the de Broglie wavelength associated with the reduced mass of the H_2 system having as an average relative kinetic energy of $2k$T, T=290°K is $\lambda_{rms}=7.9a$. Also, during the collision the interaction energy surely reaches a value around the relative translational energy. A classical treatment of the H_2 collision should not be used, partly because the de Broglie wavelength of the reduced mass particle is larger than the interaction distance. Mariens[14] used classical techniques to calculate theoretically relaxation times for H_2. His calculations led to close agreement with experimental values.

In a nonclassical treatment of the H_2 collision one should expect the Born approximation to lead to poor results since the interaction energy here is not always small compared to the relative translational energy. The method of distorted waves should be applicable to the collision proposed even though the interaction energy during the collision is not small compared to the relative translational energy, provided the change of the distance of closest approach during one full rotation of the molecule is small compared to the interaction distance. This condition is nearly satisfied in the case of H_2 since it was shown that the change is only $0.53a$. It will be shown in the next section, wherein a brief outline of the distorted wave method applied to the one-dimensional H_2 collision is presented, that in view of the above fact, the off-diagonal matrix components of the interaction energy $V(x, \varphi)$ are small compared to the diagonal terms. The off-diagonal matrix components are the average interaction energy over the free plane rotator wave functions of the initial and final states. This circumstance justifies the use of the method.[15]

OUTLINE OF DISTORTED WAVE METHOD APPLIED TO THE H_2 COLLISION

The time independent Schroedinger wave equation for the one-dimensional H_2 collision problem proposed is

$$\left\{\frac{\hbar^2}{2\mu}\frac{\partial^2}{\partial x^2}+E+\frac{\hbar^2}{2I}\frac{\partial^2}{\partial\varphi^2}-V_0e^{-x/a}\cosh(b\cos\varphi)\right\}\Psi(x,\varphi)=0,$$

where μ is the reduced mass of the colliding H_2 system, I is the moment of inertia of the H_2 molecule, and E is the total energy of the system. The solution can be expressed in the form

$$\Psi(x,\varphi)=F_m^{(1)}(x)\Phi_m(\varphi)+\sum_{m''}F_{m''}^{(2)}(x)\Phi_{m''}(\varphi),$$

where $\Phi_{m''}(\varphi)$ is one of the orthonormal set of wave functions for a free rotator in a plane belonging to the rotational energy eigenvalue $E_{m''}$. The translational wave functions, $F_m^{(1)}(x)$ and $F_{m''}^{(2)}(x)$, can be obtained when the distorted wave method is permissible by solving the equations:

$$\left[\frac{d^2}{dx^2}+K_m^2-\frac{2\mu}{\hbar^2}R_{mm}V_0e^{-x/a}\right]F_m^{(1)}(x)=0, \qquad (2)$$

and

$$\left[\frac{d^2}{dx^2}+K_{m'}^2-\frac{2\mu}{\hbar^2}R_{m'm'}V_0e^{-x/a}\right]F_{m'}^{(2)}(x)$$
$$=\frac{2\mu}{\hbar^2}R_{mm'}V_0e^{-x/a}F_m^{(1)}(x),\ (m'\neq m), \qquad (3)$$

where

$$K_{m''}^2=\frac{2\mu}{\hbar^2}(E-E_{m''}),$$

and

$$R_{mm'}=\int^{2\pi}\Phi_m^*(\varphi)\cosh(b\cos\varphi)\Phi_{m'}(\varphi)d\varphi.$$

This integral was evaluated by Jackson and Howarth[12] and has a value such that

$$|R_{mm'}|=I_{|m-m'|}(b);\quad \text{for}\quad |m-m'|=\text{even integers},$$

and

$$|R_{mm'}|=0;\quad \text{for}\quad |m-m'|=\text{odd integers}.$$

$I_{|m-m'|}(b)$ is the modified Bessel function of the first kind of order $|m-m'|$. Exact solutions for equations having the form of Eq. (2) and Eq. (3) were first obtained by Jackson and Mott.[16] The total wave function $\Psi(x, \varphi)$ is required to have the asymptotic behavior

$$\Psi(x\to+\infty,\varphi)\sim 2\cos(K_mx+\alpha)\Phi_m(\varphi)$$
$$+\sum_{m''}A_{m''}e^{+iK_{m''}x}\Phi_{m''}(\varphi),$$

[14] P. Mariens, *Colloquium Over Ultrasonore Trillingen* (Mededelingen Koninklijke Zaamsche Academie voor Wetenschappen, Brussels, June 7–8–9, 1951), p. 74.

[15] For further discussion see N. F. Mott and H. S. W. Massey, *Theory of Atomic Collisions* (Oxford University Press, London, 1949), second edition, p. 145.

representing an incident and elastically reflected wave of unit amplitude belonging to the initial rotational state m, and inelastically reflected waves with amplitude designated by $A_{m''}$.

The diagonal matrix components appearing in Eq. (2) and Eq. (3) are clearly all equal, and using the value of $b=1.13$ obtained previously for interaction, one can show that the nearest off-diagonal matrix components which correspond to jumps by two rotational quantum numbers are about $\frac{1}{10}$ the strength of the diagonal terms. The next nearest off-diagonal matrix components of the interaction energy are about 1/200 of the diagonal terms. This circumstance leads one to expect reasonable results using the method of distorted waves. The equations (2) and (3) indicate the method of approximation. The homogeneous wave equation is solved for the initial wave function $F_m(x)$, where the potential energy term has no component in other states. This distorted wave function, together with the interaction matrix component connecting the initial and final states considered, is treated as a perturbation leading to transitions. Designating $P_{mm'}(v, v')$ as the probability that on collision the rotational quantum number goes from m to m', while the relative velocity goes from v to v', the expression for this transition probability can be written down utilizing the results of calculations by Mott and Jackson[16] and Jackson and Howarth[12] in the form

$$P_{mm'}(v, v')=\frac{|R_{mm'}|^2}{4\pi^2}\left[\frac{\frac{1}{2}\mu(v'^2-v^2)}{\frac{1}{2\mu}(\hbar/2\pi a)^2}\right]^2 f(g, g'), \qquad (4)$$

where

$$f(g, g')=\frac{\sinh g' \sinh g}{[\cosh g'-\cosh g]^2},$$

in which $g=2\pi a\mu v/\hbar$ and $g'=2\pi a\mu v'/\hbar$.

Since energy is conserved in the collision, v and v' are connected by the relation

$$\frac{\mu}{2}(v'^2-v^2)=\Delta E=\frac{\hbar^2}{2I}(m^2-m'^2), \qquad (5)$$

where ΔE is the rotational energy given to translational motion during the collision. This relation is used to eliminate v' of the expression $P_{mm'}(v, v')$, which is then averaged over the fraction of reduced mass particles in a Maxwellian beam at temperature T, which have velocities lying between v and $v+dv$.

$$\mathcal{P}_{mm'}=2\left(\frac{\mu}{2k\mathrm{T}}\right)^2\int_0^\infty P_{mm'}(v, \Delta E)v^3e^{-\mu v^2/2k\mathrm{T}}dv \qquad (6)$$

is the probability that during a collision between H_2 molecules of a gas at temperature T, rotational energy is transferred to translation motion as the rotational energy of the molecule jumps from state E_m down to state $E_{m'}$. $P_{mm'}(v, \Delta E)$ is an increasing function of v and a decreasing function of ΔE. At high velocities the integrand of Eq. (6) is dominated by the rapidly decreasing exponential. Using the dimensionless variable $g=2\pi a\mu v/\hbar$, and the conservation of energy relation Eq. (5), the expression for $\mathcal{P}_{mm'}$ can be written as

$$\mathcal{P}_{mm'}=\frac{|I_{|m-m'|}(b)|^2}{2\pi^2}\left(\frac{\Delta E}{k\mathrm{T}}\right)^2\int_0^\infty f(g, g')g^3e^{-\epsilon g^2/k\mathrm{T}}dg, \qquad (7)$$

where

$$\epsilon=\frac{1}{2\mu}(\hbar/2\pi a)^2, \quad \text{and} \quad g'=\left(g^2+\frac{\Delta E}{\epsilon}\right)^{\frac{1}{2}}.$$

ϵ is a constant having the dimensions of energy and depending only on the interaction distance and the reduced mass. It is smaller than ΔE for H_2. From the fact that ΔE and ϵ are inversely proportional to μ, one can see by inspection of the expression for $\mathcal{P}_{mm'}$, Eq. (7), that $(\mu\mathrm{T})$ always appear together. Since the interaction distance is only slightly dependent on temperature, the effect of increasing μ can be compensated by decreasing the temperature so as to keep the product $\mu\mathrm{T}$ constant. A change from a hydrogen gas to a deuterium gas might be considered as a change of μ without significant changes in other quantities, a, b, and L, contained in the expression for $\mathcal{P}_{mm'}$. The temperature dependence of $\mathcal{P}_{mm'}$ is dominated by the exponential, and thus an increase of μ also produces an increase of $\mathcal{P}_{mm'}$. The rotational states of D_2 are more easily deactivated than those of H_2 at the same temperature solely because of the mass effect.

EVALUATION OF THE INTEGRAL OVER THE VARIABLE g

An estimate of the size of the arguments in the function $f(g, g')$ can be found by taking the root mean square velocity for the beam of reduced mass particles. This gives $g_{\mathrm{rms}}=2\pi a\mu v_{\mathrm{rms}}/\hbar=4\pi a(\mu k\mathrm{T})^{\frac{1}{2}}/\hbar$ which has a value of 5.3 for H_2 gas $\mathrm{T}=290°\mathrm{K}$, and about half this value when H_2 is at temperature 90°K. This means that the integral cannot be evaluated by using a limiting form for the function $f(g, g')$. The integral was evaluated by putting

$$\ln\{g^3f(g, g')\}=-Ag^2+Bg-C \qquad (8)$$

and determining the non-negative coefficients, A, B, and C, by requiring that the function pass through three values of g, covering the important range. The error in fitting was less than 0.15 on the natural logarithmic scale over the important range of the variable g. Therefore, the function $\{g^3f(g, g')\}$ is expressible in exponential form which is probably not in error by more than factor 1.2.

The integral in the expression for $\mathcal{P}_{mm'}$, Eq. (7), using

[16] J. M. Jackson and N. F. Mott, Proc. Roy. Soc. **A137**, 703 (1932).

the approximation Eq. (8), can be written as

$$\mathcal{F}(T, \Delta E/\epsilon)=\int_0^\infty \exp\{-(A+\epsilon/kT)g^2+Bg-C\}dg. \quad (9)$$

By the method of completing the square of the exponent and changing integration variable to $Z=g-\frac{1}{2}B(A+\epsilon/kT)^{-1}$, one obtains the value of the integral:

$$\mathcal{F}(T, \Delta E/\epsilon)=\tfrac{1}{2}\sqrt{\pi}(A+\epsilon/kT)^{-\frac{1}{2}}\left[1+\operatorname{erf}\frac{B}{2}(A+\epsilon/kT)^{-\frac{1}{2}}\right]$$

$$\times\exp\left\{-C+\frac{B^2}{4(A+\epsilon/kT)}\right\} \quad (10)$$

and the deactivation probability:

$$\mathcal{P}_{mm'}=\frac{|I_{|m-m'|}(b)|^2}{2\pi^2}\left(\frac{\Delta E}{kT}\right)^2\mathcal{F}(T, \Delta E/\epsilon). \quad (11)$$

Using this formula, Eq. (11), one finds for H_2 gas at 90°K the deactivation probability $\mathcal{P}_{20}=0.028$, and by doubling the reduced mass, one finds for D_2 at the same temperature that $\mathcal{P}_{20}$ is 2.24 times greater than that of H_2, i.e., $\mathcal{P}_{20}=0.062$, and $\mathcal{P}_{31}=0.057$. In view of the small occupation numbers of H_2 molecules in rotational states above quantum number $m=2$, at this low temperature, practically the whole rotational specific heat is associated with the 2–0 rotational levels.[17] This means that one relaxation time should be sufficient to account for ultrasonic absorption experiments in H_2 at 90°K.

The situation is not simple for H_2 at the higher temperature T=290°K. At this temperature values of the deactivation probability were found to be $\mathcal{P}_{20}=0.077$, $\mathcal{P}_{31}=0.076$, and $\mathcal{P}_{42}=0.068$, which are seen to decrease slowly. Although the numbers of H_2 molecules in rotational states above $m=4$ are negligible, it is clear that more than one relaxation time will be required to describe ultrasonic dispersion and absorption experiments in H_2 at room temperatures. The value of the deactivation probability $\mathcal{P}_{40}$ is considerably smaller partly because of the much smaller value of the factor $|I_{|m-m'|}(b)|^2$.

Pure *ortho*-D_2 at 90°K will also require only one relaxation time associated with the 2–0 rotational levels. However, in the equilibrium mixture of *ortho* and *para* D_2 at this low temperature the contribution to the specific heat due to the *para*-D_2 modification is small but not negligible.[17] Therefore, a relaxation time must be associated with the 3–1 rotational levels, besides that of the 2–0 rotational levels in order to account for relaxation phenomena in the equilibrium mixture at 90°K of D_2.

In order to compute relaxation times according to Eq. (1), one needs to know the ratio of the equilibrium numbers of molecules in the upper and lower rotational states. Somewhat inconsistently a three-dimensional diatomic gas was used, for which the ratio is given by

$$\frac{N_J^0}{N_{J'}^0}=\left(\frac{2J+1}{2J'+1}\right)\exp\left[-\frac{(E_J-E_{J'})}{kT}\right], \quad (13)$$

where

$$E_J=\frac{\hbar^2}{2I}J(J+1).$$

Putting the lower rotational quantum number $J'=J-2$, then this ratio N_J^0/N_{J-2}^0 is a decreasing function of J. The ratios calculated using Eq. (13) for H_2 at T=290°K are

$$N_2^0/N_0^0=0.863;\ N_3^0/N_1^0=0.125;\ \text{and}\ N_4^0/N_2^0=0.03.$$

It should be noted that since all of the ratios are less than one, the deactivation probabilities for H_2 will be larger than the activation probabilities. This will not be the case for the gases of the heavier molecules N_2 and O_2, if one uses Eq. (13) for the population ratio.

Table I. Calculated and experimental relaxation times.[a]

$J-J'$	Gas	Temp.	$\tau_{calc.}$	$\tau_{exp.}$
2–0	H_2	90°K	1.2×10^{-9} sec.	2.5×10^{-8} sec.[b]
2–0	D_2	90°K	0.58×10^{-9} sec.	
3–1	D_2	90°K	0.8×10^{-9} sec.	1.5×10^{-8} sec.[b]
2–0	H_2	290°K	0.49×10^{-9} sec.	1.7×10^{-8} sec.[c]
3–1	H_2	290°K	0.82×10^{-9} sec.	
4–2	H_2	290°K	1.0×10^{-9} sec.	

[a] Values of the viscosity needed to compute the time between collisions were taken from Table V, Hirschfelder, *et al.*[9] The time between collisions for D_2 was taken as $\sqrt{2}$ times that of H_2.
[b] A. van Itterbeek and R. Vermaelen, Physica, **9**, 345 (1942). See also A. van Itterbeek and L. Verhaegen, *Colloquium over Ultrasonore Trillingen* (Mededlingen Koninklyke Zaamsche academie voor Wetenschappen, Brussels) **61**, (1951); Nature **167**, 477 (1951).
[c] E. E. Swomley, Phys. Rev. **69**, 632 (1946).

COMPARISONS WITH EXPERIMENTS

The calculated relaxation times for H_2 and D_2 at 90°K, and for H_2 at T=290°K, required in the description of sound absorption and dispersion experiments, are presented in Table I along with experimental values. The calculated relaxation times range between a factor 15 to 35 shorter than the experimental values. This is expected in view of the simplified collision model used; it is within the range of ratios found for transfer of vibrational energy with a one-dimensional model.[3] Relative values of the calculated relaxation times will be considerably more accurate. The ratio τ_{20} for H_2 to τ_{31} for D_2 at 90°K is 1.5. This is close to the ratio of the experimental values, 1.65. This ratio was chosen for comparison with the experimental ratio because the absorption measurements were made on normal D_2 at a low sound frequency.

Rhodes[18] (1946), who experimented on *para*-H_2, normal-H_2, and 50–50 *para-ortho* H_2 at temperatures

[17] H. C. Urey and G. K. Teal, Revs. Modern Phys. **7**, 35 (1935), pp. 50–51 and Fig. 2, p. 51.

[18] J. Rhodes, Phys. Rev. **70**, 932 (1946).

TABLE II. Relaxation times and deactivation probabilities calculated using Eq. (14).[a]

$J-J'$	Gas	Temp.	$\mathcal{P}_{mm'}$	$\tau_{calc.}$
2–0	H_2	90°K	0.013	2.58×10^{-9} sec.
2–0	D_2	90°K	0.020	1.77×10^{-9} sec.
3–1	D_2	90°K	0.020	2.24×10^{-9} sec.
2–0	H_2	290°K	0.042	0.9×10^{-9} sec.
3–1	H_2	290°K	0.038	1.66×10^{-9} sec.
4–2	H_2	290°K	0.030	2.27×10^{-9} sec.

[a] The author is grateful to Miss R. A. Weiss of the Mathematics Department, Bell Telephone Laboratories, Murray Hill, New Jersey, who evaluated the integral in Eq. (14) on IBM machines.

around 300°K and 200°K definitely found broader sound dispersion curves than expected from one relaxation time, as well as a shift of the dispersion curves to lower frequency to pressure ratios for the lower temperature. He was the first to present a paper treating pure *para*-H_2 gas at room temperatures as essentially a three-level gas to which he assigned two relaxation times associated with the 2–0 and 4–2 rotational transitions. However, it is clear from the results of calculations in this paper that he erroneously associated a shorter relaxation time with the 4–2 transition rather than the 2–0 transition. He assumed correctly that only jumps by two quantum numbers need be considered and developed equations which can lead to the dependence of rotational specific heat on the sound frequency of *para*-H_2 having two relaxation times.

Normal H_2 at room temperatures, which consists of $\frac{1}{4}$ *para*-H_2 molecules essentially occupying levels $J=0$, 2, 4 and $\frac{3}{4}$ *ortho*-H_2 molecules as principally occupying levels $J=1$, 3, requires three relaxation times. For temperatures such that rotational states above $J=4$ become appreciably occupied, more than three relaxation times will be needed to describe ultrasonic experiments in H_2.

RELAXATION TIMES COMPUTED USING THE ONE-DIMENSIONAL VELOCITY DISTRIBUTION

From theoretical considerations to be published soon, R. N. Schwartz suggests that the appropriate velocity distribution for a one-dimensional collision model is the one-dimensional velocity distribution and not that of a Maxwellian beam of particles at temperature T, used in the body of this paper. In this section calculations for H_2 and D_2 are presented in order to indicate the effects of the suggested change.

Since kT and not $2k$T is now the average relative translational energy of collision, the interaction potential constants determined by fitting an exponential to the Lennard-Jones potential for H_2 at the classical turning point will be different. The interaction distance for H_2 is now $a=0.1515$A at T=290°K and $a=0.1241$A at T=90°K. Using the same value of the potential parameter b found from Margenau's calculations, one can find the deactivation probabilities which are now given by the formula

$$\mathcal{P}_{mm'}=\frac{|R_{mm'}|^2}{2\pi^2}\left(\frac{\Delta E}{\epsilon}\right)^2\frac{\epsilon}{k\mathrm{T}}\int_0^\infty f(g,g')ge^{-\epsilon g^2/k\mathrm{T}}dg, \quad (14)$$

where the notation is as in Eq. (7). Calculated deactivation probabilities and relaxation times using this formula are presented in Table II. They may be compared with the values given in Table I which were computed using Eq. (7).

The deactivation probabilities in Table II are smaller than those obtained using the Maxwellian velocity distribution by about a factor 2, except in the case of D_2, where the improvement is near a factor 3. There is a corresponding improvement in the calculated relaxation times, which now range from a factor 7 to 19 shorter than the experimental ones. Now, however, the ratio of τ_{20} for H_2 to τ_{31} for D_2 at 90°K from Table II is not as close to the ratio of the experimental values. The effect of using the one-dimensional velocity distribution does not require any change of interpretation.

TABLE III. Interaction potential constants.

Nitrogen	Oxygen
$x_0=3.681$A; $\epsilon_0=91.46k$[a]	$x_0=3.433$A; $\epsilon_0=113.2k$[a]
$L=1.09$A	$L=1.20$A
$a=0.180$A at $T=300$°K	$a=0.163$A at $T=300$°K
$b=0.265L/a=1.60$	$b=0.265L/a=1.96$

[a] Lennard-Jones potential constants taken from Hirschfelder, *et al.* (See reference 9.)

APPENDIX

Treatment of Collisions of Molecules N_2 and O_2

The same collision model and form of the interaction energy employed for H_2 is used here in the treatment of N_2 and O_2 collisions at temperature T=300°K. The parameter a is obtained in the same manner as for H_2. Since the angle dependence of the interaction energy between N_2 molecules, and O_2 molecules is doubtful, the parameter b is assumed to be given approximately by $0.265\ L/a$. Table III lists the pertinent quantities in the determination of the potential constants for N_2 and O_2.

The distorted wave method used to treat H_2 collisions is not applicable here since the nearest off-diagonal matrix components of the interaction energy are not small enough compared to the diagonal terms, i.e., 0.225 for N_2 and 0.295 for O_2. The method of exact resonance [15] is better since the matrix components for states separated by four rotational quantum numbers are negligible, less than 0.03 of the diagonal terms, and rotational energy changes by two quantum numbers are small compared to $2k$T for both nitrogen and oxygen collisions. (This last condition is not satisfied for H_2 collisions.)

The method of exact resonance, in which it is assumed that $K_{m'}^2=K_m^2=K^2$, leads to two equations

One is the sum of and the other the difference between the coupled translational wave equations involving the initial and final states.

$$\left[\frac{d^2}{dx^2}+K^2-\frac{2\mu}{\hbar^2}(R_{mm}\pm R_{mm'})V_0e^{-x/a}\right][F_m(x)\pm F_{m'}(x)]=0.$$

The solutions $F_m(x)+F_{m'}(x)$ and $F_m(x)-F_{m'}(x)$ are to have the asymptotic form of an ingoing and outgoing wave of unit amplitude that is identified with the initial state m and an outgoing wave of complex amplitude to be identified with the final state m'. A renormalization of the exact solution for a free particle in an exponential field, obtained by Jackson and Mott,[16] which satisfies the above asymptotic form, enables one to obtain $F_{m'}(x)\sim A_{mm'}e^{+iKx}$. The transition probability as a function of the relative velocity for rotational changes by two quantum numbers is given by

$$P(v)=A_{mm'}A_{mm'}{}^*=\sin^2\left[\frac{\mu a}{\hbar}\ln\left(\frac{I_0(b)+I_2(b)}{I_0(b)-I_2(b)}\right)v\right].$$

Averaging this over the Maxwellian velocity distribution for a beam of particles, one obtains

$$\mathcal{P}(\beta)=\tfrac{1}{2}\beta^2+(\tfrac{3}{2}-\beta^2)\beta e^{-\beta^2}\int_0^\beta e^{+u^2}du,$$

where

$$\beta=\frac{a}{\hbar}(2\mu kT)^{\frac{1}{2}}\ln\left(\frac{I_0(b)+I_2(b)}{I_0(b)-I_2(b)}\right).$$

Calculated values of $\mathcal{P}(\beta)$ for N_2 and O_2 are so large that the approximation is not good enough.

ACKNOWLEDGMENTS

The author is very grateful to Professor Karl F. Herzfeld who suggested the problem, for his continued interest, encouragement, and frequent helpful discussions. The writer also wishes to thank Professors Virginia Griffing and Francis E. Fox, O.S.F., for reading the manuscript.

THE JOURNAL OF CHEMICAL PHYSICS VOLUME 21, NUMBER 11 NOVEMBER, 1953

The Effect of Pressure and Temperature on the Absorption Spectrum of Benzene in the Near Ultraviolet

S. SAMBURSKY, A. HALPERIN, AND H. HENIG
Department of Physics, Hebrew University, Jerusalem, Israel

(Received March 23, 1953)

The absorption spectrum of benzene vapor in the near ultraviolet was photographed at temperatures varying from room temperature up to above the critical temperature (287°C), and at the corresponding pressures of the saturated vapor (from a few mm of mercury up to about 50 atmos).

Changes of the intensity distribution within each of the groups of bands were found, which gave a shift in the maxima of these groups, but even at the highest temperatures and pressures near the critical point, no measurable shift in the frequencies of the components of the groups was found. This shows that the effect of intermolecular forces on the frequencies of the bands is very small.

A short discussion of the results is also given.

INTRODUCTION

IN the present work, the absorption spectrum of benzene vapor in the near ultraviolet was examined at temperatures varying from room temperature up to above the critical temperature (287°C), and at the corresponding pressures of the saturated vapor varying from a few mm of mercury at room temperature to about 50 atmos at 290°C.

The aim of this work was to get information about the behavior of molecules near their critical point. Such information, it was expected, could be obtained from the absorption and fluorescence spectra whenever the spectra in the liquid state differ appreciably from those of the vapor. In this case transition from the spectrum of the vapor to that of the liquid could be expected when approaching the critical point, when the distinction between the two phases vanishes.

The absorption spectrum of benzene in the near ultraviolet both in the liquid state and that of the vapor, consists of eight groups of vibrational bands[1] 923 cm^{-1} apart. But in the spectrum of the vapor each group shows well resolved fine structure components, while in that of the liquid this structure is completely obliterated and only broad bands are observed. The maxima of the groups in the spectrum of the liquid are found to be shifted by about 300 cm^{-1} towards the red relative to that of the corresponding groups in the spectrum of the vapor.[1,2]

Such shifts were found[3] in the spectra of various molecules, and were attributed by the authors to intermolecular forces (Van der Waals forces, Lorentz' field of polarization, etc.). If this is really the case, each of the components of a group in the spectrum of the liquid

[1] V. Henri, J. phys. radium **3**, 181 (1922).
[2] A. Kronenberger and P. Pringsheim, Z. Physik **40**, 75 (1926).
[3] P. K. Seshan, Trans. Faraday Soc. **32**, 689 (1936). S. Samburský and G. Wolfsohn, Phys. Rev. **62**, 357 (1942).

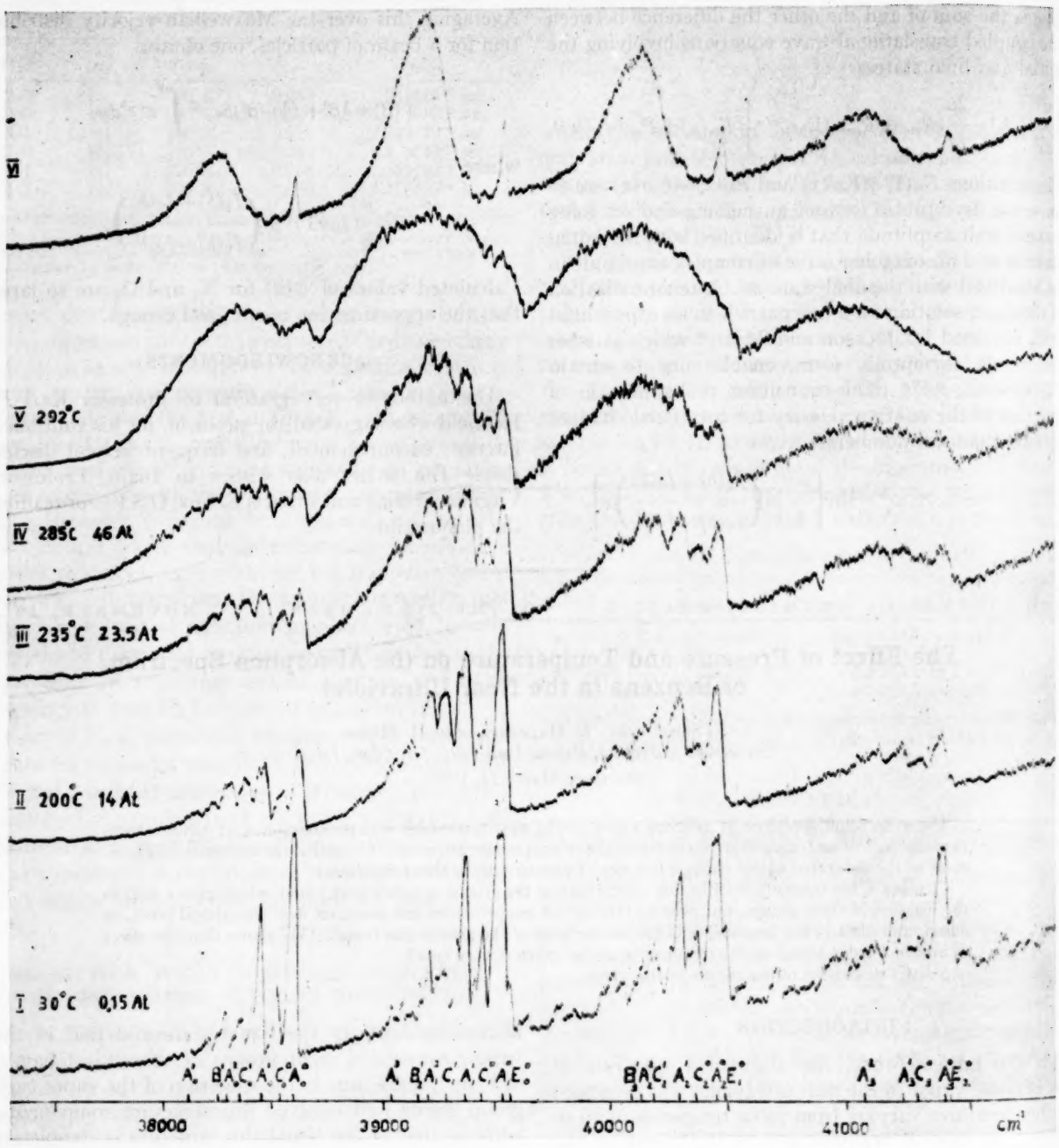

FIG. 1. The effect of temperature and pressure on the absorption spectra of benzene vapor. (Curves I to V.) Temperatures and corresponding pressures are indicated on the left side of each curve. Curve VI shows the spectrum of the liquid with that of the vapor (the sharp small peaks) superimposed.

should have been shifted relative to that of the spectrum of the vapor. This cannot be ascertained experimentally because the component bands of each group in the spectrum of the liquid are thoroughly blurred, so that only one broad band appears.

The spectrum of solid benzene resembles that of the liquid at room temperature, but differs from it at very low temperatures. This spectrum was investigated at $-180°C$[2] and even at $-259°C$[4] and was found to consist of narrow bands similar to that of the vapor. A red shift of about 285 cm^{-1} relative to the vapor was found in this spectrum.[5] Even in this case it is not easy to decide about the nature of the shift. Sponer, *et al.*[5] claim their analyses of the spectra of solid benzene and of the vapor show that each of the fine components of each group is really shifted, and attributed this shift to intermolecular and crystalline forces. On the other hand,

[4] P. Kronenberger, Z. Physik 63, 494 (1930).

[5] Sponer, Nordheim, Sklar, and Teller, J. Chem. Phys. 7, 207 (1939).

Kronenberger[4] argued that the interpretation of the two spectra would be more consistent if it were assumed that there is almost no shift in each of the components of the groups, while he attributed the apparent shift in the maxima of the groups to changes in the relative intensities of the components in each group.

The examination of the changes in the absorption spectrum of benzene vapor subjected to high pressures may throw light on the mechanism of the above-mentioned shift. For, if the shift is due to intermolecular forces, this should increase gradually with pressure, since the intermolecular distances become smaller and consequently the intermolecular forces grow larger.

EXPERIMENTAL ARRANGEMENTS

The benzene vapor was introduced into the optical path between the light source and the spectrograph by means of a specially built absorption cell. This cell consisted of two hollow brass cylinders of 6-mm internal diameter each with a parallel quartz window cemented to one end. These cylinders were screwed into a massive brass body forming a cell with an adjustable absorption path in the space between the two windows. Rings of soft copper pressed by a screw mechanism ensured tight closing of the cell preventing leakage of the benzene vapor. The whole apparatus was surrounded by a resistance regulated furnace. The temperature in the cell was indicated by a thermometer inserted into a hole in the brass body near to the cell. Saturated benzene vapor was obtained in the optical path of the cell by filling it with liquid benzene through an opening in the cell, heating it to about 80°C (the boiling point of benzene) and then allowing part of the liquid to evaporate until the light path became free from the liquid, upon which the opening was tightly closed. Approaching the critical point, smaller and smaller parts of the liquid were evaporated in this way. Heating of the cell elevated the vapor pressure in it to the corresponding saturation pressure. The absorption spectra were then photographed at various temperatures. The corresponding pressures up to about 20 atmos were read on a manometer attached to the absorption cell. For higher pressures the values were taken from a table of the saturated-vapor pressures of benzene.[6]

A hydrogen discharge lamp of the ordinary type was employed as a light source. An image of the source was cast by means of a quartz lens on the absorption cell, while another lens gave an image of the cell on the slit of the spectrograph.

The spectrograph used was a medium Schmidt & Haensch Quartz spectrograph ($f=60$ cm). The spectra were taken on Ilford Zenith H & D 700 photographic plates. An iron arc spectrum superimposed in part of the absorption spectrum served for comparison of wavelengths. The dispersion on the photographic plates in the spectral region under investigation (2400–2700A) was about 7A per mm.

The spectra were recorded with a microphotometer of the Moll type manufactured by Kipp & Zonen. Two records were made for each of the absorption spectra, one without the iron spectrum and the other with the superimposed iron spectrum recorded parallel to the first. This enabled determination of the wavelengths of the maxima of the absorption bands with an error of less than ±1A. When photographing the spectra at the higher pressures it was necessary to shorten the absorption path. As it was not easy to obtain these small absorption paths, it was found necessary to increase the exposure time from 1 min and a few mm absorption path at room temperature to about 15 min and only about 0.01 mm absorption path for the highest pressures.

RESULTS

Figure 1 represents the microphotometer records of the absorption spectra of benzene vapor for various temperatures and pressures (curves I to V). The absorption spectrum of liquid benzene at room temperature is also shown for comparison (curve VI). On this curve the sharp small peaks belong to the spectrum of the vapor, and was obtained by introducing a small amount of vapor into the optical path. The above-mentioned red shift is the distance between each peak in the spectrum of the liquid and the corresponding peak in the spectrum of the vapor.

The four groups of bands in each of the curves are the *B*, *C*, *D*, and *E* groups (an assignment due to Henri), and the indication at the bottom of Fig. 1 (A_0^0, A_0^1, B_1^1, etc.) are in accordance with the assignment of Sponer, *et al.*[5]

Curves I to V show a gradual transition from the resolved components in each of the groups in curve I (30°C; 0.15 atmos) to unresolved broad bands in curve V (292°C; about 50 atmos). This transition is accompanied also with a shift of the intensity maximum from that corresponding to the vapor at room temperature to about the maximum in the spectrum of the liquid (curve VI). But, there is no measurable real shift in the frequencies of each of the components, and only changes in the distribution of intensities of the various components of the bands were found. These changes were accompanied by broadening of the bands, which together give an apparent shift to the red of about 320 cm^{-1} in the maxima of the bands.

Taking for instance the group *C* (at about 39000–39570^{-1}) we see that the A_1^0 band is the dominating one at room temperature (curve I). At 235°C and 23.5 atmos (curve III) the A_1^1 band is already stronger than the A_1^0, and at 285°C; 46 atmos the peak coincides with A_1^2.

It seems that this shift in the maxima is partly caused by the broadening of each of the components which affects more the intensities in the center of the groups where the broadened bands are superimposed.

[6] Landolt-Börnstein, *Physikalisch-Chemische Tabellen* (Julius Springer, Berlin, 1923), fifth edition, Vol. II, p. 1370.

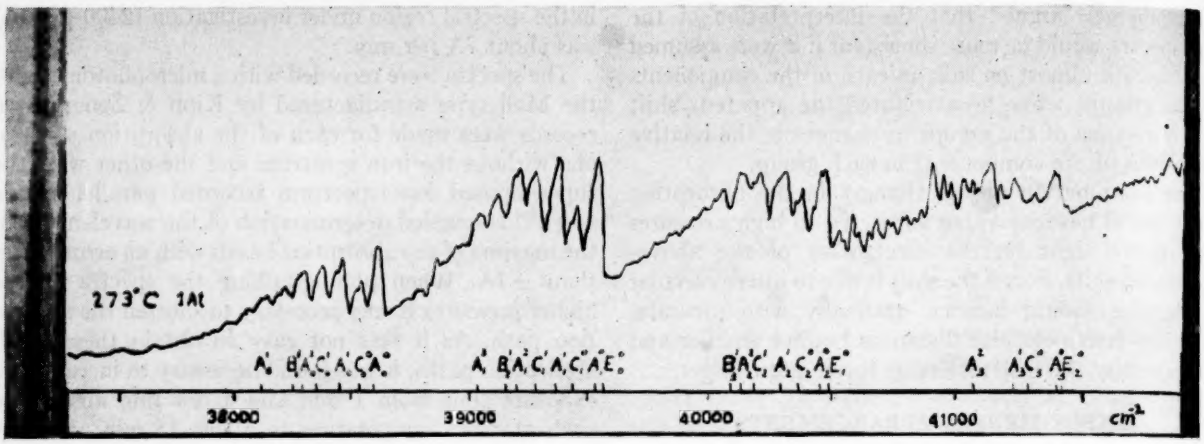

FIG. 2. Absorption spectrum of benzene vapor at 273°C, 1 atmos.

This broadening is continued at higher temperatures, and at 292°C (above the critical point; curve V), only slight traces of the components of each group are to be noticed, and the spectrum, though rather broadened, resembles that of the liquid.

In order to show the effect of temperature isolated from that of pressure, a series of photographs of the absorption spectra was made, at various temperatures and constant vapor pressure of about one atmos. This low pressure was obtained by slowly letting out the excess vapor while the cell was being heated. The spectrum at 273°C and one atmos (Fig. 2) was found to resemble in intensity-distribution a state between the spectra II and III of Fig. 1 (about 220°C and 19 atmos).

DISCUSSION

It is known that rise of temperature should influence the Boltzmann factor of each band and thus alter the intensity distribution. For example, the relative intensity of an A^0 band originating in the vibrationless ground state[5] should decrease with heating, while the intensities of bands originating in higher vibrational levels such as A^1; A^2; B^1 should continue to increase with temperature and obtain their relative maxima only at higher temperatures. Measurements of the effect of the Boltzmann factor were also carried out on some of the component-bands of the spectrum of benzene vapor.[7]

The comparison of the spectra in Fig. 1 with the spectrum in Fig. 2 clearly indicates that the changes cannot be attributed solely to this effect of temperature.

The effect of pressure is mainly a broadening effect, which, as mentioned above, increases the shift of the maxima towards the center of the groups.

No measurable shift in the frequencies of each of the components of the groups was obtained even at the highest pressures near the critical point. This shows that the intermolecular forces affect only slightly, if at all, the frequencies of the bands. Now, what about the red shift in the liquid relative to the spectrum of the vapor? In this case the shift is obtained at ordinary temperatures so that the effect of temperature on the intensity distribution within the groups is eliminated. If there exists no real shift due to intermolecular forces, there remains only the assumption that the intermolecular forces give an apparent shift by changing the relative intensities of the components in the groups. This assumption fits that of Kronenberger[4] for the spectrum of solid benzene at low temperatures, but is in contradiction to the assumption of Sponer, *et al*,[5] which is based upon a full analysis of the energy levels of benzene. Further experimental work is needed before the nature of these shifts could be fully understood. Measurements of the spectra of liquid benzene at high pressures, more work on the spectra of the solid at low temperatures, and perhaps also measurements of the spectra of the vapor mixed with foreign gases at high pressures, may help in solving this problem.

An additional point of view which should be borne in mind in trying to interpret the spectra is connected with the theory of heterophase fluctuations.[8] This theory shows that heterogenous fluctuations must become especially important in the neighborhood of the transition points. It has also been shown that the number of liquid droplets in saturated vapor should increase with temperature. If this number is not negligible for the saturated benzene vapor near the critical point, the spectrum obtained should appear as superposition of the spectrum of the vapor on that of the liquid. This interpretation seems somewhat speculative until an estimate of the number of this liquid droplets will show that it cannot be neglected.

[7] F. W. Radle and C. A. Beck, J. Chem. Phys. 8, 507 (1940).

[8] J. Frenkel, J. Chem. Phys. 7, 538 (1938).

The Quantum Mechanics of Collisions between Diatomic Molecules*

C. F. CURTISS
The Naval Research Laboratory, the Department of Chemistry, the University of Wisconsin, Madison, Wisconsin
(Received February 13, 1953)

The quantum mechanics of collisions between diatomic molecules is discussed. Explicit expressions for the angular transition probabilities are obtained. These expressions are in terms of a set of coefficients which are defined by the asymptotic form of the solutions of a set of coupled differential equations in one variable, the separation of the molecules. The coupled differential equations involve integrals of the intermolecular potential function, which may be of any form. A solution of the coupled differential equations by a perturbation method, which is valid in the case of low-energy collisions, in which transitions occur rarely, is discussed.

A KNOWLEDGE of the detailed dynamics of collisions between molecules is required for an understanding of various nonequilibrium properties of gases. The angular-dependent transition probabilities enter into the kinetic theory of gases made up of molecules. The magnitude of these quantities is of particular importance in estimating the thermal conductivity of such a gas and in estimating the magnitude of various quantities associated with the time lag in the establishment of thermal equilibrium among the various degrees of freedom of the molecules. In the present paper we discuss, from a quantum-mechanical point of view, the detailed dynamics of collisions between diatomic molecules. This discussion is a generalization of that presented previously on the scattering of atoms by diatomic molecules.[1]

The wave function describing the scattering of a plane wave of molecules by a single molecule consists of functions representing a plane wave of incoming molecules and a set of outgoing waves each representing a pair of transitions in the states of the molecules. The angular dependence of the outgoing waves may be described by an analysis in terms of the spherical harmonics. The asymptotic form of the wave function may then be written in terms of a set of scattering amplitudes representing the angular dependence of the transition probabilities. These coefficients are evaluated by an analysis of the asymptotic form of a solution of the wave equation representing the over-all system.

Group theoretical methods have been used to separate the rotational coordinates from the Schrödinger equation of the system and obtain results which are particularly convenient in the present problem.[2] A wave function of the system is written in terms of a set of functions which are solutions of a set of coupled differential equations involving three coordinates: the separation of the molecules, and the distances between the atoms in each of the molecules. The angular transition probabilities are obtained in terms of the asymptotic behavior of the well behaved solutions of these equations. If the transition probabilities are small, solutions of these equations may be obtained by the method of distorted waves. Recently, Takayanagi[3] has used the method of distorted waves to evaluate the probabilities of transitions in the rotational levels in collisions of H_2 molecules in the first few rotational states.

I. THE ASYMPTOTIC FORM

Asymptotically, at large separations, the two molecules behave independently. In terms of a space fixed coordinate system, let $\mathbf{r}_a$ and $\mathbf{r}_b$ denote the position vectors of the centers of gravity of molecules a and b; let ξ_a and ξ_b denote the separation of the atoms in molecules a and b; and let θ_a, φ_a and θ_b, φ_b be the polar angles specifying the directions of the axes of the two molecules. Furthermore, let $Z(n|\xi)$ be an harmonic oscillator wave function, and $Y(lm|\theta\varphi)$ be a normalized spherical harmonic. Then in the region of no interaction between the molecules a wave function can be written in the form

$$\Psi^{(0)}=\exp(i\mathbf{k}_a\cdot\mathbf{r}_a)\exp(i\mathbf{k}_b\cdot\mathbf{r}_b)Z^{(a)}(n_a|\xi_a)\times Z^{(b)}(n_b|\xi_b)Y(l_am_a|\theta_a\varphi_a)Y(l_bm_b|\theta_b\varphi_b). \quad \text{(I-1)}$$

Here, $l_am_an_a$ and $l_bm_bn_b$ are quantum numbers representing the internal states of the two molecules, and $\mathbf{k}_a$ and $\mathbf{k}_b$ are the vectorial wave numbers associated with the translational motion of the two molecules.

The wave function for the system of two molecules may easily be factored into functions describing the motion of the center of gravity of system and the relative motion of two molecules. Let M_a and M_b be the masses of molecules a and b, respectively. Then in terms of the position vector of molecule a with respect to molecule b,

$$\boldsymbol{\varrho}=\mathbf{r}_a-\mathbf{r}_b, \quad \text{(I-2)}$$

and the vectorial wave number associated with the relative motion,

$$\mathbf{k}=(M_b\mathbf{k}_a-M_a\mathbf{k}_b)/(M_a+M_b), \quad \text{(I-3)}$$

the wave function

$$\psi^{(0)}=\exp(i\mathbf{k}\cdot\boldsymbol{\varrho})Z^{(a)}(n_a|\xi_a)Z^{(b)}(n_b|\xi_b)\times Y(l_am_a|\theta_a\varphi_a)Y(l_bm_b|\theta_b\varphi_b) \quad \text{(I-4)}$$

* This work was carried out at the University of Wisconsin Naval Research Laboratory under contract with the Office of Ordnance Research, U. S. Army.
[1] C. F. Curtiss and F. T. Adler, J. Chem. Phys. **20**, 249 (1952).
[2] C. F. Curtiss, J. Chem. Phys. **21**, 1199 (1953).
[3] K. Takayanagi, Progr. Theoret. Phys. (Japan) **8**, 497 (1952).

involving only nine coordinates, represents the motion of the system of two molecules in a center of gravity coordinate system.

It is convenient to analyze the plane wave as given by the last equation into "spherical harmonic waves." Let θ and φ be the direction angles of the vector $\boldsymbol{\rho}$, that is, the direction of the line between the molecules, and let Θ and Φ be the direction angles of the vector $\mathbf{k}$, that is, the direction of the relative velocity. In terms of these quantities it may be readily shown that for large values of the separation ρ, the wave function given by Eq. (I-4) is of the form

$$\psi^{(0)}\rightarrow-\frac{2\pi i}{k\rho}Z^{(a)}(n_a|\xi_a)Z^{(b)}(n_b|\xi_b)Y(l_am_a|\theta_a\varphi_a)$$
$$\times Y(l_bm_b|\theta_b\varphi_b)\sum_{l\nu}[\exp(ik\rho)-(-1)^l\exp(-ik\rho)]$$
$$\times Y(l\nu|\theta\varphi)Y(l\nu|\Theta\Phi)^*. \quad \text{(I-5)}$$

This wave function represents, asymptotically, in a center of gravity coordinate system, the relative motion of two molecules. The quantum states of molecules a and b are represented by the quantum numbers $l_am_an_a$ and $l_bm_bn_b$. The direction of the relative velocity is denoted by Θ and Φ and its magnitude is represented by k.

Let us consider the scattering of a plane wave of molecules a in the quantum state $\bar{l}_a\bar{m}_a\bar{n}_a$ with the relative velocity associated with the wave number $\bar{k}$ from a molecule of kind b in quantum state $\bar{l}_b\bar{m}_b\bar{n}_b$. The wave function representing, asymptotically, the incoming plane wave, in the direction of the positive z axis, is obtained from Eq. (I-5), by putting Θ equal to zero. Since

$$Y(l\nu|0\Phi)=\left(\frac{2l+1}{4\pi}\right)^{\frac{1}{2}}\delta(\nu,0), \quad \text{(I-6)}$$

the resulting expression is

$$-\frac{i\sqrt{\pi}}{\bar{k}\rho}Z^{(a)}(\bar{n}_a|\xi_a)Z^{(b)}(\bar{n}_b|\xi_b)Y(\bar{l}_a\bar{m}_a|\theta_a\varphi_a)$$
$$\times Y(\bar{l}_b\bar{m}_b|\theta_b\varphi_b)\sum_l(2l+1)^{\frac{1}{2}}$$
$$\times[\exp(i\bar{k}\rho)-(-1)^l\exp(-i\bar{k}\rho)]Y(l0|\theta\varphi). \quad \text{(I-7)}$$

It is convenient to use the symbol n to represent collectively the quantum numbers, $l_am_an_al_bm_bn_b$, describing the states of the two molecules. In terms of this symbol, the last expression represents an incoming plane wave in which the "two molecule quantum state" is $\bar{n}$.

The terms in $\exp(ik\rho)$ and $\exp(-ik\rho)$ of the wave function of Eq. (I-5) are, of course, separately valid solutions of the wave equation, representing the two independent solutions. Asymptotically, the scattered wave, a wave going out from the origin, contains only terms in $\exp(ik\rho)$. Let $f(\bar{n}|n|\Theta\Phi)$ describe the angular dependence of the scattered wave in which a transition from the two molecule quantum state $\bar{n}$ to the state n has taken place. In terms of this function, and in view of the expression given by Eq. (I-5), we can write for the asymptotic form of the total scattered wave the expression

$$-2\pi i\sum_{l\nu n}\frac{e^{ik\rho}}{k\rho}Z^{(a)}(n_a|\xi_a)Z^{(b)}(n_b|\xi_b)$$
$$\times Y(l_am_a|\theta_a\varphi_a)Y(l_bm_b|\theta_b\varphi_b)Y(l\nu|\theta\varphi)$$
$$\times\int\int f(\bar{n}|n|\Theta\Phi)Y(l\nu|\Theta\Phi)^*\sin\Theta d\Theta d\Phi. \quad \text{(I-8)}$$

In the sum, k is such a function of $\bar{k}$, $\bar{l}_a$, $\bar{n}_a$, $\bar{l}_b$, $\bar{n}_b$, l_a, n_a, l_b, and n_b that the total energy of the system is conserved. (Because of the usual degeneracy, k does not depend on $\bar{m}_a$, m_a, $\bar{m}_b$, and m_b.) It is convenient to analyze the scattered wave in terms of the spherical harmonics rather than in terms of plane waves. Hence we define the

$$\alpha(\bar{n}|n|l\nu)$$
$$=\int\int f(\bar{n}|n|\Theta\Phi)Y(l\nu|\Theta\Phi)^*\sin\Theta d\Theta d\Phi \quad \text{(I-9)}$$

as the amplitudes of the various spherical harmonic waves. If we use this definition, the asymptotic form of the complete wave function, which is the sum of the expressions given by Eqs. (I-7 and I-8), is

$$\psi\rightarrow-2\pi i\sum_{l\nu n}Z^{(a)}(n_a|\xi_a)Z^{(b)}(n_b|\xi_b)$$
$$\times Y(l_am_a|\theta_a\varphi_a)Y(l_bm_b|\theta_b\varphi_b)Y(l\nu|\theta\varphi)$$
$$\times\left[\frac{e^{ik\rho}}{k\rho}\left\{\alpha(\bar{n}|n|l\nu)+\left(\frac{2l+1}{4\pi}\right)^{\frac{1}{2}}\delta(\bar{n},n)\delta(\nu,0)\right\}\right.$$
$$\left.-(-1)^l\frac{e^{-ik\rho}}{k\rho}\left(\frac{2l+1}{4\pi}\right)^{\frac{1}{2}}\delta(\bar{n},n)\delta(\nu,0)\right]. \quad \text{(I-10)}$$

This wave function is to be distinguished from the wave function $\psi^{(0)}$. The function $\psi^{(0)}$ represents a single plane wave of molecules a approaching a molecule b with the quantum states of both molecules well specified. The wave function ψ represents the actual situation of an incoming plane wave and outgoing scattered waves. Because of the transitions, the states of the molecules cannot be specified.

The constants $\alpha(\bar{n}|n|l\nu)$, which are interpreted as scattering amplitudes, are obtained by considering the asymptotic form of a wave function which satisfies the requirements of the interaction potential. That is, one obtains a valid solution of the true wave equation which is asymptotically of the form of Eq. (I-10). The constants, $\alpha(\bar{n}|n|l\nu)$, are then well specified.

II. THE SOLUTION OF THE WAVE EQUATION

The relative configuration and orientation of two diatomic molecules in a center-of-gravity coordinate system may be described by either of two sets of coordinates. In either method one uses the two distances ξ_a and ξ_b between the atoms in the diatomic molecules. In the first method, as used in the previous section, one uses in addition the two polar angles of the axes of each of the two molecules and those of the line between the centers of gravity of the two molecules. These angles are denoted symbolically by the rotations $R^{(a)}$, $R^{(b)}$, and R, respectively. It is now convenient to use an alternative description. The angle between the axis of molecule a and the intermolecular axis is represented by the rotation $S^{(a)}$. The two angles representing the relative orientation of molecule b, i.e., the angle between the axis of molecule b and the intermolecular axis and the angle between the planes containing the axes of each of the molecules and the intermolecular axis (the azimuthal angle), is represented by the rotation $S^{(b)}$. The orientation of the entire system in space is described by the rotation R. This representation is convenient since the potential energy of the system depends only on the three angles describing the rotations $S^{(a)}$ and $S^{(b)}$.

The wave equation for the system consisting of two diatomic molecules has been discussed in a previous paper,[2] the results of which are summarized here. In the present discussion, it is convenient to consider the potential energy of the entire system as the sum of three terms,

$$V=V^{(a)}(\xi_a)+V^{(b)}(\xi_b)+V^{(ab)}(\xi_a\xi_b\rho S^{(a)}S^{(b)}), \quad \text{(II-1)}$$

the potential energy of molecules a and b separately, $V^{(a)}(\xi_a)$ and $V^{(b)}(\xi_b)$, and an interaction potential, $V^{(ab)}(\xi_a\xi_b\rho S^{(a)}S^{(b)})$. Clearly, $V^{(a)}$ and $V^{(b)}$ are independent of the relative orientations of the two molecules and $V^{(ab)}$ approaches zero at large separations ρ. Then it follows from the orthogonality of the representation coefficients that the matrix element of the total potential, $W(l_a'l_b'\nu'|l_al_b\nu)_s$, defined by Eq. (III-10) of reference 2, is

$$W(l_a'l_b'\nu'|l_al_b\nu)_s=\frac{\delta(l_a,l_a')\delta(l_b,l_b')\delta(\nu,\nu')}{(2l_a+1)(2l_b+1)}\times[V^{(a)}+V^{(b)}]+W^{(ab)}(l_a'l_b'\nu'|l_al_b\nu)_s, \quad \text{(II-2)}$$

where

$$W^{(ab)}(l_a'l_b'\nu'|l_al_b\nu)_s=\frac{1}{\int\int dS^{(a)}dS^{(b)}}\times\int\int D^{l_a'}(S^{(a)})_{0,-s-\nu'}{}^*D^{l_b'}(S^{(b)})_{0\nu'}{}^* \times V^{(ab)}D^{l_a}(S^{(a)})_{0,-s-\nu}D^{l_a}(S^{(b)})_{0\nu}dS^{(a)}dS^{(b)} \quad \text{(II-3)}$$

is the matrix component of the interaction potential.

It has been shown in a previous paper,[2] that the wave function in a center-of-gravity coordinate system representing a state with a total angular momentum quantum number J and a z component of the angular momentum quantum number μ may be written in the form

$$\psi(J\mu)=\sum_{\substack{Lvs\\ l_al_b}} s(l_a,l_b|L,-s-\nu,\nu)s(J,L|l,s,-s)\times D^J(R)_{s\mu}D^{l_a}(S^{(a)})_{0,-s-\nu}{}^*D^{l_b}(S^{(b)})_{0\nu}{}^*\times F^J(Ll l_al_b|\xi_a\xi_b\rho). \quad \text{(II-4)}$$

Here, the $s(l,j|L,s,\nu)$ are the coefficients defined by Wigner,[4] the $D^J(R)_{s\mu}$ are the representation coefficients of the three-dimensional rotation group, and the $F^J(Ll l_al_b|\xi_a\xi_b\rho)$ are solutions of a set of coupled differential equations described below.

If one uses the expression for the matrix component of the total potential, $W(l_a'l_b'\nu'|l_al_b\nu)_s$ in terms of the matrix component of the interaction potential, $W^{(ab)}(l_a'l_b'\nu'|l_al_b\nu)_s$, as given by Eq. (II-2), it follows directly from the previous results[2] that the coupled equations for the $F^J(Ll l_al_b|\xi_a\xi_b\rho)$ are

$$\left[\frac{\hbar^2}{2\mu\rho^2}\left[\frac{\partial}{\partial\rho}\left(\rho^2\frac{\partial}{\partial\rho}\right)-l(l+1)\right]+E+\frac{\hbar^2}{2\mu_a\xi_a{}^2}\left[\frac{\partial}{\partial\xi_a}\left(\xi_a{}^2\frac{\partial}{\partial\xi_a}\right)-l_a(l_a+1)\right]-V^{(a)}+\frac{\hbar^2}{2\mu_b\xi_b{}^2}\left[\frac{\partial}{\partial\xi_b}\left(\xi_b{}^2\frac{\partial}{\partial\xi_b}\right)-l_b(l_b+1)\right]-V^{(b)}\right]\times F^J(Ll l_al_b|\xi_a\xi_b\rho)$$
$$=(2l_a+1)(2l_b+1)\sum_{L'l'l_a'l_b'}F^J(L'l'l_a'l_b'|\xi_a\xi_b\rho)\times\sum_{\nu\nu's}s(l_a,l_b|L,-s-\nu,\nu)s(l_a',l_b'|L',-s-\nu',\nu')\times s(J,L|l,s,-s)s(J,L'|l',s,-s)\times W^{(ab)}(l_a'l_b'\nu'|l_al_b\nu)_s. \quad \text{(II-5)}$$

In this equation, E is the total energy, μ is the reduced mass of the two molecule system,

$$\mu=M_aM_b/(M_a+M_b), \quad \text{(II-6)}$$

and μ_a and μ_b are the reduced masses of the molecules separately.

The sets of functions $Z^{(a)}(n_a|\xi_a)$ and $Z^{(b)}(n_b|\xi_b)$ form complete sets of functions in the spaces of ξ_a and ξ_b, respectively. Hence we expand the functions

[4] Eugene Wigner, *Gruppentheorie and Ihre Andwendung auf die Quantum Mechanik der Atomspektren* (Edwards Brothers, Inc., Ann Arbor, 1944), p. 206.

$F^J(Lll_al_b|\xi_a\xi_b\rho)$ in the double series,

$$F^J(Lll_al_b|\xi_a\xi_b\rho)$$
$$=\sum_{n_an_b} g^J(q|\rho)Z^{(a)}(n_a|\xi_a)Z^{(b)}(n_b|\xi_b), \quad \text{(II-7)}$$

where the symbol q is used to represent collectively the quantum numbers, $Lll_an_al_bn_b$. The functions $Z^{(a)}(n_a|\xi_a)$, of course, satisfy the equation for the nonrotating free molecule,

$$-\frac{\hbar^2}{2\mu_a\xi_a^2}\frac{\partial}{\partial\xi_a}\left(\xi_a^2\frac{\partial}{\partial\xi_a}\right)Z^{(a)}(n_a|\xi_a)$$
$$+V^{(a)}Z^{(a)}(n_a|\xi_a)=E_{n_a}{}^{(a)}Z^{(a)}(n_a|\xi_a), \quad \text{(II-8)}$$

where $E_{n_a}{}^{(a)}$ is the energy of the vibrational state n_a of molecule a. These functions are taken to be real and are orthogonal in that

$$\int Z_{n_a'}{}^{(a)}(\xi_a)Z_{n_a}{}^{(a)}(\xi_a)\xi_a^2d\xi_a=\delta(n_a, n_a'). \quad \text{(II-9)}$$

Similar relations apply to the $Z^{(b)}(n_b|\xi_b)$.

If we neglect the coupling between the rotational and vibrational motion of the molecules, as has already been implied by the form of the wave function of Eq. (I-1), the terms representing the centrifugal potential in Eq. (II-5), i.e., $l_a(l_a+1)\hbar^2/2\mu_a\xi_a^2$ and $l_b(l_b+1)\hbar^2/2\mu_b\xi_b^2$ may be replaced by similar terms involving the equilibrium separations ξ_a^0 and ξ_b^0. Then if the expansion [Eq. (II-7)] is introduced into the equations for the F^J [Eq. (II-5)] and use is made of the orthogonality [Eq. (II-9)], the equations become

$$\frac{\hbar^2}{2\mu\rho^2}\left[\frac{\partial}{\partial\rho}\left(\rho^2\frac{\partial}{\partial\rho}\right)-l(l+1)+k^2\rho^2\right]g^J(q|\rho)$$
$$=\sum_{q'}W^J(q'|q|\rho)g^J(g'|\rho), \quad \text{(II-10)}$$

where

$$W^J(q'|q|\rho)$$
$$=(2l_a+1)(2l_b+1)\sum_{\nu\nu's}s(l_a, l_b|L, -s-\nu, \nu)$$
$$\times s(l_a', l_b'|L', -s-\nu', \nu')s(J, L|l, s, -s)$$
$$\times s(J, L'|l', s, -s)\int\int Z^{(a)}(n_a'|\xi_a)Z^{(b)}(n_b'|\xi_b)$$
$$\times W^{(ab)}(l_a'l_b'\nu'|l_al_b\nu)_sZ^{(a)}(n_a|\xi_a)$$
$$\times Z^{(b)}(n_b|\xi_b)\xi_a^2\xi_b^2d\xi_ad\xi_b, \quad \text{(II-11)}$$

and

$$\frac{\hbar^2k^2}{2\mu}=E-E_{n_a}{}^{(a)}-\frac{l_a(l_a+1)\hbar^2}{2\mu_a(\xi_a{}^0)^2}-E_{n_b}{}^{(b)}-\frac{l_b(l_b+1)}{2\mu_b(\xi_b{}^0)^2} \quad \text{(II-12)}$$

is the kinetic energy associated with the relative translational motion of the two molecules. As in the previous section, k is the wave number associated with the relative translational motion.

The Eqs. (II-10) possess an infinitude of sets of solutions. In addition to the continuous quantum number k, associated with the coordinate ρ, additional quantum numbers associated with each of the coupling indices appear. Let us denote by $g^J(q^0|q|\rho)$ the "qth" member of the set of functions forming the solution described by the set of quantum numbers q^0.

If $k^2>0$ and if the $W^J(q'|q|\rho)$ approach zero sufficiently rapidly as ρ becomes large, the solutions of the Eqs. (II-10) asymptotically consist of linear combinations of $(1/k\rho)\exp(ik\rho)$ and $(1/k\rho)\exp(-ik\rho)$. The quantum numbers q^0 are defined in such a manner that asymptotically only the "diagonal" functions contain terms in $(1/k\rho)\exp(-ik\rho)$. Furthermore, the normalization is taken arbitrarily in such a manner that asymptotically

$$g^J(q^0|q|\rho)\rightarrow\delta(q^0, q)\frac{e^{-ik\rho}}{k\rho}+Q^J(q^0|q)\frac{e^{ik\rho}}{k\rho}. \quad \text{(II-13)}$$

The constants $Q^J(q^0|q)$ are determined by the nature of the functions in the region of interaction and depend upon the intermolecular potential through the values of the coupling functions $W^J(q'|q|\rho)$.

An approximate solution to a set of equations completely analogous to the Eqs. (II-10) has been discussed elsewhere.[1] The approximate solution is valid in the limit that the coupling is weak, and transitions occur only rarely. In this approximation the $Q^J(q^0|q)$ may be evaluated in the following manner: First we define the $U^J(q|\rho)$ as the solutions of the auxiliary equations

$$\frac{\hbar^2}{2\mu\rho^2}\left[\frac{\partial}{\partial\rho}\left(\rho^2\frac{\partial}{\partial\rho}\right)-l(l+1)+k^2\rho^2\right]U^J(q|\rho)$$
$$=W^J(q|q|\rho)U^J(q|\rho), \quad \text{(II-14)}$$

which are bounded at the origin and which are asymptotically of the form

$$U^J(q|\rho)\rightarrow\frac{1}{k\rho}\sin[k\rho+\theta^J(q)]. \quad \text{(II-15)}$$

These solutions define the set of phase angles $\theta^J(q)$. Then

$$Q^J(q^0|q)=-\exp[2i\theta^J(q)]$$
$$\times[\delta(q^0,q)-(1-\delta(q^0,q))2i\beta^J(q^0|q)], \quad \text{(II-16)}$$

where

$$\beta^J(q^0|q)=\frac{2\mu k}{\hbar^2}$$
$$\times\int_0^\infty U^J(q^0|\rho)W^J(q^0|q|\rho)U^J(q|\rho)\rho^2d\rho. \quad \text{(II-17)}$$

III. THE SCATTERING COEFFICIENTS

We now proceed to evaluate the scattering amplitudes, $\alpha(\bar{n}|n|l\nu)$ in terms of the constants $Q(q^0|q)$ which are determined by the intermolecular potential. The asymptotic form of a wave function which represents a plane wave of molecules of type a scattered by a molecule of type b is given by Eq. (I-10). A particular solution of the wave equation of the two molecule system is described by Eq. (II-4). Since the solution as given by Eq. (I-10) is, of necessity, a linear combination of solutions of the type given by Eq. (II-4), corresponding to a fixed value of the total energy, a comparison of the two forms provides an evaluation of the $\alpha(\bar{n}|n|l\nu)$.

The transformation of an expression for the wave function in terms of the rotations $S^{(a)}$, $S^{(b)}$, and R to one in terms of $R^{(a)}$, $R^{(b)}$, and R is discussed in a previous paper.[2] If this transformation is carried out on the expression for the wave function as given by Eq. (II-4) and if the series for the functions F^J in terms of the g^J, Eq. (II-7), is used, the expression becomes

$$\psi(J\mu q^0)=\sum_{qm_am_b} s(l_a, l_b|L, -m_a, -m_b)\times s(J, L|l, \mu, -m_a-m_b)\times D^l(R)_{0,\,\mu-m_a-m_b} D^{l_a}(R^{(a)})_{0,\,-m_a}{}^* \times D^{l_b}(R^{(b)})_{0,\,-m_b}{}^* Z^{(a)}(n_a|\xi_a)\times Z^{(b)}(n_b|\xi_b) g^J(q^0|q|\rho). \quad \text{(III-1)}$$

This wave function is specified by the nine quantum numbers $J\mu q^0$ and k. Any wave function of specified energy may be written as a linear combination of these functions,

$$\psi=\sum_{J\mu q^0} A(J\mu q^0)\psi(J\mu q^0), \quad \text{(III-2)}$$

where, in the sum, k is taken as a function of the quantum numbers in such a manner that the energy is conserved. The constants $A(J\mu q^0)$ will be chosen so that this wave function is asymptotically of the same form as that described by Eq. (I-10).

The representation coefficients with the first index zero are related to the spherical harmonics in the following manner:

$$D^l(R)_{0m}=\left(\frac{4\pi}{2l+1}\right)^{\frac{1}{2}} Y(lm|\theta\varphi). \quad \text{(III-3)}$$

Furthermore, the spherical harmonics as defined in reference 2 are such that

$$Y(lm|\theta\varphi)^*=(-1)^m Y(l, -m|\theta\varphi), \quad \text{(III-4)}$$

so that

$$D^l(R)_{0,-m}{}^*=(-1)^m\left(\frac{4\pi}{2l+1}\right)^{\frac{1}{2}} Y(lm|\theta\varphi). \quad \text{(III-5)}$$

The asymptotic form of the wave function, Eq. (III-2), is obtained by using Eq. (III-1) and the equation for the asymptotic form of the $g^J(q^0|q|\rho)$, Eq. (II-13). If the resulting expression is equated to the wave function as given by Eq. (I-10), and use is made of the last relations and the orthogonality of the spherical harmonics and the harmonic oscillator wave functions, it follows that

$$-(-1)^{m_a+m_b}\frac{i}{4\sqrt{\pi}}[(2l+1)(2l_a+1)(2l_b+1)]^{\frac{1}{2}} \times\left[\frac{e^{ik\rho}}{k\rho}\left\{\alpha(\bar{n}|n|l,\,\mu-m_a-m_b)+\left(\frac{2l+1}{4\pi}\right)^{\frac{1}{2}} \times\delta(\bar{n}, n)\delta(\mu, m_a+m_b)\right\}-(-1)^l\frac{e^{-ik\rho}}{k\rho} \times\left(\frac{2l+1}{4\pi}\right)^{\frac{1}{2}}\delta(\bar{n}, n)\delta(\mu, m_a+m_b)\right]$$
$$=\sum_{JLq^0} A(J\mu q^0)s(l_a, l_b|L, -m_a, -m_b)\times s(J, L|l, \mu, -m_a-m_b)\times\left[\frac{e^{ik\rho}}{k\rho}Q^J(q^0|q)+\frac{e^{-ik\rho}}{k\rho}\delta(q^0,q)\right]. \quad \text{(III-6)}$$

The constants $A(J\mu q^0)$ and $\alpha(\bar{n}|n|l\nu)$ are fixed by the fact that this last equation is an identity in ρ.

If one equates the coefficients of $(1/k\rho)\exp(-ik\rho)$ in the last equation, one obtains a set of equations for the $A(J\mu q)$. This set of equations may be solved by making use of the orthogonality properties of the $s(l, j|L, s, \nu)$, to obtain an explicit expression for $A(J\mu q)$. Similarly, if one equates the terms in $(1/k\rho)\exp(ik\rho)$, one obtains a set of equations for scattering amplitudes, $\alpha(\bar{n}|n|l\nu)$. Upon use of the expression for the $A(J\mu q)$, and solution of this result one finds that

$$\alpha(\bar{n}|n|l\nu)=-\delta(\bar{n}, n)\delta(\nu, 0)\left(\frac{2l+1}{4\pi}\right)^{\frac{1}{2}}-(-1)^l\frac{\delta(\nu, \bar{n}-m)}{(4\pi)^{\frac{1}{2}}} \times\left[\frac{(2\bar{l}_a+1)(2\bar{l}_b+1)}{(2l_a+1)(2l_b+1)}\right]^{\frac{1}{2}}\sum_{JLL^0l^0}(2l^0+1)^{\frac{1}{2}} \times s(l_a, l_b|L, -m_a, -m_b)s(\bar{l}_a, \bar{l}_b|L^0, -\bar{m}_a, -\bar{m}_b) \times s(l, L|J, \nu, m)s(l^0, L^0|J, 0, \bar{m}) \times Q^J(L^0l^0\bar{l}_a\bar{n}_a\bar{l}_b\bar{n}_b|Lln_an_al_bn_b), \quad \text{(III-7)}$$

where by definition $m=m_a+m_b$ and $\bar{m}=\bar{m}_a+\bar{m}_b$. This expression gives explicitly the values of the scattering amplitudes. The states of the two molecules are described by the "quantum number" n, which represents symbolically the set of quantum numbers, $l_am_an_a\bar{l}_b\bar{m}_b\bar{n}_b$.

The scattering amplitude, $\alpha(\bar{n}|n|l\nu)$, is the contribution to the scattered wave with angular dependence given by the $(l\nu)$ spherical harmonic due to transitions in the two molecule quantum state from $\bar{n}$ to n.

Because of the properties of the $s(j,l|L,s,\nu)$ it follows that in the expression for the $\alpha(\bar{n}|n|l\nu)$ [Eq. (III-7)] the index l^0 takes on all integer values (0 to ∞) while the indices L and L^0 are limited by the conditions, $|l_a-l_b| \leqslant L \leqslant (l_a+l_b)$ and $|\bar{l}_a-\bar{l}_b| \leqslant L^0 \leqslant (\bar{l}_a+\bar{l}_b)$. Similarly the index J is limited by both the conditions, $|l-L| \leqslant J \leqslant (l+L)$ and $|l^0-L| \leqslant J \leqslant (l^0+L)$. Each term in the sum of Eq. (III-7) may be interpreted, loosely, as the contribution of a particular type of collision. The index l^0 refers to the angular momentum associated with the relative translational motion of the two molecules. This index is a manifestation of the classical "impact parameter." From the classical point of view, because of the lack of spherical symmetry, three additional parameters are necessary to describe the collision. These parameters appear here as the indices J, L, and L^0. The indices L and L^0 measure the vector sum of the angular momentum associated with the rotation of molecules a and b in space before and after the collision, respectively. The index J measures the total angular momentum of the two molecule system, that is, the vector sum of the angular momenta associated with the rotation of the two molecules and that associated with the translational motion. This quantity of course is a constant of motion and is the same before and after the collision.

This coefficients $Q^J(q^0|q)$ are defined by Eq. (II-13) in terms of the asymptotic behavior of the set of coupled differential equations, Eqs. (II-10). An approximate evaluation of the $Q^J(q^0|q)$ valid under conditions such that transitions occur relatively seldom is discussed in the previous section. A more general evaluation of the $Q^J(q^0|q)$ will be discussed in a later paper.

THE JOURNAL OF CHEMICAL PHYSICS VOLUME 21, NUMBER 11 NOVEMBER, 1953

The Statistical Mechanical Theory of Transport Processes. VI. A Calculation of the Coefficients of Shear and Bulk Viscosity of Liquids*

ROBERT W. ZWANZIG, JOHN G. KIRKWOOD, KENNETH F. STRIPP, AND IRWIN OPPENHEIM
The Sterling Chemistry Laboratory, Yale University, New Haven, Connecticut

(Received March 11, 1953)

The theory of the coefficients of shear and bulk viscosity of liquids developed in the third article of this series is applied to the calculation of the coefficients of viscosity of liquid argon at its normal boiling point. The theory of the bulk viscosity, including a previously omitted term due to the rate of dilatation, is presented. With the use of the Lennard-Jones potential, a radial distribution function which is a much better approximation than the previously used one, and a new approximation to the friction constant, values are obtained for the coefficients of viscosity.

I. INTRODUCTION

IN the third article of this series[1] (SMT III) Kirkwood, Buff, and Green presented a statistical mechanical theory of the coefficients of bulk and shear viscosity of liquids, and reported a calculation of the coefficient of shear viscosity of liquid argon at its normal boiling point. Their calculation was performed with a special approximation to the equilibrium radial distribution function, chosen to represent the experimentally observed shape of its first peak, and containing parameters which were adjusted to give correct calculated values for the equilibrium pressure and internal energy. Since then, more accurate equilibrium radial distribution functions have been obtained by solving the appropriate integral equations[2,3] in the superposition approximation. In the present article, the coefficients of bulk and shear viscosity are calculated using the new radial distribution functions. The special analytic form of the peak approximation used in SMT III permitted exact solution of the differential equations for the perturbation to the equilibrium radial distribution function due to fluid flow. With the new distribution functions, the differential equations must be solved numerically. The method of solution used here is described in appendices I and II.

The theory of the coefficient of bulk viscosity given in SMT III was incomplete. In Sec. II, the complete theory, including an omitted term due to the rate of dilatation, is presented.

The friction constant used in SMT III was obtained by a very rough approximation. The friction constant used here was obtained by the more detailed linear trajectory analysis, which will be described in a later paper.

The numerical value obtained for the coefficient of shear viscosity η of liquid argon at its normal boiling

* This work was carried out under contract Nonr-410(00) with the U. S. Office of Naval Research.

[1] Kirkwood, Buff, and Green, J. Chem. Phys. **17**, 988 (1949).

[2] Kirkwood, Lewinson, and Alder, J. Chem. Phys. **20**, 929 (1952).

[3] Zwanzig, Kirkwood, Stripp, and Oppenheim, J. Chem. Phys. (to be published).

point is $\eta=0.73\times10^{-3}$ poise. This differs from the result $\eta=1.27\times10^{-3}$ poise given in SMT III, and is smaller than the experimental value $\eta=2.39\times10^{-3}$ poise by a factor of about three. The friction constant is $\zeta=2.85\times10^{-10}$ g/sec which is also smaller than the value $\zeta=4.84\times10^{-10}$ g/sec used in SMT III. The sensitivity of the friction constant and the coefficients of bulk and shear viscosity to the shape of the equilibrium radial distribution function is investigated. The friction constant and the coefficient of shear viscosity are insensitive, but the bulk viscosity φ is quite sensitive. The result $\varphi=0.36\times10^{-3}$ poise is less reliable than the calculated shear viscosity.

II. BASIC EQUATIONS

The equations of continuity and motion of a viscous fluid are

$$\frac{\partial\rho}{\partial t}+\nabla_R\cdot\rho\mathbf{u}=0,$$
$$\frac{\partial}{\partial t}\rho\mathbf{u}=\mathbf{X}+\nabla_R\cdot\boldsymbol{\sigma}, \tag{1}$$

where ρ is the mass density of the fluid, $\mathbf{u}$ is the fluid velocity, $\mathbf{X}$ represents external body forces, and $\boldsymbol{\sigma}$ is the stress tensor of the fluid. The Newtonian stress tensor depends on pressure P, rate of strain $\dot{\boldsymbol{\epsilon}}$, and divergence of velocity $\nabla\cdot\mathbf{u}$ in this way,

$$\boldsymbol{\sigma}=-\left\{P+\left[\frac{2\eta}{3}-\varphi\right]\nabla\cdot\mathbf{u}\right\}\mathbf{1}+2\eta\dot{\boldsymbol{\epsilon}}, \tag{2}$$

where $\mathbf{1}$ is the unit dyad and η and φ are the coefficients of shear and bulk viscosity. In the statistical mechanical theory of transport processes, the stress tensor may be expressed in terms of molecular variables,

$$\boldsymbol{\sigma}=-\rho^{(1)}\left[\frac{\langle\mathbf{pp}\rangle_{Av}}{m}-m\mathbf{uu}\right]+\tfrac{1}{2}\int\frac{\mathbf{R}_{12}\mathbf{R}_{12}}{R_{12}}\frac{dV(R_{12})}{dR_{12}}\rho^{(2)}(\mathbf{R},\mathbf{R}_{12})d^3R_{12} \tag{3}$$

$$\rho^{(1)}\langle\mathbf{pp}\rangle_{Av}=N\int\mathbf{pp}f^{(1)}(\mathbf{R},\mathbf{p})d\mathbf{p},$$

where m is the mass of an individual molecule, N is Avogadro's number, $V(R_{12})$ is the potential of intermolecular force of a pair of molecules separated by the distance R_{12}, $\rho^{(1)}(\mathbf{R})$ is the average number density of molecules at $\mathbf{R}$, $\rho^{(2)}(\mathbf{R},\mathbf{R}_{12})$ is the average number density of pairs of molecules when one is at $\mathbf{R}$ and the other is at $\mathbf{R}+\mathbf{R}_{12}$, and $\bar{f}^{(1)}(\mathbf{R},\mathbf{p})$ is the probability that a given molecule has momentum $\mathbf{p}$ and is at position $\mathbf{R}$. To convert this expression for the stress tensor to the Newtonian form, it is necessary to expand $\bar{f}^{(1)}$ and $\rho^{(2)}$ in $\nabla\cdot\mathbf{u}$ and $\dot{\boldsymbol{\epsilon}}$. When this is done, the momentum transport contribution becomes

$$\rho^{(1)}\left[\frac{\langle\mathbf{pp}\rangle_{Av}}{m}-m\mathbf{uu}\right]=\rho^{(1)}kT\mathbf{1}-\frac{\rho^{(1)}kT}{\zeta}\left[\dot{\boldsymbol{\epsilon}}-\frac{\nabla\cdot\mathbf{u}}{3}\mathbf{1}\right], \tag{4}$$

where ζ is the Brownian motion friction constant. With the definition of the pair correlation function,

$$g^{(2)}(\mathbf{R},\mathbf{R}_{12})=\rho^{(2)}(\mathbf{R},\mathbf{R}_{12})/\rho^{(1)}(\mathbf{R})\rho^{(1)}(\mathbf{R}+\mathbf{R}_{12}), \tag{5}$$

and the expansion in spherical harmonics,

$$g^{(2)}(\mathbf{R}_{12})=g_0^{(2)}(R_{12})\left\{1+\frac{\zeta}{kT}\times\left[\frac{\mathbf{R}_{12}\cdot\dot{\boldsymbol{\epsilon}}\cdot\mathbf{R}_{12}}{R_{12}^2}-\tfrac{1}{3}\nabla\cdot\mathbf{u}\right]\psi_2(R_{12})+\frac{\zeta}{6kT}(\nabla\cdot\mathbf{u})\psi_0(R_{12})\right\}, \tag{6}$$

expressions for the pressure and coefficients of shear and bulk viscosity are

$$P=\rho^{(1)}kT-\frac{2\pi}{3}[\rho^{(1)}]^2\int_0^\infty R^3\frac{dV}{dR}g_0^{(2)}(R)dR, \tag{7}$$

$$\eta=\frac{\rho^{(1)}kT}{2m\zeta}+\frac{\pi\zeta}{15kT}[\rho^{(1)}]^2\int_0^\infty R^3\frac{dV}{dR}g_0^{(2)}(R)\psi_2(R)dR, \tag{8}$$

$$\varphi=\frac{\pi\zeta}{9kT}[\rho^{(1)}]^2\int_0^\infty R^3\frac{dV}{dR}g_0^{(2)}(R)\psi_0(R)dR. \tag{9}$$

The function $g_0^{(2)}(R_{12})$ is the equilibrium radial distribution function of the fluid, and $\psi_0(R_{12})$ and $\psi_2(R_{12})$ describe the perturbation of $g^{(2)}$ caused by fluid flow.

The perturbed $g^{(2)}$ satisfies the differential equation

$$\nabla_R\cdot\{\nabla_R g^{(2)}-g^{(2)}\nabla_R\log g_0^{(2)}\}-\frac{\zeta}{kT}\frac{\partial g^{(2)}}{\partial t}=\frac{\zeta}{2kT}\mathbf{R}\cdot\dot{\boldsymbol{\epsilon}}\cdot\nabla_R g^{(2)}, \tag{10}$$

together with boundary conditions resulting from requirements imposed on the excess current density in pair configuration space. When $g^{(2)}$ is expanded in spherical harmonics (Eq. 6), the equation is linearized with respect to the rate of strain $\dot{\boldsymbol{\epsilon}}$, and only the stationary state is considered, differential equations are obtained for $\psi_0(R)$ and $\psi_2(R)$. The equation for ψ_2 is

$$\frac{d}{dR}\left(R^2g_0^{(2)}(R)\frac{d\psi_2(R)}{dR}\right)-6g_0^{(2)}(R)\psi_2(R)=R^3\frac{dg_0^{(2)}(R)}{dR}$$
$$\lim_{R\to0}R^2g_0^{(2)}(R)\frac{d\psi_2(R)}{dR}=0, \tag{11}$$
$$\lim_{R\to\infty}\psi_2(R)=0.$$

The differential equation given in SMT III for $\psi_0(R)$ is not complete:† the correct form is

$$\frac{d}{dR}\left(R^2 g_0^{(2)}(R)\frac{d\psi_0(R)}{dR}\right) = R^3\frac{dg_0^{(2)}(R)}{dR} - 3R^2\frac{\partial g_0^{(2)}(R)}{\partial \log\rho^{(1)}},$$

$$\lim_{R\to 0} R^2 g_0^{(2)}(R)\frac{d\psi_0(R)}{dR} = 0, \tag{12}$$

$$\lim_{R\to\infty}\frac{d\psi_0(R)}{dR} = 0.$$

In SMT III, the second term on the right-hand side of the differential equation does not appear. This correction is due to the physical impossibility of having a stationary state of dilatation, so that $\partial g^{(2)}/\partial t$ must not be neglected. Actually,

$$\frac{\partial g^{(2)}}{\partial t} = \frac{\partial g^{(2)}}{\partial \rho^{(1)}}\frac{\partial \rho^{(1)}}{\partial t} = \left(\frac{\partial g^{(2)}}{\partial \log\rho^{(1)}}\right)_T \nabla\cdot\mathbf{u}, \tag{13}$$

when the equation of continuity is used. The boundary conditions are not affected by this correction.

In this article, the Lennard-Jones intermolecular potential,

$$V(R) = \epsilon\gamma_L(x),$$
$$x = R/a, \tag{14}$$
$$\gamma_L = 4\left(\frac{1}{x^{12}} - \frac{1}{x^6}\right),$$

will be used. With the parameters a and ϵ one may construct a dimensionless or reduced pressure P^*, volume v^*, and temperature T^*,

$$P = P^*(\epsilon/a^3)$$
$$v = v^*(Na^3) \tag{15}$$
$$T = T^*(\epsilon/k).$$

Dimensionless quantities will be denoted by asterisks throughout this article. The differential equations are transformed by the substitution $x = R/a$ to

$$\frac{d}{dx}\left(x^2 g_0^{(2)}(x)\frac{d\psi_0^*(x)}{dx}\right) = x^3\frac{dg_0^{(2)}(x)}{dx} + 3v^* x^2\frac{\partial g_0^{(2)}(x)}{\partial v^*}, \tag{16}$$

$$\frac{d}{dx}\left(x^2 g_0^{(2)}(x)\frac{d\psi_2^*(x)}{dx}\right) - 6g_0^{(2)}(x)\psi_2^*(x) = x^3\frac{dg_0^{(2)}(x)}{dx}, \tag{17}$$

† The authors are indebted to Professor F. P. Buff for pointing this out to them.

where

$$\psi_0^*(x) = \frac{1}{a^2}\psi_0(x), \tag{18}$$

$$\psi_2^*(x) = \frac{1}{a^2}\psi_2(x). \tag{19}$$

These equations are now dimensionless. In terms of reduced variables, the coefficients of bulk and shear viscosity are

$$\varphi = \left(\frac{\zeta}{a}\right)I_0^*, \tag{20}$$

$$\eta = \left(\frac{\zeta}{a}\right)I_2^*, \tag{21}$$

where

$$I_0^* = \frac{\pi}{9T^*v^{*2}}\int^\infty x^3\gamma_L'(x)g_0^{(2)}(x)\psi_0^*(x)dx, \tag{22}$$

$$I_2^* = \frac{\pi}{15T^*v^{*2}}\int_0^\infty x^3\gamma_L'(x)g_0^{(2)}(x)\psi_2^*(x)dx. \tag{23}$$

The momentum contribution to η will be neglected, since it is numerically dominated by the potential contribution in the liquid state.[1] The bulk viscosity does not contain a momentum contribution. Values of a and ϵ were determined for argon by Michels[4] from second virial coefficient data. They are

$$a = 3.405\times10^{-8}\text{ cm},$$
$$\epsilon = 1.653\times10^{-14}\text{ erg}.$$

The numerical value of the friction constant will be presented in Sec. V.

The equilibrium radial distribution function $g_L(cx)$ used in these calculations was described in detail in a recent publication.[3] This function was obtained by solving the appropriate integral equation with the Lennard-Jones potential. In the present article, the viscosity coefficients will be calculated at the boiling point of argon under atmospheric pressure, where the reduced variables of state are $T^* = 0.7454$ and $v^* = 1.223$. The parameter c is introduced into the radial distribution function $g_L(x)$ in order to obtain better agreement between calculated and experimental thermodynamic properties. In particular, the equilibrium pressure of the fluid is calculated by substituting $g_L(cx)$ for $g_0^{(2)}$ in Eq. (7), and the value of c is determined which leads to the experimental pressure. This value is $c = 1.026$ at the normal boiling point. In SMT III, a similar procedure was carried out, with two adjustable parameters, and the experimental pressure and internal energy were used to determine the parameters. In the present article, a much better initial approximation to $g_0^{(2)}$ is used, and only one parameter is adjusted.

[4] Michels, Wijker, and Wijker, Physica **15**, 627 (1949).

When $g_L(cx)$ is substituted for $g_0^{(2)}(x)$ in the differential equation for $\psi_0^*(x)$ and $\psi_2^*(x)$, a simple transformation leads to

$$\psi_0^*(x;\text{ with } g_L(cx)) = (1/c^2)\psi_0^*(cx;\text{ with } g_L(x)) \quad (24)$$

and an exactly similar expression for ψ_2^*. Therefore it is necessary to solve the differential equations only with $g_L(x)$, or $c=1$. Then, the appropriate substitutions lead to,

$$I_0^*(c) = cI_0^*(1) - \frac{16\pi}{3T^*v^{*2}}(c^6-1)c \times \int_0^\infty x^{-10} g_L(x)\psi_0^*(x)dx, \quad (25)$$

$$I_2^*(c) = cI_2^*(1) - \frac{16\pi}{5T^*v^{*2}}(c^6-1)c \times \int_0^\infty x^{-10} g_L(x)\psi_2^*(x)dx, \quad (26)$$

where $I_0^*(c)$ and $I_2^*(c)$ are the values of these functions obtained using $g_L(cx)$ throughout, $I_0^*(1)$ and $I_2^*(1)$ are the values obtained using $g_L(x)$ throughout, and $\psi_0^*(x)$ and $\psi_2^*(x)$ are the functions obtained by solving the differential equations with $g_L(x)$.

III. BULK VISCOSITY

The differential equation (Eq. (16)) for $\psi_0^*(x)$ may be integrated directly. For convenience, $\psi_0^*(x)$ is split into two parts,

$$\psi_0^*(x) = C_1(x) + C_2(x), \quad (27)$$

where

$$C_1(x) = -\int_x^\infty \frac{ds}{s^2 g_0^{(2)}(s)} \int_0^s u^3 \frac{dg_0^{(2)}(u)}{du} du, \quad (28)$$

and

$$C_2(x) = -3v^* \int_x^\infty \frac{ds}{s^2 g_0^{(2)}(s)} \int_0^s u^2 \left(\frac{\partial g_0^{(2)}(u)}{\partial v^*}\right)_T du. \quad (29)$$

These integrals were evaluated numerically, using the radial distribution function $g_L(x)$. The details of this computation are presented in Appendix I. The contributions of $C_1(x)$ and $C_2(x)$ to the integral I_0^* are

$$I_0^* = 0.187 + 0.360 = 0.547.$$

The effect on I_0^* of the correction to the differential equation for ψ_0 is considerable.

In order to calculate $I_0^*(c)$ as a function of the scale factor c, the integral

$$\int_0^\infty x^{-10} g_L(x)\psi_0^*(x)dx = 0.204$$

is needed. Table I, which contains $I_0^*(c)$ as a function of c, was constructed using these values in Eq. (25). The results show that $I_0^*(c) = a\varphi/\zeta$ is quite sensitive to the value of c and therefore to the shape of the radial distribution function. At $c=1.026$, $I_0^*(c)=0.038$. For a slightly higher value of c, $I_0^*(c)$ becomes negative.

In section V, numerical values for ζ and a will be introduced, and the calculation of φ will be completed.

IV. SHEAR VISCOSITY

The differential equation (Eq. 17) for $\psi_2^*(x)$ may be converted into an integral equation,

$$\psi_2^*(x) = C_1(x) - 3k(0)G(x) + 6G(x)\int_x^\infty g_0^{(2)}(s)\psi_2^*(s)ds - 6\int_x^\infty G(s)g_0^{(2)}(s)\psi_2^*(s)ds, \quad (30)$$

where $C_1(x)$ is part of $\psi_0^*(x)$, defined in Sec. III,

$$k(0) = \int_0^\infty x^2[g_0^{(2)}(x) - 1]dx \quad (31)$$

TABLE I.

c	$I_0^*(c)$	$I_2^*(c)$	$\varphi(c)/\eta(c)$
1.000	0.547	0.0696	7.9
1.010	0.362	0.0729	5.0
1.020	0.163	0.0763	2.1
1.026	0.038	0.0784	0.5
1.030	−0.073	0.0799	−0.9
peak	...	0.090	...

and

$$G(x) = \int_x^\infty \frac{1}{u^2 g_0^{(2)}(u)} du. \quad (32)$$

This equation was solved numerically with the radial distribution function $g_L(x)$. The method of solution is described in detail in Appendix II. The function $\psi_2^*(x)$ leads to numerical values

$$I_2^*(1) = 0.06964,$$
$$\int_0^\infty x^{-10} g_L(x)\psi_2^*(x)dx = -0.00451.$$

The column labeled $I_2^*(c)$ in Table I was constructed by substituting these numerical values into Eq. (26). This function is less sensitive to c than $I_0^*(c)$. The peak approximation of SMT III leads to a value I_2^* (labeled "peak" in Table I) which is close to the value obtained using $g_L(cx)$ with $c \approx 1.06$.

The ratio

$$\varphi(c)/\eta(c) = I_0^*(c)/I_2^*(c) \quad (33)$$

is independent of the friction constant, and depends only on the reduced parameters of state v^* and T^*. It is given as a function of c in Table I. The ratio varies

TABLE II.

c	$\zeta(c)\times10^{10}$ g/sec	$\varphi(c)\times10^{3}$ poise	$\eta(c)\times10^{3}$ poise
1.00	3.53	6.34	0.81
1.01	3.27	3.89	0.78
1.02	3.01	1.61	0.75
1.026	2.85	0.36	0.73
1.03	2.74	−0.66	0.72
peak	...	...	0.84
expt	...	...	2.39

considerably with c: at $c=1.026$ it has the value $\varphi/\eta\approx0.5$. There are no reliable experimental results with which to compare this.

In Sec. V, numerical values of ζ, a, and ϵ will be introduced and the calculation of the shear viscosity will be completed.

V. FINAL RESULTS

In Secs. III and IV, computations of the quantities $a\varphi/\zeta$ and $a\eta/\zeta$ were described. In order to complete the calculation of the coefficients of bulk and shear viscosity, the friction constant ζ must be known. The value $\zeta=4.84\times10^{-10}$ g/sec used in SMT III was obtained from an approximate expression for the friction constant using the peak approximation for the radial distribution function. In a forthcoming article, another calculation of the friction constant, by the method of linear trajectories, will be described. This value is

$$\zeta=\left(\frac{m\epsilon}{a^2}\right)^{\frac{1}{2}}\zeta^*, \tag{34}$$

$$\zeta^*=\begin{cases}11.49; & c=1\\ 9.27; & c=1.026,\end{cases}$$

where ζ^* is the friction constant in dimensionless form, at the normal boiling point. This calculation was performed with $g_L(cx)$, for scale factors $c=1$ and $c=1.026$: $\zeta(c)$ is obtained by linear interpolation. In Table II, $\zeta(c)$, $\varphi(c)$, and $\eta(c)$ are tabulated. The coefficient of shear viscosity obtained using this friction constant (with $c=1.026$) and the integrals I_2^* computed with the peak approximation of SMT III is also given in this table. The calculated coefficients of shear viscosity are all too small by a factor of about three. The calculated coefficients of bulk viscosity depend strongly on the value chosen for c.

APPENDIX I

The procedure used in the calculation of $I_0^*(c)$ will be described in detail. Equation (28) was rearranged and integrated by parts to yield

$$C_1(x)=\int_x^\infty\left[\frac{u}{g_0^{(2)}(u)}-u\right]du +3G(x)[k(0)-k(x)]+3h(x); \tag{35}$$

where

$$G(x)=\int_x^\infty\frac{du}{u^2g_0^{(2)}(u)},$$

$$k(x)=\int_x^\infty u^2[g_0^{(2)}(u)-1]du, \tag{36}$$

$$h(x)=\int_0^\infty G(u)u^2[g_0^{(2)}(u)-1]du.$$

The integrals were calculated, and tabulated separately, and then added. For all the numerical integrations, the trapezoidal rule was used, with the intervals 0.01 for $1.00\leqslant x\leqslant1.12$, 0.02 for $1.12\leqslant x\leqslant1.28$, and 0.04 for $1.28\leqslant x\leqslant8.80$. For $x\geqslant8.80$, $g_L(x)$ is uniformly unity and the integrals were therefore evaluated analytically. The values of $g_L(x)$ at 0.01 and 0.02 intervals were obtained by a numerical interpolation on the values at 0.04 intervals.

Although this method may be used to calculate $C_1(x)$ for $x<1$, it was found to be more practical to use the alternative expression

$$C_1(x)=C_1(1)-\int_x^1\frac{du}{u^2g_0^{(2)}(u)}\int_0^u v^3\frac{dg_0^{(2)}(v)}{dv}dv, \tag{37}$$

or, after integrating by parts,

$$C_1(x)=C_1(1)+\frac{x^2-1}{2} +3\int_x^1\frac{du}{u^2g_0^{(2)}(u)}\int_0^u v^2g_0^{(2)}(v)dv. \tag{38}$$

The integral was evaluated numerically, using the trapezoidal rule and an 0.01 interval, for $x<1$.

In order to calculate $C_2(x)$, it is necessary to evaluate the derivative $\partial g_0^{(2)}(x)/\partial v^*$. Since the radial distribution function $g_L(x)$, which was obtained for only four unequally spaced values of v^*, is to be used, the differentiation was performed using Lagrange's interpolation formula. Due to numerical inaccuracies in $g_L(x)$, the resulting derivative is not a smooth function. To remove this roughness, Spencer's analytic smoothing formula[5] was used. For the integrations leading to $C_2(x)$, the trapezoidal rule was used with the same intervals as in the calculation of $C_1(x)$.

APPENDIX II

Equation (17), together with its boundary conditions, is equivalent to the integral equation

$$\psi_2^*(x)=-6\int_x^\infty\frac{dt}{t^2g_0^{(2)}(t)}\int_0^t g_0^{(2)}(s)\psi_2^*(s)ds -\int_x^\infty\frac{dt}{t^2g_0^{(2)}(t)}\int_0^t s^3\frac{dg_0^{(2)}(s)}{ds}ds. \tag{39}$$

[5] E. Whittaker and G. Robinson, *The Calculus of Observations* (Blackie and Sons, London, 1947), p. 290.

When $\int_0^t$ is replaced by $\int_0^\infty - \int_t^\infty$ in the first term of the right-hand side, and the order of integration is changed, this equation is transformed to

$$\psi_2^*(x) = C_1(x) - 3k(0)G(x) + 6G(x)\int_x^\infty g_0^{(2)}(s)\psi_2^*(s)ds - 6\int_x^\infty G(s)g_0^{(2)}(s)\psi_2^*(s)ds, \quad (40)$$

where $C_1(x)$, $G(x)$, and $k(0)$ were defined in Appendix I. In solving this integral equation, the integrals were replaced by sums, using the trapezoidal rule. When the interval is 0.04, the equation becomes

$$\psi_2^*(x) = C_1(x) - 3k(0)G(x) + 0.24\{G(x)\sum_{x+.04}^{\infty} g_0^{(2)}(s)\psi_2^*(s) - \sum_{x+.04}^{\infty} G(s)g_0^{(2)}(s)\psi_2^*(s)\}. \quad (41)$$

Since $C_1(x)$, $G(x)$, $k(0)$, and $g_0^{(2)}(x)$ are known functions, it is clear that if $\psi_2^*(s)$ is known for all s greater than x, then the value of ψ_2^* at x can be obtained directly.

When $x>8.80$, the radial distribution function used here is equal to unity, and the differential equation has an asymptotic solution

$$\psi_2^*(x) \sim b/x^3. \quad (42)$$

If a value of b is chosen arbitrarily, a function $\psi_2^*(x, b)$ may be constructed by integrating analytically from infinity to $x=8.80$ and then step by step to $x=0$. This procedure gives a family of functions, each arising from a different value of b. If the correct b is selected, the resulting $\psi_2^*(x, b)$ is the solution of the integral equation. If the correct b is not used, the resulting $\psi_2^*(x, b)$ does not satisfy the boundary condition at $x=0$. This condition may be converted to a normalization condition. The differential equation for ψ_2^* is integrated once,

$$x^2 g_0^{(2)}(x)\frac{d\psi_2^*(x)}{dx} = 6\int_\infty^x g_0^{(2)}(s)\psi_2^*(s)ds + \int_\infty^x s^3\frac{dg_0^{(2)}(s)}{ds}ds,$$

and the boundary condition is applied, so that,

$$-6\int_0^\infty g_0^{(2)}(s)\psi_2^*(s)ds = \int_0^\infty s^3\frac{dg_0^{(2)}(s)}{ds}ds,$$

or,

$$\int_0^\infty g_0^{(2)}(s)\psi_2^*(s)ds = \tfrac{1}{2}k(0). \quad (43)$$

Therefore, the correct value of b may be found by solving the equation

$$\int_0^\infty g_0^{(2)}(s)\psi_2^*(s, b)ds = \tfrac{1}{2}k(0). \quad (44)$$

Since $\psi_2^*(x, b)$ is linear in b, it is sufficient to evaluate this function for two values of b, solve a linear equation in b, and then interpolate to get the correct $\psi_2^*(x)$.

This procedure was carried out with the radial distribution function $g_L(x)$. When the trapezoidal rule was used to replace integrals by sums, the intervals were the same as in Appendix. I. The functions $\psi_2^*(x, 0)$ and $\psi_2^*(x, -1)$ were calculated, and the correct value of b was found to be $b=1.5209$. This was used to obtain the correct $\psi_2^*(x)$, and the integrals needed to calculate $I_2^*(c)$ were evaluated.

On the Theory of the Virial Development of the Equation of State of Monoatomic Gases

R. J. RIDDELL, JR.,* *Department of Physics and Radiation Laboratory, University of California, Berkeley, California*

AND

G. E. UHLENBECK, *H. M. Randall Laboratory of Physics, University of Michigan, Ann Arbor, Michigan*

(Received May 26, 1953)

The problem of the condensation of a gas is intimately related to the asymptotic behavior of the virial coefficients, B_m, as $m\to\infty$. The problem of the evaluation of the virial coefficients may be divided into two distinctly different ones. The first of these, which is purely combinatorial in nature and is independent of the intermolecular force law, is that of determining the number of a certain type of connected graphs of l points and k lines which are called "stars." This problem is solved by means of generating functions, with the result that the total number of such stars is asymptotically equal to

$$\binom{\frac{1}{2}l(l-1)}{k},$$

for almost all k. Arguments are also presented which indicate that the total number of topologically different stars is

$$\frac{1}{l!}\binom{\frac{1}{2}l(l-1)}{k}.$$

With these results the combinatorial problem is essentially solved.

The second problem is that of evaluating certain integrals of functions which depend on the intermolecular potential. This problem is not so near to a solution. For a purely repulsive force, asymptotic expressions are obtained for $k=l$, and $k=l+1$. The partial contributions to the virial coefficient in these two cases are:

$$(-1)^l\cdot\frac{5}{3}\left(\frac{5}{2\pi}\right)^{\frac{1}{2}}(2b)^{l-1}\frac{(l-1)}{l^{5/2}},$$

and

$$(-1)^l\frac{2\cdot 5^3}{24\pi\sqrt{3}}(2b)^{l-1},$$

respectively. Results for some simple one-dimensional rigid lines are also given.

I. INTRODUCTION

MOST of the explicit theories of the condensation of gases are based on the development of the thermodynamic quantities of the gas in powers of the density or of the inverse of the specific volume.[1] This leads to the well-known virial development of Kamerlingh Onnes for the equation of state:

$$pv=RT\left[1+\frac{B_2(T)}{v}+\frac{B_3(T)}{v^2}+\cdots\right], \qquad (1)$$

in which the deviations of the ideal gas law due to the interaction of the molecules in pairs, triples, etc., are taken successively into account in the successive virial coefficients $B_2(T)$, $B_3(T)$, etc. The theory gives explicit expressions for these virial coefficients in terms of the intermolecular forces, but the actual evaluation of the integrals is notoriously involved and seems quite out of the question for the higher coefficients. The condensation phenomenon depends on the convergence of the series (1),[2] however, and therefore on the asymptotic behavior of the $B_l(T)$ for high l, and we thought that this asymptotic behavior might be simpler to determine, especially for simple force laws, as, for instance, for a gas of elastic spheres.

The motivation to consider especially the case of elastic spheres was the striking and paradoxical result of Kirkwood and co-workers[3] who showed that on the basis of the so-called superposition approximation, a gas of elastic spheres has a transition point at a volume of about 1.24 times the volume of close packing. Although perhaps hard to believe, one must admit that there is no rigorous argument which disproves the existence of such a condensation point, and, since the work of Onsager, one has learned to be rather skeptical about intuitive and approximate arguments. In addition there is the suggestion that perhaps the Kirkwood transition has something to do with the solidification of helium, which is known to occur at temperatures many times the critical temperature, so that it is hard to ascribe it to the weak attractive forces between the helium atoms which are of the order kT_{crit}. The solidification of a gas is

* U. S. Atomic Energy Commission Predoctoral fellow, University of Michigan, 1950–1951.

[1] We have especially in mind the theory of J. E. Mayer; for a summary see his book: *Statistical Mechanics* (John Wiley and Sons, Inc., New York, 1940), Chap. 13. Compare also B. Kahn and G. E. Uhlenbeck, Physica **5**, 399 (1938); B. Kahn, dissertation, University of Utrecht, 1938; J. de Boer, dissertation, University of Amsterdam, 1940; K. Husimi, J. Chem. Phys. **18**, 686 (1950).

[2] Or better on the convergence of the series $\Sigma b_l z^l$, where b_l are the Mayer cluster integrals from which the virial coefficients follow. See Sec. II.

[3] J. G. Kirkwood and E. Monroe, J. Chem. Phys. **9**, 514 (1941); Kirkwood, Maun, and Alder, J. Chem. Phys. **18**, 1040 (1950). See also M. Born and H. S. Green, *A General Kinetic Theory of Liquids* (Cambridge University Press, Cambridge, 1949).

perhaps a general consequence of the sharp repulsive forces, which in first approximation may well be idealized by the elastic sphere model.

On the other hand, the argument of Kirkwood is surely not rigorous either, since it depends on his superposition approximation,[4] and the only way we know of to arrive at a rigorous result is through the convergence discussion mentioned above. Unfortunately, we have not been able to solve the problem of the asymptotic behavior of the b_l and B_l, so that the question of the existence of a transition point for a gas of elastic spheres remains open. We would like to report on some partial results. In Sec. II we will recapitulate the general formula for the cluster integrals b_l and for the virial coefficients B_l, always with the assumption that the intermolecular forces are additive. In this case the expressions for b_l and B_l consist, for large l, of a great number of different integrals over the configuration space of l particles. Therefore two problems can be distinguished; the first one is to determine the number of different integrals and their multiplicities, and the second is to calculate the value of each "irreducible" integral. Such a distinction is of course common to any successive approximation method, and from the Feynman diagrams used in the perturbation theory of quantum mechanics it has become a familiar fact that the first problem can always be formulated as a problem in the theory of linear graphs. One has to count all possible topologically different graphs of a certain kind. In Sec. III the precise formulation of the combinatorial problems will be given in the language of the theory of graphs, and in Secs. IV and V the solution of these problems will be discussed, with special emphasis on the asymptotic behavior for large l of the different numbers involved.[5] The results are of course independent of the form of the intermolecular potential. This enters in the second and more difficult problem, the calculation of the irreducible integrals. We have made no progress with this problem, and in Sec. VI only some remarks and suggestions will be presented.

II. GENERAL EXPRESSIONS FOR THE CLUSTER INTEGRALS AND VIRIAL COEFFICIENTS

For additive intermolecular forces one can write the partition function for N particles in the volume V, followlng Mayer, in the form:

$$Z=\frac{1}{N!}\left(\frac{2\pi mkT}{h^2}\right)^{3N/2}\times\int_V\cdots\int_V d^3r_1\cdots d^3r_N\prod_{i<j=1}^{N}(1+f_{ij}) \quad (2)$$

where $f_{ij}=\exp(-\phi(r_{ij})/kT)-1$, and the product goes over all possible pairs. Consider first the product:

$$\prod_{i<j=1}^{N}(1+f_{ij}),$$

for l particles. If one expands the product, one clearly gets $2^{\frac{1}{2}l(l-1)}$ terms, and each term can be represented by a linear graph if one indicates each particle by a point and each factor f_{ij} by a line between particles i and j. The different terms can first be grouped according to the number of factors f_{ij}, that is, according to the number, k, of lines in the graph. One can further distinguish between

(a) *Separated graphs*, consisting of two or more graphs which are not connected together, and

(b) *Connected graphs*. The so-called cluster function $U_l(\mathbf{r}_1, \mathbf{r}_2, \cdots, \mathbf{r}_l)$ is the sum of all terms represented by connected graphs of l points and the cluster integral is then defined by:

$$b_l=\frac{1}{l!V}\int_V\cdots\int_V d^3r_1\cdots d^3r_l U_l(\mathbf{r}_1, \mathbf{r}_2, \cdots, \mathbf{r}_l). \quad (3)$$

For fixed l and large volume the b_l become asymptotically independent of V, and one can show then that Z becomes a polynomial of degree N in V, given by:

$$Z=\left(\frac{2\pi mkT}{h^2}\right)^{3N/2}\sum_{(m_l)}{}'\prod_l\frac{(Vb_l)^{m_l}}{m_l!} \quad (4)$$

where the round summation sign indicates a sum over all sets of integers $m_1, m_2, \cdots$ with the condition (indicated by the prime):

$$\sum_{l=1}^{N} lm_l=N.$$

Since for large N the partition function Z is related to the free energy per particle $\psi(v, T)$, with $v=\lim(V/N)$ by:[6]

$$Z=\exp(-N\psi/kT) \quad (5)$$

one can then derive the well-known Mayer equations:

$$\begin{aligned} p&=kT\textstyle\sum_l b_l z^l,\\ \frac{1}{v}&=\textstyle\sum_l l b_l z^l, \end{aligned} \quad (6)$$

which express the pressure and the specific volume as power series in the variable z, which is related to the chemical potential of the gas.

To obtain the virial development for the equation of state one must elimlnate z between the two Eqs. (6).

[4] For a criticism of this approximation with regard to the radial distribution function and the value of the fourth virial coefficient for a gas of elastic spheres see B. R. A. Nijboer and L. van Hove, Phys. Rev. **85**, 777 (1952).

[5] Thanks to a communication of Professor G. Pólya the actual counting problems for finite l are almost completely solved also. We will mention the results but omit the proofs, since the asymptotic behavior can be seen by more intuitive arguments. For a similar investigation of the number of different Feynman diagrams in various field theories, see C. A. Hurst, Proc. Roy. Soc. (London) **214**, 44 (1952); also, R. J. Riddell, Jr., Phys. Rev. **91**, 1243 (1953).

[6] For a rigorous proof of these statements, see L. van Hove, Physica **15**, 951 (1949).

Formally this can be done as follows: define a set of quantities $\beta_\nu(T)$, $\nu=1, 2, \cdots$ by the prescription that $l^2 b_l$ is to be the coefficient of t^{l-1} in $\exp(l\sum \beta_\nu t^\nu)$. This gives, for instance:

$$b_2=\tfrac{1}{2}\beta_1,$$
$$b_3=\tfrac{1}{3}\beta_2+\tfrac{1}{2}\beta_1^2,$$
$$b_4=\tfrac{1}{4}\beta_3+\beta_1\beta_2+\tfrac{2}{3}\beta_1^3,$$

and so on. One can solve successively for the β_ν in terms of the b_l, and thus one sees that the two sets of quantities b_l and β_ν are uniquely related to each other. Then one can show[7] that from (6) follows:

$$\frac{p}{kT}=\frac{1}{v}-\sum_{\nu=1}^{\infty}\frac{\nu}{\nu+1}\beta_\nu\frac{1}{v^{\nu+1}}, \tag{7}$$

so that the l'th virial coefficient B_l is given by

$$B_l=-\frac{(l-1)}{l}\beta_{l-1}. \tag{8}$$

The question arises how to express the β_ν as an integral over the configuration space of ν particles, analogous to the expression (3) for b_l. To do this one has to separate the terms represented by connected graphs, which enter in U_l, in two groups in the following way. An *articulation point* of a graph is a point where the graph could be cut[8] into two or more separated graphs by cutting all the lines going to this point. A connected graph which has no articulation points will be called a *star*. From the terms represented by connected graphs of l points, select the terms which are represented by stars. The sum of these terms will be called the *star function*, $V(\mathbf{r}_1, \mathbf{r}_2, \cdots, \mathbf{r}_l)$, and Mayer proves that:

$$\beta_\nu=\frac{1}{\nu!V}\int_V\cdots\int_V d^3\mathbf{r}_1\cdots d^3\mathbf{r}_{\nu+1}V(\mathbf{r}_1, \cdots, \mathbf{r}_{\nu+1}). \tag{9}$$

Equations (3) and (9) are the starting point of our considerations.

III. COMBINATORIAL PROBLEMS IN THE THEORY OF GRAPHS[9]

The simplest type of connected graph is the so-called *Cayley tree*. They consist of l points and $l-1$ lines, from which follows that there are no closed loops in a Cayley tree. A more general type of connected graph may be called *Husimi trees*, since they were first introduced in a paper by Husimi.[10] A Husimi tree is a connected graph in which no line lies on more than one cycle. It is characterized by the numbers $n_2, n_3, n_4, \cdots$ of lines, triangles, quadrilaterals, etc., out of which it is built up. The number of points, l, is equal to $1+n_2+2n_3+\cdots$. A *pure* Husimi tree is one which consists of only one type of figure. Clearly a Cayley tree is a special case of a pure Husimi tree.

A general connected graph is divided by its articulation points into a number of stars. If in each star one would disregard all internal lines and consider only the "outline" one would obtain a Husimi tree. In this sense the general connected graph is a generalization of the Husimi tree, just as a star is a generalization of a polygon.

There are two kinds of combinatorial problems connected with each type of graph. The *first* and simplest kind of problem is to find the number of different graphs if *all* points are distinguished from each other. For Cayley trees of l points, the answer[11] is simply l^{l-2}. For Husimi trees of l points and type $n_2, n_3, \cdots$ the answer[10] is:

$$\frac{l!}{\prod_{i=2}^{l}[(i-1)!]^{n_i}n_i!}\,l^{\sum_{i=2}^{l}n_i-2} \tag{10}$$

which clearly specializes to l^{l-2} for Cayley trees. In the next section we will determine the numbers $d(l, k)$ and $c(l, k)$ of separated (or disjoint) and of connected graphs of l points and k lines, always assuming that all points are distinguished from each other. Clearly:

$$d(l, k)+c(l, k)=\binom{\frac{1}{2}l(l-1)}{k}. \tag{11}$$

In addition we will find the fraction of the connected graphs which are stars. Let $s(l, k)$ denote their number.

The numbers $c(l, k)$ and $s(l, k)$ for all possible values of k indicate how many terms are involved in the cluster and star function of l points. However if one integrates over the configuration space of the l points, all terms which differ only in the labelling of the l points will clearly give the same results. To find the number of "irreducible" integrals in (3) and (9) one has to determine the number of connected graphs and stars which are really different. This brings us to the *second* and more difficult kind of problem: to find the number of topologically different graphs of a certain type if the points are *not* distinguishable. For Cayley trees the problem has been solved in all details,[12] and a beginning has been made for the case of Husimi trees of type $n_2, n_3, \cdots$.[13] In Sec. V we will give the answer for the numbers $\delta(l, k)$ and $\gamma(l, k)$ of separated and of con-

[7] For the proof see B. Kahn and G. E. Uhlenbeck, reference 1.
[8] Therefore it is also often called a "cutting point."
[9] For the general topological theory of linear graphs see the book of Koenig, *Theorie der Endlichen und Unendlichen Graphen* (Leipzig, 1936). Combinatorial questions are not discussed in this book. For these the basic reference is the paper of G. Pólya, Acta Math. **68**, 145 (1938).
[10] K. Husimi, J. Chem. Phys. **18**, 682 (1950).
[11] A. Cayley, *Collected Mathematical Papers* (Cambridge 1889-1898) Vol. 13, p. 26; other proofs are given by Pólya, reference 9, and by G. Bol, Abhardl. Math. Seminar Hamburg **12**, 242 (1938).
[12] R. Otter, Ann. Math. **49**, 583 (1948).
[13] F. Harary and G. E. Uhlenbeck, Proc. Natl. Acad. U. S. **39**, 315 (1953).

nected graphs of l points and k lines which are topologically different. The corresponding number, $\sigma(l, k)$, for stars is not yet known.

We will denote by $d_i(l, k)$, $c_i(l, k)$, and $s_i(l, k)$ the number of separated graphs, connected graphs, and stars of l points and k lines and of a definite topological type indicated by the index i, so that:

$$d(l,k)=\sum_{i=1}^{\delta(l,k)} d_i(l,k),$$

$$c(l,k)=\sum_{i=1}^{\gamma(l,k)} c_i(l,k), \tag{12}$$

$$s(l,k)=\sum_{i=1}^{\sigma(l,k)} s_i(l,k).$$

As an example we have drawn in Fig. 1 all topologically different graphs of five points, arranged according to the value of k. The numbers in parentheses refer to the number of times the graph occurs, and represent therefore the $d_i(5, k)$, $c_i(5, k)$, $s_i(5, k)$. One can also read off the numbers $\delta(5, k)$, $\gamma(5, k)$, and $\sigma(5, k)$. For instance, $\delta(5, 6)=1$, $\gamma(5, 6)=5$ of which two are stars so $\sigma(5, 6)=2$. In terms of these numbers one can then express the cluster integrals and the virial coefficients as follows:

$$b_l=\frac{1}{l!V}\sum_{k=l-1}^{\frac{1}{2}l(l-1)}\sum_{i=1}^{\gamma(l,k)} c_i(l,k)\mathfrak{F}_c^{(i)}(l,k),$$

$$B_l=-\frac{(l-1)}{l!V}\sum_{k=l}^{\frac{1}{2}l(l-1)}\sum_{i=1}^{\sigma(l,k)} s_i(l,k)\mathfrak{F}_s^{(i)}(l,k). \tag{13}$$

$\mathfrak{F}_c^{(i)}(l, k)$ and $\mathfrak{F}_s^{(i)}(l, k)$ are the irreducible integrals for the connected graph and star of l points, k lines, and of the i'th topological type.

IV. THE NUMBERS $d(l,k)$, $c(l, k)$, AND $s(l, k)$

Let us begin with the separated configurations. Since a separated configuration is made up of a number (at least two) of connected graphs, and since the numbers $d(l, k)$ and $c(l, k)$ are related by Eq. (11), it is evident that one must be able to express $d(l, k)$ in the d's involving smaller numbers of particles. To formulate this relation, let the separated configuration of l points and k lines consist of n_1 isolated points, n_2 connected pairs of points, n_3 connected triples of points, etc. Let j be an index which distinguishes between the n_i different connected graphs of i particles, and let k_{ij} be the number of lines in the j'th graph. Clearly one must have:

$$\sum_{i=1}^{l-1} in_i=l,\quad \sum_{i=2}^{l-1}\sum_{j=1}^{n_i} k_{ij}=k. \tag{14}$$

The upper limit of i is $l-1$, since one must have at least one point separated from the rest of the graph. One then

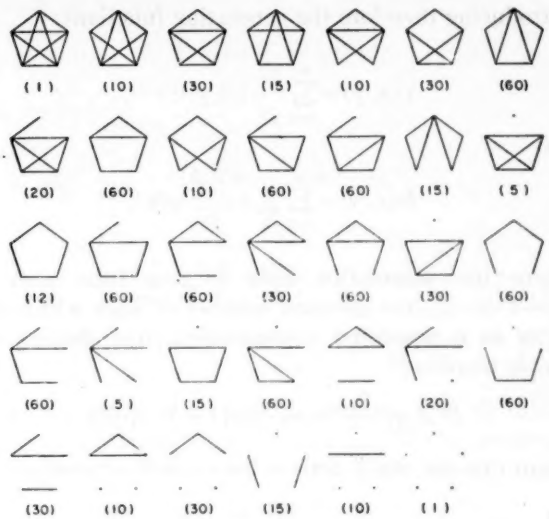

FIG. 1. Topologically different graphs of five points.

can convince oneself that:

$$d(l,k)=S'_{(n_i)}\prod_{i=1}^{l-1}\frac{l!}{(i!)^{n_i}n_i!}\times S'_{(k_{ij})}\prod_{j=1}^{n_i}\left\{\binom{\frac{1}{2}i(i-1)}{k_{ij}}-d(i,k_{ij})\right\}, \tag{15}$$

where the round summation signs go over all sets of numbers n_i and k_{ij} consistent with the relations (14), of which one is reminded by the primes. One can remove these restrictions by multiplying (15) by $x^l y^k$, and one can then write:

$$\frac{d(l,k)}{l!}=\text{coefficient of } x^l y^k \text{ in:}$$

$$S_{(n_i)}\prod_{i=1}^{l-1}\frac{1}{(i!)^{n_i}n_i!}S_{(k_{ij})}\prod_{j=1}^{n_i}\left\{\binom{\frac{1}{2}i(i-1)}{k_{ij}}-d(i,k_{ij})\right\}x^{i}y^{k_{ij}}.$$

The sums over the k_{ij} are readily carried out, to give:

$$\frac{d(l,k)}{l!}=\text{coefficient of } x^l y^k \text{ in:}$$

$$S_{(n_i)}\prod_{i=1}^{l-1}\frac{1}{n_i!}\left\{(1+y)^{\frac{1}{2}i(i-1)}\frac{x^i}{i!}-\sum_{k=0}^{\frac{1}{2}(i-1)(i-2)}\frac{d(i,k)}{i!}x^i y^k\right\}^{n_i}.$$

If one adds and subtracts the term for $i=l$, then the product may be taken to infinity since terms with $i>l$ will not contribute to the coefficient of x^l. One thus obtains:

$$\frac{1}{l!}\binom{\frac{1}{2}l(l-1)}{k}=\text{coefficient of } x^l y^k \text{ in:}$$

$$\exp\left[\sum_{i=1}^{\infty}\frac{x^i}{i!}(1+y)^{\frac{1}{2}i(i-1)}-\sum_{i,k}\frac{d(i,k)}{i!}x^i y^k\right].$$

Introducing therefore the generating functions:

$$N(x,y)=\sum_{i=1}^{\infty}\frac{x^i}{i!}(1+y)^{\frac{1}{2}i(i-1)},$$

and

$$D(x,y)=\sum_{l=1}^{\infty}\sum_{k}\frac{d(l,k)}{l!}x^l y^k,$$

where the summation over k goes from zero to $\frac{1}{2}(l-1)(l-2)$, the greatest number of lines which can occur in a separated configuration, one obtains the simple relation:[14]

$$D(x,y)=N(x,y)-\ln\{1+N(x,y)\}. \tag{16}$$

From this one easily derives the explicit expression:

$$d(l,k)=\sum_{r=2}^{l}\frac{(-1)^r}{r}\underset{(li)}{S'}\frac{l!}{l_1!l_2!\cdots l_r!}\binom{\sum_{i=1}^{r}\frac{1}{2}l_i(l_i-1)}{k}, \tag{17}$$

where in the round sum the l_i all start from one and the prime means the condition $l_1+l_2+\cdots+l_r=l$. For k near the upper limit, $\frac{1}{2}(l-1)(l-2)$, only the terms with $r=2$, $l_1=1$, $l_2=l-1$, or vice versa, contribute, so that for $k>\frac{1}{2}(l-2)(l-3)+1$:

$$d(l,k)=l\binom{\frac{1}{2}(l-1)(l-2)}{k}. \tag{18}$$

For smaller k one gets corrections to this number, the first of which are:

$$\tfrac{1}{2}l(l-1)\binom{\frac{1}{2}(l-2)(l-3)+1}{k}-l(l-1)\binom{\frac{1}{2}(l-2)(l-3)}{k}. \tag{19}$$

For large l this can be written:

$$d(l,k)\cong l\binom{\frac{1}{2}(l-1)(l-2)}{k}\left[1-\frac{l}{2}e^{-2k/l}+\cdots\right], \tag{20}$$

so that for $k>l\log l$ the correction goes to zero for $l\to\infty$. In the main range of values for k, Eq. (18) gives the asymptotic behavior for large l of the number of separated configurations. Only for small k, for which $d(l,k)$ is small anyway, does Eq. (18) fail for large l.

Turning now to the numbers of stars, $s(l,k)$, among the connected graphs of l points and k lines, we first derive a recurrence relation for the number of connected graphs, $c(l,k)$, which is based on the idea that any connected graph can be considered to be built up out of stars which are connected to each other at the articulation points. To formulate this more precisely, let the connected graph consist of n_2 stars of two points (bars), n_3 stars of three points (triangles), n_4 stars of four points (rectangles with zero, one or two diagonal lines), etc. Let j distinguish between the n_i different stars of i points, and let k_{ij} be the number of lines in the j'th star. One must have of course:

$$\sum_{i=2}^{l}(i-1)n_i=l-1,\quad \sum_{i=2}^{l}\sum_{j=1}^{ni}k_{ij}=k. \tag{21}$$

The upper limit for i is l since the connected graph may just be one star of points. Similarly to Eq. (15), one now has:

$$c(l,k)=\underset{(ni)}{S'}H(n_2,n_3,\cdots)\underset{(kij)}{S'}\prod_{i=1}^{l}\prod_{j=2}^{ni}s(i,k_{ij}), \tag{22}$$

where $H(n_2,n_3,\cdots)$ is the number of Husimi trees of type $n_2, n_3, \cdots$ given by Eq. (10), and the two primes refer to the two conditions (21). Removing these conditions again by multiplying with $x^{l-1}y^k$, one obtains:

$c(l,k)=$ coefficient of $x^{l-1}y^k$ in:

$$\frac{l!}{l^l}\exp\left\{l\sum_{i=2}^{\infty}\sum_{k=i}^{\frac{1}{2}i(i-1)}\frac{s(i,k)}{(i-1)!}x^{i-1}y^k\right\}. \tag{23}$$

If we now introduce the generating function:

$$S(x,y)=\sum_{l=2}^{\infty}\sum_{k=l}^{\frac{1}{2}l(l-1)}\frac{s(l,k)}{l!}x^l y^k,$$

and use Eq. (11), one can write (23) in the form:

$\binom{\frac{1}{2}l(l-1)}{k}-d(l,k)=$ coefficient of $x^{l-1}y^k$ in:

$$\frac{l!}{l^l}\exp\left\{l\frac{\partial S(x,y)}{\partial x}\right\}. \tag{24}$$

If we multiply this equation by $(l/l!)x^l y^k$, sum over all l and k, and use Eq. (16), we get:

$$z(x,y)=\sum_{l=1}^{\infty}\frac{x^l}{l!}\left\{\frac{d^{l-1}}{d\xi^{l-1}}\exp\left[l\frac{\partial S(\xi,y)}{\partial\xi}\right]\right\}_{\xi=0},$$

where $z(x,y)$ is defined as:

$$z(x,y)=x\frac{\partial}{\partial x}\ln\{1+N(x,y)\}. \tag{25}$$

From Lagrange's theorem[15] then follows:

$$\frac{\partial S(z,y)}{\partial z}=\ln\frac{z}{x}. \tag{26}$$

[14] We assume the convention that $d(1,0)=0$.

[15] See for instance Whittaker and Watson, *Modern Analysis*, Chap VII (Macmillan, New York, 1944). In order that Eq. (26) is valid for all l and k, we assume the following conventions: $s(1,0)=0$, $c(1,0)=1$; $s(2,1)=c(2,1)=1$.

It is not possible to obtain from (25) and (26) an explicit expression for $s(l, k)$, since expressing x in terms of y and z through (25) involves the inversion of a power series. However, one can obtain an asymptotic expression for large l. To do this it is easier to start from Eq. (24). By developing the exponential function and by taking in the different powers of $l\partial S/\partial x$ always the coefficients of the highest powers of y, one obtains a recurrence relation of the form:

$$\binom{\frac{1}{2}l(l-1)}{k}-d(l,k)=s(l,k)+l(l-1)s(l-1,k-1)$$
$$+\tfrac{1}{2}l(l-1)(l-2)s(l-2,k-3)$$
$$+\tfrac{1}{2}l^2(l-1)(l-2)s(l-2,k-2)+\cdots,$$

in which the further terms depend on the number of stars with less than $l-2$ points. From this one sees that in first approximation for large l:

$$s(l,k)\cong\binom{\frac{1}{2}l(l-1)}{k}. \tag{27}$$

In second approximation, using (18):

$$s(l,k)\cong\binom{\frac{1}{2}l(l-1)}{k}-l\binom{\frac{1}{2}(l-1)(l-2)}{k}$$
$$-l(l-1)\binom{\frac{1}{2}(l-1)(l-2)}{k-1}. \tag{28}$$

This expression is exact for $k>\frac{1}{2}(l-2)(l-3)+1$. In the next approximation one finds further correction terms which contribute for smaller values of k. Just as for the $d(l, k)$, we can conclude that for large l and almost all k (in fact again for $k>l\log l$), Eq. (27) will give the number of stars, or in other words for large l practically all graphs of k lines are stars. From Eq. (28) one can see further that for large l the number of connected graphs with at least one articulation point is asymptotically:

$$l(l-1)\binom{\frac{1}{2}(l-1)(l-2)}{k-1}. \tag{29}$$

V. THE NUMBERS $\delta(l, k)$, $\gamma(l, k)$, and $\sigma(l, k)$.

The first problem is to determine the total number:

$$\pi(l,k)=\delta(l,k)+\gamma(l,k), \tag{30}$$

of topologically different graphs of l points and k lines, which is the analogue of the binomial coefficient $\binom{\frac{1}{2}l(l-1)}{k}$ in Eq. (11). This problem has been solved by Pólya.[16] He expresses his result in terms of the generating function:

$$F_l(y)=\sum_k \pi(l,k)y^k$$

and he finds:

$$F_l(y)=\sum_{(j_r)}{}' \frac{1}{\prod_r j_r!r^{j_r}} \prod_{r=\text{odd}} (1+y^r)^{\frac{1}{2}(r-1)j_r}$$
$$\cdot \prod_{r=\text{even}} [(1+y^{r/2})(1+y^r)^{\frac{1}{2}(r-2)}]^{j_r}$$
$$\cdot \prod_r (1+y^r)^{\frac{1}{2}rj_r(j_r-1)} \cdot \prod_{r<s} (1+y^{m(r,s)})^{t(r,s)j_rj_s}. \tag{31}$$

Here the round summation sign goes over all sets of integers j_r, starting from zero, which fulfill the condition:

$$\sum_{r=1}^{l} rj_r=l.$$

$m(r, s)$ is the least common multiple and $t(r, s)$ the greatest common divisor of r and s. Take for example $l=5$; the sum consists then of seven terms corresponding to the seven partitions $5=1+1+1+1+1$, $5=1+1+1+2$, $5=1+1+3$, $5=1+2+2$, $5=1+4$, $5=2+3$, $5=5$, for which one finds:

$$5!F_5(y)=(1+y)^{10}+(1+y)^4(1+y^2)^3+20(1+y)(1+y^3)^3$$
$$+15(1+y)^2(1+y^2)^4+30(1+y^2)(1+y^4)^2$$
$$+20(1+y)(1+y^3)(1+y^6)+24(1+y^5)^2.$$

This leads to:

$$F_5(y)=1+y+2y^2+4y^3+6y^4+6y^5$$
$$+6y^6+4y^7+2y^8+y^9+y^{10},$$

from which one can read off $\pi(5, k)$, which can be checked with Fig. 1.

From Eq. (31) one can also derive the asymptotic behavior of $\pi(l, k)$ for large l. Taking only the partitions of l in l one's and in $l-2$ one's and one two, one gets:

$$l!F_l(y)=(1+y)^{\frac{1}{2}l(l-1)}$$
$$+\tfrac{1}{2}l(l-1)(1+y)^{\frac{1}{2}(l-2)(l-3)+1}(1+y^2)^{l-2}+\cdots \tag{32}$$

from which one sees that for large l the main contribution to $\pi(l, k)$ comes from the first term, so that:

$$\pi(l,k)\cong\frac{1}{l!}\binom{\frac{1}{2}l(l-1)}{k}. \tag{33}$$

From the second term in (32) one can find corrections to this result, which however vanish for large l and for k not too near the two ends of its range, zero and $\frac{1}{2}l(l-1)$.[17]

[16] We are greatly indebted to Professor G. Pólya for communicating his result to us. In this section we will omit the proofs, since they would take up too much space, and since we hope that they will appear elsewhere. They can be found in the dissertation of R. J. Riddell (Ann Arbor, 1951, p. 57.)

[17] We are indebted to Dr. P. Erdös for communicating to us various estimates for the range of k for which our asymptotic results are valid. With regard to Eq. (33) he thinks that k must lie in the range

$$k>(1+\epsilon)l(\log l)>\tfrac{1}{2}l(l-1)-k,$$

just as for Eqs. (18) and (27).

The next question is the determination of the number $\delta(l, k)$ of separated configurations, which are topologically different. The answer[18] can be expressed as follows: Define the double generation functions as

$$P(x, y)=\sum_{l=0}^{\infty} F_l(y)x^l=\sum_l \sum_k \pi(l, k)x^l y^k,$$
$$\Delta(x, y)=\sum_l \sum_k \delta(l, k)x^l y^k. \tag{34}$$

Then one can prove the relation

$$\sum_\nu \frac{1}{\nu}\Delta(x^\nu, y^\nu)=\sum_\nu \frac{1}{\nu}\{P(x^\nu, y^\nu)+(-1)^\nu P^\nu(x, y)\}, \tag{35}$$

from which one can find the $\delta(l, k)$ in terms of the known $\pi(l, k)$. Especially one can show from Eq. (35) that for large l and a suitable range of k, one has

$$\delta(l, k)\cong\frac{1}{(l-1)!}\binom{\frac{1}{2}(l-1)(l-2)}{k}. \tag{36}$$

We have not succeeded in splitting the number of topologically different stars $\sigma(l, k)$ from the number of connected graphs $\gamma(l, k)=\pi(l, k)-\delta(l, k)$. However, there is no doubt that for large l, $\sigma(l, k)\cong\pi(l, k)$, and that the number of topologically different connected graphs with at least one articulation point is asymptotically

$$\frac{1}{l!}l(l-1)\binom{\frac{1}{2}(l-1)(l-2)}{k-1}. \tag{37}$$

The reason is simply that for large l the great majority of all graphs are stars as we saw in Sec. IV, and that only very rarely will a graph have some kind of symmetry. As a result for large l the numbers $d_i(l, k)$, $c_i(l, k)$, $s_i(l, k)$ will be just $l!$ for practically all i, so that (see Eq. (12)) asymptotically $\delta(l, k)$, $\gamma(l, k)$, and $\sigma(l, k)$ will be $(1/l!)$ times $d(l, k)$, $c(l, k)$, and $s(l, k)$.

Finally we will consider a few special cases, which have some interest for themselves and which will illustrate further the relation between the numbers $s(l, k)$, $s_i(l, k)$, and $\sigma(l, k)$. First consider the case $k=l$. All stars are in the form of a ring, so $\sigma(l, l)=1$. The points can be put on the ring in any order, which gives a factor $l!$ in $s(l, l)$. However we may choose any point as the starting point, and we may count either clockwise or counter-clockwise around the ring without changing the configuration. This gives a "symmetry number" $2l$ by which the $l!$ has to be divided. So:

$$s(l, l)=\tfrac{1}{2}(l-1)! \tag{38}$$

If $k=l+1$ the stars take the form of three chains connected at their ends, in which there may be l_1 particles in the first chain, l_2 in the second, and l_3 in the third (not counting the end particles), so that $l_1+l_2+l_3=l-2$. Not more than one chain may have $l_i=0$. Any partition therefore of $l-2$ in two or three summands will correspond to a star of a definite topological type. The number $\sigma(l, l+1)$ is the number of such partitions and these can be found by standard methods. One can show that $\sigma(l, l+1)$ is the coefficient of y^{l-2} in

$$\frac{1}{(1-y)(1-y^2)(1-y^3)}-\frac{1}{1-y},$$

and explicit expressions can easily be obtained. Especially for large l one finds that $\sigma(l, l+1)\cong l^2/12$. To find $s_i(l, l+1)$, note that if all chains are different there is only a mirror symmetry between left and right, but if some chains are alike, then these chains may be interchanged as well. Thus we obtain:

$$s_i(l, l+1)=l!/2n_i!$$

where n_i is the number of chains which are alike. Since for large l it will be a rare case if two or more chains are alike, it is clear that asymptotically $s(l, l+1)\cong l!l^2/24$, and it is also not difficult to show that exactly

$$s(l, l+1)=(l!/24)(l-3)(l-2). \tag{39}$$

The fact that for $k=l+1$ all stars take the form of three chains is expressed in the theory of graphs by saying that all stars are *homeomorphic* to each other. If k increases, the number of homeomorphic types increases too. For instance for $k=l+2$ there are four homeomorphisms, as shown in Fig. 2. To find for each type the number of topologically different stars, is again a partition problem of $l-2$, $l-3$, or $l-4$ in four, five, or six parts. The $s_i(l, l+2)$ are $l!/s_i$ where s_i is the number of symmetry operations which may be performed on the star without changing it. For instance if in the four types (a), (b), (c), and (d) the chains are all alike s_i will have the values $2\cdot 4!(a)$; $2^3(b)$; $4!(c)$; $2^4(d)$. Finally by summing over all partitions one can determine $s(l, l+2)$ for each of the four types. We will not write down the explicit numbers, and mention only that altogether

$$s(l, l+2)=\frac{l!}{48\cdot 4!}(l-3)(l^4+4l^3-15l^2-46l-40). \tag{40}$$

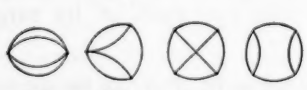

FIG. 2. Homeomorphic types of graphs for $k=l+2$.

[18] For the proof, see R. J. Riddell, dissertation, University of Michigan, 1951, p. 65.

VI. REMARKS ON THE INTEGRAL PROBLEM

1. If the intermolecular force is always repulsive the $f_{ij}(r)$ of Eq. (2) will always by negative. Hence the sign of all the irreducible integrals $\mathfrak{J}^{(i)}(l, k)$ will be $(-1)^k$. With regard to the absolute magnitude it is clear that the star integrals must decrease with increasing k, be-

cause adding a line between two points means that we introduce a factor in the integrand which requires the two points to be less than a certain distance apart. Thus with increasing k the integrand will differ from zero over a smaller region of the $3l$ dimensional phase space. This is illustrated for the three stars of four points by the following known results for the integrals:[19]

$$\square = 2.5905b^3; \quad \frac{16}{3}b^3,$$

$$\boxslash = -1.8894b^3; \quad -\frac{14}{3}b^3, \tag{41}$$

$$\boxtimes = 1.2728b^3; \quad \frac{12}{3}b^3.$$

The second column gives the values of the integrals in one dimension; b is the van der Walls' b equal to four times the proper volume of a molecule in three dimensions, and equal to just the volume in one dimension.

2. In three dimensions the cluster integrals b_l and virial coefficients B_l for a gas of elastic spheres are only known up to $l=4$. In one dimension on the other hand one knows that:

$$B_l = b^{l-1},$$
$$b_l = \frac{(-1)^l l^{l-1}}{l!} b^l. \tag{42}$$

Note that the B_l are all positive and the b_l are alternating in sign. Whether this is also so in three dimensions is not known, but is plausible.

One might hope to gain insight into the relation between the numbers $s(l, k)$ and the integral $\mathfrak{z}_s(l, k)$ by considering the one-dimensional case in greater detail. For all configurations the integrals are elementary and can be calculated successively. For instance for $l=5$ the results for $\mathfrak{z}_s^{(i)}(l, k)$ together with the $s_i(l, k)$ are given in Table I. It would be of interest to do the calculation for arbitrary l and k, and to see especially what the asymptotic behaviour of the $\mathfrak{z}_s(l, k)$ is for large l. But we have not succeeded in doing that.[20]

3. Because of the alternating sign of the $\mathfrak{z}_s(l, k)$ for repulsive forces the alternating moments of the $s(l, k)$ may be of interest. These can all be calculated from the general formulas, Eq. (25) and Eq. (26). Defining

$$M_s^{(n)}(l) = \sum_{k=l}^{\frac{1}{2}l(l-1)} (-1)^k k^n s(l, k),$$

TABLE I. Decomposition of the 5th virial coefficient for one-dimensional rigid lines.

TYPE	⬠	⬟	⋈	⬠	⋈	⋈	⬟	⋈	⬟	★
$b^{-4}\times s_S^{(i)}(5,k)$	$-\frac{115}{12}$	$+\frac{49}{6}$	$+8$	$-\frac{29}{4}$	$-\frac{41}{6}$	$-\frac{15}{2}$	$+6$	$+\frac{19}{3}$	$-\frac{11}{2}$	$+5$
$S_i(5,k)$	12	60	10	60	30	10	15	30	10	1

one finds for instance:

$$M_s^{(0)}(l) = -(l-2)!,$$
$$M_s^{(1)}(l) = -\tfrac{1}{2}l!, \tag{43}$$
$$M_s^{(2)}(l) = -\tfrac{1}{8}l!(l^2+3l-6).$$

Analogous formulas can be found for the alternating moments of $d(l, k)$ and therefore of $c(l, k)$. However, we have not been able to exploit these results for the general problem.

4. Since for repulsive forces the f_{ij} have always the same sign one may interpret f_{ij} as the (unnormalized) probability of going from the point i to the point j. For a linear chain of n particles the integral,

$$I(\mathbf{r}_1, \mathbf{r}_n) = \int \cdots \int d^3r_2 \cdots d^3r_{n-1} f_{12} f_{23} \cdots f_{n-1,n}, \tag{44}$$

can then be considered as the probability of going from $\mathbf{r}_1$ to $\mathbf{r}_n$ by a random walk of $n-1$ steps, and from the central limit theorem one knows that $I(\mathbf{r}_1, \mathbf{r}_n)$ will become a Gaussian distribution for large n. In fact for the case of elastic spheres ($f(|\mathbf{r}_i-\mathbf{r}_j|)=-1$ for $|\mathbf{r}_i-\mathbf{r}_j|<d$ and zero otherwise) one easily shows that asymptotically

$$I(\mathbf{r}_1, \mathbf{r}_n) \cong (-1)^n \frac{(2b)^n}{(2\pi)^3} \left(\frac{10\pi}{nd^2}\right)^{\frac{3}{2}} \exp\left(-\frac{5r^2}{2nd^2}\right), \tag{45}$$

with $b=2\pi d^3/3$ and $r=|\mathbf{r}_1-\mathbf{r}_n|$. For $n=3$, Eq. (45) already gives a close approximation.

If, therefore, the star consists of a number of connected chains, which are long enough so that (45) can be applied, then the integrand of the star integral becomes a Gaussian distribution in the linkage points of the chains, and the evaluation becomes straightforward.[21] For instance, for the ring integrals $\mathfrak{z}_s(l, l)$ one gets simply:

$$\mathfrak{z}_s(l, l) \cong I(0) = (-1)^l \frac{(2b)^{l-1}}{l^{\frac{3}{2}}} \frac{5}{3} \left(\frac{10}{\pi}\right)^{\frac{3}{2}},$$

so that, if one writes Eq. (13) in the form

$$B_l = \sum_{k=l}^{\frac{1}{2}l(l-1)} B(l, k), \tag{46}$$

[19] The irreducible integrals in two dimensions have also been evaluated by Harris, Sells, and Guth (to be published).

[20] Using Eq. (13) one finds from Table I $B_5=b^4$ in agreement with (42). For $l=4$ the numbers $s(l, k)$ are 3, 6, 1 and from (41) then follows $B_4=b^3$, again in agreement with (42).

[21] The fact that for a single chain the integral (44) can always be reduced to a single integral by a Fourier transformation (since (44) is obtained by folding the function $f(r)$ $(n-1)$ times) was first noted by E. W. Montroll and J. E. Mayer [J. Chem. Phys. 9, 626 (1941)]. Also Eq. (45) and the results for the ring and three chain integrals can be found essentially in this paper.

one gets, using (38):

$$B(l,l)\cong(-1)^{l-1}\frac{l-1}{l!}(2b)^{l-1}\frac{5}{3}\left(\frac{5}{2\pi}\right)^{\frac{1}{2}}. \quad (47)$$

For $l=3$, this differs from the well known exact value $5b^2/8$ by 22 percent; for $l=5$, the error is only 12 percent. For the case $k=l+1$, where the stars take the form of three chains linked at their ends, the integral becomes

$$\mathfrak{I}_*^{(i)}(l,l+1)\cong(-1)^{l+1}\frac{250}{9\pi}(2b)^{l-1}$$
$$\times[(l_1+1)(l_2+1)+(l_2+1)(l_3+1)+(l_3+1)(l_1+1)]^{-\frac{1}{2}},$$

where l_1, l_2, l_3 are the numbers of particles in the chains, so that $l_1+l_2+l_3=l-2$. Using the result of Sec. V on the $s_i(l,l+1)$, one can show that for large l:

$$B(l,l+1)=(-1)^l\frac{250}{9}(2b)^{l-1}. \quad (48)$$

In principle one can go on in this way. For $k=l+2$ one has to consider the four homeomorphisms shown in Fig. 2, and the calculation (especially the summation over all the numbers of particles in the different chains) becomes rapidly more involved, so that we have not been able to go further.

THE JOURNAL OF CHEMICAL PHYSICS VOLUME 21, NUMBER 11 NOVEMBER, 1953

Dynamics of the Graphite Lattice*

HERBERT B. ROSENSTOCK
U. S. Naval Research Laboratory, Washington, D. C.

(Received July 7, 1953)

The distribution of frequencies of normal vibrations in the graphite lattice has been obtained in closed form for low temperatures in the two-dimensional approximation for the values $(\alpha,\beta,0)$ and $(\alpha,\beta,\alpha/2)$ of the force constants (α,β,γ) for nearest, second-nearest, and third-nearest neighbors. The frequencies run from 0 to a finite value ω_{max}, with two logarithmic peaks in their density. The specific heat has been calculated for two special sets of force constant ratios. Deviations from T^2 dependence set in at temperatures much lower than predicted by Debye theory. Comparison with experiment leads to a numerical value for $\theta=\hbar\omega_{max}/k$, from which ω_{max}, and therefore also α and one of the macroscopic elastic constants, c_{44}, may be calculated. θ and ω_{max} appear very sensitive to the assumed force constant ratios, c_{44} less so.

I. INTRODUCTION

ONE plane in a graphite lattice is shown in Fig. 1. On account of the wide separation of planes, it is believed[1] that the interaction between atoms in different planes is so slight that each crystallite consists of only a few (12–17) planes. It follows that no vibrational waves will be propagated perpendicular to the planes (or, at any rate, none with a wavelength long enough to be of importance at low temperatures). Gurney[1] further argues that of the remaining possible waves only those that are propagated in the planes but consist of vibrations perpendicular to the planes will be appreciably excited at low temperatures, since the restoring forces for "in-plane" motion will be much greater than for "transverse" motion. The principal object of Gurney's paper is to point out that the two-dimensional problem so resulting leads to a T^2-law (instead of the T^3-law obtained for three-dimensional solids) for the specific heat at low temperatures if the Debye approximation is used for the frequency distribution, and that this agrees with experiment.

It is, however, possible to calculate the frequency distribution of transverse vibrations of the two-dimensional "graphite" lattice exactly for certain values of the force constants α, β, and γ for nearest, 2nd-nearest, and 3rd-nearest neighbors. The purpose of this paper is, then, to carry out this calculation where possible, to calculate the specific heat using several special cases of this exact distribution, rather than using the approximate Debye distribution; and by comparison with experiment to try to infer the values of the force constants and the related "elastic constants" which should in principle be experimentally measurable.

II. THE FREQUENCIES

Let w_{ij} be the displacement, perpendicular to the plane, of atom ij of Fig. 1, and m be the mass of each atom. The kinetic energy of the lattice of N^2 particles is then

$$T=\tfrac{1}{2}m\sum_{\text{all } i,j}^{N,N}\dot{w}_{ij}^2$$

and the potential energy

$$V=\tfrac{1}{2}\alpha\sum_{\substack{\text{nearest}\\ \text{neighbors}}}(w_{ij}-w_{kl})^2$$
$$+\tfrac{1}{2}\beta\sum_{\substack{\text{2nd}\\ \text{nearest}}}(w_{ij}-w_{kl})^2+\tfrac{1}{2}\gamma\sum_{\substack{\text{3rd}\\ \text{nearest}}}(w_{ij}-w_{kl})^2$$

* Results reported at the North Carolina meeting of the American Physical Society, March, 1953 (H. B. Rosenstock, Phys. Rev. 91, 233(A) (1953).

[1] R. W. Gurney, Phys. Rev. 88, 465 (1952).

which defines the force constants α, β and γ (see Fig. 1) in the usual fashion. From this a Lagrangian equation of motion may be derived for each atom; the equations for all atoms for which $i+j=$even ("even" atoms) are formally identical, and the equations for all atoms for which $i+j=$odd ("odd" atoms) are formally identical; the fact that the equations of motion for "even" atoms cannot be the same as for "odd" atoms is most easily seen by observing that "even" atoms in Fig. 1 have a nearest neighbor to their right, while "odd" atoms have a nearest neighbor to their left. The equations of motion may be solved by standlng waves:

$$w_{kl}=Ge^{i(\omega t+kx+ly)} \quad \text{if} \quad k+l=\text{even},$$

$$w_{kl}=Ue^{i(\omega t+kx+ly)} \quad \text{if} \quad k+l=\text{odd},$$

where $x=p\pi/N$, $y=q\pi/N$; $p, q=1, 2, 3, \cdots, N$, with N^2 so large that x and y may be treated as continuous variables $0<x, y<\pi$. Observe that the solutions obey periodic boundary conditions and that this also leads to the right number N^2 of frequencies. Substituting our solutions into the equations of motion yields two simultaneous linear homogeneous equations in G and U, for which the compatibility condition is that the determinant of the coefficients vanish. The determinantal equation, a quadratic in ω^2, then gives the normal frequencies when solved, using $u=\cos x$, $v=\cos y$:

$$\omega^2=\psi(u,v)$$

$$\equiv\frac{\alpha}{m}\left\{3+3\frac{\gamma}{\alpha}+4\frac{\beta}{\alpha}(2-u^2-uv) \pm\left[(4u^2+4uv+1)+\frac{\gamma}{\alpha}(16u^3v+8u^2+4v^2-4uv-6)+\frac{\gamma^2}{\alpha^2}(16u^4+16u^2v^2-24u^2-8v^2+9)\right]^{\frac{1}{2}}\right\}. \quad (1)$$

The frequency distribution $g(\omega^2)d\omega^2$, defined as the fractional number of frequencies whose value lies between ω^2 and $\omega^2+d\omega^2$, is formally given by[2]

$$g(\omega^2)=g_+(\omega^2)+g_-(\omega^2),$$

$$g_\pm(\omega^2)=\frac{1}{2\pi^2}\int_0^\pi\int_0^\pi\delta(\omega^2-\psi_\pm(u,v))dxdy, \quad (2)$$

where the $\pm$ subscript refers to the choice of $+$ or $-$ in (1). This formula can be understood directly: integration is over $x-y$ space, because the frequencies are uniformly spaced there, and the Dirac δ function is inserted so that we might count only those frequencies for which $\psi(u, v)$ is really equal to ω^2. The factor $\frac{1}{2}\pi^2$ is inserted for correct normalization, $\int g(\omega^2)d\omega^2=1$.

[2] W. A. Bowers and H. B. Rosenstock, J. Chem. Phys. **18**, 1056 (1950).

Formula (2) has been previously evaluated for transverse vibrations of a square lattice,[2] for arbitrary values of the force constants. Let us attempt to do the same for the present case of the hexagonal lattice. We can write (2) as

$$g_\pm(\omega^2)=\frac{1}{2\pi^2}\int_{-1}^{1}\frac{I_\pm(u)du}{(1-u^2)^{\frac{1}{2}}}, \quad (3)$$

where, with $z=(u+v)u$ and $\varphi(z)\equiv\psi(u, v)$, formally at least

$$I_\pm(u)=\int_{u(u-1)}^{u(u+1)}\frac{\delta(\omega^2-\varphi_\pm(z))dz}{\{[z-u(u-1)][u(u+1)-z]\}^{\frac{1}{2}}}. \quad (4)$$

Equation (4) may be evaluated by use of Eq. (A2)

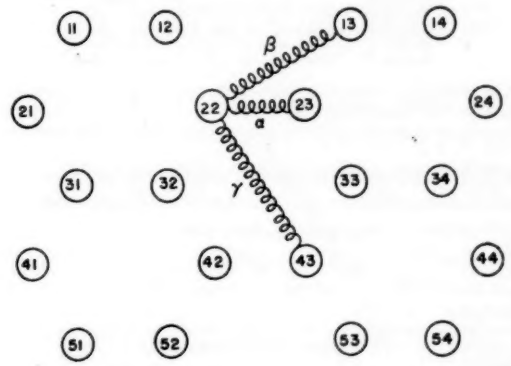

FIG. 1. A plane in the graphite lattice. Distance between nearest neighbors, 1.42A. Distance between neighboring planes, 3.35A.

(Appendix I) to give

$$I_\pm(u)=\begin{cases}\xi_\pm'(0)/P(\xi_\pm(0),u) & P(\xi_\pm(0),u)>0\\ 0 & \text{otherwise,}\end{cases}$$

where $P(x, u)=[x-u(u-1)][u(u+1)-x]$, $z=\xi_\pm(y)$ is the solution of $y=\omega^2\pm\varphi(z)$ and $'$ means differentiation with respect to the argument. The integral (3) can then be done easily (by letting $u^2=p$ and using formula 553 of Peirce[3]) if $\xi(z)$ is not an explicit function of u. This is the case when $\gamma/\alpha=0$ (as is seen by a glance at (1)), and when $\gamma/\alpha=\frac{1}{2}$, (in which case the discriminant becomes a perfect square,[4] $(2z+\frac{1}{2})^2$). β may take on any value without affecting the feasibility of the computation. The results are:

$$g(\omega^2)=g_+(\omega^2)+g_-(\omega^2),$$

$$g_\pm(\omega^2)=\frac{\xi_\pm'(0)}{\pi^2}\begin{cases}\sigma_{\pm 12} & \text{range } A_\pm,\\ \sigma_{\pm 21} & \text{range } B_\pm.\end{cases} \quad (5)$$

[3] B. O. Peirce, *A Short Table of Integrals* (Ginn and Company, 1929), 3rd edition.

[4] E. W. Montroll, J. Chem. Phys. **15**, 575 (1947).

Range $A_\pm$ means $\xi_\pm(0)>0$, range $B_\pm$ means $\xi_\pm(0)<0$,

$$\sigma_{\pm ij}=K(f_{\pm i}/f_{\pm j})/(f_{\pm i})^{\frac{1}{2}},$$
$$f_{\pm 1}=(4\xi_\pm(0)+1)^{\frac{1}{2}},$$
$$f_{\pm 2}=\tfrac{1}{4}(1+f_{\pm 1}+2\xi_\pm(0))(1+f_{\pm 1}-2\xi_\pm(0)),$$

TABLE I. Explicit values of the functions in Eq. (5) when $\gamma/\alpha=0$.

Functions involved in $g_-(\omega^2)$				
Range of β/α	$\xi_-(0)$	$\xi_-'(0)$	$m\omega_{-\min}^2$	$m\omega_{-\max}^2$
$0<\beta/\alpha<\infty$	P_-	Q_-	0	$9\beta+3\alpha$

Functions involved in $g_+(\omega^2)$				
Range of β/α	$\xi_+(0)$	$\xi_+'(0)$	$m\omega_{+\min}^2$	$m\omega_{+\max}^2$
$0<\beta/\alpha<\frac{1}{6}$	P_-	Q_-	$9\beta+3\alpha$	6α
$\frac{1}{6}<\beta/\alpha<\frac{1}{3}$	P_-	Q_-	$9\beta+3\alpha$	$9\beta+3\alpha+\alpha^2/4\beta$
$\frac{1}{3}<\beta/\alpha<\infty$	$\begin{cases}P_+ \text{ in range } C\\ P_- \text{ in range } D\end{cases}$	$\begin{cases}Q_+ \text{ in range } C\\ Q_- \text{ in range } D\end{cases}$	6α	$9\beta+3\alpha+\alpha^2/4\beta$

Range A_- $\quad \omega_{-\min}^2<\omega^2<(8\beta+2\alpha)/m$
Range A_+ $\quad \omega_{+\min}^2<\omega^2<(8\beta+4\alpha)/m$
Range B_- $\quad (8\beta+2\alpha)/m<\omega^2<\omega_{-\max}^2$
Range B_+ $\quad (8\beta+4\alpha)/m<\omega^2<\omega_{+\max}^2$
Range C $\quad \omega_{+\min}^2<\omega^2<(9\beta+3\alpha)/m$
Range D $\quad (9\beta+3\alpha)/m<\omega^2<\omega_{+\max}^2$

$$P_\pm=(\alpha^2/8\beta^2)[1+6\beta/\alpha+16\beta^2/\alpha^2-2m\beta\omega^2\pm([6\beta/\alpha+1]^2-4m\beta\omega^2)^{\frac{1}{2}}]$$
$$Q_\pm=(m/4\beta)[1\pm([6\beta/\alpha+1]^2-4m\beta\omega^2)^{\frac{1}{2}}]$$

TABLE II. Explicit values of the functions in Eq. (5) when $\gamma/\alpha=\frac{1}{2}$.

Functions involved in $g_-(\omega^2)$				
Range of β/α	$\xi_-(0)$	$\xi_-'(0)$	$m\omega_{-\min}^2$	$m\omega_{-\max}^2$
$0<\beta/\alpha<\infty$	P_1	Q_1	0	$9\beta+9\alpha/2$

Functions involved in $g_+(\omega^2)$				
Range of β/α	$\xi_+(0)$	$\xi_+'(0)$	$m\omega_{+\min}^2$	$m\omega_{+\max}^2$
$0<\beta/\alpha<\frac{1}{2}$	P_2	Q_2	$9\beta+9\alpha/2$	9α
$\beta/\alpha=\frac{1}{2}$	special case (see below)			
$\frac{1}{2}<\beta/\alpha<\infty$	P_2	$-Q_2$	9α	$9\beta+9\alpha/2$

Range A_- $\quad \omega_{-\min}^2<\omega^2<(8\beta+4\alpha)/m$
Range A_+ $\quad \omega_{+\min}^2<\omega^2<(8\beta+5\alpha)/m$
Range B_- $\quad (8\beta+4\alpha)/m<\omega^2<\omega_{-\max}^2$
Range B_+ $\quad (8\beta+5\alpha)/m<\omega^2<\omega_{+\max}^2$

$$P_1=2-m\omega^2/(4\beta+\alpha/2) \qquad Q_1=m/(4\beta+\alpha/2)$$
$$P_2=(8\beta+5\alpha-m\omega^2)/(4\beta-\alpha/2) \qquad Q_2=m/(4\beta-\alpha/2)$$

When $\beta/\alpha=\frac{1}{2}$, $g_+(\omega^2)=\frac{1}{2}\delta((9\alpha/m)-\omega^2)$

ξ has been previously defined and K is the complete elliptic integral of the first kind in the notation of Milne-Thompson,[5] $K(m)=\int_0^1 dx/[(1-x^2)(1-mx^2)]^{\frac{1}{2}}$. The various quantities involved in (5) are given explicitly in Table I (for $\gamma/\alpha=0$) and in Table II (for $\gamma/\alpha=\frac{1}{2}$). A special case arises for g_+ if $\beta/\alpha=\frac{1}{2}$, $\gamma/\alpha=\frac{1}{2}$, as can be seen directly from (1). Except for this special case, each g_- distribution and each g_+ distribution has one logarithmic peak, at $\xi_\pm(0)=0$, since $m=f_1/f_2$ approaches unity there.[6] Every g_--distribution runs from $\omega_{-\min}^2=0$ to a finite value, $\omega_{-\max}^2$, and each g_+ distribution runs from a finite value, $\omega_{+\min}^2$ to a finite value $\omega_{+\max}^2$; in some cases the g_+ and the g_- distributions overlap, in others they do not. These general features of the distributions as a function of β/α are shown in Table III and illustrated in Figs. 2 and 3.

For concrete illustration of the nature of the distributions and for use in the subsequent sections, two cases have been worked out in detail, *viz.* $\gamma/\alpha=0$, $\beta/\alpha=0$, which leads to[7]

$$\left.\begin{aligned} g(\tilde\omega^2)&=g_+(\tilde\omega^2)+g_-(\tilde\omega^2)\\ g_+(\tilde\omega^2)&=g_-(1-\tilde\omega^2)\\ g_-(\tilde\omega^2)&=\frac{9(1-2\tilde\omega^2)}{\pi^2}\begin{cases}K(f_2/f_1)/f_1^{\frac{1}{2}} & 0<\tilde\omega^2<\frac{1}{3}\\ K(f_1/f_2)/f_2^{\frac{1}{2}} & \frac{1}{3}<\tilde\omega^2<\frac{1}{2}\end{cases}\\ f_1&=3(1-2\tilde\omega^2)\\ f_2&=3(2-3\tilde\omega^2)^3\tilde\omega^2\end{aligned}\right\} \quad (6)$$

and is shown graphically in Fig. 4, and $\gamma/\alpha=\frac{1}{2}$, $\beta/\alpha=\frac{1}{2}$, which leads to

$$\left.\begin{aligned} g(\tilde\omega^2)&=g_+(\tilde\omega^2)+g_-(\tilde\omega^2)\\ g_+(\tilde\omega^2)&=\tfrac{1}{2}\delta(1-\tilde\omega^2)\\ g_-(\tilde\omega^2)&=\frac{9}{4\pi^2}\begin{cases}K(f_2/f_1)/f_1^{\frac{1}{2}} & 0<\tilde\omega^2<8/9\\ K(f_1/f_2)/f_2^{\frac{1}{2}} & 8/9<\tilde\omega^2<1\end{cases}\\ f_1&=3(1-\tilde\omega^2)^{\frac{1}{2}}\\ f_2&=\tfrac{3}{4}[1+2(1-\tilde\omega^2)^{\frac{1}{2}}-3(\tfrac{3}{2}\tilde\omega^2-1)^2]\end{aligned}\right\} \quad (7)$$

TABLE III. General features of the frequency distributions of $g_\pm(\omega^2)$ for $\gamma/\alpha=0$ and $\gamma/\alpha=\frac{1}{2}$ as a function of β/α. These results are also shown in Figs. 2 and 3.

γ/α	β/α	$m\omega_{-\min}^2$	$m\omega_{-\text{peak}}^2$	$m\omega_{-\max}^2$	$m\omega_{+\min}^2$	$m\omega_{+\text{peak}}^2$	$m\omega_{+\max}^2$
0	$0<\beta/\alpha<\frac{1}{6}$	0	$8\beta+2\alpha$	$9\beta+3\alpha$	$9\beta+3\alpha$	$8\beta+4\alpha$	6α
	$\frac{1}{6}<\beta/\alpha<\frac{1}{3}$	0	$8\beta+2\alpha$	$9\beta+3\alpha$	$9\beta+3\alpha$	$8\beta+4\alpha$	$9\beta+3\alpha+\alpha^2/4\beta$
	$\frac{1}{3}<\beta/\alpha<\infty$	0	$8\beta+2\alpha$	$9\beta+3\alpha$	6α	$8\beta+4\alpha$	$9\beta+3\alpha+\alpha^2/4\beta$
$\frac{1}{2}$	$0<\beta/\alpha<\frac{1}{2}$	0	$8\beta+4\alpha$	$9\beta+9\alpha/2$	$9\beta+9\alpha/2$	$8\beta+5\alpha$	9α
	$\frac{1}{2}<\beta/\alpha<\infty$	0	$8\beta+4\alpha$	$9\beta+9\alpha/2$	9α	$8\beta+5\alpha$	$9\beta+9\alpha/2$

[5] L. M. Milne-Thomson, *Jacobian Elliptic Function Tables* (Dover Publications, New York, 1950).

[6] L. van Hove, Phys. Rev. **89**, 1189 (1953) shows that such singularities are to be expected for a very general class of two-dimensional crystals. I am indebted to Prof. van Hove for a prepublication copy of his paper.

[7] This result was obtained independently by C. M. Askey, thesis, University of North Carolina (1951); by J. P. Hobson and W. A. Nierenberg, Phys. Rev. **89**, 662 (1953); and by C. A. Coulson and R. Taylor, Proc. Phys. Soc. (London) **A65**, 815 (1952), the last in connection with a calculation of the density of energy states in the two-dimensional "tight binding" approximation. (It is known that such a calculation leads to a problem mathematically equivalent to finding the frequency distribution; W. A. Bowers, private communication; see also "concluding remarks" of van Hove, reference 6.) I am indebted to Professor Nierenberg for correspondence.

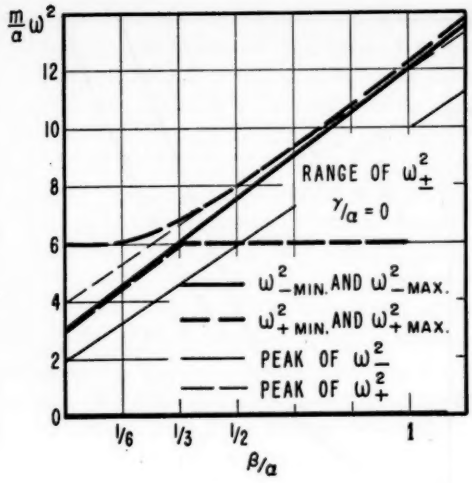

FIG. 2.

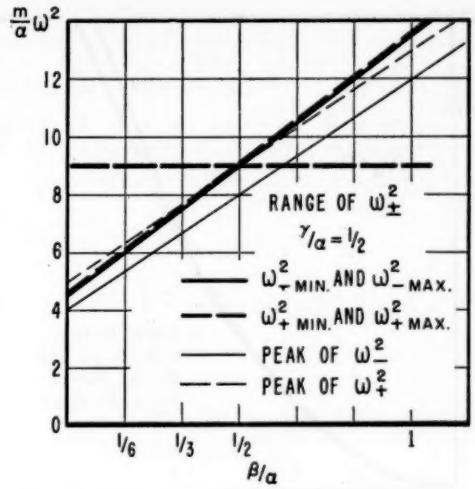

FIG. 3.

FIG. 2 and FIG. 3. General features of the frequency distributions $g_\pm(\omega^2)$ for $\gamma/\alpha=0$ and $\gamma/\alpha=\frac{1}{2}$ as a function of β/α. The minimum and maximum values taken on by ω^2, as well as the value at which the logarithmic peak occurs, are indicated in each case.

and is shown graphically in Fig. 5. For future convenience we use $\tilde{\omega}^2=\omega^2/\omega_{+\max}{}^2$ as our variable, hence $g(\tilde{\omega}^2)=\omega_{+\max}{}^2 g(\omega^2)$ as our distribution function.

In contrast to the above distributions, the Debye theory leads to a distribution $g_D(\tilde{\omega}^2)$ which is constant throughout:[7]

$$g_D(\tilde{\omega}^2)=\begin{cases} g(0) & 0<\tilde{\omega}^2<1/g(0) \\ 0 & \tilde{\omega}^2>1/g(0). \end{cases} \tag{8}$$

III. THE SPECIFIC HEAT

The specific heat per mole of a solid with one degree of freedom per particle is given by

$$C_V=NK\int_0^1 E(p)g(\tilde{\omega}^2)d\tilde{\omega}^2, \tag{9}$$

where

$$p=\tilde{\omega}\theta/T, \quad \theta=\hbar\omega_{+\max}/k, \tag{10}$$

$2\pi\hbar$, N and k are Planck's, Avogadro's, and Boltzman's constants, $E(x)=x^2e^x(e^x-1)^{-2}$ is the "Einstein function" which has been conveniently tabulated,[8] and $g(\tilde{\omega}^2)$ is in our case given by (5). According to Debye theory the specific heat is

$$C_V{}^D=Nk\int_0^{1/g(0)} E(p)g_D(\tilde{\omega}^2)d\tilde{\omega}^2,$$

or with (8)

$$C_V{}^D=2Nkg(0)(T/\theta)^2\int_0^{\theta/T(g(0))^{\frac{1}{2}}} E(p)pdp. \tag{11}$$

Both C_V and $C_V{}^D$ approach Nk at high temperatures (we are not concerned with high temperatures in this paper), but at low temperatures their behavior differs: (11) leads to a strict T^2 law as soon as T is small enough for the integrand of (11) to be negligible at the upper limit, but (9) leads to a strict T^2 law only if T is so small that all non-negligible contributions come from the immediate neighborhood of the origin (i.e., from a neighborhood so small that $g(\omega^2)$ can be approximated correctly by a constant there).[9] More precisely, by expanding the distribution as given by (5) in a Taylor

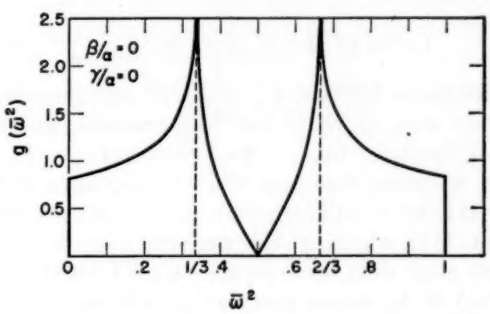

FIG. 4. Frequency distribution, $\gamma/\alpha=0$, $\beta/\alpha=0$.

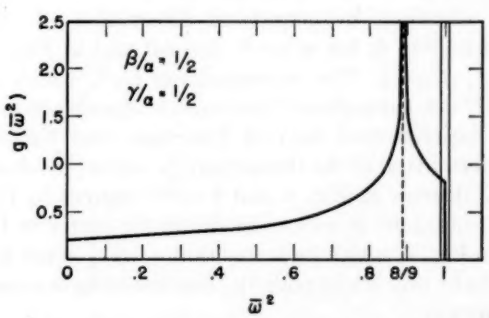

FIG. 5. Frequency distribution, $\gamma/\alpha=\frac{1}{2}$, $\beta/\alpha=\frac{1}{2}$.

[7] J. Sherman and R. B. Ewell, J. Phys. Chem. 46, 641 (1942).

[9] The replacement of $g(\tilde{\omega}^2)$ by $g(0)$ [Hobson and Nierenberg (reference 7)] at temperatures up to 60°K may thus be justified as a Debye approximation. In the case they consider (our Fig. 6), resulting discrepancies are small, but they would become larger (~30 percent) for $\gamma/\alpha=\beta/\alpha=\frac{1}{2}$ (Fig. 7).

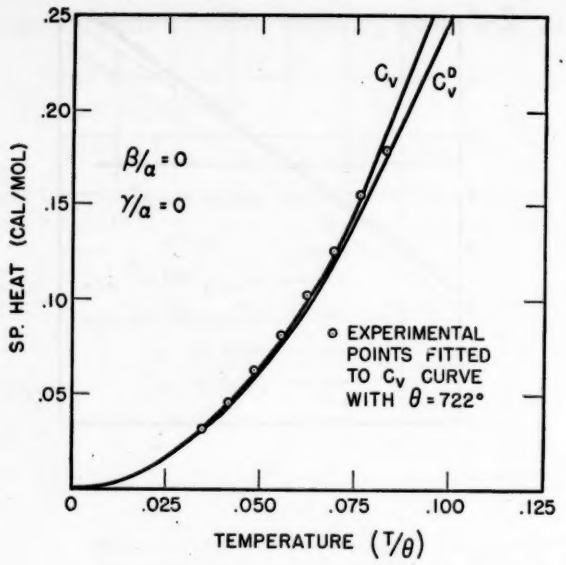

FIG. 6.

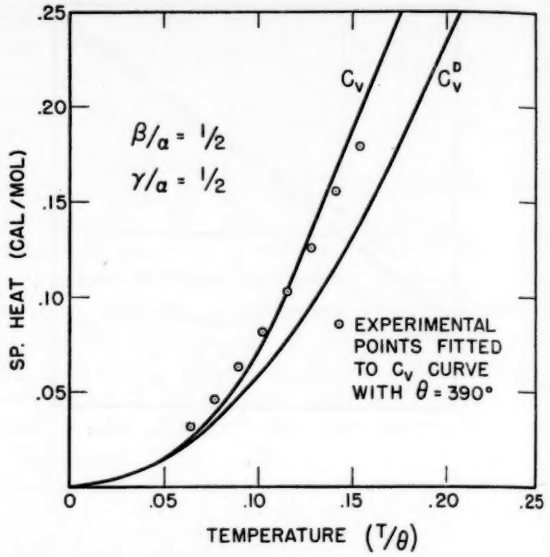

FIG. 7.

FIG. 6 and FIG. 7. Specific heat as function of temperature (see text). Experimental points, from reference 10, correspond to 25, 30, 35, 40, 45, 50, 55, 60°K.

series

$$g(\tilde{\omega}^2)=g(0)[1+b_1\tilde{\omega}^2+b_2(\tilde{\omega}^2)^2+\cdots]$$

we can show, by replacing the upper limit of integration in (9) and (11) by ∞, that in the range where C_V^D is proportional to $(T/\theta)^2$, C_V is given by

$$C_V=C_V^D[1+17.3b_1(T/\theta)^2+\cdots]. \qquad (12)$$

The difference between C_V and C_V^D can thus be considerable even at these low temperatures. For a numerical example, take $T/\theta=1/9=0.111\cdots$. As $E(9)\cong 0.01$, replacing the upper limit of integration in either (9) or (11) by ∞ will introduce an error of only about 1 percent, (12), which in this range therefore is good to 1 percent also, then leads to $C_V=C_V^D[1+0.21b_1+\cdots]$ for $T=1/9$. b_1, whose exact value will depend on the values of α, β, γ, may be assumed to be of the order unity. (When $\beta=\gamma=0$, we find $b_1=2$).

C_V, obtained by numerical integration of (9), is shown in Fig. 6, for $\gamma/\alpha=0$, $\beta/\alpha=0$ and in Fig. 7 for $\gamma/\alpha=\frac{1}{2}$, $\beta/\alpha=\frac{1}{2}$. The corresponding C_V^D, which is an exact T^2 law throughout this range, is also shown in each case. Experimental data of Esterman and Kirkland[10] have been fitted to the theoretical C_V curves by choosing $\theta=722$ degrees in Fig. 6 and $\theta=392$ degrees in Fig. 7. The fit obtained is seen to be distinctly better in Fig. 6 than in Fig. 7, which indicates that $\gamma/\alpha=\frac{1}{2}$ is too high a value to be physically realistic; one would have expected this anyway.

It is doubtful whether the present data are precise enough to enable one to determine whether they can be better fitted to the C_V or the C_V^D curve of Fig. 6. When more precise specific heat data become available, they should enable one to find β/α by comparing the data with theoretical specific heat curves obtained from using a $g(\tilde{\omega}^2)$'s calculated by (5) with various β/α ratios; provided, of course, that there exists a temperature range in which our assumption, that (a) interaction between atoms in different planes and wave propagation in the z direction, and (b) in-plane vibrations are negligible, holds. Should no fit be obtainable, the effect of these various neglected quantities would have to be investigated. Both (a)[11] and (b)[12] can, in fact, be taken into account, although at the expense of considerably greater complexity of the distribution function.

IV. THE ELASTIC CONSTANTS

θ having been determined by comparison of the calculated C_V with experiment, $\omega_{+\max}$ can be found from (10) and the force constants α, β, and γ from Tables I or II. α, β, and γ may be related to these macroscopic so-called "elastic constants" c_{ij} in the Voigt notation by replacing the difference quotients in our equations of motion by differential coefficients and comparing the resulting differential equation with the usual equation of motion of elasticity theory.[13] One obtains

$$\left.\begin{aligned} c_{33}&=0 \\ c_{44}&=\frac{2}{\sqrt{3}b}[\alpha+6\beta+4\gamma] \end{aligned}\right\}, \qquad (13)$$

[10] Esterman and Kirkland, as quoted by R. W. Gurney, Phys. Rev. 88, 465 (1952).

[11] J. A. Krumhansl, Knolls Atomic Power Laboratory, report KAPL-730.

[12] G. F. Newell (private communication).

[13] The process is illustrated in M. Born and T. von Karman, Physik. Z. 13, 297 (1912). On account of the assymetry of our equations of motion referred to in Sec. II, it is best in our case to add the equations of motion for two neighboring atoms before proceeding.

where b is the distance between crystal planes (3.35A). $c_{33}=0$ is merely a restatement of Gurney's assumption, upon which this paper is based, of absence of interaction between atoms in different planes; the ratio (1, 6, 4) of the coefficients of (α, β, γ) in (13) can be understood as the product of the ratio of numbers of nearest, 2nd nearest, and 3rd nearest neighbors (3, 6, 3) and the ratio of the squares of the distances between them (1, 3, 4).

Numerical results are given in Table IV. They are of the expected order of magnitude; no experimental results with which they could be compared seem to be available at this time, however. A direct measurement of the elastic constants, in conjunction with specific heat data, would, then, give considerable information concerning the values of α, β, γ, besides providing a direct check on the assumption of weakness of interaction between planes.

TABLE IV. Numerical results.

Assumption	θ (degrees)	$Q_{+\max}$ ($\sec^{-1}$)	α (dynes/cm)	c_{44} (dynes/cm^2)
$\beta/\alpha=0,\ \gamma/\alpha=0$	722	9.44×10^{13}	2.96×10^{4}	1.02×10^{12}
$\beta/\alpha=\frac{1}{2},\ \gamma/\alpha=\frac{1}{2}$	390	5.12×10^{13}	0.588×10^{4}	1.22×10^{12}

ACKNOWLEDGMENTS

I acknowledge with gratitude discussions with Dr. J. Karle, Professor W. A. Bowers, Dr. H. Friedman, Mr. L. S. Birks, and Mrs. H. M. Rosenstock.

APPENDIX I

The integral

$$J=\int_a^b \delta(p(z))f(z)dz$$

may be evaluated by defining

$$y=p(z) \tag{A1}$$

and calling the solution of this equation $z=q(y)$, so that $dz=q'(y)dy$. Then

$$J=\int_{p(a)}^{p(b)} \delta(y)f(q(y))q'(y)dy,$$

which with use of the defining property

$$\int_\alpha^\beta \delta(x)F(x)dx=\begin{cases}F(0) & \alpha\beta<0\\ 0 & \text{otherwise}\end{cases}$$

of the Dirac delta function gives

$$J=\begin{cases}f(q(0))q'(0) & p(a)p(b)<0\\ 0 & \text{otherwise.}\end{cases} \tag{A2}$$

When $\gamma/\alpha=0$ (see discussion just preceding Eq. (5)), the expression $\varphi_\pm(z)$ which corresponds to $p(z)$ of Eq. (A1) contains both z and $(4z+1)^{\frac{1}{2}}$. Equation (A1) therefore may have two, one, or no formal solutions, depending on the values of the parameters β/α and ω^2. It can be shown, however, that each of the equations $y=\varphi_+(z)$ and $y=\varphi_-(z)$ has, for each value of β/α and ω^2 that is physically significant (both β/α and ω^2 real and >0), one and only one solution.

When $\gamma/\alpha=\frac{1}{2}$ Eqs. (A1) are linear in z and the application of (A2) is straightforward.

Letters to the Editor

THIS section will accept reports of new work, provided these are terse and contain few figures, and especially few half-tone cuts. The Editorial Board will not hold itself responsible for opinions expressed by the correspondents. Contributions to this section should not exceed 600 words in length and must reach the office of the Editor not later than the 15th of the second month preceding that of the issue in which the Letter is to appear. No proof will be sent to the authors. A publication charge of $10.00 per Letter is made which, when honored, will entitle the Institution to 100 free reprints.

A New Relation between Potential Energy and Internuclear Distance*

ELLIS R. LIPPINCOTT
Department of Chemistry, Kansas State College, Manhattan, Kansas
(Received August 24, 1953)

MANY investigators have given potential energy functions describing the internuclear law of force.[1] However most of these have been of little use in predicting bond dissociation energies and anharmonicity constants either because of the approximate nature of the function or because of inadequate means of evaluating the necessary parameters. Recently Rittner has given a function which allows the quantitative prediction of the binding energy and other properties for alkali halide and hydride molecules,[2,3] but when applied to other diatomic molecules the results have been unsatisfactory.

This author has been using a number of potential energy functions for the calculation of bond dissociation energies and anharmoncity constants. One of these seems to be quite generally applicable to both diatomic and polyatomic molecules in their ground states and it seems worthwhile to give here a preliminary report of some of the results. The function is

$$V=D_e(1-e^{-n(\Delta r)^2/2r})(1+af(r)), \tag{1}$$

where D_e and r have their usual meaning and a and n are constants. $\Delta r=r-r_e$. $f(r)$ is a function of the internuclear distance chosen such that $f(r)=\infty$ when $r=0$ and $f(r)=0$ when $r=\infty$. For many purposes the $f(r)$ term is unimportant.

With $a=0$ and using the condition that $V''=k_e$ the following relation may be readily derived from (1).

$$D_e(\text{ergs/molecule})=k_e r_e/n. \tag{2}$$

Here n may be evaluated by means of the following empirical relation:

$$n=6.32\cdot 10^8(I/I_0)_A^{\frac{1}{2}}(I/I_0)_B^{\frac{1}{2}}\ \text{cm}^{-1}. \tag{3}$$

$(I/I_0)_A$ and $(I/I_0)_B$ are the ionization potentials of atoms A and B respectively relative to those of the corresponding atoms in the same row and first column of the periodic table. For H atoms I/I_0 has been assigned the value 0.88 rather than 1. Relation (2) has been used to calculate D_e values and these in turn used to obtain bond dissociation energies (D_0^0 values) for the 22 diatomic molecules given in Table I. The results are quite reasonable when compared with spectroscopically determined D_0^0 values. However, the average percent deviation of 4.5 for D_0^0 is considerably larger than the experimental error in obtaining r_e, k_e and (I/I_0) which is of the order of 0.1 percent. Most of the observed discrepancies may be attributed to the approximate nature of the relation but part may be due to the uncertainties associated with the correct dissociation energies of a number of important diatomic molecules.

Relation (2) has also been applied to a number of polyatomic molecules where the bond stretching force constants have been determined by assuming a simple valence force model. With the polyatomic molecules tested the predicted bond energies agree with the corresponding thermochemically determined quantities within an average error of about 6 percent. Thus the potential energy function (1) may have a wide range of application.

TABLE I. Bond dissociation energies and anharmonicity constants calculated from k_e, r_e and n.[a]

Molecule	Observed D_0^0(kcal/mole)	Calculated D_0^0(kcal/mole)	Deviation percent	Observed $\omega_e x_e$	Calculated $\omega_e x_e$	Deviation percent
As_2	91.3	85.1	6.7	1.12	1.19	6.2
Br_2	45.5	46.6	2.5	(?)	1.25	
CH	80.0	79.6	0.5	64.3	61.4	4.5
ClBr	52.0	48.4	6.9			
Cl_2	57.0	57.8	1.5	(?)	2.98	
ClF	60.2	58.0	3.7	(?)	6.25	
ClI	49.6	49.7	0.2	1.46	1.61	9.2
CO	210.5[b]	208.8	0.8	13.5	12.7	5.9
HBr	86.4	81.5	5.6	45.2	47.3	4.7
HCl	102.0	95.9	6.0	52.0	50.7	2.5
H_2	103.2	103.4	0.2	118.0	117.5	0.4
HI	70.4	73.9	5.0	39.7	41.3	4.0
IBr	41.8	44.1	5.2	0.78	0.92	17.9
I_2	35.6	41.5	16.8	0.61	0.63	3.3
N_2	224.8[c]	209.7	6.7	14.5	14.8	2.1
NO	149.4[d]	156.1	4.5	14.0	12.8	6.0
OH	100.5	109.1	8.2	82.8	72.1	13.2
O_2	117.0	123.9	5.9	12.1	11.1	8.3
P_2	116.0	111.5	3.9	2.80	3.02	7.8
S_2	101.4	104.8	3.4	2.85	2.77	2.1
SO	118.5	116.9	1.3	6.12	5.96	2.6
Se_2	81.9	78.0	4.7	1.06	1.08	1.9

[a] Data for the computations in this table were taken from G. Herzberg, *Spectra of Diatomic Molecules* (D. Van Nostrand Company, Inc., New York, 1950), pp. 502–58.
[b] For the purpose of calculating percent deviation D_0^0 for CO has been taken as 210.5 rather than the alternative possible values of 256 or 221.5 kcal/mole respectively.
[c] For the purpose of calculating percent deviation D_0^0 for N_2 has been taken as 224.8 rather than the alternative value of 170 kcal/mole.
[d] For the purpose of calculating percent deviation the D_0^0 for NO has been taken as 149.4 rather than the alternative value of 122 kcal/mol.

As a further check on this function the results of a second order perturbation treatment of the Schrödinger wave equation have been used to obtain energy expressions from which anharmonicity constants may be calculated. The cubic and quartic terms of (1) after expansion in series with $a=0$ were used as the perturbing potential while the square term was used for the zeroth order harmonic oscillator approximation. With this treatment the following expression for $\omega_e x_e$ is readily obtained.

$$\omega_e x_e=3h(n/r_e+1/r_e^2)/64\pi^2 c\mu. \tag{4}$$

The $\omega_e x_e$ values given in Table I have been obtained from this equation. A comparison with $\omega_e x_e$ values determined spectroscopically shows that the average percent deviation is 5.7. This agreement is quite satisfactory in view of the difficulty in obtaining agreement between D_0^0 and $\omega_e x_e$ values simultaneously for a number of other potential functions. For example the Morse function is very unsatisfactory for this purpose while one proposed by Linnett[4] gives an average deviation of about 20–30 percent in both $\omega_e x_e$ and D.

TABLE II. Dissociation energies calculated from $\omega_e x_e$, k_e and r_e.[a]

Molecule	Calculated D_0^0(kcal/mole)	Deviation percent	Molecule	Calculated D_0^0(kcal/mole)	Deviation percent
As_2	90.4	0.4	N_2	214.0	4.5[c]
CH	71.6	10.5	NO	142.2	5.0[d]
ClI	54.7	10.3	OH	93.9	6.1
CO	195.0	7.4[b]	O_2	114.0	2.5
HBr	85.7	0.7	P_2	119.0	1.9
HCl	95.7	6.1	S_2	102.0	0.6
H_2	102.0	1.3	SO	114.0	3.8
HI	71.9	2.0	Se_2	79.5	2.9
I_2	40.9	14.9			

[a] See (a) Table I.
[b] See (b) Table I.
[c] See (c) Table I.
[d] See (d) Table I.

By combining Eqs. (2) and (4) one may eliminate the constant n and obtain the relation

$$D_e(\text{ergs/molecule})=k_e/[(64\pi^2 c\mu\omega_e x_e/3h)-1/r_e^2]. \tag{5}$$

Since values of D_e calculated from (5) depend only on k_e, r_e and $\omega_e x_e$ this equation offers a check on the potential function independent of the empirically evaluated constant n. D_0^0 values calculated in this way for some 17 diatomic molecules where the $\omega_e x_e$ values are known accurately are tabulated in Table II along with the spectroscopically determined D_0^0 values. The average percent error is 4.8.

The above potential function should be useful in predicting unknown bond dissociation energies and anharmonicity constants for both diatomic and polyatomic molecules. Where two or more alternative values for a dissociation energy have been proposed (such as N_2 and CO) this function should suggest which is the correct one. In addition it is hoped that (1) indirectly will enable the prediction of such quantities as heats of sublimations, hydrogen bond energies, and molecular ionization potentials, as well as suggest new forms for wave functions useful in the quantum theory of chemical binding. A more detailed report of this and related work will be given at a later date.

* This work was assisted in part by the U. S. Office of Ordnance Research under contract DA23-072-ORD-677.

[1] For a brief discussion of a number of these with references see G. Herzberg, *Spectra of Diatomic Molecules* (D. Van Nostrand Company, Inc., New York, 1950), pp. 102 and 459.

[2] E. Rittner, J. Chem. Phys. **19**, 1030 (1951).

[3] W. A. Klemperer and J. L. Margrave, J. Chem. Phys. **20**, 527 (1952).

[4] J. W. Linnett, Trans. Faraday Soc. **36**, 1123 (1940); **38**, 1 (1942).

Note on the Quantum-Mechanical Calculation of Reaction Rates

SIDNEY GOLDEN
Brandeis University, Waltham, Massachusetts
(Received July 6, 1953)

A PREVIOUS quantum-mechanical treatment[1] of the reaction: $H_2+Br \rightarrow H+HBr$, is similar in some respects to the recent treatment by Bauer and Wu.[2] Nevertheless, the two treatments differ enough to perhaps justify additional comment.

Both treatments seek to employ: (a) the adiabatic approximation of neglecting electronic transitions; (b) the interchange of energy between certain translational, rotational, and vibrational modes of motion as determining the rate of chemical change; (c) localization of the interaction deemed responsible for chemical transitions; (d) an averaging of quantum-mechanical transition probabilities in accordance with a Boltzmann distribution-in-energy of the reactants to provide a rate expression to be compared with experiment.

The treatment in reference (1) is evaluated by noting that it corresponds, in the main, to the Born approximation for rearrangement collisions and possesses thereby the limitations of the latter.[3] Perhaps its most serious shortcoming lies in the wave functions used for the reactants and products. Among other things, interactions associated with purely physical (i.e., nonchemical) scattering have been neglected in their choice. This can be important when the zero-point energy difference between reactants and products is small,[4] but is probably not too serious for the hydrogen-bromine reaction, above.

However, within these limitations and certain numerical approximations, the treatment of reference (1) takes fully into account the interchange of energy between all modes of motion (excepting electronic) of the reacting system in (b), above. The wave functions employed for both reactants and products permit localization of the interaction in (c), above, to be justified. Finally, because all modes of nuclear motion have been retained, the averaging is executed in a complete manner, corresponding to (d), above.

In reference (2) by contrast, somewhat greater detail is ascribed to the interaction between the hydrogen molecule and the bromine atom, even "prior" to chemical reaction (see below, however). The computations are executed, however, at the expense of neglecting rotational motion and approximating the problem by a linear one. Since the transition probabilities are conditional probabilities, the average chemical transition probability depends upon an estimate of the probability of an essentially linear configuration HHBr. This may be made as indicated by Pelzer and Wigner in their classic work,[5] although a non quantum statistical mechanical procedure would be involved. It would seem that the steric factor of reference (2) can be too large on this account.

Another difficulty with the collinear model of reference (2) lies in the choice of the wave functions for vibratory motion. For the symmetrical potential and the wave functions employed, *the central atom has an equal probability of being on either side of the potential barrier even in the initial state*, a seemingly inadequate description of the reactants, at least. This difficulty can be minimized by employing only that linear combination of the *degenerate* (or nearly so) initial wave functions which corresponds to a bromine atom approaching a hydrogen molecule. For the present case the interaction may be expected to be unsymmetrical, which would effect an even greater modification in the form of the initial wave functions. With some asymmetry introduced thereby into the initial wave functions, the matrix elements of the perturbation may be affected appreciably. Thus, matrix elements which would be related to those on the bottom of column 1, page 731, of reference (2) would not be expected to vanish as a consequence.

To make some estimate of the influence of asymmetry, one may restrict the initial states to those for which the likelihood of finding the central hydrogen atom in the vicinity of the other hydrogen atom is appreciably greater than of finding it, initially, in the vicinity of the bromine atom. As previously indicated, this can be accomplished by utilizing the appropriate linear combination of (degenerate) ground-state wave functions. With the phases indicated by Morse and Stueckelberg,[6] this means that an antisymmetric linear combination (or one essentially so) of ground-state functions alone should be employed. The needed matrix element of the perturbation is then obtained readily from Table II of reference (2). It is found that the resulting probability coefficient will then be diminished by a factor of one hundred.

It would seem on this account, and contrary to the point of view expressed by Bauer and Wu, that their result for the steric factor may be expected to be too large.

In connection with the translational matrix elements, it is interesting to note that the approximations which are made to effect their simplification virtually eliminate the influence of the assumed interaction between the bromine atom and hydrogen molecule. Thus, Eq. (19) of reference 2 reduces for zero phase shift to the same form (to the order of approximation used in reference 2) obtainable from free particle wave functions of zero angular momentum. Indeed, by ascribing to the final translational state a kinetic energy necessary to make the final total translational energy zero in the presence of a slight attractive potential, precisely the same values are obtained. While for the final translational state which has been selected, a purely Born-approximation treatment (i.e., no initial interaction) would set the kinetic energy equal to zero, the subsequent averaging over a Boltzmann distribution of initial translational energies will have the effect of introducing final states of nonzero kinetic energy. Because the attractive potential is of the same order of magnitude as kT, it would seem that a Born-approximation treatment should yield results for the translational matrix elements which would correspond closely with those of Bauer and Wu.

An additional difficulty arises because transitions which have excited states *as their origin* have been neglected. One cannot simply neglect these by virtue of a small Boltzmann factor (as in the case of an excited state J) since for the same *total* energy precisely the same Boltzmann factor obtains. A detailed examination of the matrix elements for excited initial states appears essential to settle the matter. In any case, the steric factor would be increased on this account.

In view of the presence of several compensatory factors, the order-of-magnitude reasonableness of the steric factor value obtained by Bauer and Wu would seem to be fortuitous.

The subject matter of the present note has received helpful clarification from correspondence with Dr. Bauer, which is gratefully acknowledged. In addition, Dr. Bauer and Dr. Wu have kindly let me see a copy of their reply prior to publication.

[1] S. Golden and A. M. Peiser, J. Chem. Phys. **17**, 630 (1949); **17**, 842 (1949).
[2] E. Bauer and T. Y. Wu, J. Chem. Phys. **21**, 726 (1953).
[3] See, for example, L. I. Schiff, *Quantum Mechanics* (McGraw-Hill Book Company, Inc., New York, 1949), pp. 230–235.
[4] In an unpublished investigation on the ortho-para conversion of hydrogen, the approximation employed in reference (1) led to a negative apparent activation energy. Modification of the plane-waves in the Born approximation to take into account the physical scattering process led to much more reasonable results. The latter have been summarized in an U. S. Office of Naval Research report: "The thermal ortho-para conversion of hydrogen," by Golden, Peiser, and Katz, issued February 4, 1952, under NR-010-101.
[5] H. Pelzer and E. Wigner, Z. physik. Chem. 15B, 445 (1932).
[6] P. M. Morse and E. C. G. Stueckelberg, Helv. Phys. Acta **4**, 337 (1931).

The Quantum-Mechanical Calculation of Reaction Rates: A Reply to the Preceding Note

E. BAUER
Mathematics Research Group, New York University, New York, New York
AND
TA-YOU WU
Division of Physics, National Research Council, Ottawa, Canada
(Received July 20, 1953)

IN the preceding note[1] S. Golden mentions his recent calculations.[2] We had studied this article, but did not refer to it in our recent paper[3] because we do not agree with his treatment for the following fundamental reason. Golden supposes that a chemical reaction proceeds straight from the initial state to the final state, and calculates the rate constant by first order perturbation theory between these two states. Now, the essential contribution of the phenomenological theory is its introduction of the "activated state" as a real state, having a finite (though short) lifetime. If a detailed knowledge is available of the complete interaction potential (the manifold of potential surfaces of the usual type corresponding to all possible relative orientations of the three particles), it is in principle possible to get this activation energy from a detailed theory. In the absence of any such knowledge, on account of the impracticability of a detailed calculation, it is necessary to introduce the concept of an activated state directly into the physical model of the theory. In Golden's work, the concept of this activated state is not used and his activation energy arises as a mere function of an averaging with a Boltzmann factor over translational, rotational, and vibrational states. It is by no means clear how, without a detailed knowledge of the interaction potential or a physical model, such an averaging can give rise to any definite activation energy. We have tried to give a clear discussion of the status of the activated state in our article[3] (Secs. I, II).

Golden then proceeds in his note to give a number of criticisms of our article. It is clear that in any calculation of a problem as complicated as the present one it will be necessary to make approximations of two kinds, namely physical ones dealing with the model involved, and technical ones referring merely to the details of evaluating matrix elements.

Regarding the physical assumptions, Golden criticizes the neglect of rotation, and of excited states. As far as rotation is concerned, it is well known[4] that the transfer of energy between translational and rotational degrees of freedom is very easy. We are here calculating the probability for transfer of energy E_A ($\sim\frac{1}{2}$ ev) from translation to vibration: and this probability will certainly not be changed fundamentally if some or even all of E_A comes initially from rotation, rather than translation. Taking these effects into account would merely involve us in lengthy calculations with unsatisfactory interaction potentials.

Reactions involving excited states, when most or all of E_A comes from or goes into the vibration of one of the separating molecules, present slightly different problems that seem to have also been neglected in most if not all the phenomenological calculations. From general considerations of the nature of energy transfer between the coordinates r and ρ involved, it seems that the matrix elements and hence the cross sections for such processes are of the same general order of magnitude as that calculated by us, and thus our rate constant could be too small by a factor of two or so on this account. In any case it appears unlikely that including them would change the general order of magnitude of the cross section (i.e., introduce a factor $\sim$10–100, rather than $\sim$2).

Regarding technical approximations, Golden criticizes our use of a symmetrical two-minimum potential. The thing to remember is that there exists no good quantitative potential, and thus to use any one unsymmetrical potential is quite as arbitrary as to use a symmetrical potential. It is of course true that some particular matrix elements which vanish for a symmetrical potential will not vanish for an unsymmetrical one, but the cross section we are interested in does not depend on those particular matrix elements alone. It should perhaps be emphasized that the general order of magnitude of the cross section depends on the nature of the transition (translation-vibration in this case) and on the amount of energy transferred, rather than on the detailed shape of the potential.

Golden's detailed arguments about superposition of vibrational wave functions seem to overlook the basic limitations imposed by the uncertainty principle. If one specifies the energy of the system, then one must use our kind of wave function, which means that the vibrational motion is not localized. We start with a system having a two-minimum potential, and we want to find the transition probability between two *definite* energy states. For this one must not superpose wave functions belonging to *different* energy states. If one localizes the particle in one potential valley by using combinations of wave functions of different energies, then one is not able to specify the energy.

Finally, Golden makes some remarks concerning the translational wave functions, which imply that our results are essentially equivalent to the use of the Born approximation. The point here is that we examined the general character of the eigenfunctions of the appropriate potential, and found that in a certain region they could be represented by *sin* waves of suitable wave number, with a phase difference δ that we could not estimate in view of our lack a detailed knowledge of the potential. We examined our results, and found that the total matrix element depends rather little on δ, although individual terms do depend critically on the precise value of δ[3] (footnote 8).

To sum up, as we pointed out in the discussion of our paper, the treatment given there is admittedly very crude on account of the many approximations that have to be made both in formulating the physical model and in the calculation, but we do not believe that Golden's criticisms are relevant.

[1] S. Golden, J. Chem. Phys. (preceding letter). We are grateful to Professor Golden for letting us see his note before publication.
[2] S. Golden and A. M. Peiser, J. Chem. Phys. **17**, 630 (1949).
[3] E. Bauer and Ta-You Wu, J. Chem. Phys. **21**, 726 (1953).
[4] N. F. Mott and H. S. W. Massey, *Theory of Atomic Collisions* (Clarendon Press, Oxford, 1949), second edition, Chap. XII, p. 294.

The Rotational Spectrum of ND_3 between 60 and 200 K

RICHARD E. STROUP,* ROBERT A. OETJEN, AND ELY E. BELL
Department of Physics, The Ohio State University, Columbus, Ohio
(Received September 8, 1953)

THE far infrared spectrograph at The Ohio State University[1] has been used to obtain 14 lines of the rotational spectrum of deuterated ammonia. Six of the 14 lines reported here have previously been reported by Barnes;[2] eight new lines are reported.

ND_3 is a symmetric top molecule and its rotational spectrum in absorption can be represented by the equation

$$=2B(J+1)-4D_J(J+1)^3-2D_{JK}(J+1)K^2$$

and the selection rules $\Delta J=+1$ and $\Delta K=0$. J and K are the quan-

tum numbers associated with the total angular momentum of the molecule and with the component of angular momentum directed along the symmetry axis, respectively, B is a constant determined by the moment of inertia of the molecule about an axis perpendicular to the symmetry axis, and D_J and D_{JK} are the constants of centrifugal distortion. D_J and D_{JK} are of the same order of magnitude and quite small compared to B. J refers to the lower state.

The rotational lines which were observed are listed in Table I. The spectrum was obtained using spectral slit widths of from 0.3 to 0.6K and there was no indication of inversion doubling.

The rotational constants B and D_J have been determined from the observed spectrum by neglecting the contribution of the $2D_{JK}(J+1)K^2$ term. This procedure introduces but a small error as the K components of the lines could not be resolved and thus the contribution of this term is small. The value of B has been determined to be 5.143 ± 0.002K. The value for the centrifugal distortion coefficient D_J was found to be 0.00018 ± 0.00003K. The calculated line positions given in Table I are those obtained using the derived constants. The fit of the calculated spectrum to the observed is indicated by their difference.

TABLE I. Positions of main absorptions in far infrared spectrum of ND_3.

J value		Frequency		Difference calculated-observed
Lower	Upper	Calculated	Observed	
5	6	61.60K	61.58K	0.02K
6	7	71.81	71.69	0.12
7	8	82.01	82.03	−0.02
8	9	92.18	92.17	0.01
9	10	102.32	102.28	0.04
10	11	112.43	112.48	−0.05
11	12	122.49	122.51	0.02
12	13	132.52	132.65	−0.13
13	14	142.51	142.70	−0.19
14	15	152.45	152.49	−0.04
15	16	162.36	162.37	−0.01
16	17	172.20	172.03	0.17
17	18	181.98	181.94	0.04
18	19	191.73	191.78	−0.05

The values of these centrifugal stretching constants may be calculated by the method of Slawsky and Dennison[3] from the molecular geometry and force constants. The calculated values are $D_J=+0.000135$K and $D_{JK}=-0.000195$K. The experimental value of D_J is in fair agreement with the calculated value but is smaller than the true value because of the unresolved line splittings due to the D_{JK} term. The experimental value of B is slightly too large for this same reason; however, the magnitudes of these two errors are small.

* Present address: Eastern New Mexico University, Portales, New Mexico.

[1] Oetjen, Haynie, Ward, Hansler, Schauwecker, and Bell, J. Opt. Soc. Am. **42**, 559 (1952).

[2] R. B. Barnes, Phys. Rev. **47**, 658 (1935).

[3] Z. I. Slawsky and D. M. Dennison, J. Chem. Phys. **7**, 509 (1939).

Some Theorems in the Theory of Brownian Motion Which Apply to the Excluded Volume Problem in Polymer Chains*

ROBERT J. RUBIN
Applied Physics Laboratory, The Johns Hopkins University, Silver Spring, Maryland
(Received September 11, 1953)

THE purpose of this letter is twofold: first, to bring attention to the fact that the following results in the theory of Brownian motion can be applied to the excluded volume problem in polymer chains; and second, to use the theorems to indicate extensions of the results of Rubin.[1] The theorems are:[2]

(1) In a 2-dimensional Brownian motion, almost all paths (except for a set of measure zero) constitute an everywhere dense set and come back to any neighborhood of any given point infinitely many times for infinitely large time.

(2) In an n-dimensional Brownian motion ($n\geqslant3$), almost all paths constitute a nowhere dense set.

(3) In a 2- or 3-dimensional Brownian motion, almost all paths have infinitely many double points (points where the path crosses itself).

(4) In an n-dimensional Brownian motion ($n\geqslant4$), almost all paths have no double points.

The result of Rubin[1] that the increase (due to excluded volume) in the mean square distance, $\langle R_N^2\rangle$, between any two steps in a random walk in two dimensions is a constant independent of the number of intermediate steps, is consistent with theorem (1). One can conjecture from (1) that in 2 dimensions, $\langle R_N^2\rangle\sim N^{1+C}$ where N is the number of steps and $C>0$.

In view of theorem (2) and especially theorem (4) one can definitely conclude that in 4 dimensions $\langle R_N^2\rangle\sim N$. This conclusion is based on the fact that the strength and effect of excluded volume interaction depend on the number of double points.

However, it does not follow from theorem (3) that $\langle R_N^2\rangle\sim N^{1+C}$ in 3 dimensions because theorem (2) suggests that the higher order interactions will not be important. The only statement which can be made is that the 3-dimensional case is a borderline one. Thus, more refined methods are needed to find the dependence of $\langle R_N^2\rangle$ on N for $n=3$ when there is a finite excluded volume.

* This work was supported by the U. S. Navy Bureau of Ordnance under contract NORD-7386.

[1] R. J. Rubin, J. Chem. Phys. **20**, 1940 (1952).

[2] Various cases of theorems (1)–(4) are contained in: P. Levy, Amer. J. Math. **62**, 487 (1940); S. Kakutani, Proc. Imp. Acad. (Tokyo) **20**, 648 (1944); **20**, 706 (1944); Dvoretzky, Erdos, and Kakutani, Szeged Egyetem Acta Universitatis Szegediensis Acta Scientarium Mathematicarum **12**, 75 (1950); P. Levy, *Processus Stochastiques et Mouvement Brownien* (Gauthier-Villars, Paris, 1948).

Pure Quadrupole Spectra of Some Nitrochlorobenzenes*

T. L. WEATHERLY AND QUITMAN WILLIAMS
School of Physics, Georgia Institute of Technology, Atlanta, Georgia
(Received August 19, 1953)

CHLORINE quadrupole resonances have been observed in 1,2-dichloro-4-nitrobenzene and 1,4-dichloro-2-nitrobenzene at liquid nitrogen temperature using a frequency modulated regenerative detector. Frequencies were measured with a Signal Corps BC-221 frequency meter which has been recalibrated.

The Cl^{35} resonance frequencies are listed in Table I. The two resonance frequencies observed for each compound are presumably produced by chlorine atoms occupying different positions in the molecule.

In 1,4-dichloro-2-nitrobenzene the NO_2 group occupies the *ortho*-position with respect to chlorine 1 and the *meta*-position with respect to chlorine 4. By comparing the resonance frequencies of ClC_6H_5, o-$NO_2C_6H_4Cl$, and m-$NO_2C_6H_4Cl$, reported by Dean and Pound[1] one finds that the presence of an NO_2 group in the *ortho*-position increases the resonance frequency by a larger amount than an NO_2 group in the meta-position. This would indicate that the resonance at 37.874 Mc is produced by chlorine 1 and that the resonance at 35.921 Mc is produced by chlorine 4. Quantitative estimates of the resonance frequencies obtained by adding the frequency shifts produced by NO_2 and Cl are in reasonable agreement with the observed frequencies. Such estimates are compli-

TABLE I. Cl^{35} quadrupole resonance frequencies at −196°C.

Compound	Frequency (Mc)	Produced by
1,4-Dichloro-2-nitrobenzene	35.921	Chlorine 4
	37.874	Chlorine 1
1,2-Dichloro-4-nitrobenzene	36.488	
	37.055	

cated by differences in crystal structure and the temperature dependence of quadrupole resonance.

In 1,2-dichloro-4-nitrobenzene the NO_2 group occupies the meta-position with respect to chlorine 2 and the para-position with respect to chlorine 1. Since quadrupole resonance has not been observed in *p*-nitrochlorobenzene, the frequency shift produced by a para-NO_2 group is unknown. This frequency shift is difficult to estimate with accuracy due to presence of the resonance effect described by Pauling.[2] For this reason we are unable to identify the two resonance frequencies in this molecule.

* Supported in part by Engineering Experiment Station, Georgia Institute of Technology.

[1] C. Dean and R. V. Pound, J. Chem. Phys. **20**, 195 (1952).

[2] L. Pauling, *The Nature of the Chemical Bond* (Cornell University Press, Ithaca, New York, 1948), second edition, p. 151.

Dipole Moments of Gaseous Thallous Halides

AUBREY P. ALTSHULLER
1911 Clover Street, Cleveland, Ohio
(Received September 8, 1953)

THE dipole moments of gaseous alkali halides have recently been calculated by Rittner[1] who has taken into full consideration the distortion polarization of the ions. The thallous halides (excluding TlF) offer another opportunity for the application of this method to a class of highly polar molecules with negligible covalent bonding. The recent determination of the product $I\mu^2$, and I the moment of inertia, μ the dipole moment, and a the internuclear distance for TlCl by the molecular beam electrical resonance method[2] increases the interest in a theoretical calculation. In former measurements by the electric resonance method on the alkali halides[2] only m_j transitions in the presence of an electric field have been detectable. As a result only $I\mu^2$ has been determinable with both I and μ values being of much lower accuracy.[1] In the investigation of TlCl, a rotational transition ($J=0\rightarrow J=1$) at zero field strength could also be measured making it possible to determine I, a, and μ with much improved accuracy.

The theoretical equation employed is the one given by Rittner,[1]

$$\mu_1=ea\left[1-\frac{a^3(\alpha_1+\alpha_2)+4\alpha_1\alpha_2}{a^6-4\alpha_1\alpha_2}\right]. \quad (1)$$

When $4\alpha_1\alpha_2$ is an unimportant quantity, this expression reduces to

$$\mu_2=ea[1-(\alpha_1+\alpha_2)/a^3], \quad (2)$$

that is, only the first terms in the expansions of the induced moments in α/a^3 are employed.

The values of a determined by electron diffraction for the thallous halides[3] are as follows: TlCl 2.55 ± 0.03A, TlBr 2.68 ±0.03A and TlI 2.87 ± 0.03A. The electron diffraction value found for TlCl and the value arrived at from band spectra[2] of 2.53A are in excellent agreement with the value of 2.541 ± 0.002A obtained from microwave spectroscopy.[2] This fact increases further the reliability of the dipole moment of $4.444\pm0.014D$ for TlCl obtained from the microwave method.

The values used for the polarizabilities of Cl^-, Br^-, and I^- are those given by Pauling[4] and Fajans and Joos.[5] A polarizibility value of 3.50×10^{-24} cm^3 for Tl^+ in the solid state has been given.[6] For highly polarizable cations such as Tl^+, $[\Sigma\alpha]_{crys}-[\Sigma\alpha]_{gas}$ is positive.[5] It may be estimated that the value of Tl^+ in the gaseous state will be approximately 0.2 to 0.4×10^{-24} cm^3 less than in the solid by comparison with the known differences for the alkali halides.[5] A value for α_1 of 3.2×10^{-24} cm^3 should be a fair approximation and will be employed in the calculations.

Values of the dipole moments calculated from the approximate Eq. (2) are listed in column 2 and those calculated from Eq. (1) are listed in column 3. The value of the dipole moment of TlCl from the electric resonance method is given in column 4 along with the approximate value for TlI found in early work using the molecular beam method.[7]

The values of the dipole moments calculated from Eq. (2) are almost twice as large as those calculated from Eq. (1). The value of μ_2 for TlCl is much higher than the experimental value due to the neglect of higher order terms in the expansion of the induced moments in α/a^3. The quantity $4\alpha_1\alpha_2$ is even more significant for compounds with positive ions having highly polarizable 18-electron shells than for the alkali halides. The fact that $\mu_1<\mu_{exp}$ could not be due to TlCl having a partially covalent nature since then $\mu_1>\mu_{exp}$. Since the experimental values of a, μ_1, and α_2 for TlCl are all fairly accurate, the polarizability of the Tl^+ must be too large. If the calculation employing Eq. (1) is inverted, a value of 2.9×10^{-24} cm^3 is found for the polarizability of the thallous ion. In column 5 the values of the dipole moments of TlBr and TlI are recalculated using this value for α_1. It may well be that this difference of 0.3×10^{-24} cm^3 is due both to a somewhat high estimate for α_{Tl^+} in the solid state and a too small correction for the change in state upon the polarizability.

An investigation of the microwave spectra of TlI which would include the determination of the dipole moment of TlI to the same accuracy as that of TlCl would give added support to the method employed if a difference in dipole moment of $0.16D$ were found between the dipole moments of TlCl and TlI, as is predicted in column 5 of Table I.

TABLE I. Comparison of dipole moments.

Compound	μ_2	μ_1	μ_{exp}	μ_1'	ea
TlCl	7.21	3.77	4.44[a]	4.44	12.19
TlBr	7.49	3.81	···	4.49	12.86
TlI	7.77	3.94	<10[b]	4.60	13.77

[a] Reference 2.
[b] Reference 6.

[1] E. S. Rittner, J. Chem. Phys. **19**, 1030 (1951).
[2] Carlson, Lee, and Fabricand, Phys. Rev. **85**, 784 (1952).
[3] W. Grether, Ann. Physik **26**, 1 (1936).
[4] L. Pauling, Proc. Roy. Soc. (London) **A114**, 181 (1927).
[5] K. Fajans and G. Joos, Z. Physik **23**, 1 (1924).
[6] J. E. Mayer, J. Chem. Phys. **1**, 327 (1933).
[7] E. Wrede, Z. Physik **44**, 261 (1927).

Polarizability of the Hydride Ion and the Dipole Moments and Binding Energies of the Alkali Metal Hydrides

AUBREY P. ALTSHULLER
1911 Clover Street, Cleveland, Ohio
(Received September 8, 1953)

RECENTLY Klemperer and Margrave[1] have made calculations of the binding energies and dipole moments of gaseous alkali metal hydrides applying the method suggested by Rittner.[2] It should be pointed out that the polarizability of the hydride ion used by them[3] of 1.80×10^{-24} cm^3 is very different from other values given in the literature.[4,5] The molar refractivity and hence the polarizability has been calculated quantum mechanically for hydrogen-like ions by several independent methods[6-8] and the resulting formula has been modified by Pauling[4] by the inclusion of screening constants so as to be applicable to nonhydrogen-like ions. Employing a mole refraction screening constant of 0.4, one may calculate $\alpha(H^-)$ as 10.2×10^{-24} cm^3. Henrich[5] more recently has applied the variation method to the calculation of $\alpha(H^-)$ employing a third-order and a sixth-order Hylleraas type wave function. The calculations resulted in $\alpha(H^-)$ values of 11.6×10^{-24} cm^3 (third-order function) and 14.6×10^{-24} cm^3 (sixth-order function). Also if the value for the ionic radius of H^- given by Pauling[4] is employed in the relationship $\alpha\cong r^3$, a polarizability of 9.0×10^{-24} cm^3 is calculated. All of these values of $\alpha(H^-)$ are much larger than that employed by Klemperer and Margrave[1] and obtained from Bode.[3] This value was calculated from the refractive indices of solid crystalline alkali metal hydrides. It may be possible that such a difference as is found might exist between $\alpha(H^-)$ in the solid and

gaseous states (quantum mechanical calculations should apply to gaseous ions) despite the fact that it is such an extremely large difference.

If either the value of $\alpha(H^-)$ of 14.6×10^{-24} cm³ calculated by Henrich[5] or the value of 10.2×10^{-24} cm³ given by Pauling[4] is used in the calculation of the dipole moments of the gaseous alkali metal hydrides, negative dipole moments result. This situation arises from $a^3(\alpha_1+\alpha_2)+4\alpha_1\alpha_2>a^6-4\alpha_1\alpha_2$ and also in most of the calculations from $\alpha_1+\alpha_2>a^3$. Such negative values for the dipole moments are physically impossible and must result from an incorrect assumption being made at some point in the calculations.

Since Pauling's values[4] have been applied satisfactorily in numerous computations involving the need for the polarizabilities of gaseous ions, the value given for H^- should also be applicable. It is true that the possibility exists that the quantum mechanical calculations are grossly incorrect. In view of the fact that a variety of approximation methods give results which are in fair agreement with each other, this seems highly unlikely. Furthermore, the same functions when employed in calculatlng the polarizability of He give results which are in quite good agreement with each other and with the experimental value.[10] This leaves the possibility that the classical electrostatic model used fails when it is applied to the alkali metal hydrides. This alternative is quite possibly the one responsible for the results obtained.

Rittner[2] has given an argument based on a model of a diatomic molecule consisting of a point charge $+e$ at a distance a from a metal sphere of charge $-e$ of radius R when $\alpha_1\ll\alpha_2$, and has applied the method of images. This model is satisfactory for the alkali halides. The model is not satisfactory for the alkali metal hydrides because the condition that $a>R$ is not satisfied. If a $R(H^-)$ of 2.08A is accepted[9] then the condition is not satisfied for LiH and NaH. If an $\alpha(H^-)=14.6\times10^{-24}$ cm³ is employed in the expression $R=a^3$, then $R(H^-)=2.44$A and the condition is not satisfied by LiH, NaH, KH, or RbH, and is just barely satisfied by CsH. It seems likely then that the electrostatic model used[1,2] fails for the alkali metal hydrides because of actual interpenetration of the large hydride ion by the alkali metal ion.

The reasonable agreement between the calculated and experimental binding energies is quite likely fortuitous. If an $\alpha(H^-)=14.6\times10^{-24}$ cm³ is now employed in the calculation of the contribution to the binding energy made by the electrostatic terms, in the case of KH an increase of about 109 Kcal/mole is found over that obtained employing 1.80×10^{-24} cm³ for the $\alpha(H^-)$. Furthermore, since the value of the compressibility ρ is dependent on the assumed model and the correspondlng expression for the binding energy, use of a poor model resulting in an incorrect expression for the binding energy would also result in an incorrect compressibility and repulsive energy. Owing to this interdependence, a nearly correct binding energy might result from a cancellation of errors.

[1] W. A. Klemperer and J. L. Margrave, J. Chem. Phys. **20**, 527 (1952).
[2] E. R. Rittner, J. Chem. Phys. **19**, 1030 (1951).
[3] H. Bode, Z. physik. Chem. **6B**, 251 (1930).
[4] L. Pauling, Proc. Roy. Soc. (London) **A114**, 181 (1927).
[5] L. R. Henrich, Phys. Rev. **62**, 545 (1942).
[6] P. S. Epstein, Phys. Rev. **28**, 695 (1926).
[7] G. Wentzel, Z. Physik **38**, 518 (1926).
[8] I. Waller, Z. Physik **38**, 635 (1926).
[9] L. Pauling, *The Nature of the Chemical Bond* (Cornell University Press, Ithaca, New York, 1940), p. 346.
[10] L. Pauling and E. B. Wilson, *Introduction to Quantum Mechanics* (McGraw-Hill Book Company, Inc., New York, 1935), pp. 228–229.

Mechanism of the Hg ($^3P_1$) Photosensitized Decomposition of Ethylene*

A. G. MITCHELL† AND D. J. LE ROY
Department of Chemistry, University of Toronto, Toronto, Canada

(Received May 4, 1953)

SOME years ago Le Roy and Steacie[1] proposed the following mechanism for the mercury photosensitized decomposition of ethylene at room temperature:

$$Hg(^1S_0)+h\nu=Hg(^3P_1) \quad (1a)$$

$$Hg(^3P_1)=Hg(^1S_0)+h\nu \quad (1b)$$

$$Hg(^3P_1)+C_2H_4=C_2H_4^*+Hg(^1S_0) \quad (2)$$

$$C_2H_4^*+C_2H_4=2C_2H_4 \quad (3)$$

$$C_2H_4^*=C_2H_2+H_2. \quad (4)$$

The corresponding rate equation may be written in the form

$$1/(\phi q)=1+(k_2/k_3)(C_2H_4), \quad (5a)$$

in which $\phi=(1/I_a)d(H_2)/dt$=quantum yield of hydrogen production, and $q=\{k_b/k_1+(C_2H_4)\}/(C_2H_4)$. From the quenching data of Steacie[2] the value of k_b/k_1 at 25°C is 0.367 mm.

This mechanism has recently been criticized by Darwent[3] on the basis that the data may be fitted more accurately to the equation

$$\phi/(\gamma-\phi)=(k_3/k_2)/(C_2H_4)+(k_4/k_2)/(C_2H_4)^2, \quad (5b)$$

in which γ is defined as the product of the "efficiencies" of reactions (1) and (4), and in which $k_4/(C_2H_4)$ is defined as the rate of heterogeneous decomposition of $C_2H_4^*$. It should be noted, however, that *at constant temperature* each of the three parameters in Eq. (5b), γ, (k_3/k_2), and (k_4/k_2), was found to vary with the concentration of mercury in the cell, although only k_4 would be expected to change. A further difficulty was the fact that the maximum value of ϕ occurred at an ethylene pressure considerably higher than one would expect from quenching data.

We have re-investigated the reaction with emphasis on the accurate determination of rates and using a true resonance lamp as the light source, rather than a low pressure arc with noble gas carrier as used previously.[1,3] The light originated as fluorescent radiation from a small quartz cell containing mercury vapor at a pressure of 1.8×10^{-4} mm and irradiated by a low pressure arc. The emission line should therefore be much narrower than that from a low pressure arc.

The radiation from the true resonance lamp was essentially all absorbed in a 60 mm cell containing mercury vapor at a pressure of 1.8×10^{-3} mm, whereas only 85 percent of the 2537A radiation from the low pressure arc was absorbed under the same conditions, although the arc was operated at less than half the current used previously.[1] The absorption of light from the low-pressure arc increased to 95 percent, however, in the presence of 23.5 mm of ethylene, which suggests that pressure broadening of the absorption line is appreciable at these pressures.

If a low pressure arc were used one might expect, therefore, that the maximum would be shifted to higher ethylene pressures and that the rate *vs* (C_2H_4) curve would become distorted because of the effect of ethylene pressure on the rate of light absorption.

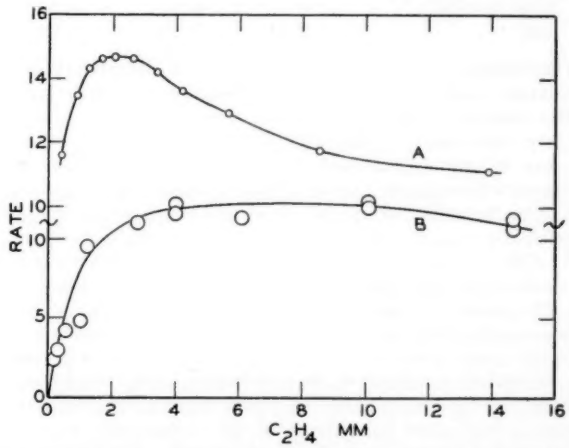

FIG. 1. Effect of line structure on the rate curve. *A*: present data; *B*: data of Le Roy and Steacie (reference 1). The ordinates are mm min^{-1} $\times10^4$ and mm $hr^{-1}\times10^2$, respectively.

These effects would not be expected if the emission line were narrow relative to the absorption line. A comparison of our present results (curve *A*, Fig. 1) with those obtained previously[1] (curve *B*) appears to confirm this theory. With the true resonance lamp the maximum in the curve is quite sharp and occurs at the approximate position predicted from quenching data; in the previous work[1,3] the maxima were very broad.

Darwent[3] has suggested that some of the ($^3P_1$) atoms are quenched to the metastable ($^3P_0$) state by ethylene, and on this basis has predicted that the maximum rate should occur at ethylene pressures greater than two mm but at successively lower pressures as the mercury concentration is decreased. This interpretation is not borne out by the present measurements. We have found the maximum to occur at 2 mm with a mercury pressure of 1.8×10^{-3} mm, while he found it to occur at a considerably higher ethylene pressure with a mercury pressure of 1.8×10^{-4} mm.

We hesitate at this time to suggest a suitable modification of the original mechanism of Le Roy and Steacie, but it is interesting to note that whereas a plot of $1/(\phi q)$ *vs* (C_2H_4) using the data of Le Roy and Steacie or of Darwent is convex toward the (C_2H_4) axis even at the lowest pressures, the analogous plot using the present data is concave toward the (C_2H_4) axis. This might mean that deactivation, rather than decomposition of C_2H_4* can occur at the wall but further work will be necessary to settle the point.

* This work was supported by a grant from the National Research Council of Canada.

† Present address: McColl-Frontenac Oil Company Limited, Toronto, Canada.

[1] D. J. Le Roy and E. W. R. Steacie, J. Chem. Phys. **9**, 829 (1941).
[2] E. W. R. Steacie, Can. J. Research **B18**, 44 (1940).
[3] B. de B. Darwent, J. Chem. Phys. **20**, 1673 (1952).

Remarks on Mechanism of the Hg($^3P_1$) Photosensitized Decomposition of Ethylene

B. deB. Darwent
Olin Industries, Inc., New Haven, Connecticut
(Received June 15, 1953)

THE communication from Mitchell and Le Roy indicates the necessity for correcting and explaining some points in my paper.

A. Pressure of ethylene for maximum rate (p_{max}).—The statement, "The results given in Tables I and II seem to indicate that the maximum rate occurs at progressively decreasing pressures as the mercury concentration decreases" is misleading since there are no data which allow estimates to be made of p_{max}, in the experiments at the two highest mercury concentrations. The pertinent results at the lowest concentration of mercury were

pHg (mm Hg):	6.98	4.78	2.54
ϕH_2:	0.223	0.227	0.219

The accuracy of these results is probably not greater than ±5 percent so that conclusions about p_{max} would be very uncertain.

The statement quoted above was prompted by the fact that Le Roy and Steacie (pHg$=18\times10^{-4}$ mm) found $p_{max}=9$ mm, whereas in my experiments with pHg$=1.8\times10^{-4}$ mm, p_{max} appeared to lie between 2.5 and 7.0 mm. I may add here that I was not primarily concerned, in that investigation, with the relationship between p_{max} and such factors as concentration of mercury.

B. Effect of (Hg) *on* p_{max}.—The statement was, "Since the rate of reaction (*e*) depends on the average distance through which the ($^3P_0$) atoms diffuse before they strike a wall, it is not difficult to see, qualitatively, that the maximum rate of the reaction will occur at smaller pressures as the distance of diffusion is increased (i.e., as the concentration of mercury is decreased)." Reaction (*e*) represented the deactivation of ($^3P_0$) atoms at the wall. The foregoing statement was offered as an explanation of (i) the effect of (Hg) on p_{max}, and (ii) the fact that p_{max} (in Le Roy and Steacie's experiments) was 9 to 10 mm. Now if ($^3P_0$) atoms are formed and if they are capable, after many collisions, of causing ethylene to decompose, they will have a greater chance of decomposing ethylene when they are formed far from the walls than when they are formed near to the wall. This means that, other conditions being equal, the quantum yield should increase with decreasing mercury concentration. But it is difficult to see what effect, if any, the change in (Hg) should have on p_{max}, unless a detailed study is made of the kinetics. Furthermore, it is by no means certain that the ($^3P_0$) atoms are capable of inducing the decomposition of ethylene and, if they are not, the change in mercury concentration should have no effect on either ϕ or p_{max}. Hence, I consider the statement in question to be inaccurate and it should be withdrawn.

Mitchell and Le Roy have found (1) that only 85 percent of the light from the low-pressure lamp is absorbed by a 60-mm path of mercury at 1.8×10^{-3} mm, and that this figure increases to 95 percent in the presence of 23.5 mm of ethylene; (2) that the maximum rate occurs at 2 mm with the resonance lamp, whereas Le Roy and Steacie had found it to occur at 9 mm with the broader line; (3) that with the resonance lamp the graph of $1/\phi H_2$ *vs* (C_2H_4) is concave towards the (C_2H_4) axis, whereas previous data with a broader line gave a convex curve. They conclude or suggest (1) that pressure broadening was important in the experiments with the broadened source; (2) that quenching to the metastable state ($^3P_0$) is unimportant or at least not in accordance with the results; and (3) that excited ethylene molecules are deactivated and do not decompose on the wall.

Their first conclusion appears to be reasonable and may account for the change in p_{max} from the broad to the narrow line, though it is not obvious why this should be the case.

The second conclusion is not necessarily valid (it has been discussed above). The evidence for quenching to the metastable state was based on quite separate experiments[1] and, as mentioned previously, the photosensitized experiments may not be capable of providing evidence either for or against this type of quenching.

The third conclusion is perhaps the most interesting and important. If we accept Mitchell's and Le Roy's statement that 95 percent of the radiation is absorbed in a 60-mm path, when the pressure of ethylene is 23.5 mm, then in a 100-mm path such as was used in my experiments, we should expect that pressure broadening would be without effect provided that the ethylene pressure was above about 25 mm. Hence, if Le Roy and Steacie's mechanism were correct, there should be no difference above 25 mm between the results obtained with a broad or narrow line and the $1/\phi$ *vs* (C_2H_4) graph should be a straight line. There is no doubt that Le Roy and Steacie's results and my own, when plotted in this manner, deviated considerably from a straight line. It is true that my results, over a limited range (40 to 96 mm), appear to give a linear relationship between $1/\phi$ and (C_2H_4); however, the best line through those points extrapolate to $1/\phi \lesssim 0.5$ at (C_2H_4)$=0$. This is incompatible with the "original mechanism" which demands the extrapolated value of $1/\phi$ to be $\gtrsim 1.0$ and suggests strongly that the linear relationship over the limited range of pressure is only illusory and that we are really dealing with a continuous curve.

Mitchell and Le Roy now find that the $1/\phi$ *vs* (C_2H_4) curve, with the narrow line, deviates from linearity in the opposite sense to that obtained previously. Judging by their Fig. 1, the highest pressure was about 14 mm, and one wonders if they would continue to get this type of deviation at much higher pressure since the linear relationship is strictly valid only in the region of high pressures where the life time of Hg($^3P_1$) is quite negligible.

By using the narrow line, Mitchell and Le Roy have obtained the important result that $p_{max}=2$ mm, which is much more understandable than the previous value; but this can shed no light on the fate of the excited ethylene molecule unless the detailed kinetics are solved. Information about the fate of C_2H_4* can be obtained by working at high pressures where the kinetics become manageable and where pressure broadening should not complicate the picture.

[1] B. deB. Darwent and F. G. Hurtubise, J. Chem. Phys. **20**, 1684 (1952).

Isotope Effect and Thermal Expansion Coefficients of Crystals

CHRISTER E. NORDMAN AND WILLIAM N. LIPSCOMB
School of Chemistry, University of Minnesota, Minneapolis, Minnesota
(Received August 24, 1953)

WHEN H is replaced by D a contraction occurs in the LiH crystal,[1] whereas an expansion occurs in those crystals containing short hydrogen bonds.[2] A simple explanation in terms of the amplitudes of vibration of H or D in idealized one-dimensional potential fields has been given,[3] and the temperature dependence of the effect has been discussed qualitatively[4] for H_2O and D_2O. We wish to outline[5] a quantitative discussion of the thermal expansion coefficients of LiH, LiD, and LiT.

Assume that the interatomic forces in LiH and LiD are the same when the lattice constants d are the same. At 293°K, however, these parameters are different;[1] for LiH, $d=4.085kX$, and for LiD, $d=4.065kX$. Since the one-dimensional potential function $U(d,x)=V(d+x)+V(d-x)$ is probably nearly parabolic,[3] we assume that

$$V(d+x)=\frac{b}{3}(d+x)^3+\frac{c}{2}(d+x)^2+e(d+x)+g \qquad (1)$$

so that the integral,[3] which is also equal to $f(d)$, becomes

$$\int_{-\infty}^{\infty}P(x,d,m,T)\frac{\partial V(d+x)}{\partial x}dx=\frac{bh}{4\pi^2 m\nu}\coth\left(\frac{h\nu}{2kT}\right)+cd+e. \qquad (2)$$

We now choose a temperature for LiD such that its lattice constant is equal to the lattice constant of LiH at 293°K. The $f(d)$ terms for LiH and LiD then are equal, and since, by assumption, the constants in the potential function are equal,

$$\frac{1}{m_H\nu_H}\coth\left(\frac{h\nu_H}{2kT_H}\right)=\frac{1}{m_D\nu_D}\coth\left(\frac{h\nu_D}{2kT_D}\right), \qquad (3)$$

where $\nu=(1/2\pi)(4bd+2c)^{\frac{1}{2}}m^{-\frac{1}{2}}$, and thus $\nu_H^2 m_H=\nu_D^2 m_D$. From the value of $T_H=293$°K and of $\nu_H=1.575\times10^{13}$ sec^{-1}, obtained from the Debye characteristic temperature of LiH, the value of $T_D=379$°K is found for which the lattice parameter of LiD is $4.085kX$. Hence, the thermal expansion coefficient of LiD is 5.7×10^{-5} deg^{-1}.

With the use of this result the lattice parameter of LiD at 350°K is found to be $4.078kX$, and we then find $T_H=250$°K from Eq. (3). Hence, $d=4.078kX$ for LiH at 250°K, and the thermal expansion coefficient of LiH is 3.9×10^{-5} deg^{-1}.

The lattice parameter of LiT, which has not been determined experimentally, is calculated from Eq. (3) as $4.085kX$ at 400°K and $4.065kX$ at 322°K. The predicted thermal expansion coefficient of LiT is 6.3×10^{-5} deg^{-1}, and the value of its lattice parameter at room temperature should be close to $4.058kX$.

Support of this work by the U. S. Office of Naval Research is gratefully acknowledged.

[1] E. Zintl and A. Harder, Z. physik. Chem. **28B**, 478 (1935). See R. E. Rundle, J. Am. Chem. Soc. **69**, 1719 (1947).
[2] J. M. Robertson and A. R. Ubbelohde, Proc. Roy. Soc. (London) **A170**, 222 (1939); A. R. Ubbelohde, Proc. Roy. Soc. (London) **A173**, 417 (1939); A. R. Ubbelohde and I. Woodward, Proc. Roy. Soc. (London) **A179**, 399 (1942); D. H. W. Dickson and A. R. Ubbelohde, Acta Cryst. **3**, 6 (1950).
[3] C. E. Nordman and W. N. Lipscomb, J. Chem. Phys. **19**, 1422 (1951).
[4] R. E. Rundle, J. Chem. Phys. **21**, 937 (1953).
[5] Abstracted from the Ph.D. Thesis of Christer E. Nordman, University of Minnesota, March, 1953.

A One-Dimensional Wave Equation for Hydrogen Bonds

CHRISTER E. NORDMAN AND WILLIAM N. LIPSCOMB
School of Chemistry, University of Minnesota, Minneapolis, Minnesota
(Received August 24, 1953)

IN the absence of more complete quantum mechanical discussions of symmetrical hydrogen bonds, an idealized one-dimensional representation, with or without a central maximum, is ordinarily assumed.[1] Solution of the wave equation should be of interest in connection with the isotope effect,[2] expansion coefficients,[3] the frequencies and intensities of the infrared spectrum, as well as more general applications of single or double minima problems.

Assume that the O−H potential has the form of a Morse function

$$V(x)=D\{1-\exp[-\beta(x-r_e)]\}^2,$$

and that the potential energy of a hydrogen atom between two oxygen atoms at $\pm d$ may be represented by

$$U(d,x)=V(d+x)+V(d-x).$$

It follows that

$$U(d,x)=2D\{1-2\exp[-\beta(d-r_e)]\cosh\beta x+\exp[-2\beta(d-r_e)]\cosh2\beta x\}.$$

The Schrödinger equation for a particle of mass m in the potential well $U(d,x)$ can be written as

$$\psi''(\xi)+[a+b\cosh(\beta\xi/\alpha)-b^2\cosh^2(\beta\xi/\alpha)]\cdot\psi(\xi)=0,$$

where

$$b=\exp[-\beta(d-r_e)],\quad \alpha=(4\pi/h)(2Dm)^{\frac{1}{2}},$$
$$a=E/4D-(1-b^2)/2,\quad \xi=\alpha x.$$

Choosing the new variables

$$z=\tanh^2(\beta\xi/2\alpha),\quad \psi(\xi)=\phi(z),$$

we find

$$(\beta/\alpha)^2z(1-z)^2\phi''(z)+(1/2)(\beta/\alpha)^2(1-z)(1-3z)\phi'(z)+[a+b(1+z)/(1-z)-b^2(1+z)^2/(1-z)^2]\phi(z)=0.$$

Substitution of $\phi(z)=(1-z)^p f(z)$ then yields,

$$(\beta/\alpha)^2z(1-z)^2f''(z)+(\beta/\alpha)^2[(1/2)(1-z)(1-3z)-2pz(1-z)]f'(z)+[a+b(1+z)/(1-z)-b^2(1+z)^2/(1-z)^2+(\beta/\alpha)^2p(p-1)z-(1/2)(\beta/\alpha)^2p(1-3z)]f(z)=0.$$

Further substitution of

$$f(z)=\exp[-(\alpha/\beta)b(1+z)/(1-z)]g(z),$$

then gives

$$z(1-z)^2g''(z)+[(1/2)(1-z)(1-3z)-2pz(1-z)-4(\alpha/\beta)bz]g'(z)+[(\alpha/\beta)^2(a-b^2)-(\alpha/\beta)b(1+z)/(1-z)+(\alpha/\beta)^2b(1+z)/(1-z)+p(p-1)z-(1/2)p(1-3z)+4p(\alpha/\beta)bz/(1-z)]g(z)=0.$$

If we choose

$$p=-(1/2)(\alpha/\beta)+1/2,$$

this equation simplifies to

$$z(1-z)^2g''(z)+[1/2+(-4b\alpha/\beta+\alpha/\beta-3)z+(5/2-\alpha/\beta)z^2]g'(z)+[A+(1/4)(\alpha^2/\beta^2-3\alpha/\beta+2)z]g(z)=0,$$

where

$$A=(\alpha/\beta)^2(a-b^2+b-b\beta/\alpha+(1/4)\beta/\alpha-(1/4)\beta^2/\alpha^2).$$

Now, if $g(z)$ is expanded in a power series in z,

$$g(z)=\sum_{\nu=0}^{\infty}c_\nu z^{\nu+\lambda},$$

it is found that the coefficients c_ν are related by a three-term recursion formula,

$$(\nu+\lambda+1)(\nu+\lambda+1/2)c_{\nu+1}+[A-(\nu+\lambda)(2\nu+2\lambda+1+4b\alpha/\beta-\alpha/\beta)]c_\nu+[(\nu+\lambda-1)(\nu+\lambda+1/2-\alpha/\beta)+(1/4)(\alpha^2/\beta^2-3\alpha/\beta+2)]c_{\nu-1}=0,$$

where $\lambda=0$ or $1/2$ for even and odd solutions, respectively.

Consequently, the solutions can be obtained in the form

$$\psi(\xi)=(1-z)^p\exp[-(\alpha/\beta)b(1+z)/(1-z)]\sum_{\nu=0}^{\infty}c_\nu z^{\nu+\lambda}.$$

When $\nu=0$ the recursion formula gives $c_1/c_0=-2A$ in the case of $\lambda=0$. On the other hand, c_1/c_0 can be expressed as an infinite

continued fraction by dividing this formula by c_ν and expressing $c_\nu/c_{\nu-1}$ in terms of $c_{\nu+1}/c_\nu$. This gives an equation which is satisfied by an infinite number of discrete values of A. The orders of magnitude of the constants involved indicate that the convergence of the continued fraction is fairly rapid. Thus, the eigenvalues of the energy E may be obtained by determining the appropriate values of A by a process of successive approximations.

[1] See M. L. Huggins, J. Phys. Chem. **40**, 723 (1936); A. R. Ubbelohde and I. Woodward, Proc. Roy. Soc. (London) **185**, 462 (1946).
[2] C. E. Nordman and W. N. Lipscomb, J. Chem. Phys. **19**, 1422 (1951).
[3] See the preceding letter.

Ozone Catalysis of Isotope Exchange between Molecular Oxygen Species

RICHARD A. OGG, JR., AND WILLIAM T. SUTPHEN
Department of Chemistry, Stanford University, California
(Received September 8, 1953)

SAMPLES of gaseous oxygen containing approximately 30 atomic percent O^{18} were made available through the courtesy of Professor A. O. Nier of the University of Minnesota. The samples had been stored at moderate pressure in sealed glass bulbs at room temperature for several years. Over this period no significant change had occurred in the mass ratios 34/32 (approximately 1.0) and 36/34 (approximately 0.01). Thus there is indicated under the stated conditions a negligible rate of attainment of the isotope exchange equilibrium

$$O^{16}O^{16}+O^{18}O^{18}\rightleftarrows 2O^{16}O^{18}$$

with the expected limiting value of 4.0 for the product of the mass ratios 34/32 and 34/36.

The simplest method of establishing the above equilibrium in the oxygen samples proved to be the passage of an electric discharge, as from a Tesla coil. It would appear likely that the mechanism of this process involves the atomic oxygen exchange reaction to be discussed below. Of considerably greater interest is the observation that gaseous ozone proves an extremely effective homogeneous catalyst for establishment of this equilibrium. The ozone was prepared from isotopically normal oxygen and separated by low-temperature fractional distillation. Suitable samples were mixed with portions of the enriched oxygen in Pyrex glass vessels. At the conclusion of each experiment the ozone was separated by low-temperature fractionation and then completely pyrolyzed. Mass spectrometer analyses were performed on this product oxygen, as well as on the highly O^{18} enriched gas sample after separation from the ozone.

Under our representative experimental conditions (partial pressures of ozone from 30 to 150 mm Hg, partial pressure of oxygen some 20 mm Hg, temperature 0°C) the rate of homogeneous decomposition of pure ozone is negligible.[1] The slight irreversible decomposition of the ozone noticed in the present experiments was probably due to surface catalysis. The most rapid homogeneous reaction observed was the approach to the above equilibrium. Contact periods of the order of ten minutes yielded a mass ratio product $34/32\times34/36$ of the order of 6.0 to 10.0 (compare original 100). The O^{18} isotope exchange between molecular oxygen and ozone proved under the stated conditions to be extremely slow—of the order of one-thousandth of the rate of the equilibration. The addition of chemically indifferent gases appears to be without effect on the rate of the equilibration processes, but to cause a marked enhancement of the O^{18} exchange between ozone and oxygen.

The extraordinary slowness of O^{18} exchange with ozone precludes the reaction

$$OOO+OO^{18}\rightarrow OO+OOO^{18}, \text{ etc.} \qquad (1)$$

as being significantly responsible for the catalysis of the oxygen equilibration, and it must be concluded that (1) has a large activation energy. The catalysis would appear to result from the presence of atomic oxygen, the species responsible for homogeneous ozone decomposition.[1] The proposed mechanisms follow:

$$O_3\rightarrow O+O_2, \qquad k_2; \qquad (2)$$
$$O+O_2\rightarrow O_3, \qquad k_3; \qquad (3)$$
$$O+OO^{18}\rightarrow OO+O^{18}, \text{ etc. } k_4. \qquad (4)$$

The observed rate constant for the ozone catalyzed reaction is interpreted as $(k_2/k_3)k_4$. The known thermodynamic properties of O_3, O_2, and O permit evaluation of the equilibrium constant k_2/k_3 at the temperatures employed, and hence of the rate constant k_4. The latter proves to be of the magnitude 10^{14} $(\text{Mole/cc})^{-1}$ sec^{-1}, indicative of a practically zero activation energy for step (4). Aside from a moderate statistical factor, k_4 is the rate constant for the formation of an energy-rich ozone molecule by collision of oxygen and ozone—a molecule which in the absence of stablizing collisions may dissociate randomly. The quasi-bimolecular association reaction (3) derives from this same energy-rich intermediate. The ratio k_3/k_4 constitutes that fraction of collisions between O and O_2 which are effectively stablizing collisions with a "third body." The experimental observation of the extremely slow isotope exchange with ozone indicates this ratio to be of the order of 10^{-3} at the above gas pressures. The systematic study of the enhancement by foreign gases of the rate of O^{18} exchange between ozone and oxygen promises a uniquely powerful experimental approach to the study of the quasi-bimolecular association (3).

The isotope enrichment under Professor Nier's direction was made possible by a grant from the American Cancer Society. Grateful acknowledgement of mass spectrometer analyses is made to Drs. Amos Newton and Constant Delwich, respectively, of the Radiation Laboratory and Department of Plant Biochemistry of the University of California, and to Professor Francis E. Blacet and Mr. Robert Vanselow, of The Department of Chemistry, University of California at Los Angeles.

[1] O. R. Wulf, J. Am. Chem. Soc. **54**, 156 (1932).

Chlorine Photosensitized Isotope Exchange between Molecular Oxygen Species

RICHARD A. OGG, JR.
Department of Chemistry, Stanford University, California
(Received September 17, 1953)

THE highly O^{18} enriched oxygen described in another communication[1] has been found to undergo a chlorine photosensitized isotopic exchange between the molecular oxygen species. Samples of the enriched oxygen (partial pressures of the order of 5-mm Hg) and of chlorine (partial pressures of the order of 200 mm Hg) were mixed in a 100-cm^3 Pyrex glass bulb and exposed to the unfiltered radiation from a General Electric H-4 mercury lamp. After a measured irradiation period of the order of a few hours, the bulb was chilled in liquid nitrogen, and an oxygen sample was withdrawn for mass spectrometer analysis. In a typical experiment the product of mass ratios 34/32 and 34/36 had been reduced to about 30 (compare the initial value of approximately 100). The rate appeared to depend (at least approximately) on the first power of the light intensity, the latter being varied by use of screens and by altering the distance from the source. The temperature coefficient has not yet been determined with great precision, but in the range 0°–100°C it appears to be appreciably negative. The absolute magnitude of the quantum yield is very much less than unity.

These experiments appear explicable only by the formation of ClO radical, first observed in the striking flash photolysis experiments of Norrish and Porter.[2] In its essential details the following mechanism resembles that proposed by these investigators. By "ClO_2" is meant the peroxy isomer ClOO.

$$Cl_2+h\rightarrow 2Cl, \qquad E_{abs}; \qquad (1)$$
$$2Cl+M\rightarrow Cl_2+M, \qquad k_2; \qquad (2)$$

$$Cl+O_2 \rightarrow ClO_2, \qquad k_3=f((M)); \qquad (3)$$

$$ClO_2 \rightarrow Cl+O_2, \qquad k_4=f((M)); \qquad (4)$$

$$Cl+ClO_2 \rightarrow 2ClO, \qquad k_5; \qquad (5)$$

$$2ClO \rightarrow Cl+ClO_2, \qquad k_6. \qquad (6)$$

Reaction (3) followed by (5), (6), and (4) necessarily leads to "scrambling" of molecular oxygen species. From the above mechanism the corresponding rate (aside from a small statistical factor) is

$$\frac{k_3k_5}{k_2k_4}\cdot\frac{E_{abs}(O_2)}{(M)}.$$

This is in agreement with data so far obtained, although the inhibitory effect of inert gas "M" has not yet been unambiguously demonstrated.

From the thermal data[2] for ClO, the reaction

$$2ClO \rightarrow 2Cl+O_2$$

is endoenergetic by about 8 kcal per mole. The extremely short life of ClO in flash photolysis[2] suggests that (6) has a negligible activation energy, and hence is exoenergetic, or at least thermoneutral. This would suggest that reaction (3) is at least 8 kcal per mole exoenergetic, and that (5) cannot be exoenergetic. Since k_3/k_4 is the equilibrium constant for the formation of ClO_2, and reaction (2) is expected to have a negligible activation energy, the overall activation energy corresponding to the above derived rate expression should be *negative* by 8 kcal per mole. That a negative temperature coefficient is in fact observed is indicative of the essential correctness of the mechanistic details. It appears unlikely that any other steps, as,

$$2ClO \rightarrow Cl_2+O_2,$$

can contribute appreciably to the overall process. Continuing studies of the reaction in question are aimed at greater precision, and are expected to cast further light on the properties of the peroxy ClO_2 species. Possibly the quasiunimolecular character of step (4) may be demonstrated.

The above experiments were suggested to the author in a personal discussion with Professor R. G. W. Norrish of Cambridge University. Acknowledgement is made to Professor A. O. Nier and to the American Cancer Foundation for the O^{18} enriched oxygen, and to Dr. Constant Delwich of the University of California for mass spectrometer analyses.

[1] R. A. Ogg, Jr., and W. T. Sutphen, J. Chem. Phys. **21**, 2078 (1953).
[2] See, for example, G. Porter, Discussions Faraday Soc. **1950**, No. 9, pp. 60–69.

Kinetic Evidence for the Gas Phase Existence of the Peroxy Radicals NO_4 and NO_3

RICHARD A. OGG, JR.
Department of Chemistry, Stanford University, Stanford, California
(Received September 17, 1953)

THE highly O^{18} enriched oxygen described in another communication[1] has been found to undergo changes in isotopic constitution on mixing with the vapor of isotopically normal dinitrogen pentoxide, N_2O_5. Gas samples were contained in 50-cm³ Pyrex glass bulbs maintained at 0° or 25°C. Analysis was performed by periodically chilling the bulbs in liquid nitrogen and removing an oxygen sample for mass spectrometer analysis. With comparable reactant pressures, of the order of 20 mm Hg, the principal reaction proved to be an O^{18} exchange with the N_2O_5, a process considerably more rapid than the pyrolysis of N_2O_5. If O_2 is in considerable molar excess over N_2O_5, further progress of the exchange is evidenced by changes in the 32, 34, and 36 abundances in the O_2, approaching the final equilibrium relations discussed elsewhere.[1] The rate of the exchange was not affected by the initial addition of NO_2. Separate experiments indicated that under the above temperature conditions NO_2 is without effect on O_2, either as regards O^{18} exchange or the disturbance of the 32, 34, 36 constitution. The exchange data so far obtained conform best to a rate expression first order in both N_2O_5 and O_2. The activation energy is approximately 20 kcal/mole.

The following mechanism for the exchange reaction appears to be the only one compatible with experimentally known facts. The formula NO_3 refers to the structural isomer $^{O}_{O}NO$ previously shown[2] to be important in N_2O_5 pyrolysis. The apparently novel species NO_4 is suggested to have a peroxide structure $^{O}_{O}NOO$. For clarity, reaction (5) is repeated with structural formulas, and seen to be an O atom transfer.

$$N_2O_5 \rightarrow NO_3+NO_2, \qquad k_1; \qquad (1)$$

$$NO_3+NO_2 \rightarrow N_2O_5, \qquad k_2; \qquad (2)$$

$$NO_2+O_2 \rightarrow NO_4, \qquad k_3; \qquad (3)$$

$$NO_4 \rightarrow NO_2+O_2, \qquad k_4; \qquad (4)$$

$$NO^{18}{}_4+NO_3 \rightarrow NO^{18}{}_3+NO_4, \qquad k_5; \qquad (5)$$

$$^{O}_{O}NO^{18}O \quad ON_O{}^{O} \rightarrow {}^{O}_{O}NO^{18} \quad OON_O{}^{O}.$$

The rate of the O^{18} exchange reaction between N_2O_5 and O_2 derived from this mechanism is (aside from a small statistical factor)

$$\frac{k_1k_3k_5}{k_2k_4}(N_2O_5)(O_2),$$

in agreement with the observed order. Since the energy change[2] associated with the equilibrium constant k_1/k_2 is approximately 20 kcal/mole, from the presently observed activation energy reaction (3) is exoenergetic by an amount equal to the activation energy of (5). Some structurally related reactions have associated activation energies of the magnitude of 6 kcal/mole. As a crude guess it may thus be suggested that reaction (3) is exoenergetic by about 6 kcal/mole. The standard entropy change for reaction (3) should be similar to that for the formation of N_2O_3 from NO and NO_2. These estimates suggest rough magnitudes of the equilibrium constant k_3/k_4 which enable appraisal of possible direct physical detection of the proposed species NO_4 in an O_2-NO_2 mixture. The conclusion is that no appreciable gas law deviations due to NO_4 formation are probable, but that there appears to be considerable promise in the direct search for the infrared spectrum of NO_4 in a high-pressure O_2-NO_2 mixture, employing a long optical path.

The peroxy NO_4 is seen to be formed from the "free radicals" NO_2 and O_2. Similarly, it might be expected that NO and O_2 would form an energetically stable peroxide ONOO, isomeric with the NO_3 discussed above. Provisional evidence for the existence of the peroxy NO_3 is found from isotopic exchanges accompanying the oxidation of NO with an excess of the O^{18} enriched oxygen described above. The results appear compatible only with the following mechanism.

$$(a) \quad NO+O_2 \rightarrow ONOO, \qquad k_a;$$

$$(b) \quad ONOO \rightarrow NO+O_2, \qquad k_b;$$

$$(c) \quad ONO^{18}O+ONO \rightarrow ONO^{18}+OONO, \qquad k_c.$$

In the order written the reactions are seen to be comparable, respectively, to (3), (4), and (5) of the previous mechanism. Positive evidence for the existence of ONOO strongly suggests it as the intermediate in the homogeneous oxidation of NO, the "rate determining step" being

$$(d) \quad ONOO+NO \rightarrow ONO+ONO.$$

If $k_b \gg k_d(NO)$ the familiar termolecular rate expression results, with rate constant $(k_a/k_b)k_d$. The negative overall activation energy indicates reaction (a) to be exoenergetic by an amount greater than the activation energy of reaction (d).

Acknowledgment is made to Professor A. O. Nier and to the American Cancer Foundation for the O^{18} enriched oxygen, and to Dr. Constant Delwich of the University of California for mass spectrometer analyses.

[1] R. A. Ogg, Jr., and W. T. Sutphen, J. Chem. Phys. **21**, 2078 (1953).
[2] Richard A. Ogg, Jr., J. Chem. Phys. **15**, 337, 613 (1947).

The Homomolecular Exchange of Oxygen*†

W. H. JOHNSTON AND C. J. O'SHEA‡
Department of Chemistry, Purdue University, Lafayette, Indiana
(Received September 18, 1953)

STABLE isotopes and a mass spectrometer make possible the study of exchange reactions between identical molecules. It is proposed that these be called homomolecular exchange reactions. In the case of a diatomic molecule such as oxygen, an initial non-equilibrium distribution of the three molecular species will approach equilibrium in a simple exchange reaction according to

$$\ln(1-\alpha)=\frac{-2Qt}{N}, \tag{1}$$

where Q is the rate of exchange in pairs of molecules exchanged per unit time, N is the number of molecules, and t is the time for a fraction of exchange, α. The expression for α is

$$\alpha=\frac{f_i^0-f_i}{f_i^0-f_i^\infty} \tag{2}$$

in terms of the change in the molecular fraction f_i of any one of the molecular species i and its complete change to the equilibrium fraction corresponding to a random isotopic distribution. Here f_i^0 and f_i^∞ are the initial and equilibrium fractions, respectively. Similar expressions apply to a two-element molecule such as nitric oxide, however, they necessarily involve the use of an enriched isotope of each element.

The study of the homomolecular exchange of oxygen was made with a sample of 25 percent oxygen-18 which was kindly provided by Professor A. O. C. Nier. Measurements of the molecular fractions were made with a Consolidated-Nier Mass Spectrometer, Model 21-201. No thermal exchange was observed in five months at room temperature. Using a quartz cell and a General Electric AH-4 mercury arc without the envelope a photochemical exchange was observed as shown in Fig. 1. The irradiation between 20 and 40 minutes consisted of alternating one-minute periods of irradiation and darkness. The absence of a deviation from a straight line suggests negligible exchange through a long-lived specie.

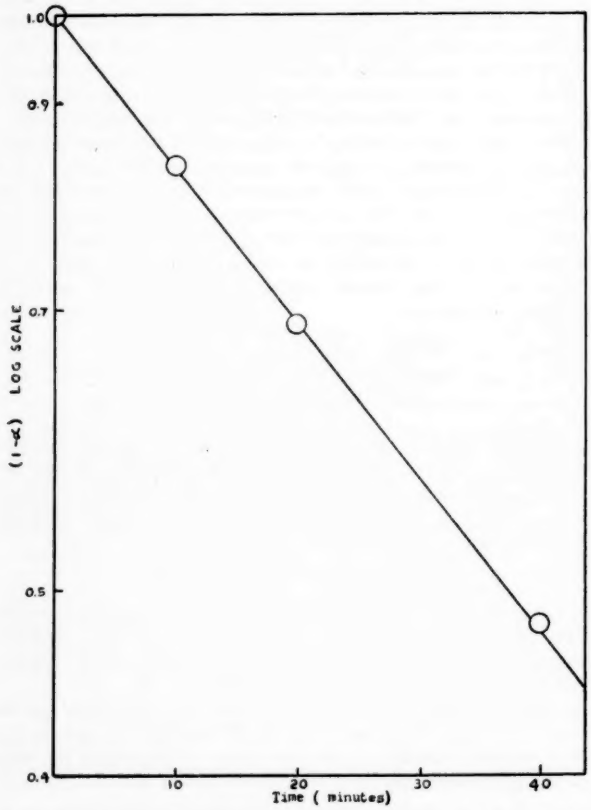

FIG. 1. Homomolecular exchange of O_2 during irradiation by a mercury arc.

A first-order exchange was also observed with 2537A radiation in the presence of mercury vapor. The half-time of exchange was 102 hours corresponding to a rate of exchange of 5.6×10^{13} sec^{-1}. A Gaertner quartz vacuum thermopile was used to calibrate the radiation which was isolated with a Bausch and Lomb Grating Monochromator. The determination of the absorption of radiation was difficult because of the large inversion of the 2537A radiation of the AH-4. An initial measurement of this fraction suggested a low quantum yield. However, a more precise measurement gave an absorption of 4.5×10^{11} quanta·sec^{-1} corresponding to a quantum yield of 125. This suggests that the mechanism of exchange is the chain reaction initiated by the mercury sensitized production of oxygen atoms,

$$O+O_2\rightarrow O+O_2. \tag{3}$$

This confirms the suggestion of Ogg[1] who proposed this reaction to account for his observation of an equilibration of oxygen by ozone.

* Presented in part before the 123rd Meeting of the American Chemical Society, Los Angeles, California, March 17, 1953.

† Supported in part by the U. S. Atomic Energy Commission under Contract AT(11-1)-166.

‡ Taken in part from the master's thesis of C. J. O'Shea, Purdue University, May, 1953.

[1] Richard A. Ogg, Jr., Comments during discussion of the paper at presentation (123rd American Chemical Society Meeting, Los Angeles, California, March 1953).

Gravitational Effects in PVT Measurements in the Critical Region

W. G. SCHNEIDER AND H. W. HABGOOD
Division of Pure Chemistry, National Research Laboratories, Ottawa, Canada
(Received September 18, 1953)

PVT measurements in the liquid-vapor critical region of a substance contained in a bomb of any considerable height may be seriously affected by gravitational effects. Until fairly recently corrections for such effects have been largely ignored with the result that the true nature of the critical isotherm was obscured.[1] The effect of the gravitational field on the nature of the liquid-vapor co-existence curve was previously demonstrated by observing the co-existence curve of xenon contained alternately in a long vertical bomb and in a very short bomb;[2,3] the long vertical bomb gave rise to a co-existence curve having a flat top over a wide density range, whereas with the short bomb a narrower curve with a rounded apex was obtained. It was shown that these results could be satisfactorily explained by assuming the existence of a unique critical point, as in classical theory, and taking into account the density distribution within the bomb imposed by the presence of the gravitational field. These conclusions have recently been confirmed by other workers.[4,5] To demonstrate the corresponding effect on PVT measurements, we have determined the critical isotherm of xenon contained first in a glass bomb, 25 cm by 10 mm, mounted horizontally, and then in a similar bomb mounted vertically. Here also, the results found with the vertical bomb can be explained in terms of the density distribution based on the isotherm measured in the horizontal bomb.

The detailed measurements with the horizontal bomb will be published shortly. For the measurements with the vertical bomb provision was made for measuring the pressure at any desired height within the bomb. This was accomplished by means of a mercury U-tube which could be moved up and down along the length of the bomb within the thermostat; the electrical contact point of the mercury surface in the U-tube served as the reference level for the pressure measurements.[6] The measurements at the critical temperature of xenon, 16.590°C, are given in Table I.

TABLE I. Measurements in vertical bomb at 16.590°C.[a]

Density, gm/ml	Meniscus level, cm	Hg contact level, cm	Pressure, atmos
1.3170	···	25.4	57.7068
			57.7086
		12.7	57.7245
			57.7240
		2.5	57.7369
			57.7367
1.2463	···	25.4	57.6398
		2.5	57.6661
			57.6651
1.2219	23.7	23.7	57.6355
			57.6355
			57.6361
			57.6350
		3.3	57.6596
1.1837	20.0	25.4	57.6307
		20.0	57.6360
		10.8	57.6460
		2.4	57.6563
1.1296	14.8	14.8	57.6353
1.0868	10.5	10.5	57.6356
1.0421	5.05	25.4	57.6144
		12.7	57.6284
		5.05	57.6353
1.0171	3.6	25.4	57.6153
		3.6	57.6348
0.9934	1.0	1.0	57.6350
0.9774	···	25.4	57.6071
		0	57.6270
			57.6260

[a] Note: Total height of bomb 25.4 cm.

At each density the contents of the bomb were thoroughly stirred and then allowed to settle for 4 to 24 hours. In Fig. 1 the circles indicate the pressures measured at the meniscus level, the height of which is of course dependent on the filling density. Within the limits of experimental error (± 0.0005 atmos) these points yield a horizontal portion, *BE*, on the critical isotherm, and in this range of densities the meniscus can be observed to disappear within the length of the bomb. This is exactly the behavior to be anticipated on the basis of the classical idea of a unique set of critical parameters, T_c, P_c, ρ_c, if the added effects of a gravitational field are taken into account.

From the critical isotherm determined in the horizontal bomb, also shown in Fig. 1, the variations of density and pressure with

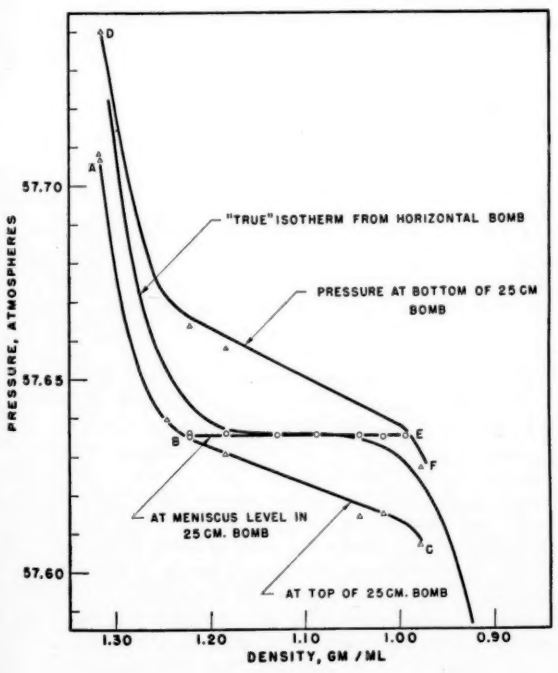

FIG. 1.

height above and below the meniscus were calculated. These are shown as smooth curves in Fig. 2. The directly measured pressures are indicated by circles and are seen to agree reasonably well. The density distribution curve shows good agreement with a similar curve obtained previously by means of a radioactive tracer technique,[7] while the pressure curve is in fair agreement with that deduced by Palmer[8] using optical interferometer measurements. Finally, the calculated range of average filling densities for which a meniscus may be expected to disappear within the length of the bomb was from 0.99 to 1.24 gm/cc, in good agreement with the observed values.

To illustrate the possible forms of isotherms which might be obtained from measurements in a vertical bomb as compared with the "true" isotherm obtained from the measurements in the horizontal bomb, the curves of Fig. 1 have been constructed using the relationships mentioned above. *ABC* is the isotherm which would be obtained if pressure measurements were made at the top of a 25 cm bomb; *DEF* that resulting from pressure measurements at the bottom; while *ABEF* would be obtained if the pressure were measured at the top for high densities, at the meniscus level for densities yielding a meniscus, and at the bottom for low densities. In each case the density plotted is the measured

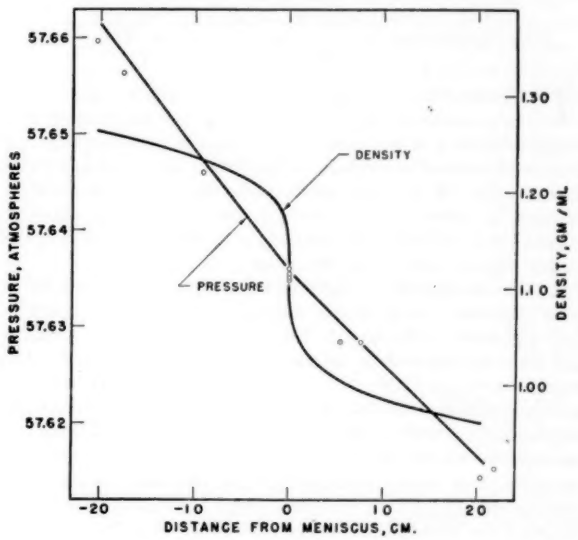

FIG. 2.

average density of the filling. Experimental points taken from Table I are shown for the three curves, three measurements at a height of 2.5 cm having been corrected to 0 cm.

The precise shape and the degree of flatness of the isotherms at, and just above the critical temperature are questions of some current interest. It can be seen that any uncorrected measurements made in a bomb as tall as 25 cm would be virtually useless on such a point. Furthermore, for such measurements it is doubtful whether corrections of the required magnitude could be determined accurately enough to reach any useful conclusion. In applying the necessary corrections, the question arises to what point (height) in the experimental bomb the pressures are to be corrected. At first sight it would appear that a proper choice would be the meniscus level, and this has been used.[6,9] However, on the basis of the present interpretation, this will necessarily result in a flat portion in the isotherm since the pressure at the level where the meniscus disappears (for different filling densities) is the unique pressure, P_c. What is wanted is the true isotherm which is characteristic of the substance in the absence of a gravitational field. To approximate such an isotherm we believe it is preferable to correct the measured pressures to that height in the bomb at which the local density is equal to the mean filling density of the

bomb. If the bomb is of small height, the uncorrected isotherm can be used to plot a density distribution curve, as illustrated in Fig. 2, and the inflection point of this curve is made to coincide with the meniscus level. From this curve the height where the local density is equal to the filling density is obtained and the necessary pressure correction can then be deduced. This was the procedure followed in obtaining the "true" isotherm of xenon shown in Fig. 1 from pressure measurements in the horizontal bomb. Since the effective height in this case was 10 mm, the pressure corrections were small.

[1] Schneider, "Changement de Phases" (Soc. chim. phys., Paris 1952), p. 69.
[2] Weinberger and Schneider, Can. J. Chem. **30**, 422 (1952).
[3] Weinberger, Habgood, and Schneider, Can. J. Chem. **30**, 815 (1952).
[4] Whiteway and Mason, Can. J. Chem. **31**, 569 (1953).
[5] Murray and Mason, Can. J. Chem. **30**, 550 (1952).
[6] MacCormack and Schneider, Can. J. Chem. **29**, 699 (1951).
[7] Weinberger and Schneider, Can. J. Chem. **30**, 847 (1952).
[8] Palmer, Ph.D. thesis, University of Wisconsin, 1952.
[9] Wentorf, University of Wisconsin Naval Research Laboratory, NO-ORD 9938, Report No. CM-724, May (1952), p. 56.

Microwave Spectrum of Pyridine*

K. E. McCulloh and Gilbert F. Pollnow
Department of Chemistry, State University of Iowa, Iowa City, Iowa
(Received August 13, 1953)

THE recent letter by Bak and Rastrup-Andersen[1] has prompted us to raise a question concerning the correctness of the interpretation of the microwave spectrum of pyridine as given by these authors and to indicate briefly the results of our independent investigation of the same problem. In the above-cited letter, an attempt to assign the spectrum on the basis of the asymmetry parameter $\kappa=0.6875$ failed to yield close agreement of calculated frequencies with the observed value.

In our investigation, 124 lines in the region 22.1–27.3 kmc have been observed, including the two highest frequencies reported by Bak and Rastrup-Andersen. Thirty-one Q-transitions with $J\leq 18$ and three R-branch lines have been assigned, corresponding to the case in which the dipole moment lies in the axis of least moment of inertia. Using the derived constants $\kappa=0.84777$, $(a-c)/2=1539.94$ mc, $(a+c)/2=4499.19$ mc, and taking centrifugal distortion into account by means of the symmetric rotor approximation, frequencies have been calculated for the assigned transitions, the average deviation from observed values amounting to less than 0.1 mc. The rotational constants listed above indicate a planar structure. Observed intensities, clearly dependent upon the parity of K_{-1}, required the presence of a twofold axis of symmetry; therefore, the point group must be C_{2v}. The excellent agreement between observed and calculated frequencies reported herein is taken as a strong argument for accepting the present interpretation of the microwave spectrum of pyridine, in preference to that proposed by Bak and Rastrup-Andersen. The complete results of our investigation will be submitted for publication in the near future.

* Work supported by the U. S. Office of Naval Research, Contract N8-onr-79400.
[1] B. Bak and J. Rastrup-Andersen, J. Chem. Phys. **21**, 1305 (1953).

Some Aspects of the Dissociation of Benzene Under Electronic Impact

J. L. Franklin and F. H. Field
Refining Technical and Research Divisions, Humble Oil and Refining Company, Baytown, Texas
(Received August 14, 1953)

HUSTRULID, Kusch and Tate[1] have published values for the appearance potentials of a large number of ions from benzene. When the work was done not enough was known about the energies of the gaseous ions for them to interpret their data; however, it is now possible to draw some conclusions about the ionization processes in benzene and the energies of certain of the fragments that are formed. The ions and their appearance potentials (corrected for the change in the $cm^{-1}-ev$ conversion factor) which we propose to discuss are listed in Table I.

TABLE I. Benzene ion appearance potentials.[a]

Ion	AP (ev)
$C_6H_6^+$	9.9
$C_6H_5^+$	14.6
$C_6H_4^+$	15.1
$C_4H_4^+$	15.6
$C_3H_3^+$	16.2
$C_2H_3^+$	21.2
$C_2H_2^+$	18.0

[a] Taken from Hustrulid, Kusch, and Tate, Phys. Rev. **54**, 1037 (1938).

$C_6H_5^+$.—The only ionization mechanism possible is $C_6H_6\rightarrow C_6H_5^++H$ from which it follows that $\Delta H_f(C_6H_5^+)=305$ kcal/mole. Some recent experimental work in this laboratory on benzene gives a value of 14.3 ev for the appearance potential of $C_6H_5^+$, which corresponds to a phenyl ion heat of formation of 298 kcal/mole. Furthermore, Honig[2] and Morrison and Nicholson[3] using electron impact methods have recently determined the ionization potential of benzene to be 9.43 and 9.52 ev, respectively. These are to be compared with Hustrulid, Kusch, and Tate's value of 9.9 ev. We mention these comparisons to illustrate the fact that the Hustrulid, Kusch and Tate data, while old, are probably reasonably accurate.

$C_6H_4^+$.—Two ionization mechanisms are possible: $C_6H_6\rightarrow C_6H_4^++H_2$, $\Delta H_f(C_6H_4^+)=368$ kcal/mole; and $C_6H_6\rightarrow C_6H_4^++2H$, $\Delta H_f(C_6H_4^+)=264$ kcal/mole. Comparing these heats of formation with that for phenyl ion, one must almost certainly come to the conclusion that the first ionization mechanism is the correct one. The carbon-hydrogen bond dissociation energy of the benzene molecule-ion is easily calculated by taking the difference of $A(C_6H_5^+)$ and $I(C_6H_6)$ to be 108 kcal/mole. If one assumes that the second carbon-hydrogen bond dissociation energy in benzene molecule-ion has about the same value, one calculates that the heat of formation of $C_6H_4^+$ ion is about 361 kcal/mole. Even taking into account the uncertainties in the assumption, the agreement indicates that the value of 368 kcal/mole which results from the first ionization mechanism is of a reasonable magnitude.

$C_4H_4^+$.—We postulate the reaction mechanism to be $C_6H_6\rightarrow C_4H_4^++C_2H_2$, $\Delta H_f(C_4H_4^+)=326$ kcal/mole. One can estimate the energy of the ion with structure

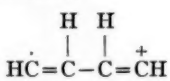

to be 329 kcal/mole by means of Franklin's[4] method of group equivalents. While this estimate is admittedly rather rough, the agreement of the estimated energy with that found experimentally leads us to believe that the postulated mechanism is correct and indicates that the $C_4H_4^+$ ion may have the butadiene radical ion structure.

$C_3H_3^+$.—We postulate the ionization mechanism $C_6H_6\rightarrow C_3H_3^++C_3H_3\cdot$, $\Delta H_f(C_3H_3\cdot)=109$ kcal/mole. The heat of formation of the $C_3H_3^+$ ion is well established,[5] and consequently we calculate the heat of formation of the neutral fragment formed in the ionization process. The choice of $C_3H_3\cdot$ as the neutral fragment formed can be made reasonable on the following grounds. The C—H bond dissociation energy in ethylene is known to be 122 kcal/mole,[6] and the choice of a value of about this order of magnitude for the C—H bond dissociation energy in allene is probably justifiable. Taking the value of 120 kcal/mole we calculate that the heat of formation of the $C_3H_3\cdot$ radical is 114 kcal/mole. The agreement with the experimental value is satisfactory. Reversing the argument, if it be assumed that the proposed ionization mechanism is the correct one, the C—H bond dissociation energy

in allene is 115 kcal/mole, which in turn tends to provide some support for the relatively high value of 122 kcal/mole which has been advanced for the C−H bond dissociation energy in ethylene. It is noteworthy that little activation energy seems to be involved in the ionization process even though two hydrogens must be shuffled around to form the $C_3H_3^+$ ion and $C_3H_3\cdot$ radical.

$C_2H_2^+$.—For this ion the energies are compatible with the ionization mechanism $C_6H_6 \rightarrow C_2H_2^+ + 2C_2H_2$, $\Delta H_f(C_2H_2) = 59$ kcal/mole. The satisfactory agreement with the known heat of formation of acetylene, 54 kcal/mole, constitutes quite good evidence for the correctness of the postulated ionization mechanism. Here again no very large amount of activation energy seems to be involved.

$C_2H_3^+$.—The ionization mechanism which requires the least energy is $C_6H_6 \rightarrow C_2H_3^+ + C_2H_2 + C_2H\cdot$; $\Delta H_f(C_2H\cdot) = 173$ kcal/mole. The value of 173 kcal/mole for $\Delta H_f(C_2H\cdot)$ corresponds to a C−H bond strength in acetylene of 171 kcal/mole, which is much higher than any previous estimates[7] of this value. It may be that the high value is the result of activation energy in the ionization process, but as has been pointed out in connection with some of the ions previously discussed, benzene decompositions involving only small activation energies do occur. In addition, Kusch, Hustrulid, and Tate[8] report data from which the C−H bond strength in $C_2H_2^+$ can be calculated $[D(CH{\equiv}C{-}H^+) = A(C_2H^+) - I(C_2H_2)]$, and the value that results is 152 kcal/mole. Similar results have been obtained in some very recent measurements on acetylene.[9] For ethylene it can be shown in the same way that the C−H bond strength in $C_2H_4^+$ is 76 kcal/mole, which is to be compared with 122 kcal/mole in neutral ethylene. If a similar relationship exists in the case of acetylene the value of 173 kcal/mole for the heat of formation of $C_2H\cdot$ is not unreasonable.

[1] Hustrulid, Kusch, and Tate, Phys. Rev. **54**, 1037 (1938).
[2] R. E. Honig, J. Chem. Phys. **16**, 105 (1948).
[3] J. D. Morrison and A. J. C. Nicholson, J. Chem. Phys. **20**, 1021 (1952).
[4] J. L. Franklin, Ind. Eng. Chem. **41**, 1070 (1949); J. Chem. Phys. (to be published).
[5] J. Delfosse and W. Bleakney, Phys. Rev. **56**, 256 (1939); F. H. Field, J. Chem. Phys. **20**, 1734 (1952).
[6] F. H. Field, J. Chem. Phys. **21**, 1506 (1953).
[7] J. S. Roberts and H. A. Skinner, Trans. Faraday Soc. **45**, 339 (1949).
[8] Kusch, Hustrulid, and Tate, Phys. Rev. **52**, 843 (1937).
[9] Private communication from Professor R. C. Anderson, University of Texas.

Valence Stabilization in Crystals

DIETER M. GRUEN
Chemistry Division, Argonne National Laboratory, Lemont, Illinois
(Received September 17, 1953)

IT is often possible to stabilize certain valency states of multiple valency cations in solid solutions with fixed valency cations. The phenomenon has been called "valence inductivity" by Selwood.[1] However, it appears that no attempt has been made as yet to correlate the observations with modern theories of nonstoichiometric compounds. The purpose of this note is to propose a model for the effect.

Consider for simplicity a binary compound MX (e.g., NiO) in which the cation M carries a formal charge of $+1$, the anion X a formal charge of -1. Assume that in the compound MX_{1+x} containing an excess of anions, but preserving the crystal structure of the stoichiometric MX phase, a fraction x of cations has been oxidized from M^+ to M^{++} and that the excess of anions is accommodated by the creation of holes on M^+ sites, the X^- lattice being taken as perfectly ordered. In the most favorable state energetically there will be $(Z-1)M^+$ and $1M^{++}$ nearest neighbors surrounding each positive ion vacancy, with electronic interchange taking place easily only between these Z ions (Z being of order of magnitude 10) which are adjacent to a lattice hole. A mechanism called *double exchange* has recently been proposed by Zener[2] which is of the sort required here. The exchange energy involved in the process $M^+{-}X^-{-}M^{++} \rightleftharpoons M^{++}{-}X^-{-}M^+$ may be of the order of several tenths of electron volts,[3] and is presumably increased by the possibility of resonance among Z sites. The ease of formation of positive ion vacancies must be closely associated with the energy of the ionization process $M^+ \rightarrow M^{++} + e$. Indeed, the most marked deviations from stoichiometry occur in compounds of the transition metals in which the metal ions have valency states separated by energies of a few volts. Thus, we see in the double exchange energy a mechanism for making a higher valency state more accessible.

Consider now the random replacement of M^+ ions in the MX phase by fixed valency cations A^+ having an ionic radius very close to that of M^+ (e.g., the isomorphous substitution of Ni^{++} in NiO by Mg^{++}). Each M^+ in the mixed crystal $M(A)X$ will be surrounded by $(Z-n)M^+$ and nA^+ nearest neighbors where n is a statistical function of the concentration of A. The creation of positive ion vacancies by the addition of excess X will become increasingly difficult with increasing concentration of A since the obvious result will be a progressive loss of exchange energy: A^+ cannot enter into double exchange with M^{++}. Suppose that the concentration of A is so large that most of the M^+ ions have only A^+ nearest neighbors. To preserve electroneutrality in the crystal, the creation of a positive ion vacancy by the addition of excess X now requires the oxidation of a next nearest neighbor M^+ to M^{++}. Roughly the energy for this process will increase as $-r^{-1}$ where r is the distance from the vacancy to the nearest M^+ ion.

The increased difficulty in oxidizing M^+ in lattices in which M^+ is being replaced by A^+ will, on the basis of this picture, be due to (1) loss of double exchange energy (2) increase in coulombic energy. Part (2) of the effect will become important at very low concentrations of M, where all of the M^+ nearest neighbors have been replaced by A^+ nearest neighbors. The M^+ valency state will thus have been "stabilized." A typical example of the effect has been observed by Prandtl and Huttner[4] in the Pr-oxide system. When pure Pr_2O_3 is heated in air, one obtains $PrO_{1.83}$. In this oxide 66 percent of the Pr is in the +4 valency state. Solid solutions of $La_2O_3 - Pr_2O_3$ containing 10 mole percent Pr when heated in air, yield an oxide in which only 10 percent of the Pr is in the +4 state. In this case we would say that the +3 state of Pr has been stabilized.

Studies have been made in this laboratory on solid solutions of UO_2 and ThO_2 in which similar effects have been observed. A detailed account of this work is to be published elsewhere.

[1] P. W. Selwood, J. Am. Chem. Soc. **70**, 883 (1948).
[2] C. Zener, Phys. Rev. **82**, 403 (1951).
[3] R. R. Heikes, "Ferromagnetism in non-metallic alloys," Ph.D. thesis, University of Chicago, 1953.
[4] W. Prandtl and K. Huttner, Z. anorg. u. allgem. Chem. **149**, 235 (1925).

The Sites of the Amino-Acid Residues on a Cyclol Model of Insulin*

GLADYS A. ANSLOW
Department of Physics, Smith College, Northampton, Massachusetts
(Received August 8, 1953)

IF consideration is given to the interaction of the ions of the medium, in which a protein develops, with the amino-acid cations and anions, it appears[1] that three types of protein skeletons may result: at high pH the polypeptide chain; at intermediate pH the modified Wrinch cyclol cage;[2] and at low pH the earlier Wrinch fabric.[3] Consequently the structure of many proteins, particularly the globulins, may be of the second type; i.e., a cage comprised of 48 members, 24 residues on 12 diazine rings linked through 24 single or higher linear peptides, thus forming eight interlocked hexapeptides, the linear peptides also being members of tetrapeptide rings. The infrared spectra resulting from such structures should consist of contributions from amide and carbonyl groups in the linear peptides, from hydroxyls in the diazine ring hydrogen-bonded to neighboring carbonyls, and from the chromophores in the side-chains. These frequencies appear in protein spectra, but

have been attributed to polypeptide chains by investigators, who assume the chain structure as characteristic of all proteins.

Consequent to the identification by Sanger *et al.*[4] of the amino-acid sequences, which appear in peptide fractions produced by the hydrolysis of oxidized insulin, and the interpretation of their origin as two pairs of polypeptide chains with 21 and 30 residues constituting the 12 000 *MW* monomer, attempts are being made to identify the cystine linkages between these chains and sequences of structural significance.[5]

Wrinch[6] has proposed that insulin monomers consist of two 48-unit cyclol cages of *MW* about 6000, which are bonded to form the 12 000 *MW* monomer. With this suggestion the subsequent report by Frederic and Neurath[7] that the 12 000 *MW* unit dissociates into subunits of 6000 *MW* fitted very neatly. To test the Wrinch hypothesis cyclol models of the subunit have been built by the author utilizing Fisher-Taylor-Hirschfelder atom units, assigning diazine sites to the more basic residues and linear peptide sites to

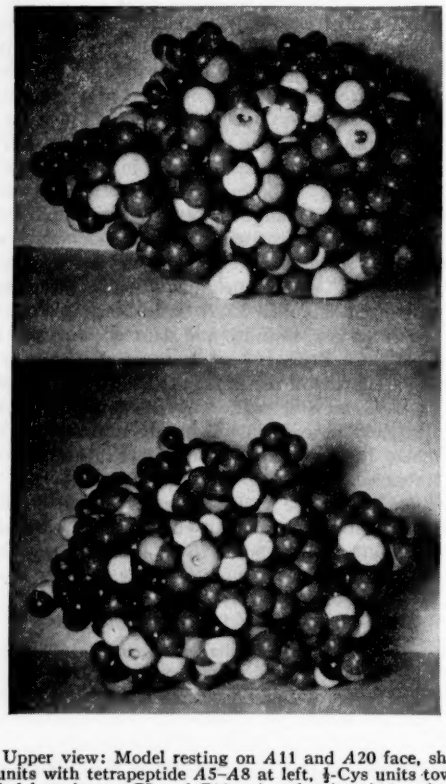

FIG. 1. Upper view: Model resting on *A*11 and *A*20 face, showing *B*7 and *B*19 units with tetrapeptide *A*5–*A*8 at left, ½-Cys units toward rear. Lower: Model resting on *B*7 and *B*19 units, showing *A*11 and *A*20 units, tetrapeptide at right.

the more acidic, while placing the Sanger fractions on connected rings so that these fractions would naturally result from the specific oxidation and hydrolysis processes.

In the arrangement depicted in Fig. 1 the six ½-cystine residues appear as three sets of neighboring pairs, suggesting that S–S bonds between two subunits produce the monomer and between adjacent monomers form dimers and other polymers. These pairs are *A*11 and *A*20, diametrically opposite on a relatively flat face, *A*6 and *A*7 in the flexible tetrapeptide, *A*5–*A*8 occupying a linear peptide site, and *B*7 and *B*19. When not involved in cross-bonding *A*5–*A*8 may become Gly-Cys-Ala. On the outer surface appear clusters of tyrosine and phenylalanine and the majority of the more basic residues. Hydrolysis fractions, which Sanger *et al.* designated as mixtures, appear as continuous sequences; additional recurring sequences, of possible significance for synthesis, are recognized.

Using the scale of the F-T-H atom units, 1 cm = 1A, approximate dimensions of the subunit are: diameter of the hexapeptide rings, 10A; distance between skeletal units on opposite faces, 15A; between the end groups on these faces, 22–24A, (30A to face containing *A*5–*A*8); distance between opposite tetrapeptide rings, 19.5A. The volume of the subunit is approximately 7.5×10^3A^3: the dimer is bounded by a rhombohedral cell approximately 44A×50A×30A. These are dimensions which appear in x-ray crystallography.[8,9]

* Supported by the U. S. Office of Naval Research.

[1] G. A. Anslow (to be published).
[2] D. Wrinch, Science **107**, 445 (1948); **116**, 562 (1952).
[3] D. Wrinch, Nature **139**, 972 (1937) and following.
[4] F. Sanger *et al.*, Biochem. J. **44**, 126; **45**, 563 (1949); **49**, 463, 481 (1951); **53**, 353, 366 (1953).
[5] C. Robinson, Nature **172**, 27 (1953).
[6] D. Wrinch, J. Chem. Phys. **16**, 1007 (1948).
[7] E. Frederic and H. Neurath, J. Am. Chem. Soc. **72**, 2684 (1950).
[8] D. Crowfoot Hodgkin, Proc. Roy. Soc. **A164**, 580 (1938); Nature **144**, 1011 (1939); Cold Spring Harbor Symposia on Quant. Biol. **14**, 65 (1950).
[9] B. W. Low, Nature **169**, 955 (1952).

Neutron Diffraction Study of Tetragonal Potassium Dihydrogen Phosphate*

S. W. PETERSON AND HENRI A. LEVY
Chemistry Division, Oak Ridge National Laboratory, Oak Ridge, Tennessee
AND
S. H. SIMONSEN,† *University of Texas, Austin, Texas*
(Received August 17, 1953)

THE position of hydrogen atoms in the crystal structure of tetragonal KH_2PO_4 has been studied by neutron diffraction. Three sets of single-crystal data were collected:

(*hk*0) zone, room temperature, λ = 1.16A and 0.93A.
(*hk*0) zone, ~140°K, λ = 1.062A.
(*h*0*l*) zone, room temperature, λ = 1.16A.

Indexes are based on a body-centered unit cell. Fourier projections were prepared from each set, phases being assigned from West's[1] parameter values for K, P, and O with the assumption that the hydrogen atoms are situated near the midpoints of the hydrogen bonds. A convergence factor having approximately the form of an artificial temperature factor was applied to ameliorate termination-of-series errors.

Each projection showed peaks assignable to hydrogen atoms centered at the midpoints of the hydrogen bonds and pronouncedly elongated along the hydrogen bonds. Detailed analysis of the peak shapes showed them to be equally consistent with two alternative descriptions of the hydrogen atom distribution:

(a) Mean location at the midpoint of the hydrogen bond with enhanced thermal motion along the bond direction (centered model).

(b) Mean locations at random about 0.15A from the midpoint with little or no asymmetric temperature motion (uncentered model).

Comparison of calculated and observed structure factors confirmed that both descriptions are consistent with the data.

Refinement of parameters included the following steps:

(1) Correction of parameters for residual termination-of-series errors by the back-shift method.[2]

(2) Computation of a difference synthesis with coefficients proportional to $(F_{obs}-F_c')$, in which F_c' includes calculated contributions from K, P, and O but not from H, without use of a convergence factor. Although this synthesis utilized the full resolving power of the data to detail the peak due to hydrogen, it did not permit a choice between the centered and uncentered models.[3]

(3) In the case of the 140°K data, a least squares refinement of the following parameters for hydrogen: displacement from the midpoint along the hydrogen bond, isotropic temperature factor coefficient, and anisotropic temperature factor coefficient perpendicular to the hydrogen bond. Initial values of these param-

eters were obtained from analysis of the peak in the $(F_{obs}-F_c')$ synthesis assuming an uncentered model.

The agreement factors $\Sigma|F_{obs}-F_{calc}|/\Sigma|F_{obs}|$ achieved for $(hk0)$ data are 8 percent at room temperature and 3.8 percent at low temperature. Refinement based on $(h0l)$ data is not yet complete.

The results of the study include several points of interest. Parameters for oxygen are essentially identical at both temperatures and are closer to those given by the x-ray study of Frazer and Pepinsky[4] at 126°K than to those from the study of West[1] at room temperature. The length of the hydrogen bond was found to be 2.48A at both temperatures. While the diffraction study alone does not distinguish between centered and uncentered hydrogen positions, the latter description is strongly favored by infrared spectral data[5] and by the existence of excess entropy.[6] The O−H distance, based on the uncentered model and the 140°K data, is 1.085A with an uncertainty (standard deviation) of 0.013A, and is thus considerably longer than that observed in other substances; e.g., 1.01A in ice[7] and 0.958A in H_2O gas.[8] The unusual length seems likely to be correlated with the unusually short hydrogen bond. (This uncertainty for the O−H distance is derived from the least squares calculation; the distance quoted might best be provisionally regarded as a lower limit, inasmuch as the variation in the least squares agreement as the centered model is approached has not been studied in detail.) The room temperature $(hk0)$ data, but not those at low temperature, require an asymmetric temperature factor for oxygen corresponding to enhanced motion along each projected P−O bond direction. A bending mode of the PO_4 group with large amplitude is thereby indicated; the existence of such a mode of easy deformation may be of interest in connection with the dielectric properties of KH_2PO_4.

The coherent neutron scattering amplitude of phosphorus evaluated from the data is 0.54×10^{-12} cm, positive phase.

* This work was performed under the auspices of the U. S. Atomic Energy Commission.

† Research participant, Oak Ridge Institute of Nuclear Studies, 1953.

[1] J. West, Z. Krist. **74**, 306 (1930).

[2] A. D. Booth, Proc. Roy. Soc. (London) **A188**, 77 (1946).

[3] R. Pepinsky, Science **117**, 1 (1953), also reference (5), has reported that a Fourier projection prepared from neutron diffraction data from KH_2PO_4 at room temperature shows the protons to be in double minima between oxygen atoms. Examination of the data and maps shows however that the apparently divided hydrogen peak is an artifact resulting from use of incomplete data and large errors due to non convergence. We thank Dr. Pepinsky for the opportunity to examine his maps and data.

[4] B. C. Frazer and R. Pepinsky, Acta Cryst. **6**, 273 (1953).

[5] R. E. Rundle and M. Parasol, J. Chem. Phys. **20**, 1487 (1952).

[6] C. C. Stephenson and J. G. Hooley, J. Am. Chem. Soc. **66**, 1397 (1944).

[7] S. W. Peterson and H. A. Levy, Bull. Am. Phys. Soc. (Albuquerque meeting, 1953).

[8] D. M. Dennison, Revs. Modern Phys. **12**, 175 (1940).

On the Influence of the Packing on the Atomformfactor Based on the Thomas-Fermi Theory*

KWAI UMEDA AND YASUO TOMISHIMA
Department of Physics, Faculty of Science, Okayama University, Okayama, Japan

(Received August 7, 1953)

As many investigators[1] have remarked, the atomformfactor for the atom at rest, f_0, will be in the crystal somewhat different from that in free space. In determining the form of the f_0 curve, the inner electrons which are not influenced by the exterior are of prime importance, while the outer electrons will play a role only for small values of $\sin\theta/\lambda$, since their effects cancel so rapidly by interference as $\sin\theta/\lambda$ increases. The juxtaposition of the atoms in the crystal must disturb principally the outer electrons, so that its influence on the shape of the f_0 curve should be noticeable only for small values of $\sin\theta/\lambda$. Since for atoms with $Z>25$ the f_0 curves calculated from the Thomas-Fermi (abbreviated as TF) field are accurate enough, we have investigated the influence of the packing on the shape of the f_0 curve on the basis of the TF theory.

For a TF atom Z, f_0 is given by

$$f_0(k)=\frac{Z}{k\mu}\int_0^{x_0}\sin(k\mu)x\cdot\phi^{\frac{1}{2}}/x^{\frac{1}{2}}\cdot dx$$

with $k=4\pi\sin\theta/\lambda$, $\phi=$the TF function, and $x_0=$the atom radius, or the lattice spacing, in the TF unit μ. The values of the TF functions for a number of lattice spacings have been tabulated previously by Slater and Krutter,[2] then by Feynman, Metropolis, and Teller,[3] and recently with higher accuracy by March.[4] By means of these values we have calculated numerically the values of f_0 for ten different values of $k\mu$ (see Table I) as well as for thirteen different lattice spacings ($x_0=1.19$ to 8.015) using the Filon[5] formula for evaluating the Fourier integrals. Since the f_0 curve for any TF atom Z can be obtained from that for a standard atom Z_0 simply by a change of scale, we have illustrated in Fig. 1 three f_0

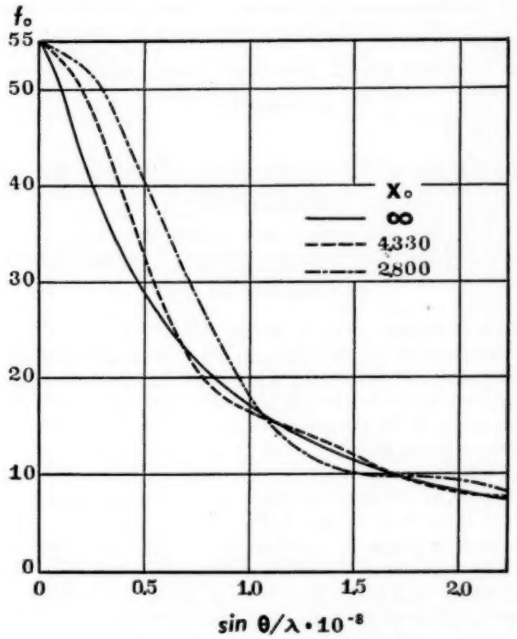

FIG. 1. f_0 curves for Cs atom in free space as well as in crystals with different lattice spacings.

curves as examples for caesium ($Z_0=55$) taken as the standard atom as usual. The packed f_0 curves ($x_0=$finite) converge to the free one ($x_0=\infty$) fluctuating about this more rapidly with increasing lattice spacing. From the figure we see that the expected properties mentioned above have been verified theoretically. The systematic fluctuating course of the value of $\delta f_0=f_{0\,\mathrm{exp}}-f_{0\,\mathrm{Hartree}}$ with increasing $\sin\theta/\lambda$, in particular the positive values of δf_0 for smallest values of $\sin\theta/\lambda$, observed by Wasastjerna[6] (see his Fig. 1), seems to be in favor of our results.

The free f_0 curve calculated by Bragg and West[1] from the charge distribution given by Thomas primitively has been hitherto always referred as the standard of the TF free f_0 curve, while that has in the region of larger values of $\sin\theta/\lambda$ somewhat too small values for the convergence limit of the sequence of the packed f_0 curves.

TABLE I. Atomformfactor for the free caesium atom at rest, f_0, calculated anew from Miranda's values of the TF function.

$k\mu$	0°	12.5°	25°	37.5°	50°	75°
$\sin\theta/\lambda\cdot10^{-8}$	0	0.141	0.282	0.423	0.564	0.845
f_0	55	47.53	38.69	32.09	26.97	19.97
$k\mu$	100°	125°	150°	175°	200°	
$\sin\theta/\lambda\cdot10^{-8}$	1.127	1.409	1.601	1.973	2.254	
f_0	15.50	12.46	10.28	8.67	7.43	

Thus we have recalculated that anew from Miranda's[7] most accurate values of the TF function. The results are given in Table I. There is our free f_0 curve just in the position expected from the sequence of the packed f_0 curves.

The tables of the numerical values of f_0 for finite lattice spacings obtained by us will be published shortly in the Research Notes of the Department of Physics, Faculty of Science, Okayama University, Okayama, Japan.

* Supported by the Scientific Research Expenditure of the Japanese Ministry of Education.

[1] W. L. Bragg and J. West, Z. Krist. **69**, 118 (1928); R. W. James and G. W. Brindley, Z. Krist. **78**, 470 (1931).

[2] J. C. Slater and H. M. Krutter, Phys. Rev. **47**, 559 (1935); P. Gombás, *Die statistische Theorie des Atoms und ihre Anwendungen* (Springer-Verlag, Vienna, 1949), p. 357. We have taken only three cases $x_0=1.19$, 1.69, and 2.20.

[3] Feynman, Metropolis, and Teller, Phys. Rev. **75**, 156 (1949).

[4] N. H. March, Proc. Camb. Phil. Soc. **48**, 665 (1952). We have taken all ten cases given in his Table 1.

[5] I. N. G. Filon, Proc. Roy. Soc. Edinburgh **A49**, 38 (1929).

[6] J. A. Wasastjerna, Soc. Sci. Fennica, Commentationes Phys.-Math. **13**, 1 (1946).

[7] C. Miranda, Mem. reale accad. naz. Lincei, Classe sci. fis. mat. e nat. **5**, 285 (1934).

The Rate of Recombination of Iodine Atoms in Solution*

ROYAL MARSHALL AND NORMAN DAVIDSON
Gates and Crellin Laboratories of Chemistry, California Institute of Technology, Pasadena, California
(Received August 8, 1953)

THE technique already used[1a,b] for the rapid photoelectric observation of the rate of the homogeneous three-body recombination of iodine atoms produced by the flash photolysis of molecular iodine in the gas phase has now been applied to the measurement of the rate of recombination of iodine atoms in the nonpolar solvents $n-C_7H_{16}$ and CCl_4.

The solution experiment is more difficult than the gas phase one because, at the same concentration of iodine atoms, the recombination rates in CCl_4 and C_7H_{16} are about 40 and 130 times faster than in argon at 1 atmos pressure. By increasing the cell length by a factor of 3 over that previously used (10 cm), the reaction rate for a given total number of iodine atoms per cm² in the spectrophotometer light path was decreased threefold. The flash lamp energies (200–400 joules; 4 μf, 10–15 kv) were also greater than those (50–70 joules) previously used. The flash lamp had a $1/e$ time of $\sim$25 μsec; nevertheless, amplifier blocking due to electrical and optical pickup from the flash prevents the required sensitive observation of iodine molecule concentration until about 200 μsec after the flash. Typical half-times for the recombination were in the range of 100–400 μsec, so that the early stages of the reaction were not observed. Typical initial changes in iodine molecule concentration for a 200 joule flash were $\sim 1-3\times10^{-7}M$ (M=mole/liter) (1–3 percent photodissociation) and the values of the fractional changes in photocurrent to be measured were $\sim 3-23\times10^{-4}$, whereas noise fluctuation was $\sim 5\times10^{-5}$. The solvents used were Phillips Petroleum Company pure grade n-heptane and Eastman Kodak spectrophotometer grade carbon tetrachloride. The former was further purified. Poorer grades of solvents gave anomalous results. The data for any one trace are not highly accurate and can be fitted to either a second- or a first-order integrated rate equation, but the smallness of the effects due to changing iodine molecule concentration and flash lamp energy show that the expected second order rate equation is indeed correct.

By extrapolation to zero time, the initial degree of dissociation of iodine was estimated. By comparison with the initial degree of dissociation for a gas cell where the quantum yield for photodissociation is known to be 1, rough estimates of the quantum yield ϕ for photodissociation in solution are obtained. The flash light passed through a filter which removed wavelengths less than 500 mμ and the quantum yields quoted are averages for the wavelengths greater than this emitted by the lamp and absorbed by iodine.

The values of k at room temperature for the equation

$$I+I\rightarrow I_2, \quad d(I_2)/dt=k(I)^2$$

are 2.2 ($\pm$0.4, mean deviation)$\times10^{10}M^{-1}$ sec^{-1} for C_7H_{16}; and 0.72 ($\pm$0.11)$\times10^{10}M^{-1}$ sec^{-1} for CCl_4. The rough estimation of the quantum yields are $\phi=0.41$ ($\pm$0.32) for C_7H_{16} and $\phi=0.19$ ($\pm$0.07) for CCl_4.

Measurement of the steady state concentration of atoms in illuminated solutions of iodine gives values of $k/\phi=2.4$ ($\pm$1.8) $\times10^{10}$ and 6 ($\pm$2)$\times10^{10}M^{-1}$ sec^{-1} for hexane and CCl_4.[2] This has been combined with the measurement of $k\phi$ by a chopped light measurement of the lifetime of photochemically produced iodine atoms in hexane to give $k=1.1\times10^{10}M^{-1}$ sec^{-1}, $\phi_{578}=0.37$, $\phi_{436}=0.59$.[3] A new direct determination of ϕ for iodine, using allyl iodide as a scavenger in air saturated solutions, gives at 25°, $\phi_{436}=0.66$ ($\pm$0.04) and 0.14 ($\pm$0.01) for C_6H_{14} and CCl_4.[4] In view of the difficulties in all of the various experiments, the measure of agreement between them should be regarded as satisfactory.

The ratio of three between the rate constants for recombination in heptane and CCl_4 may be compared to the ratio of 2.0 for the diffusion coefficients of molecular iodine in the two solvents at 20° ($D\times10^5=2.386$ and 1.177 cm² sec^{-1}).[5] Since the recombination reaction itself presumably has no activation energy, the over-all recombination process is diffusion controlled and $k=2\pi D\sigma$,[6] where D and σ are the diffusion coefficient and diameter of the iodine atoms. This formula applied to our results gives $D\sigma=58\times10^{-13}$ cm³ sec^{-1} (C_7H_{16}) and 19×10^{-13} (CCl_4), indicating rather large values of the effective collision diameter σ.

* Research supported by the U. S. Office of Naval Research, Project NR051-248.

[1a] R. Marshall and N. Davidson, J. Chem. Phys. **21**, 659 (1953); [1b] for independent measurements by this technique see Christie, Norrish, and Porter, Proc. Roy. Soc. (London) **A216**, 152 (1952); K. E. Russell and J. Simons, Proc. Roy. Soc. (London) **A217**, 271 (1953).

[2] E. Rabinowitch and W. C. Wood, Trans. Faraday Soc. **32**, 547 (1936), (some of the numerical data given here are incorrect and have been recalculated).

[3] J. Zimmerman and R. M. Noyes, J. Chem. Phys. **18**, 658 (1950).

[4] R. M. Noyes, private communication.

[5] C. C. Miller, Proc. Roy. Soc. (London) **A106**, 724 (1924).

[6] E. A. Moelwyn-Hughes, *Kinetics of Reactions in Solution* (Oxford University Press, Oxford, 1947), 2nd edition, p. 245.

Reaction of Optically Excited Mercury Vapor with Oxygen

DAVID H. VOLMAN
Department of Chemistry, University of California, Davis, California
(Received August 31, 1953)

RECENT discussions in this journal pertaining to the mercury photosensitized oxidation of hydrocarbons[1,2] have brought into consideration the reaction of optically excited mercury vapor with oxygen. Darwent[1] assumes that the reaction

$$Hg(^3P_1)+O_2\rightarrow HgO+O \qquad (1)$$

is an important process. Gray[2] has given evidence that this is probably not an important reaction. Results pertinent to this discussion obtained several years ago but hitherto unpublished are presented here.

The experimental technique has been described previously.[3] Oxygen at atmospheric pressure and 40° with mercury vapor at 0.0013 mm, corresponding to its saturation vapor pressure at 20°, was irradiated in a flowing system with a helical quartz mercury resonance lamp. The cylindrical reaction vessel, 20 mm in diameter, was coated on the outside with mineral oil to eliminate light of wavelength shorter than 2500A. The flow rate was 600 ml per minute corresponding to a linear velocity of 3.2 cm per second in the reaction vessel. Under these conditions approximately 10^{-4} mole of ozone was formed per liter of oxygen passed, and the quantum yield based on uranyl oxalate actinometry was approximately 0.03.

Calculations from these results show that, for every mercury atom entering the reaction zone, about 40 molecules of ozone are finally obtained. The number of ozone molecules formed is somewhat higher than this value since photodecomposition of ozone and reaction of ozone with mercury vapor have not been considered in the calculations. Mercuric oxide was deposited for a distance of about 5–8 cm from the start of the irradiation zone which had a total length of 25 cm. The deposit was most heavy at the start and then tapered off. These results are consistent with those of Dickinson and Sherrill[4] who were the first to report ozone synthesis by mercury photosensitization. They reported 7 molecules of ozone per mercury atom. This lower value may easily be accounted for by incomplete saturation with mercury, lower light intensity, and lower linear velocity of flow.

It is difficult to see how reaction (1) could account for the major results. Even on the basis of the results of Dickinson and Sherrill this reaction is highly improbable. However, on the basis of only 7 ozone molecules per mercury atom and the exothermicity of Eq. (1), some hope for an explanation based on an energy chain perhaps existed.

From the evidence presented here, it seems that mercury must undergo a large number of fruitful cycles to produce as much ozone as is actually found. The actual number of all cycles involving mercury may be even greater on account of the low quantum efficiency found. However, since mercury is actually eliminated from the gas phase in the first portion of the irradiation zone and ozone is being decomposed all along the reaction zone, the actual efficiency of ozone formation from $Hg(^3P_1)$ could be somewhat greater than the quantum yield indicates.

Mechanisms alternative to (1) will not be discussed here since Noyes and Leighton[5] have presented an excellent review of this topic. However, we hope to shed additional light on the mechanism by experiments now under way in these laboratories.

[1] B. deB. Darwent, J. Chem. Phys. **20**, 1979 (1952).
[2] J. A. Gray, J. Chem. Phys. **21**, 1300 (1953).
[3] D. H. Volman, J. Chem. Phys. **14**, 707 (1946).
[4] R. G. Dickinson and M. S. Sherrill, Proc. Natl. Acad. Sci. **12**, 175 (1926).
[5] W. A. Noyes and P. A. Leighton, *The Photochemistry of Gases* (Reinhold Publishing Corporation, New York, 1941).

On the Reaction Field of Polar Liquids

TH. G. SCHOLTE
Centraal Laboratorium der Staatsmijnen, Geleen, The Netherlands
(Received August 17, 1953)

RECENTLY, Frood and Dekker[1] published a computation of the reaction field of spherical molecules with an eccentric dipole moment. They found that the average reaction field of an extended dipole μ of arbitrary position and direction in a spherical particle with radius R and with dielectric constant ϵ_i, embedded in a homogeneous dielectric with dielectric constant ϵ_0, can be given by the equation:

$$E_r=\frac{2(\epsilon_0-1)}{R^3(2\epsilon_0+\epsilon_i)}\mu.$$

So E_r has the same value as if there were a mathematical dipole μ in the center of the particle.

It seemed useful to mention that this can be considered as a special case of the general problem of a spherical particle with an arbitrary distribution of charge in a homogeneous dielectric. This problem has been examined in my thesis[2] and has also been dealt with in Böttcher's new book.[3] It has appeared that if one considers the charge as the sum of an electrical point charge, a mathematical dipole with three components, a mathematical quadrupole with five components, and so on, all in the center of the particle, the reaction field can be computed as the sum of the reaction fields of these parts. Since the point charge has no reaction field and the quadrupole and the poles of higher order give a reaction field with an average value equal to zero, only the dipole contributes to the average reaction field.

With a polarizable particle this conclusion also holds if the polarizability is evenly distributed over the entire particle. For, in that case, only the average reaction field gives rise to an induced dipole moment.

So only the dipole part of the whole charge distribution has to be taken into account for the average reaction field and for the dielectric constant of a polar liquid if the Onsager-Böttcher model is used.

[1] D. G. Frood and A. J. Dekker, J. Chem. Phys. **20**, 1030 (1952).
[2] Th. G. Scholte, Thesis, University of Leiden (1950), p. 11.
[3] C. J. F. Böttcher, *Theory of Electric Polarisation* (Elsevier Publishing Company, Amsterdam, Houston, London, New York, 1952), p. 94.

The Molecular Structure of B_5H_{11}

LOUIS R. LAVINE AND WILLIAM N. LIPSCOMB
School of Chemistry, University of Minnesota, Minneapolis, Minnesota
(Received August 24, 1953)

ANALYSIS by three-dimensional Fourier and least squares methods of 298 x-ray diffraction maxima from single crystals of B_5H_{11} has yielded its molecular structure. There are four molecules in a monoclinic unit cell having parameters $a=6.76$, $b=8.51$, $c=10.14$A and $\beta=94.3°$. The space group, $P2_1/n$, is unique. Boron positions were located unambiguously from analysis of the three-dimensional Patterson function. The hydrogen atoms appeared as the eleven highest peaks in the asymmetric unit, containing one molecule, in a three-dimensional Fourier series from which the contributions of boron atoms were subtracted. Although no molecular symmetry is required the molecular dimensions indicate C_s symmetry. Within our limits of error all B—H (nearly single bond) distances are equal, and all B—H_b (bridge) bonds are equal. The unusual hydrogen atom, Hu, at the center of Fig. 1

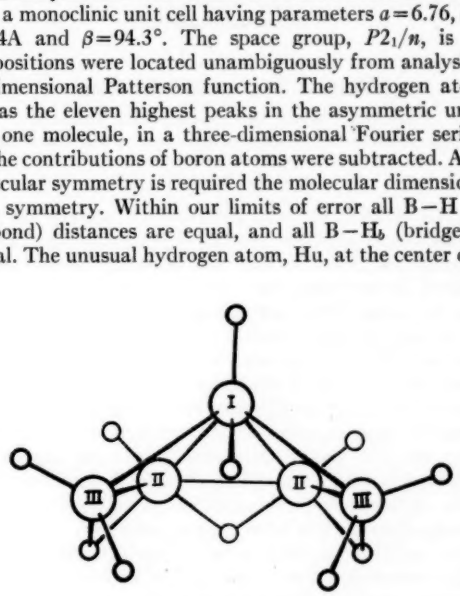

FIG. 1. The molecular structure of B_5H_{11}.

is singly bonded to B_I, but also can be said to form very weak bonds, bond order about $\frac{1}{6}$, to the neighboring B_{III} atoms. Molecular parameters, and their average deviation from the mean when more than one is averaged, are two $B_IB_{III}=1.86_5\pm0.00_5$A, two $B_{II}B_{III}=1.75\pm0.02$A, two $B_IB_{II}=1.72\pm0.02$A, one $B_{II}B_{II}=1.77$A, seven B—H$=1.07\pm0.04$A, six B—$H_b=1.24\pm0.07$A, one B_I—Hu$=1.00$A, and two B_{III}—Hu$=1.67\pm0.09$A. While these average deviations may be comparable with probable errors, it is possible that the incompleteness of our Fourier series may give rise to some systematic shortening of the B—H distances. This shortening is slightly greater than that[1] for B_4H_{10} where the Fourier series was more complete. However, the molecular geometry seems to be established.

That the boron atoms are a fragment from the icosahedron seems to have been generally expected from the principles previously realized from studies of $B_{10}H_{14}$[2] and B_5H_9.[3] Although one cannot predict the hydrogen positions with confidence an arrangement close to that in Fig. 1 can be obtained by taking apart the $B_{10}H_{14}$ structure, and by adding onto the B_4H_{10} structure,[1,4] as has been pointed out to us.[5] Both of the highly reactive B_5H_{11} and B_4H_{10} molecules have relatively open structures as compared

with the compact arrangements in $B_{10}H_{14}$ and B_5H_9. The geometrical properties of these fragments of the icosahedron or octahedron, the occurrence of bridge hydrogens at open edges, and the ligancy of five or six for boron are principles now common to all of the boron hydrides whose structures are established. The unusual hydrogen atom in B_5H_{11} may, however, be an intermediate type, between a normal "singly bonded" hydrogen and a bridge hydrogen, perhaps not too dissimilar to the unsymmetrical hydrogen bridges previously established in $B_{10}H_{14}$[2] and in B_4H_{10}[0,1].

Support of this work by the Office of Naval Research is gratefully acknowledged. The three-dimensional Fourier work was carried out on the X-RAC at Pennsylvania State College, and the least squares treatment at the Computing Center of the University of Minnesota. We wish to thank Dr. L. V. McCarty of the General Electric Company, Schenectady, New York, for supplying us with a sample of pure B_5H_{11}.

[1] C. E. Nordman and W. N. Lipscomb, J. Am. Chem. Soc. (to be published).
[2] Kasper, Lucht, and Harker, Acta Cryst. **3**, 436 (1950).
[3] W. J. Dulmage and W. N. Lipscomb, Acta Cryst. **5**, 260 (1952). Hedberg, Jones, and Schomaker, Proc. Nat. Acad. Sci. U. S. **38**, 679 (1952).
[4] Jones, Hedberg, and Schomaker, J. Am. Chem. Soc. (to be published).
[5] M. E. Jones, private communication.

Triplet States in Solution

GEORGE PORTER AND MAURICE W. WINDSOR
Department of Physical Chemistry, University of Cambridge, Cambridge, England
(Received August 19, 1953)

PHOTOCHEMICAL and fluorescence studies of aromatic molecules in solution indicate that metastable biradicals in the lowest triplet level, formed by a radiationless transition from the excited singlet state, may be intermediates in the chemical change. At present the observed kinetic laws of the over-all reaction do not allow a choice to be made between the several possible mechanisms and direct observations on the triplet molecule itself are lacking. While absorption from triplet levels can be observed by using steady cross illumination in glasses at very low temperatures,[1,2] under which conditions the lifetime approaches the true radiative lifetime, the rapid deactivation or reaction makes this method inapplicable in solution. The high efficiency of photochemical oxidation in solution[3] coupled with the observations of McClure[2] suggest, however, that if time intervals of the order of 10^{-5} second could be resolved and a high intensity source used, the direct study of triplet-state molecule reactions in solution might become possible.

We have applied the method of flash photolysis and flash spectroscopy[4] to the study of the photolysis of aromatic molecules in solution and in all polynuclear compounds so far investigated we have detected transient absorption spectra which are attributed to absorption from the lowest triplet level. The example in the accompanying figure was obtained with a 10^{-5} molar solution of anthracene in hexane from which dissolved gases had been carefully removed. Each spectrum was recorded by a flash lasting 25 μsec. The fluorescence resulting from the photolysis flash alone is shown in the first spectrum. The second spectrum, taken before the photolysis flash, shows the absorption of normal anthracene in the ground singlet state and subsequent spectra were taken in arbitrary order at increasing time intervals after photolysis. Immediately after photolysis there is a decrease in the absorption of the singlet state accompanied by the appearance of new absorption bands at 4203 and 3980A and a continuous absorption beginning at 2800A which increases to lower wavelengths until it overlaps the second singlet system. The bands are attributed to absorption from the lowest triplet level to two vibrational levels of an excited triplet state, the continuum arising from the transition to a second electronically excited triplet state. The triplet spectra disappear, and the singlet absorption returns to its original intensity, with a half time of about 100 μsec. The conversion time is unchanged in ethanol solution but is increased by a factor of ten in the more viscous solvent, glycerol. Similar spectra have been obtained with solutions of naphthalene, phenanthrene, naphthacene, triphenylene, chrysene, pyrene, 3,4-benzphenanthrene, 1,2-benzanthracene, 1,2,5,6-dibenzanthracene, perylene, rubrene, coronene, β-bromonaphthalene, α-chloroanthracene and also diacetyl. All have lifetimes in hexane of 100 μsec or less and there is no obvious correlation of lifetime with molecular structure.

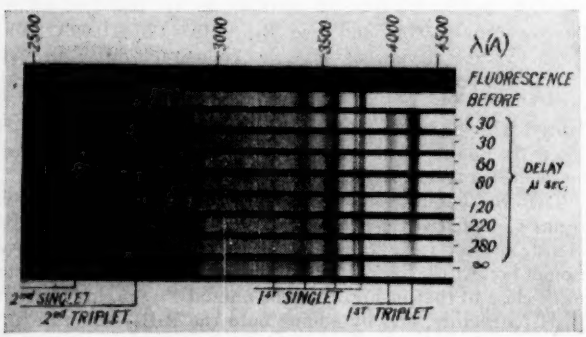

FIG. 1. Flash photolysis of a 10^{-5} molar solution of anthracene in hexane.

It is clear that the formation of triplet states by photolysis in solution is a general phenomenon. It is also one of major importance, as is shown by the fact that in some cases about 50 percent conversion to the triplet state is produced by a single flash. These high conversions make possible the direct measurement of absolute concentrations and hence of extinction coefficients and transition probabilities of the triplet transitions. Of most promise to the chemist is the fact that the reactions of triplet molecules in solution become amenable to direct kinetic investigation.

We are grateful to the British Rayon Research Association for financial support and to Dr. E. J. Bowen and Professor J. W. Cook for samples of hydrocarbons.

[1] Lewis, Lipkin, and Magel, J. Am. Chem. Soc. **63**, 3005 (1941).
[2] D. S. McClure, J. Chem. Phys. **19**, 670 (1951).
[3] E. J. Bowen, Faraday Soc. Discussions **14**, 143 (1953).
[4] G. Porter, Proc. Roy. Soc. (London) **A200**, 284 (1950).

Quenching of Organic Phosphorescence

M. KOIZUMI AND S. KATO
Institute of Polytechnics, Osaka City University, Osaka, Japan
(Received August 20, 1953)

FROM the standpoint of photochemistry, it is important, as we believe, to measure the quenching action of many substances upon the organic phosphors and especially to determine whether the action affects the singlet (S') or triplet state (T). Concerning this problem, we have derived the kinetic formulas for the initial intensity I_{p0} and natural life τ (or decay constant $\alpha=1/\tau$) on the ground of Lewis' model.[1]

The results obtained are as follows: (The approximation was made in consideration of the fact that the life of S' state is very short compared with that of T state.)

$$I_p=I_{p0}e^{-\alpha t},$$

$$I_{p0}=\frac{n_uQ}{(n_e+n_i+n_u+q)(n_e'+n_i'+n_u'+q')-n_un_u'}\times\left(n_e'+\frac{n_u'n_e}{n_e+n_i+n_u+q}\right), \quad (1)$$

$$\alpha=n_e'+n_i'+q'+\frac{n_u'(n_e+n_i+q)}{n_e+n_i+n_u+q}. \quad (2)$$

In the foregoing equations, Q is the number of photons absorbed

per sec during illumination. The various transitions probabilities from S' (Fig. 1) are: n_e, transition with radiation to the ground

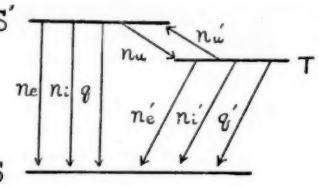

FIG. 1. Lewis' scheme o phosphorescence.

state; n_i, transition caused by the inner quenching effect; q, transition caused by the action of a quenching substance; and n_u, transition to the triplet state. The analogous quantities from T are n_e', n_i', q', and n_u'.

When there is no quenching action of any kind, Eqs. (1) and (2) are expressed as follows:

$$I_{P_0}^{(0)}=\frac{Q}{\alpha^{(0)}}\times\frac{n_u\{n_e'(n_e+n_i+n_u)+n_en_u'\}}{(n_e+n_i+n_u)^2}, \tag{1a}$$

$$\alpha^{(0)}=n_e'+n_i'+\frac{n_u'(n_e+n_i)}{n_e+n_i+n_u}. \tag{2b}$$

As a special case, when the quencher only affects T state, (1) and (2) will be simplified as follows:

$$\alpha^{(q')}=\alpha^{(0)}+q',$$

$$I_{P_0}^{(q')}=\frac{Q}{\alpha^{(q')}}\times\frac{n_u\{n_e'(n_e+n_i+n_u)+n_en_u'\}}{(n_e+n_i+n_u)^2}$$

$$=I_{P_0}^{(0)}\times\frac{\alpha^{(0)}}{\alpha^{(q')}}.$$

Thus when the quencher acts only on T state, the initial-intensity of phosphorescence ought to be proportional to its life.

As another special case, when the quencher only operates on S' state, Eqs. (1) and (2) are written as follows:

$$\alpha^{(q)}=n_e'+n_i'+\frac{n_u'(n_e+n_i+q)}{(n_e+n_i+n_u+q)},$$

$$I_{P_0}^{(q)}=\frac{Q}{\alpha^{(q)}}\times\frac{n_u\{n_e'(n_e+n_i+n_u+q)+n_en_u'\}}{(n_e+n_i+n_u+q)^2}$$

$$=I_{P_0}^{(0)}\frac{\alpha^{(0)}}{\alpha^{(q)}}\times\frac{(n_e+n_i+n_u)^2}{(n_e+n_i+n_u+q)^2}\times\frac{n_e'(n_e+n_i+n_u+q)+n_en_u'}{n_e'(n_e+n_i+n_u)+n_en_u'}.$$

In this case, any simple relation does not hold. But, it is expected that the intensity is reduced remarkably in contrast to a rather small change of α.

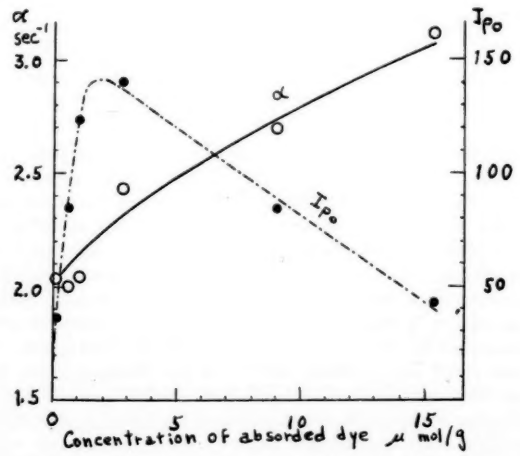

FIG. 2. Initial intensity and natural life as a function of concentration of adsorbed dye.

On the ground of the above deduction, we examined as a first step, the concentration quenching in the trypaflavine-filter paper phosphor. Decay curves of phosphorescence were measured by means of an oscillograph, and from them, the initial intensity and α were calculated. (LogI_{P_0}~t curve gave a straight line and from its inclination α was obtained.)

Some typical results are shown in Fig. 2. As is seen in the figure, I_{P_0} at high concentration of dye is about 1/3~1/4 of the maximum of I_{P_0} value, while α decreases only about 30 percent or so.

Tentatively assuming that q and q' can represent the concentration quenching and further assuming that all the transition probabilities remain constant, we can deny the possibility that T state is chiefly affected in the phenomenon of self-quenching.

Details will be reported in the *Journal of the Institute of Polytechnics*, Osaka City University.

[1] G. N. Lewis and M. Kasha, J. Am. Chem. Soc. **66**, 2100 (1944); Lewis, Calvin, and Kasha, J. Chem. Phys. **17**, 804 (1949).

The Slow Neutron Cross Section of Water

MILTON DANZKER
Westinghouse Electric Corporation, Pittsburgh, Pennsylvania
(Received September 18, 1953)

A CALCULATION of the total cross section of neutrons for hydrogen in water vapor has been made as a function of incident neutron energy in the thermal range. Curve I in Fig. 1

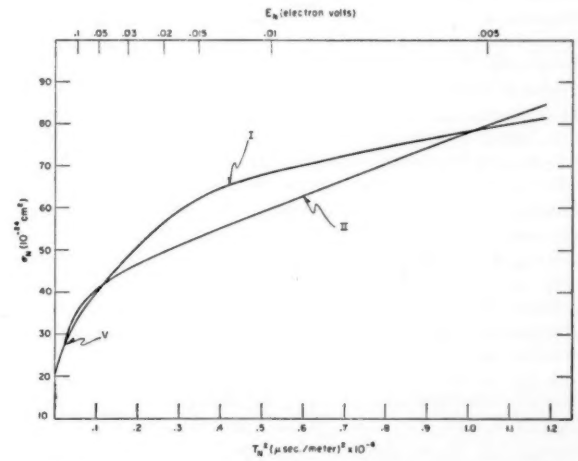

FIG. 1. Curve I—experimental for liquid water; Curve II—calculated for water vapor; and point V is where the first vibrational level of water vapor is excited.

represents this calculation where the total neutron cross section, σ_N, is plotted against the time of neutron flight squared, T_N^2. The energy of the neutron E_N is related to T_N^2 by the relationship, $T_N^2E_N=5227$, where E_N is in electron volts and T_N is in μsec/meter. The point V on the curve corresponds to the neutron energy that is just able to excite the first vibrational level of the water vapor molecule.

The calculation was made with the semi-classical MTV theory of Messiah[1] which is based on the classical reduced mass tensor method of Sachs and Teller. A linear molecular model was used whose fundamental frequencies were fitted to the experimental values for water vapor. The calculated curve differs significantly from the experimental curve found for liquid water at room temperature by Melkonian,[2] which is Curve II of Fig. 1.

In the experimental study by Melkonian on the thermal neutron cross section of liquid and gaseous n-butane no difference was observed between the curves for the two phases of butane.[2] This can be correlated with the relative constancy of the infrared spectra of hydrocarbons of this type in the solid, liquid, and

gaseous forms.[3] Apparently the molecular interaction energies are small compared to the carbon and hydrogen binding energies within the molecule; hence the molecular vibrational levels are only slightly perturbed in going from the gaseous to a condensed state. The case of water is different, however. There is a considerable shift of frequency and change of intensity as well as introduction of new bands in the infrared spectrum of water in proceeding from the gaseous to the condensed state. Thus the total neutron cross section might well be expected to be different for these two states, and the difference between Curves I and II is not unreasonable. In fact, the association of water molecules in the liquid state makes its neutron cross section for hydrogen similar to that for cetane, where curve for water vapor, as calculated, appears similar to that for methane.[2]

[1] A. M. L. Messiah, Phys. Rev. **84**, 204 (1951).
[2] E. Melkonian, Phys. Rev. **76**, 1750 (1949).
[3] G. B. Carpenter and R. S. Halford, J. Chem. Phys. **15**, 99 (1947).

Measurement of Electrode Polarization by the Current-Interrupter Method

SIDNEY BARNARTT
Westinghouse Research Laboratories, East Pittsburgh, Pennsylvania
(Received August 19, 1953)

RECENT potential-mapping studies[1,2] concerning the measurement of electrolytic polarization by the so-called direct method, wherein the tip of the capillary from the reference electrode is brought close to the polarized electrode, have clarified the two sources of error inherent in this method: (1) distortion of the electric field at the electrode, (2) inclusion in the measurement of an I.R. drop between the capillary tip and the electrode, since the measurement is made while current flows. It may be concluded from these studies that a considerable volume of published polarization data obtained by the direct method is inaccurate.

In order to avoid these two errors, many authors have utilized interrupted currents, whereby measurements are made during the open-circuit interval and are extrapolated to the instant of current interruption. It is clear that, if the electrode has been polarized with uniform current density over its surface, no I.R. drop is included in the measurement; and the connecting tube from the reference electrode may be terminated at some distance from the polarized electrode to eliminate the field-distortion error.

In the actual experimental cells, however, the current density over the electrode was not uniform. We wish to point out, and illustrate herein, that such nonuniformity itself leads to I.R. drops through the electrolyte, and therefore the polarization readings obtained will be dependent upon the positioning of the reference electrode.

An electrode over which the current density varies will generally become polarized to different potentials at different points on its surface. Just after the current is interrupted, the electrode surface may be conceived as being composed of many small areas of different potentials, the values of which will determine the electric field in the electrolyte. A potential map of such a field has been made in a model which approximately represents a disk electrode over which the polarization voltage increases linearly with radius from the center of the disk to the edge. The disk (radius R) was centrally situated against the closed end of an insulating tube (radius $3.44R$) which was filled with electrolyte. Figure 1 shows a map of the equipotential lines in a plane containing the axis of symmetry. The potential mapping was carried out in a wedge-shaped tank, with apparatus previously described.[2]

The electrode in the model was composed of eleven separate conducting elements, representing rings 1.0 cm wide and 0.5 cm apart. The total potential difference applied from the inner to the outer element was distributed in 10 percent steps among the intermediate elements. The equipotential lines in the electrolyte are also labeled as percentages of the potential difference from the center to the edge of the electrode. They show how the potential

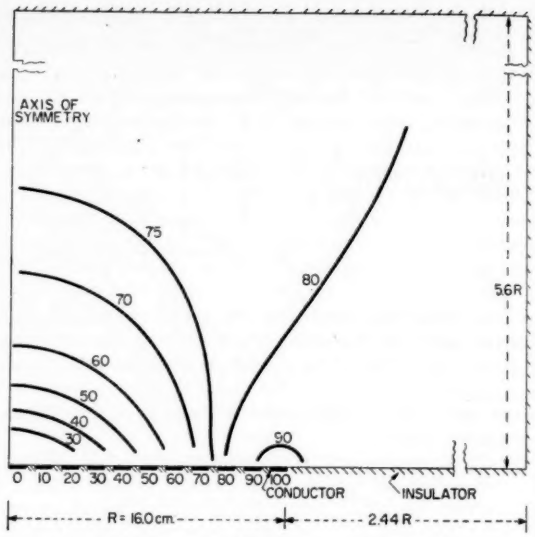

FIG. 1. Equipotential lines in the electrolyte around a disk electrode over which the potential varies linearly with radius from center to edge.

measured by a probe would vary with the positioning of the probe. Most of this variation takes place inside a hemisphere whose center is at the center of the electrode and whose radius is only slightly greater than that of the electrode.

In practice, the potential at the surface of a polarized disk would not generally vary linearly with radius. It is clear, however, that the potential measured by the reference probe will depend in general upon the positioning of the latter. When the reference electrode is in a fixed position relative to the polarized electrode, the polarization measurement may be readily duplicated, but the current density to which the measurement corresponds will not usually be known.

For accurate polarization measurements by the current-interrupter method, therefore, one should use an electrode over which the current density is uniform.

[1] R. Piontelli and G. Bianchi, Gazz. chim. ital. **80**, 581 (1950); Proc. Intern. Comm. Electrochem. Thermodynam. and Kinet., 2nd meeting (Milan, 1951), p. 379; Piontelli, Bianchi, and Aletti, Z. Elektrochem. **56**, 86 (1952); Aletti, Bertocci, Bianchi, Guerci, Piontelli, Poli, and Serravalle, Proc. Intern. Comm. Electrochem. Thermodynam. and Kinet., 3rd meeting (Milan, 1952).
[2] S. Barnartt, J. Electrochem. Soc. **99**, 549 (1952).

The Direct Production of Molecular Electron Spectra Using the Mass Spectrometer

J. D. MORRISON
Chemical Physics Section, Division of Industrial Chemistry, Commonwealth Scientific and Industrial Research Organization, Melbourne, Australia
(Received August 24, 1953)

FOR any process of ionization by electron collision, the second derivative of the ionization efficiency with respect to the electron energy scale is closely related to the term scheme of electronic energy levels for the resulting ion. If the electron beam used to produce the ionization were very closely mono-energetic, the second derivative of the ionization efficiency would consist of a series of sharp peaks at the energy levels of the ion, provided that the ionization probability for each process is a linear function of the excess energy above its ionization potential. This appears to be the case in all the processes studied so far. When a beam with a Maxwellian energy spread is used, each peak is spread out into a distribution which is the same as that of the electron energy but is reversed on the energy scale.[1]

In the previous work, the direct ionization efficiency I for the process studied was measured at electron energy intervals of ΔV

volts, and the differential ionization efficiency curves $\Delta I/\Delta V$ and $\Delta^2 I/\Delta V^2$ obtained by subtraction. This called for a high order of accuracy, not only in the measurement of I, but also in the equality of the intervals ΔV. Even with large analysed ion beam currents, the maximum accuracy which can be attained in the direct measurement of I is about 1 in 300. Accordingly, as the value of I increases, the scatter in the values of $\Delta I/\Delta V$ increases also, rapidly becoming as large as the values themselves. As ΔV requires to be as small as possible, it is difficult to obtain accurate differential *ie* curves over a range of more than a few volts above the initial onset of ionization.

If the mass spectrometer system is adjusted to detect a given ionic fragment, and the energy of the ionizing beam is set to some value V_1, a constant ion current I_1 is recorded which is proportional to the ionization efficiency for the process at that energy. If now a sinusoidal waveform of small amplitude and frequency f is superposed on V_1, a wave of the same frequency will be detected superposed on I_1. The peak-to-peak amplitude of the wave will be proportional to the first differential of the ionization efficiency at the energy V_1, and its phase with respect to the incident wave will be either 0° or 180°, depending on whether the sign of the differential is + or −. A detecting system which responds only to ac and is phase-sensitive will record this differential signal with an accuracy which is not dependent on the dc level of I_1. If V is now varied at a rate slow compared to f, the first differential *ie* curve will be traced out.[2] Further, if the ac detecting system is tuned to the second harmonic of the wave, i.e. $2f$, a voltage is obtained which is proportional to the second differential of the ionization efficiency at energy V_1, and by varying V the second differential curve can be traced out.[3]

This method of producing the second differential makes much less rigorous demands on the accuracy of the recording system, and the second differential ionization efficiencies can be recorded to as high an electron energy as desired. By its use the molecular electron spectra for a large number of molecules have been studied, and in all cases some details of structure are evident. The measurement of the lowest ionization potential of molecules is particularly simple, in that a sharp peak is obtained, the maximum of which gives a definite energy value.

In the figure are shown galvanometer traces of the first and second differential curves for the process $Hg \rightarrow Hg^+ + e$. The signal applied to the ionizing electron energy consists of a dc component, a periodic staircase waveform containing 60 steps which is repeated every 20 seconds, and a pure filtered sine wave. The gross details of the curve are recorded photographically using sine wave amplitudes of up to 1.0 volt peak-to-peak (ptp). This amplitude is then reduced to 0.1–0.2 volt ptp, the signal converted to digital form and correlated over a number of sweeps using the method described elsewhere,[4] in order to detect fine structure.[5] A fuller description of this technique and of the spectra obtained is being prepared for publication.

The author is indebted to Professor van der Pol for a discussion which contributed to the development of this method.

[1] J. D. Morrison, J. Chem. Phys. (to be published).
[2] This method was proposed by Rutherford, and applied by E. G. Dymond, Proc. Roy. Soc. (London) **A107**, 291 (1925).
[3] B. van der Pol and T. J. Weijers, Physica **1**, 78, and 481 (1933–34).
[4] J. D. Morrison, Rev. Sci. Instr. (to be published).
[5] The mass spectrometer used in this work was a modified Consolidated Engineering Corporation *type* 21.102.

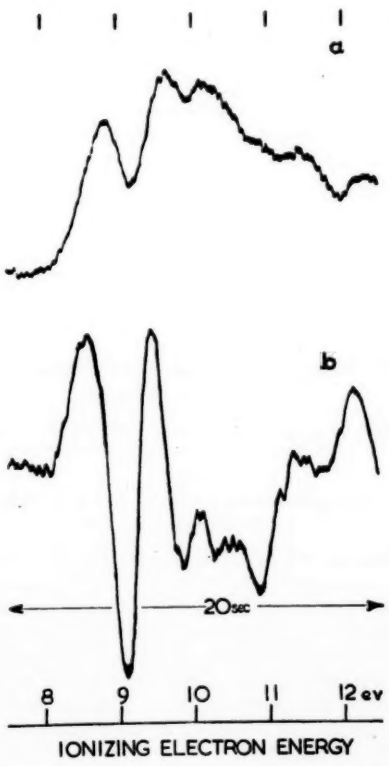

FIG. 1. First and second differential ionization efficiency curves for the process $Hg \rightarrow Hg^+ + e$ recorded directly with the mass spectrometer galvanometers over the range 7.5–12.5 ev. (a) First differential, sweep 5.0 volt, scanning sine wave, voltage 0.18 v, ptp 50 cps. (b) Second differential, sweep 5.0 volt, scanning sine wave, voltage 0.55 v, ptp 25 cps. Detecting system is tuned to 50 cps. Duration of sweep 20 seconds. The energy scale is not corrected for contact potential difference, etc.

The Photochemical Decomposition of Nitric Oxide by Absorption in the (0,0) and (1,0) γ Bands*

GORDON E. MOORE,† OLIVER R. WULF,‡ AND RICHARD M. BADGER
Gates and Crellin Laboratories of Chemistry, California Institute of Technology, Pasadena, California
(Received August 28, 1953)

THE abnormally large pressure broadening observed in the γ bands of NO[1,2] was interpreted by Wulf[3] as indicating a pressure-induced predissociation of the upper electronic state ($A^2\Sigma$). In an attempt to check this hypothesis Gaydon[4] irradiated NO at atmospheric pressure with the light from an iron arc and observed no evidence of decomposition after "long exposures."

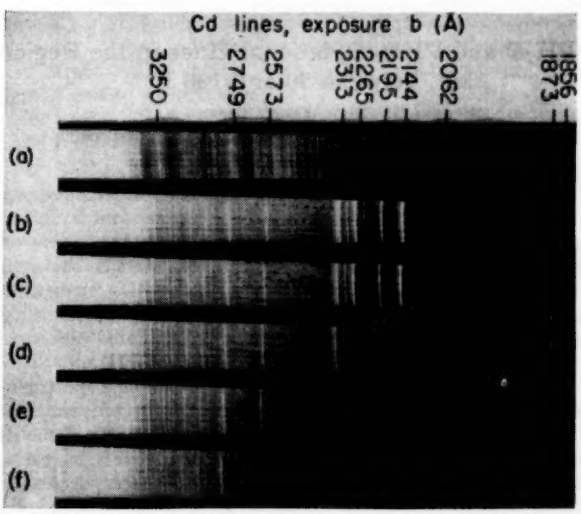

FIG. 1. All exposures were 100 seconds on a small Hilger spectrograph with the same slit width and source location. No lens was used between source and slit. (a) Iron arc, (b) Cadmium spark, (c) Cadmium spark filtered through 5.7 mm of NaCl, (d) Source as in (c) through a 25-cm absorption cell filled with NO to a pressure of 80 cm of Hg, (e) Through absorption cell after 15 minutes of irradiation, (f) Through absorption cell after 1 hour of irradiation.

Since the iron arc is a relatively weak source in the region of the γ bands (Fig. 1, exposure (a)), it was decided to repeat this experiment using a source with considerably more emission in this region.

A condensed spark between cadmium electrodes was chosen (exposure (b)) because of two strong lines at 2144 and 2265A, which overlap the (1,0) and (0,0) γ bands, respectively, (exposure (d)). In order to eliminate weak lines of higher frequency, the light was filtered through an NaCl plate, which was shown to eliminate effectively light of wavelength shorter than 2050A without appreciably weakening the desired lines (exposure (c)).

Decomposition was followed by observing the continuous absorption of N_2O_3,[5] which is formed as an end reaction product. Exposures (e) and (f) show the increase of this absorption after 15 minutes and 1 hour, respectively. That this decomposition was a photo effect by light in the region of the γ bands was demonstrated by experiments designed to rule out such possibilities as air leaks, induced electrical discharges, and light of higher frequency producing the decomposition products.

The observation of this decomposition is of interest because of its possible connection with the heat of dissociation of nitrogen. The absorbed lines have energies 5.77 and 5.46 electron-volts, considerably below the higher value for the heat of dissociation of nitric oxide (6.49 ev) as calculated from thermochemical data[6] and the two possibilities for the dissociation energy of nitrogen,[7] but more than the lower value (5.29 ev).

If the mechanism of this photo-decomposition of NO were shown to be predissociation, the lower value of the dissociation energy for NO and hence for N_2 would be established. Further experiments attempting to elucidate the mechanism will be undertaken.

* Contribution No. 1844 from the Gates and Crellin Laboratories, California Institute of Technology, Pasadena, California.
† E. I. DuPont Postgraduate Fellow, 1952–53.
‡ Member of the U. S. Weather Bureau.
[1] M. Lambrey, Compt. rend. **189**, 574 (1929); **190**, 261, 670 (1930); Ann. de Phys. **14**, 95 (1930).
[2] S. M. Naude, Phys. Rev. **36**, 333 (1930).
[3] O. R. Wulf, Phys. Rev. **46**, 316 (1934).
[4] A. G. Gaydon, *Dissociation Energies* (Dover Publications, Inc., New York, 1950).
[5] E. H. Melvin and O. R. Wulf, J. Chem. Phys. **3**, 755 (1935).
[6] National Bureau of Standards, *Selected Values of Chemical Thermodynamic Properties* (Washington 25, D. C., 1952).
[7] A. E. Douglas and G. Herzberg, Can. J. Phys. **29**, 294 (1951).

PH_2D and PHD_2 Rotational Lines in the Region between 50 and 100 K

RICHARD E. STROUP* AND ROBERT A. OETJEN
Department of Physics, The Ohio State University, Columbus, Ohio
(Received September 18, 1953)

THE rotational spectrum of phosphine and deuterophosphine have recently been investigated[1] by means of the far infrared spectrograph at The Ohio State University.[2] A study of the records made in attempting to obtain a spectrum of pure PD_3 shows that certain lines, not assignable to either PH_3 or PD_3, change their intensities from one record to another. The variation of intensity is so regular that certain of these lines may be associated with each of the partially deuterated phosphines, PH_2D and PHD_2.

Considerable difficulty was incurred in obtainlng a spectrogram of PD_3 and as a result a rather large number of records was made. If these records are arranged in order of the strength of the PD_3 lines one notices that some of the extra lines increase in intensity as the PD_3 concentration increases whereas others decrease in intensity. The data justify tentative identification of certain lines with PH_2D and certain others with PHD_2. Figure 1 shows a plot of the calculated PD_3 spectrum and an observed PH_3 spectrum along with two of the extreme records, a "poor sample" of PD_3 and therefore one strong in PH_3, and a "best sample" of PD_3 or one poor in PH_3. In these latter two spectra certain lines have been indicated by dots. The lines marked in the spectrogram labeled

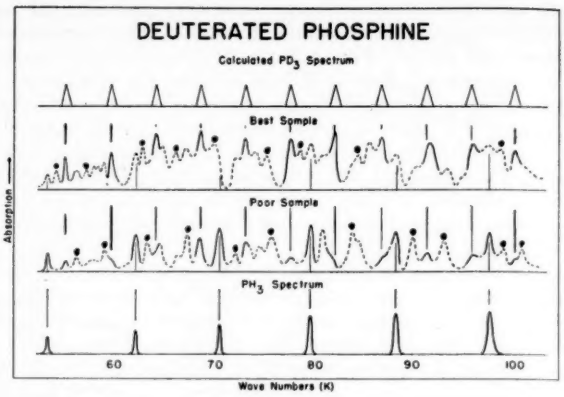

FIG. 1.

"best sample" have been assigned to PHD_2 and those lines dotted in the spectrograms labeled "poor sample" have been assigned to PH_2D. The values for the two sets of lines are listed in Table I.

TABLE I. Partially deuterated phosphine.

PH_2D	PHD_2
99.0 K	98.8 K
93.6	86.1
90.6	79.0
85.0	76.5
81.9	74.6
76.4	70.6
75.0	67.7
72.3	63.4
68.0	[57.7
63.5	[53.5
58.9	
56.1	

As the geometry of the phosphine molecule is known from the microwave investigations of Loomis and Strandberg,[3] it should be possible to predict the spectra of the partially deuterated phosphine and check the validity of the above assignments.

* Present address: Eastern New Mexico University, Portales, New Mexico.
[1] Stroup, Oetjen, and Bell, J. Opt. Soc. Am. (to be published).
[2] Oetjen, Haynie, Ward, Hansler, Schauwecker, and Bell, J. Opt. Soc. Am. **42**, 559 (1952).
[3] C. C. Loomis and M. W. P. Strandberg, Phys. Rev. **81**, 798 (1951).

Nuclear Magnetic Resonance Signals from a Tautomeric Mixture

H. S. JARRETT AND M. S. SADLER, *E. I. du Pont de Nemours & Company, Inc., Wilmington, Delaware*
AND
J. N. SHOOLERY, *Varian Associates, Palo Alto, California*
(Received August 24, 1953)

THE existence of keto-enol equilibria in β diketones and β keto esters was established by Kurt Meyer's bromine titration experiments.[1] The bromine titration technique has remained the most reliable method for determining the equilibrium ratio of the two forms. Studies of keto-enol equilibria have also been made by analysis of infrared[2] and ultraviolet[3] absorption spectra, and by refractive index measurements;[4] none of these methods has been generally applicable for providing accurate quantitative information on keto-enol equilibria.

We have succeeded in determining keto-enol equilibria in two β diketones by measurement of proton resonance with a high-resolution nuclear magnetic resonance spectrometer in the laboratory of Varian Associates at Palo Alto, California. Since this measurement cannot affect the equilibrium, it appears to be well

suited to determination of keto-enol equilibrium constants over a range of temperatures.

Nuclear magnetic resonance signals from the protons in 2,4-pentanedione (I) and 3-methyl-2,4-pentanedione (II) were observed with a resolution of a few tenths of a milligauss.

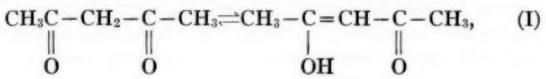

(I)

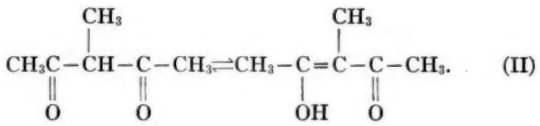

(II)

In Compound I there are four structurally nonequivalent kinds of protons in the equilibrium mixture, which can be identified with the CH_3, CH_2, CH, and OH groups. The peaks in Fig. 1 have

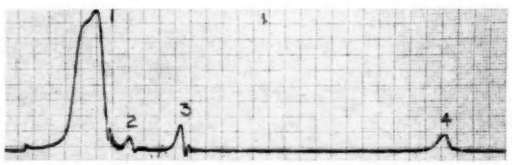

2,4-pentanedione
←H—

FIG. 1. Proton magnetic resonance from 2,4-pentanedione at 30 mc per sec in a field of 7000 gauss. Total sweep width is about 125 milligauss, the field decreasing linearly from left to right.

been assigned on the basis of relative areas under the curve. For example, peaks 3 and 4 with approximately equal areas must represent the OH and CH protons of the enol form. The signal occurring at the lowest applied field corresponds to the condition of least diamagnetic shielding and consequently should be the enolic OH proton. Peak 1 represents the CH_3 groups in both forms and peak 2 is the resonance of the CH_2 protons in the keto form.

Figure 2 is the complete spectrum obtained with 3-methyl-2,4-pentanedione (II), while Fig. 3 represents the left-hand portion of

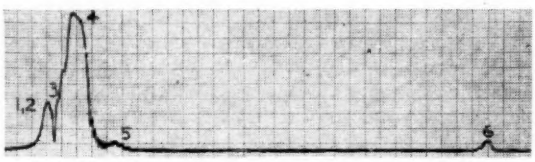

3-methyl-2,4-pentanedione
←H—

FIG. 2. Proton magnetic resonance from 3-methyl-2,4-pentanedione at 30 mc per sec in a field of 7000 gauss. Total sweep width is about 125 milligauss, the field decreasing linearly from left to right.

that spectrum with higher resolution. Peaks 1 and 2 of these figures have been assigned to the protons of the 3-methyl group in the keto form; the resonance absorption is split by spin-spin

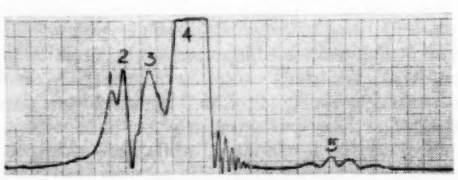

3-methyl-2,4-pentanedione
←H—

FIG. 3. Proton magnetic resonance from 3-methyl-2,4-pentanedione showing left-hand portion of Fig. 2 with higher resolution.

TABLE I.

	% Keto		% Enol	
	Proton reso-nance	Bromine titration[a]	Proton reso-nance	Bromine titration[a]
2,4-pentanedione	15	24	85	76
3-methyl-2,4-pentanedione	70	68.5	30	31.5

[a] See reference 1.

interaction with the adjacent proton. Peak 3 represents the 3-methyl group in the enol form, whereas peak 4 is identified with proton signals from the terminal CH_3 groups of both forms. Peak 5 is assigned to the CH hydrogen of the keto form, and in Fig. 3 the resonance splitting by spin-spin coupling with the CH_3 hydrogens is apparent. Peak 6 represents the enolic proton.

The relative proportions of keto and enol forms in both samples have been calculated by comparing areas under selected peaks of these spectra. In the case of 2,4-pentanedione, this calculation was made by comparing the area under peak 3 (enolic CH) with half the area under peak 2 (ketonic CH_2). In the case of 3-methyl-2,4-pentanedione, the area under peak 6 (enolic hydroxyl), Fig. 2, was compared with one-third the area under peaks 1 and 2 (ketonic 3-methyl group). The results of these calculations are shown in Table I and compared with reported values obtained by the bromine titration technique.

[1] K. H. Meyer, Ann. Physik **380**, 212 (1911); Ber. **45**, 2843 (1912); J. B. Conant and A. F. Thompson, Jr., J. Am. Chem. Soc. **54**, 4039 (1932).
[2] R. LeFevre and M. Welsh, J. Chem. Soc. **1949**, 2230; J. Powling and H. Bernstein, J. Am. Chem. Soc. **73**, 4353 (1951).
[3] P. Grossmann, Z. physik. Chem. **109**, 305 (1924); G. Briegleb and W. Strohmeier, Z. Naturforsch. **6b**, 6 (1951).
[4] K. H. Meyer and F. G. Wilson, Ber. **47**, 837 (1914).

Pre-Ignition and Flame Spectra in the Self-Combustion of Acetylene*

WM. W. ROBERTSON, N. B. HUMPHREY, AND ROBBIN C. ANDERSON
Department of Chemistry, University of Texas, Austin, Texas
(Received September 8, 1953)

EMISSION and absorption spectra of acetylene flames in the absence of oxygen have been obtained in an attempt to detect C_2 radicals and thus perhaps to clarify the kinetics of the self-combustion reactions of acetylene. The spectra were also checked for CH bands, though this is less likely as an intermediate in reactions. The spectral regions covered were the visible and the near ultraviolet, the spectra being recorded photographically on a 3-meter grating spectrograph.

The emission spectrum of the self-combustion flame was obtained by flowing preheated acetylene downward in a vertical quartz tube 3.5 cm in diameter, discharging into a large flask. The tube was heated with an external heating coil. By adjustment of the flow rate, a turbulent flame could be maintained for about 10 minutes before carbon deposited on the walls would begin to clog the tube. This was sufficiently long to obtain exposures under high resolution.

The observed emission spectrum was continuous, extending from about 3500 to 6000A with a maximum indicated at 5800A. No discrete bands or lines were observed.

The absorption spectra were recorded as acetylene flowed through a heated absorption cell, consisting of a tube 38 mm in diameter and 1 meter long having quartz windows cemented on. Cool acetylene flowed in through side-arms at each end of the cell near the windows and the hot gases were discharged through a side-arm at the center of the cell. The light source was a high-intensity Hanovia xenon arc.

Pure acetylene would ignite at a cell temperature of around 500°C and burn with the production of large quantities of carbon, plus acetylenic polymers, etc., that completely scattered and absorbed light entering the cell. Absorption spectra were recorded

at pre-ignition temperatures and showed a continuum that started in the ultraviolet and spread throughout the ultraviolet and into the visible as the cell temperature was raised from about 375° to the ignition temperature. These results are similar to those reported by Parker and Wolfhard[1] for diffusion flames and by Norrish, Porter, and Thrush[2] for oxy-acetylene flames with excess acetylene.

Samples of condensed products from the combustion cell also showed continuous absorption in the ultraviolet.

Absorption spectra at temperatures up to 500° above the normal ignition point were then recorded by using acetylene diluted with helium. (Cell temperatures around 1000°C could be reached for mixtures with 3–5 percent C_2H_2). A definite ignition of flame was not observable in mixtures containing less than 40 percent C_2H_2 by volume. At lower concentrations, however, a fairly definite temperature would still be reached at which the entering light would be effectively completely scattered by particles formed in the hot gas.

As with the pure acetylene, the absorption spectra were continuous, but with the limit extending to longer wavelengths as the temperature was increased. Typical microphotometer tracings are shown in Fig. 1.

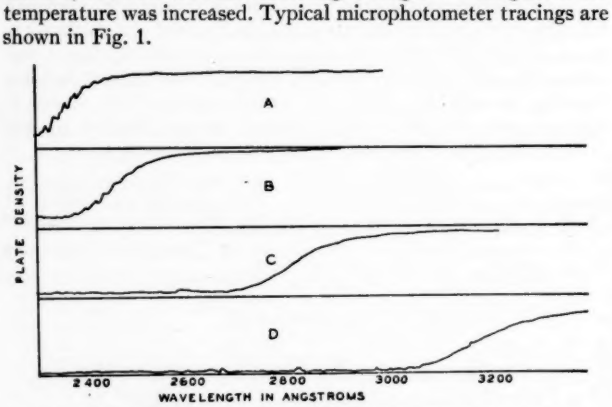

FIG. 1. Absorption spectra 50 percent C_2H_2, 50 percent He. Curve A: 400°; curve B: 450°; curve C: 500°; curve D: 555°.

The continuous absorption at lower temperatures can be attributed to conjugated unsaturated condensation products whose concentrations increase with temperature, causing extension of the region of absorption to longer wavelengths.

The fact that no C_2 or CH bands have been observed does not preclude the presence of such radicals. It is always possible that their concentrations might remain so low as to escape detection, but the experimental data give no positive evidence that these free radicals play any major role in the reaction mechanisms. The spectra do give clear evidence of the occurrence of combination reactions in the early stages of reaction, up to the ignition point and in the flame.

The authors wish to express their appreciation for the assistance of Mr. E. M. Magee and Mr. William Fain in part of the experimental work.

* This research was supported by the United States Air Force under Contracts AF 33(038)-21745 and AF 18(600)-430 monitored by Headquarters Air Research and Development Command, P. O. Box 1395, Baltimore 3, Maryland.

[1] W. G. Parker and H. G. Wolfhard, J. Chem. Soc. **1950**, 2038.
[2] Norrish, Porter, and Thrush, Proc. Roy. Soc. (London) **216**, 165 (1953).

On the Lattice Parameters and Curie Points of Unreduced Iron Catalysts

R. WESTRIK
Central Laboratory Staatsmijnen, Geleen, Netherlands
(Received August 24, 1953)

MICHEL and Pouillard[1] determined the lattice parameters and Curie points of magnetite with various amounts of Al^{3+} substituted for Fe^{3+}. They prepared their specimens by coprecipitation of the hydroxides followed by a heat treatment. The resultant mixed oxides were converted into the magnetite phases by reduction at 400°C. It was observed that, down to a given limit, both the lattice parameters and the Curie points decreased linearly with increasing amounts of Al_2O_3. This indicates that Al_2O_3 has gone into solid solution with magnetite. These results are in agreement with the older conception, based on the work of Wyckoff, Crittenden[2] and Brill[3] on iron ammonia catalysts, according to which the Al_2O_3 should have entirely dissolved in the

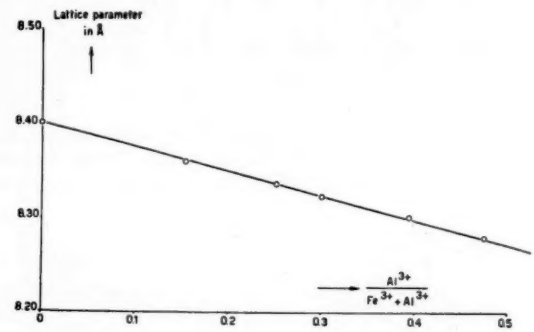

FIG. 1.

magnetite. Moreover the present knowledge of the spinel structure (Verwey and collaborators)[4] indicates that in the case of magnetite the Fe^{3+} ion can be fairly easily replaced by others, such as Al^{3+} ions, without altering the structure.

Lately, however, Maxwell, Smart, and Brunauer[5] obtained deviating results. They made an extensive thermomagnetic investigation of double and singly promoted iron catalysts for the ammonia synthesis prepared according to a melting process; these catalysts belonged to the same series as those examined by Wyckoff and Crittenden. They observed that the Curie points of unreduced singly promoted catalysts, among which there were several with different Al_2O_3 contents, differed only very little from that of pure magnetite. Considering the results found by Michel

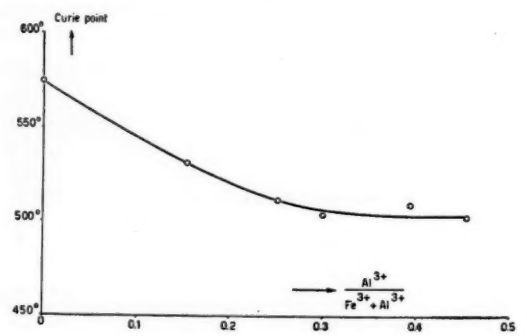

FIG. 2.

and Pouillard, they concluded that not more than about one mole percent of Al_2O_3 has gone into solid solution with Fe_3O_4.

In view of this discrepancy, we determined both the lattice parameters and the Curie points of singly promoted catalysts prepared according to a melting process and containing increasing amounts of Al_2O_3. We tried to keep the ratio between divalent and trivalent ions as close as possible to 0.50; actually it varied from 0.44 to 0.47. The x-ray photographs were made with a Guinier camera, using quartz as standard, while the Curie points were determined with a magnetic balance in an evacuated assembly. As in the latter determinations some irreproducible results were obtained owing to change occurring during the measurement, a few specimens were subjected to a temperature treatment, which did not have any significant effect on the lattice parameters.

The results are illustrated in Figs. 1 and 2. The lattice parameter decreases linearly with the ratio $Al^{3+}/(Fe^{3+}+Al^{3+})$. Extrapolating this ratio to unity, which corresponds with the spinel $FeAl_2O_4$, leads to a value of 8.14A, which is very near to the value which Verwey and Heilmann[4] found for this compound. The Curie point, the determination of which was less accurate, also shows a distinct decrease with the amount of Al_2O_3. These results clearly show that in our samples the Al_2O_3 has gone into solid solution with the magnetite.

Above 14 mole percent Al_2O_3, Michel and Pouillard found that both the lattice parameter and the Curie point do not change anymore, which should imply that in this region the Al_2O_3 no longer goes into solution. However, this has not been observed in our experiments, also the x-ray diffraction patterns did not show any trace of a new phase. It is not impossible that in the procedure followed by the latter investigators, less Fe^{3+} can be replaced by Al^{3+} than in the method used by us.

It is not clear to what cause the difference between the results of Maxwell, Smart, and Brunauer and ours is to be attributed.

[1] A. Michel and E. Pouillard, Compt. rend. **227**, 194 (1948).
[2] R. W. G. Wyckoff and E. D. Crittenden, J. Am. Chem. Soc. **44**, 2286 (1925).
[3] R. Brill, Z. Elektrochem. **38**, 669 (1932).
[4] E. J. W. Verwey and E. L. Heilmann, J. Chem. Phys. **15**, 174 (1947); Verwey, Haayman, and Romeyn, J. Chem. Phys. **15**, 181 (1947); Verwey, Braun, Gorter, and Santen, Z. Phys. Chem. **A198**, 6 (1951).
[5] Maxwell, Smart, and Brunauer, J. Chem. Phys. **19**, 303 (1951).

Some Remarks on the Equation of State and the Energy of Quantum-Liquids at the Critical Point

JOHAN VAN DRANEN
Laboratory for Analytical Chemistry, University of Amsterdam, Amsterdam, The Netherlands
(Received August 24, 1953)

THE Van der Waals equation of state gives a satisfactory qualitative representation of the behavior of a real gas. It is a well-known fact that many modifications of this equation are proposed in order to obtain a more quantitative agreement with the experimental facts. The general form for a number of these equations can be written as follows:

$$(P+aV^nT^m)(V-bV^s)=RT.$$

We shall consider in this note the equations of Berthelot ($n=-2$, $m=1$, $s=0$), of Eyring[1] ($n=-2$, $m=0$, $s=2/3$), and of Benson and Golding[2] ($n=-5/3$, $m=2/3$, $s=-1/2$).

In a series of "Letters to the Editor" we have been allowed to treat the consequences of a hypothesis concerning the critical state.[3,4] This hypothesis runs as follows: the critical state is the result of the fact that at the critical temperature the average kinetic energy (K_c) is equal to the average (negative) potential energy (U_c), or $K_c+U_c=0$, with $U_c=U_c'+P_cV_c$, where U_c' is the internal energy of gas imperfection.

With the aid of the thermodynamic relation

$$\left(\frac{dU'}{dV}\right)_T=T\left(\frac{dP}{dT}\right)_V-P,$$

it is possible to deduce from each equation an expression for U_c'. It is perhaps interesting to compare the result, given by the hypothesis $K_c=-U_c$ with the results of these equations. Van der Waals: $K_c=-2U_c$; Berthelot: $K_c=-\frac{4}{3}U_c$; Eyring: $K_c=-1.21U_c$; and Benson and Golding: $K_c=-\frac{3}{4}U_c$. We see that according to each equation the kinetic and potential energy are of the same order of magnitude but that none give the absolute equality required by this hypothesis.

We have tried to construct an equation of state, which satisfies the hypothesis. The following remarks can be made. 1.—A simple quantitative equation of state is impossible, for n, m, and s themselves are functions of P, V, and T. 2.—In view of the experimental results obtained by Michels and co-workers for U_c', and the general theoretical conclusions, the best thing is to put n equal to -2, as Van der Waals had already done in 1873. For a reasonable range of temperatures and densities $m=\frac{1}{3}$. This choice means that we take U_c' proportional to $V^{-1}T^{-1}$. 3.—According to the recent experimental results of Schneider[5] we believe that there is good evidence that under ideal circumstances (no gravitation) there is a critical point, and not a critical region, thus that we can describe the behavior of the system in the neighborhood of the critical point by an analytical function.

The results are that the simple equation with $n=1.69$, and $m=s=0$ satisfies the hypothesis and the points for $P=0$, and $P=P_c$. At very high pressures the limiting volume approaches the right value of $0.26V_c$. The value for the critical coefficient $C=P_cV_c/RT_c=0.274$ is in good agreement with the experimental value (0.294). This equation is very similar to the equation of Dietirici, with $n=1.67$, obtained as an empirical improvement of the Van der Waals equation.[6]

The more complicated expression with $n=2$, and $m=s=\frac{1}{3}$ is in agreement with the hypothesis. The value for s agrees with the fact that according to the more rigorous calculations of Kirkwood and co-workers[7] the free-volume value of Eyring for hard spheres ($s=\frac{2}{3}$) is somewhat too high. On the other hand $s=\frac{1}{3}$ is, according to Kirkwood's results, somewhat too low. The value for C (0.405) is not so good; this test is, however, a rather severe one and, by cancelling of errors (e.g., the Van der Waals equation), not always useful. Preliminary calculations, based on these equations, give a satisfactory qualitative agreement for the experimental isotherms of argon and nitrogen.

The empirical relationship $\ln p/P_c=k(1-T_c/T)$, where k is a constant and p the vapor pressure, was suggested by Van der Waals. We can deduce from the law of corresponding states that k should be a universal constant; this has been found approximately true, the value being close to 6.9 for a number of liquids.[8] With the aid of the hypothesis it is possible to calculate k theoretically. k is equal to the value for $(T/PdP/dT)$ at the critical point. We eliminate therefore, in the Clapeyron-Clausius equation, $H=L+P(V_g-V_l)$, using for L the formula given in a preceding note,[4] namely, $L=-U_c'V_c(V_l^{-1}-V_g^{-1})$. We have, according to our hypothesis, $-U_c'=3/2RT_c+P_cV_c$. Applying this relation gives for k the formula: $k=2+3/2C$, where C is the critical coefficient. We obtain therefore that k is equal to about 7, in good agreement with the experimental value. The Van der Waals equation gives $k=4$.

TABLE I. The critical constants and the various energies at the critical point of helium and hydrogen.[a]

	T_c	P_c	V_c	K_c	P_cV_c	U_c'	Z_c[b]	Z_c[c]
Helium (3)	3.34	1.15	72	11	2	−24	11	11
Helium (4)	5.20	2.26	57.8	14	3	−27	10	11
Hydrogen	33.2	13.0	67.0	98	21	−140	21	24

[a] Units: °K, atmos, cm³/mole, and cal/mole, respectively.
[b] According to the hypothesis.
[c] According to the formula of London.

It is a well-known fact that helium and hydrogen are blown up by their quantum-mechanical zero-point energies. If we apply the hypothesis at these substances we have the relation: $K_c+Z_c+P_cV_c+U_c'=0$, where Z_c is the zero-point or better Heisenberg energy. The kinetic energy can be calculated using the expressions for the total translational energy for Bose-Einstein (e.g., He^4) or Fermi-Dirac (e.g., He^3) particles. With the aid of the tables of Hirschfelder and co-workers[9] and Kirkwood and co-workers,[10] taking into account the results mentioned in references 3 and 4, we obtain a reasonably accurate value for U_c'. Then Z_c can be calculated; see Table I, seventh column. The zero-point energies of helium for different volumes have been independently calculated by London[11] and Pekeris[12] and determined experimentally by Dugdale and Simon.[13] It is a very remarkable fact that the results according to the hypothesis are in close agreement with the values of London. Table I, eighth column, shows the values for Z_c using

the following interpolation formula of London: $Z=N^2h^2d/2\pi M(R-1.12d)^2(R+0.713d)$, where M is the atomic or molecular weight, $NR^3=V$, and d the diameter of the particle (for helium $d=2.65$A, and for hydrogen $d=2.93$A).[14]

Even more remarkable is that the very accurate measurements of Dugdale and Simon give also an extremely good agreement with the values calculated by London (reference 13, Fig. 12).

With respect to the hypothesis we remark that, if true, this hypothesis can be deduced from statistical mechanical principles, if it should be possible to avoid crude approximations.

We have very much appreciated a discussion with Dr. E. D. G. Cohen on the article of Pekeris.

[1] H. Eyring and J. O. Hirschfelder, J. Chem. Phys. **5**, 249 (1937).
[2] S. W. Benson and R. A. Golding, J. Chem. Phys. **19**, 1413 (1951).
[3] J. van Dranen, J. Chem. Phys. **20**, 1175 (1952).
[4] J. van Dranen, J. Chem. Phys. **21**, 567 (1953); **21**, 1404 (1953).
[5] W. G. Schneider, Proceedings of the International Conference on Phase Transitions (written in French), Paris (1952).
[6] C. Dietirici, Drudes Ann. **5**, 51 (1901).
[7] Kirkwood, Maun, and Alder, J. Chem. Phys. **18**, 1040 (1950).
[8] S. Glasstone, *Textbook of Physical Chemistry* (D. Van Nostrand Company, Inc., New York, 1946), p. 454.
[9] Wentorf, Buehler, Hirschfelder, and Curtiss, J. Chem. Phys. **18**, 1484 (1950).
[10] Kirkwood, Lewinson, and Alder, J. Chem. Phys. **20**, 930 (1952).
[11] F. London, Proc. Roy. Soc. (London) **A153**, 576 (1936).
[12] C. L. Pekeris, Phys. Rev. **79**, 884 (1950).
[13] J. S. Dugdale and F. E. Simon, Proc. Roy. Soc. (London) **A218**, 291 (1953).
[14] R. J. Lunbeck, Ph.D. thesis (Amsterdam, 1951), p. 35 and p. 41.

Thermal Equilibrium between *F* Centers and *M* Centers in Alkali Halides*

WILLIAM A. SMITH† AND ALLEN B. SCOTT
Department of Chemistry, Oregon State College, Corvallis, Oregon
(Received August 17, 1953)

RECENT work[1] has shown that M centers may be produced thermally in alkali halides by additive coloration. Previously, these color centers had been considered primarily as an optical product[2] resulting from photo-ionization of F centers. Seitz[3] has proposed a model for the M center consisting of a pair of vacancies and an electron trapped in a negative ion vacancy. An investigation of the rate of photo-bleaching of M centers,[4] using polarized light, has given further support to Seitz's model for this center. Evidence which indicates the existence of a thermal equilibrium between M centers and F centers in additively colored KCl and KBr, has been obtained in this laboratory. The data indicate that one F center is required to produce one M center, which would be the case if Seitz's model is the correct one.

Single crystals of KCl and KBr[5] were sealed into Pyrex tubes containing potassium metal. The tubes were heated in a furnace provided with two independently controlled heating elements. The upper element maintained the crystal at 600°C, while the lower element maintained the potassium at 445°C. In order to provide a range of color center concentrations in one crystal, the crystals were heated for times shorter than that required to reach a saturation concentration of color centers. This treatment gave crystals which were quite densely colored at the exterior faces and uncolored at the center. These crystals were stored in light-proof containers and handled in red light.

A crystal holder, having a screw-activated specimen mount which moved behind a small fixed slit (about 0.4 mm wide), was constructed to fit into a Beckman Model DU spectrophotometer cell holder. Thin samples of crystals, with the longest dimension (about 3 mm) parallel to the concentration gradient, were cemented to the movable mount and absorption spectra were measured at several locations, starting with the densely colored portion and moving toward the uncolored portion. Growth of the R bands and the M band due to optical destruction of the F band was minimized by making the measurements at the red end of the spectrum first.

From the form of the Smakula[6] equation it is seen that the concentration of any color center for which this equation is valid is directly proportional to the extinction coefficient measured at the center of the absorption band. The validity of the Smakula equation for the determination of M-center concentration has not been proven experimentally, but since the M band has the same bell-like shape as the F band and is affected by temperature in just the same way, its use is justified. Ratios of the maximum extinction coefficient for the two bands were calculated for the various slit positions. These calculations are shown in Table I.

TABLE I. Extinction coefficient ratios for the M band and F band in additively colored KCl and KBr.

Crystal; heating time	Position of slit mm	Extinction coefficient ratio (M band/F band)	Average values and average deviations
K-KCl; 4.5 hours	0.00	0.218	
	0.17	0.189	
	0.35	0.196	
	0.52	0.203	
	0.71	0.189	0.199 ±0.009
K-KCl; 4.0 hours	0.00	0.254	
	0.17	0.222	
	0.35	0.229	
	0.71	0.204	
	1.06	0.232	
	1.42	0.237	0.230 ±0.011
K-KBr; 0.5 hour	0.00	0.069	
	0.17	0.071	
	0.52	0.061	0.067 ±0.004

An examination of this table shows good agreement of the extinction coefficient ratios for the individual crystals. There is also reasonable agreement between the average values of this ratio for the two KCl crystals which were prepared under comparable conditions; the small difference observed may be attributed to the lack of precise control of the coloring temperature. These results show that a thermal equilibrium exists between F centers and M centers during the coloration process; further, the attainment of the equilibrium is rapid compared with the rate of diffusion of the centers into the crystal. Since a constant ratio of the first power of the extinction coefficient is obtained throughout the concentration range from zero up to about 10^{17} centers/cc, it is evident that one M center is produced for each F center destroyed.

* Taken from the Ph.D. thesis of William A. Smith, Jr. This work supported in part by the U. S. Office of Naval Research.
† Present address: The Knolls Atomic Power Laboratory, General Physics Unit, Schenectady, New York.
[1] A. B. Scott and W. A. Smith, Phys. Rev. **83**, 982 (1951).
[2] S. Petroff, Z. Physik **127**, 443 (1950).
[3] F. Seitz, Revs. Modern Phys. **18**, 384 (1946).
[4] M. Ueta, J. Phys. Soc. Japan **7**, 107 (1952).
[5] Single crystals of these salts were obtained from the Harshaw Chemical Company.
[6] A. Smakula, Z. Physik **59**, 603 (1930).

Equal Pressure Diffusion in Porous Substances

J. HOOGSCHAGEN
Central Laboratory of Staatsmijnen, Limburg, Geleen, The Netherlands
(Received September 1, 1953)

DURING our investigations into gas diffusion through porous catalysts[1] the following question arose: If on either side of a porous tablet two different gases A and B (or mixtures of the two gases) are present, and the *total pressures and temperatures are equal*, what will be the ratio of the diffusion rates?

If the pore size is smaller than the free path of the gas molecules, the diffusion will have a Knudsen character. Then, the well-known Knudsen formula[2] leads to the relation:

$$N_A\sqrt{(M_A)}+N_B\sqrt{(M_B)}=0. \quad (1)$$

Here, N_A and N_B are the diffusion rates in moles, M_A and M_B being the molecular weights of the gases. (In general for any number of gases: $\Sigma N_i\sqrt{(M_i)}=0$.)

If the pore size exceeds the free path, bulk diffusion will occur. As far as the author knows, it is generally assumed in this case

that: $N_A+N_B=0$ (see for instance Wicke[3]). However, a theoretical estimate in which the disturbed Maxwellian velocity distribution is taken into account leads to the same relation (1) as for Knudsen diffusion. This deduction is based on the fact that the net impulse transferred to the pore walls in the direction of diffusion must be zero if no total pressure gradient exists. The impulse transferred to the wall by the diffusing molecules of A will balance the impulse transferred by the molecules of B diffusing in the opposite direction. As the peculiar velocity distribution in the vicinity of the wall has been neglected in the estimate, the theoretical conclusion might be in error. Therefore we decided to make some experiments with the arrangement according to Fig. 1.

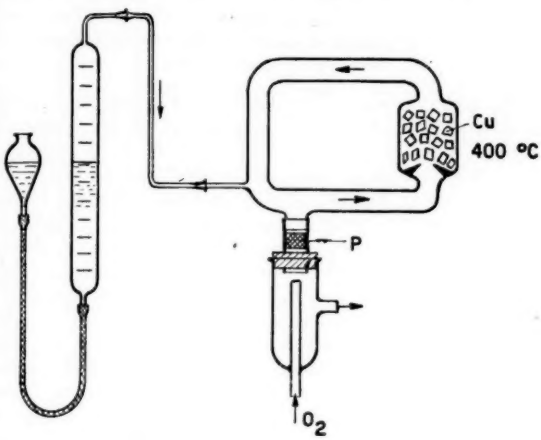

FIG. 1.

Through a porous tablet P inert gas diffuses downwards where it is carried away by a stream of oxygen. The oxygen diffusing upwards into the inert gas is continuously removed by heated active copper. The inert gas circulates through the copper by natural convection. From a gas burette, inert gas is supplemented at such a rate as to keep the pressure difference across the tablet exactly zero. The diffusion rate of the oxygen follows from the weight gain of the copper.

The diffusion through the tablet will not have a Knudsen character for two reasons: (1) the tablet consists of compressed globules of carbonyl iron ranging from 1 to 8μ in diameter. (2) the flow of nitrogen under the influence of a pressure difference highly exceeded the diffusion rate under the influence of the same partial pressure difference.

The results of a number of experiments are given in Table I.

Although the experiments were somewhat preliminary we may deduce that Eq. (1) reasonably holds.

Apparently, the ratio of diffusion rates does not enable a distinction between bulk and Knudsen diffusion in porous substances. A deviation from (1) would point to an additional transport in an adsorbed surface layer. For two commercial adsorbents with a large internal surface area this effect could be easily detected (see Table II).

TABLE I. Ratio of diffusion rates.

Gases	Ratio observed	Theor. ratio acc. to Eq. (1)
$He-O_2$	3.03:2.66:2.54	2.83
N_2-O_2	1.09: ···:1.07	1.07
CO_2-O_2	0.89: ···:0.80	0.85

The active carbon Norit R III—A has a specific surface area of 1400 m²/g and a mean pore diameter of 13.8A. For the silica gel ST 25 these figures are 1020 m²/g and 8.6A respectively.

The heavier and larger CO_2 molecules diffuse more rapidly because they are appreciably adsorbed and an additional transport in the adsorption layer is possible.

TABLE II.

Adsorbent	$-N_{CO_2}/N_{O_2}$ Observ.	$-N_{CO_2}/N_{O_2}$ Acc. to Eq. (1)	$-N_{N_2}/N_{O_2}$ Observ.	$-N_{N_2}/N_{O_2}$ Acc. to Eq. (1)
Active carbon	1.40	0.85	1.09	1.07
Silica gel	1.81	0.85	1.06$_5$	1.07

More elaborate and extensive experiments are contemplated. A detailed account of the work will be published elsewhere.

[1] C. Bokhoven and J. Hoogschagen, J. Chem. Phys. **21**, 159 (1953).
[2] M. Knudsen, Ann. Physik. **28**, 75 (1909).
[3] E. Wicke and R. Kallenbach, Kolloid Z. **97**, 135 (1941).

Erratum: Self-Diffusion in the Alkali Metals

[J. Chem. Phys. **21**, 177–178 (1953)]

D. K. C. MACDONALD
Division of Physics, National Research Council, Ottawa, Canada

IT has been pointed out to me by Dr. Dienes and Dr. Carpenter, to whom I am grateful, that after Eq. (1) in this note I should have said . . . "where U is the energy for formation of a lattice vacancy."

Crystal Class of Na_2SO_4 III

D. R. DASGUPTA
X-Ray Department, Indian Association for the Cultivation of Science, Calcutta, India

(Received September 15, 1953)

IT was reported by Fravel[1] that "altered thenardile" or Na_2SO_4 III belongs to the orthorhombic crystal class with $a=5.59$A, $b=8.93$A, and $c=6.98$A, having the space-group Pbnn. We tried to index all the lines of the powder pattern of Na_2SO_4 III with the help of the data supplied by Fravel but this was found not possible.

Moreover, Lipson's[2] method was applied to show further that Na_2SO_4 III does not certainly belong to the orthorhombic crystal class. Ultimately, with the application of the method suggested by Hesse[3] and Stosick,[4] we found that Na_2SO_4 III belongs to the tetragonal class with 16 molecules in the unit cell, having parameters $a=b=13.45$A and $C=7.879$A, respectively. It was possible to index all the lines with this data to a good degree of certainty. Further, it was observed that with the foregoing symmetry only the odd orders of (*hho*) were absent. Since the number of the reflecting planes in the case of a powder pattern is limited, it is very difficult to assign any definite space-group to Na_2SO_4 III, but from the reflections observed in the powder pattern it seems that the most possible space-group for Na_2SO_4 III is D_{2d}^{12} or $I\bar{4}2d$.

[1] L. K. Fravel, J. Chem. Phys. **8**, 290 (1940).
[2] H. Lipson, Acta Cryst. **2**, 43 (1949).
[3] R. Hesse, Acta Cryst. **1**, 200 (1948).
[4] A. J. Stosick, Acta Cryst. **2**, 271 (1949).

Madelung Constants and Coordination*

DAVID H. TEMPLETON
Department of Chemistry and Radiation Laboratory, University of California, Berkeley, California

(Received August 17, 1953)

THE major chore in the calculation of the electrostatic energy of an ionic crystal is the summation of a conditionally convergent series

$$A(R)=-0.5\sum_{i,j} Rz_iz_j/r_{ij}, \quad i\neq j$$

where $A(R)$ is called the Madelung constant for the distance R taken as unity. The index i runs up to n, the number of atoms in

the "molecule," while j includes also an infinite number of neighboring atoms. Because of the great labor involved in this computation, it is interesting that for binary crystals there exists an empirical relation between A and the coordination numbers of the ions.

The Madelung constants as usually tabulated cover a wide range of values.[1] Kapustinsky[2] pointed out that α, the Madelung constant per valence bond, is approximately the same for many substances when defined as

$$\alpha = 2A(R_0)/z_a z_c n,$$

where R_0 is the shortest anion-cation distance, and z_a and z_c are the anion and cation charge numbers. The range of α is from 1.48 to 1.76 for various structures. Large values of α correspond to large coordination numbers, as is to be expected since the leading term in the series is proportional to the coordination number. To get a correlation for various formula types, it is necessary to use some kind of average of the coordination numbers p and q of the anions and cations. The weighted harmonic mean m, defined by the relation

$$1/m = \frac{1}{n_a+n_c}\left(\frac{n_a}{p}+\frac{n_c}{q}\right)$$

seems to be the best average for this purpose. Here n_a and n_c are the numbers of anions and cations in the molecular formula. A plot of α as a function of $1/m$, Fig. 1, shows a linear relationship with an

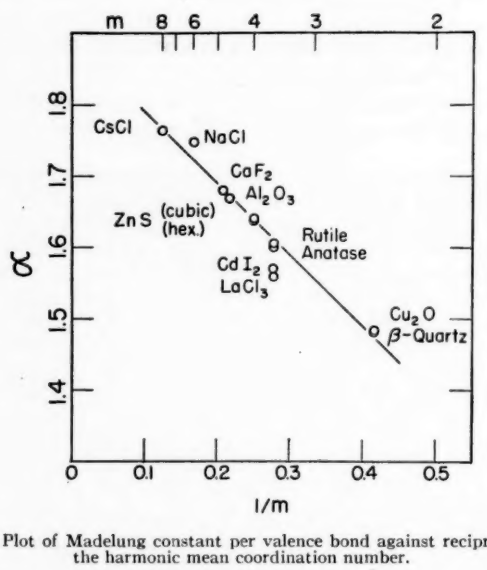

FIG. 1. Plot of Madelung constant per valence bond against reciprocal of the harmonic mean coordination number.

average accuracy of 0.9 percent for the twelve cases for which we have data. The equation of the line shown in the figure is

$$\alpha = 1.890 - 1.000/\mathrm{m}.$$

The values of A are taken from Sherman's review paper[1] except for Cu_2O[3] and $LaCl_3$.[4]

The success of this correlation reflects the fact that the electrostatic energy is very great compared with the energy differences between various solid structures and that these differences follow a trend with coordination number. No theoretical significance is known for the linearity with 1/m. It can be shown that the use of the harmonic mean is algebraically equivalent to using the curve to get a value of α for each atom, and then taking an arithmetical average of α for all the atoms in the substance.

This curve has already found application in predicting the Madelung constant of $LaCl_3$ while it was being computed by Koch, and in again calling attention to the error in the earlier value for Cu_2O.[1] The correct value for Cu_2O, computed by Sherman,[3] had escaped our attention. The curve is recommended as a check for calculated values because of the well-known pitfalls with regard to convergence and omission of terms.

I thank Professor L. Pauling for some helpful suggestions. This research was supported by the U. S. Atomic Energy Commission.

* University of California Radiation Laboratory (UCRL-2282) Contract No. W-7405-eng-48.

[1] J. Sherman, Chem. Revs. 11, 93–170 (1932).
[2] A. Kapustinsky, Z. phys. Chem. B22, 257–60 (1933).
[3] J. Sherman, Z. Krist. 87, 342 (1934).
[4] C. W. Koch (private communication).

The π-Energy Levels of Ethylene

CARL M. MOSER
Mathematical Institute, Oxford University, Oxford, England
(Received August 27, 1953)

IT is by now well-known that the best wave functions that can be obtained by an orbital approximation for the system of π electrons in unsaturated molecules predict the $N \rightarrow V$ and $V \rightarrow T$ intervals to be too large when analytical functions are used to evaluate the energy integrals. Moffitt[1] has considered the problem in detail for oxygen and has evolved a method in which the agreement with experiment of the observed transitions is certainly as good as one would wish. He has applied the method to ethylene, though the details have as yet not been published. However, it seems probable that this method would be exceedingly tedious if it were to be applied to a molecule like naphthalene. We have been working on a change in the usual ASMO procedure in the hope of improving the agreement between the calculations and the observed spectra and also with the hope that the method might be applied with ease to large molecules. We have used as the simple prototype ethylene.

The reasoning advanced by Pariser and Parr[2] that the (11|11) integral should have the value of 10.53 ev rather than the analytical value seems very sound. It is necessary to point out that the W_{2p} terms precisely cancel out in the excitation energy and one is left with only an electron repulsion term. Thus the primary assumption of our method is that whenever the (11|11) integral occurs in the *electron repulsion* integrals the analytical value is replaced by the value of 10.53 ev found from spectroscopic data.

The results are collected in Table I. In column (a) are the experimental values, in (b) the predictions of the usual ASMO calculation, and in column (c) the results of the usual ASMO calculation making the above assumption. It is seen that the $V \rightarrow T$ transition is now in excellent agreement with experiment, but the $N \rightarrow V$ transition is now much too small. If the wave functions are multiplied out it will be seen[3] that the $V \rightarrow T$ transition is independent of the method used to calculate the orbital part of the energy but the $N \rightarrow V$ transition is dependent upon the value obtained for the orbital part of the energy. Ross[4] has made a careful study of the methods used to calculate the orbital energy and has indicated that the usual assumption, due to Goeppert-Mayer and Sklar,[5] is not necessarily the best. If exchange of the core electrons with the electrons of the system being explicitly considered is included in the calculation, the agreement with experiment is a bit better [column (d)]. Also Ross has shown that if one uses an "additive" method[6] rather than a "subtractive" method to determine the orbital energy the difference in orbital energies is still larger than when exchange is included in the GMS approximation. If SCF functions were used, they should give the same results (GMS with exchange), but as only analytical func-

TABLE I.

Transition	(a)	(b)	(c)	(d)	(e)
$^1A_{1g} - {}^1B_{1u}$	7.6 ev[a]	11.4	4.8	5.8	7.2
$^3B_{1u} - {}^1B_{1u}$	1.2[b]	8.6	1.2	1.2	1.2
Change due to C.I.		1.4	0.04	0.04	0.04

[a] P. G. Wilkinson and H. L. Johnston, J. Chem. Phys. 18, 190 (1950).
[b] Potts, Ph.D. thesis, University of Chicago, 1953.

tions are used, presumably one is free to choose. It is seen [column (e)] that the agreement between experiment and calculations using the additive method, is reasonably satisfactory.

There are some difficulties in the use of this last method to calculate the orbital energies. One must assume the kinetic energies of the electrons in the bonding and anti-bonding states to be the same even though calculation with Slater orbitals gives a difference of something like 15 ev! though many people have noted that Slater orbitals are particularly bad to calculate kinetic energy values. Also it has been observed[2] that the integral which Ross defines as $(M:kl)$ is probably much too high from the calculation with analytical functions when $M=k=l$. In addition, one has here a number of integrals where there are two electrons on the same center, though in this case both electrons are not in $2p\pi$ orbitals. Thus the satisfaction that may be obtained from a comparison of columns (a) and (e) must be curtailed due to the unsatisfactory state of the calculation of orbital energies. But this reserve must apply to all calculations. Also, the last method might be rather more complicated than the GMS when applied to a larger molecule than ethylene.

In all of the modified calculations configuration interaction (C.I.) is so small that it can be safely neglected.

The interest and suggestions of Professor C. A. Coulson, F.R.S., are gratefully acknowledged.

[1] Moffitt, Proc. Roy. Soc. **A210**, 224, 246 (1951).
[2] R. Pariser and R. G. Parr, J. Chem. Phys. **21**, 466 (1953); **21**, 767 (1953).
[3] R. G. Parr and B. L. Crawford, J. Chem. Phys. **16**, 526 (1948).
[4] Ross, Trans. Faraday Soc. **48**, 973 (1952).
[5] Goeppert-Mayer and Sklar, J. Chem. Phys. **6**, 645 (1938).
[6] Reference 4, Eq. (13).

Two New Lines in the Microwave Spectrum of Heavy Water

HARRY D. CRAWFORD*
Department of Electrical Engineering, Institute of Technology, University of Minnesota, Minneapolis, Minnesota
(Received August 28, 1953)

TWO new microwave spectral lines of heavy water have been found in the X-band region with the help of a Stark modulated spectrometer using square wave modulation at 10 kc/sec in a 10-foot absorption cell.[1] A noise diode in parallel with the detector crystal provides a means of estimating the minimum detectable absorption of the instrument; this quantity was found to be 10^{-7}/cm or lower, depending somewhat on the selection of crystals and the power levels used.

King, Hainer, and Cross[2] had predicted a line for D_2O at 0.31 cm^{-1} with an absorption coefficient 5×10^{-6}/cm, due to the transition $5_{32}-4_{41}$. Using heavy water for a sample, a line indeed was found at 8884.83 ± 0.07 mc/sec with an estimated absorption coefficient of 2×10^{-6}/cm.[3] It was noted that the Stark spectrum could not be resolved indicating that the line is due to a transition between levels of relatively high J values.

Along with this line a very strong line at 8577.80 ± 0.08 mc/sec was found simultaneously in a supposedly "pure" sample of D_2O. Burke and Strandberg[4] have identified this line with the aid of Zeeman spectra as being due to HDO. The presence of HDO in our sample is understandable since heavy water is hygroscopic and undergoes exchange reactions with many hydrogen containing compounds. It was, therefore, difficult to obtain a pure D_2O sample in our absorption cell.

The question was now to which molecule this line at 8884.83 mc/sec should be assigned. Since H_2O gives no spectra in this region, we only had to discriminate between HDO and D_2O. By diluting the sample and measuring the ratio of the intensities of the 8577 mc/sec and the 8884 mc/sec we found strong indication that later absorption line was indeed due to D_2O.

Let a mixture be formed by combining a fraction X of D_2O and a fraction $(1-X)$ of H_2O; then the ratio of the concentrations of HDO and D_2O is

$$\frac{\text{HDO}}{\text{D}_2\text{O}}=\frac{2(1-X)}{X}. \tag{1}$$

The intensity of the lines should be proportional to the relative concentration.

If the 8884.83 mc/sec line were due to D_2O, the relative intensities of the lines at 8884 mc/sec and 8577 mc/sec should follow a relative like that immediately above. If the 8884.83 mc/sec were also due to HDO, the ratio above would be independent of X. In order to discriminate between the two cases, the ratio of the intensities of the two lines was measured for various values of X at constant pressure and microwave power level; X was varied by dilution of the sample. Table I gives the calculated and observed values of the ratio given in (1).

TABLE I. Calculated and observed values of the ratio given in Eq. (1).

X	$\frac{2(1-X)}{X}$	$\frac{\text{Observed intensity of 8577 mc/sec}}{\text{Observed intensity of 8884 mc/sec}}$
$\frac{1}{2}$	2	0.9
$\frac{1}{4}$	4	2.2
$\frac{1}{8}$	8	4.5

Thus, the theoretical values follow a geometric progression (determined by proper dilution) while the experimental values tend to follow one also. The intensity measurements are subject to relatively large errors and the concentration ratio in the cell may differ slightly from that in the liquid phase.

Nevertheless, the above results strongly indicate that the transitions at 8884.83 mc/sec is to be attributed to D_2O. Whether it is indeed the $5_{32}-4_{41}$ line predicted by King, Hainer, and Cross is undecided since the Stark spectrum was not resolved.

From a large number of measurements made at high frequencies the microwave spectroscopy group at the Massachusetts Institute of Technology was able to predict that HDO had an absorption line at 8835 mc/sec.[5] A search using an equilibrated sample containing equal parts of hydrogen and deuterium gave indeed a line at 8837.22 ± 0.12 mc/sec with an estimated absorption coefficient of 10^{-7}/cm.

According to the group at the Massachusetts Institute of Technology, the line corresponds to a transition between high J values. It is therefore not surprising that we did not resolve the Stark spectrum. No other lines were found in H_2O or in equilibrated samples of heavy water showing an absorption coefficient greater than 10^{-7}/cm in the frequency range 8000 to 9500 mc/sec.

The author wishes to express his appreciation to Dr. A. van der Ziel, his adviser; to Dr. H. E. Hartig for continued financial support; and finally, to Mr. William C. Smith, now of Bell Telephone Laboratories, who did much of the electronic work in the spectrometer.

* This paper constitutes part of the work performed for a Ph.D. thesis in the Department of Electrical Engineering, University of Minnesota.
[1] The construction of this instrument was supported financially by a grant from the Graduate School of the University of Minnesota to Dr. A. van der Ziel.
[2] King, Hainer, and Cross, Phys. Rev. **71**, 433 (1947).
[3] The heavy water was supplied by Norsk Hydro Elektrisk Kvoelstofakieselskab, Solligen 7, Oslo, Norway.
[4] B. F. Burke and M. W. P. Strandberg, Phys. Rev. **90**, 303 (1953).
[5] Private communication with M. W. P. Strandberg.

Evidence for Globulite Molecules in Ribonuclease*

DOROTHY WRINCH
Department of Physics, Smith College, Northampton, Massachusetts
(Received September 15, 1953)

EVIDENCE regarding the general structural types of the individual chemical units in the ribonuclease entity is contained in Carlisle and Scouloudi's vector projections of crystalline ribonuclease[1] shown in Fig. 1. In each, certain high density regions

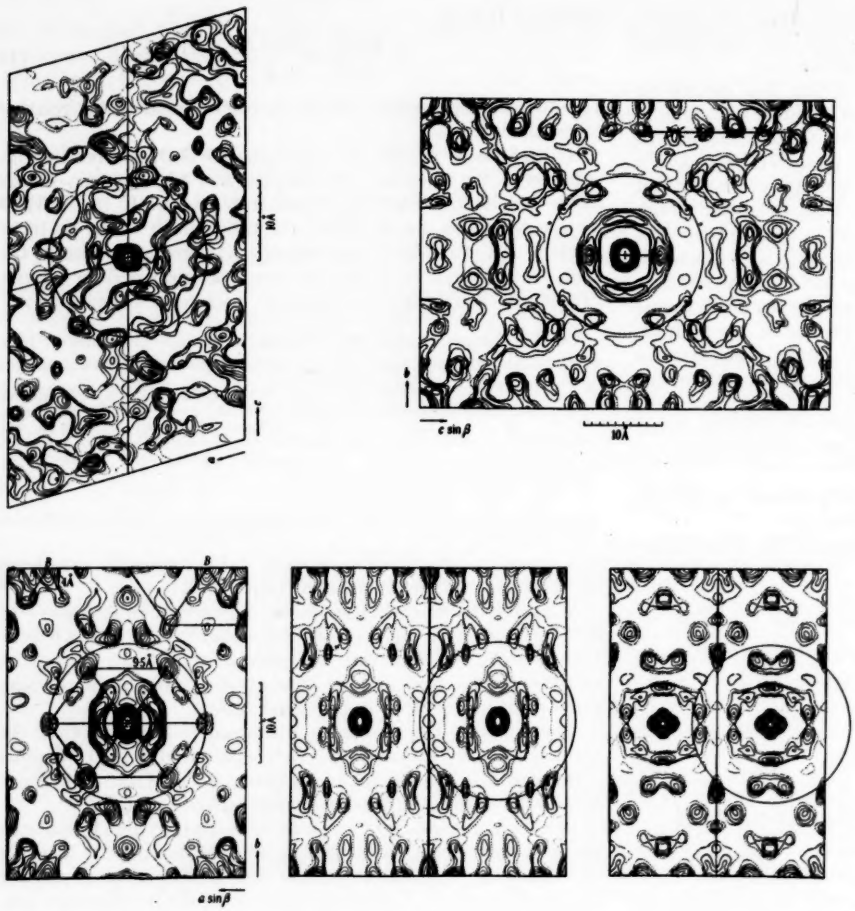

FIG. 1. The vector projections for the monoclinic wet ribonuclease crystal given by Carlisle and Scouloudi (see reference 1), on which circles of radius 10A centered at the origin have now been drawn. The projections are along [001], [201], [301], on the left, and along [010] and [100] on the right. [After Carlisle and Scouloudi, Proc. Roy. Soc. (London) **A207**, 496 (1951), Figs. 4, 5, 11, and 16.]

are seen at about 4–5A from the origin in a considerable variety of directions. An interpretation of the profusion of these 4–5A vectors in terms of actual protein molecules would require their projections in all five directions to be of impossibly small dimensions.[2] Under these circumstances, it is probable that this phenomenon is to be attributed not to the protein but to water clusters.[2,3] Necessarily proceeding further out for evidence regarding the structural type of the protein component, we remark in each projection regions of high vector density at 9–11A from the origin, also in many directions, suggesting the presence in the crystal of relatively small structures which are more or less equidimensional in shape. The notable dearth of vectors of intermediate lengths, say 6–8A, in many directions from the origin suggests that these globulite structures are cage-like in character, with interiors of relatively low density.[4,5] These specifications fit well with those obtained for individual structures in the normal wet horse monoclinic horse methemoglobin crystal. As in this case discussed earlier,[2,6] for which incomparably more information is available, i.e. 3-dimensional intensity and vector maps, we may picture individual structures which are polymerizations of $N-C_\alpha-C$ monomers in the form of relatively thin globulite shells of diameters slightly greater than 11A, say 12A. In each case the actual protein entity would contain a particular number of such shells, arranged at a set of points: each shell might then be identified with a polymer of the $N-C_\alpha-C$ monomers carrying R groups, correlated in particular ways with various subsets of the C_α atoms.

A structure for ribonuclease comprising a bundle of polypeptide chains (in the c direction) has, however, been put forward.[1,7] It has to be emphasized therefore that, just as in the case of horse hemoglobin,[2,6] the lack of evidence of some one particularly significant direction in the vector distribution, i.e., the lack of any uniaxial character in the vector distributions shown in Fig. 1, particularly in the neighborhood of the origin, points very strongly against any structure of the classical type for this protein. And this conclusion also emerges when we study the actual distribution of the high-density regions at 9–11A from the origin. Basic significance has been attributed to these high-density regions on and only on the c projection, the lines seen in Fig. 1 being drawn to emphasize the argument.[1,7] However, in point of fact, high-density regions at such distances from the origin are present on every one of the 5 sections, as is clearly seen when the 10A circles are drawn. That these high-density regions as a whole are diagnostic of the type of individual structures in the protein entities, that they are intrastructural in nature and point towards a globulite type of skeleton in the ribonuclease entity, seems highly probable.

* This work is being supported by the U. S. Office of Naval Research.

[1] C. H. Carlisle and H. Scouloudi, Proc. Roy. Soc. (London) **A207**, 496 (1951).
[2] D. Wrinch, J. Chem. Phys. **20**, 1051, 1332 (1952).
[3] D. Wrinch, Internatl. Cong. Crystallography, Abstract P7 (1951).
[4] D. Wrinch, Phil. Mag. **27**, 111 (1939).
[5] D. Wrinch, Phys. Rev. **79**, 203 (1950).
[6] D. Wrinch, Acta Cryst. **6**, 562 and 638 (1953).
[7] Carlisle, Scouloudi, and Spier, Proc. Roy. Soc. (London) **B141**, 85 (1953).